

COPY NO. 28



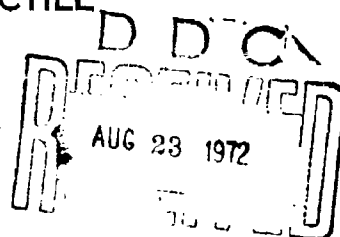
AD 746977

TECHNICAL REPORT 4300

**AERODYNAMIC CHARACTERISTICS
AND
SUBSONIC FLIGHT PERFORMANCE
OF THE
SPIN-STABILIZED, 4.2 INCH M329A1E1
MORTAR PROJECTILE**

R. KLINE
W. GAZDAYKA

JUNE 1972



APPROVED FOR PUBLIC RELEASE; DISTRIBUTION UNLIMITED

Reproduced by
NATIONAL TECHNICAL
INFORMATION SERVICE
U S Department of Commerce
Springfield VA 22151

**PICATINNY ARSENAL
DOVER, NEW JERSEY**

The findings in this report are not to be construed
as an official Department of the Army position.

DISPOSITION

Destroy this report when it is no longer needed. Do
not return it to the originator.

UNCLASSIFIED

Security Classification

DOCUMENT CONTROL DATA - R & D		
(Security classification of title, body of abstract and indexing annotation must be entered when the overall report is classified)		
1. ORIGINATING ACTIVITY (Corporate author)		2a. REPORT SECURITY CLASSIFICATION
Picatinny Arsenal, Dover, New Jersey 07801		UNCLASSIFIED
		2b. GROUP
3. REPORT TITLE		
AERODYNAMIC CHARACTERISTICS AND SUBSONIC FLIGHT PERFORMANCE OF THE SPIN-STABILIZED 4.2 INCH M329A1E1 MORTAR PROJECTILE		
4. DESCRIPTIVE NOTES (Type of report and inclusive dates)		
5. AUTHOR(S) (First name, middle initial, last name)		
R. Kline W. Gazdayka		
6. REPORT DATE	7a. TOTAL NO. OF PAGES	7b. NO. OF REFS
	443	9
8a. CONTRACT OR GRANT NO.	9a. ORIGINATOR'S REPORT NUMBER(S)	
b. PROJECT NO.	Technical Report 4300	
c. AMCMS Code 4810.16.2222.6	9b. OTHER REPORT NO(S) (Any other numbers that may be assigned this report)	
d.		
10. DISTRIBUTION STATEMENT		
Approved for public release; distribution unlimited.		
11. SUPPLEMENTARY NOTES		12. SPONSORING MILITARY ACTIVITY
13. ABSTRACT		
<p>An extensive study of the aerodynamic characteristics of the 4.2" M329A1E1 Mortar Projectile has been conducted. A spectrum of yaw levels up to 40° and Mach numbers from 0.55 to 1.025 were covered in the Ballistic Research Laboratories (BRL) Transonic Range Facility. A Magnus wind tunnel test in the Ames 12' Pressure Wind Tunnel involved boom and boattail effects on Magnus as well as static forces from moments. Mach numbers from 0.3 to 0.95 and angles of attack from 0° to 30° (for a Mach number of 0.3) and 0° to 20° (for the higher Mach numbers) were considered. Shells instrumented with yaw sondes were fired at Wallops Island Facility of NASA. The theoretical differential equation of motion then was fitted to the resulting single plane angular motion data.</p>		

DD FORM 1473

1 NOV 66

REPLACES DD FORM 1473, 1 JAN 64, WHICH IS
OBSOLETE FOR ARMY USE.

UNCLASSIFIED

Security Classification

1 w

433

UNCLASSIFIED
Security Classification

14. KEY WORDS	LINK A		LINK B		LINK C	
	ROLE	WT	ROLE	WT	ROLE	WT
Spin stabilized projectiles Aeroballistic characteristics Yaw sondes Transonic wind tunnel tests Transonic free flight range data Aerodynamic coefficients						

1b

UNCLASSIFIED
Security Classification

Technical Report 4300

AERODYNAMIC CHARACTERISTICS AND SUBSONIC FLIGHT
PERFORMANCE OF THE SPIN-STABILIZED,
4.2 INCH M329A1E1 MORTAR PROJECTILE

by

R. Kline
W. Gazdayka

JUNE 1972

Approved for public release; distribution unlimited.

AMCMS Code 4810.16.2222.6

Engineering Sciences Division
Feltman Research Laboratory
Picatinny Arsenal
Dover, N.J.

IC

The citation in this report of the trade names of commercially available products does not constitute official indorsement or approval of the use of such products.

TABLE OF CONTENTS

	Page No.
Abstract	1
Introduction	2
Test Facilities	2
BRL Transonic Range	2
NASA Ames 12' Pressure Wind Tunnel	3
Performance Flight Tests	4
Yaw Sonde Program	4
Experimental Procedure	5
BRL Transonic Range	5
NASA Ames 12' Pressure Wind Tunnel	5
Performance Flight Tests	6
Yaw Sonde Program	6
Data Reduction Techniques	7
BRL Transonic Range	7
NASA Ames 12' Pressure Wind Tunnel	7
Performance Flight Tests	7
Yaw Sonde Program	7
Presentation of Test Results	7
BRL Transonic Range	7
NASA Ames 12' Pressure Wind Tunnel	7
Performance Flight Tests	8
Discussion and Analysis (BRL Range and Ames Wind Tunnel)	9
Pitching Moment Coefficient Derivative ($C_{m_{\alpha}}$)	9

Magnus Moment Coefficient Derivative ($C_{n_{p\alpha}}$)	10
Drag Coefficient (C_D)	10
Pitching Damping Coefficient ($C_{m_q} + C_{m_{\dot{\alpha}}}$)	11
Gyroscopic Stability	11
Dynamic Stability	11
Discussion and Analysis (Yaw Sondes)	13
Conclusions and Recommendations	14
References	14
Distribution List	431
Tables	
1 Physical characteristics and launch conditions of M329A1E1 yaw sonde rounds	16
2 Ballistic Research Laboratories' range coefficients	17
Figures	
1 4.2" M329A1E1 mortar projectile (all dimensions in calibers)	19
2 4.2" M329A1 projectile	20
3 Operating characteristics of the Ames 12' pressure wind tunnel (PWT)	21
4 Configuration NBT ₁ C ₀ mounted in 12' PWT	22
5 M329A1E1 projectile equipped with yaw sonde	23

I f

6	Raw data chart from 12' PWT (pitch gauge readings vs model rpm)	24
7	Raw data chart from 12' PWT (yaw gauge readings vs model rpm)	25
8	Camera coverage for low charge high quadrant elevation firing of M329A1E1 projectile at Yuma Proving Ground	26
9	Normal force coefficient derivative vs angle of attack (BRL transonic range)	27
10	Pitching moment coefficient derivative vs angle of attack (BRL transonic range)	28
11	Pitch damping coefficient ($C_{m_q} + C_{m_{\dot{\alpha}}}$) and Magnus moment coefficient derivative vs angle of attack (BRL transonic range)	29
12-157	Normal force coefficient, pitching moment coefficient, and normal force center of pressure vs angle of attack. (Includes several configurations, Mach numbers, $pd/2V$'s and Reynolds numbers [12' PWT].)	31-177
158-333	Magnus force coefficient, Magnus moment coefficient, Magnus force center of pressure vs angle of attack. (Includes several configurations, Mach numbers, $pd/2V$'s and Reynolds numbers [12' PWT].)	179-355
334-357	Pitching moment secant slopes, Magnus moment secant slopes vs angle of attack	357-381
358	Pitching moment coefficient derivative vs Mach No. (NBT ₁ C ₁ , NBT ₁ C ₀ , NBT ₂ C ₁ , NBT ₁ C ₁)	382

359 -	Magnus moment coefficient derivative vs	
360	Mach No. ($NBT_1 C_1$, $NBT_1 C_0$, $NBT_2 C_1$)	384-385
361 -	Magnus moment coefficient derivative vs	
367	$pd/2V$ ($NBT_1 C_1$)	387-394
368 -	Muzzle velocity vs range performance flight	
369	tests at Yuma Proving Ground	396-397
370 -	Yaw data translated from camera coverage	
374	shown in Figure 8	399-404
375	M329A1E1 projectile fired at low charge, with obturator still attached	405
376	Pitching moment coefficient derivative and normal force center of pressure vs Mach No. (SPINNER and the BRL Transonic Range) ($NBG_1 C_1$, $NBT_1 C_1$)	406
377	Normal force coefficient derivative and drag coefficient vs Mach No. (SPINNER and the BRL transonic range)	407
378	Mach No. and $pd/2V$ vs time of flight for M329A1E1 six-degree of freedom trajectory computer simulations. ($QE = 60^\circ$, $V_{muzzle} = 1040$ fps)	408
379	Mach No. and $pd/2V$ vs time of flight for M329A1E1 six-degree of freedom trajectory computer simulations. ($QE = 45^\circ$, $V_{muzzle} = 1040$ fps)	409
380	Pitch damping coefficient and spin damping coefficient vs Mach No.	410
381	Muzzle gyroscopic stability factors vs Mach No.	411

1h

382-	Damping factors vs angle of attack for	
386	configuration NBT ₁ C ₁ at various Mach numbers	413-418
387-	Solar aspect angle vs time of flight for M329A1E1	
388	yaw sonde Round No. 4737	420-421
389-	Solar aspect angle vs time of flight for M329A1E1	
390	yaw sonde Round No. 4739	424-425
391-	Solar aspect angle vs time of flight for M329A1E1	
392	yaw sonde Round No. 4740	428-429

NOMENCLATURE

α	Angle of attack, degrees
β	Angle of sideslip, degrees
C_{D_0}	Axial force coefficient, $F_X/\bar{Q}S$
C_{l_p}	Roll damping moment coefficient, $L_p/\bar{Q}Sd\left(\frac{pd}{2V}\right)$
C_m	Pitching moment coefficient, $m/\bar{Q}Sd$
C_{m_α}	Pitching moment coefficient derivative, $1/\text{rad}$
$C_{m_{\dot{\alpha}}}$	Flow lag moment coefficient, $m_{\dot{\alpha}}/\bar{Q}Sd\left(\frac{\dot{\alpha}d}{2V}\right)$
C_{m_q}	Damping moment coefficient, $m_q/\bar{Q}Sd\left(\frac{qd}{2V}\right)$
C_N	Normal force coefficient, $N/\bar{Q}S$
C_{N_α}	Normal force coefficient derivative, $\partial C_N/\partial \alpha$
C_{n_p}	Magnus moment coefficient, $n_M/\bar{Q}Sd\left(\frac{pd}{2V}\right)$
$C_{n_{p\alpha}}$	Magnus moment coefficient derivative, $\partial C_{n_p}/\partial \alpha$, $1/\text{rad}$
C_{Y_p}	Magnus force coefficient, $F_Y/\bar{Q}Sd\left(\frac{pd}{2V}\right)$
$C_{Y_{p\alpha}}$	Magnus force coefficient derivative, $\partial C_{Y_p}/\partial \alpha$, $1/\text{rad}$
d, D	Diameter, ft
F_X	Axial force, lb

1 j

I_x	Axial moment of inertia, slugs - ft ²
I_y	Transverse moment of inertia, slugs - ft ²
K_1	Magnitude of nutation arm, degrees
K_2	Magnitude of precession arm, degrees
L_p	Roll damping moment, ft-lb
λ_1	Quasi linear nutation arm damping factor, 1/sec
λ_2	Quasi linear precession arm damping factor, 1/sec
N	Normal force, lb
n_M	Magnus moment, ft-lb
F_Y	Magnus force lb
M	Mach number
m_q	Damping moment, due to pitching velocity, ft-lb
$m_{\dot{\alpha}}$	Flow lag moment, ft-lb
m	Pitching moment, ft-lb
p	Roll rate, rad/sec
\bar{Q}	Dynamic pressure, lb/ft ²
q	Pitch rate, rad/sec
QE	Quadrant elevation, mils or degrees, as noted
ρ	Air density, slugs/ft ³
s_g	Gyroscopic stability factor
S	Reference area, ft ²

IK

V	Free stream or flight velocity, ft/sec
θ	Sun angle, degrees
ω_1	Nutation frequency, rad/sec
ω_2	Precession frequency, rad/sec
XCG	Center of gravity location, calibers from nose
XCP	Center of pressure of normal force, calibers from the CG
XCPM	Magnus force center of pressure, calibers from center of gravity

Subscripts

o	Initial condition
f	Final condition
2	Indicates second order coefficient of Maple-Synge polynomial expansion

Superscript

$*$	Secant slope
-----	--------------

Il

ABSTRACT

An extensive study of the aerodynamic characteristics of the 4.2", M329A1E1 Mortar Projectile has been conducted. A spectrum of yaw levels up to 40° and Mach numbers from 0.55 to 1.025 were covered in the Ballistic Research Laboratories (BRL) Transonic Research Facility. A Magnus wind tunnel test in the Ames 12' Pressure Wind Tunnel involved boom and boattail effects on Magnus as well as static forces and moments. Mach numbers from 0.3 to 0.95 and angles of attack from 0° to 30° (for a Mach number of 0.3) and 0° to 20° (for the higher Mach numbers) were considered. Shell instrumented with yaw sondes were fired at the Wallops Island Facility of NASA. The theoretical differential equation of motion then was fitted to the resulting single plane angular motion data.

INTRODUCTION

The M329A1E1 projectile is the result of an accelerated product improvement program with the objective to provide a replacement for the M329A1 projectile. Because of the accelerated nature of the program only the improvements which are within the current state of the art have been incorporated. Figures 1 and 2 are drawings of the M329A1E1 and the M329A1 projectiles. The subcaliber cylindrical sections contain the ignition cartridge; they appreciably affect the aerodynamic characteristics of the shell.

The 4.2", M329A1 has been in use since 1940. Its extension to the cartridge housing was part of an attempt to upgrade the system performance by increasing the chamber volume and enabling the use of larger charges. The M329A1 has a history of occasionally erratic flights, the propensity for which increases when the extension to the cartridge housing is present. This extension generates a larger Magnus moment than the original short boom configuration and can lead to dynamic instabilities.

Several improvements have been incorporated into the M329A1E1 design. The drag is decreased by replacing the square base of the M329A1 by a 0.65 caliber boattail and adding a longer windshield. A fixed pre-engraved rotating band has been incorporated into the new design in an attempt to improve the spin performance. A constant chamber volume propellant system makes it possible to eliminate the extension to the cartridge housing.

Cumulatively, these configurational changes mean an improvement of the M329A1E1 in both high and low range capability.

TEST FACILITIES

BRL Transonic Range

The M329A1E1 projectile was fired at subsonic and low transonic velocities in the Ballistic Research Laboratories (BRL) Transonic Range Facility described in Reference 1.

NASA Ames 12' Pressure Wind Tunnel

The Ames 12' Pressure Wind Tunnel is a variable-density, low-turbulence tunnel that operates at subsonic speeds up to slightly less than Mach number 1.0. It is powered by a two-stage axial-force fan driven by electric motors. Airspeed in the test section is controlled by variation of the rotational speed of the fan. Eight fine mesh screens in the settling chamber together with the large contraction ratio of 25 to 1 provide an airstream of exceptionally low turbulence. A special mounting drive system was available for angles of attack over 20°. Figure 3 is a plot of the operating characteristics of this wind tunnel. The full scale test configurations and strain gage balance beams were constructed by the Supersonic Wind Tunnel Branch of BRL. The two beams prepared for the test are SB228A and backup beam SB228B, but only the former was used. They are five component strain gage balances, each of which has two pitch gages and three yaw gages specifically designed for the forces and moments anticipated in this test. The exterior of the model consisted of three basic parts.:

- a. Ogive and cylindrical section
- b. Tail section (square base or boattail)
- c. Boom

Model designations are as follows:

<u>Designation</u>	<u>Drawing Number</u>	<u>Item</u>
NB	SSK2590B - 1 SSK2590A	M329A1E1 nose and cylindrical body
T ₁	SSK2590 - B2	Boattail on the aft 0.65 calibers of the model
T ₂	SSK2590 - B3	Square base (same length as boattail)
C ₁	SSK2590 - B4	Cartridge housing

C_0

No cartridge housing

$NBGT_1C_1$

Configuration NBT_1C_1 with
grit on the last inch of
cartridge housing

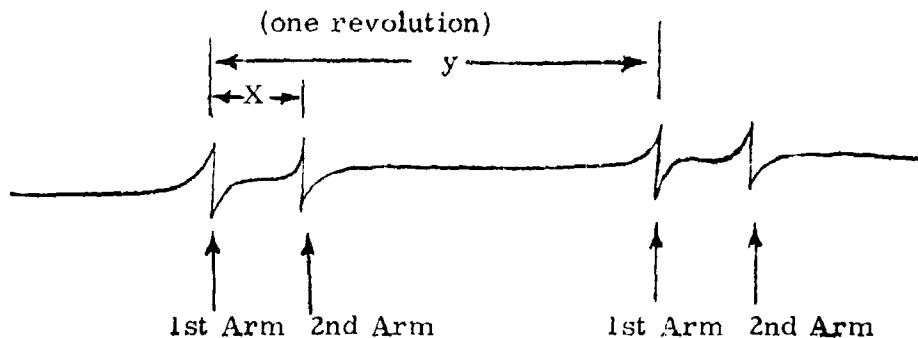
The M329A1E1 is designated by NBT_1C_1 . The configuration shown in Figure 4 is NBT_1C_0 .

Performance Flight Tests

Performance flight tests have been conducted, the majority of them at Yuma Proving Ground. Firings in January 1969 involved two preliminary designs with different boattail lengths, which will be called the "long" boattail (0.85 calibers) and the "short" boattail (0.65 calibers). The objective of subsequent firings was the development of an effective rotating band and obturator. Camera coverage was requested for some of these rounds to obtain a yaw record over and past the peak. All rounds were fired from the M30, 4.2 inch Mortar tube, which has a progressive twist resulting in one turn of the projectile in 20 calibers of linear travel.

Yaw Sonde Program

Yaw sondes and their use are fully described in Reference 2. Briefly, a yaw sonde fuze consists of two strips of photovoltaic material arranged to intercept a ray of light which is passed through a pin hole in the side of the fuze body. The strips are placed on a plane containing the axis of symmetry of the projectile in the form of an inverted V. As the projectile rotates in flight a sun ray impinges on each arm of the V. The resulting signals which take the form:



are transmitted to a recording station. As the projectile yaws while rotating, the sun ray moves up or down the axis of the projectile. Thus the ray takes a shorter or longer time to cross from the first to the second arm of the V. Therefore, as the yaw angle and the spin rate decay various values of x and y are obtained. Having previously calibrated the yaw sonde with a fixed light source and special angle measuring devices, a graph of sun angle vs a function of x and y can be determined. This calibration is then applied to the signals obtained from free flight and a plot of sun angle vs time of flight is obtained.

The yaw sonde firings of the M329A1E1 projectile were a joint effort of the BRL at Aberdeen Proving Ground and Picatinny Arsenal. Wallops Island was chosen as the site of the test, primarily because of the quality of instrumentation available there. Tracking instrumentation included a MPS-19 radar.

Six yaw sonde-equipped M329A1E1 rounds were fired on 22 and 23 October 1969 under the conditions listed in Table 1. Since the yaw sonde package is lighter than the standard fuze, the physical characteristics of the projectile differ from the standard M329A1E1 projectile. They are also listed in Table 1. Figure 5 shows a yaw sonde-equipped M329A1E1 projectile.

EXPERIMENTAL PROCEDURE

BRL Transonic Range

For small yaw angles the BRL Transonic Range test was conventional. However, to reproduce the rather large yaw levels (due to yaw of repose) which have been measured for low velocity and high quadrant elevation fire, a four-kilogram Lexan cylinder was placed 75 centimeters from the muzzle. By glancing the projectile off this cylinder, yaws in excess of 30° were produced without damage to the shell.

NASA Ames 12' Pressure Wind Tunnel

The preparations and techniques used for obtaining Magnus data in wind tunnels are outlined in Reference 3. The Reynolds number-Mach number combinations at which data was recorded in the Ames 12' Pressure Wind Tunnel are plotted in Figure 3. Where possible, the stagnation pressure was atmospheric. Reynolds numbers above and

below this value also were considered. When tunnel conditions were proper and the Mach number correct, the angle of attack was set and the model spun-up to approximately 12,000 rpm. As it was allowed to spin down, readings from all gauges were taken as a function of spin rate on Mosley X - Y Recorders. For the pitch recorders zero moment was positioned in a convenient place on the chart while static tunnel conditions existed. The tunnel then was put into operation and the model rotated through the angle of attack range. For the yaw recorders zero moment was extrapolated back to the point of zero spin rate. Figures 6 and 7 are typical raw data charts. After all Mach number and Reynolds number combinations had been run, a special mounting drive system was used to obtain data to 30° for a Mach number of 0.3 and the Reynolds numbers involved. Considerable overlap was allowed in order to maintain the continuity of the reduced data. A sand band of No. 20 grit was attached to the last inch of the boom for two Mach number - Reynolds number combinations to aid in the investigation of subcaliber after body effects. Mach numbers of 0.3 and 0.55 and their respective Reynolds numbers of 1.7×10^6 and 2.9×10^6 were involved.

Performance Flight Tests

Flight tests at Yuma Proving Ground were established to examine the performance at high and low charges as well as high and low quadrant elevations. Muzzle velocity was determined by use of velocity coils and magnetized shell. Range and deflection were measured by spotting personnel. In addition, for some rounds, cameras were positioned at the muzzle for spin and yaw measurements and under the trajectory peak of a low charge, high quadrant elevation flight for a determination of the yaw of repose (Fig 8).

Yaw Sonde Program

In setting up the yaw sonde test, the tube was positioned 1,300 ft from the radar along an azimuth of 143° . Line of fire of the low charge rounds was along an azimuth of 115° , while high charge rounds were along 130° . The muzzle velocity of each round was measured by a Fastax camera. Trajectory data, including range, altitude, and deflection, were obtained from an MPS-19 tracking radar for each projectile.

DATA REDUCTION TECHNIQUES

BRL Transonic Range

The methods used in the analysis of the transonic range data are documented in References 4 and 5. The angular orientation as well as the position of the projectile in the range are fitted to a closed form solution of the linearized equations of motion by differential correction and least square fits. If a nonlinear system is indicated, the total results must be reviewed on a quasi-linear basis to determine the aerodynamic coefficients.

NASA Ames 12' Pressure Wind Tunnel

Reduction of wind tunnel data is fairly straightforward; however, a determination had to be made concerning the extent of sting interference on the contribution of the boom to Magnus forces and moments. The circulatory flow about the boom itself was felt to be a stronger Magnus generator than boom-end effects; and since the sting was not expected to have greatly disturbed this flow (Refs 6, 7, and 8) data could be considered meaningful. Wind tunnel data reduction was performed by two independent units, the Data Reduction Section at Aberdeen Proving Ground, and a reduction unit at Picatinny Arsenal. At Picatinny Arsenal a computer program was developed to reduce readings from the Mosley recorders, shift the resulting force and moment coefficients to pass through zero at zero angle of attack, and plot the shifted coefficients. A 5th - 11th order fit (depending on the data) is represented by the solid line on each plot. Secant slopes of the Magnus and pitching moment coefficients vs angle of attack have been plotted for the reduced data points as well as the higher order fits. All moments and centers of pressure are referenced to the center of gravity (2.48 calibers from the nose) and Magnus force and moment coefficients were calculated using the nondimensional spin parameter $pd/2V$.

Performance Flight Tests

For the most part performance flight tests yielded only statistical data. Plots of range and deflection vs muzzle velocity help to indicate short rounds, and computation of standard deviations of range, velocity, and deflection are a means of comparing performance of the M329A1E1 with the M329A1. Spin rate calculations were made from

camera coverage at the muzzle for specially painted shell. Yaw histories were measured directly from the muzzle and the downrange camera records, and are discussed in the Section "Experimental Procedures/Performance Flight Tests".

Yaw Sonde Program

Raw data from the yaw sondes was transformed into sun angle and time of flight data and placed on magnetic tape by BRL. These values were then plotted (sun angle vs time of flight) with the aid of the high speed computer. The method of Chapman and Kirk (Ref 9) and a specially modified six degree of freedom trajectory program were used in an effort to reduce the angular motion output of the yaw sonde to aerodynamic coefficient form. Briefly, the size of the section of data to be fitted by the method of Chapman and Kirk was limited by the change in Mach number, since it is not yet one of the fitted parameters. This allowed Mach number variation was established by plotting wind tunnel and range data vs Mach number and then limiting the

$$\frac{\Delta C_{m\alpha}}{\Delta \text{Mach No.}}, \quad \frac{\Delta C_{mq}}{\Delta \text{Mach No.}}, \quad \frac{\Delta C_{np\alpha}}{\Delta \text{Mach No.}}$$

to $\pm 2\%$ of the value at the average Mach number of the section. Certain differential equations of angular motion were then fitted to these sections of data. Both linear and nonlinear $C_{m\alpha}$, C_{mq} , and $C_{np\alpha}$ were considered.

PRESENTATION OF TEST RESULTS

BRL Transonic Range

Data from the BRL transonic range is presented in Table 2. Coefficient values within selected Mach number ranges have been plotted vs angle of attack (Figs 9, 10 and 11).

NASA Ames 12' Pressure Wind Tunnel

The results from the Ames 12' Pressure Wind Tunnel have been plotted vs angle of attack. As was previously mentioned, the solid line through the data points represents a 5th - 11th order fit.

Figures 12 through 157 are plots of normal force coefficient, pitching moment coefficient, and normal force center of pressure vs angle of attack. Several nondimensional spin rates and Reynolds numbers are included for each Mach number.

Early in the test it was noted that the output on the forward pitch recorder was of poor quality. The difficulty was traced to a crushed lead wire to the forward pitch recorder. Normal force data on configuration NBT1C1 taken at Mach numbers of 0.3 and 0.55 at various Reynolds numbers was affected by the faulty lead wire, could not be rerun, and is not reported here.

Magnus force coefficient, Magnus moment coefficient and Magnus force center of pressure are plotted in Figures 158 through 333.

From this data, secant slopes of pitching moment and Magnus moment vs angle of attack have been calculated and are presented in Figures 334 through 357. The symbols on slope plots represent C_{m_α} 's and C_{np_α} 's for each data point. The solid line is the calculated C_{m_α} or C_{np_α} vs angle of attack from the fit to the original data. Figures 358 through 367 show the relationship of C_{m_α} and C_{np_α} to Mach number, $\frac{pd}{2V}$, and Reynolds number. Agreement between the two independent reductions of this data is excellent. An average deviation of $\pm 2\%$ was found in the check cases.

Performance Flight Tests

Results from performance flight tests include some plots displaying range vs velocity performance (Figs 368 and 369).

In addition, some of the film records were translated into pitch and yaw data at various points throughout the trajectory (Figs 370 through 374). At the time of these firings, the rubber obturator had failed to separate from the projectile at low charges. Figure 375 is a photograph of the M329A1E1 soon after exiting the muzzle at a velocity of 255 feet per second. The obturator is clearly on, although displaced from its original setting, undoubtedly causing adverse aerodynamic loads. This displacement is caused by the force of the muzzle gases as they pass over the projectile shortly after it exits the muzzle.

At high charges, the obturator is broken by the blast; but at some intermediate charges it is possible that it will be forced to a position anywhere along the projectile.

DISCUSSION AND ANALYSIS (BRL Range and Ames Wind Tunnel)

The following discussion and analysis directly compares results from the BRL Range and the Ames Wind Tunnel. Yaw Sonde results will be discussed separately, due to the unique methods by which they are obtained and the care with which they must be interpreted.

Pitching Moment Coefficient Derivative (C_{m_α})

Referring to Figure 376, the range, wind tunnel and SPINNER (Ref 10) agree well for this parameter. The increase in the transonic region is partially due to an increase in the normal force coefficient and largely due to a forward (meaning towards the nose) movement of the normal force center of pressure with increasing Mach number (Fig 376). A plot comparing C_{m_α} for the three configurations tested in the Ames Wind Tunnel appears as Figure 358. The Reynolds number effects are small (less than 3%). C_{m_α} is about 44% lower for the square base configuration NBT₂C₁. Although the normal force of NBT₂C₁ is greater, the center of pressure is considerably closer to the center of gravity than NBT₁C₁. At the lower Mach numbers the pitching moment coefficient derivative of NBT₁C₁ is greatest because its normal force center of pressure is slightly more forward of the center of gravity than for NBT₁C₀. The normal forces are the same. At the high Mach number (0.85 - 0.95) NBT₁C₁ has an 8% lower normal force than NBT₁C₀. Its center of pressure remains more forward of its center of gravity. Thus NBT₁C₁ and NBT₁C₀ have nearly the same C_{m_α} 's at $M = 0.85$ and 0.95 . The effect of angle of attack on C_{m_α} is most clearly demonstrated at $M = 0.305$ (Figs 340 and 342). This decrease in C_{m_α} is due to a rearward movement of the normal force center of pressure with an increase in angle of attack. For the other Mach numbers, the angle of attack ranges are not nearly so large, and C_{m_α} tends to remain nearly constant. A linear approximation up to 10° appears to be an accurate one here.

At high charges, the obturator is broken by the blast; but at some intermediate charges it is possible that it will be forced to a position anywhere along the projectile.

DISCUSSION AND ANALYSIS (BRL Range and Ames Wind Tunnel)

The following discussion and analysis directly compares results from the BRL Range and the Ames Wind Tunnel. Yaw Sonde results will be discussed separately, due to the unique methods by which they are obtained and the care with which they must be interpreted.

Pitching Moment Coefficient Derivative (C_{m_α})

Referring to Figure 376, the range, wind tunnel and SPINNER (Ref 10) agree well for this parameter. The increase in the transonic region is partially due to an increase in the normal force coefficient and largely due to a forward (meaning towards the nose) movement of the normal force center of pressure with increasing Mach number (Fig 376). A plot comparing C_{m_α} for the three configurations tested in the Ames Wind Tunnel appears as Figure 358. The Reynolds number effects are small (less than 3%). C_{m_α} is about 44% lower for the square base configuration NBT₂C₁. Although the normal force of NBT₂C₁ is greater, the center of pressure is considerably closer to the center of gravity than NBT₁C₁. At the lower Mach numbers the pitching moment coefficient derivative of NBT₁C₁ is greatest because its normal force center of pressure is slightly more forward of the center of gravity than for NBT₁C₀. The normal forces are the same. At the high Mach number (0.85 - 0.95) NBT₁C₁ has an 8% lower normal force than NBT₁C₀. Its center of pressure remains more forward of its center of gravity. Thus NBT₁C₁ and NBT₁C₀ have nearly the same C_{m_α} 's at M = 0.85 and 0.95. The effect of angle of attack on C_{m_α} is most clearly demonstrated at M = 0.305 (Figs 340 and 342). This decrease in C_{m_α} is due to a rearward movement of the normal force center of pressure with an increase in angle of attack. For the other Mach numbers, the angle of attack ranges are not nearly so large, and C_{m_α} tends to remain nearly constant. A linear approximation up to 10° appears to be an accurate one here.

Magnus Moment Coefficient Derivative ($C_{np\alpha}$)

Figures 193, 204, and 218 show reasonably good agreement of the BRL Range and the Ames Wind Tunnel data for this difficult-to-measure parameter. Of particular interest is the fact that the range as well as the wind tunnel data shows a negative $C_{np\alpha}$ at Mach number 0.567 and 9° angle of attack. The effect of this on stability will be discussed in a later section.

The point should here be made that small force and moment Magnus data, normally at the lower angles of attack, may contain considerable percentage error; however, relative magnitudes and consistent trends are of value. $C_{np\alpha}$ versus Mach number for the three configurations tested in the Ames Wind Tunnel are shown in Figures 359 and 360. As Mach number increases in the transonic region $C_{np\alpha}$ for Configuration NBT1C1 peaks sharply due to a sharp rise in Magnus force. NBT2C1, however, behaves quite differently, remaining nearly constant throughout the same region. It is not uncommon for square base projectiles to peak at higher Mach numbers than boattail projectiles. The boomless Configuration NBT1C0 has a lower $C_{np\alpha}$ throughout most of the Mach number range tested, supporting the belief that the boom is a Magnus generator even at low angles of attack. Figures 361 and 367 show the variation of $C_{np\alpha}$ with both $pd/2V$ and angle of attack. At the lower angles of attack and $pd/2V$'s, $C_{np\alpha}$ tends to be negative. This is primarily due to a positive Magnus force in this region of somewhat uncertain data. The trend, however, is consistent throughout the entire Mach number range.

Drag Coefficient (C_D)

The drag coefficient, for small yaws, as measured in the BRL Range, agrees well with the SPINNER data bank (Fig 317). Six-degree of freedom trajectory simulations using such drag data closely agree with full range firings at Yuma Proving Ground.

Pitch Damping Coefficient ($C_{m\dot{q}} + C_{m\dot{\alpha}}$)

($C_{m\dot{q}} + C_{m\dot{\alpha}}$) as determined by the BRL Range appears constant above 4° for Mach numbers below 0.543. Between $M = 0.638$ and 0.867, $C_{m\dot{q}} + C_{m\dot{\alpha}}$ is constant above 2° (Figs 11 and 380). Below these angles of attack, $C_{m\dot{q}} + C_{m\dot{\alpha}}$ becomes less negative, indeed, has been measured as positive at some low angles of attack. This could be caused by a dominance of the $C_{m\dot{\alpha}}$ term.

Gyroscopic Stability

Referring to Figure 381, the gyroscopic stability factor of the M329A1E1 remains within acceptable bounds throughout the Mach number range. The improvement over the M329A1 Projectile also is clear. Simulating -26.3°F lowers the gyroscopic term over 16% but it still remains well within the region of gyroscopic stability.

Dynamic Stability

Nonlinear damping factors, $\lambda_{1,2}^*$ from the quasi-linear theory, were calculated using data from the Ames Wind Tunnel, and plotted vs angle of attack in Figures 382 through 386. These parameters give an insight into what can be expected in terms of angular motion as the projectile traverses a trajectory. One may qualitatively explain the motion of a low charge high quadrant elevation round with the aid of Figure 382 in the following way: As the projectile exits the muzzle, it receives an initial disturbance resulting in an average maximum yaw of 1 or 2 degrees. At this point the precessional mode appears to be slightly undamped. Of course, due to the error in the data and the sensitivity of $\lambda_{1,2}^*$ to Magnus and damping, the precessional mode may be slightly damped. On the way to the trajectory peak a rather large yaw of repose appears and carries the projectile into a region where the precessional mode is heavily damped while the nutational mode is strongly undamped. From here on it becomes a race up to the ground impact, as the K_1 arm grows and the K_2 arm damps. The damping factors are functions of Mach number and angle of attack (Figs 382 through 386). As the Mach number decreases, there are changes in the size of the small angle precessional limit cycle until eventually a nutational limit cycle will appear.

Similarly, if the projectile is disturbed upon launch from the muzzle to an angle of attack of 12° , below $M = .75$, the angular motion will diverge due to a nutational instability. The result of this is, of course, a short range.

DISCUSSION AND ANALYSIS (Yaw Sonde)

Many attempts have been made to fit the differential equation of motion to the angular motion data obtained from the yaw sonde. While performing these fits, in addition to holding the coefficients C_{m_α} , $(C_{m_q} + C_{m_{\dot{\alpha}}})$, and $C_{n_{p_\alpha}}$ constant, various combinations of higher order terms were considered. Convergence of the equation of motion to the data was achieved for many of these combinations resulting in some reasonable fits. Some of the coefficients which generated such motion are, however, not in good agreement with those of the wind tunnel and transonic range. Among the questions raised due to these disappointing results are:

1. What accuracies are needed in yaw sonde manufacture and calibration?
2. How sensitive is the motion and thus the fit, to rather large nonlinearities in the coefficients?
3. For a given set of yaw sonde sun angle data, radar data, and projectile physical parameters, how accurately can we separate and determine the Magnus and damping moments?

While we are not ruling out fitting the equation of motion to yaw sonde data as a powerful tool in stability coefficient determination, the results of our analysis do not, at this time, merit publication until additional efforts in the area can answer some of these important questions. A qualitative discussion of the results from the yaw sonde follows.

Figures 387 through 392 show solar aspect angle data from the yaw sonde for a projectile fired at a 45° quadrant elevation and two projectiles fired at a 60° quadrant elevation. All three projectiles had a muzzle velocity of approximately 1050 feet per second.

Referring to the damping factor plots (Figs 382 through 386) one can see that the precession arm will undamp up to two degrees at a Mach number of 0.95 and up to almost five degrees for a Mach number of 0.85. We can expect, therefore, that the precessional arm should be slightly undamped near the muzzle. This is the case for the three examples shown. The initial magnitude of the nutational arm may be attributed to the muzzle disturbance. As the Mach number decreases on the up leg of the trajectory the precession damps as shown by the damping factors of Figures 382 through 386, and the nutational arm can be expected to grow to one or two degrees. This behavior will be enhanced by the increase in $C_{np\alpha}$ due to the increased $pd/2V$ in this region. The precession damps as the peak of the trajectory is traversed due to the decreasing Mach number. On the down leg of the trajectory, the combined effects of the yaw of repose, the Mach number increase, and the $pd/2V$ decrease, cause the precessional arm to reappear.

CONCLUSIONS AND RECOMMENDATIONS

The M329A1E1 has adequate damping characteristics and therefore adequate stability throughout its Mach number regime. A problem area appears in the low charge and high quadrant elevation firings due to a rather large gyroscopic term and resulting yaw of repose. When fired with a tail wind this problem becomes greater, and fuze functioning may be affected due to impact at large yaws. In addition, the rubber obturating band has been observed to remain with the round at this minimum charge. Such an occurrence will result in a decrease in accuracy and an unpredictable ground impact angle.

REFERENCES

1. Rogers, W. R., Jr., "The Transonic Free Flight Range", BRL Report 1040, June 1958 (AD 200177)
2. Amery, I. O. F., Henning, H.G.E., Lawrie, K. G. A., Latnig, E. J. M., "A Telemetry System for the Measurement of the Yaw of a Projectile Throughout the Major Part of its Trajectory (U)", RARDE, Guns and Ammunition Division, Fort Halsted, Kent, United Kingdom, Report No. 1/65 (CONF)

3. Platou, A. S., Colburn, R., and Pedgonay, J. S., "The Design and Dynamic Balancing of Spinning Models and a Testing Technique for Obtaining Magnus Data in Wind Tunnels", BRL Memorandum Report 2019, October 1969
4. Murphy, C. H., "Data Reduction for the Free Flight Spark Ranges", BRL Report 900, (AD35833) February 1954
5. Murphy, C. H., "The Measurement of Nonlinear Forces and Moments by Means of Free Flight Tests", BRL Report 974 (AD93521) February 1956
6. Tunnel, P., "An Investigation of Sting Support Interference on Base Pressure and Forebody Chord Force at Mach Numbers from 0.60 to 1.30", NACA RM A54K16, January 1955
7. Love, E., "A Summary of Interference at Transonic and Supersonic Speeds", NACA RM L53K12, January 1954
8. Zonars, D., "Large Angle of Attack Model-Sting Interference Effects at Transonic Speeds", AGARD Report 301, March 1959
9. Chapman, G., and Kirk, D., "A New Method for Extracting Aerodynamic Coefficients from Free Flight Data", AIAA Paper at 7th Aerospace Science Conference, January 1969
10. Whyte, R. H., "SPINNER - A Computer Program for Empirically Predicting the Aerodynamic Coefficients of Spin Stabilized Projectiles", Picatinny Arsenal, ESL IR 319, February 1967;
"SPINNER - A Computer Program for Predicting the Aerodynamic Coefficients of Spin Stabilized Projectiles", General Electric, Technical Information Series, No. 69APB3, August 1969

TABLE 1

Physical characteristics and launch conditions of M329A1E1 yaw sonde rounds						
Round No.	V Muzzle (fps)	Q E (deg)	I _x (lb - in. ²)	I _y (lb - in. ²)	Weight (lb)	Center of Gravity (inches from base)
4729	267	60	-----	-----	-----	-----
4731	255	60	-----	-----	-----	-----
4737	1052	45	50.89	386.7	21.0	6.432
4738	1058	45	50.84	387.9	21.01	6.437
4739	1064	60	50.84	385.8	20.96	6.427
4740	1052	60	50.93	386.2	21.0	6.43
Standard M329A1E1						
			53.0	446.0	22.2	6.8

TABLE 2

Ballistic Research Laboratories' range coefficients

MACH NO.	$\frac{W}{A}$	C_D	$C_{m\alpha}$	$C_{N\alpha}$	C_{P_N}	$C_{N_{Pa}}$	$C_{Y_{2\alpha}}$	$C_{m\alpha} + C_{m\alpha}$	S_g	$1 \begin{pmatrix} 10^3 \end{pmatrix}$	$2 \begin{pmatrix} 10^3 \end{pmatrix}$
.523	15.53	.2712	2.5441	1.6720	3.3172	.3008	-.6433	-2.5852	3.13	.0261	-.2289
.543	8.96	.1741	2.9755	1.4035	3.7357	-.1803	.0566	-2.8199	2.64	-.2317	.0328
.517	2.31	.1118	3.0460	0.9987	4.6655	.3710	-.5232	-3.8057	2.54	.0017	-.2253
.527	3.27	.1182	3.0787	1.3353	3.9212	.1282	-.7781	-.9204	2.45	.0344	-.1417
.425	1.38	.1109	2.8179	1.3287	3.7364	-1.0006	-1.0825	10.3487	2.60	.0513	.3838
.435	3.45	.1236	3.0436	1.3305	3.9031	.0404	-.9203	-1.3238	2.45	-.0352	-.0894
.538	4.42	.1277	3.1257	1.3741	3.8904	.1686	-.5095	-3.9880	2.55	-.1120	-.1409
.684	0.69	.1031	3.2735	1.4063	3.9469	-.1034	-.2408	-3.0283	2.32	-.2079	-.0043
.727	3.48	.1185	3.1450	1.2307	4.1712	.2856	.4720	-3.7092	2.40	-.0350	-.1991
.483	14.17	.2160	2.5558	1.5599	3.2541	.2265	-.7287	-1.9454	3.03	.0239	-.1913
.720	3.29	.1195	3.1980	1.6291	3.5786	.2609	.5106	-3.7596	2.43	-.0469	-.2092
.777	1.33	.1075	3.2302	1.5295	3.7275	.1104	-.8910	-2.3079	2.40	-.0493	-.1328
.776	2.31	.1093	3.2737	1.5725	3.5742	.1223	-.7027	-3.2853	2.38	-.0943	-.1408
.797	1.28	.1062	3.2025	.9917	4.8470	.0635	-1.0305	-3.0522	2.38	-.1222	-.0697

TABLE 2 (Cont'd)

MACH NO.	δ	C_D	$C_{m_{\text{ref}}}$	$C_{N_{\text{ref}}}$	C_{P_N}	$C_{n_{P_{\text{ref}}}}$	$C_{y_{P_{\text{ref}}}}$	$C_{m_q} + C_{m_{\text{ref}}}$	Sg	$1 \ (10^3)$	$2 \ (10^3)$
.815	3.90	.1252	3.3426	1.2097	4.3017	.2047	-.3038	-3.0189	2.32	-.0400	-.1607
.840	2.90	.1193	3.3211	1.9091	3.3552	.2021	.1270	-3.7254	2.22	-.0740	-.1997
.861	4.61	.1381	3.3840	1.8414	3.4534	.1800	.1627	-3.1066	2.26	-.0544	-.1867
.867	4.82	.1411	3.3973	1.6237	3.6934	.1438	-.4448	-3.6415	2.22	-.1067	-.1504

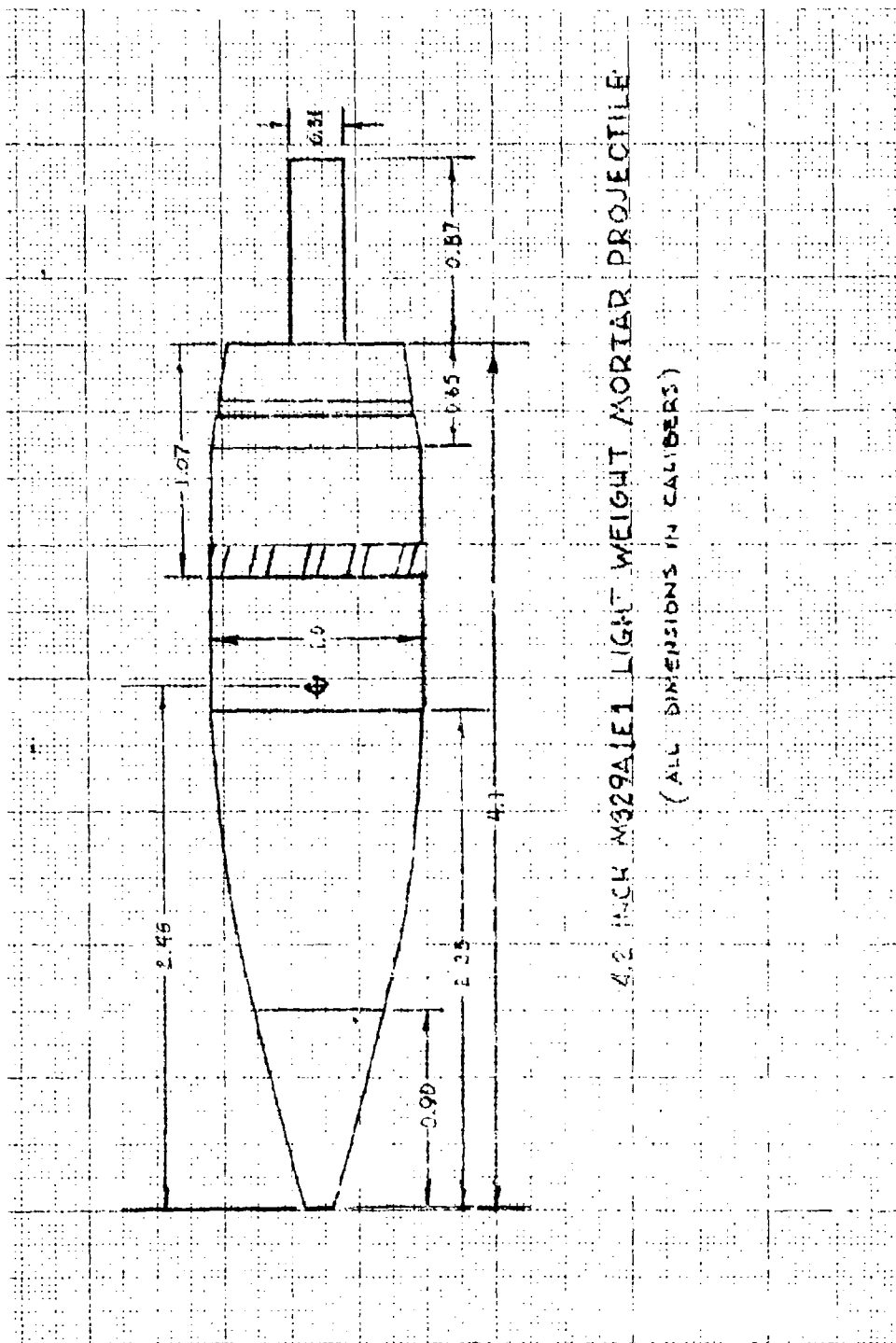
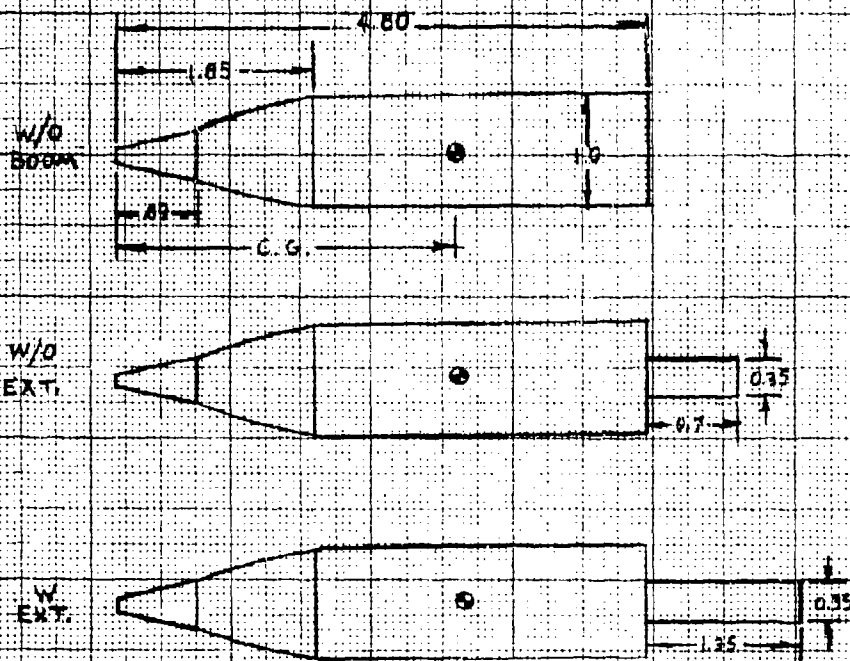


Fig 1 4.2" M329A1E1 mortar projectile
(all dimensions in calibers)

M329A1 4.2 INCH MORTAR PROJECTILE



CONFIG	WG [†] LBS	AXIAL LB-FT ²	TRANSVERSE LB-FT ²	C.G. CAL. FROM NOSE	A ² /B LB-FT ² X 10 ³
W/O BOOM	257*	0.4479*	5.208*	2.89*	.385*
W/O EXT.	239*	0.4479*	5.408*	3.01*	.471*
W EXT.	261	0.4479	5.610	3.03*	.450

* ESTIMATED

A - AXIAL MOMENT OF INERTIA

B - TRANSVERSE MOMENT OF INERTIA

(ALL DIMENSIONS IN CALIBERS)

Fig 2 4.2" M329A1 projectile

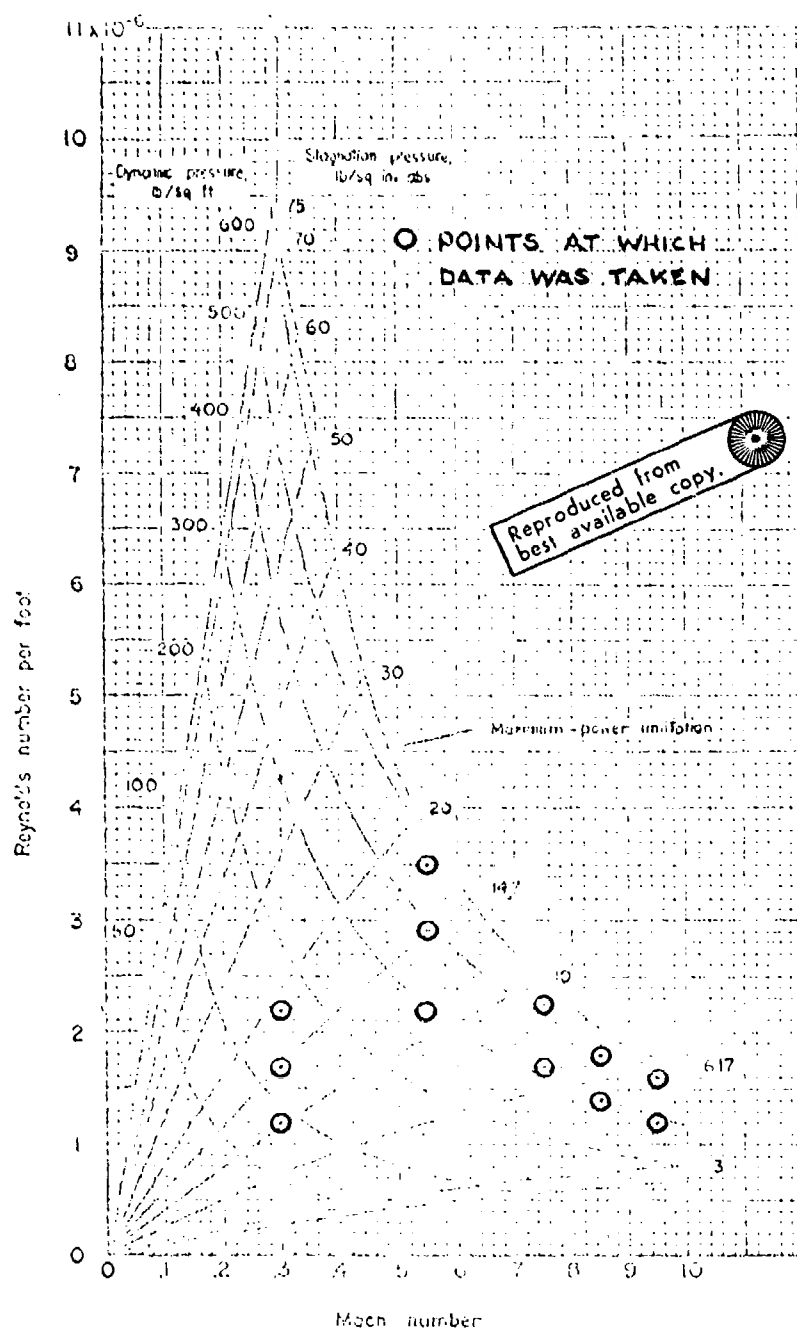


Fig 3 Operating characteristics of the Ames 12' pressure wind tunnel (PWT)

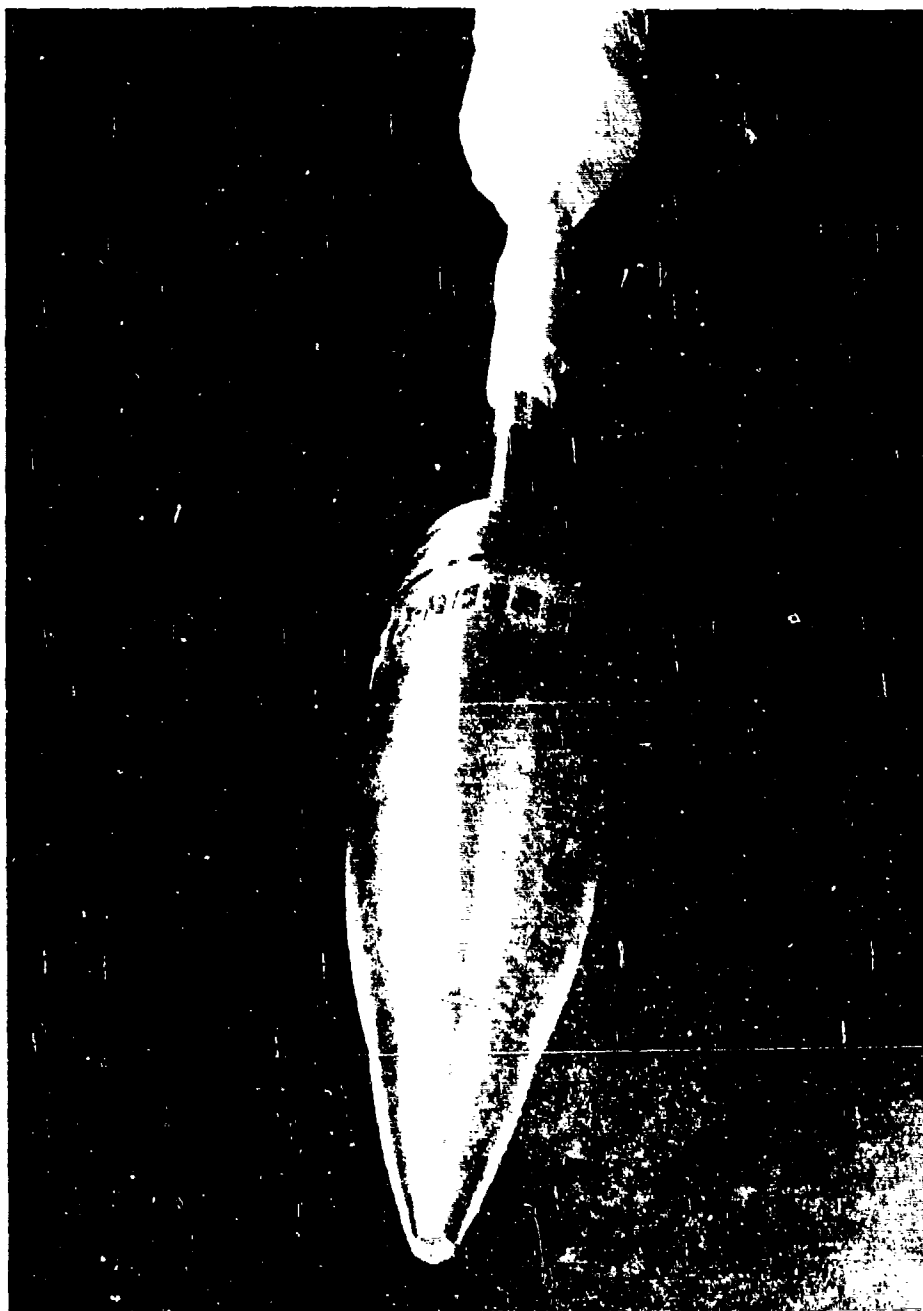


Fig 4 Configuration NBT₁C₀ mounted in 12' PWT



Fig 5 M329A1E1 projectile equipped with yaw sonde

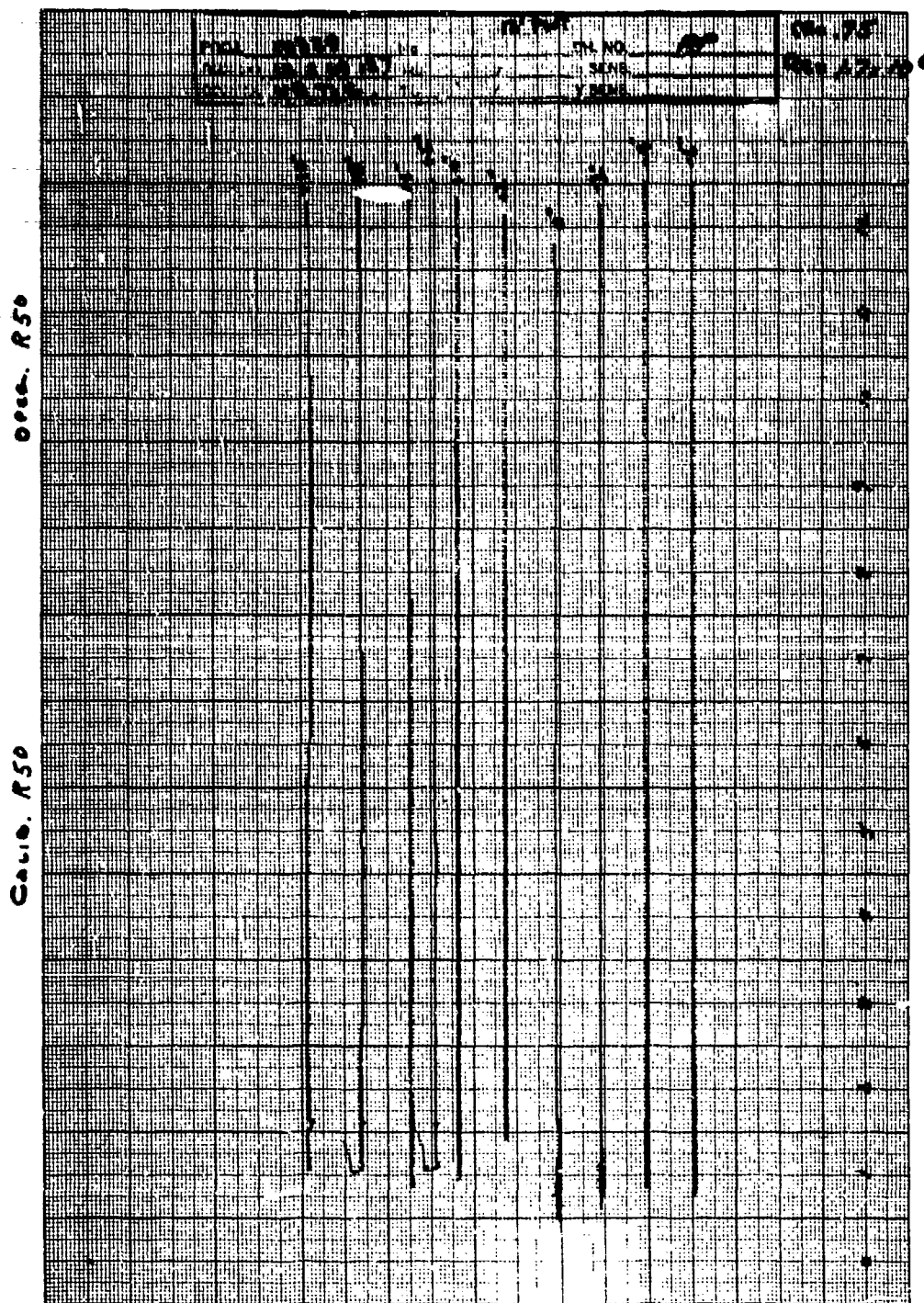


Fig 6 Raw data chart from 12' FWT (pitch gauge readings vs model rpm)

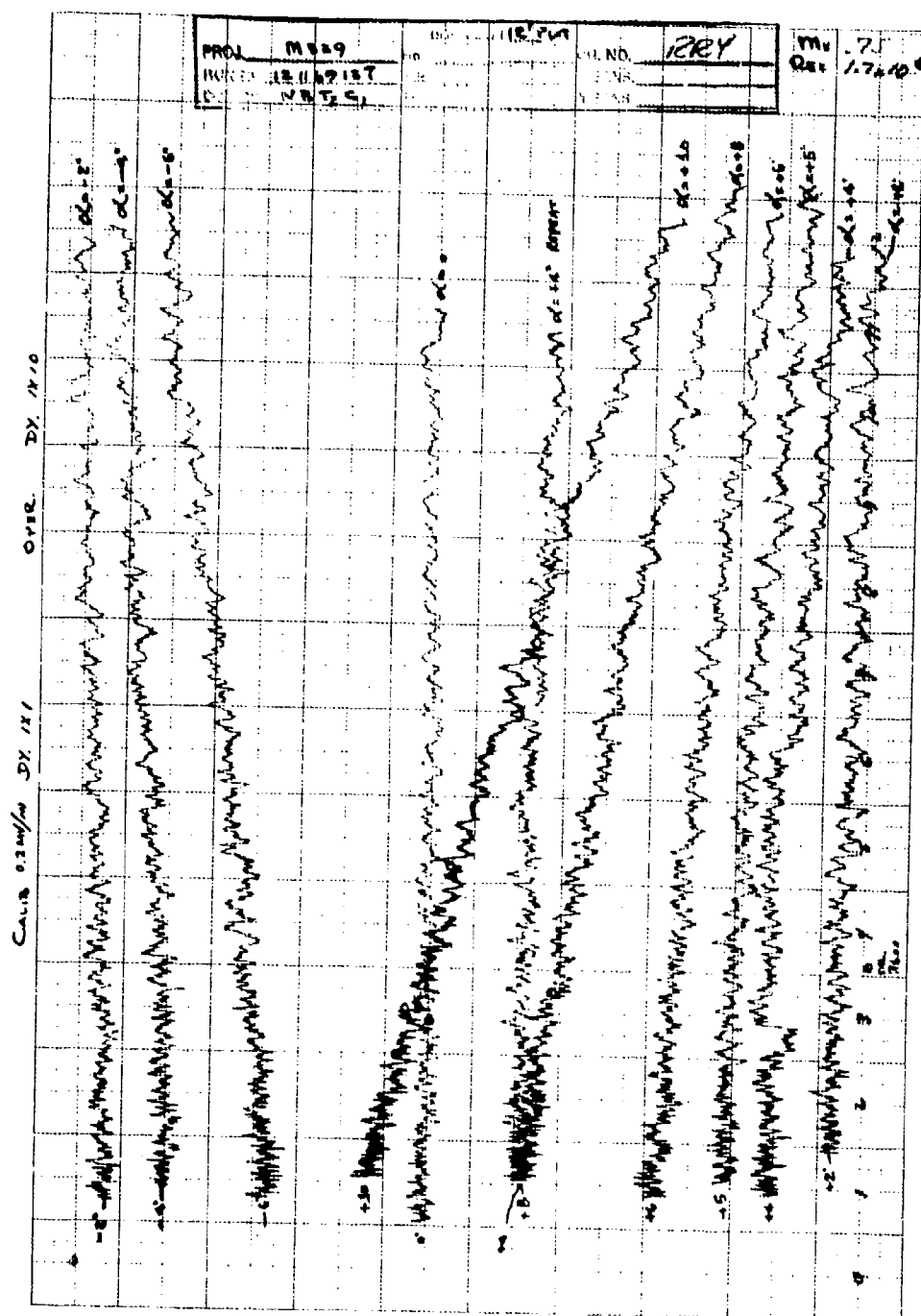


Fig 7 Raw data chart from 12' PWT (yaw gauge readings vs model rpm)

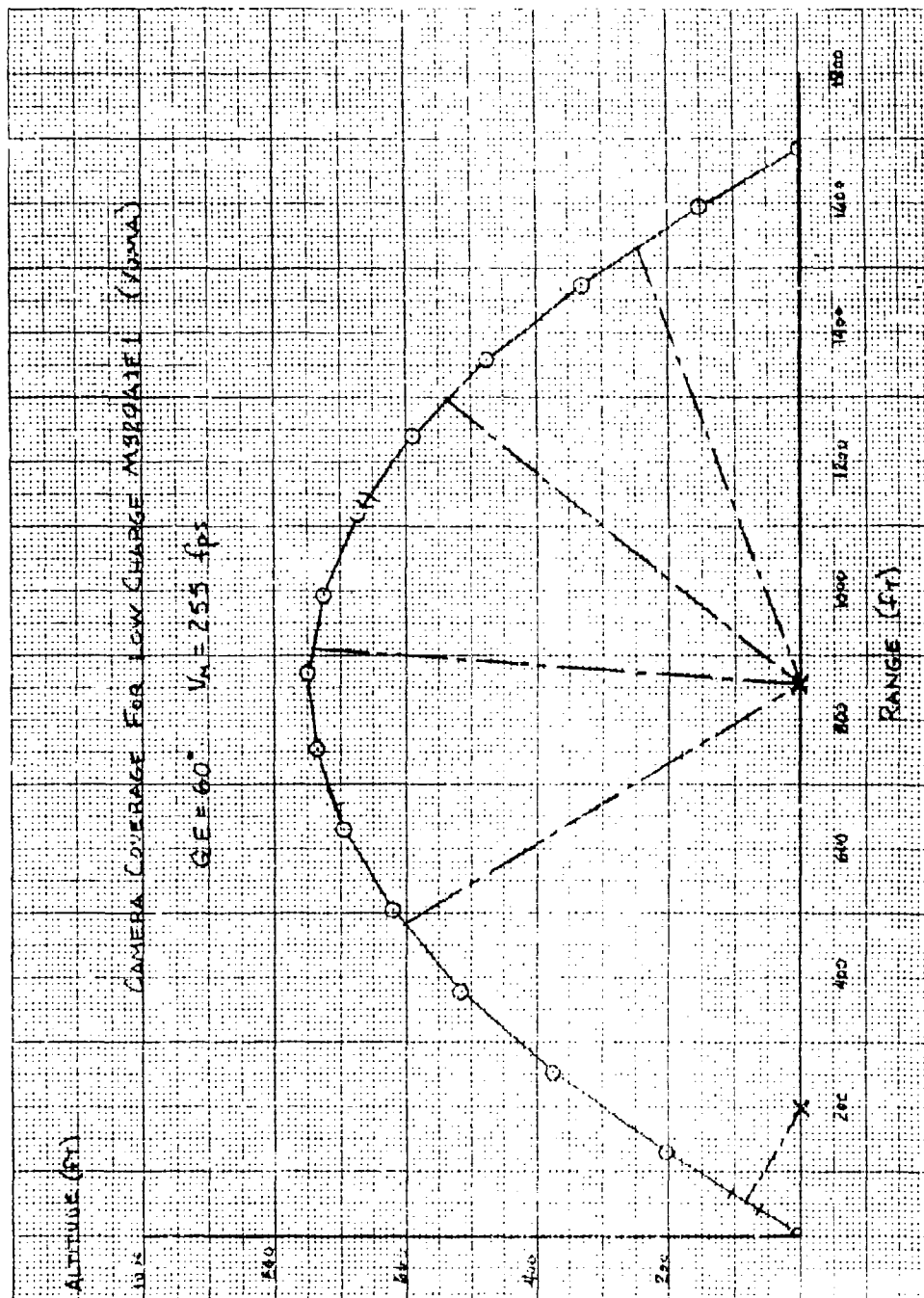


Fig 8 Camera coverage for low charge high quadrant elevation firing of M329A1E1 projectile at Yuma Proving Ground

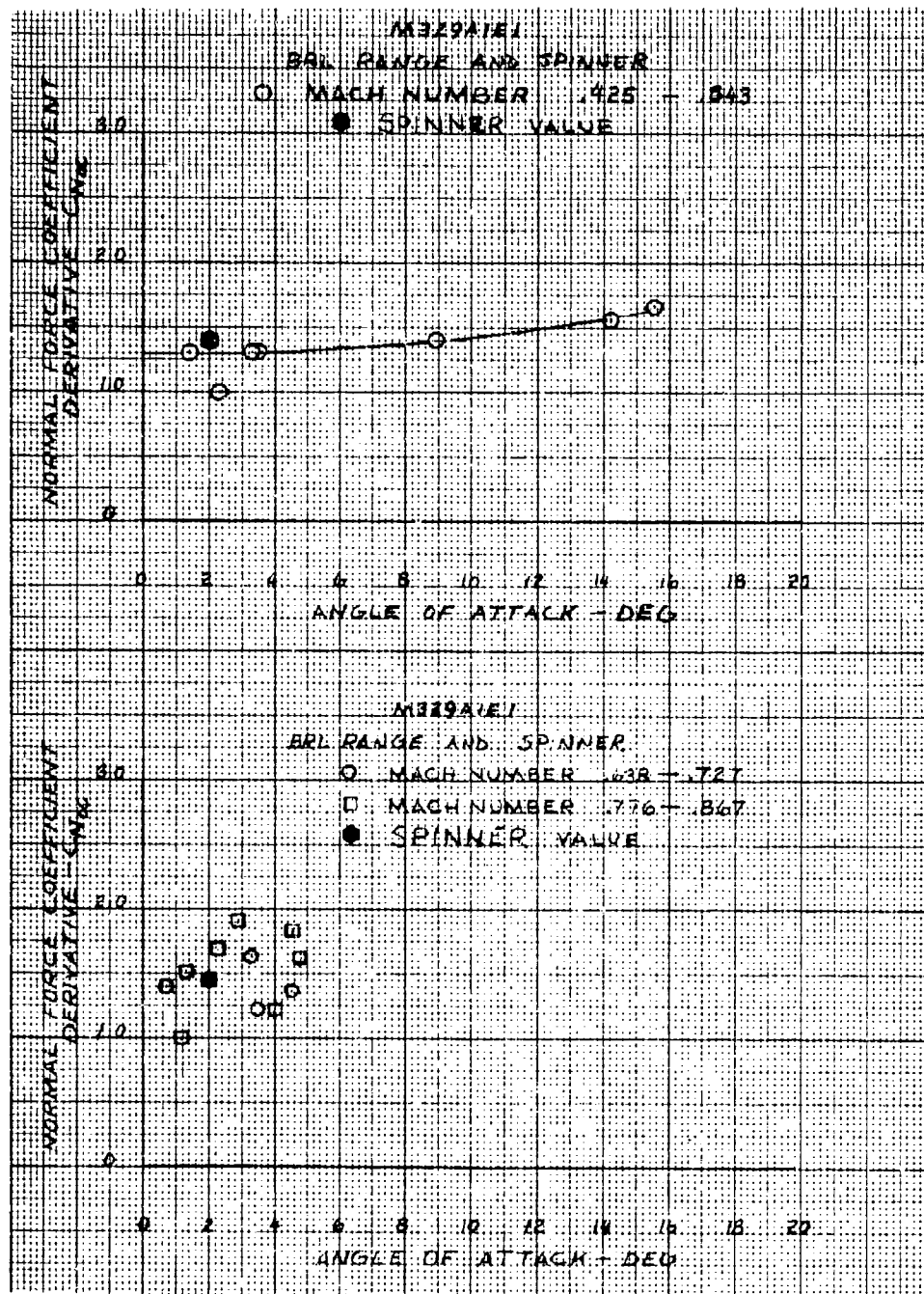


Fig 9 Normal force coefficient derivative vs angle of attack (BRL transonic range)

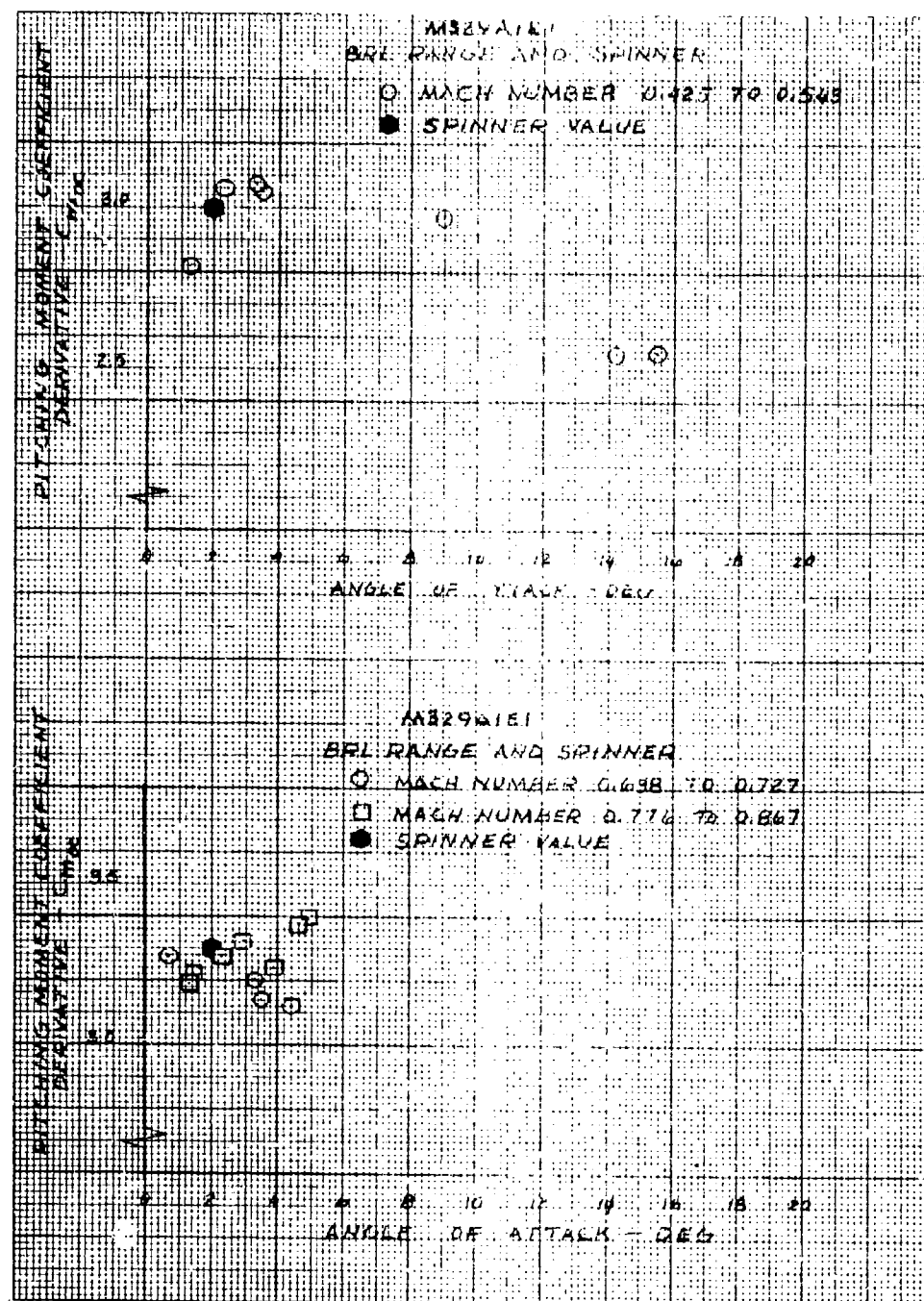


Fig 10 Pitching moment coefficient derivative vs angle of attack
 (BRL transonic range)

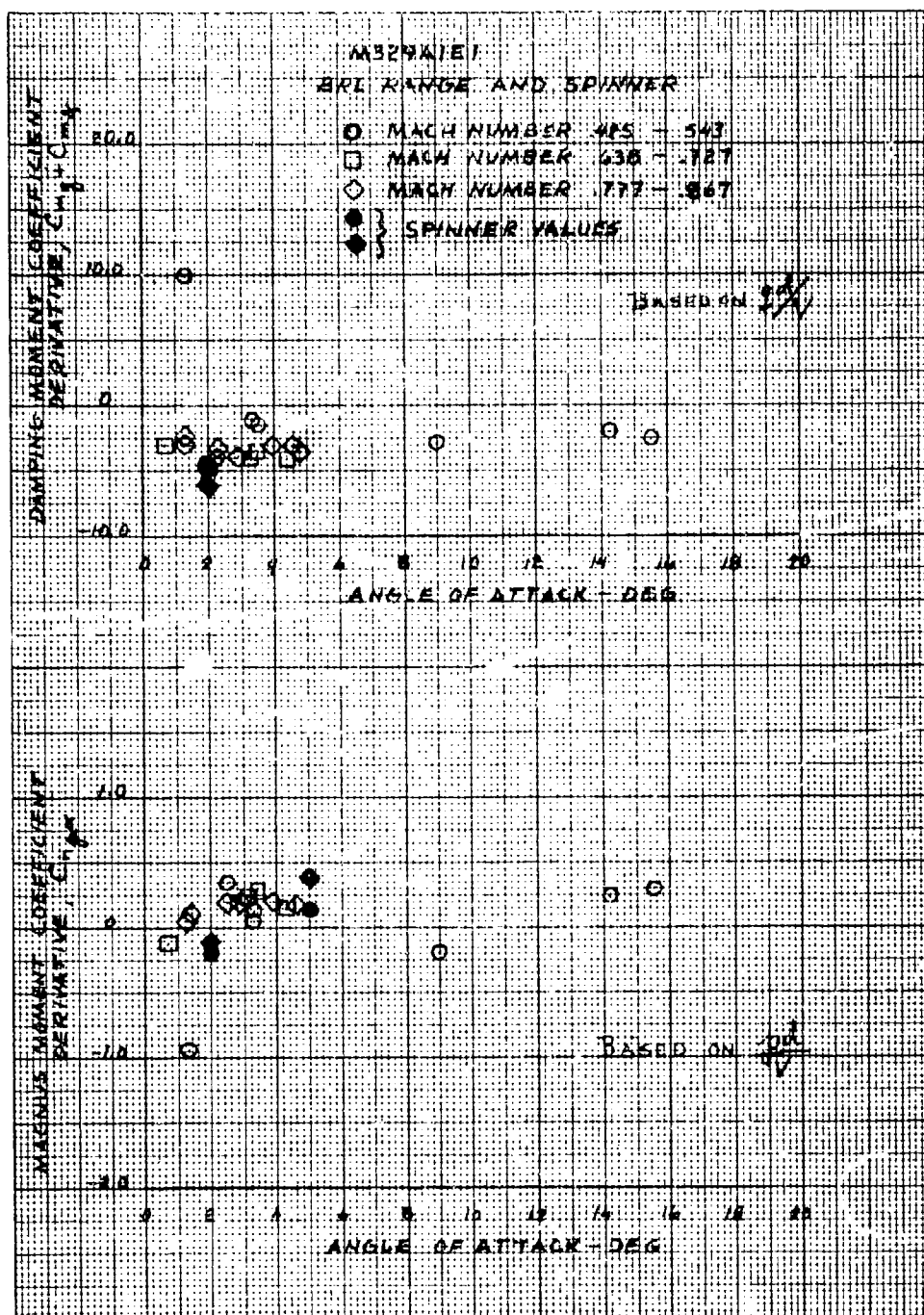
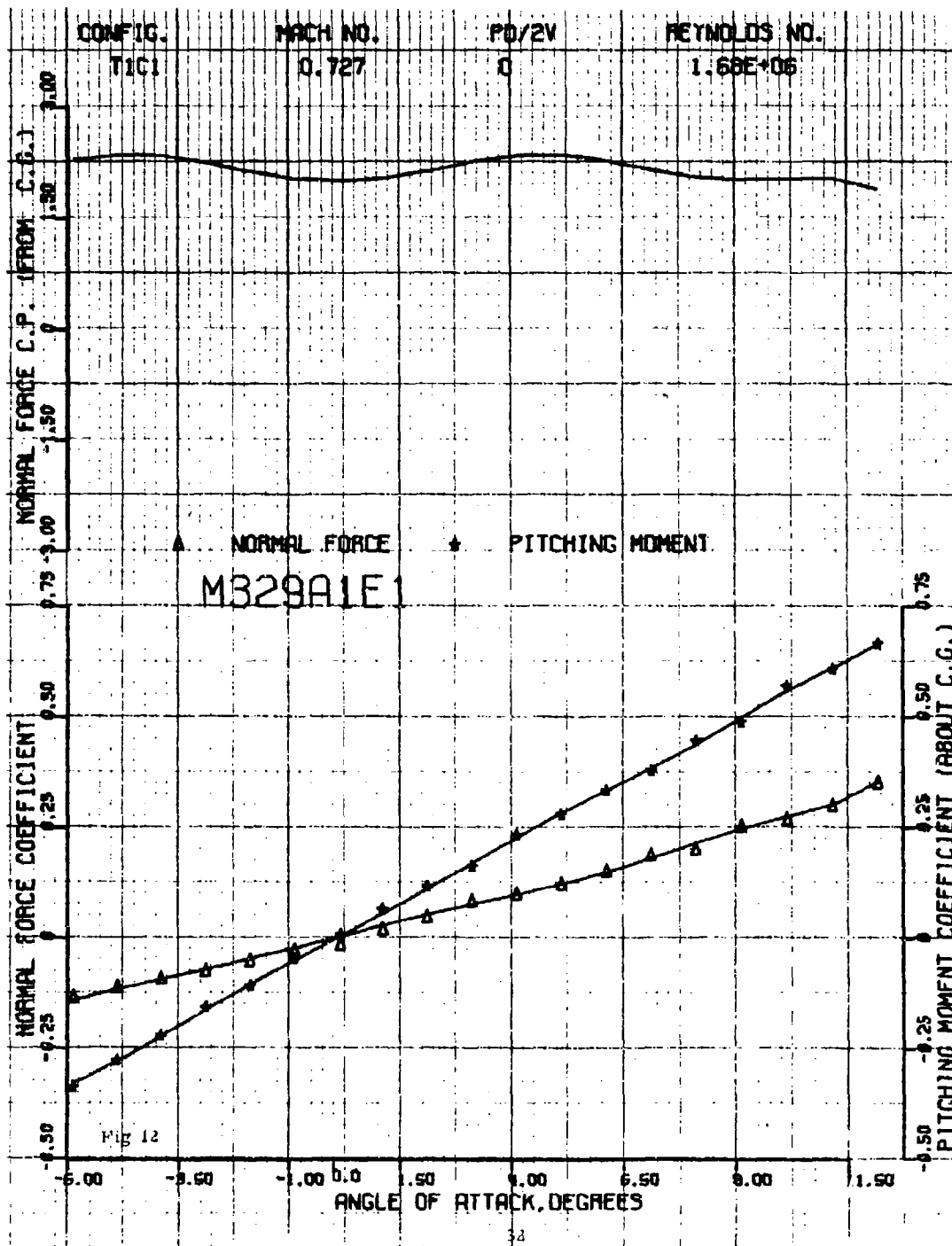


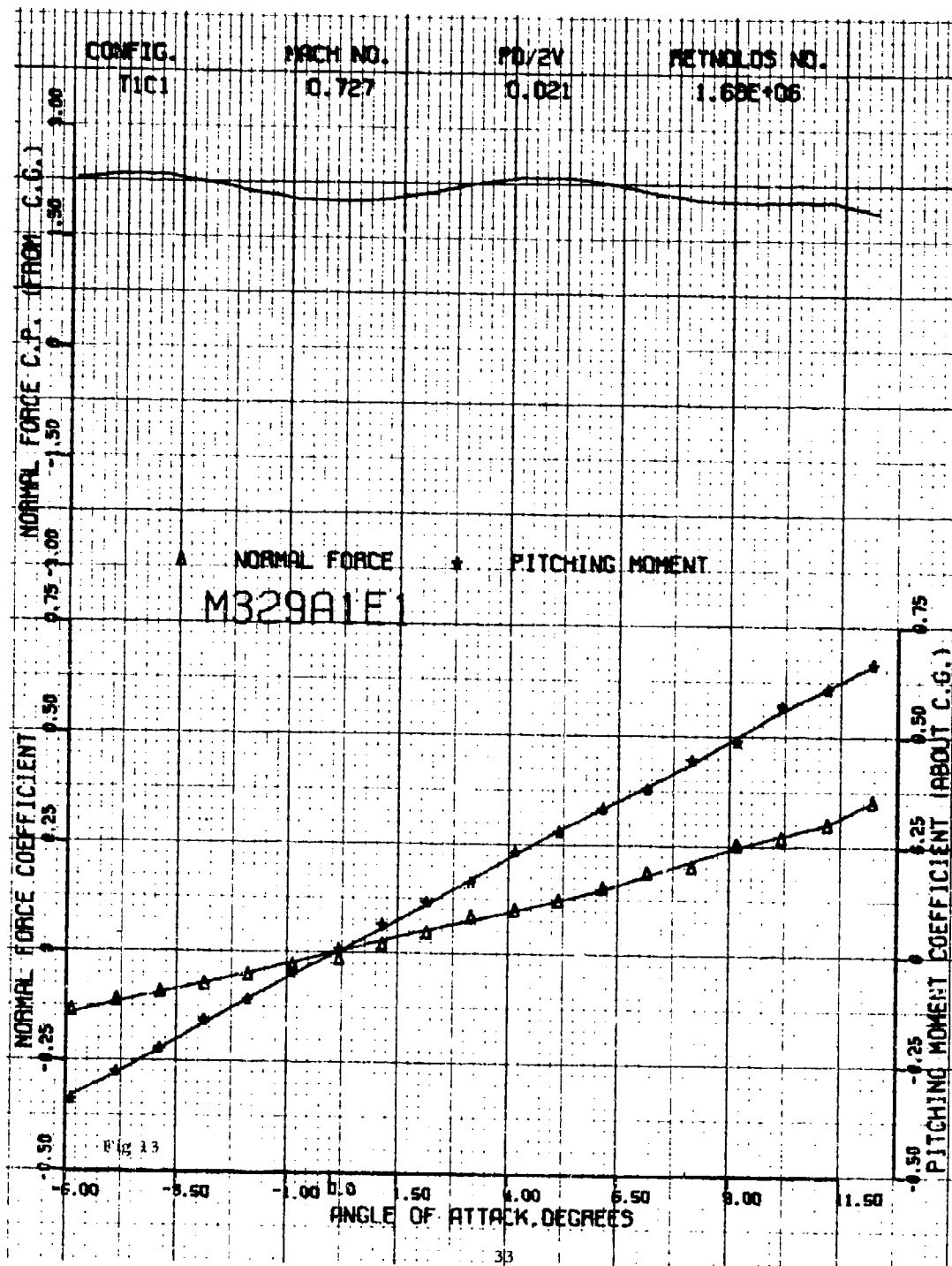
Fig 11 Pitch damping coefficient ($C_{m_q} + \dot{C}_{m_q}$) Magnus moment coefficient derivative vs angle of attack (BRL transonic range)

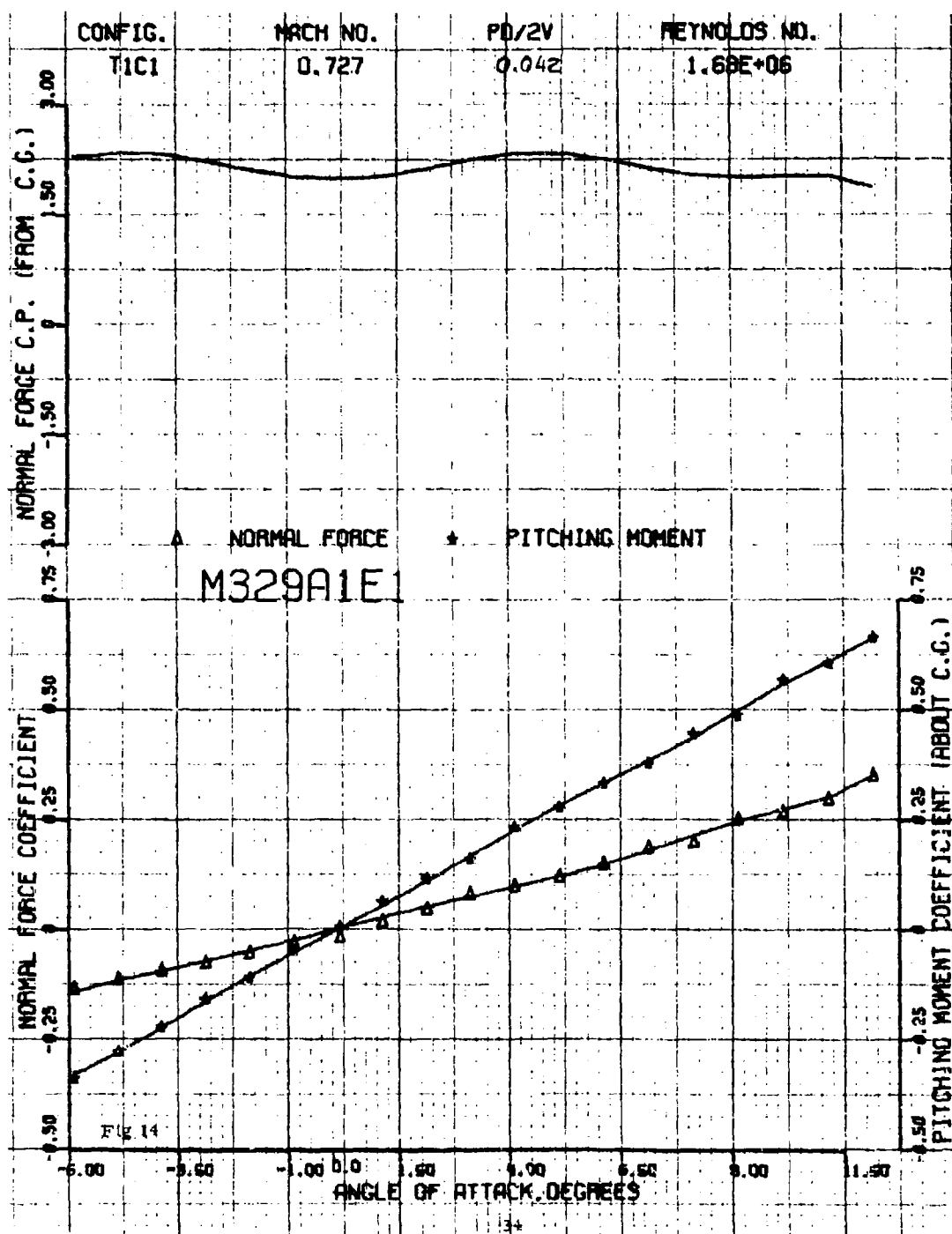
Figures 12 through 157

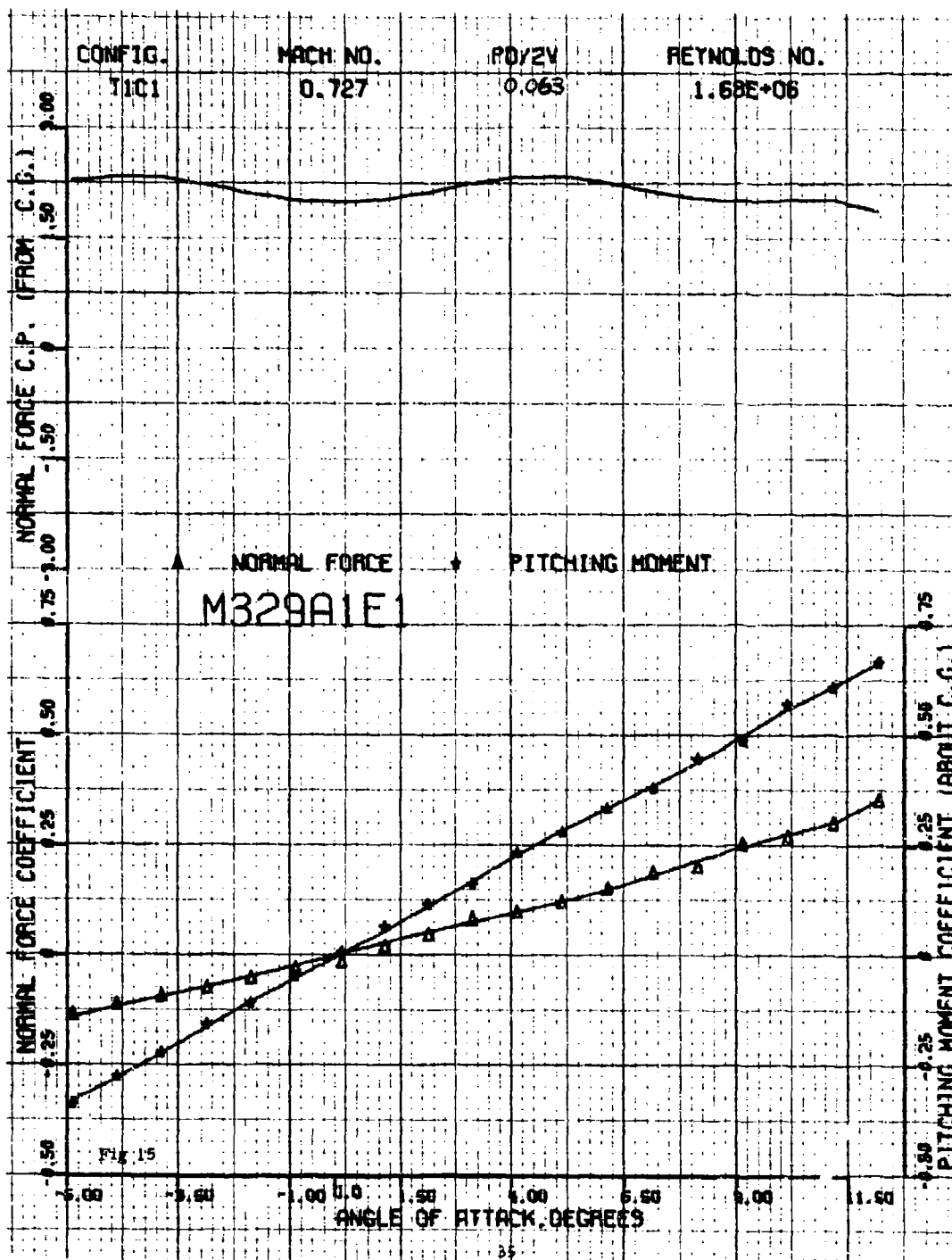
Normal force coefficient, pitching moment coefficient,
and normal force center of pressure vs angle of attack.
(Includes several configurations, Mach numbers,
pd/2V's and Reynolds numbers [12' PWT] .)

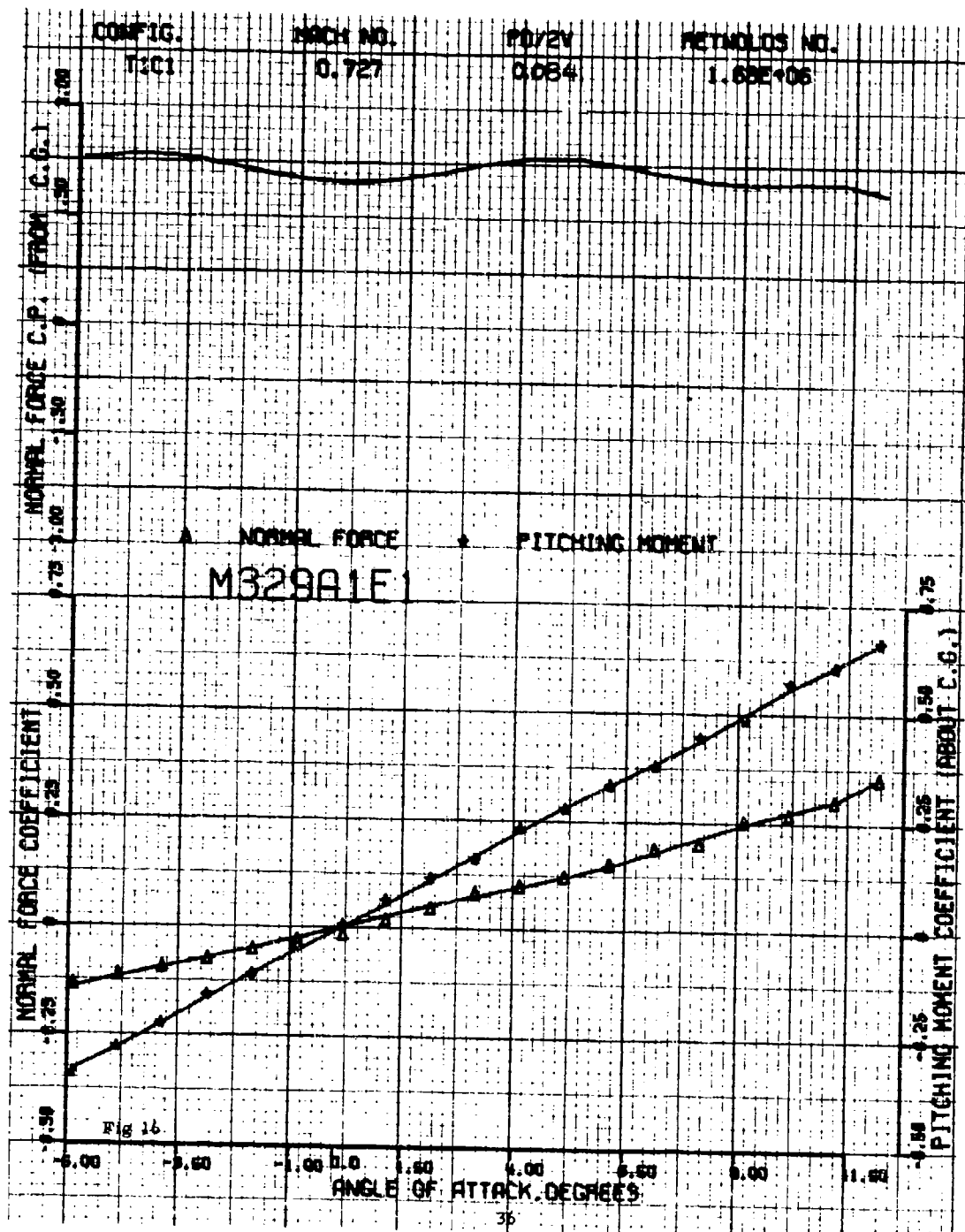
Preceding page blank

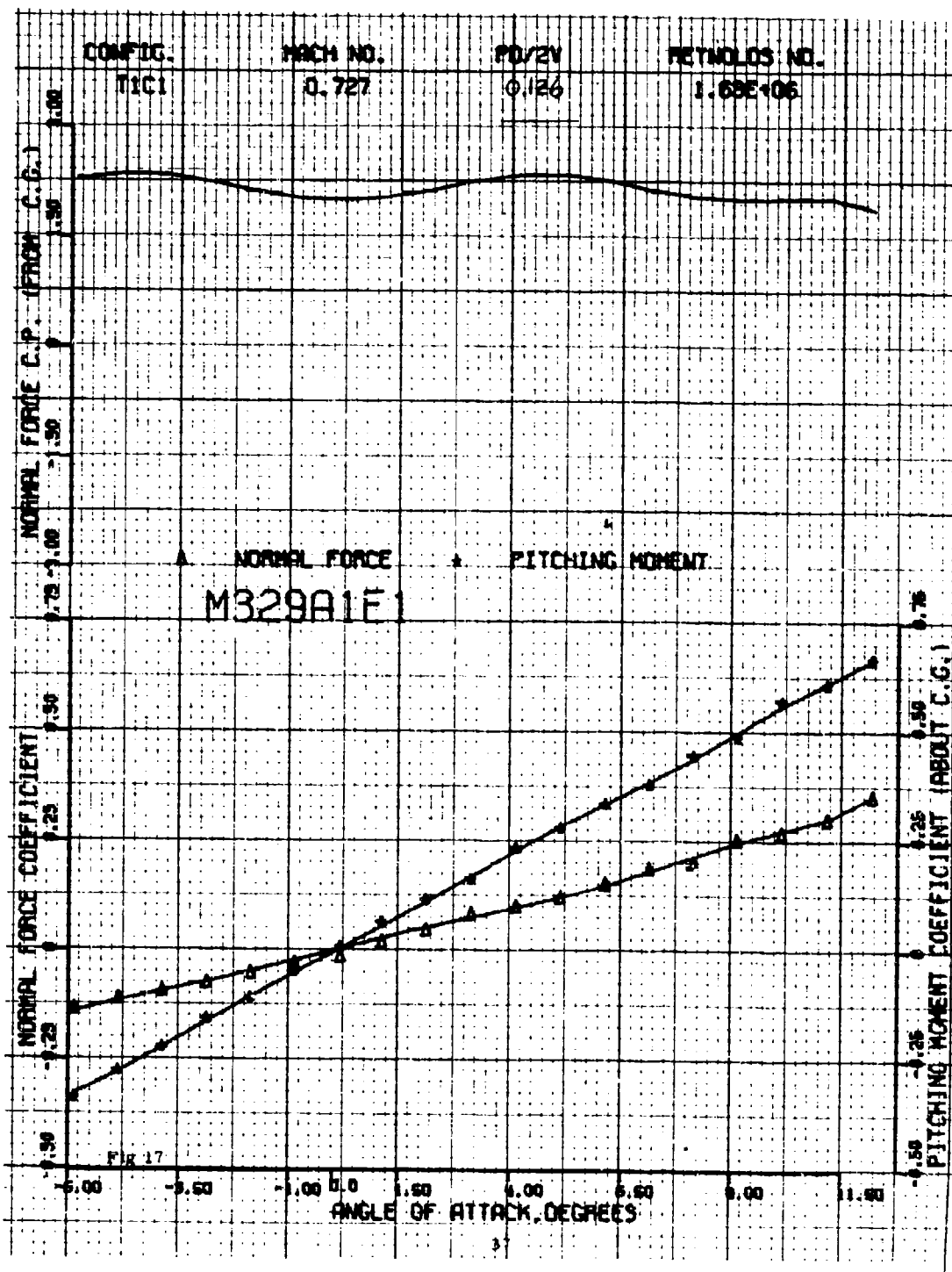


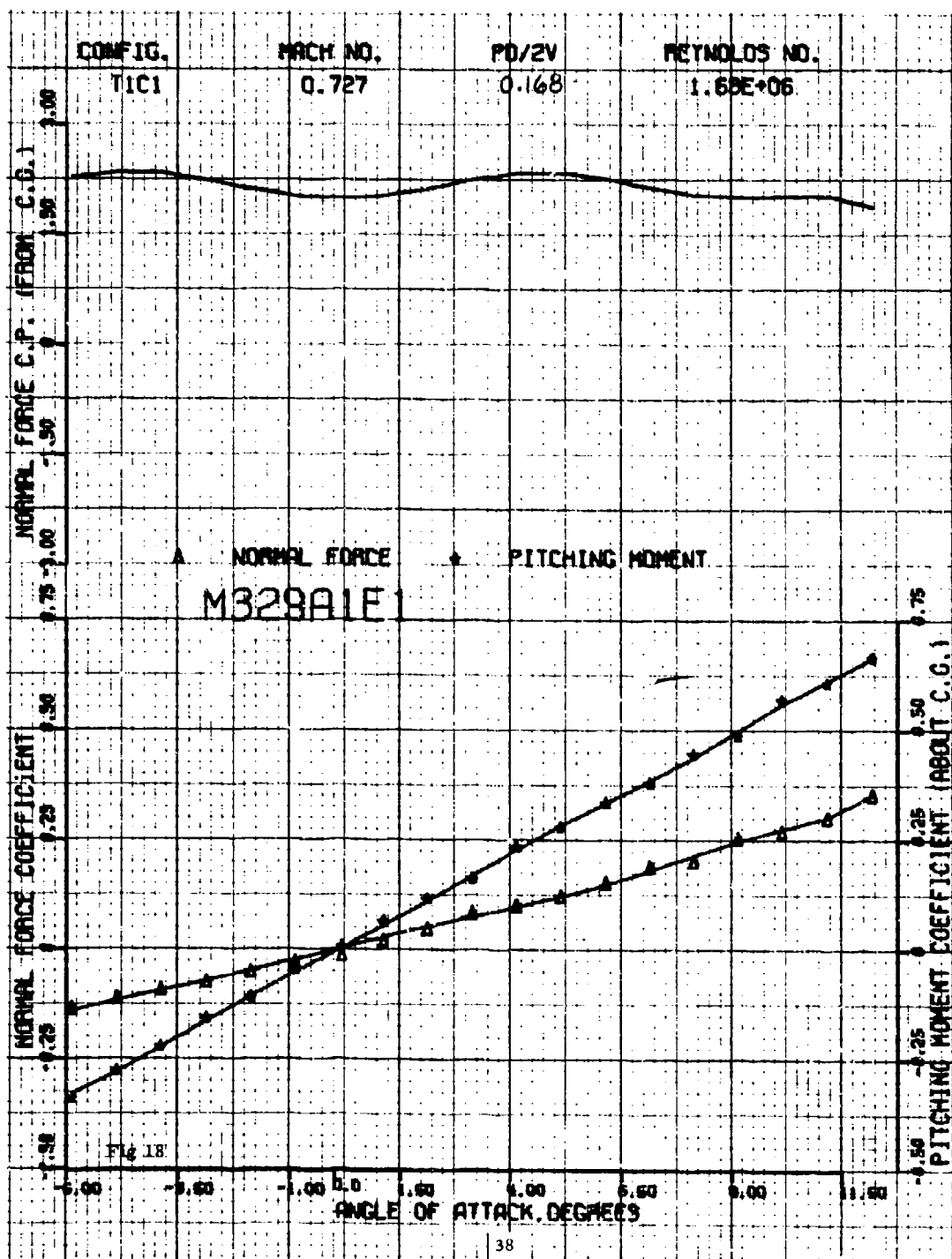


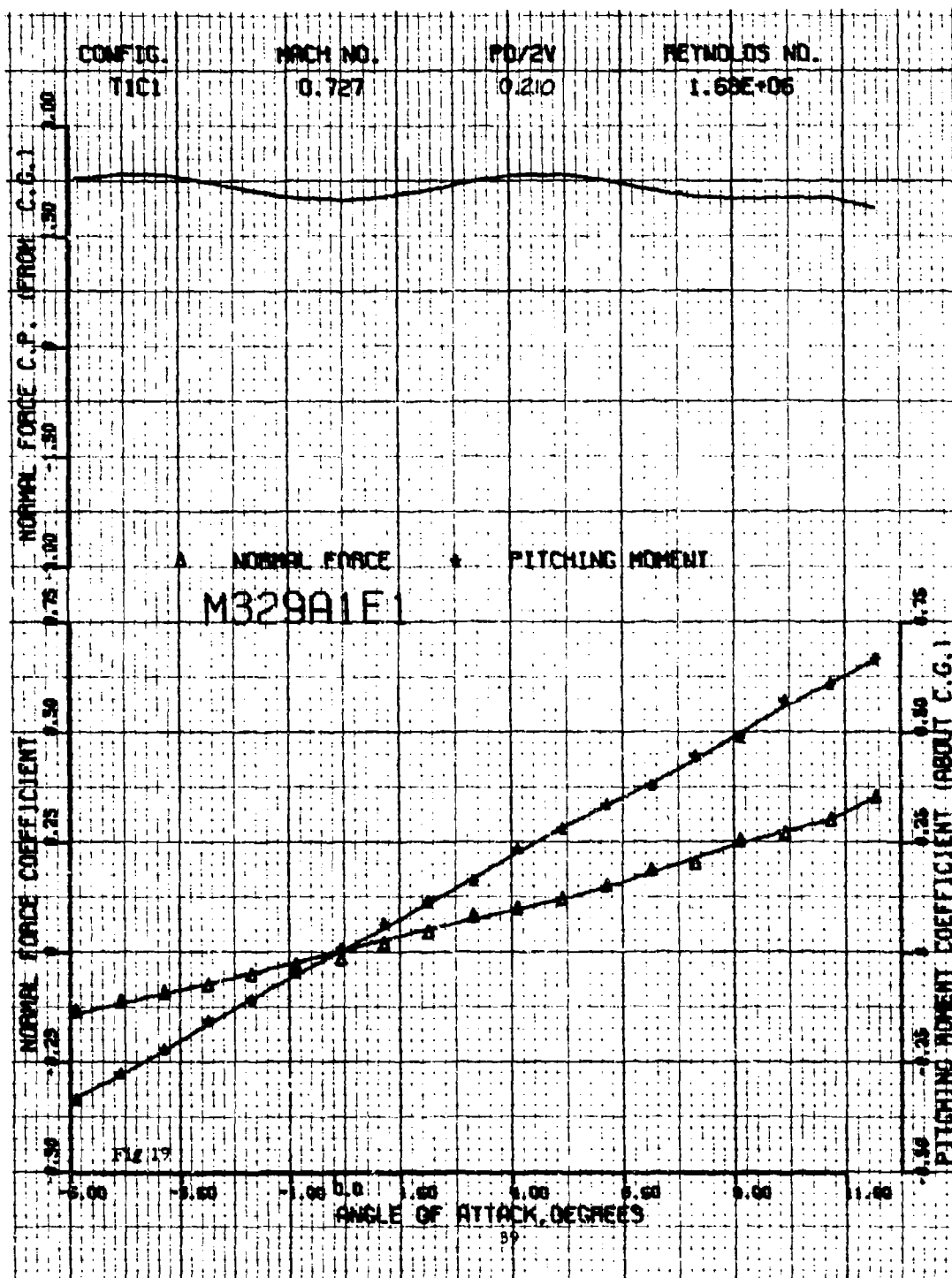


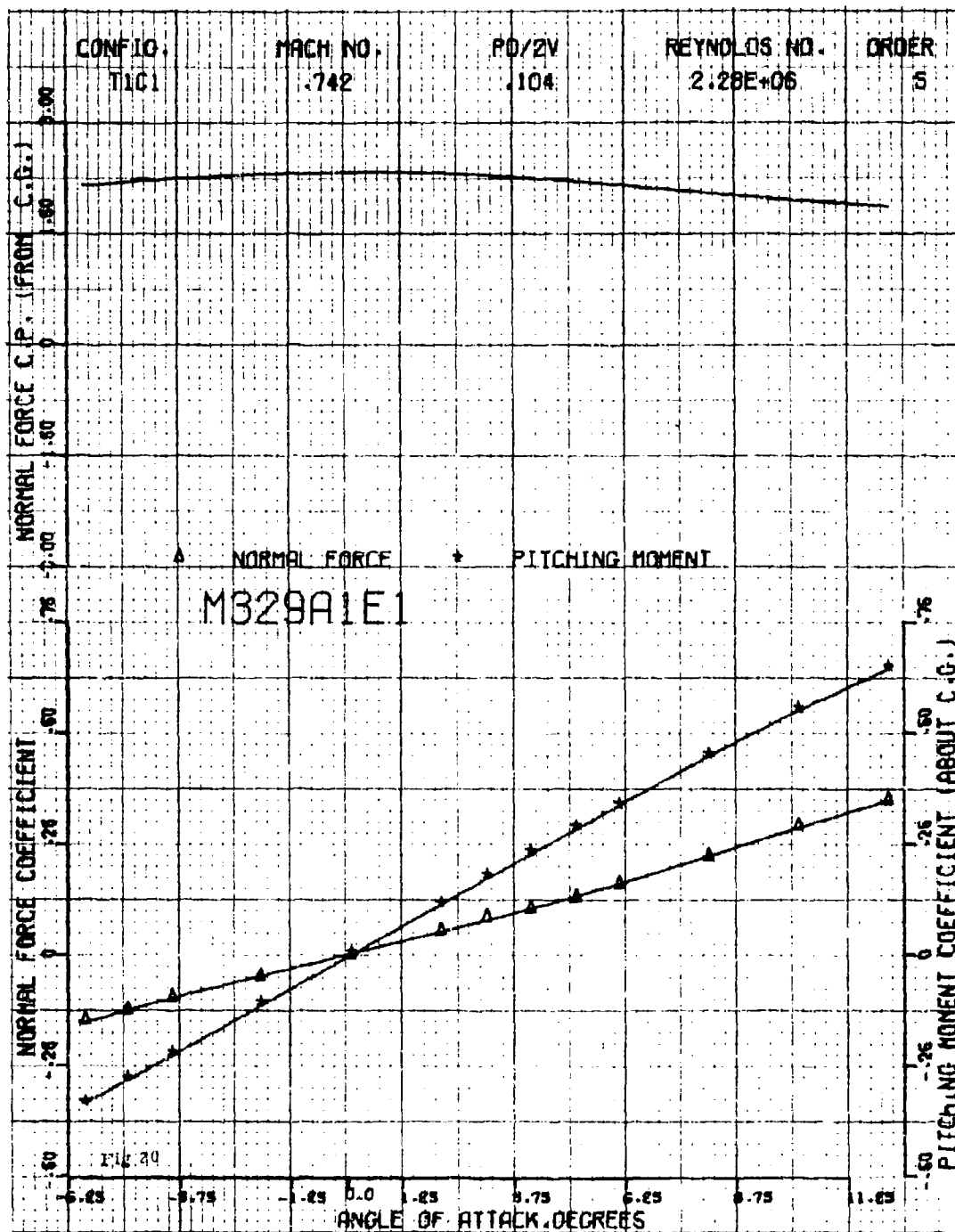


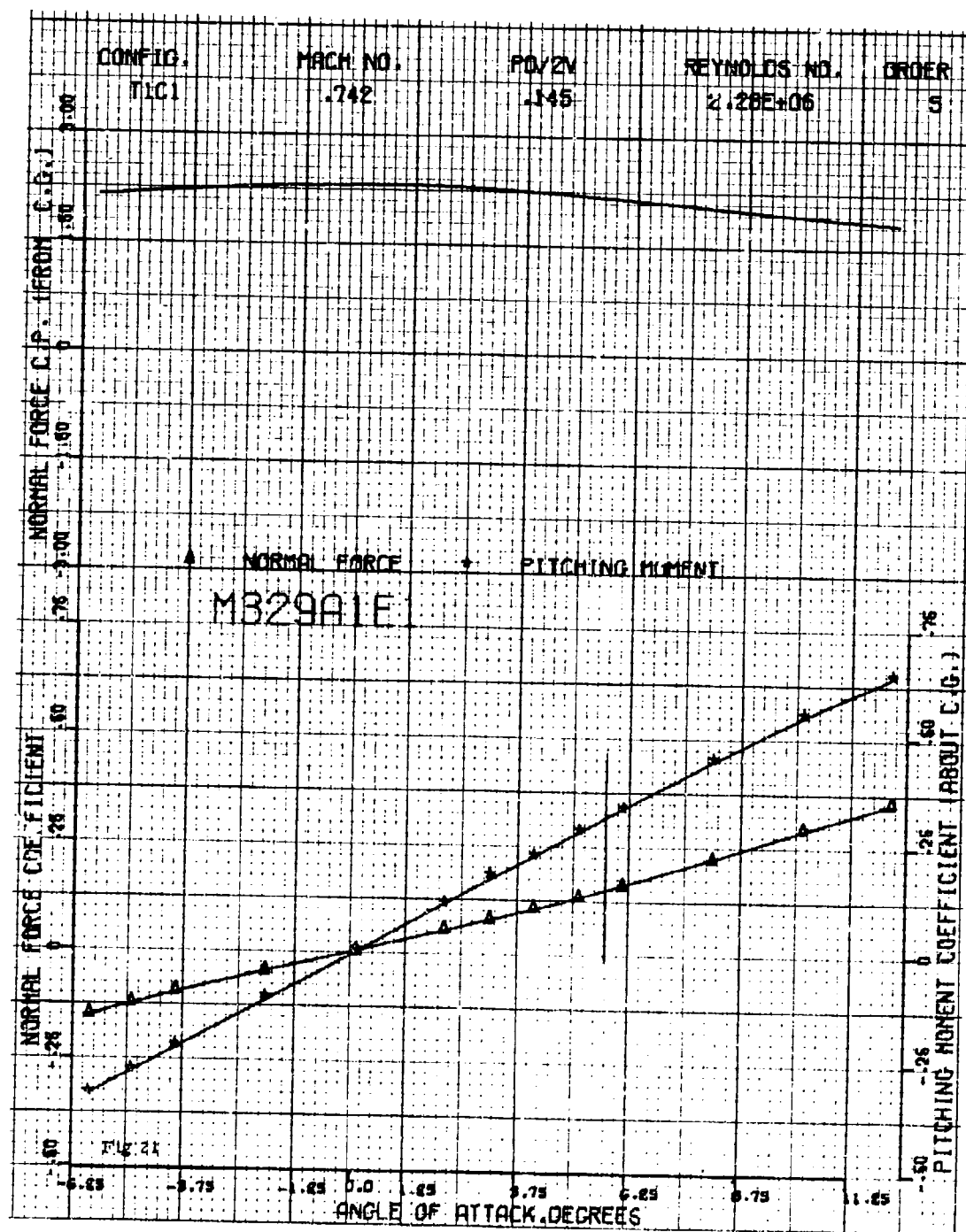


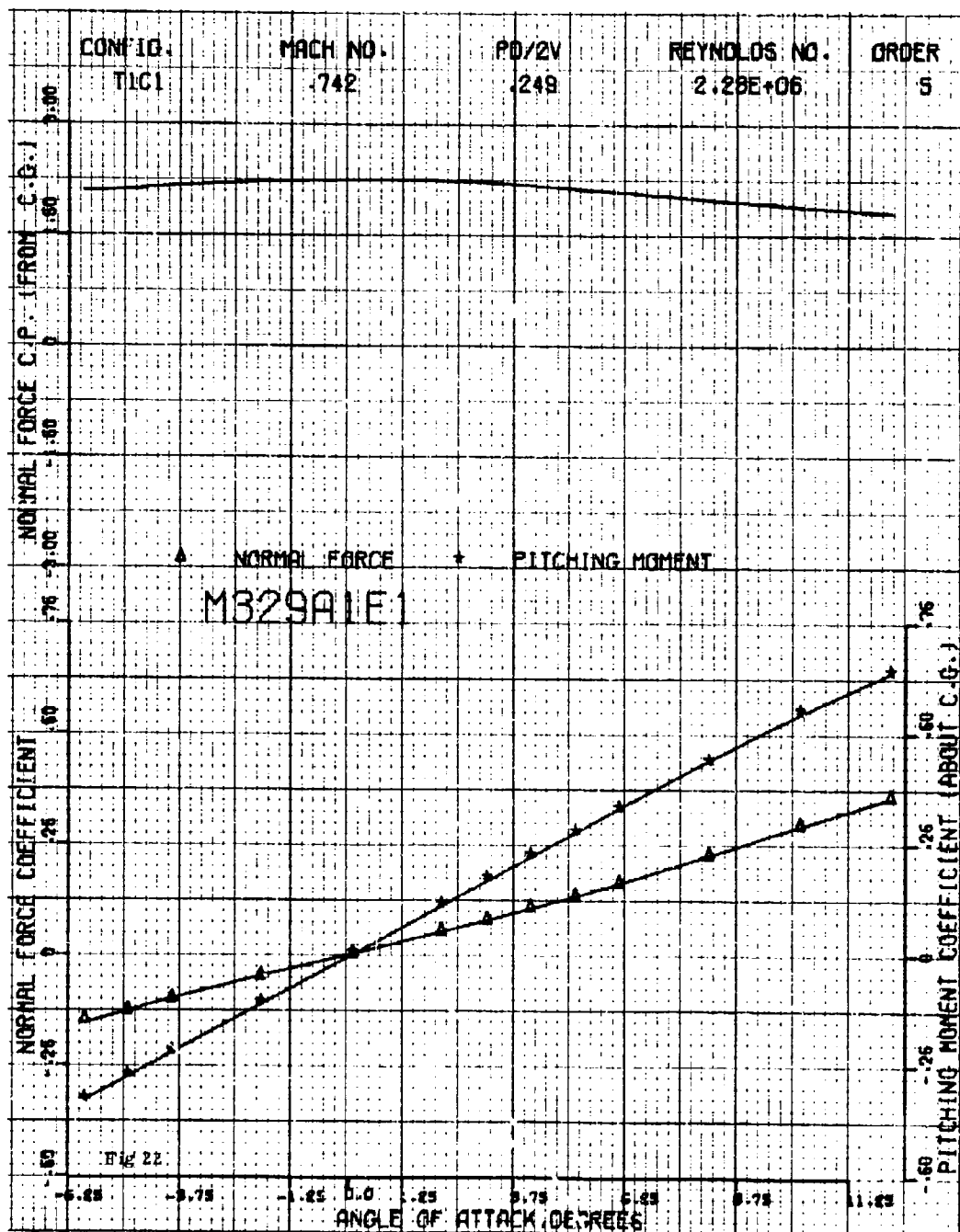


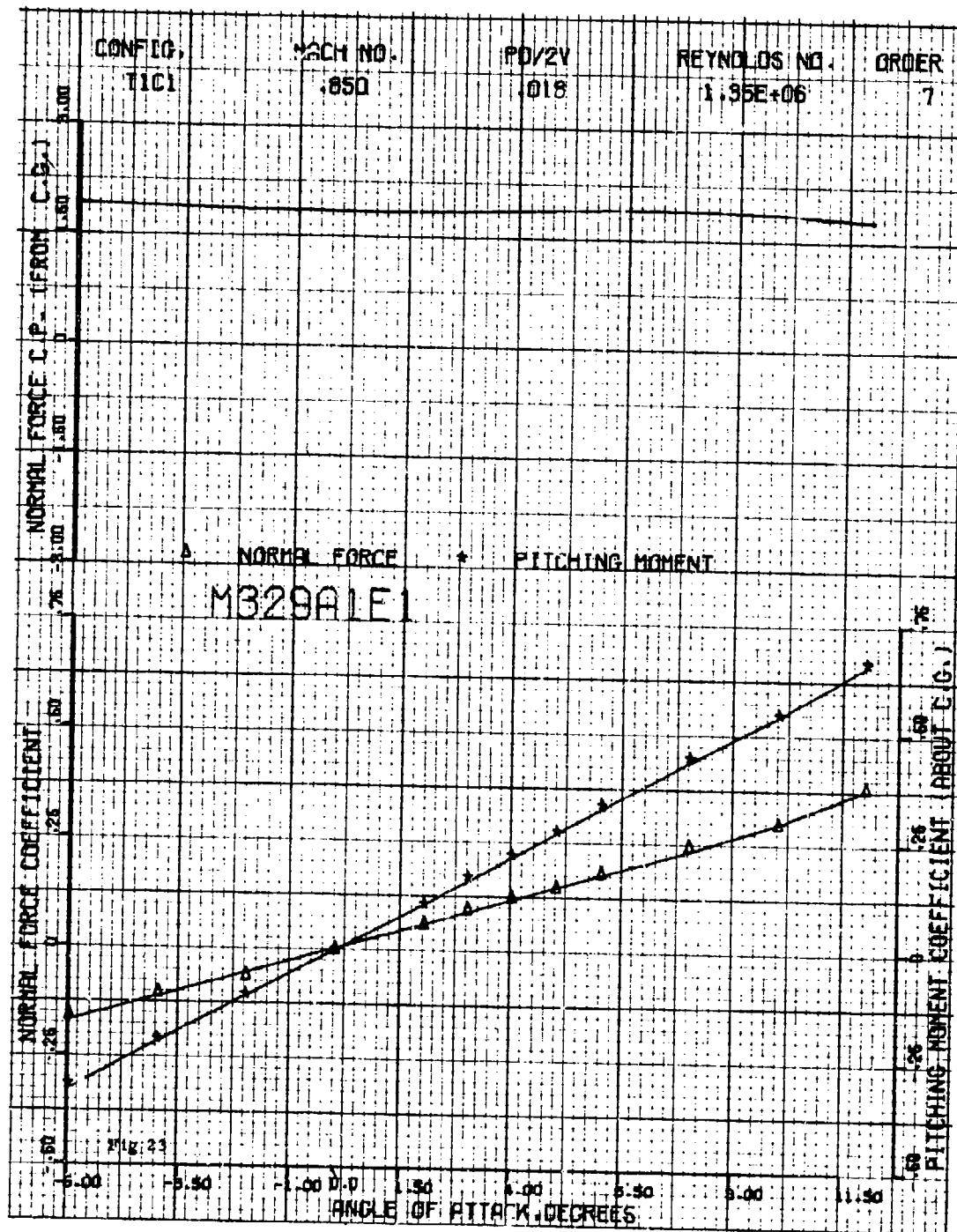


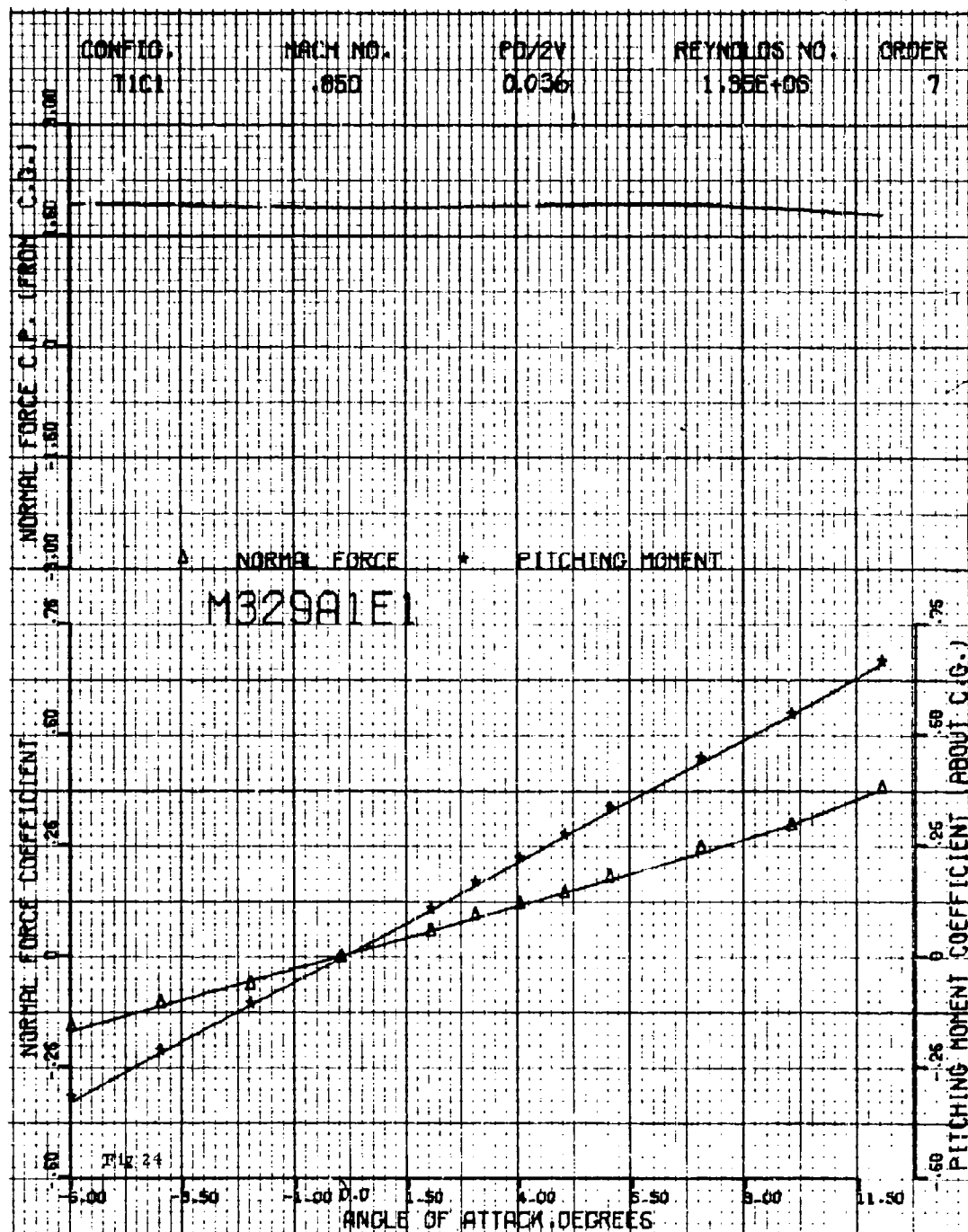


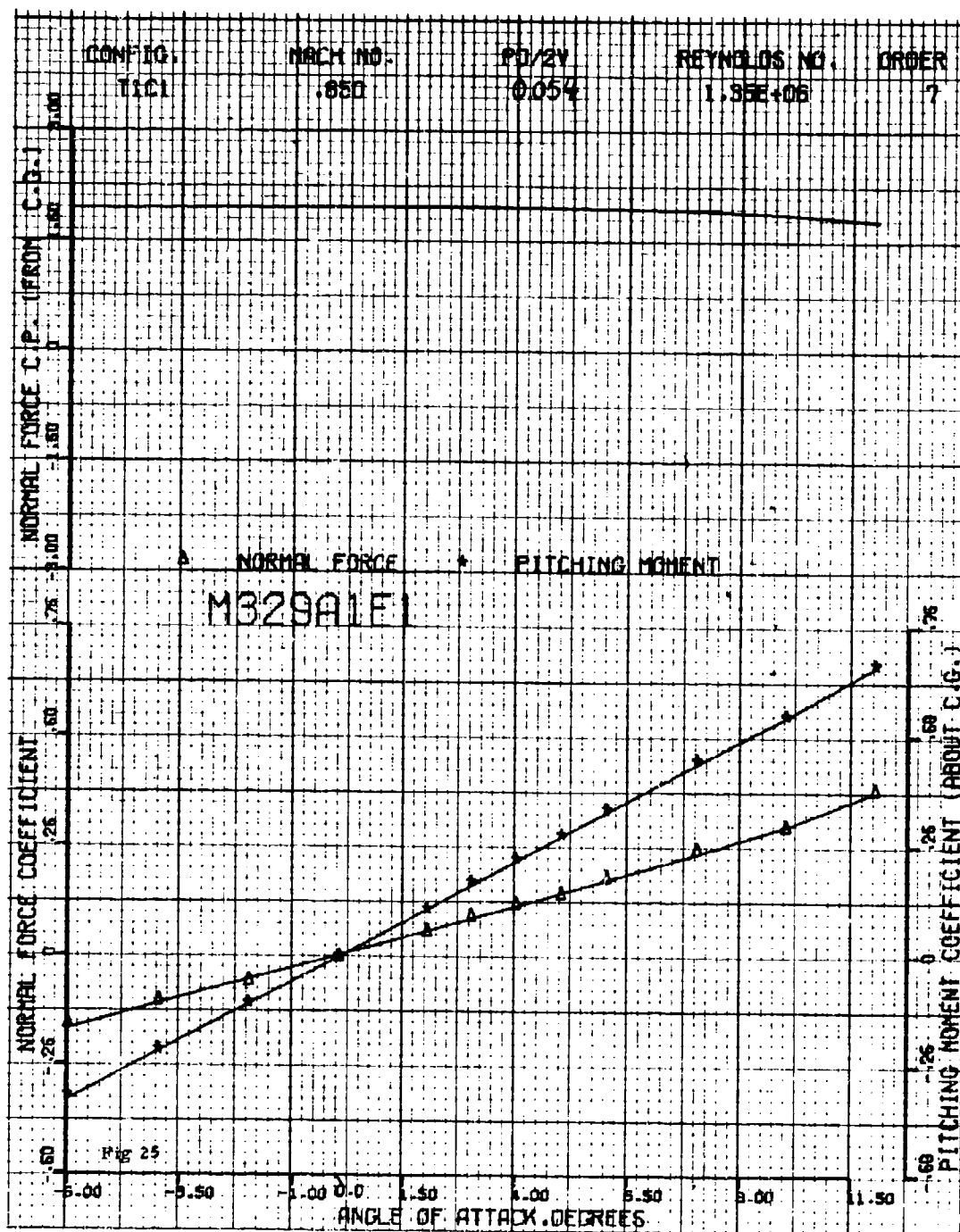


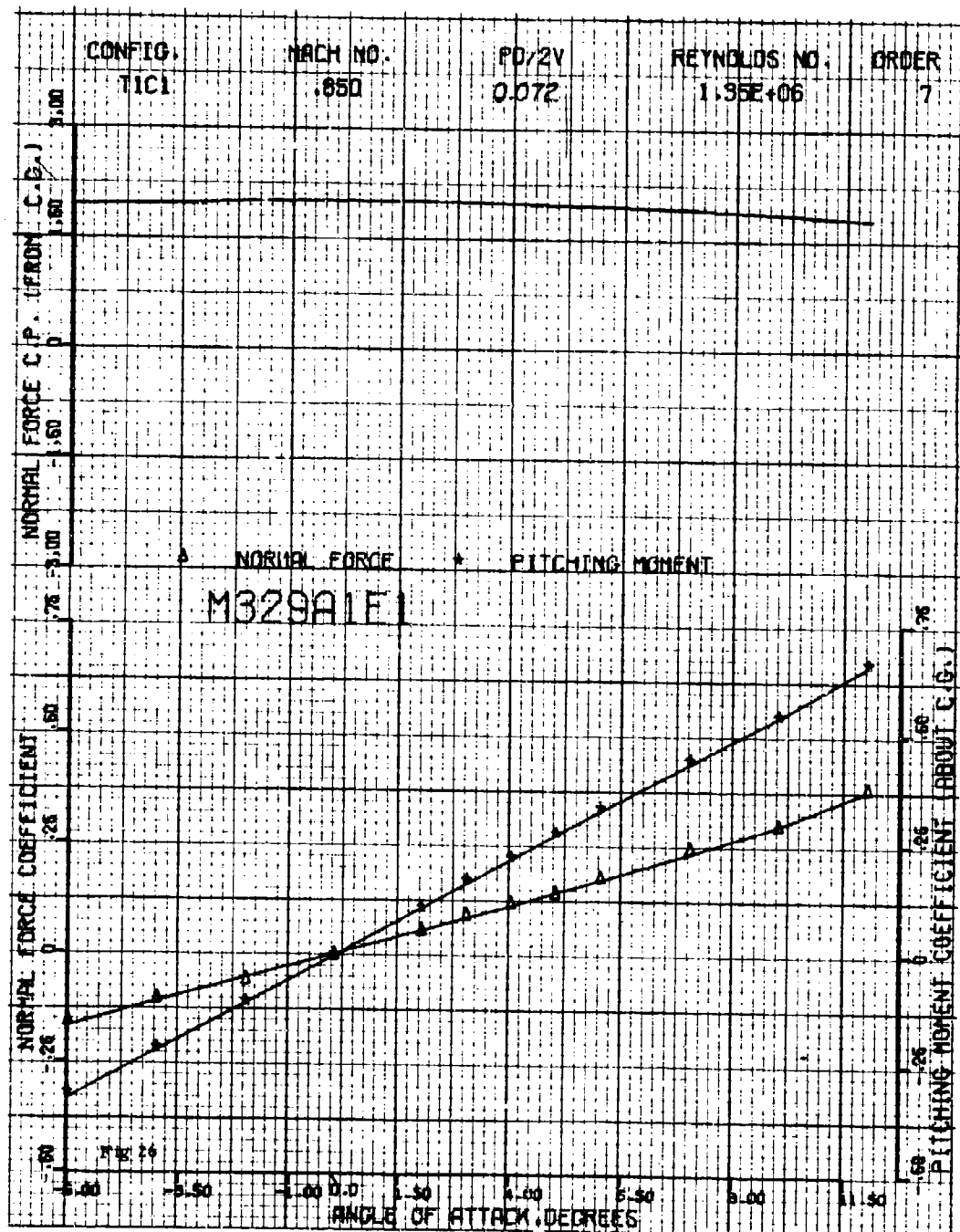


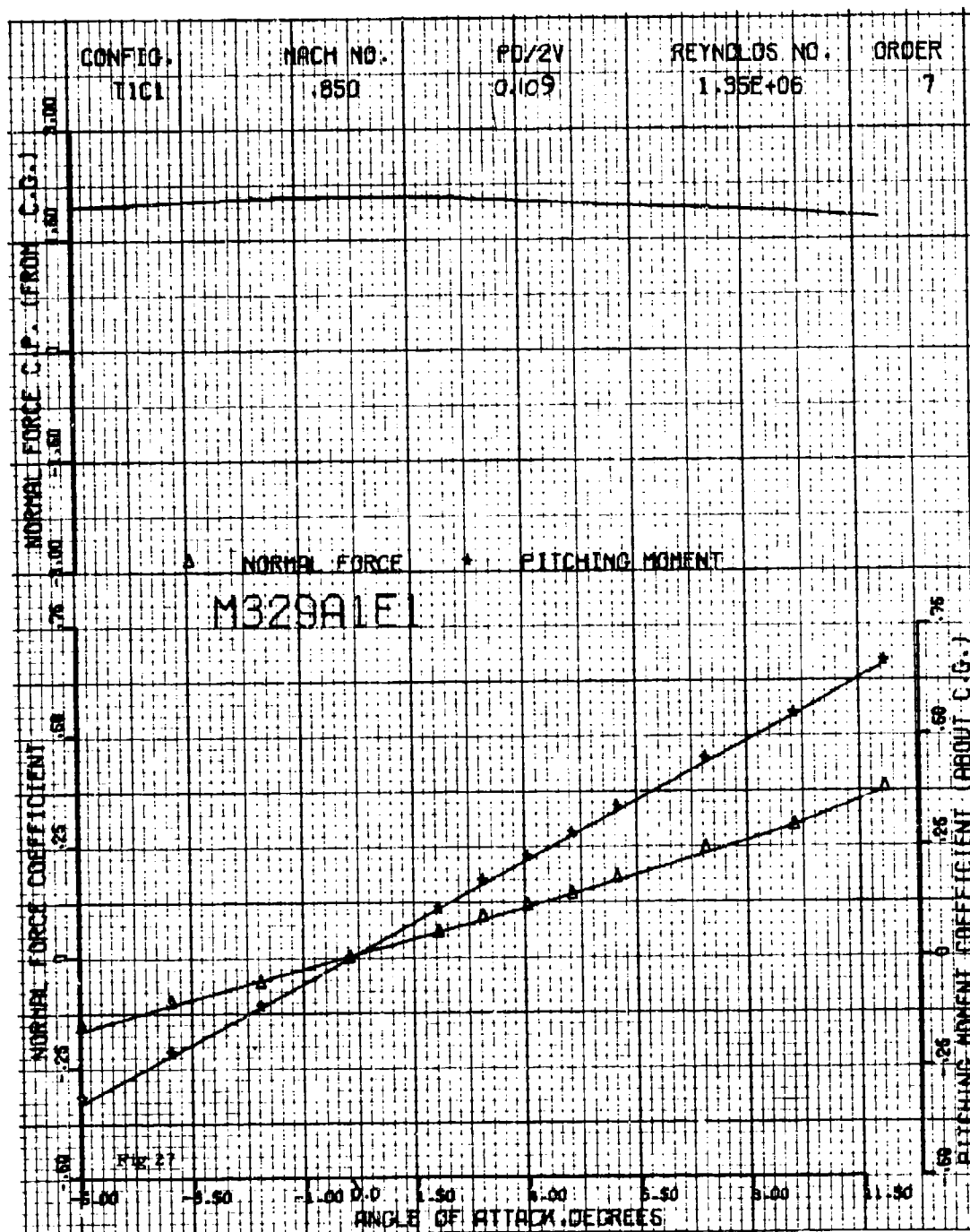


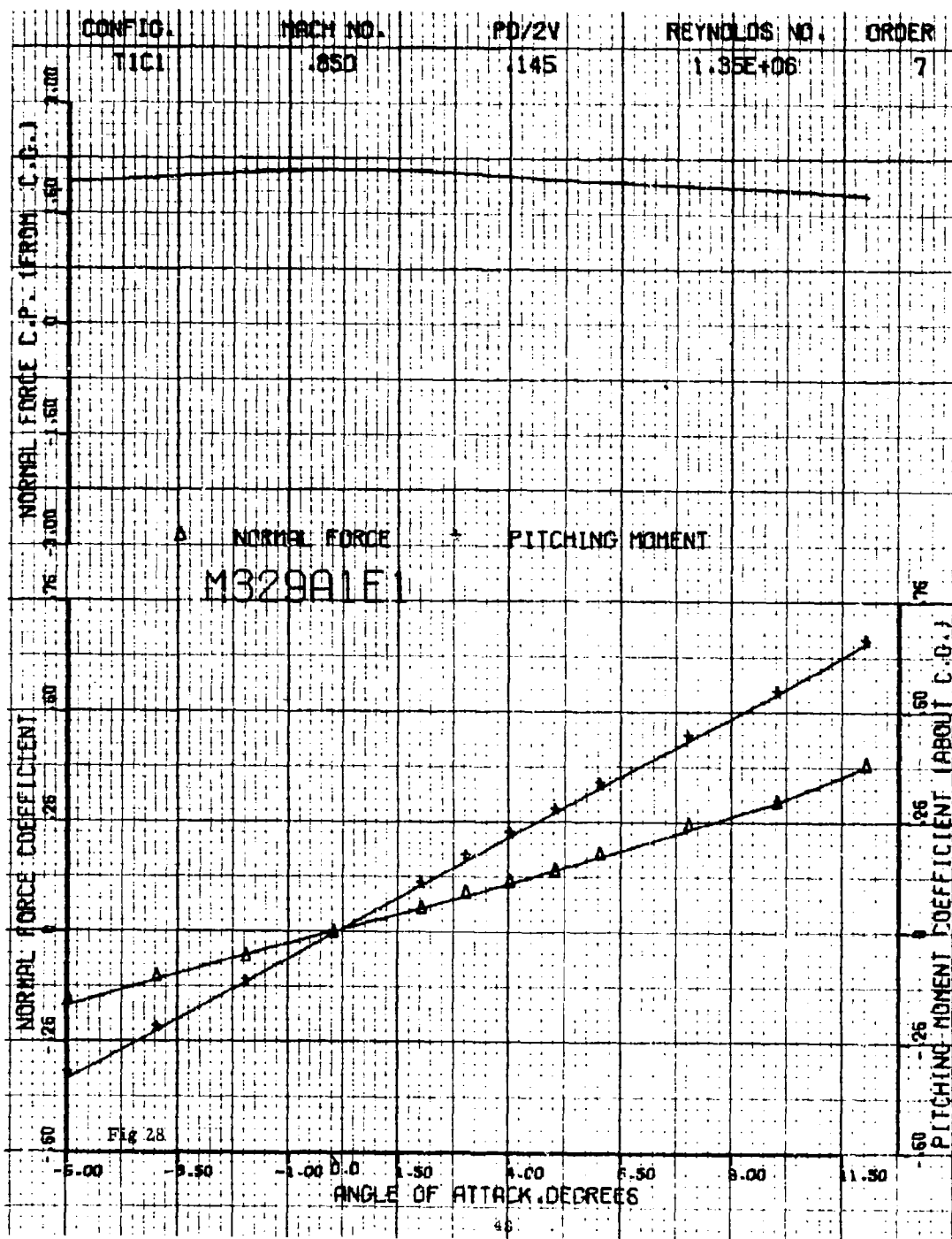


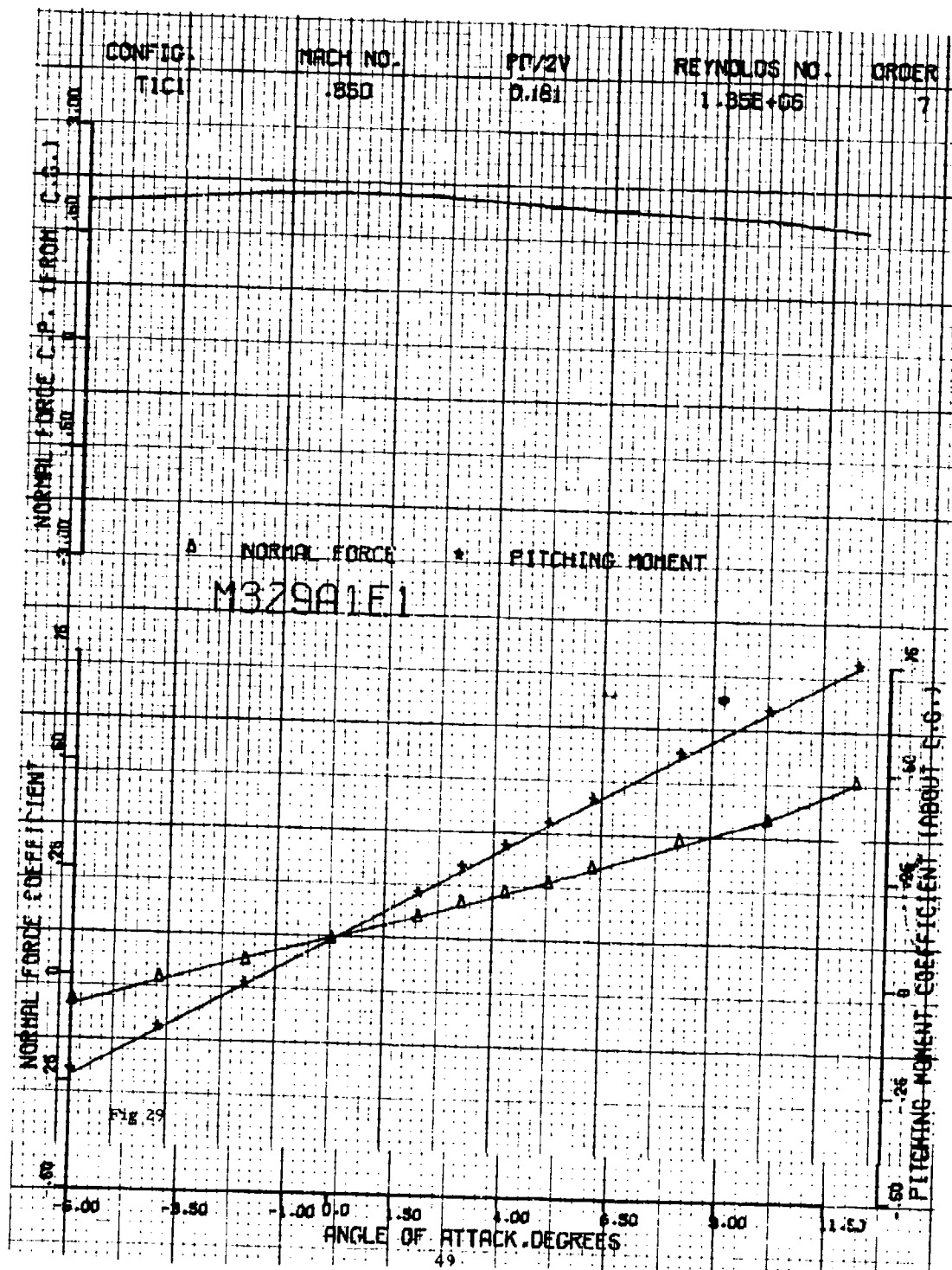


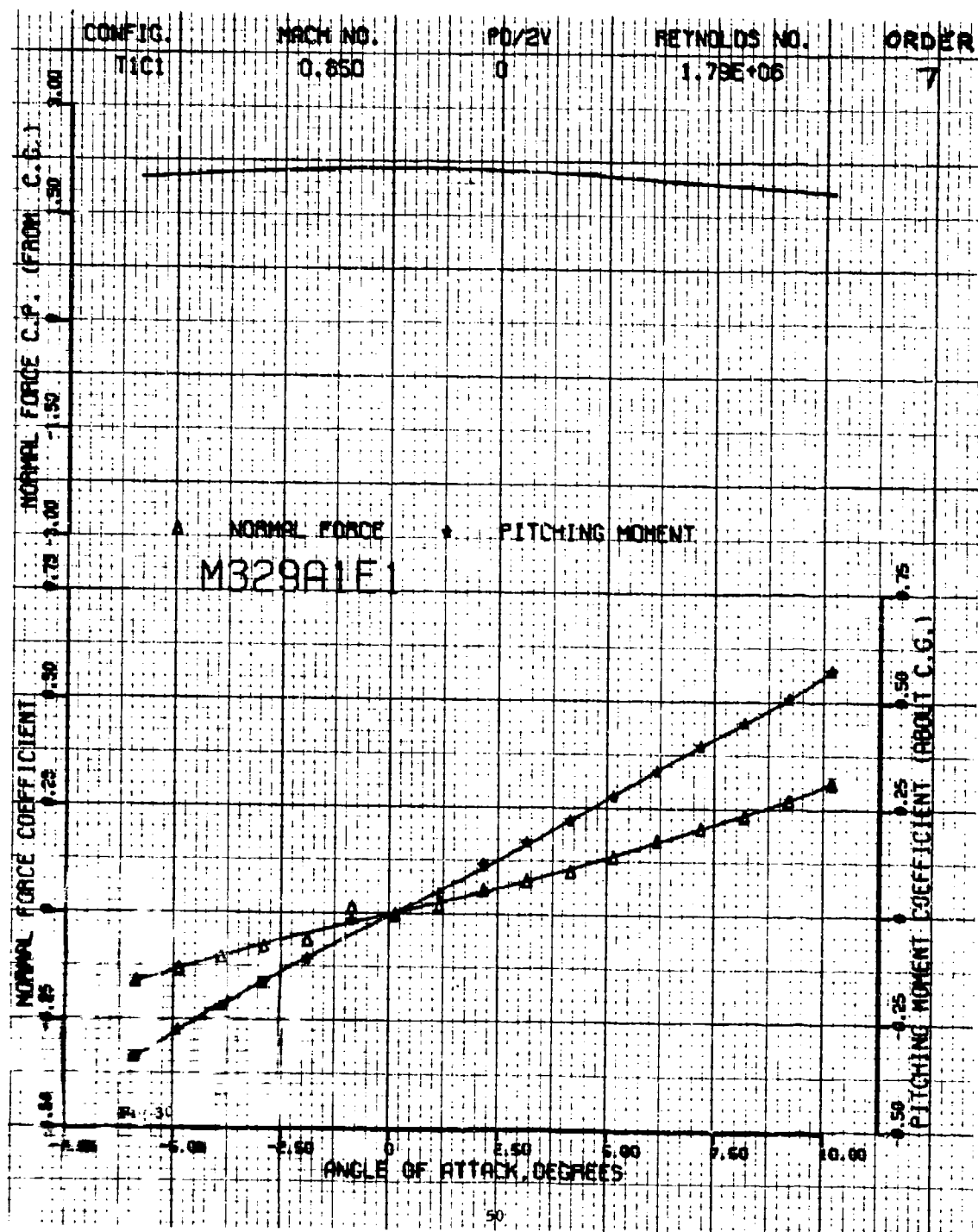


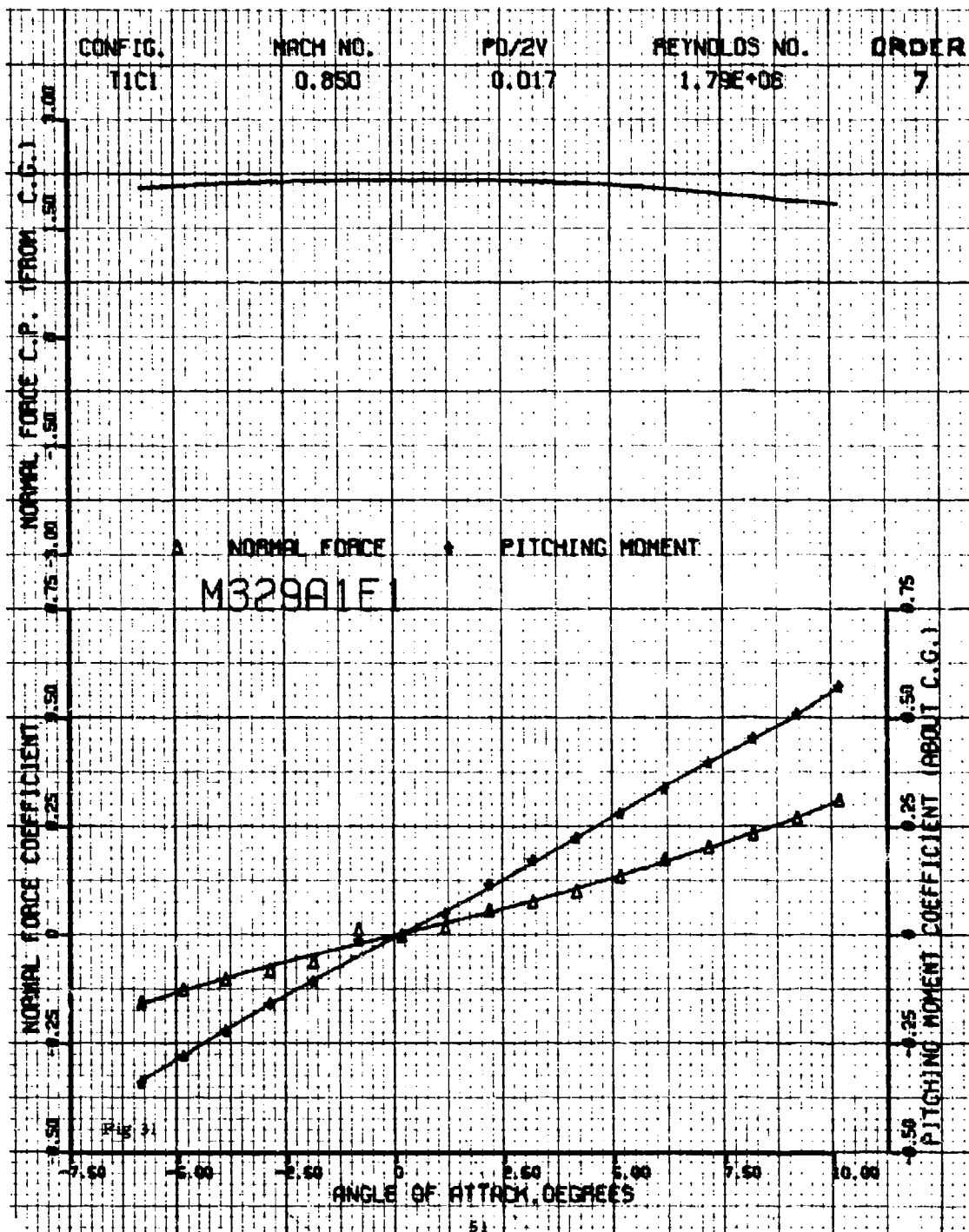


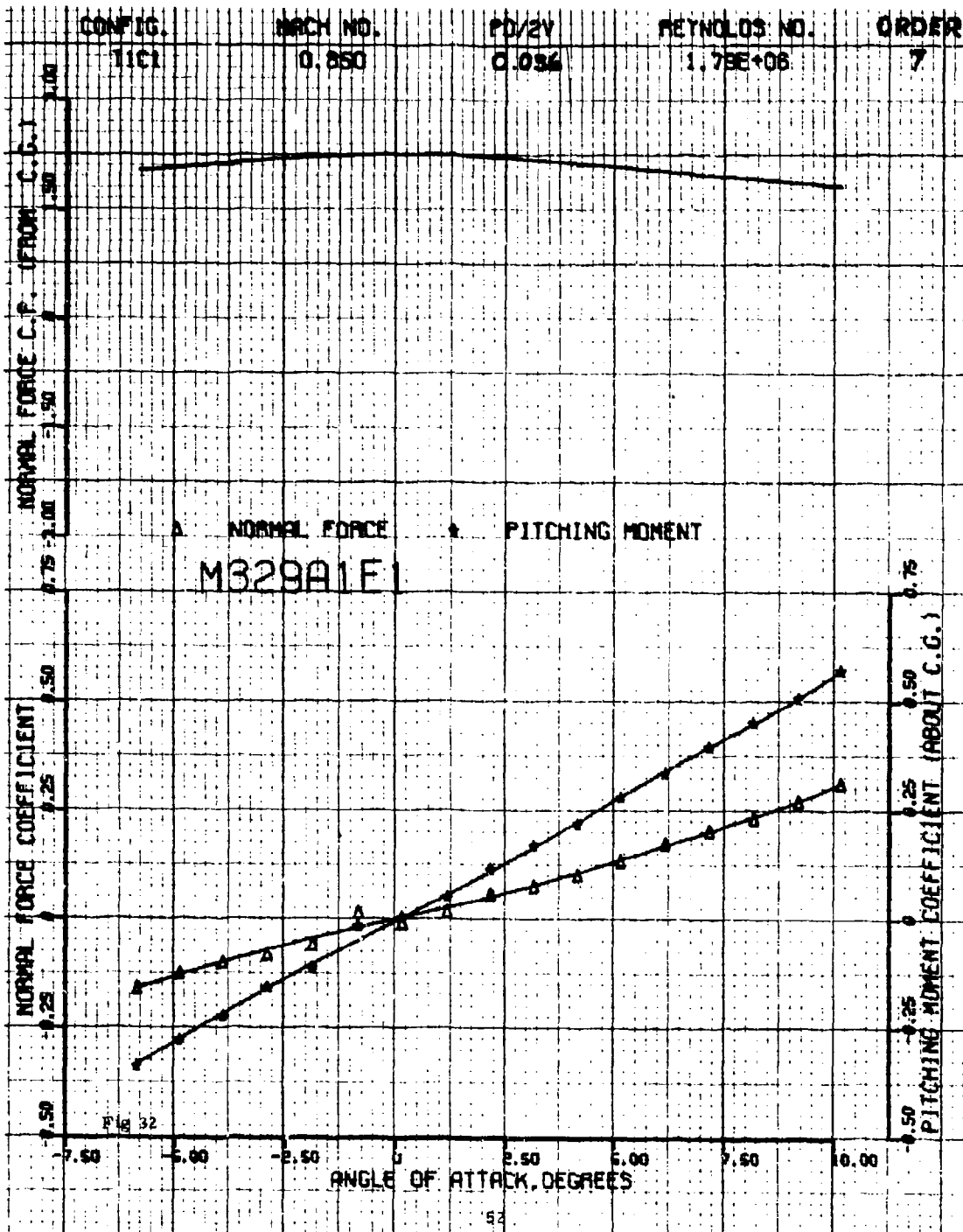


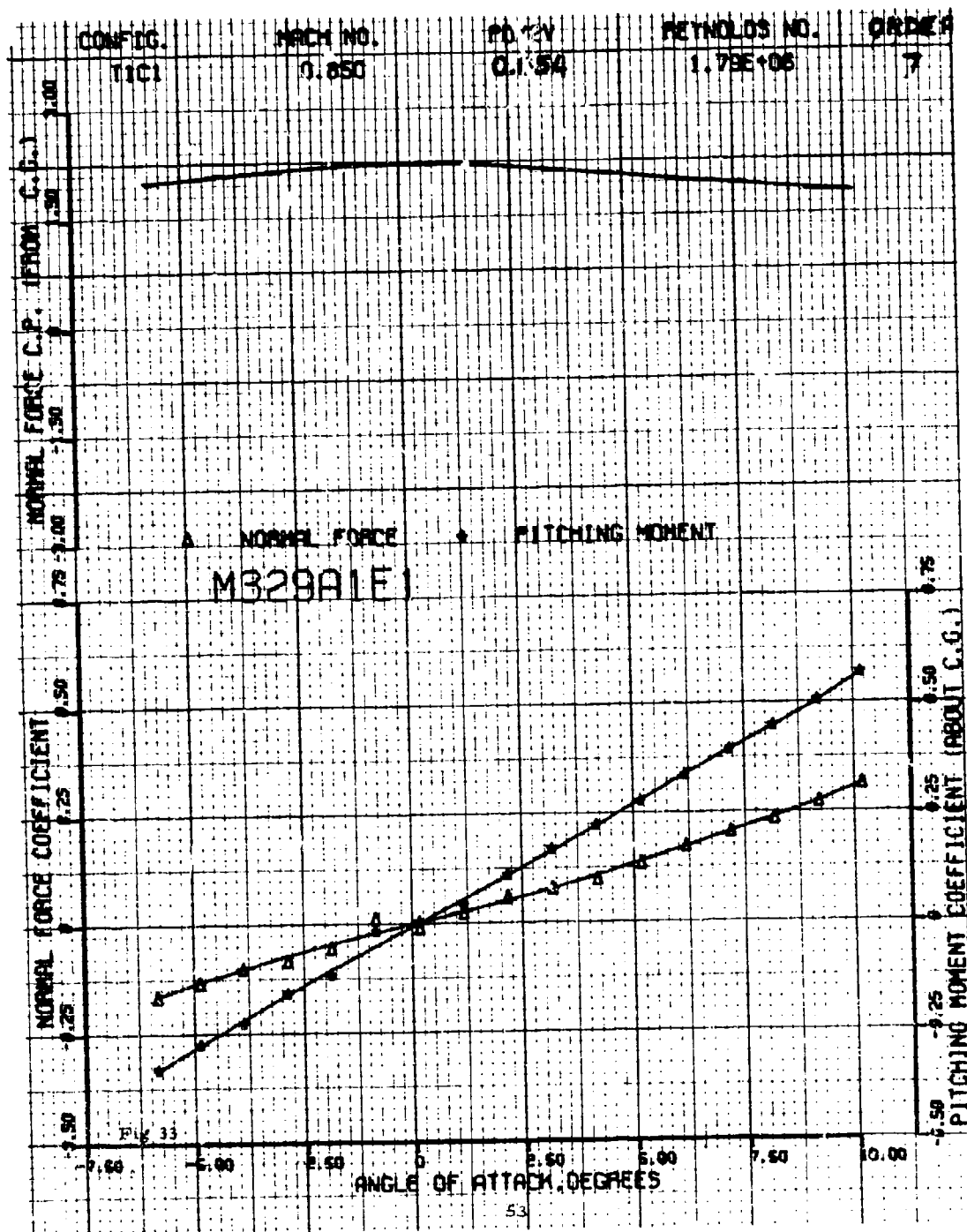


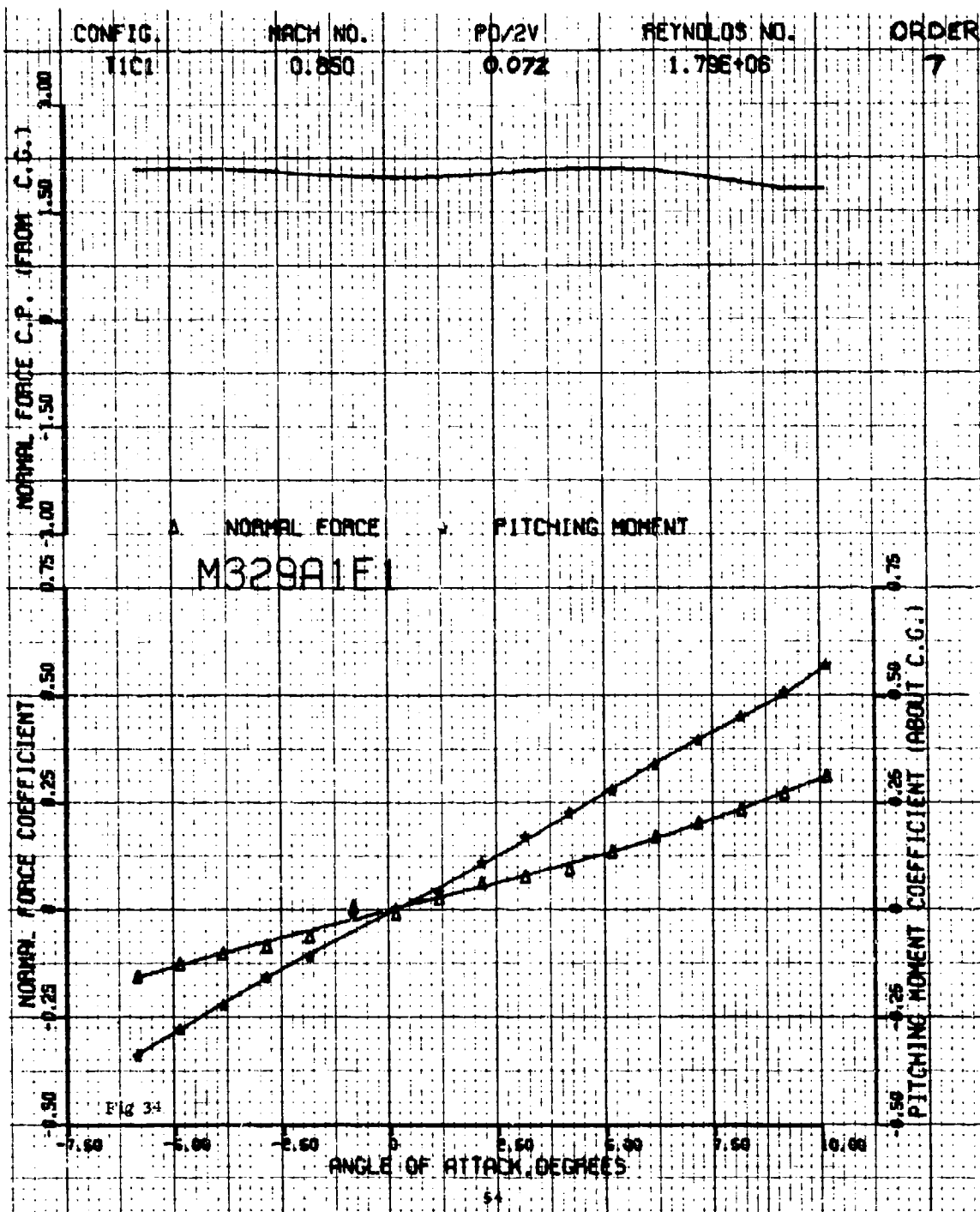


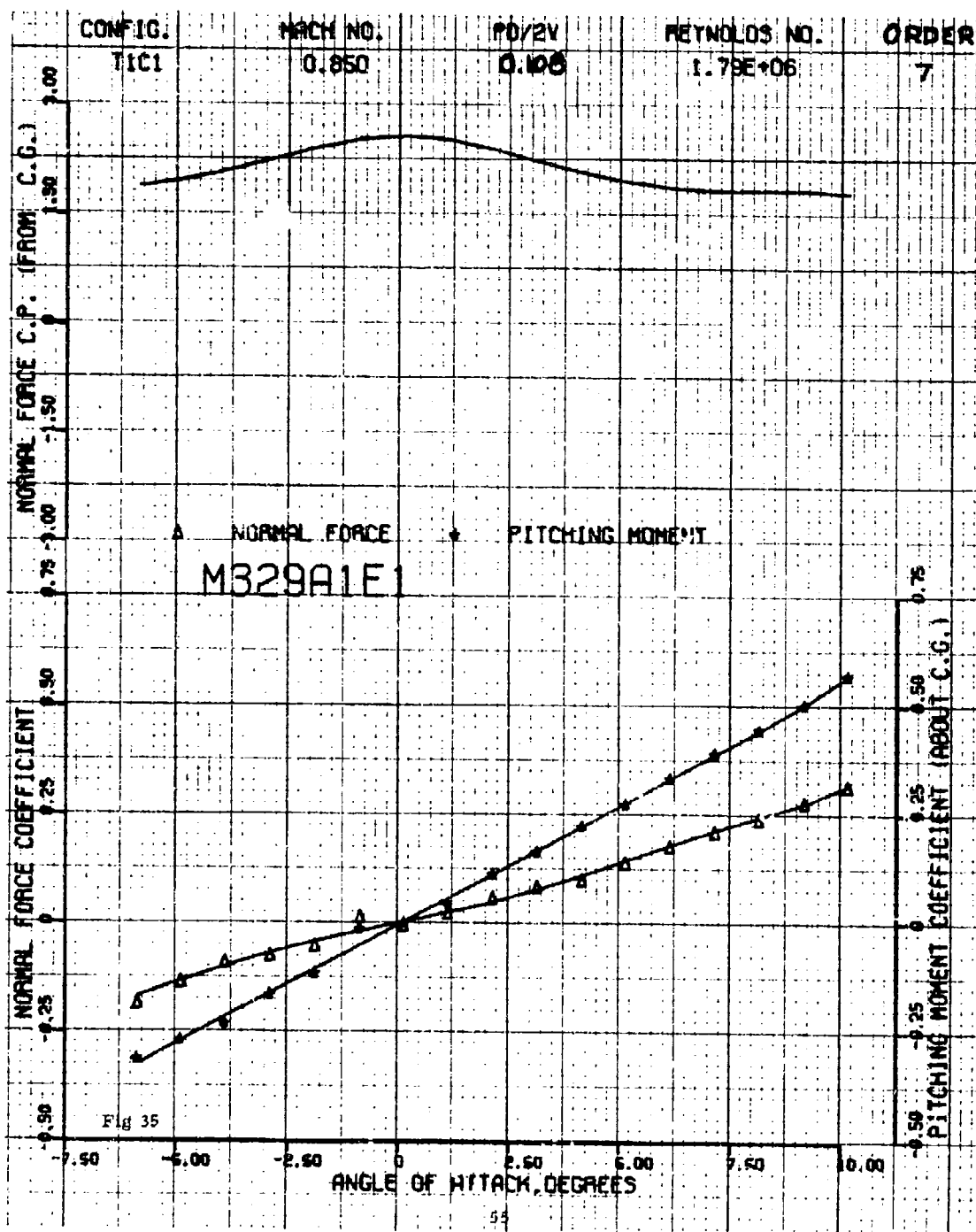


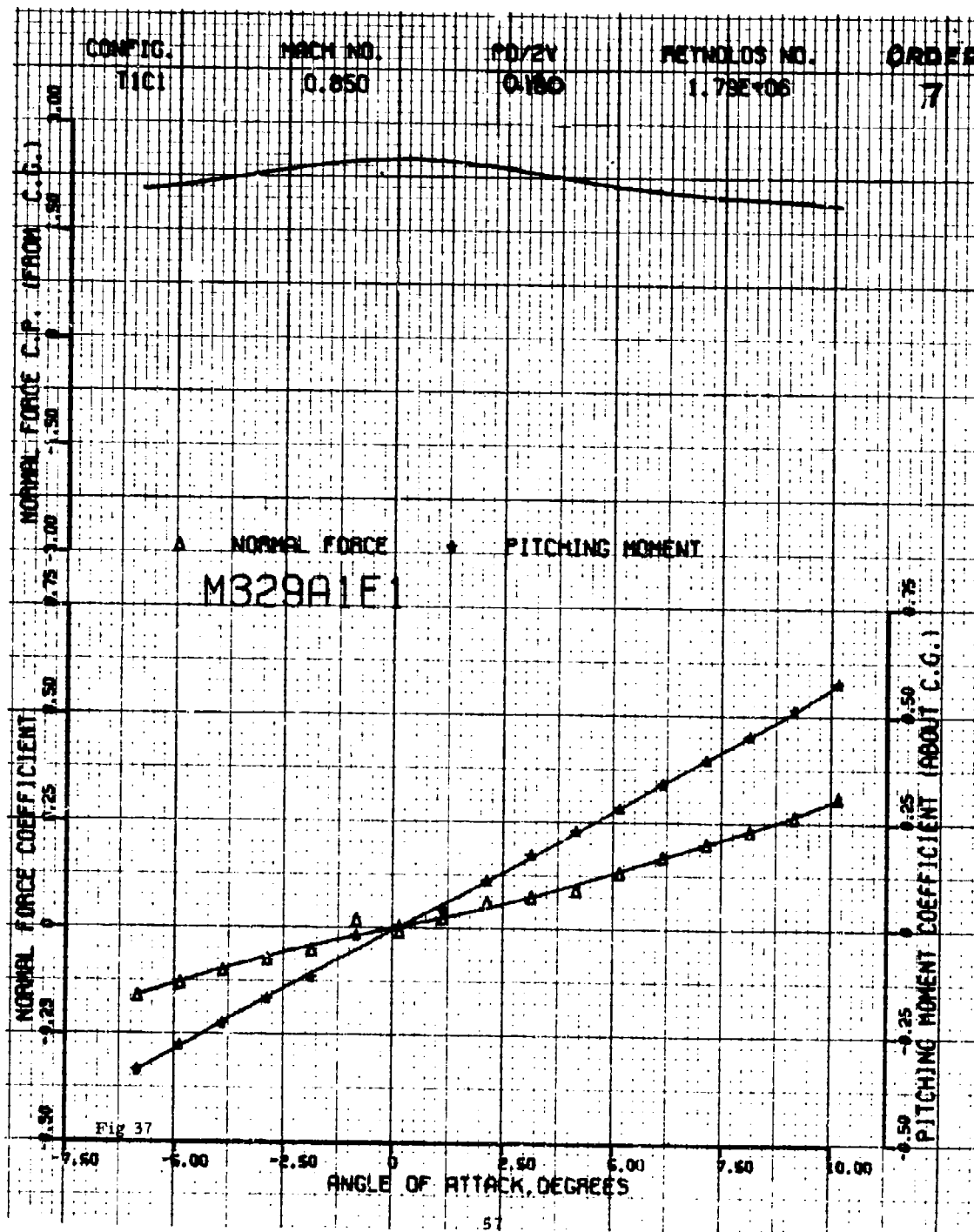


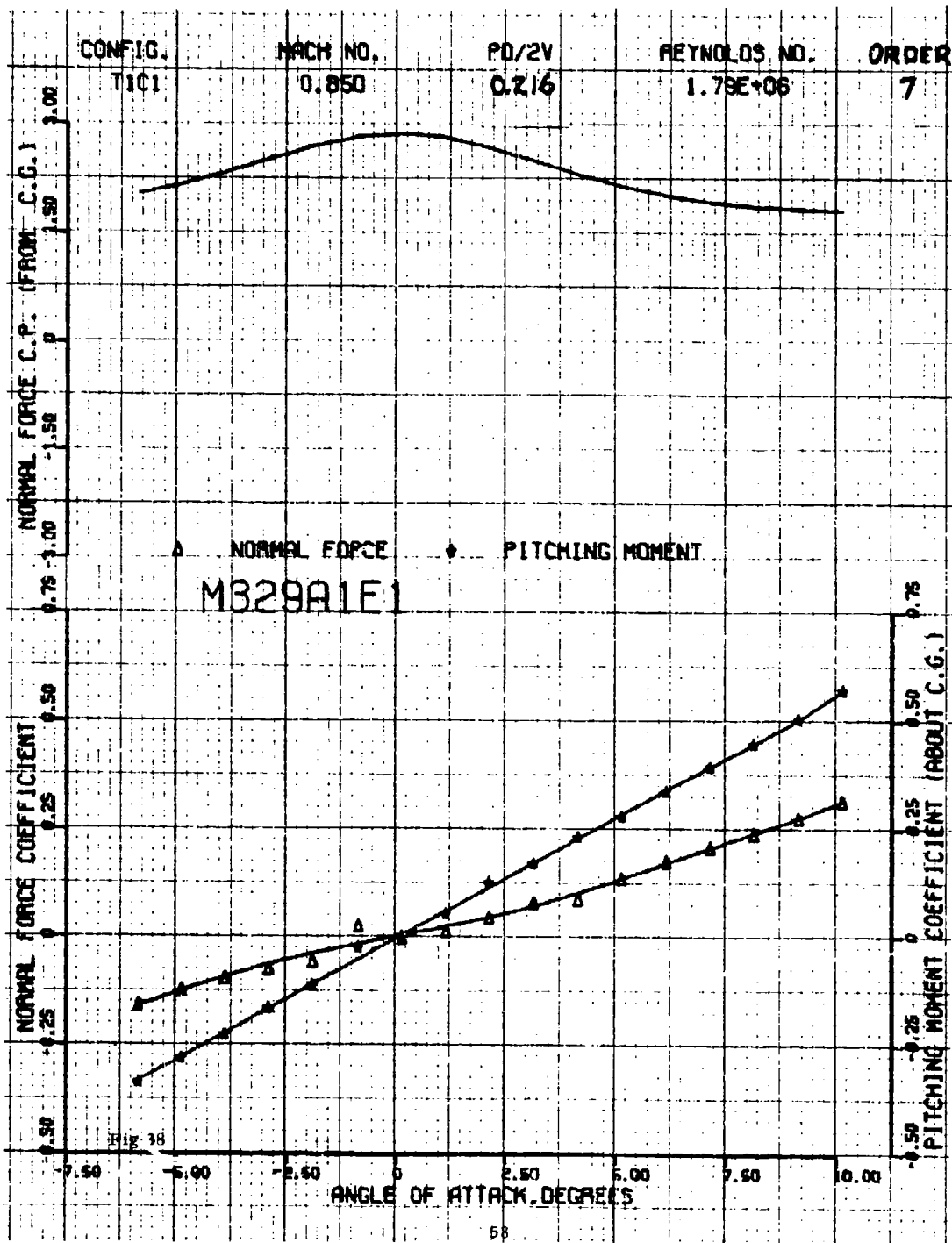


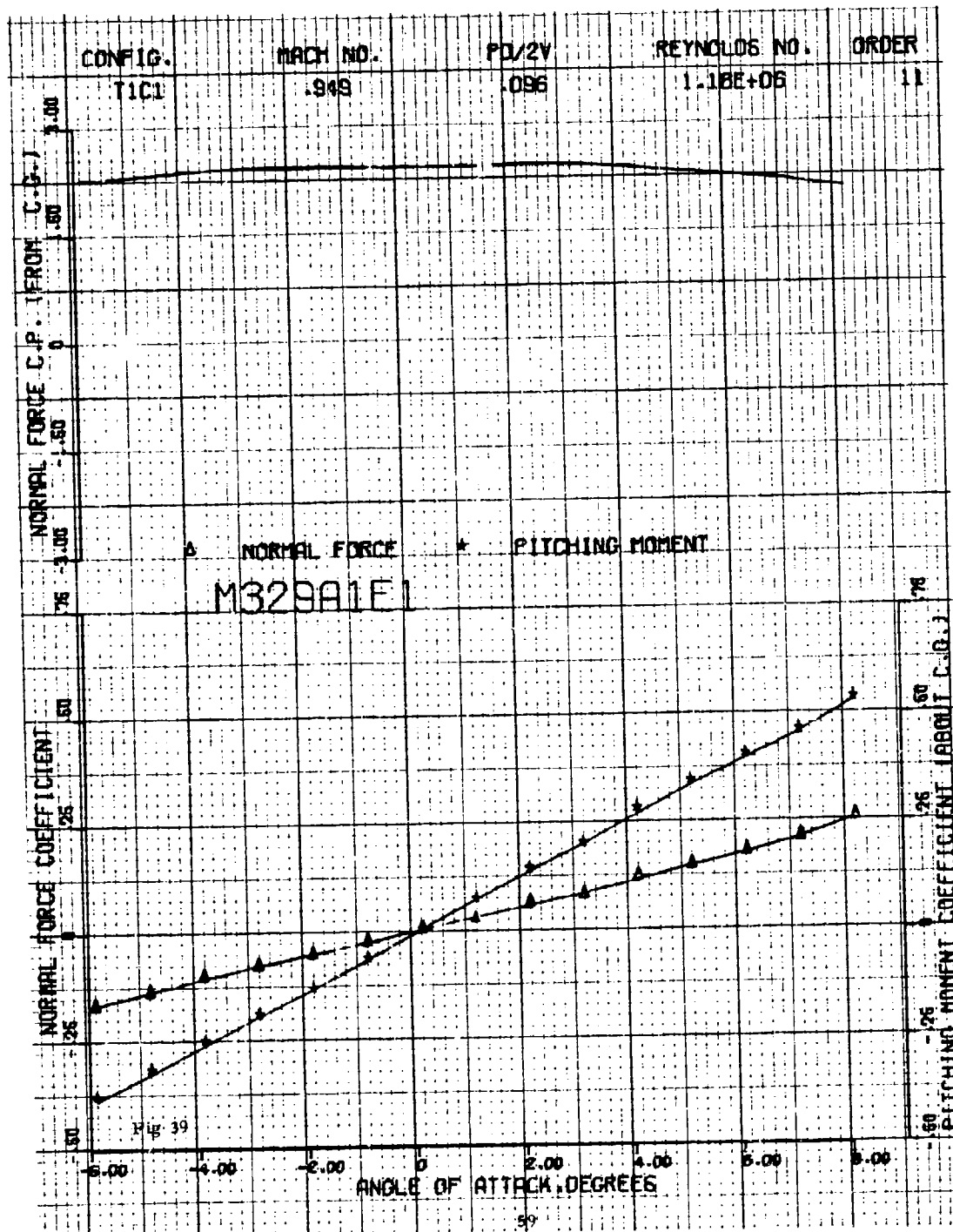


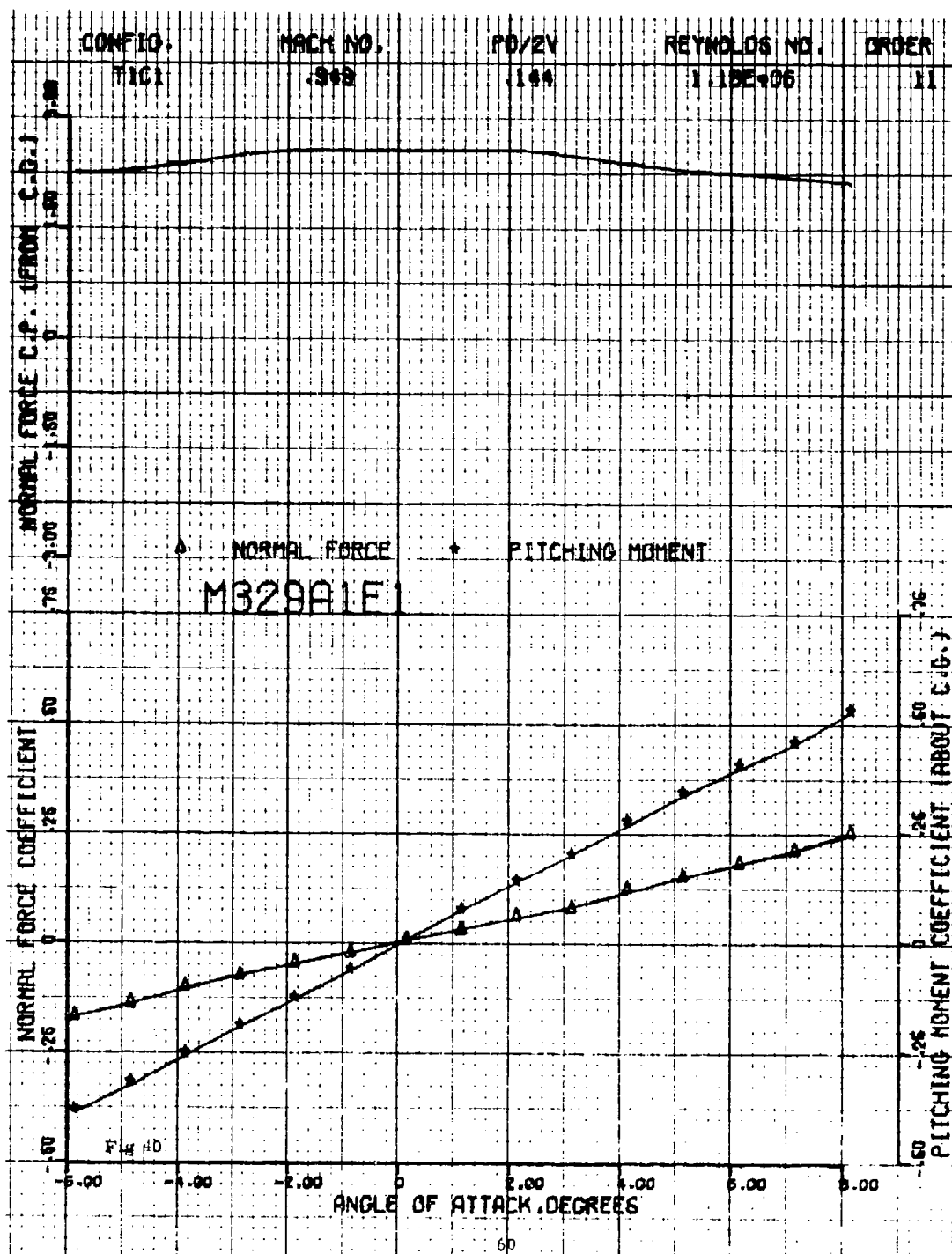


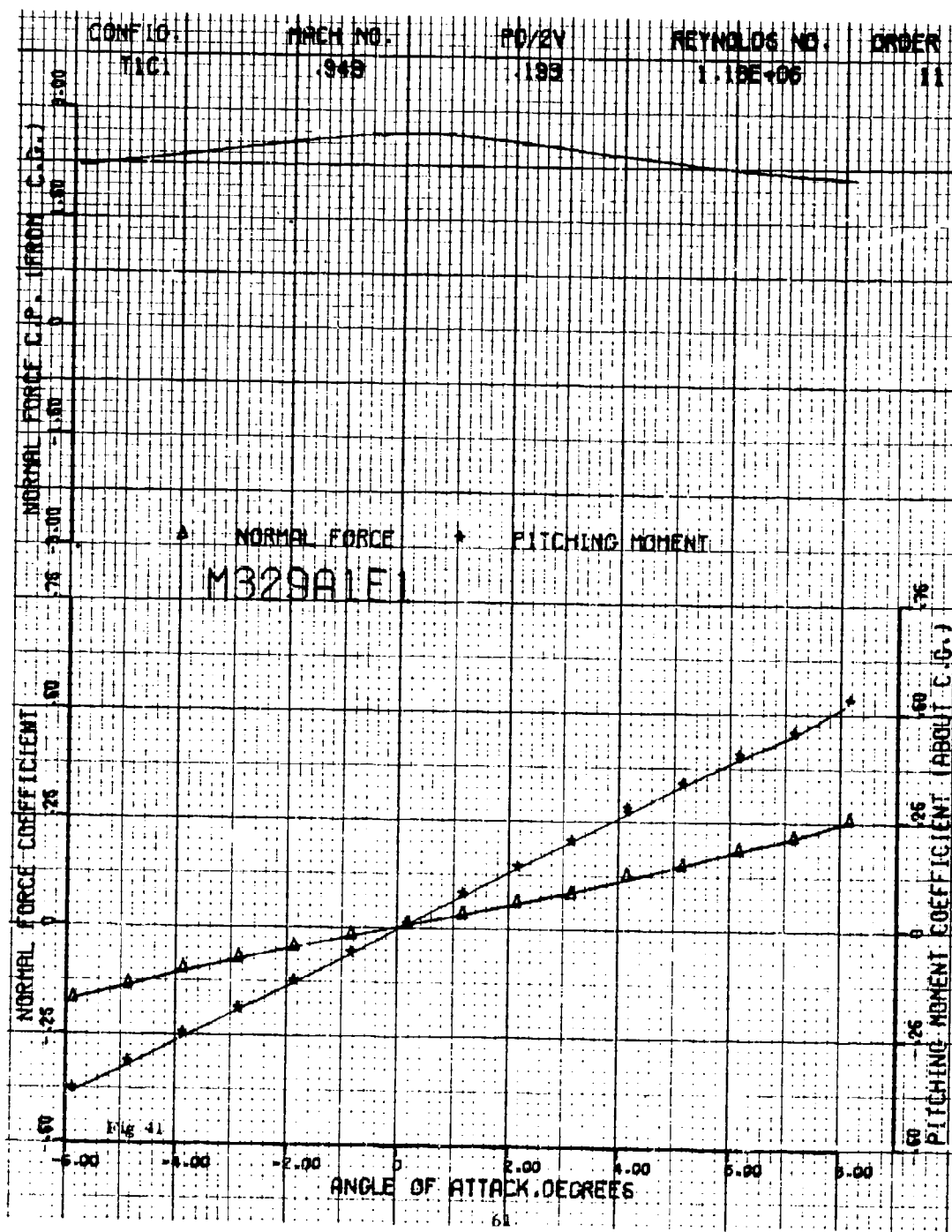


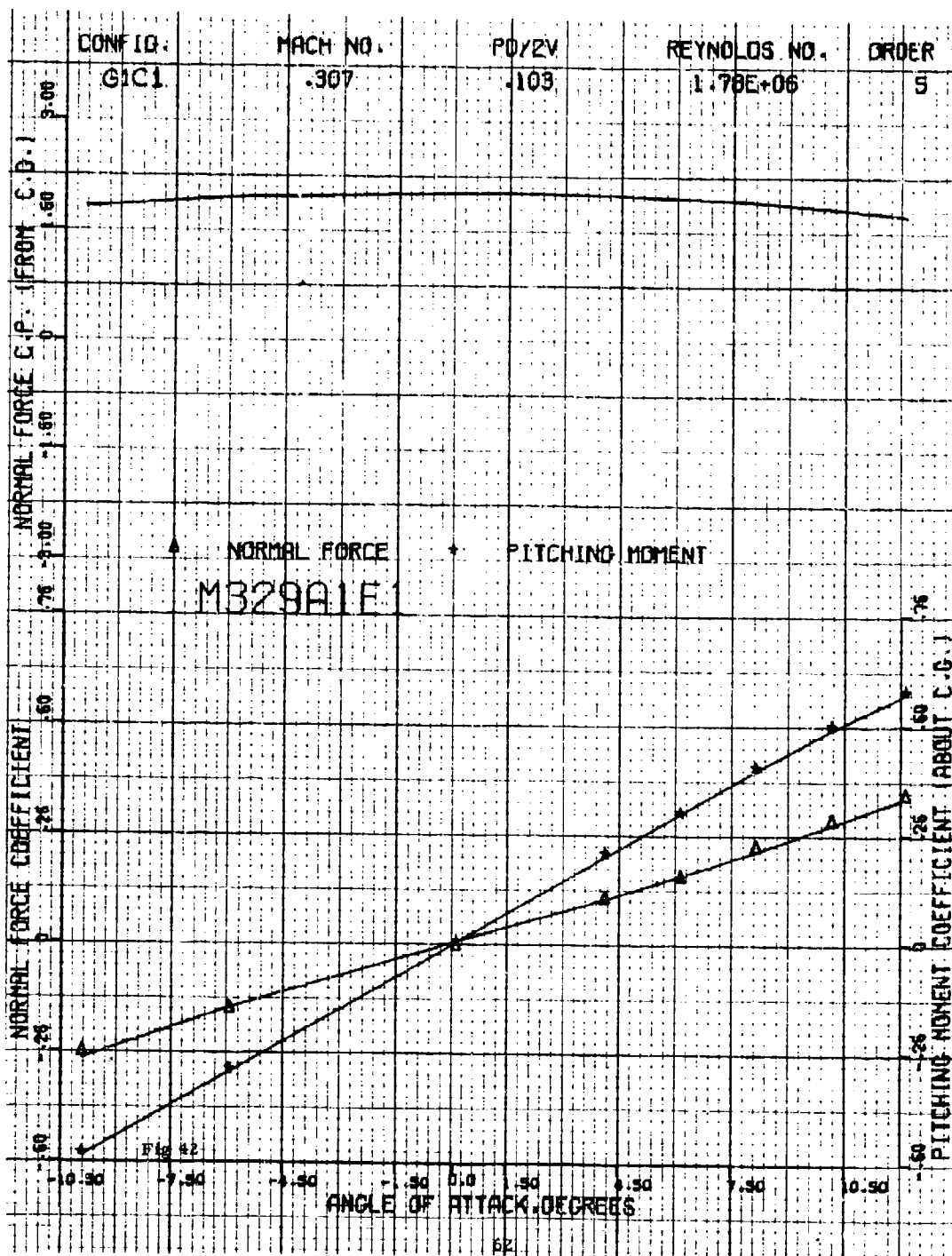


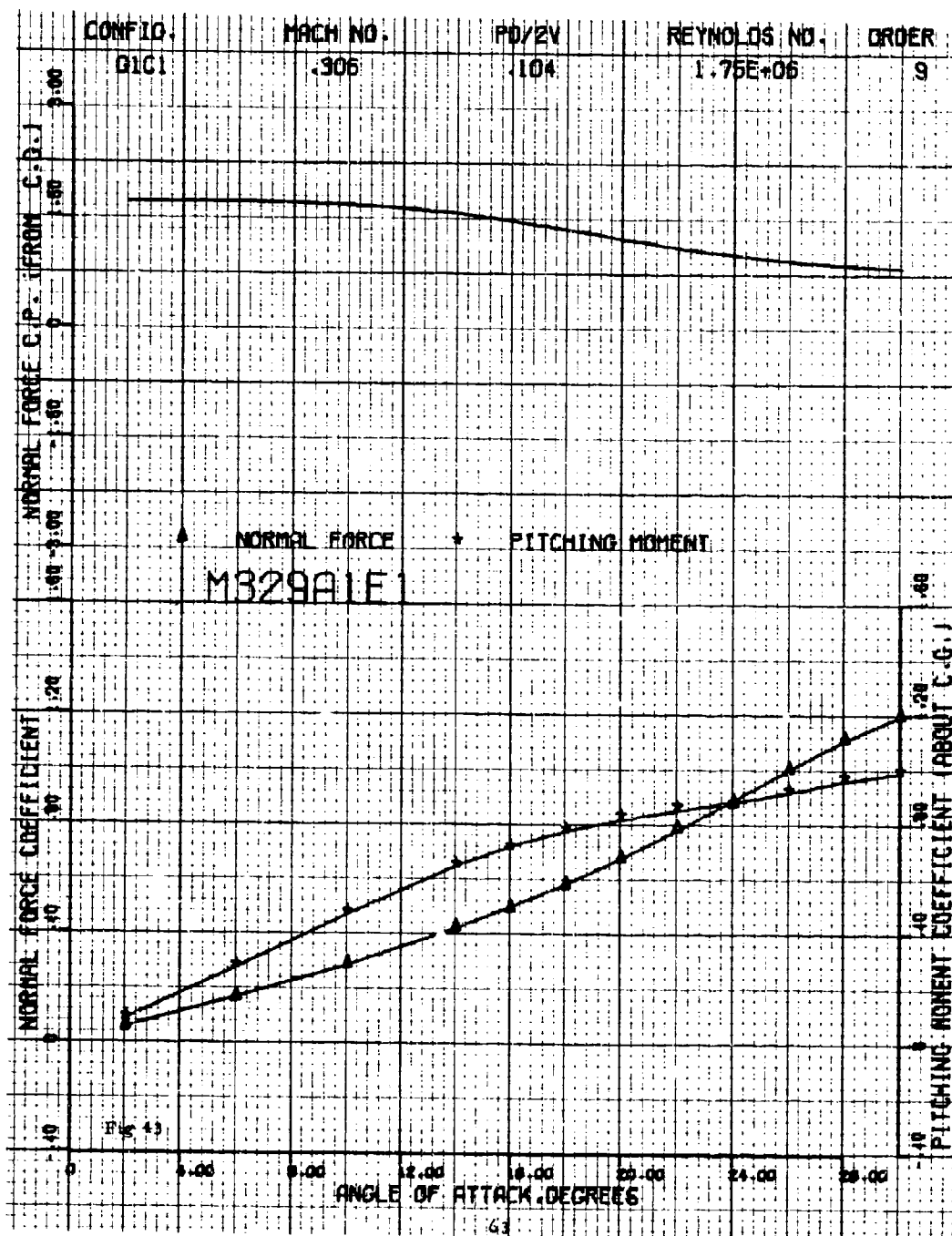


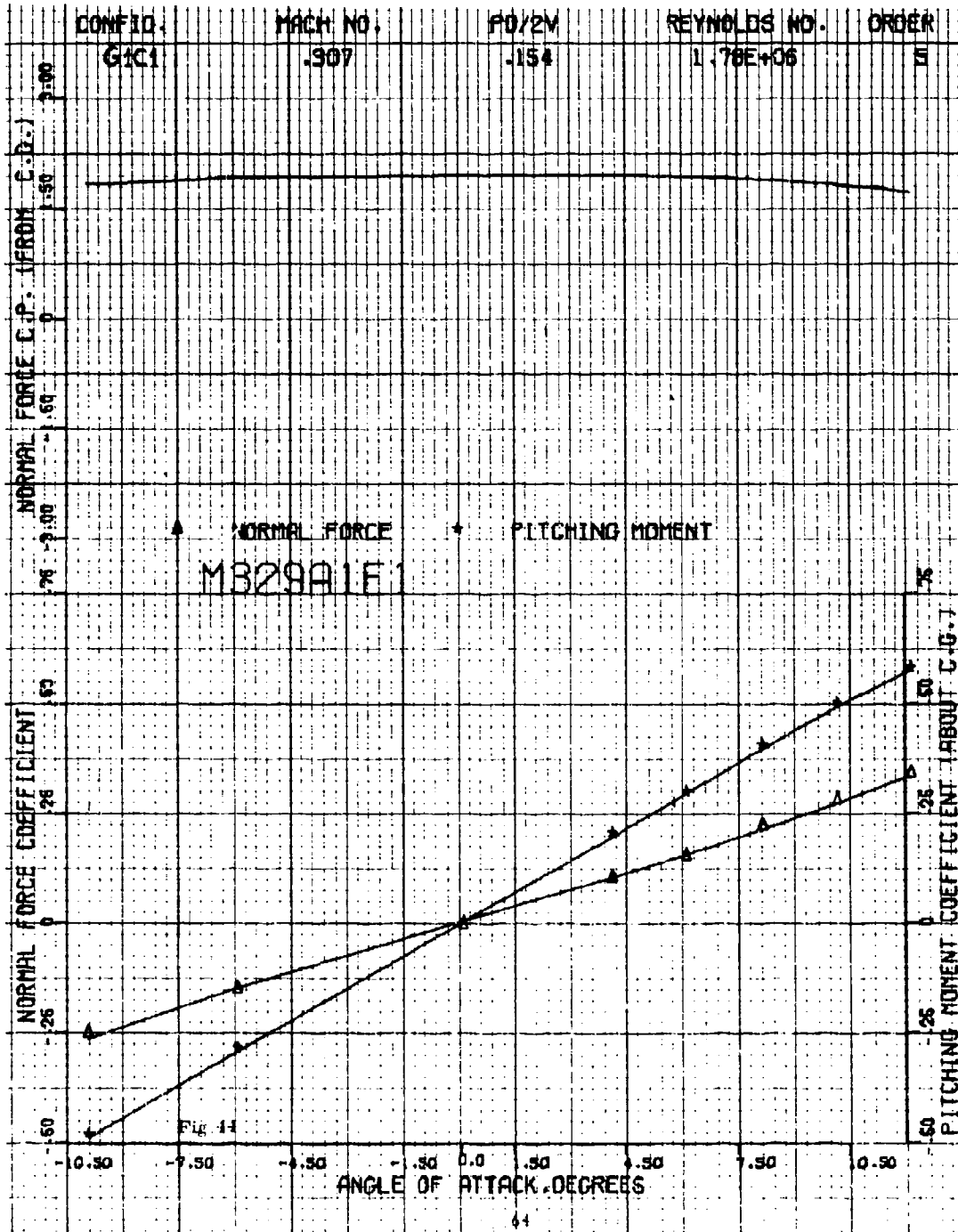


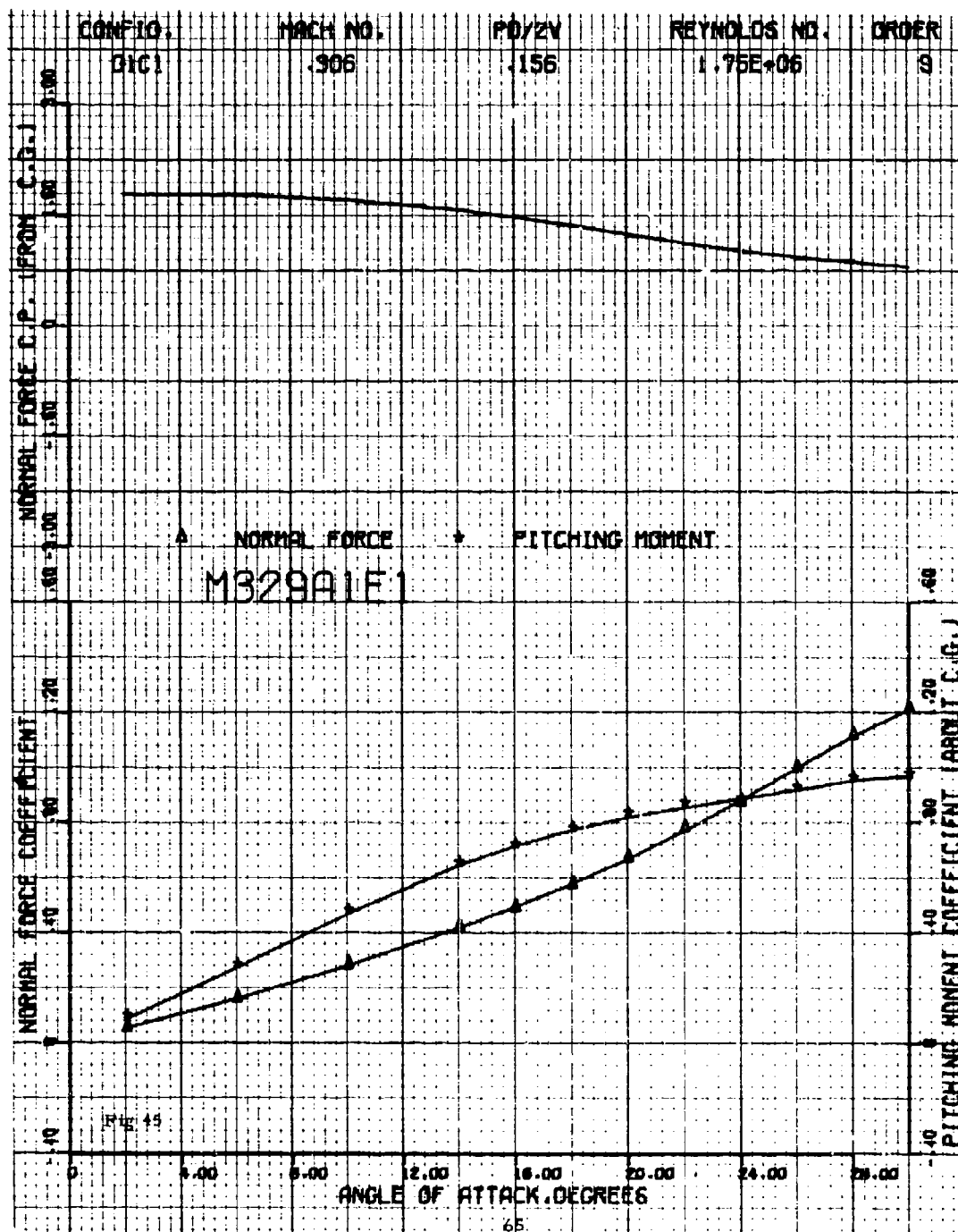


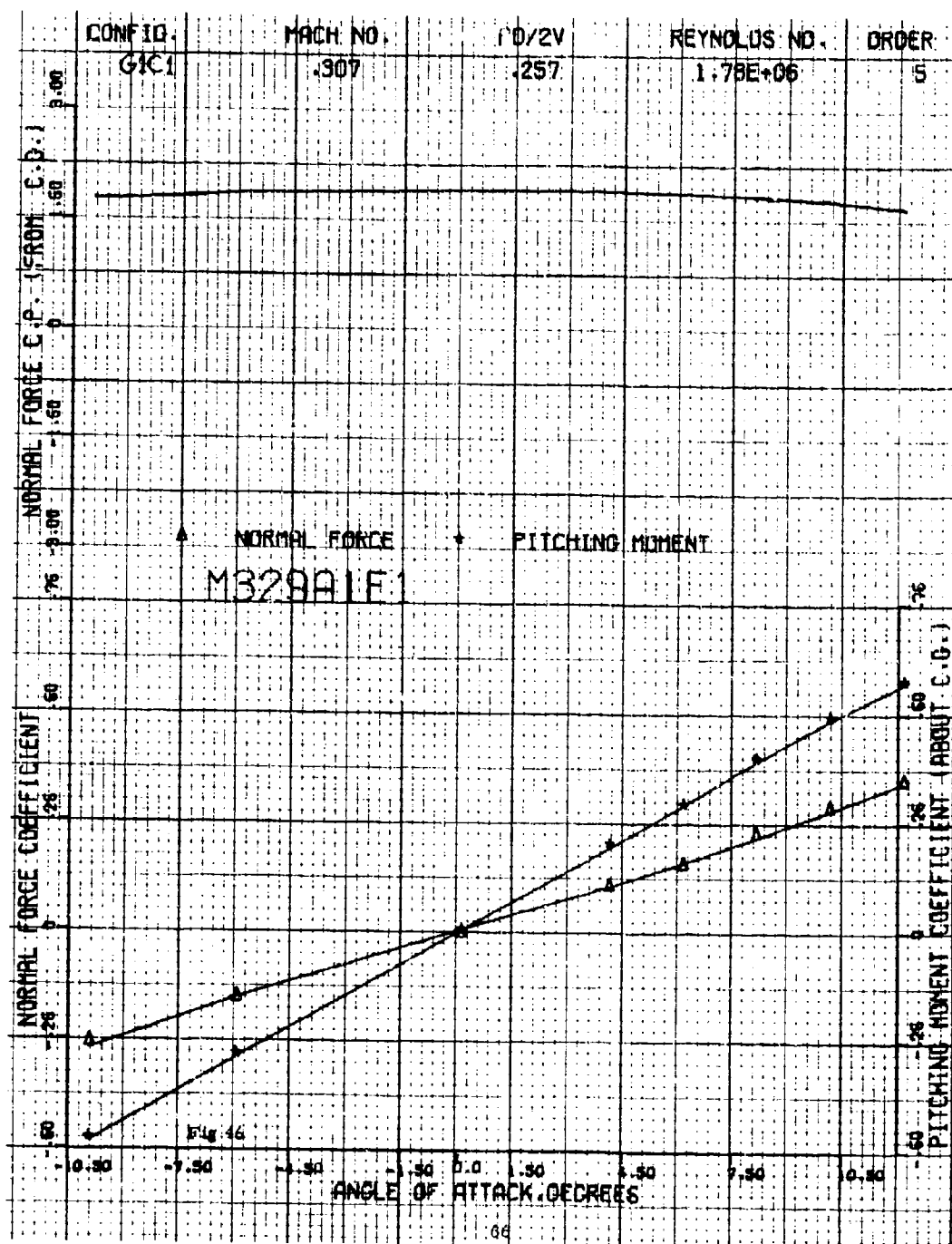


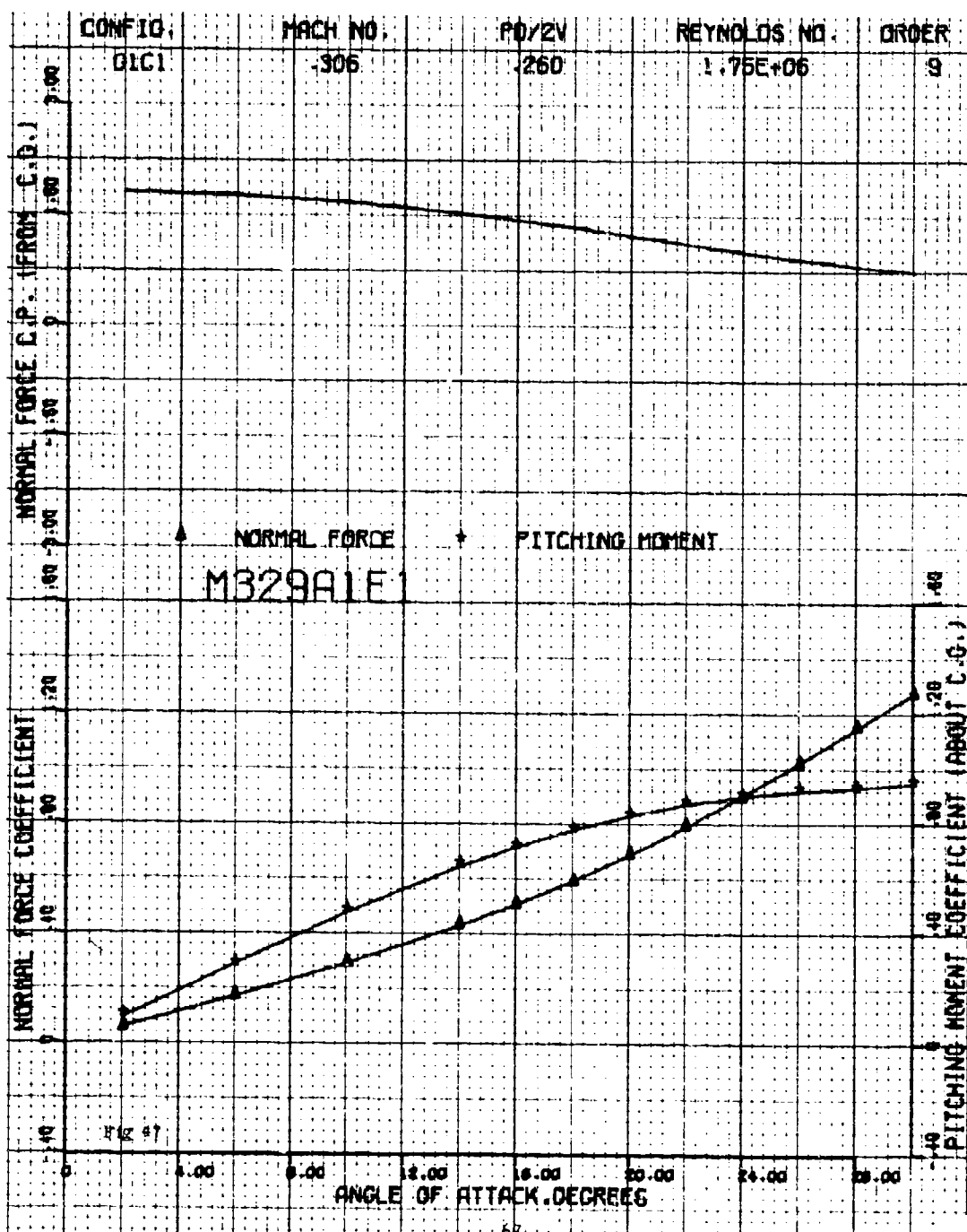


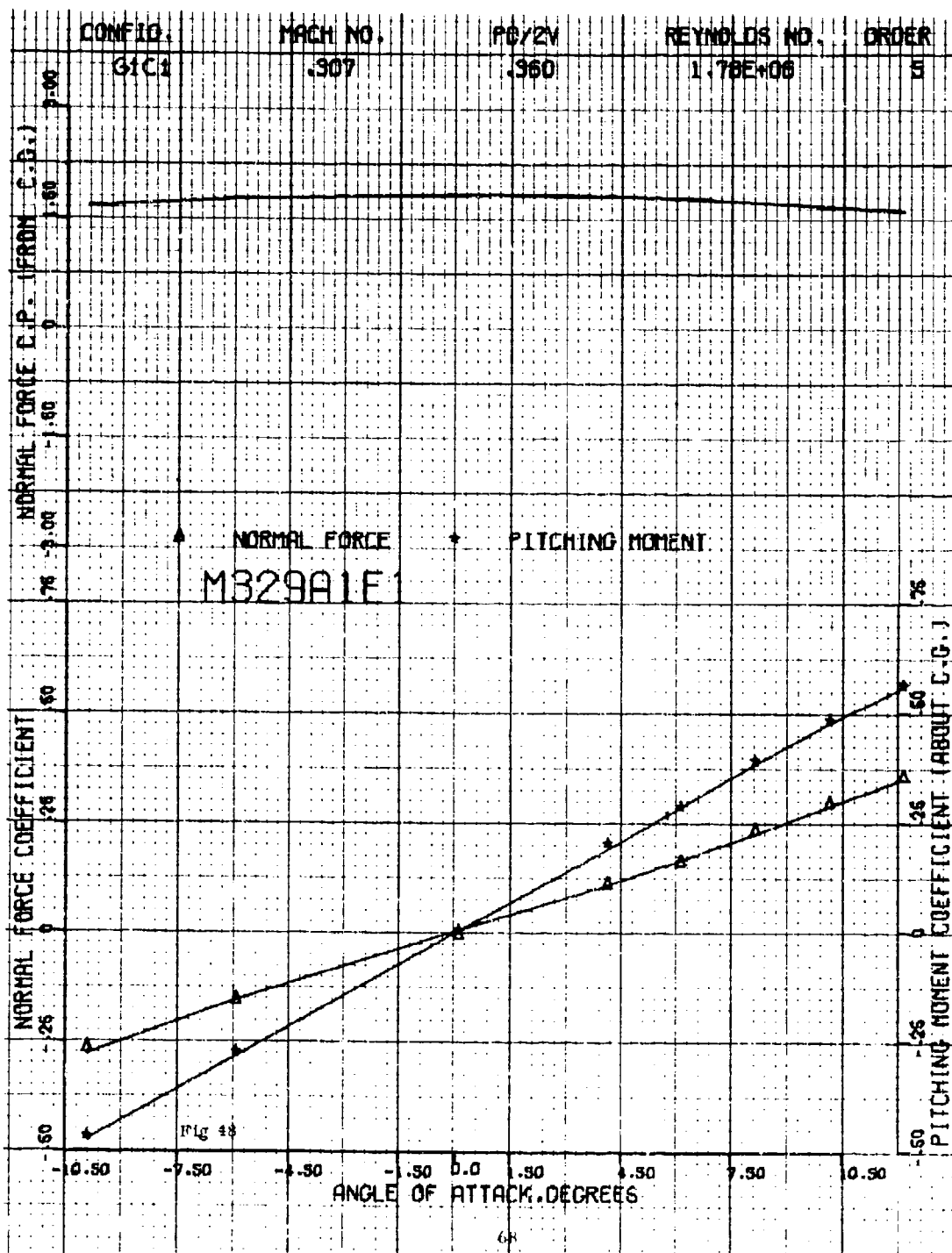


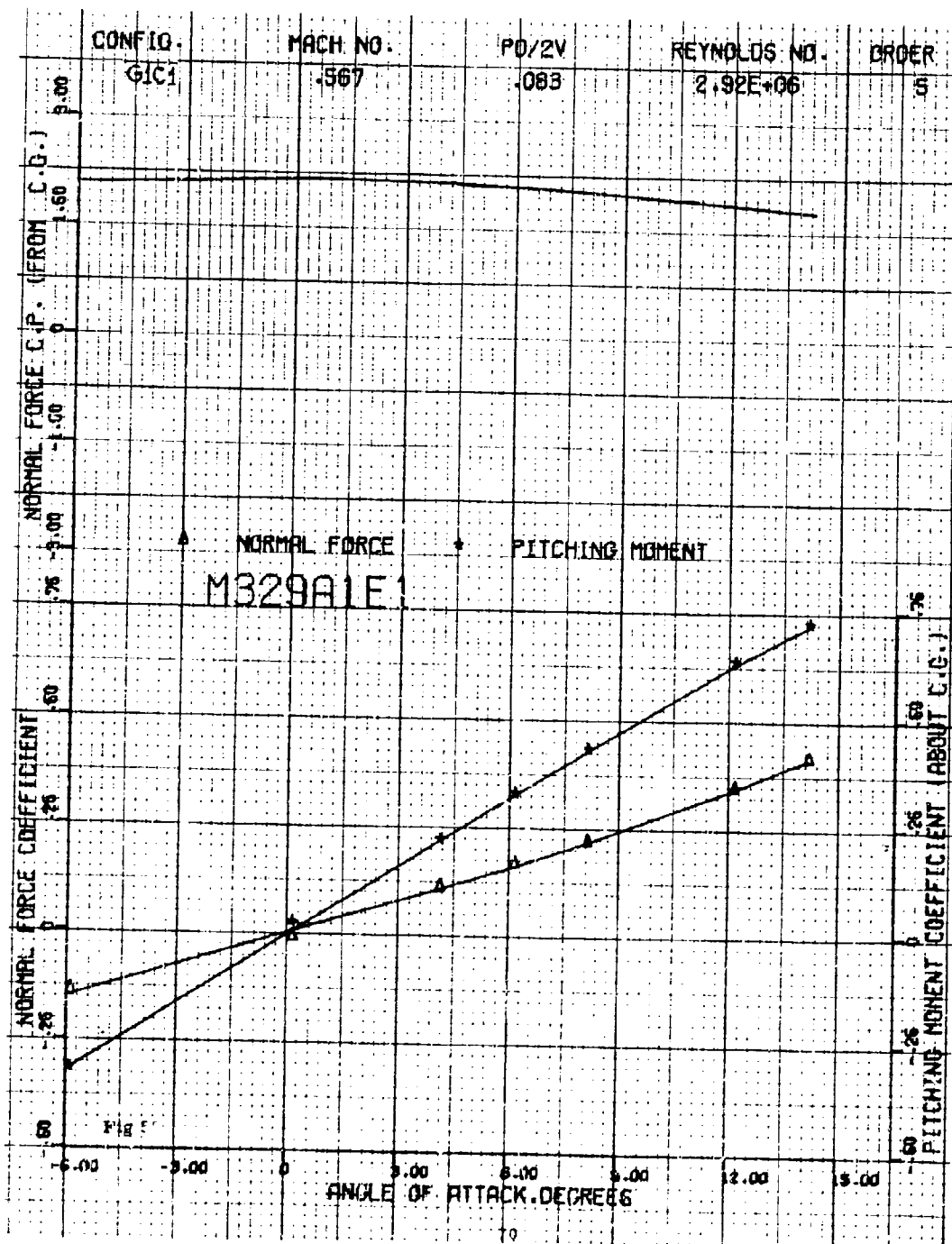


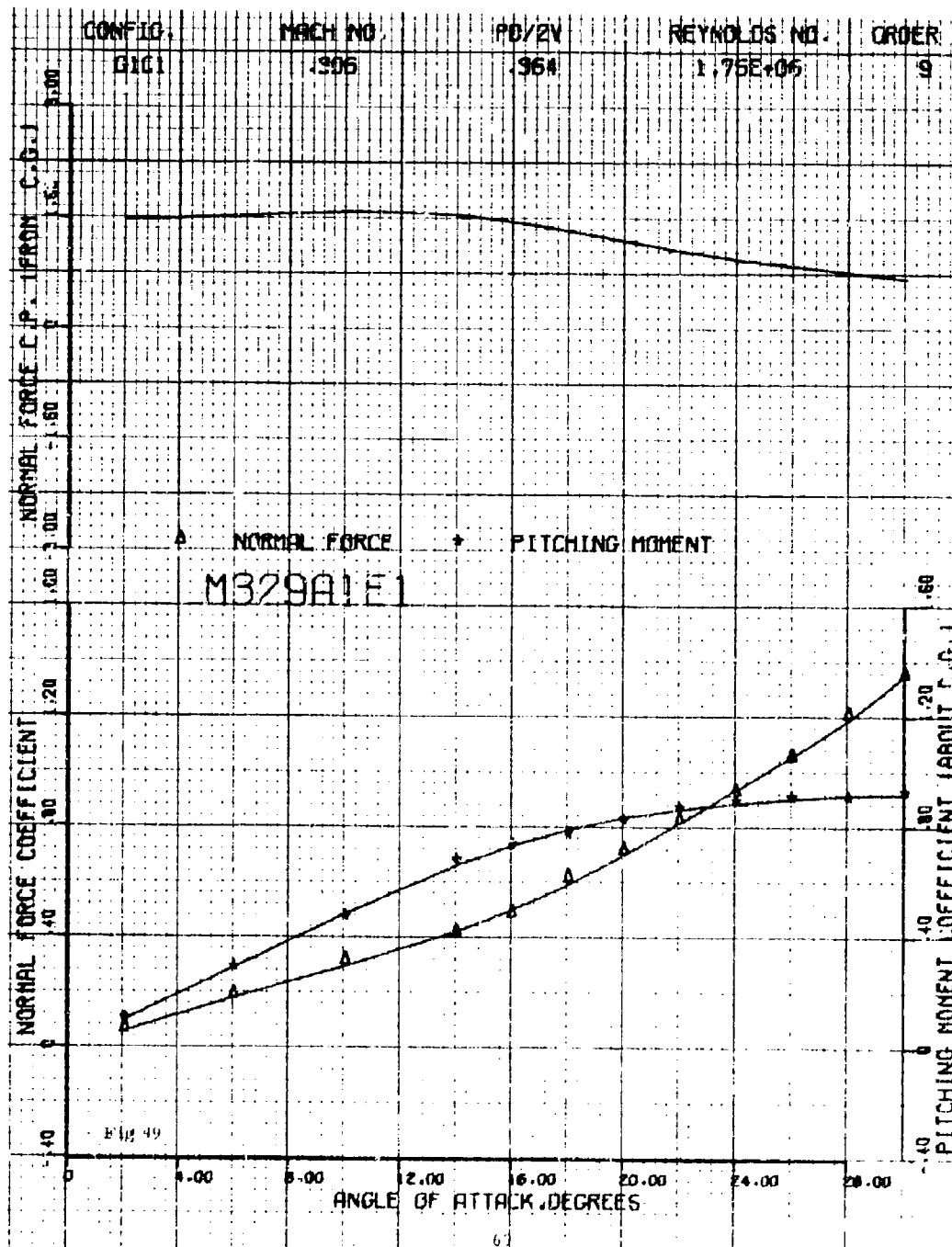


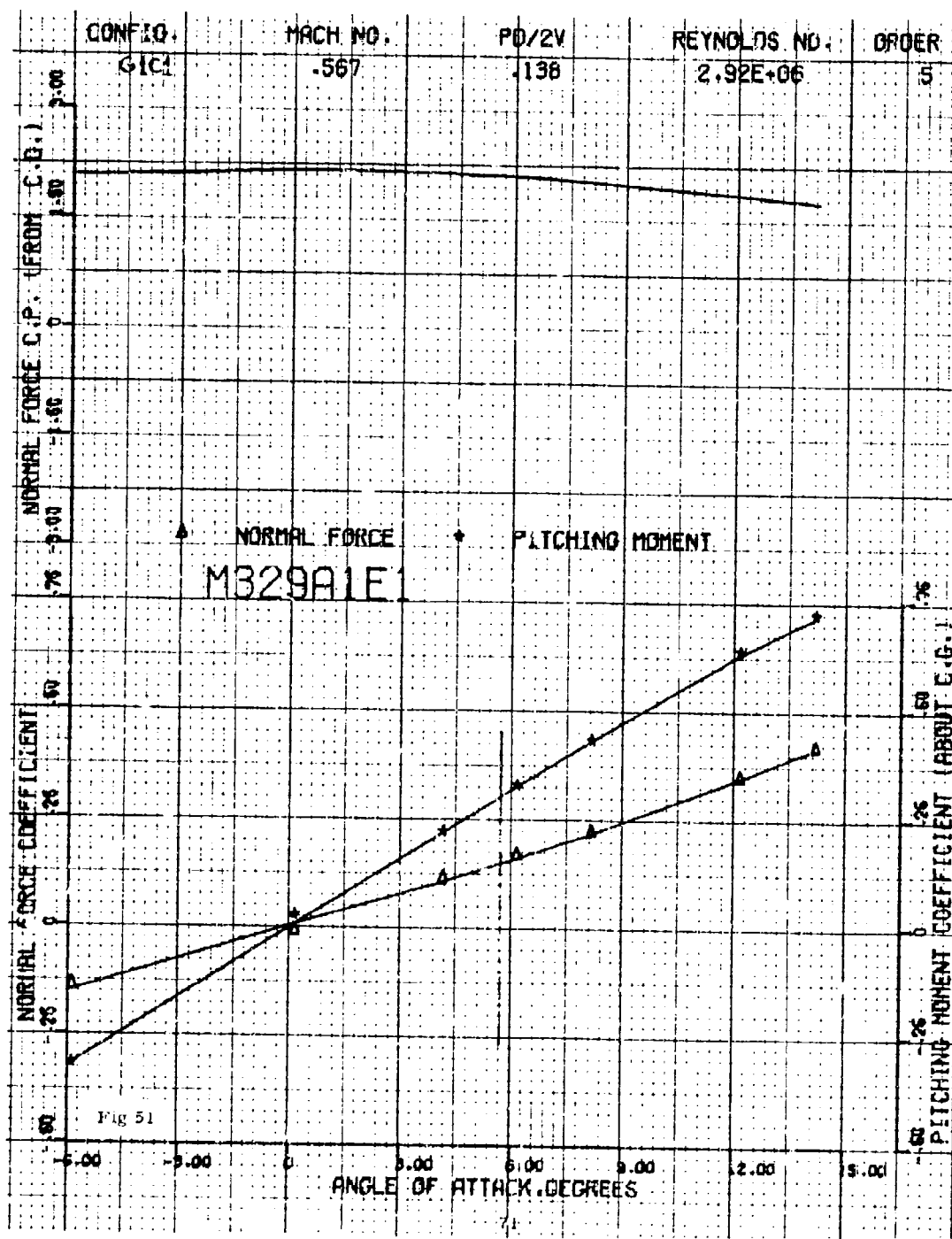


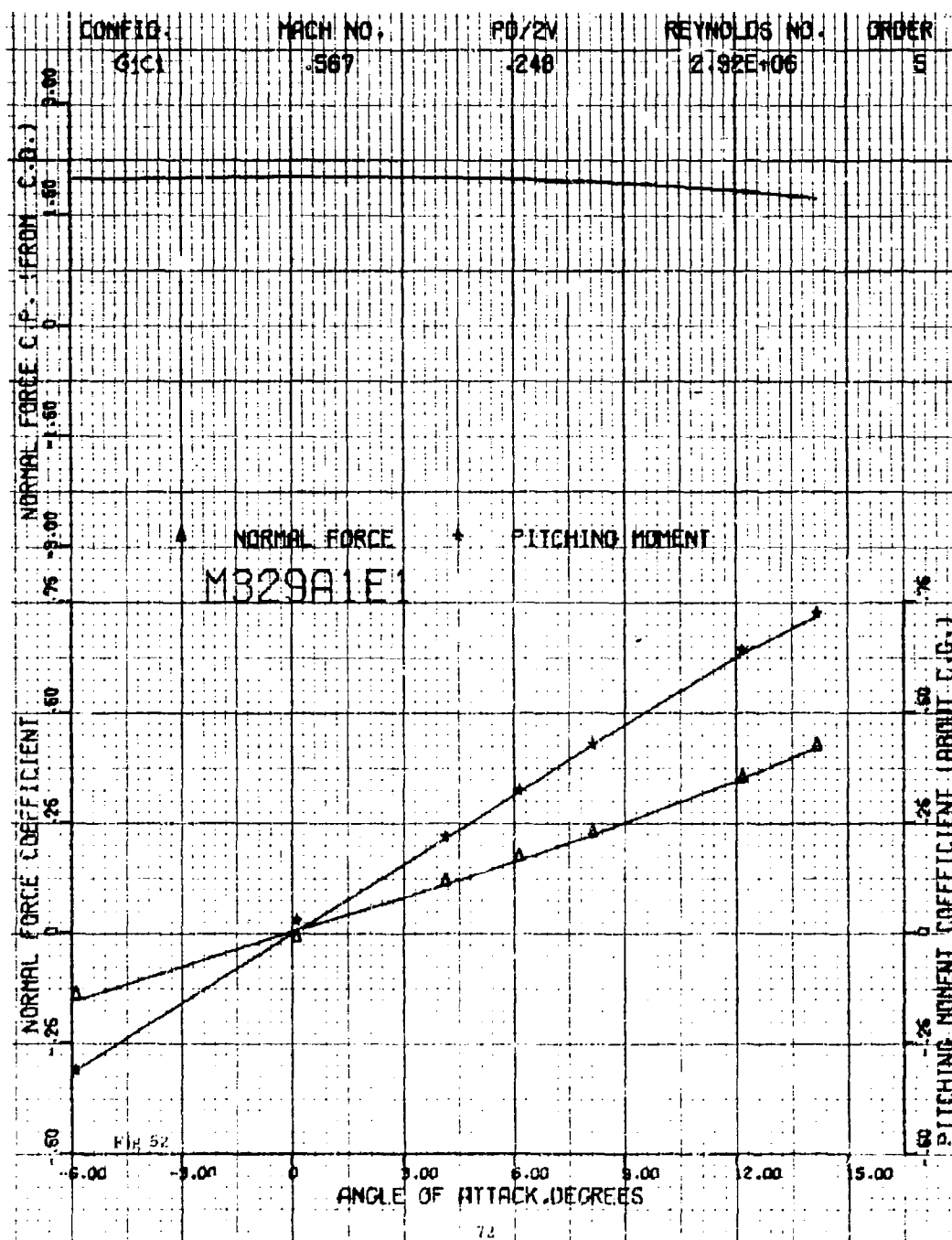


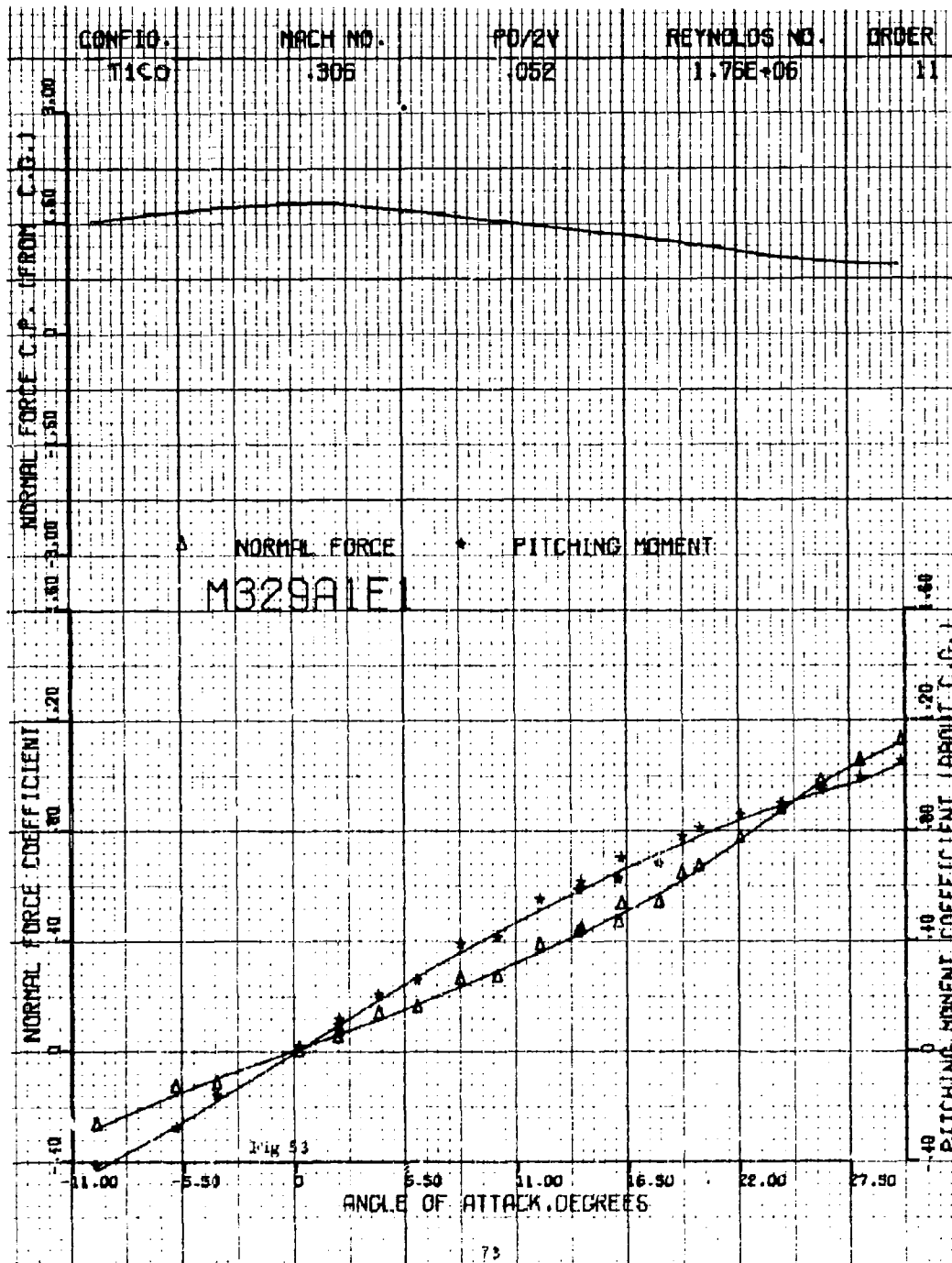


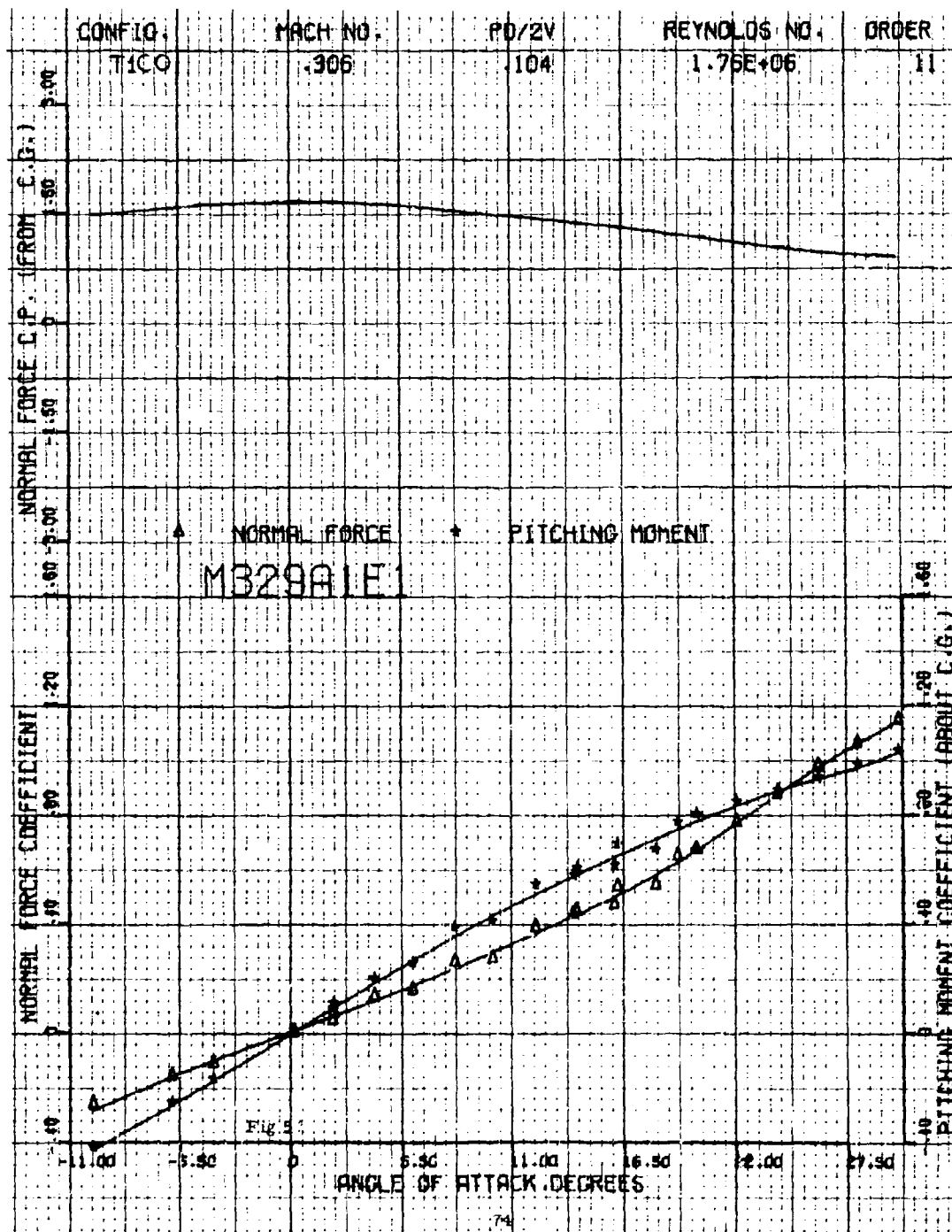


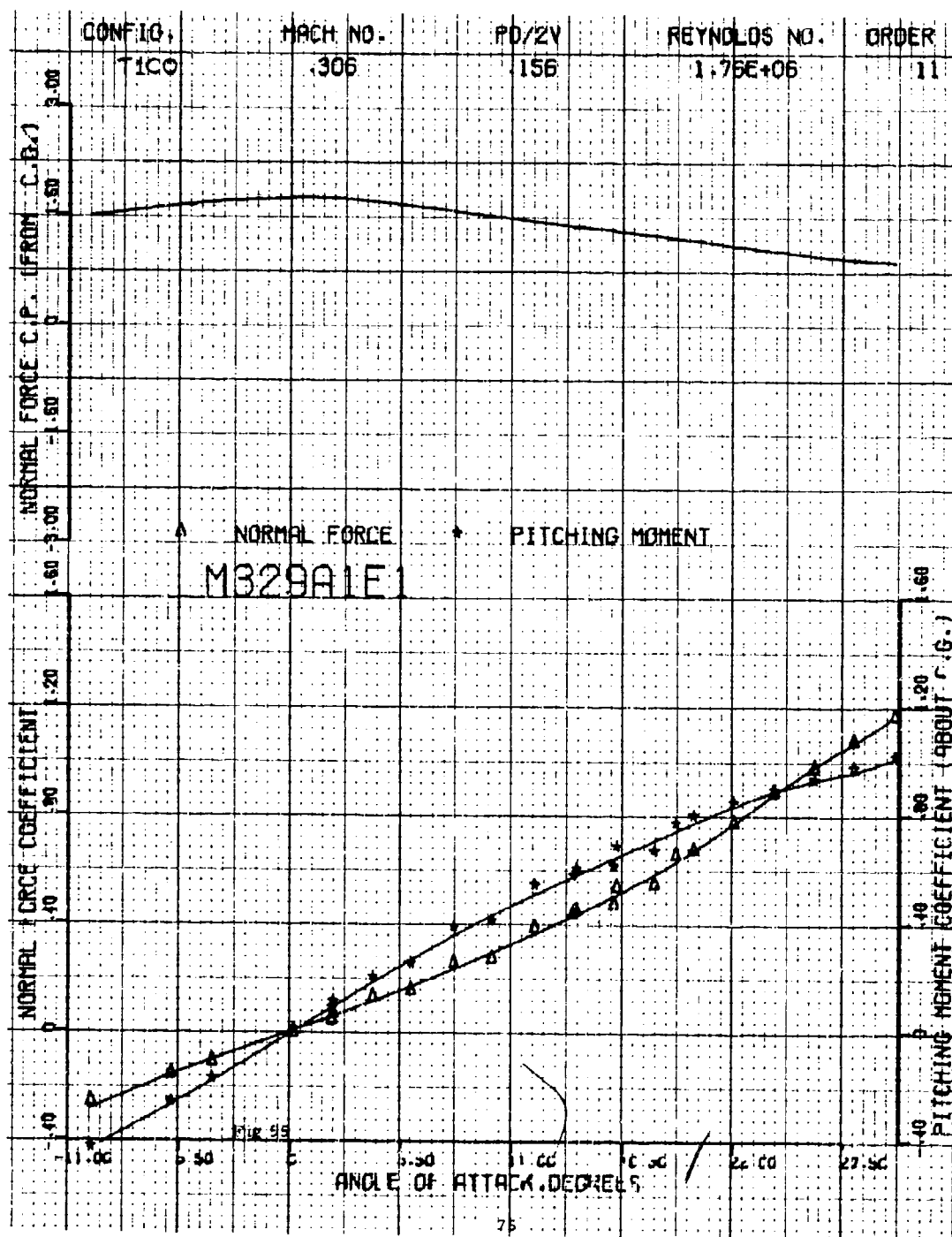


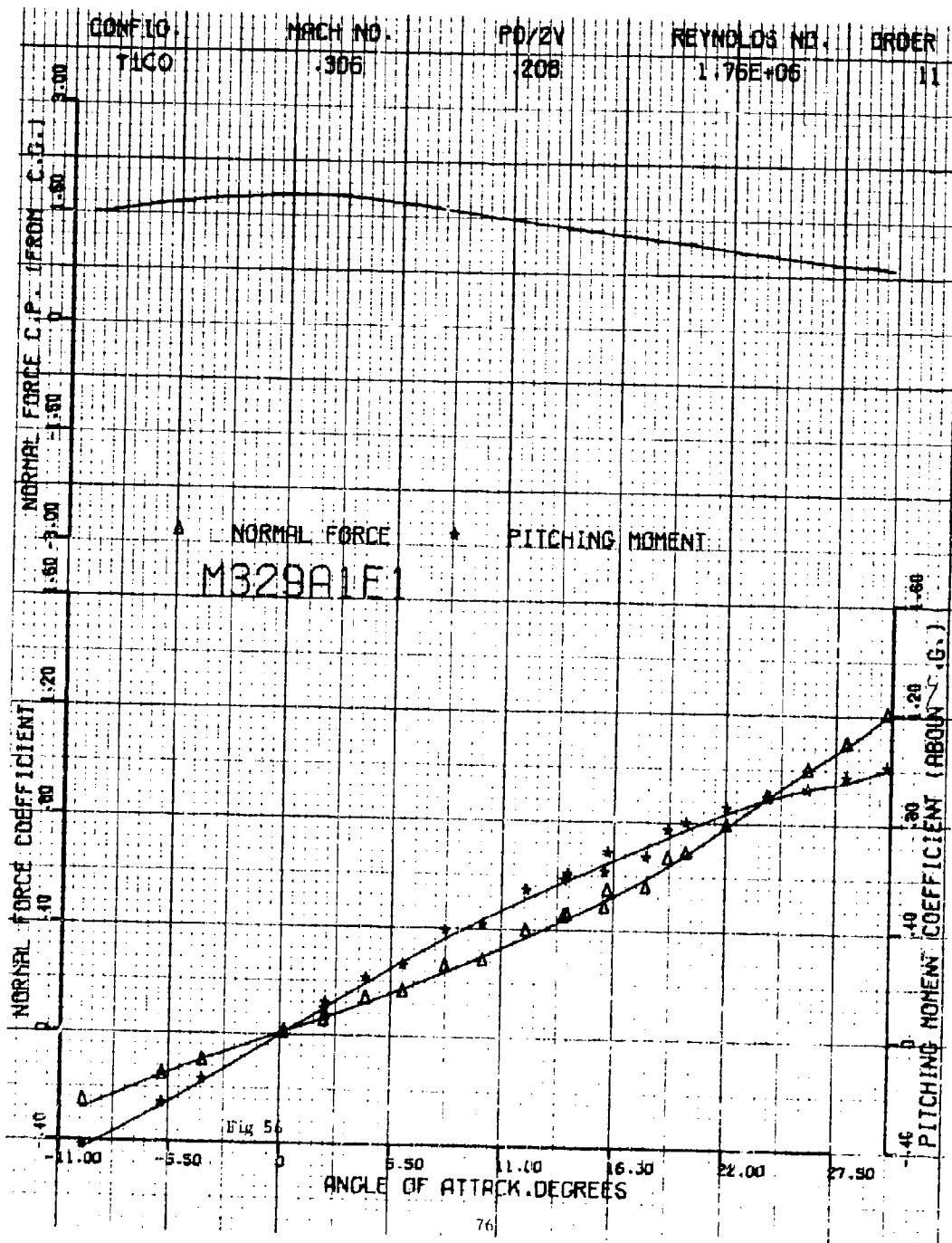


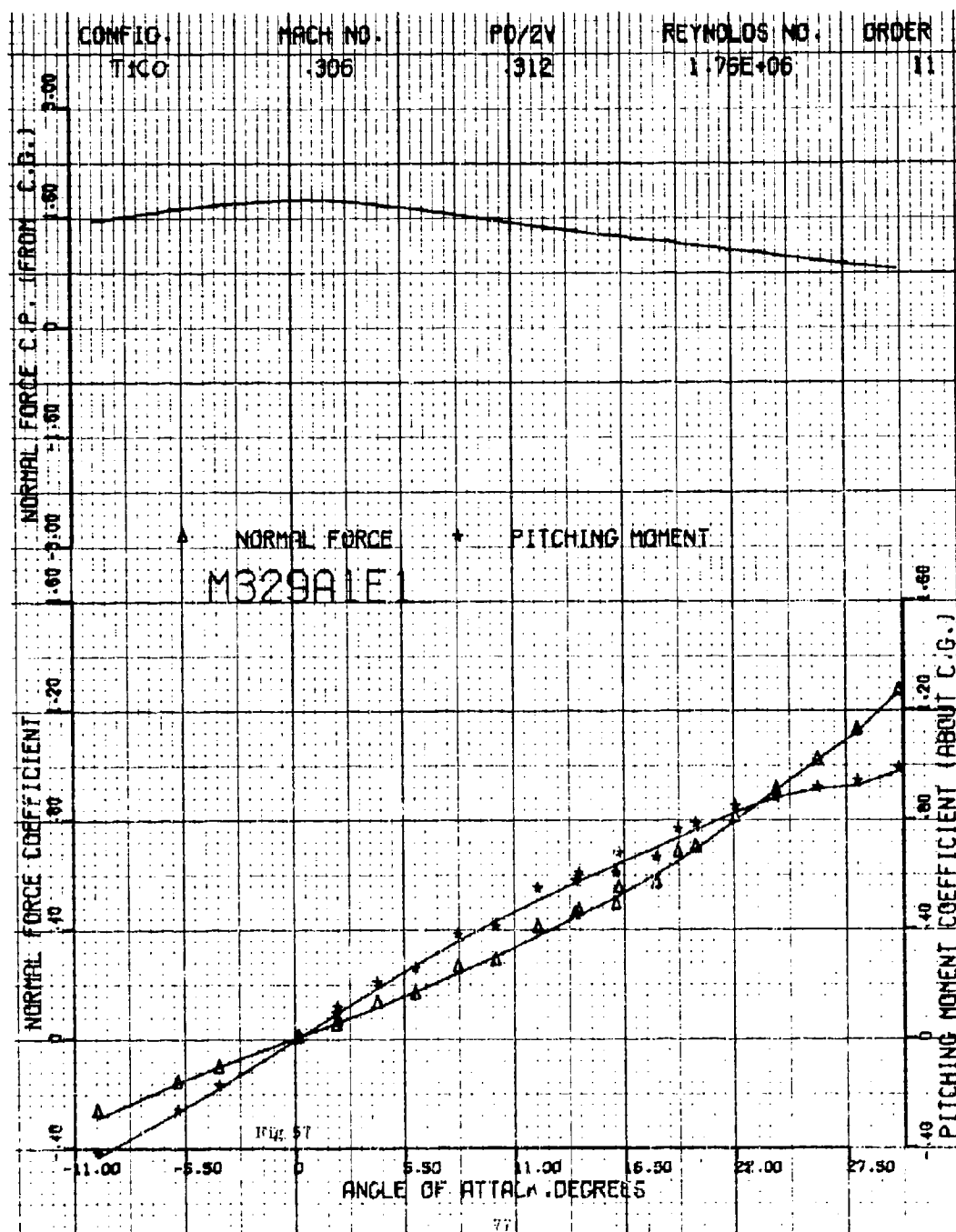


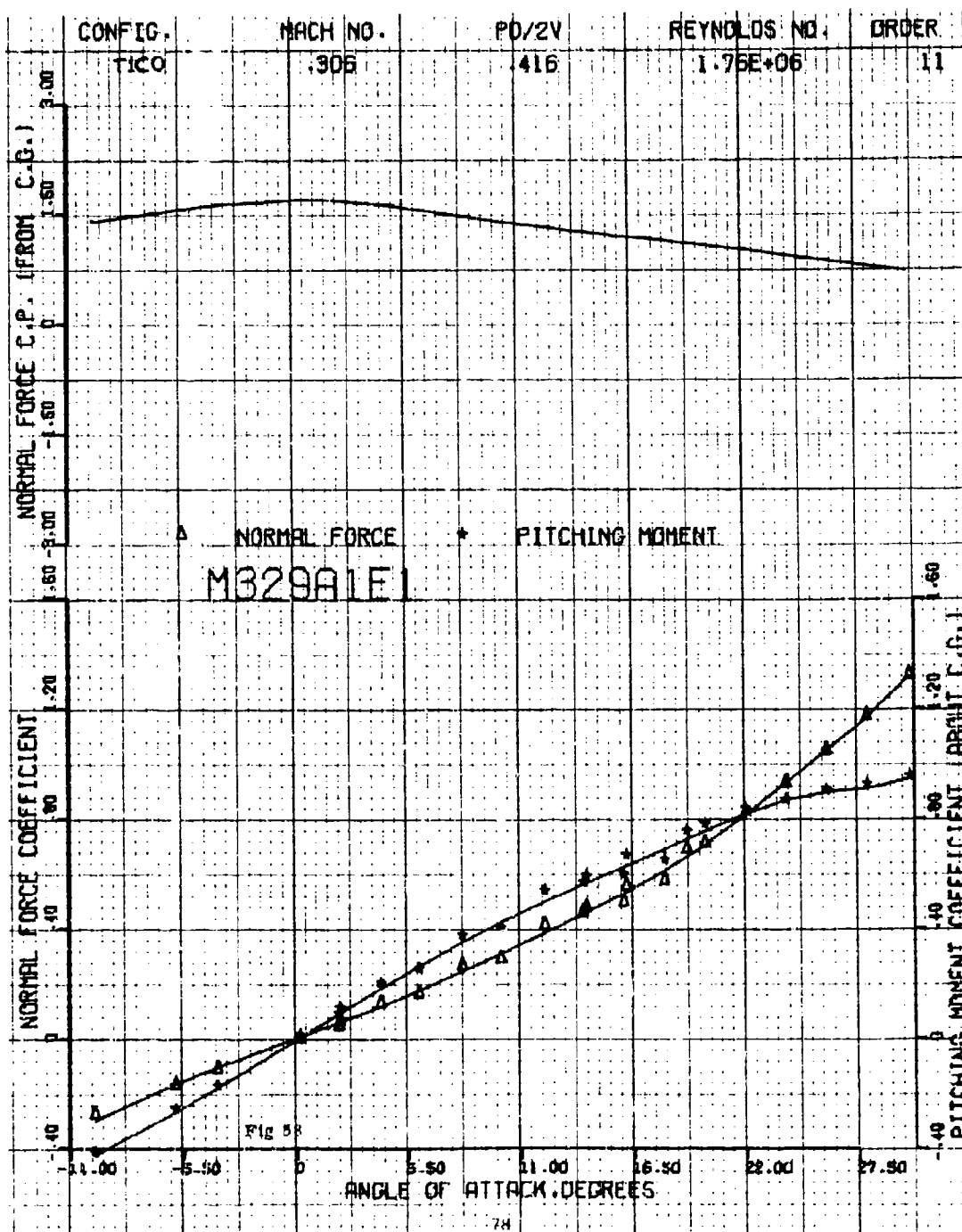


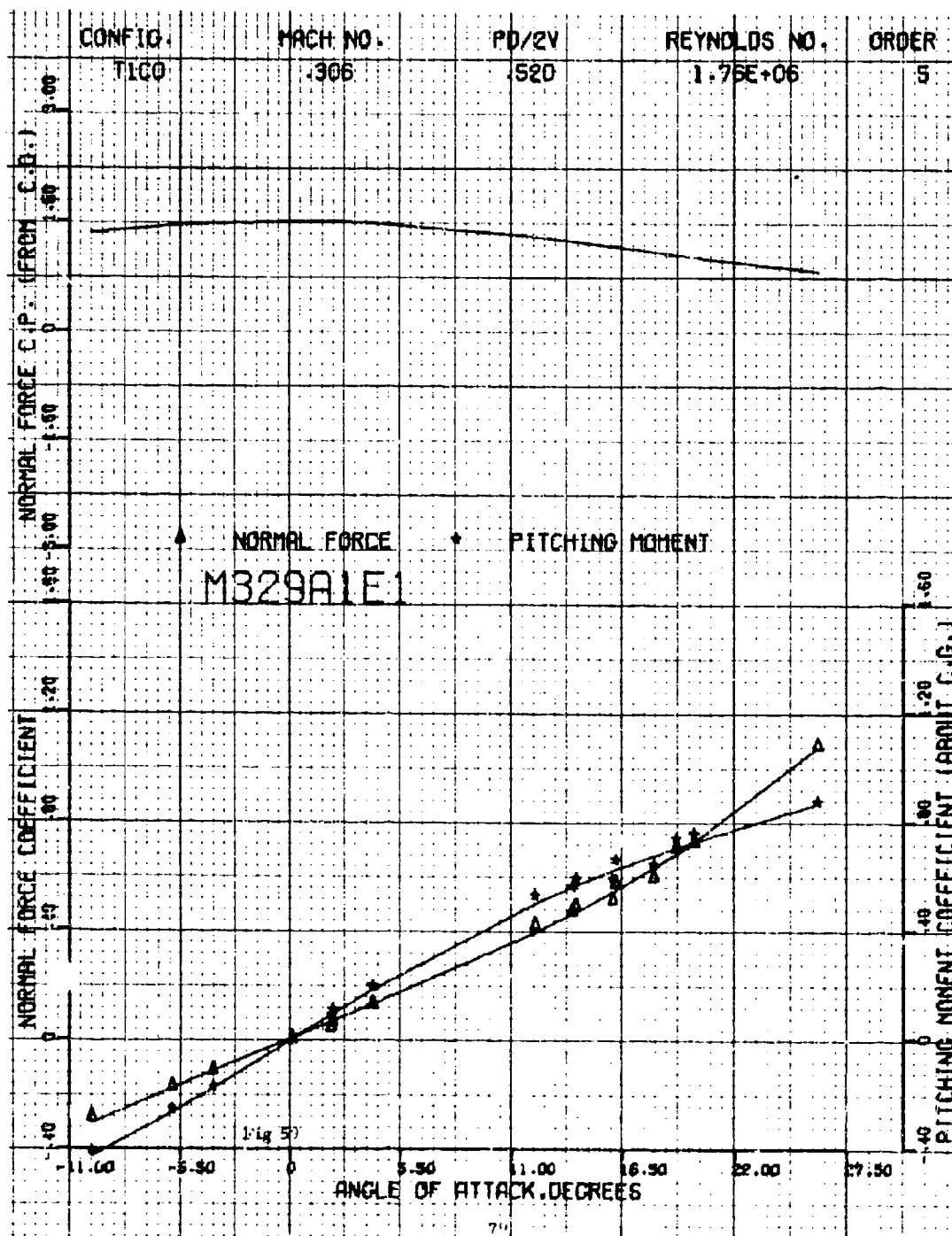


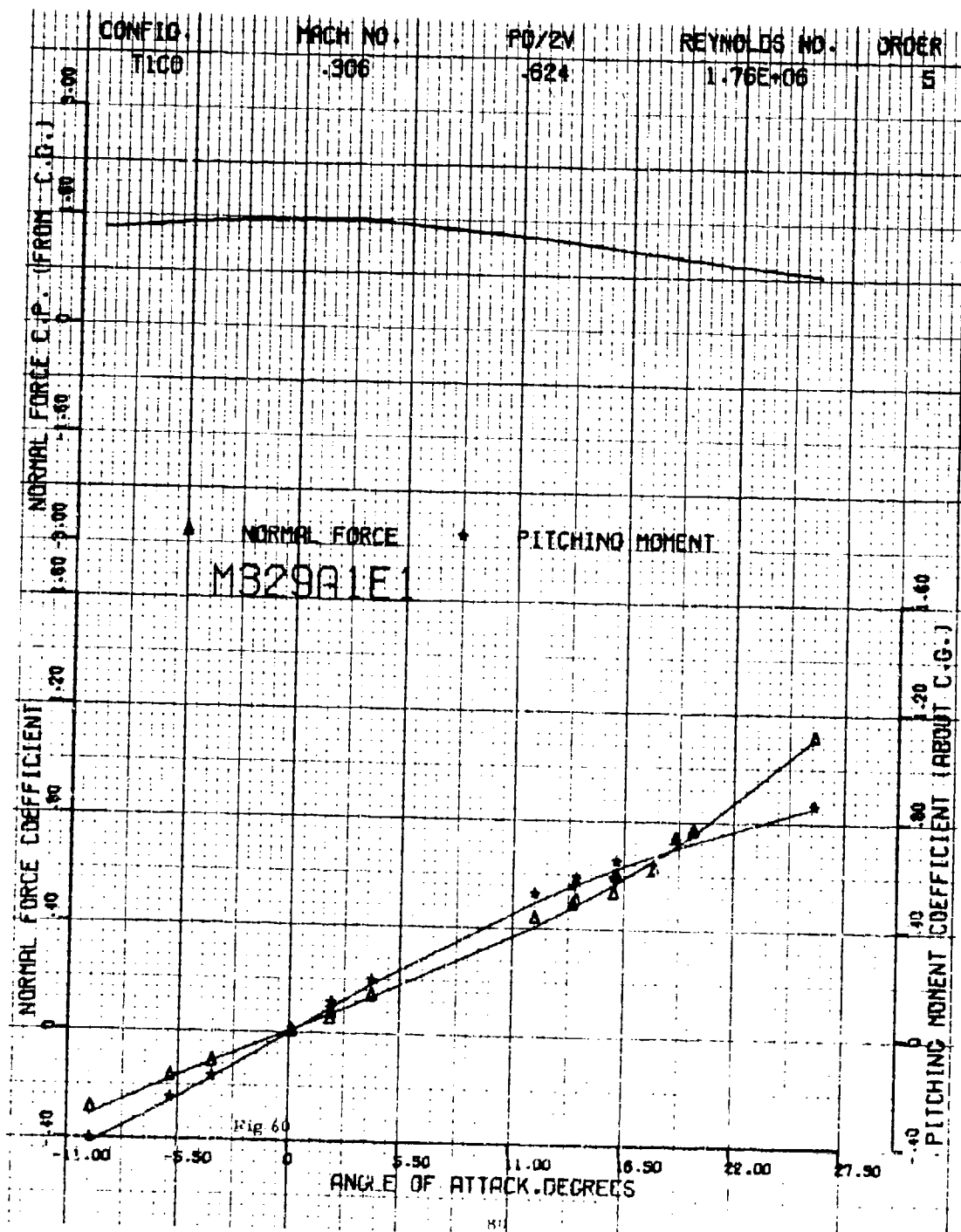


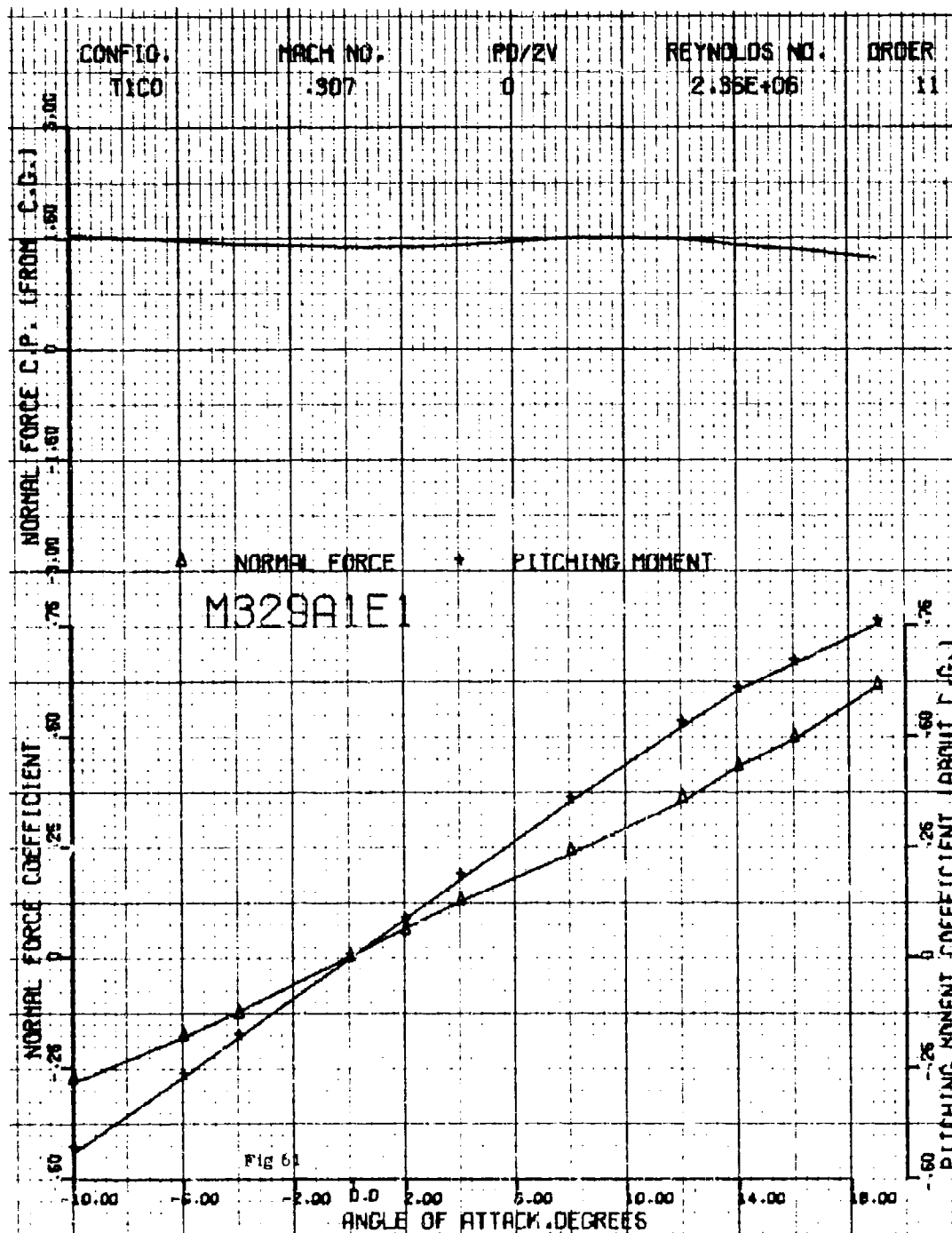


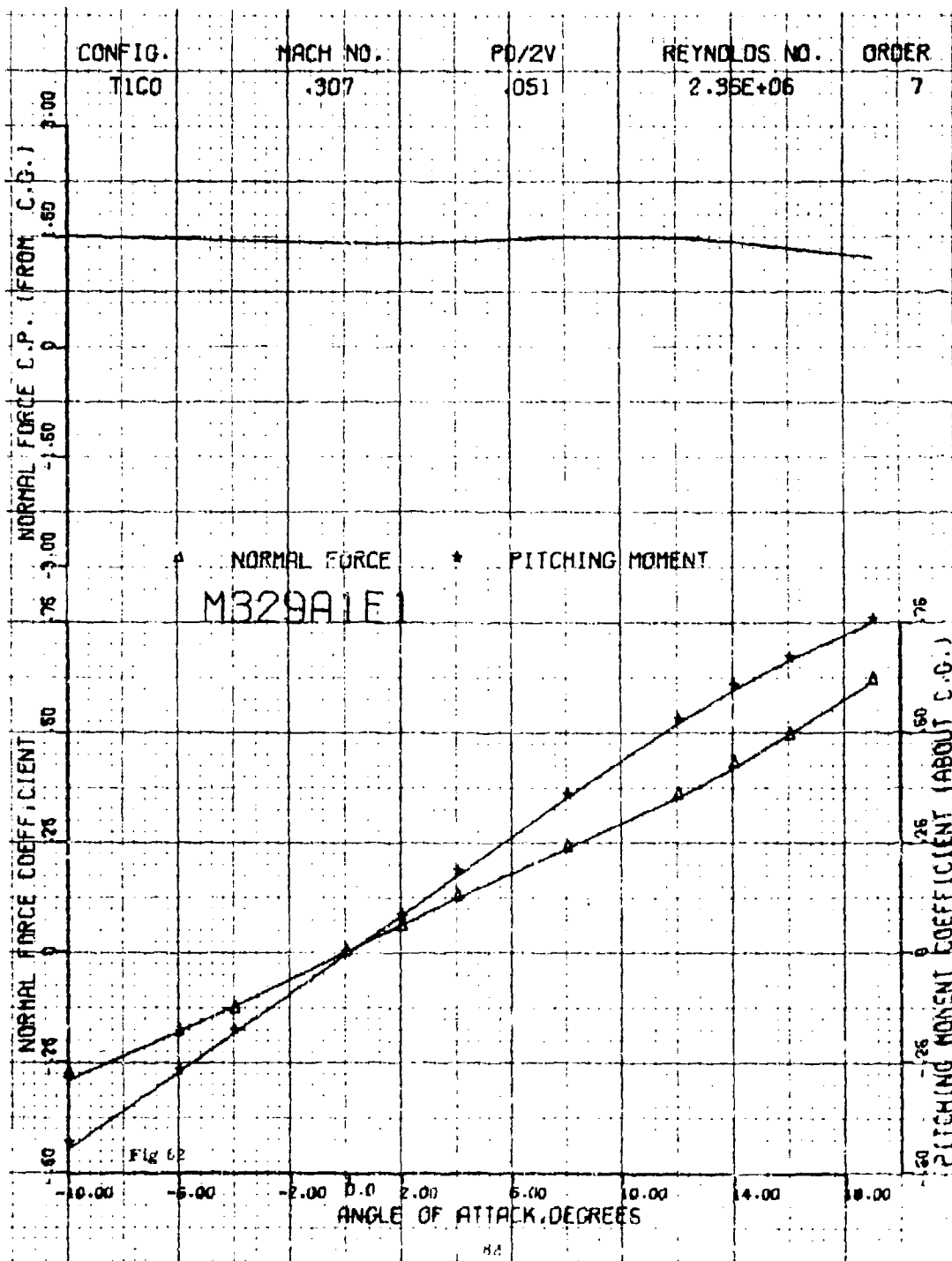


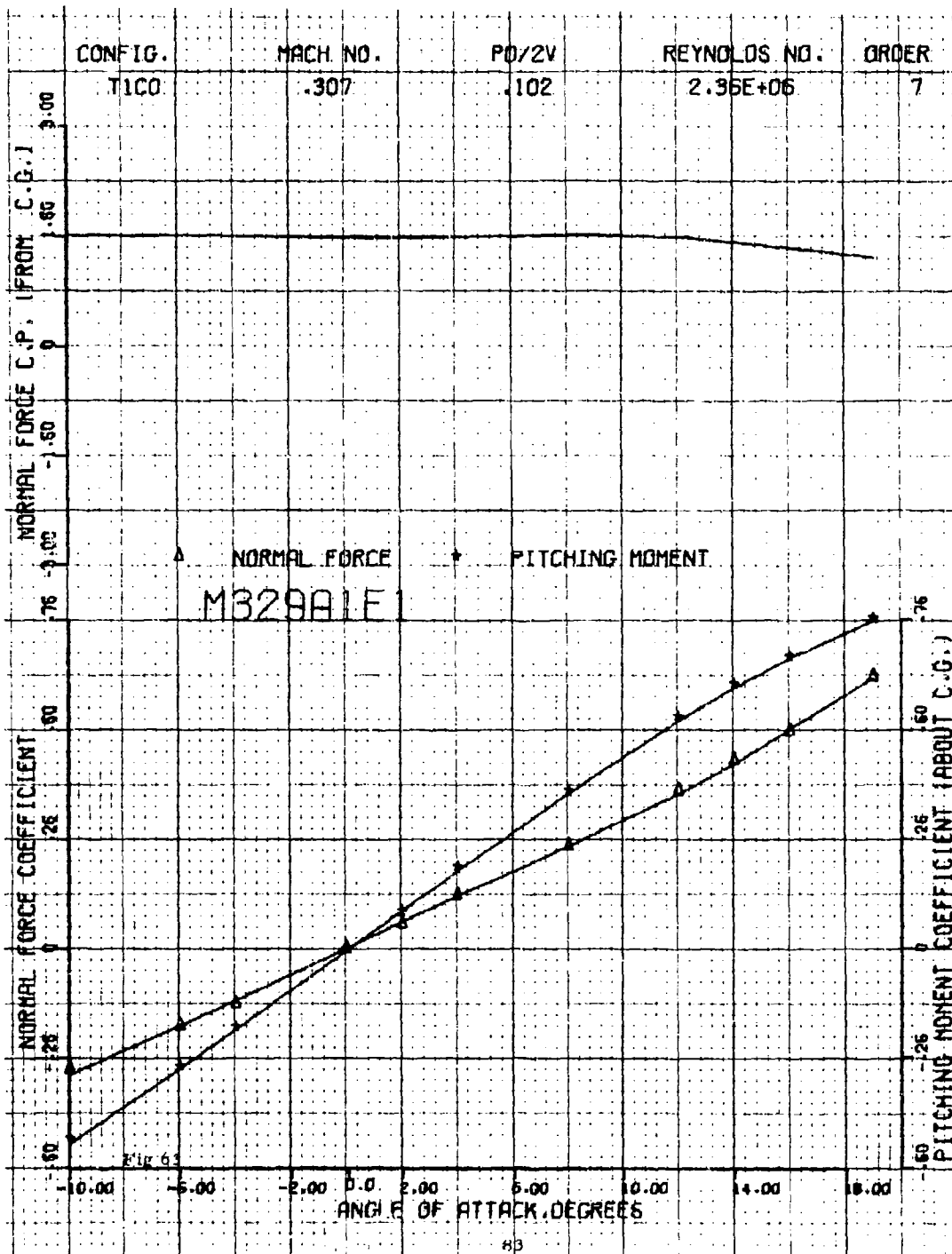


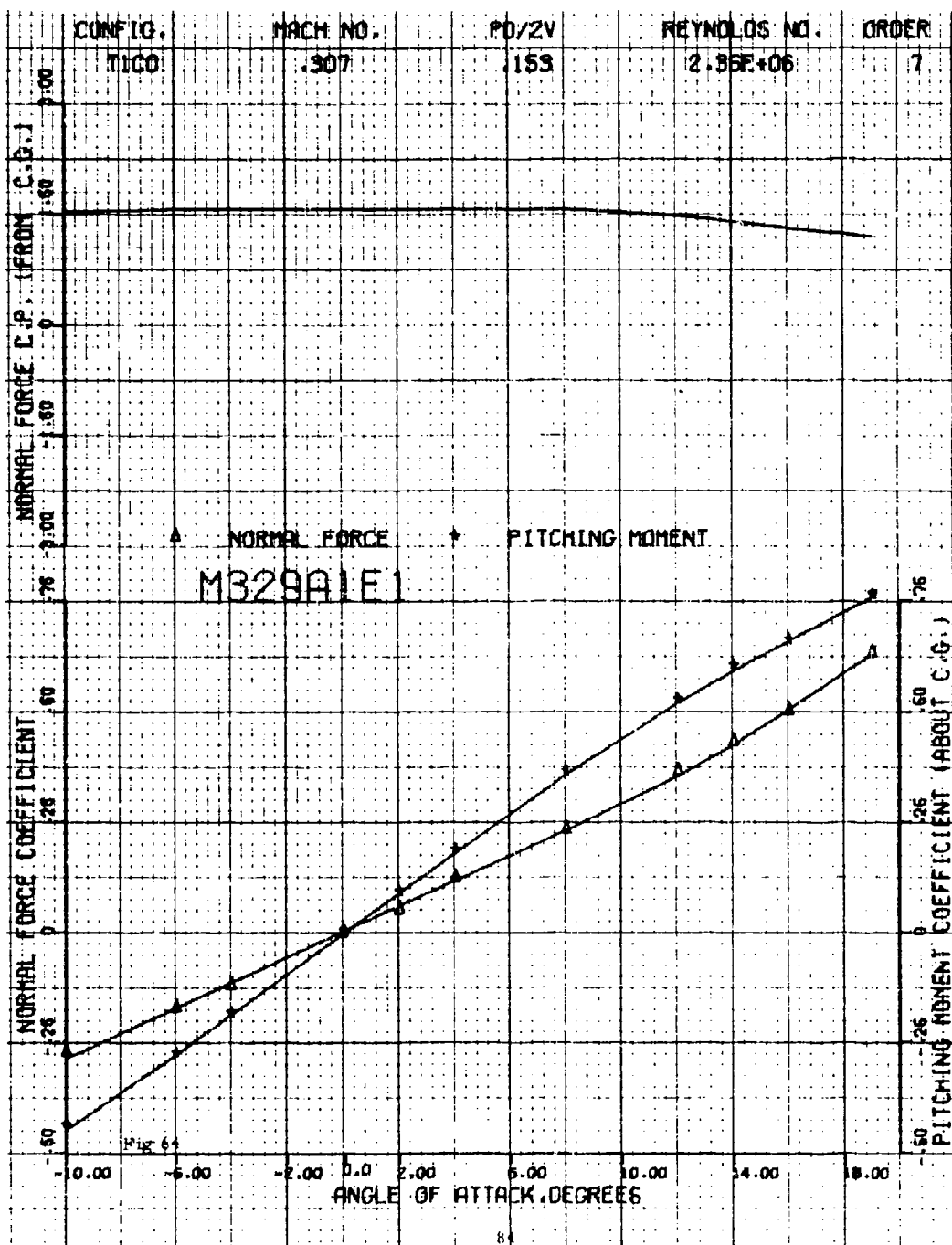


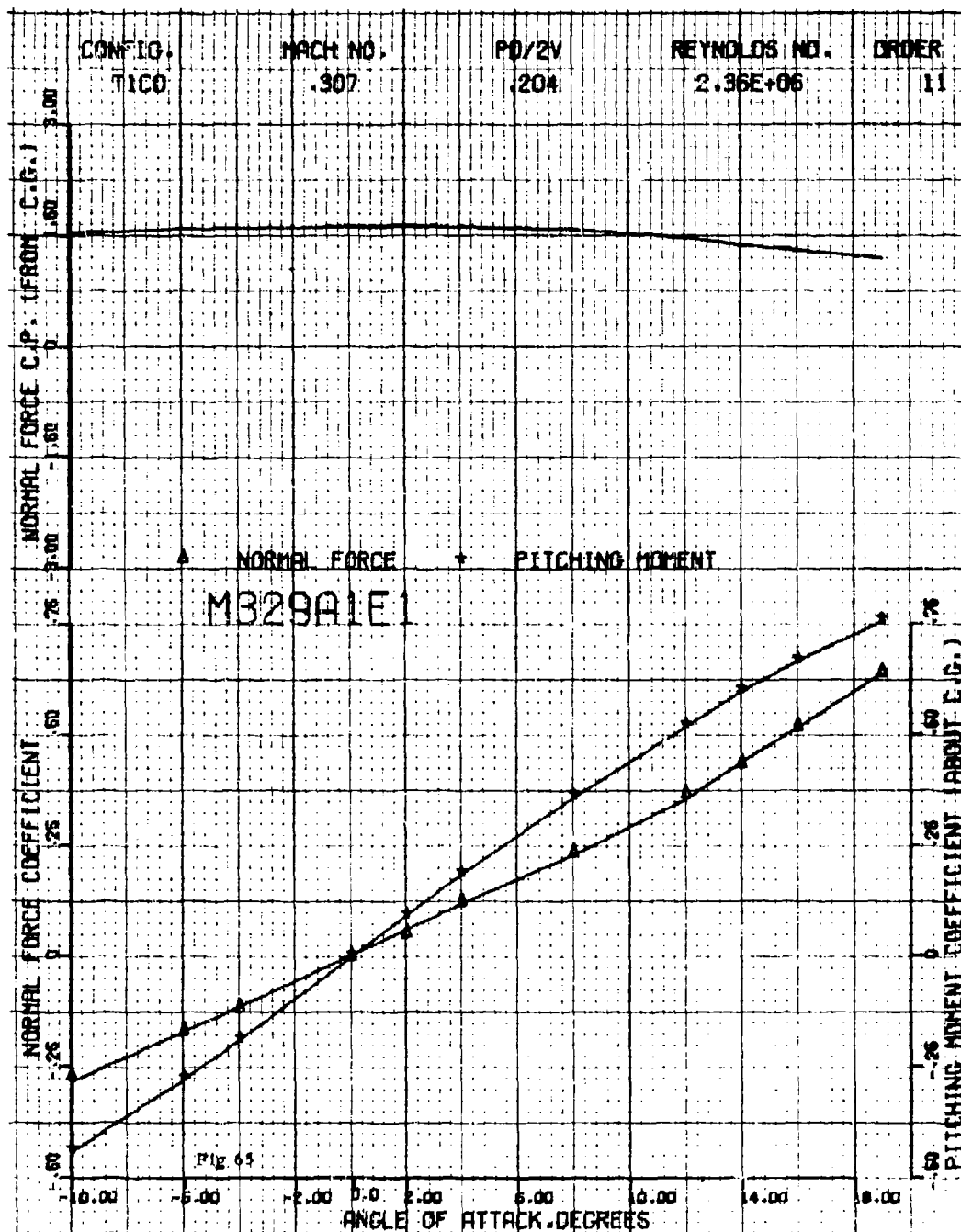


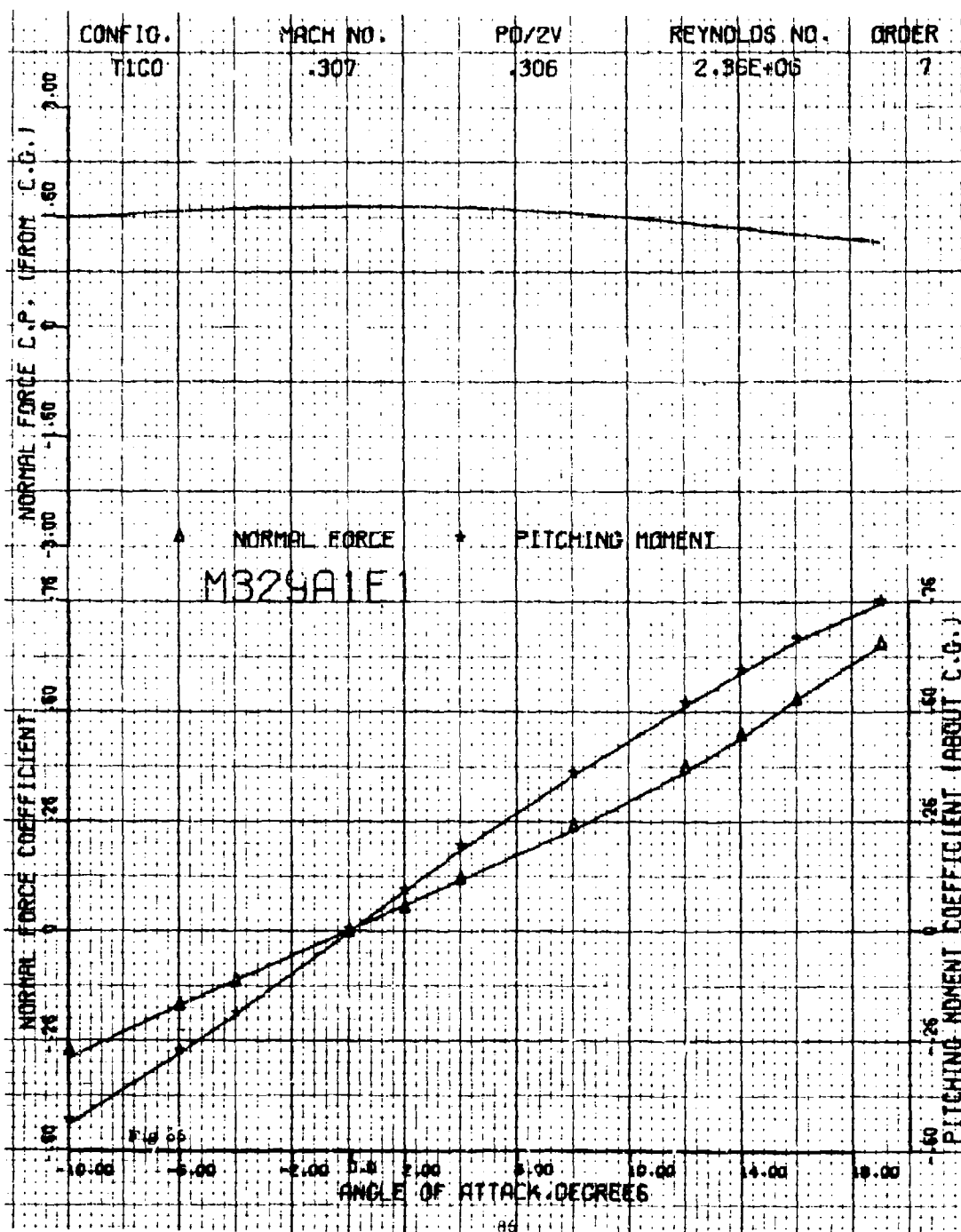


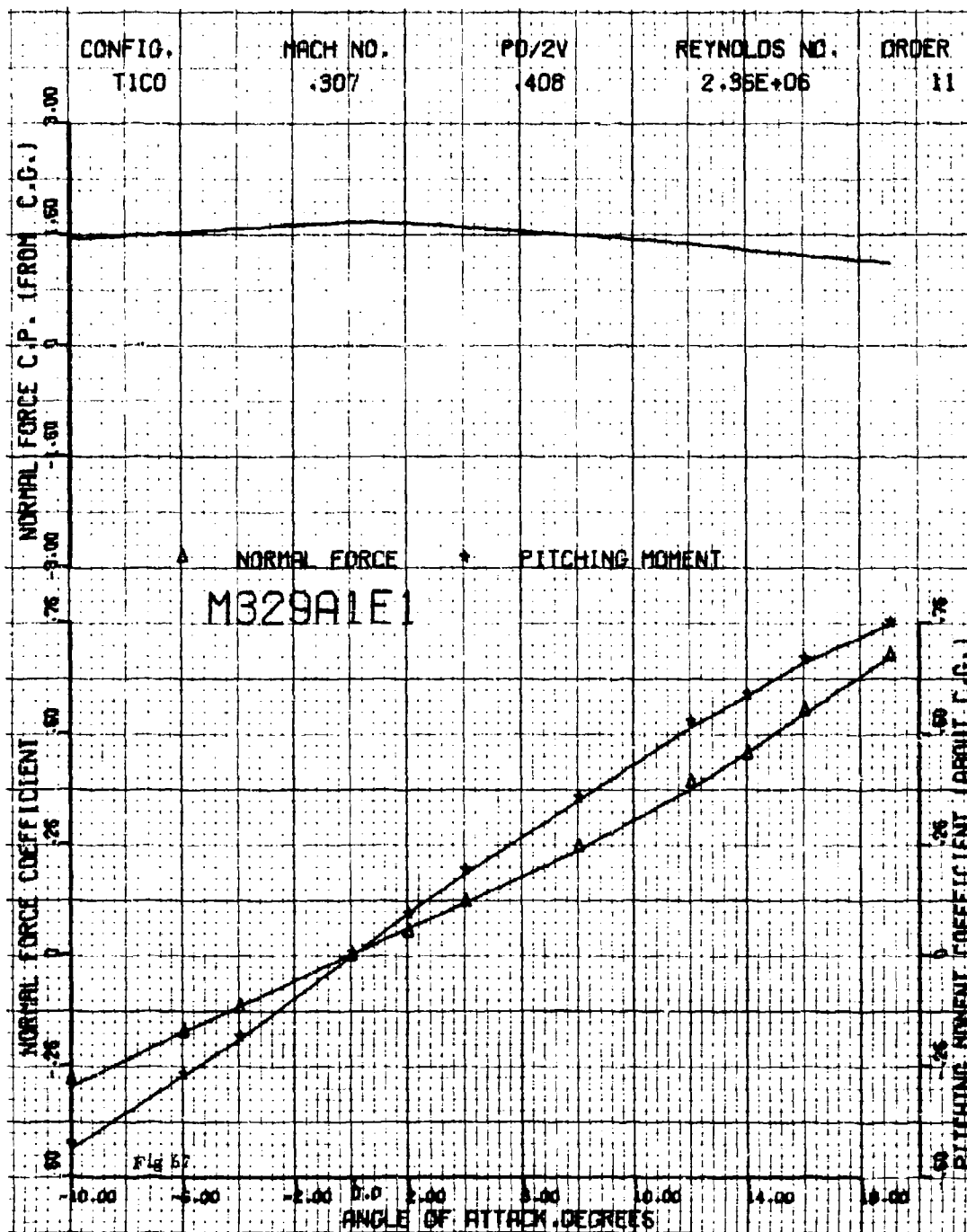


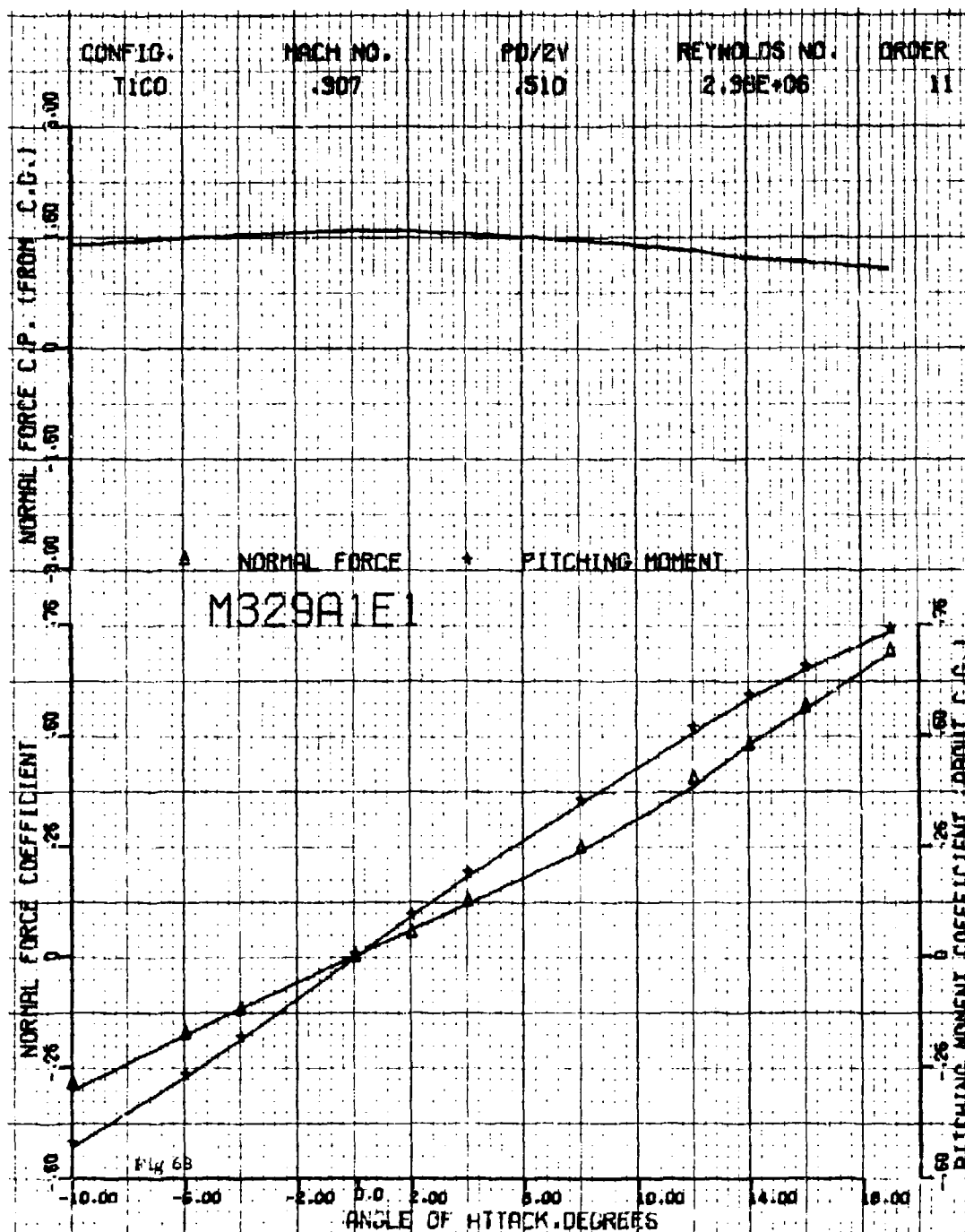


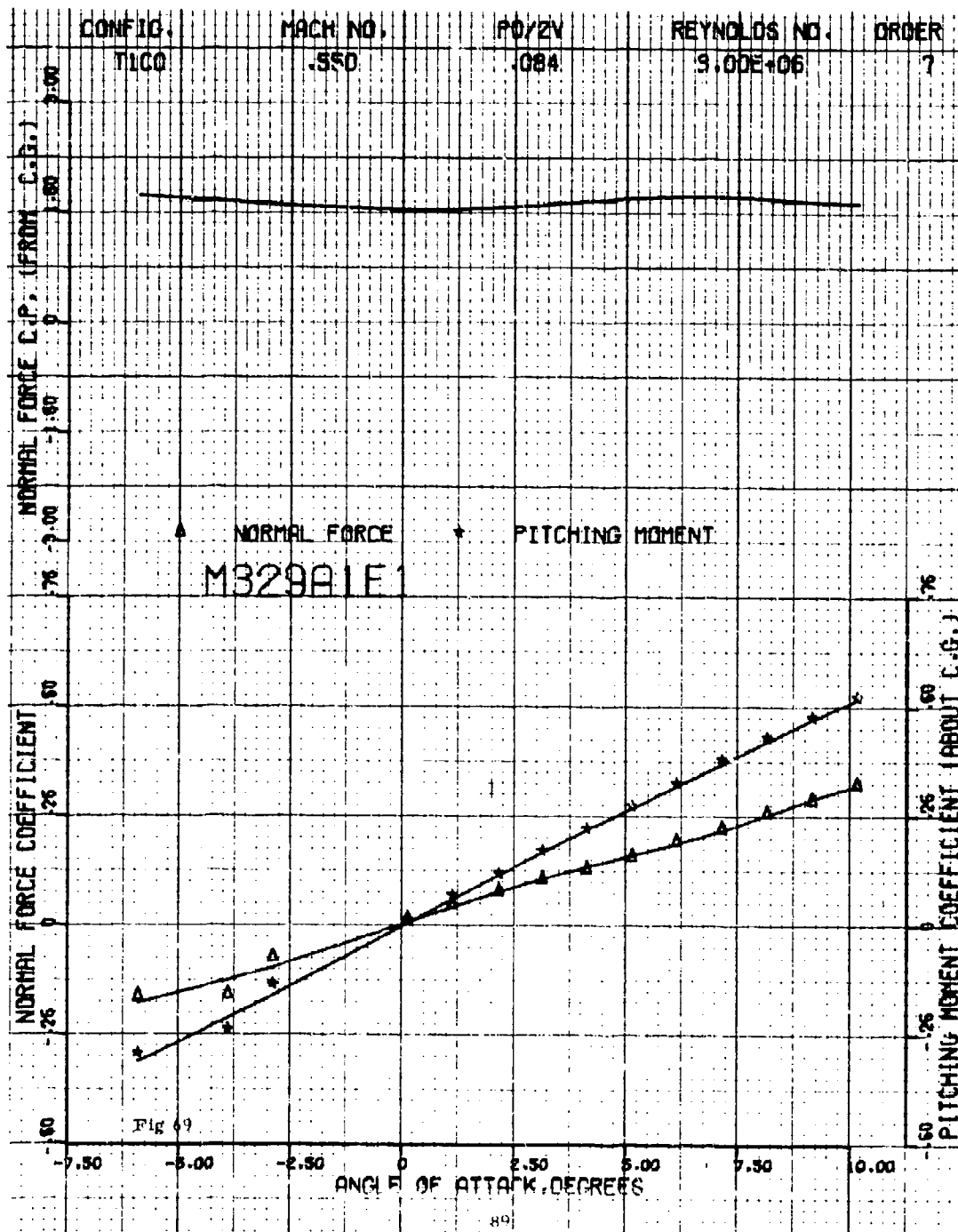


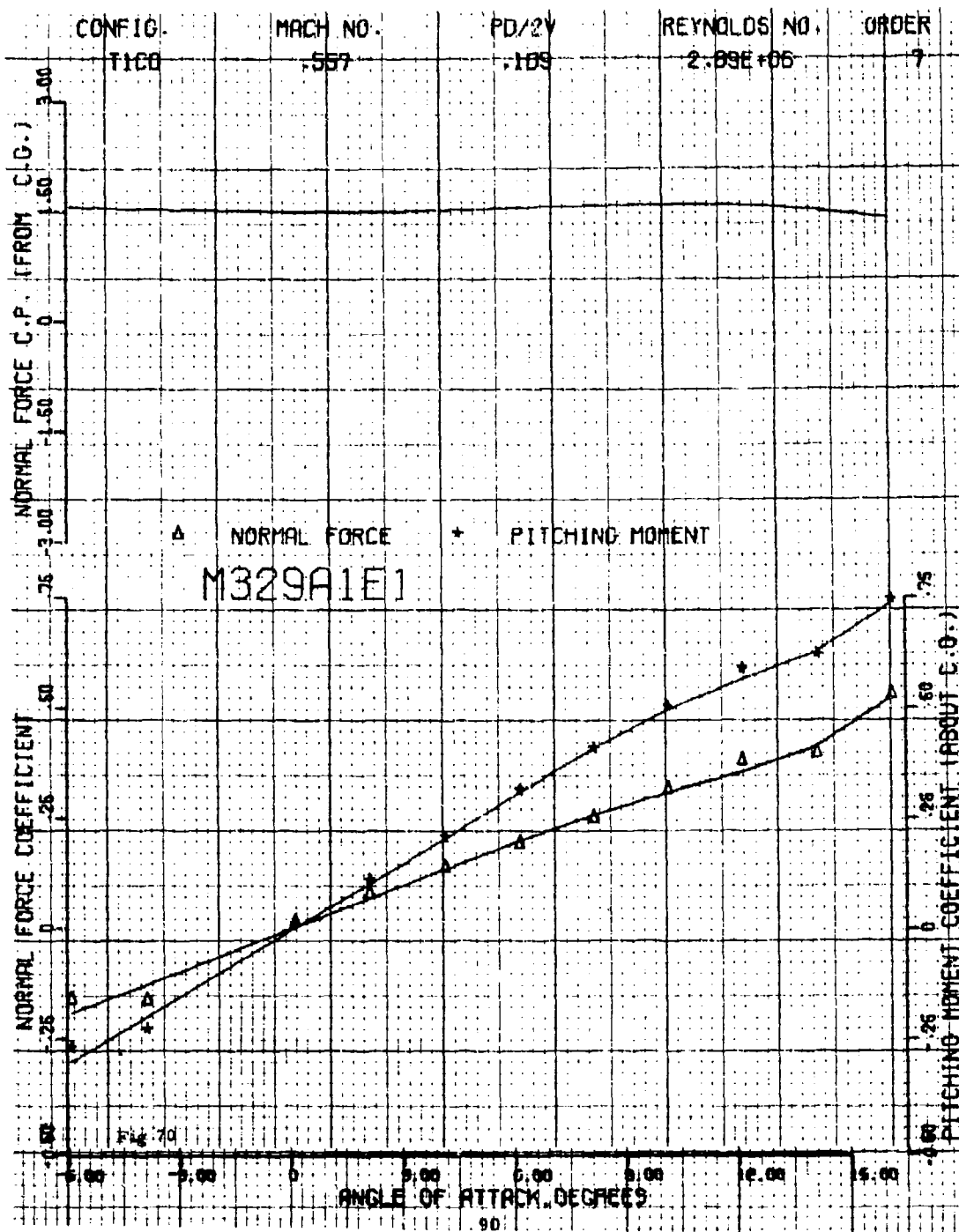


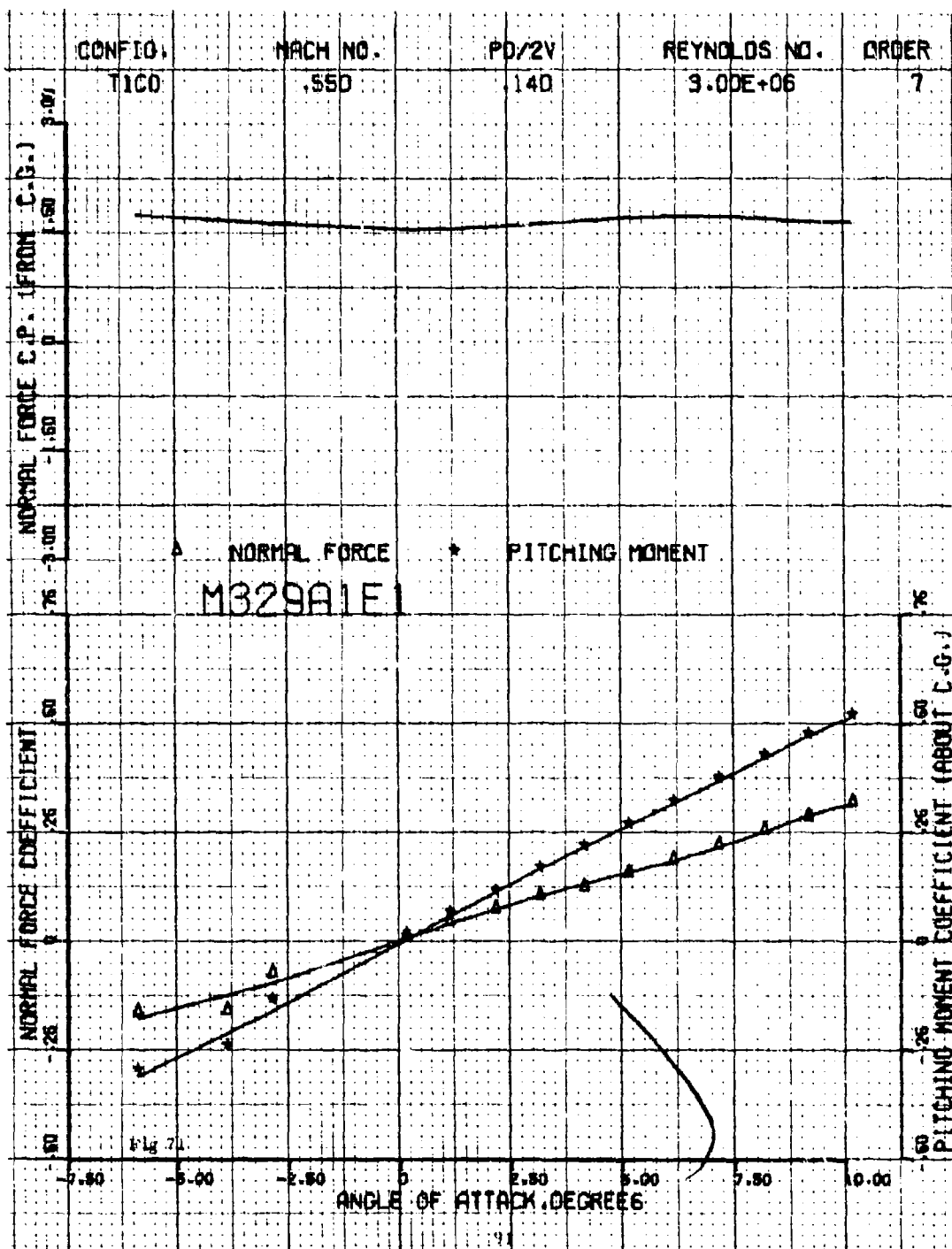


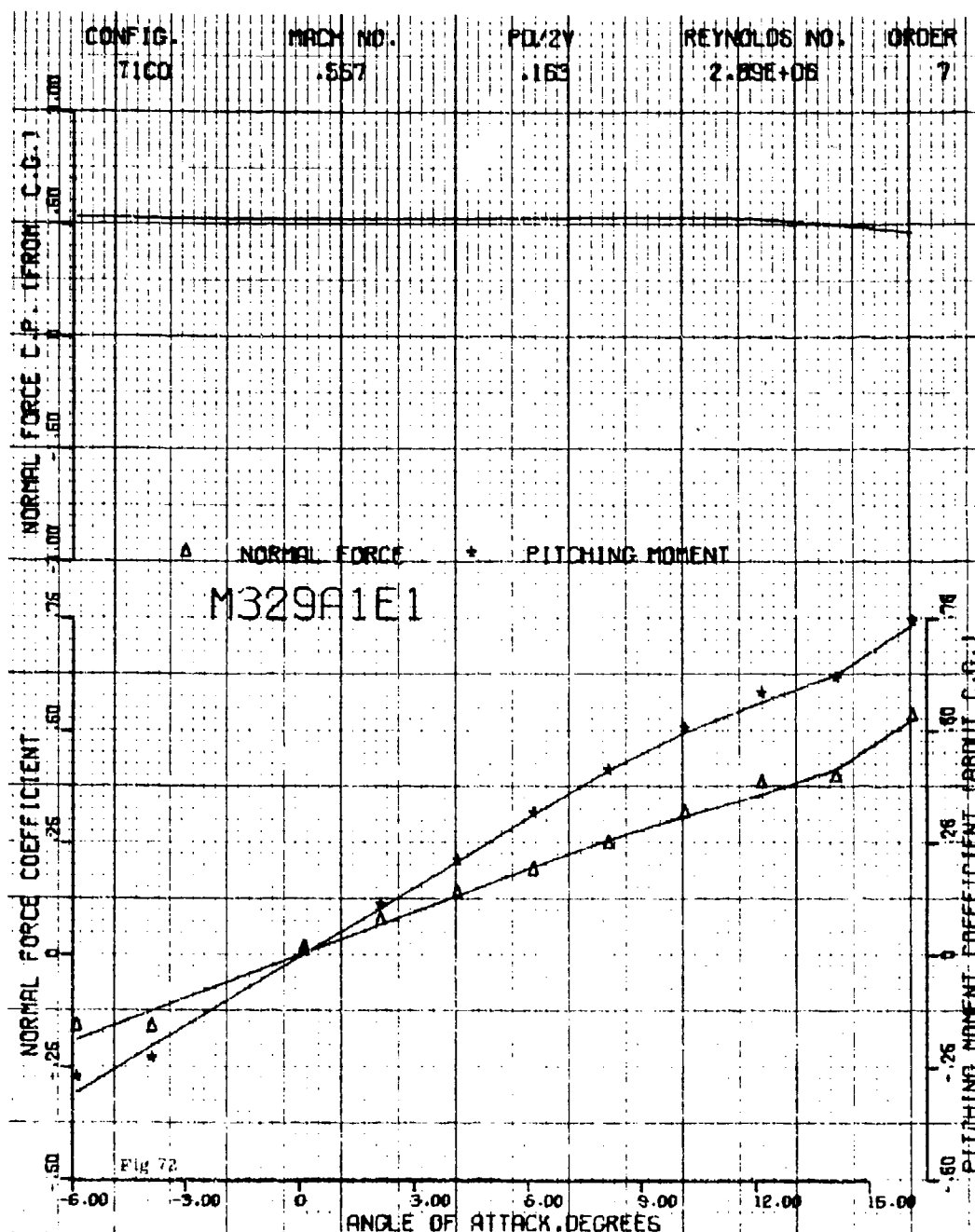


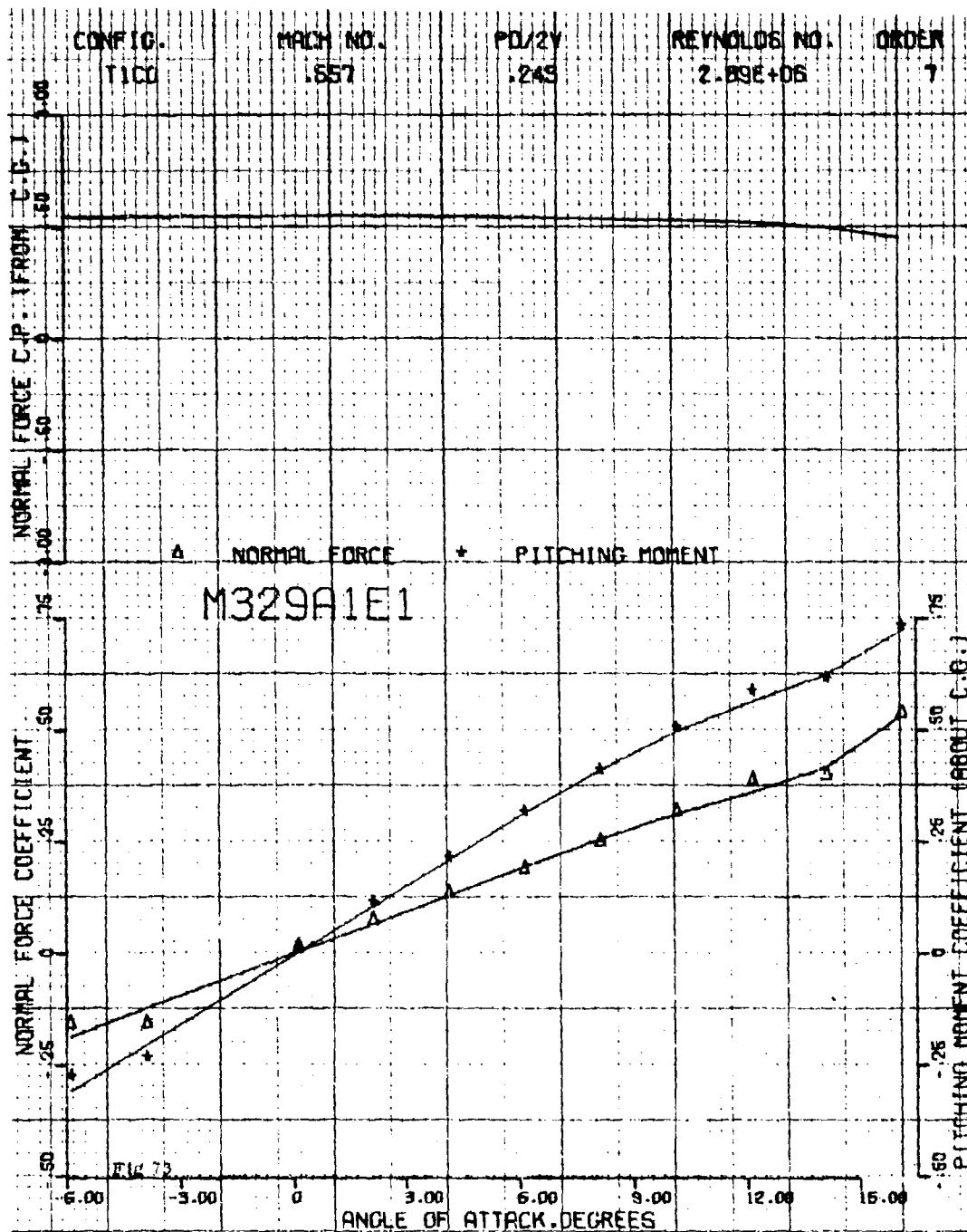


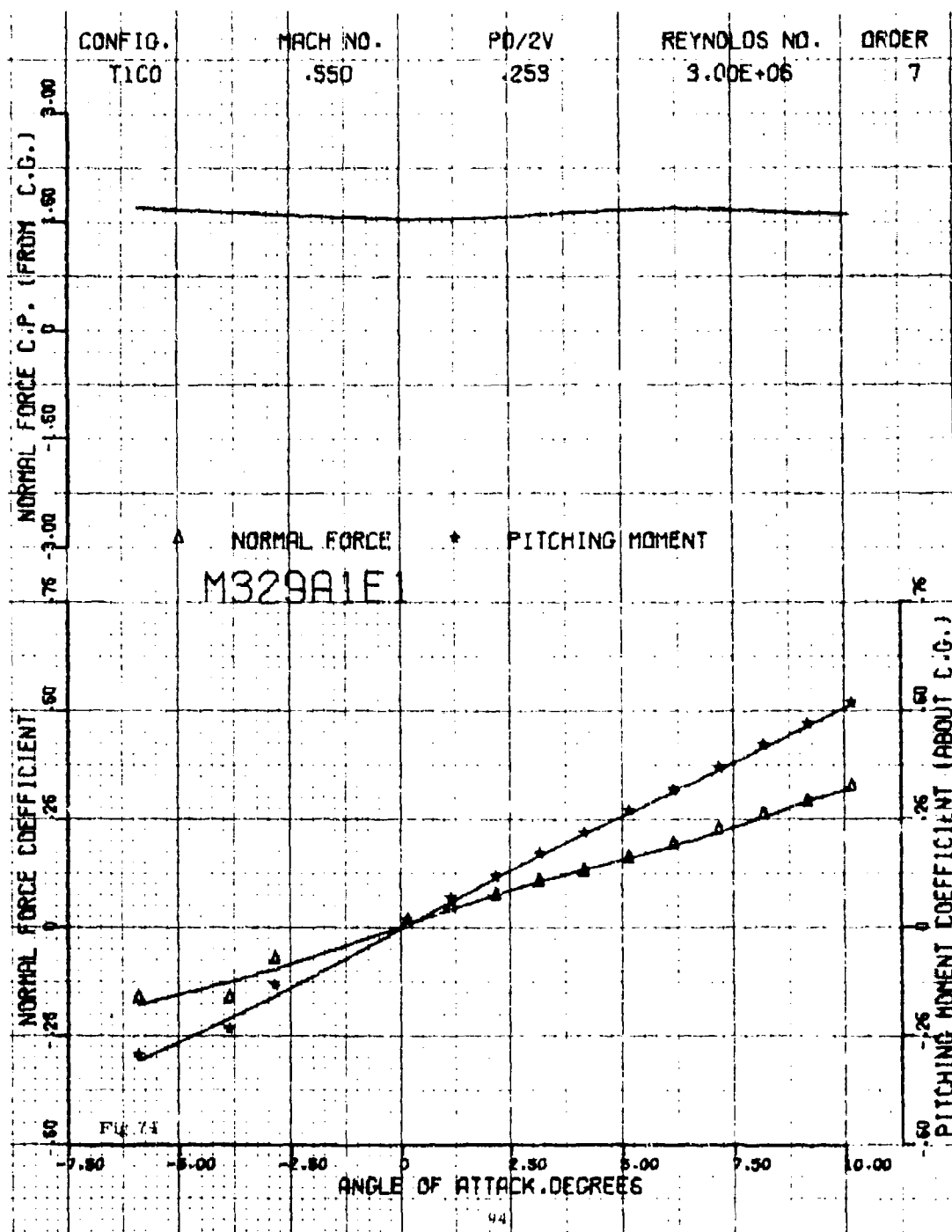


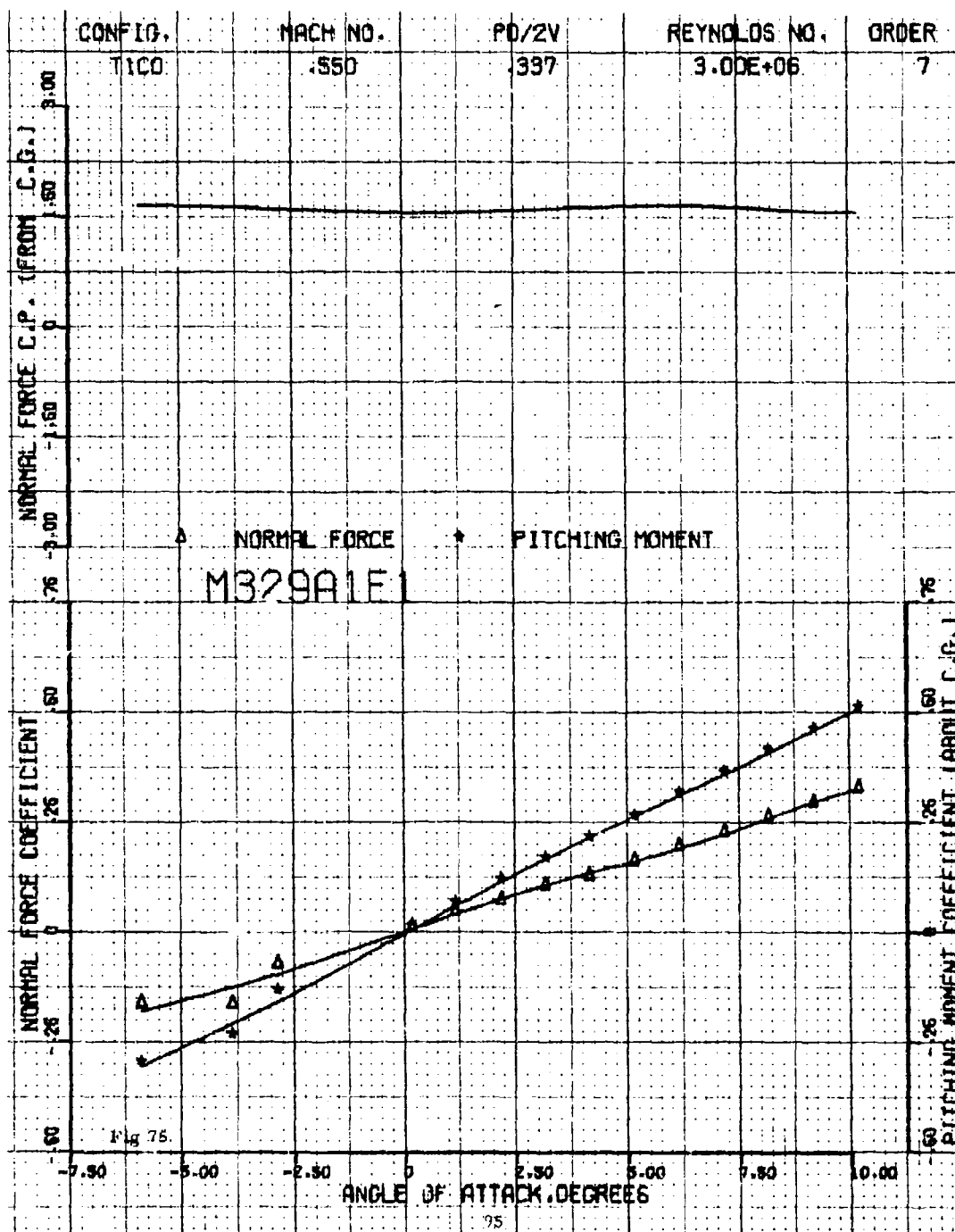


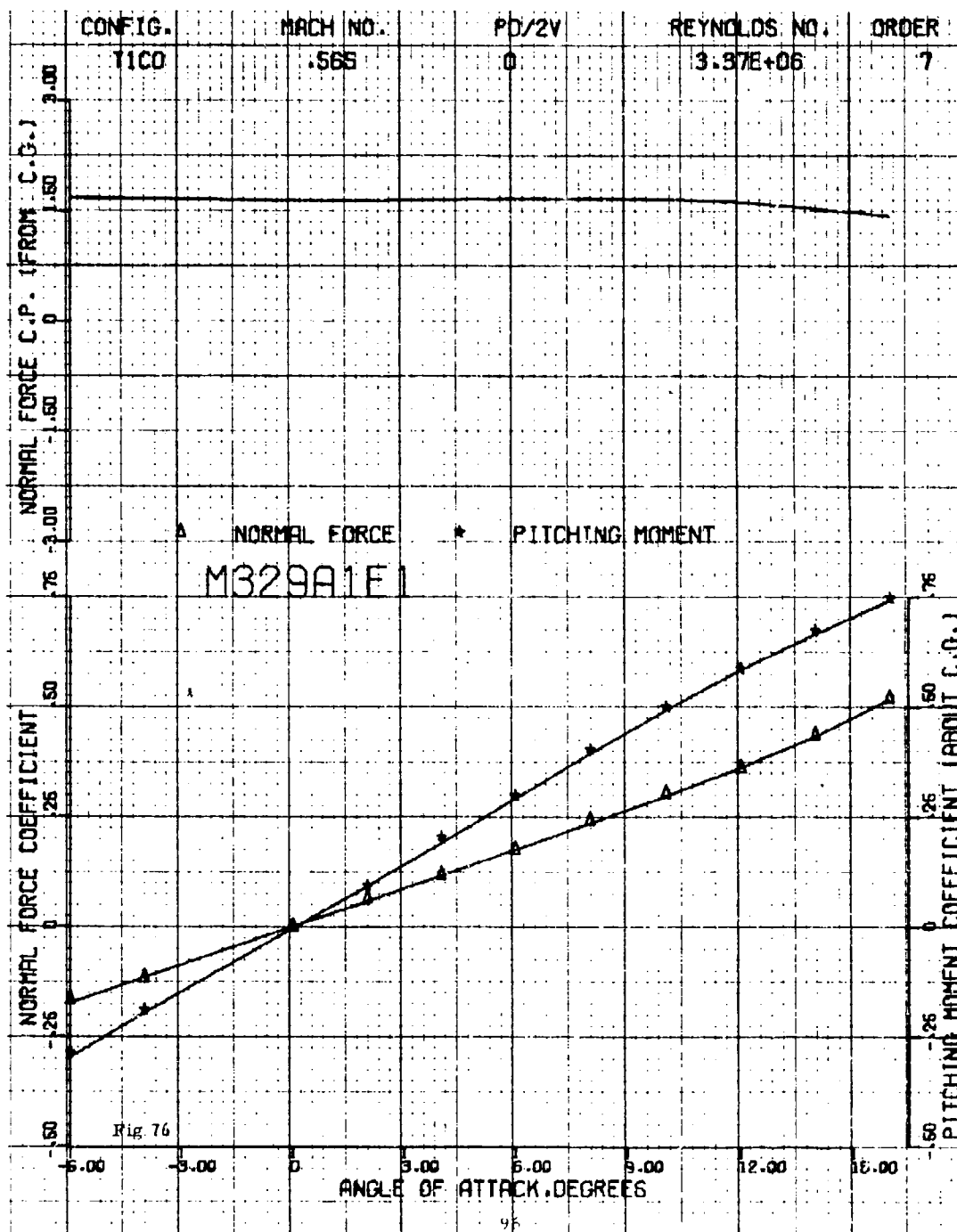


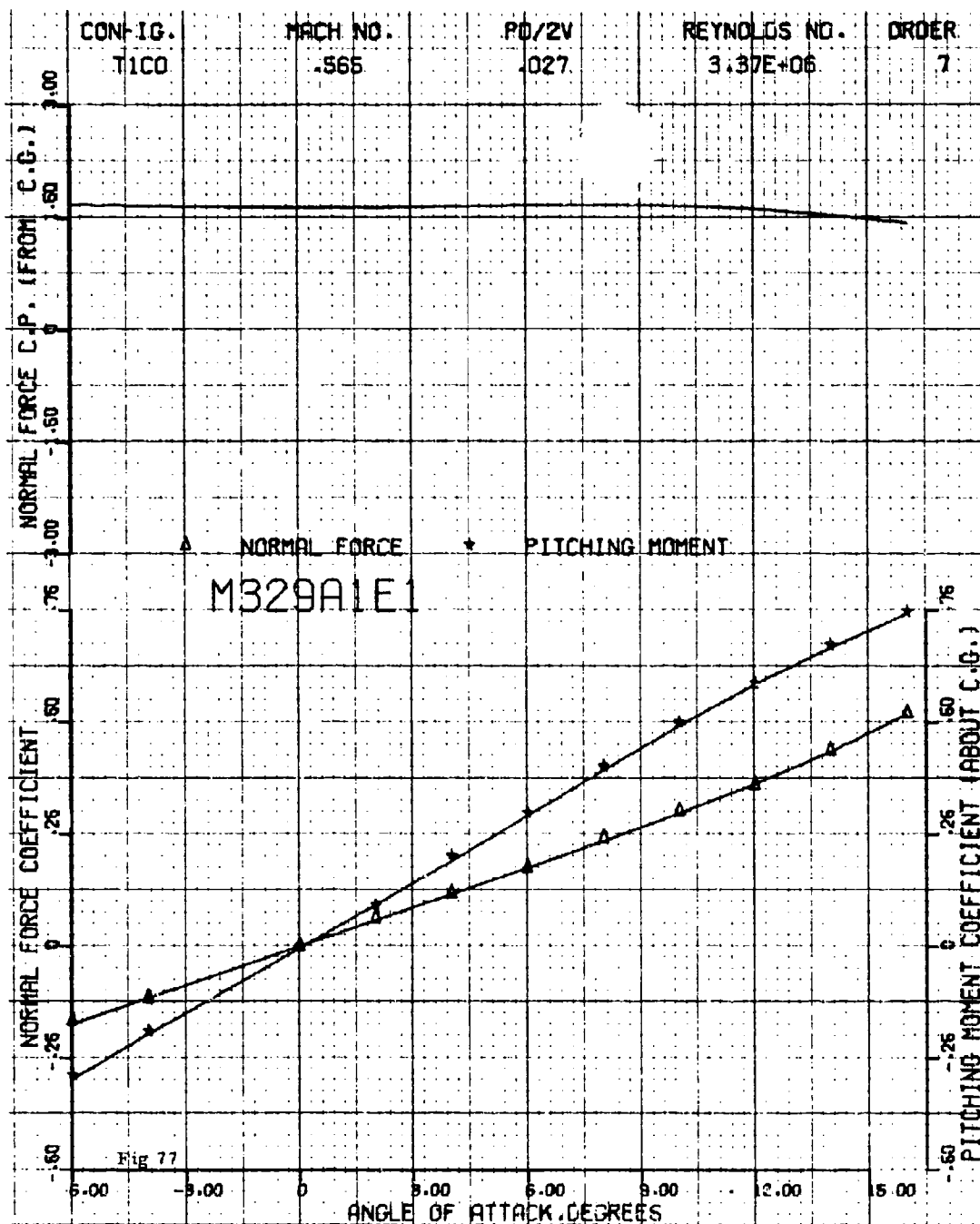


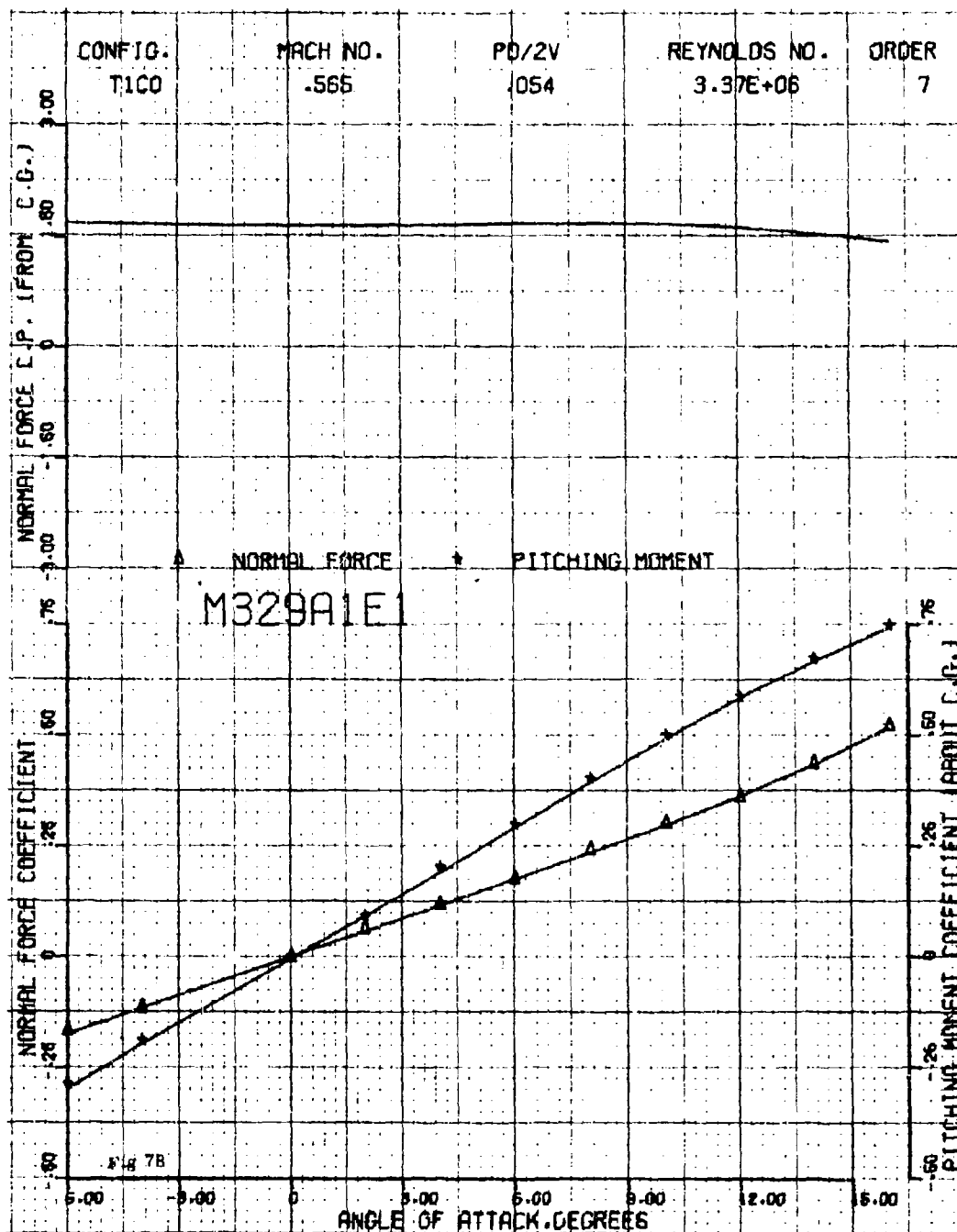


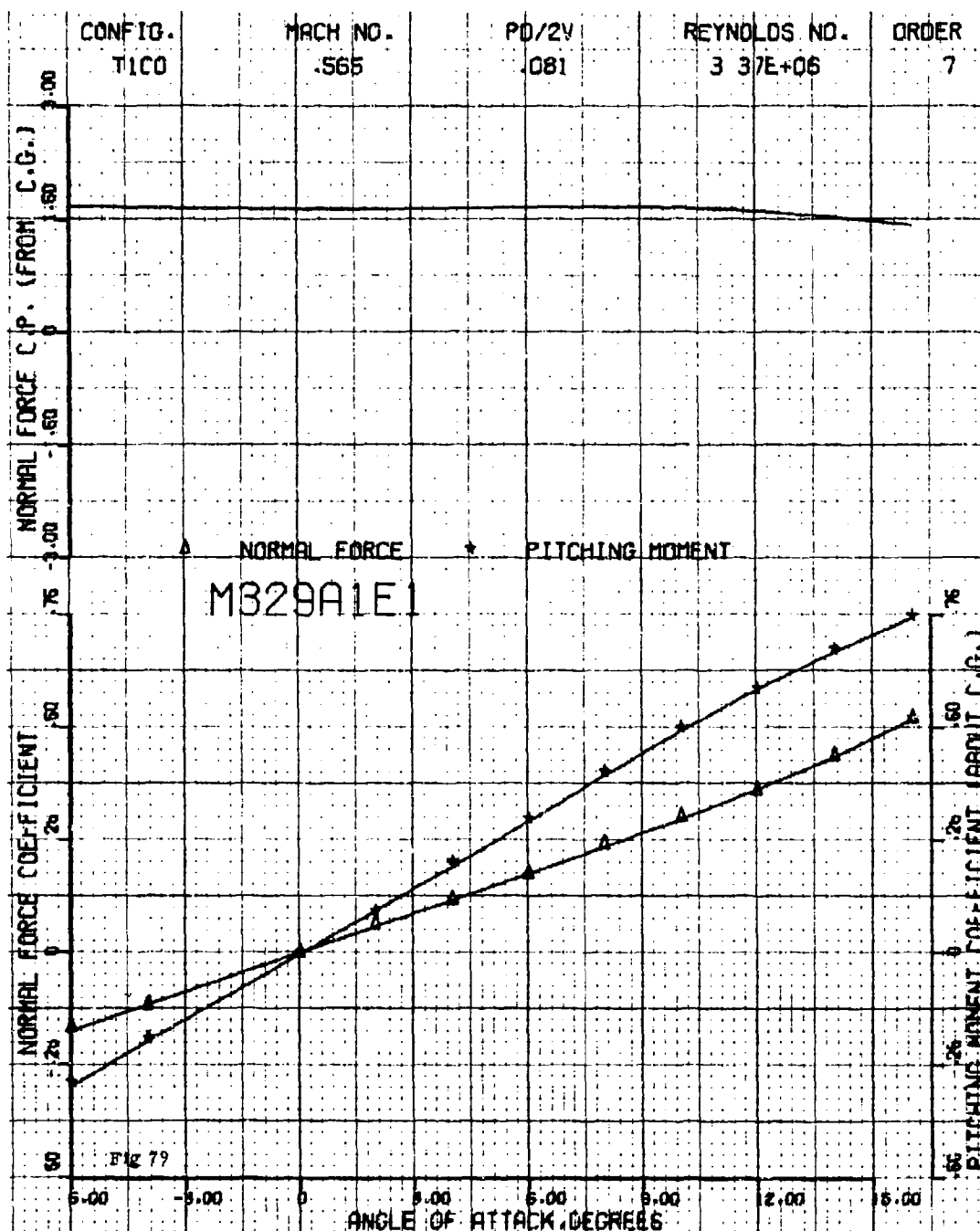


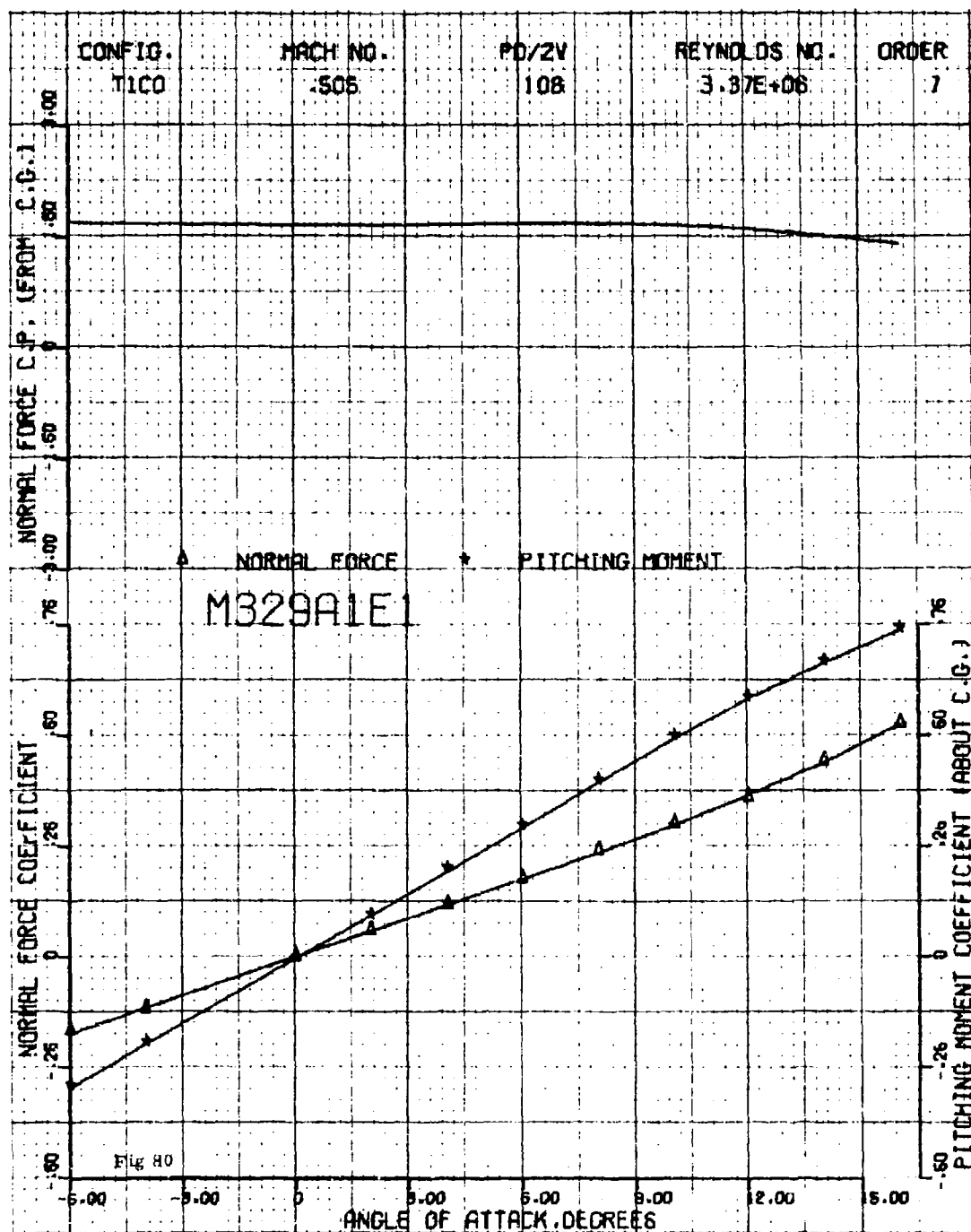


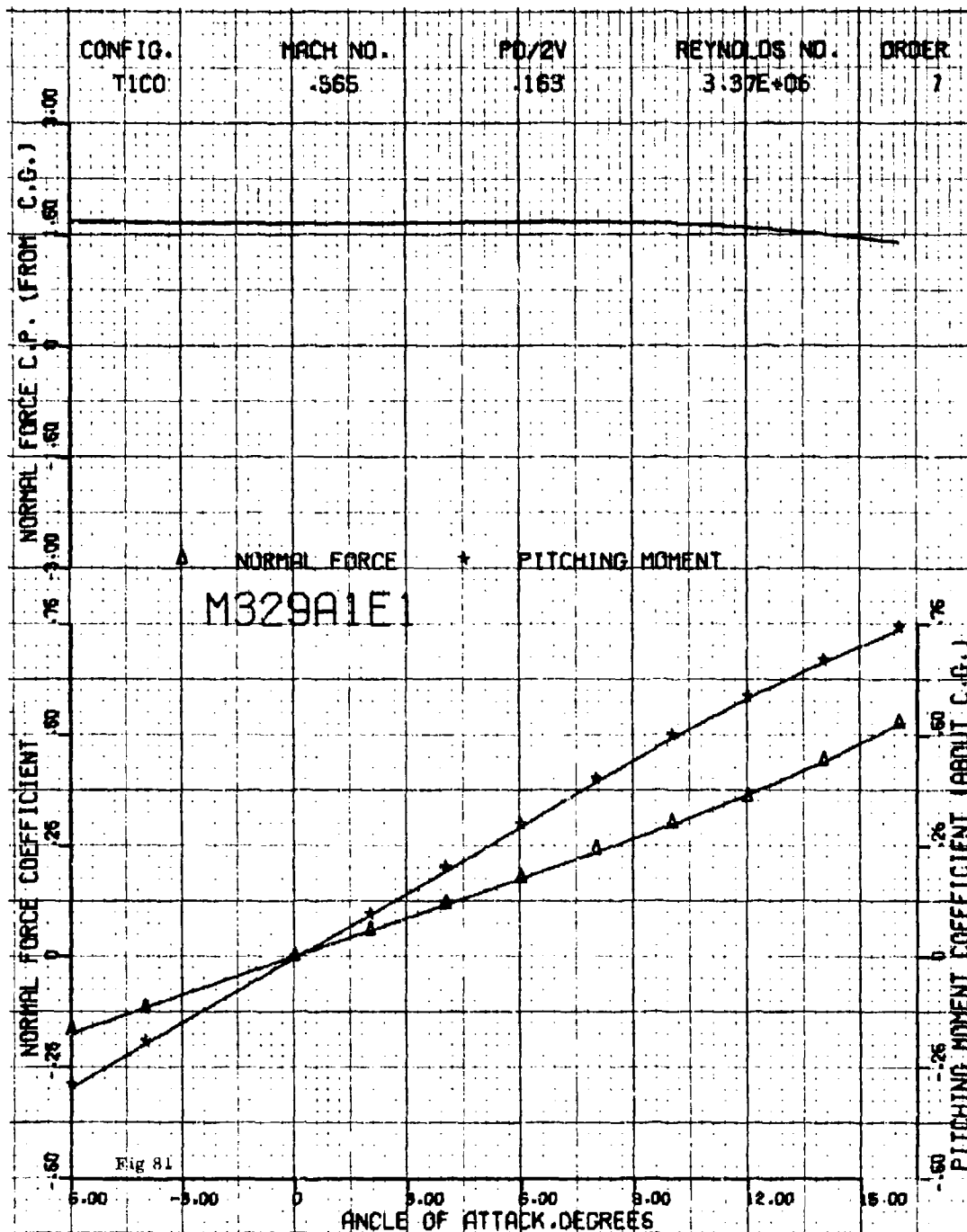


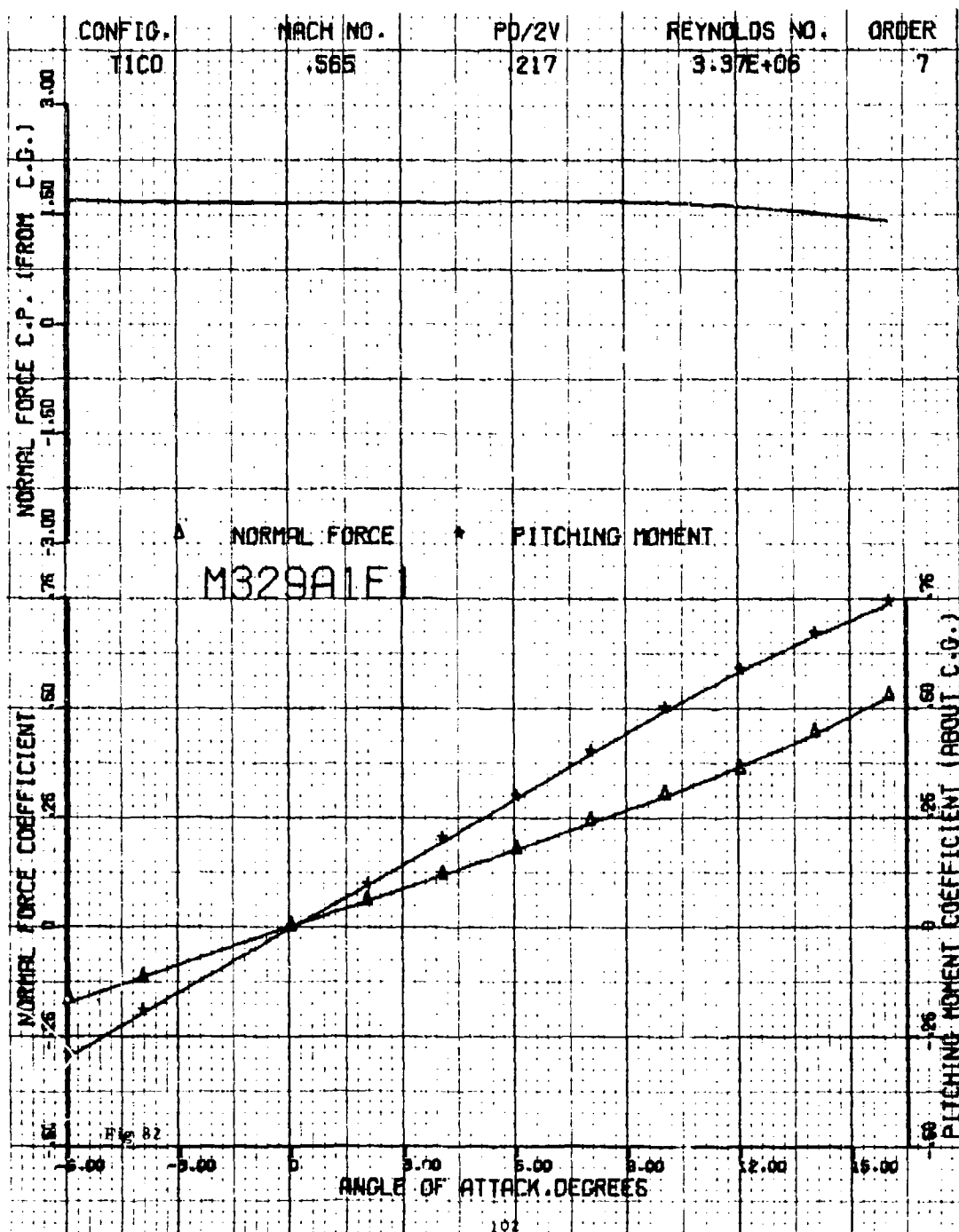


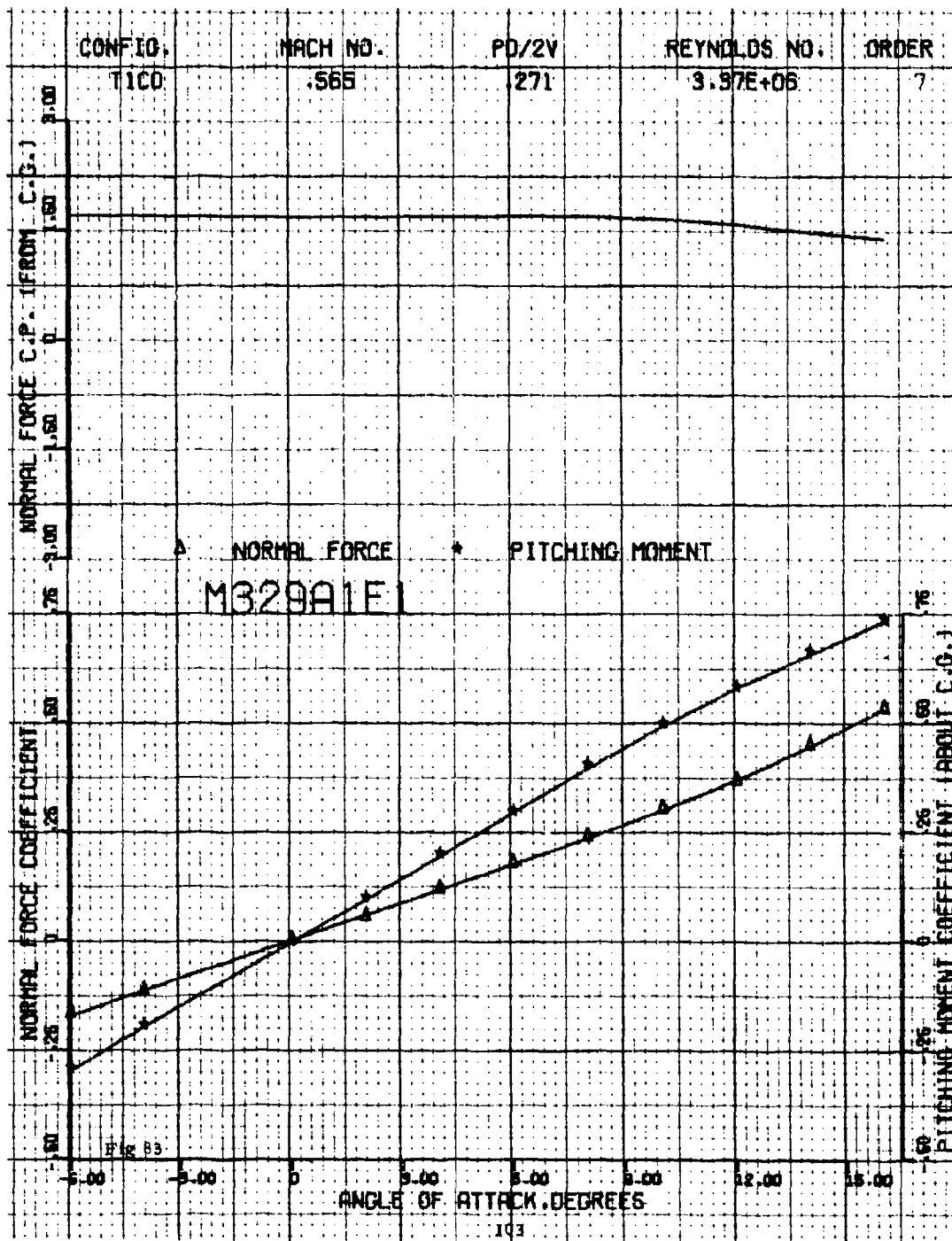


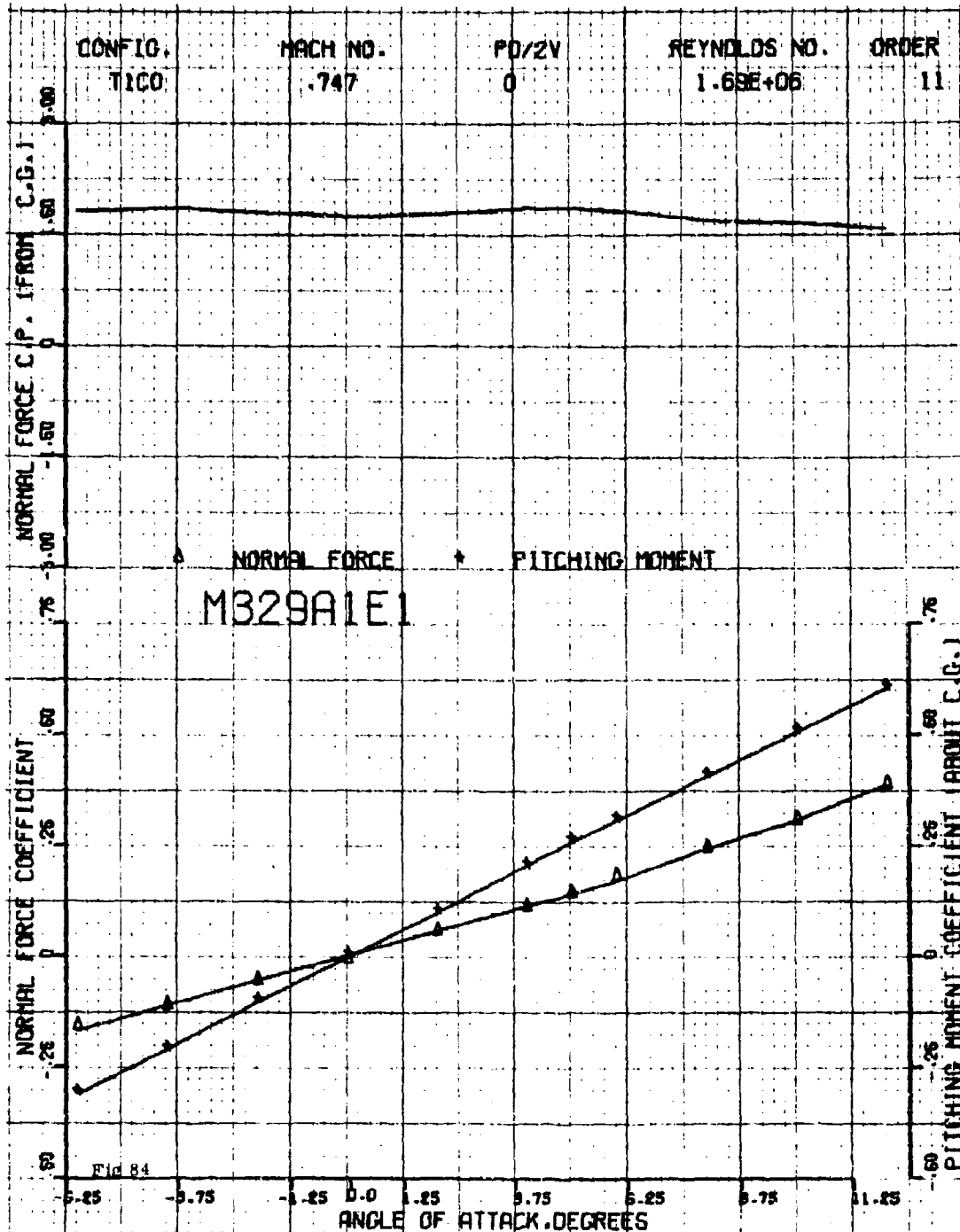


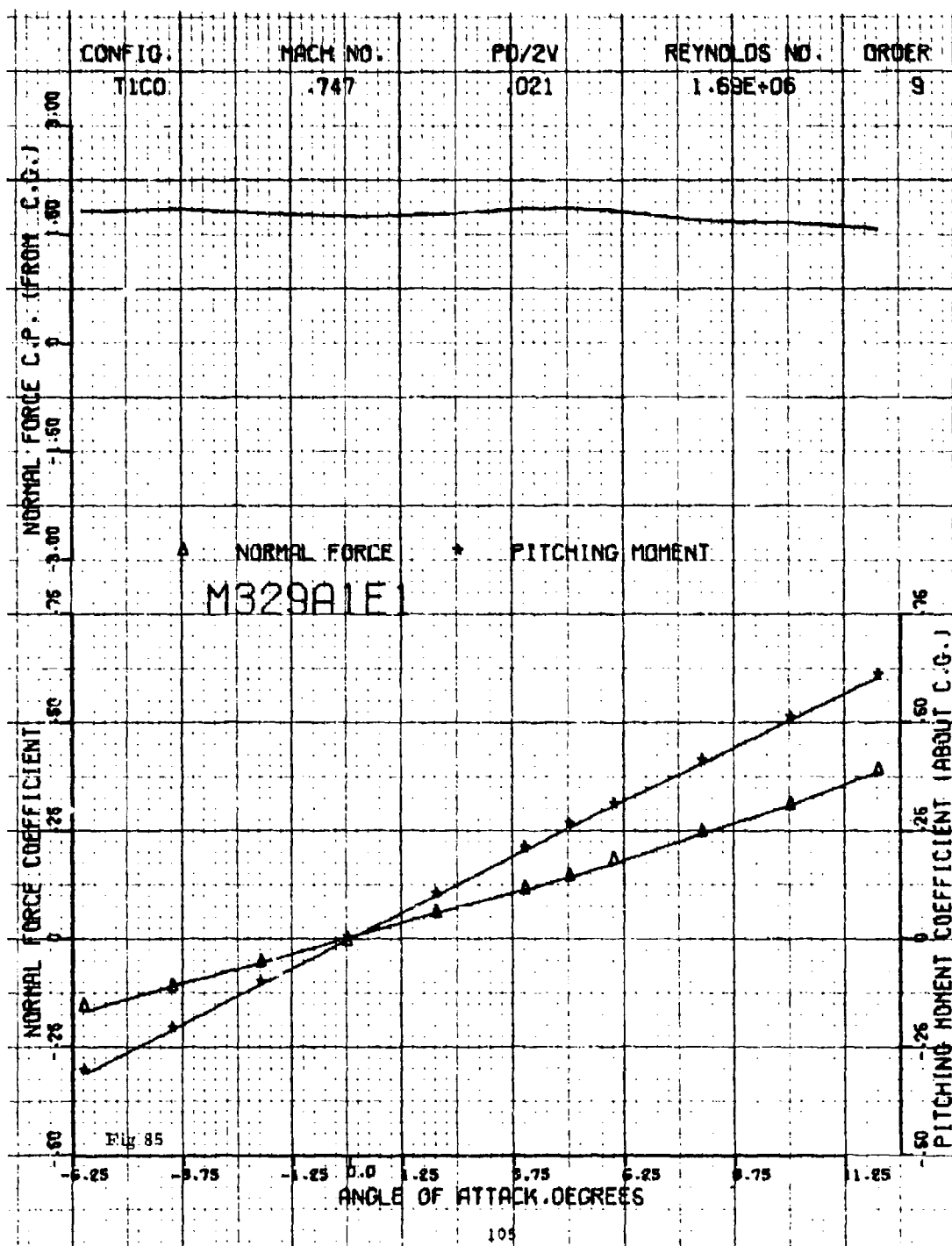


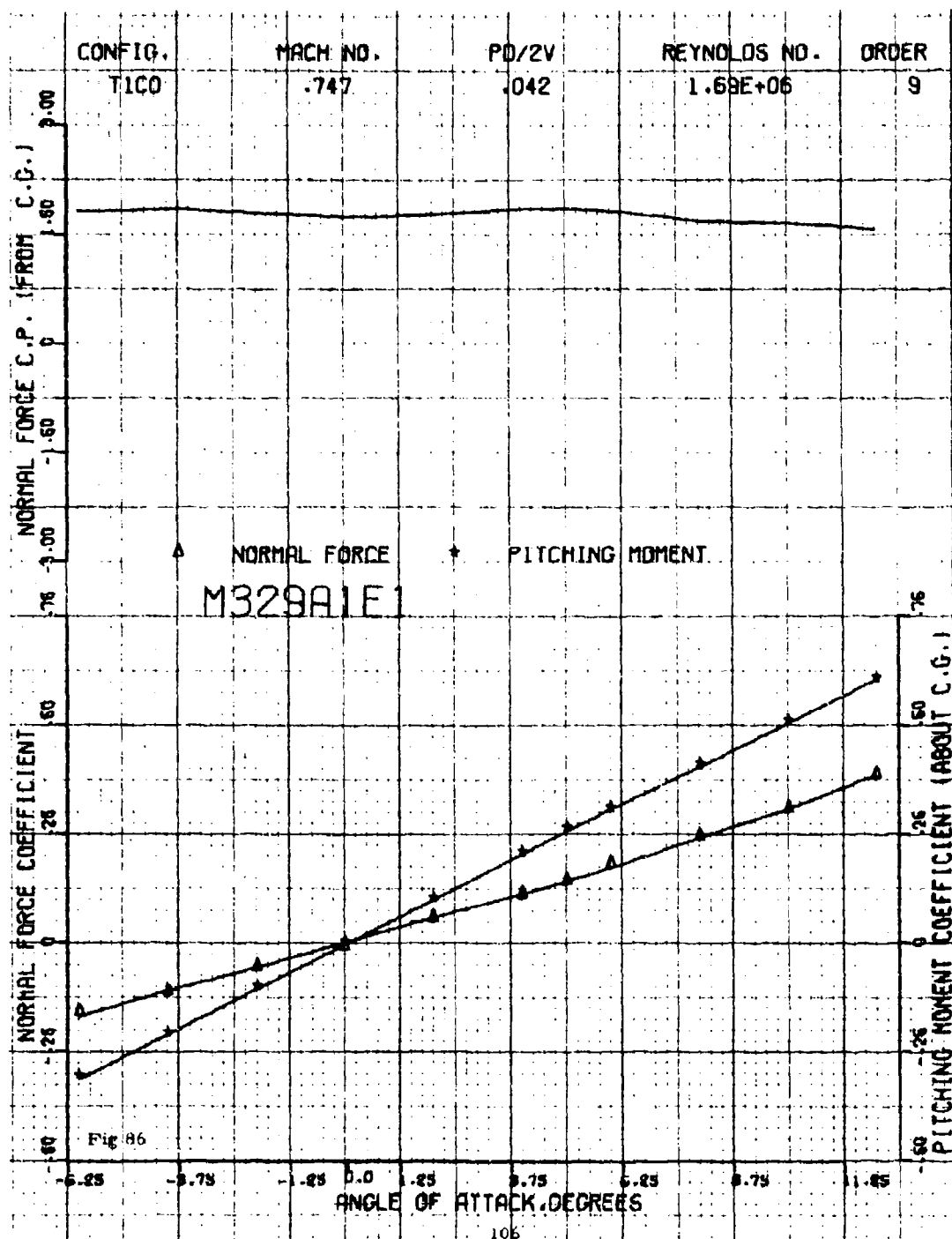


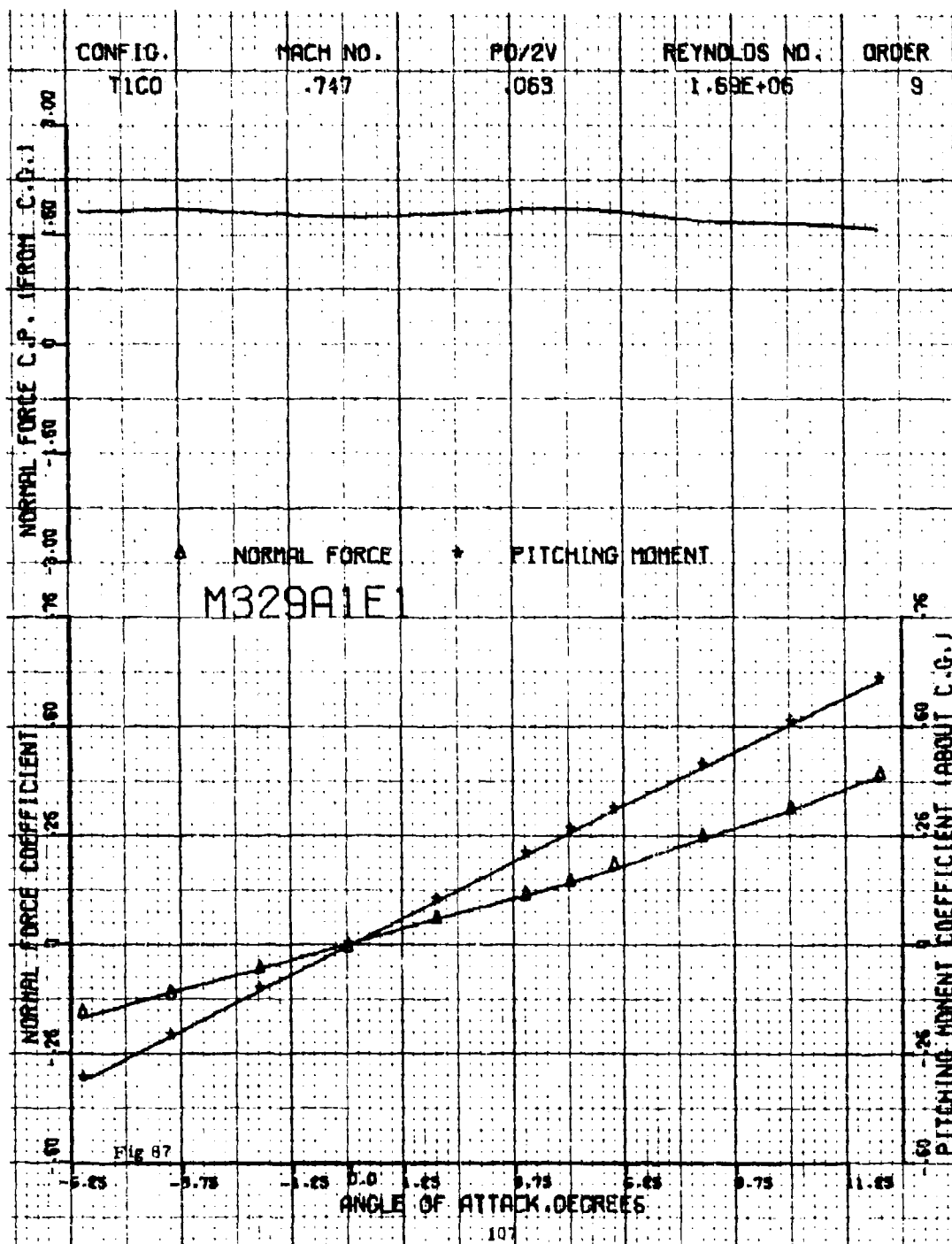


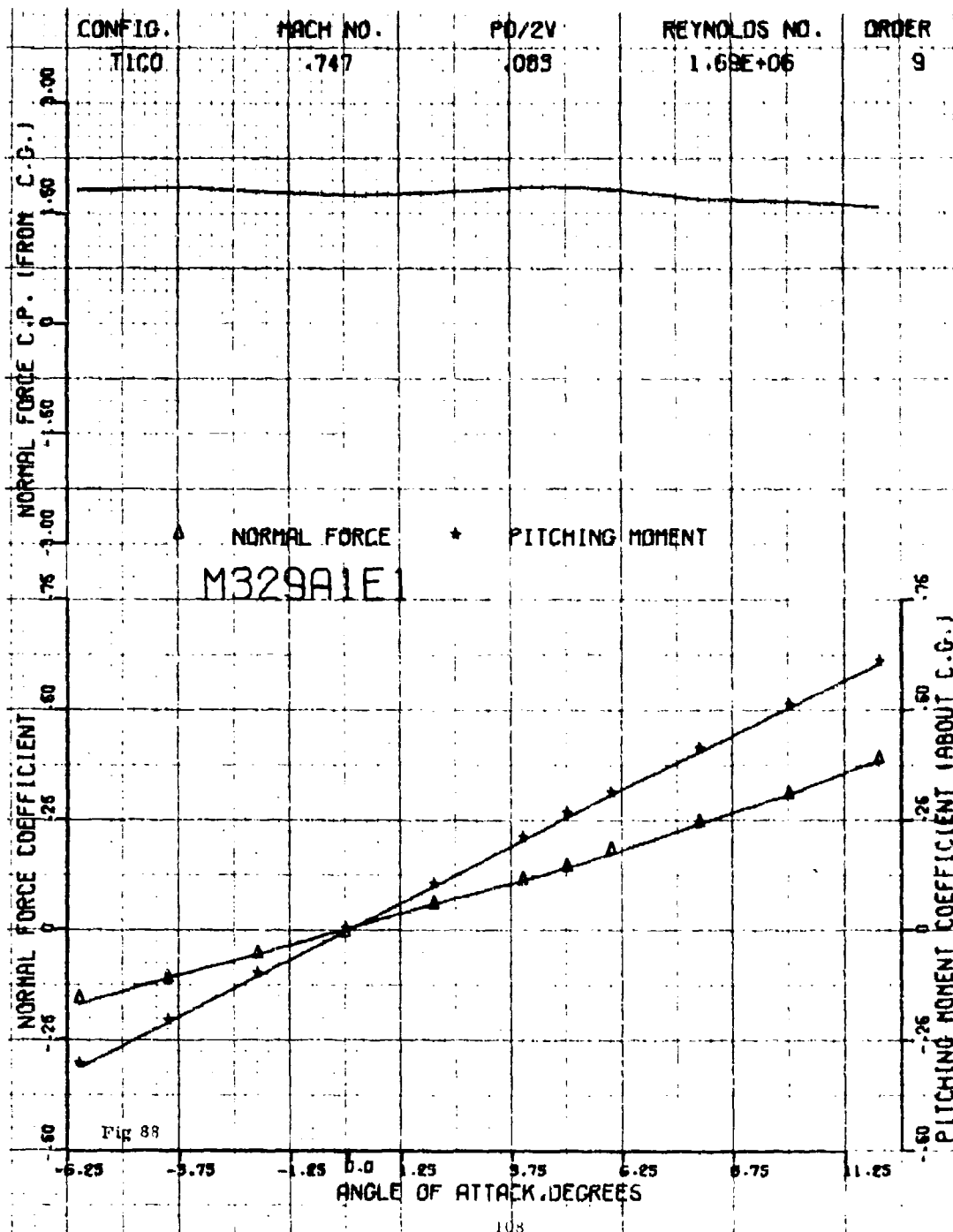


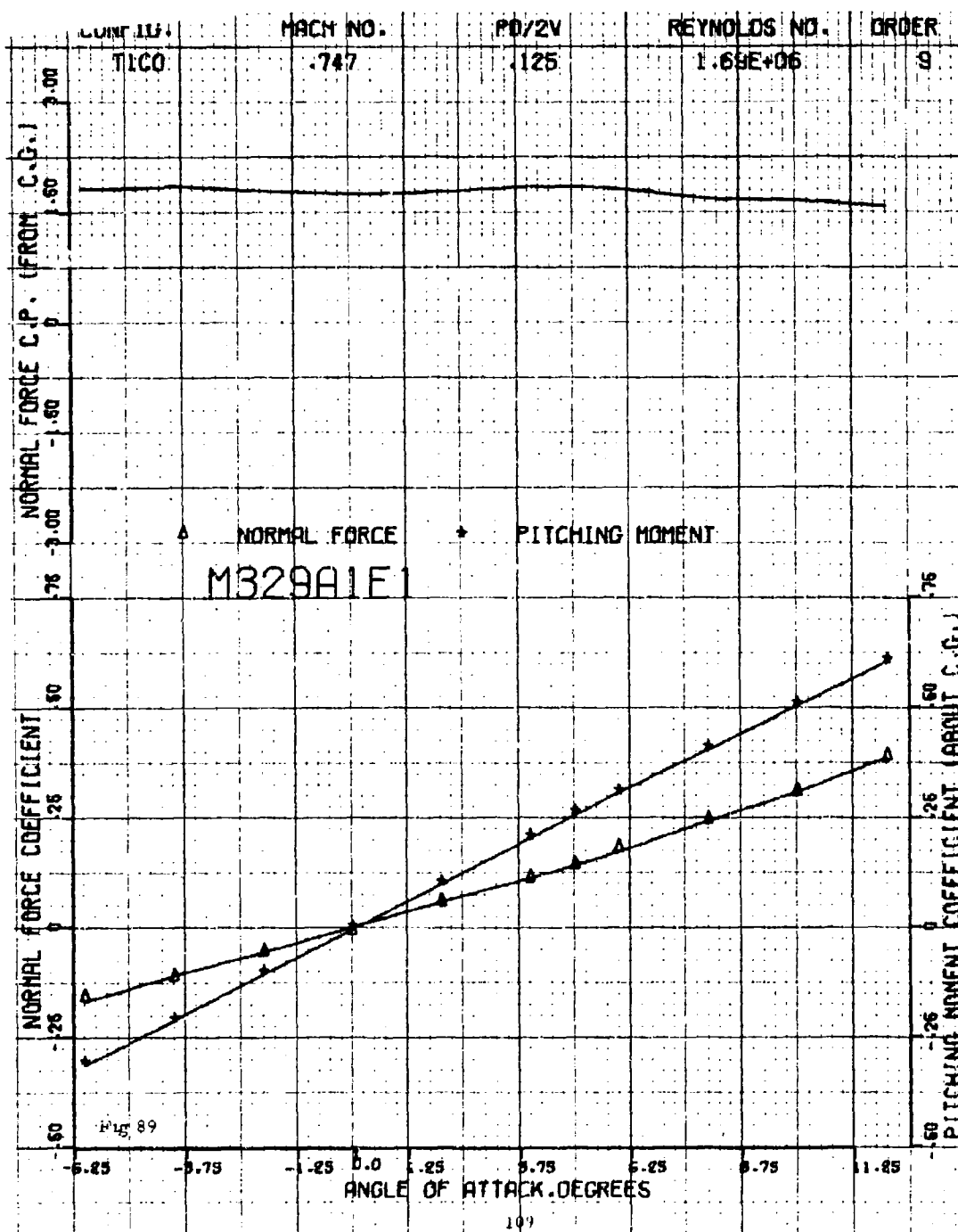


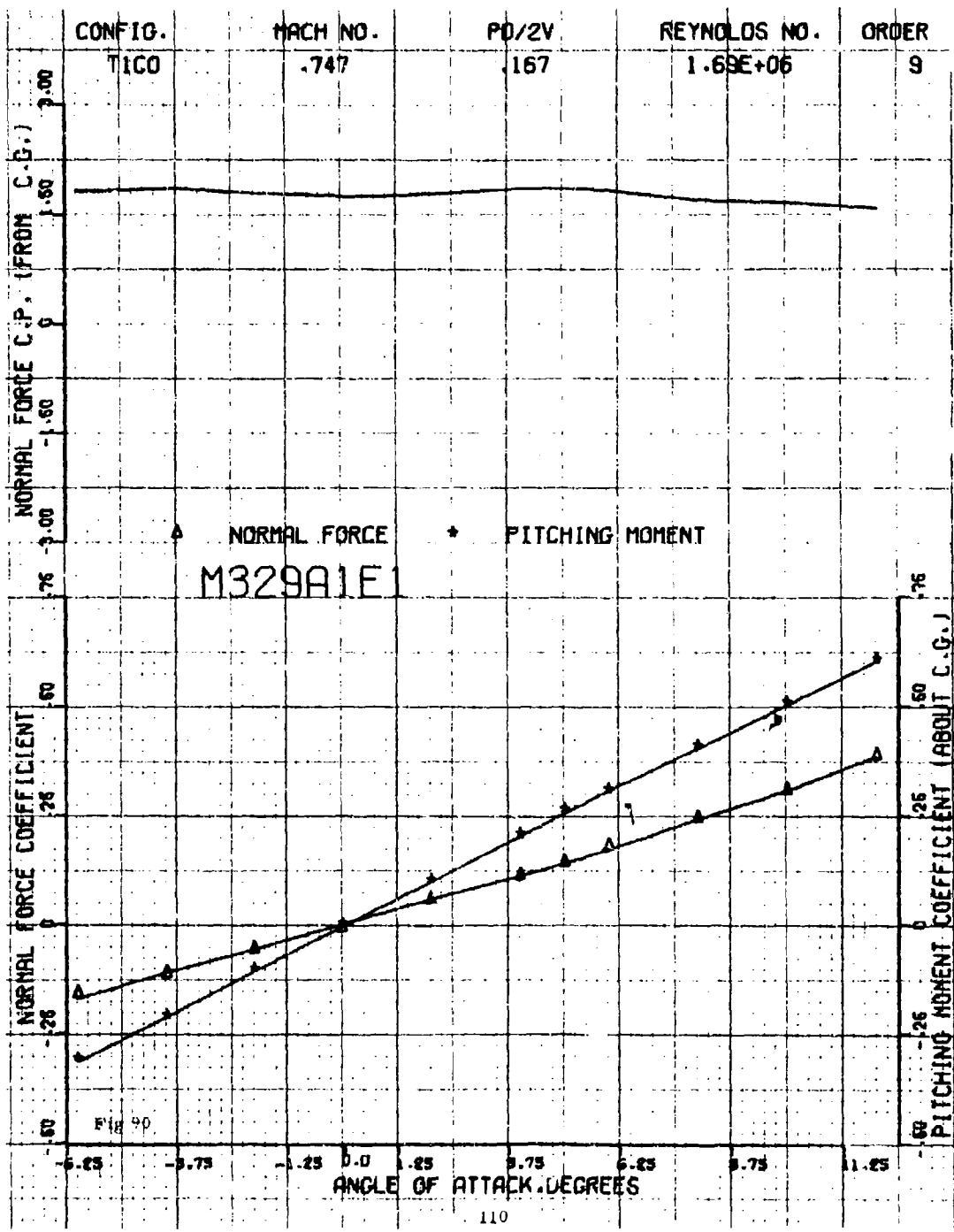


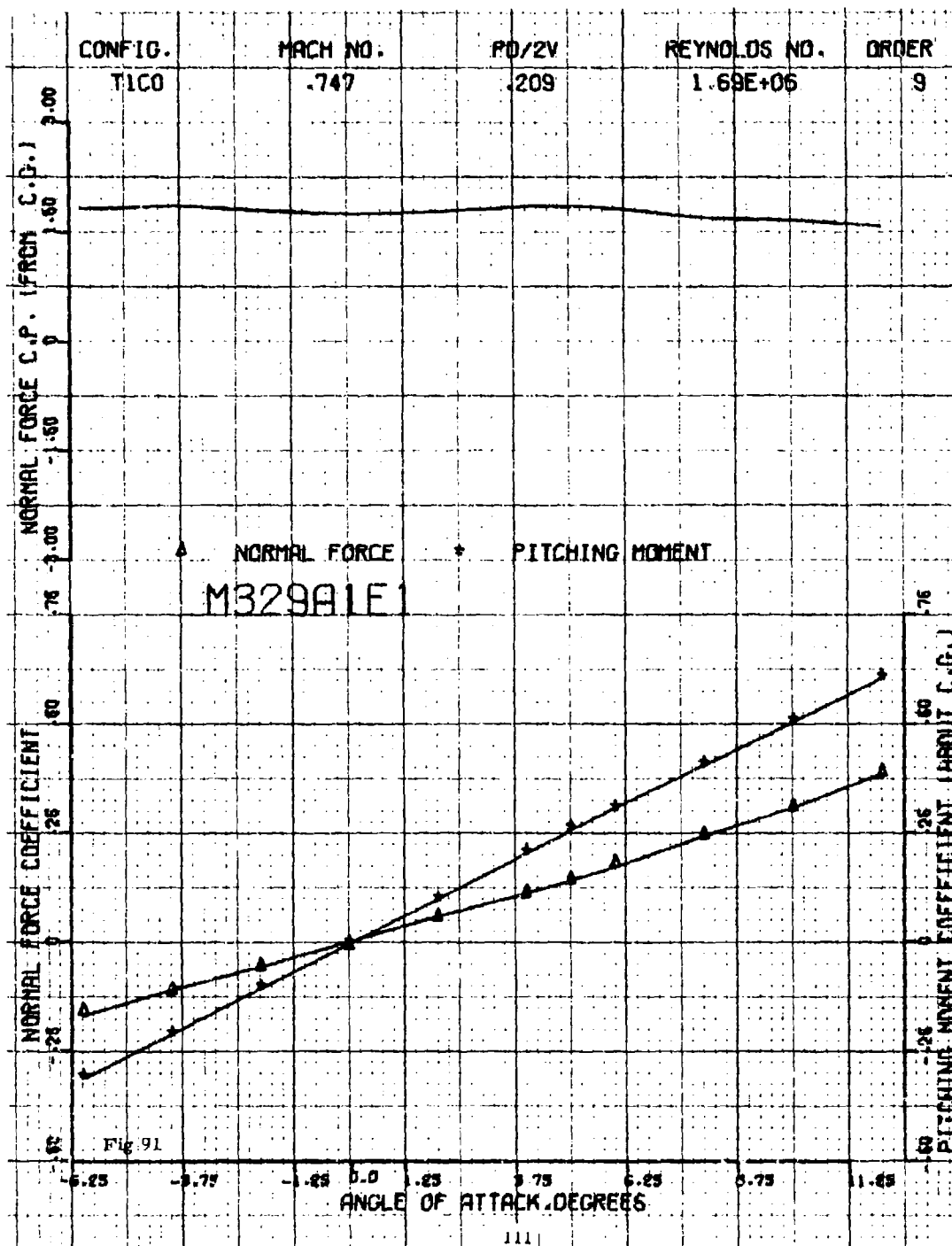


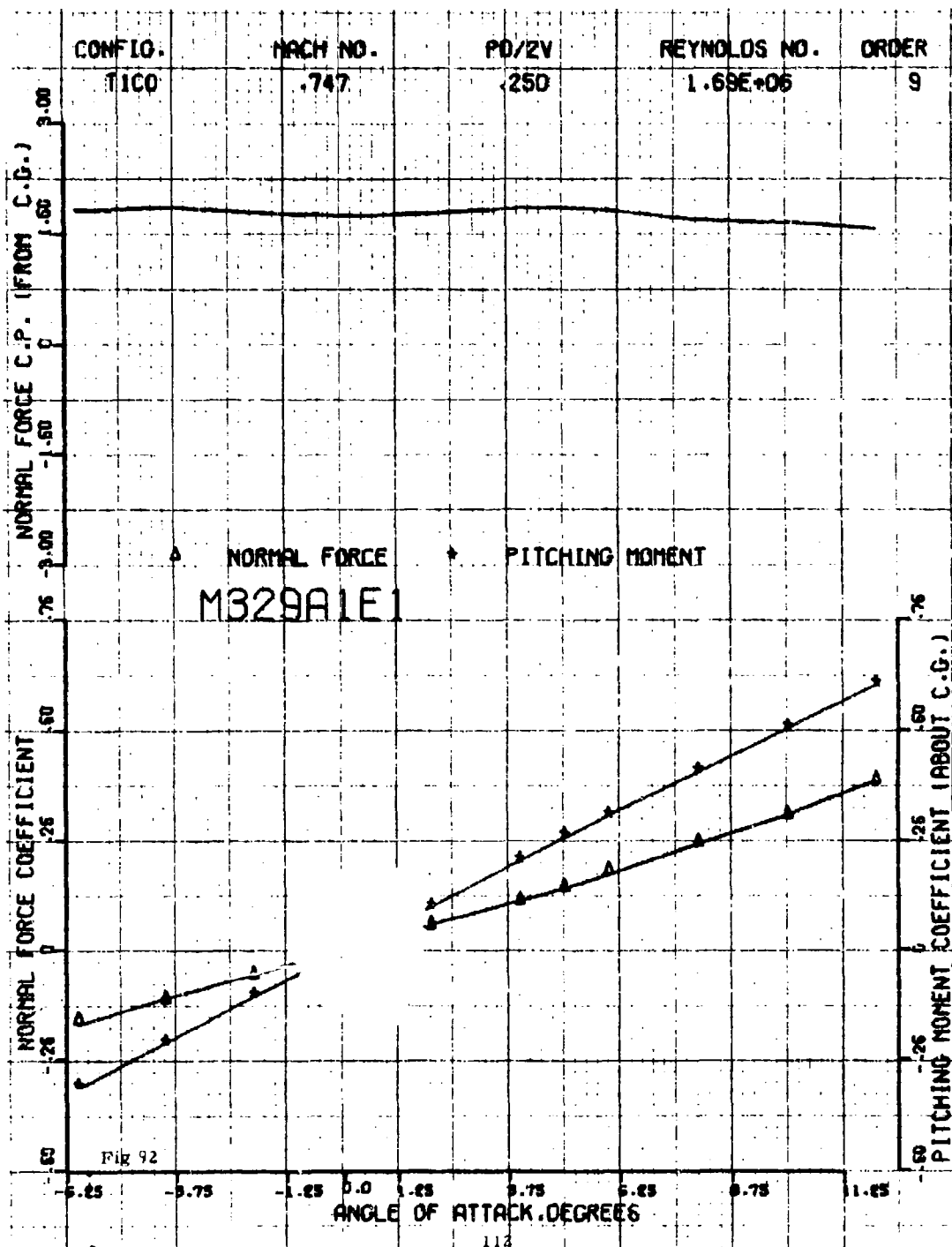


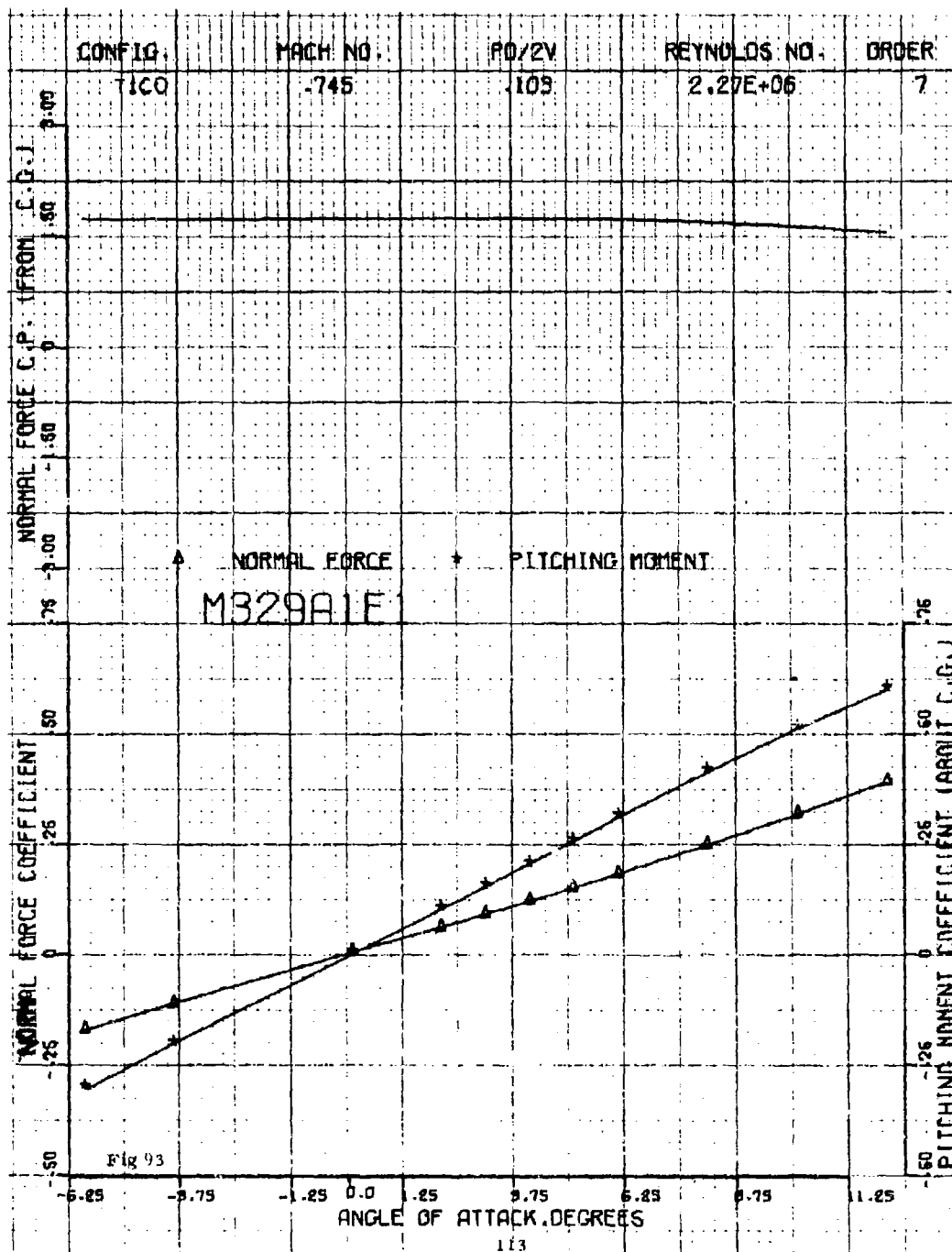


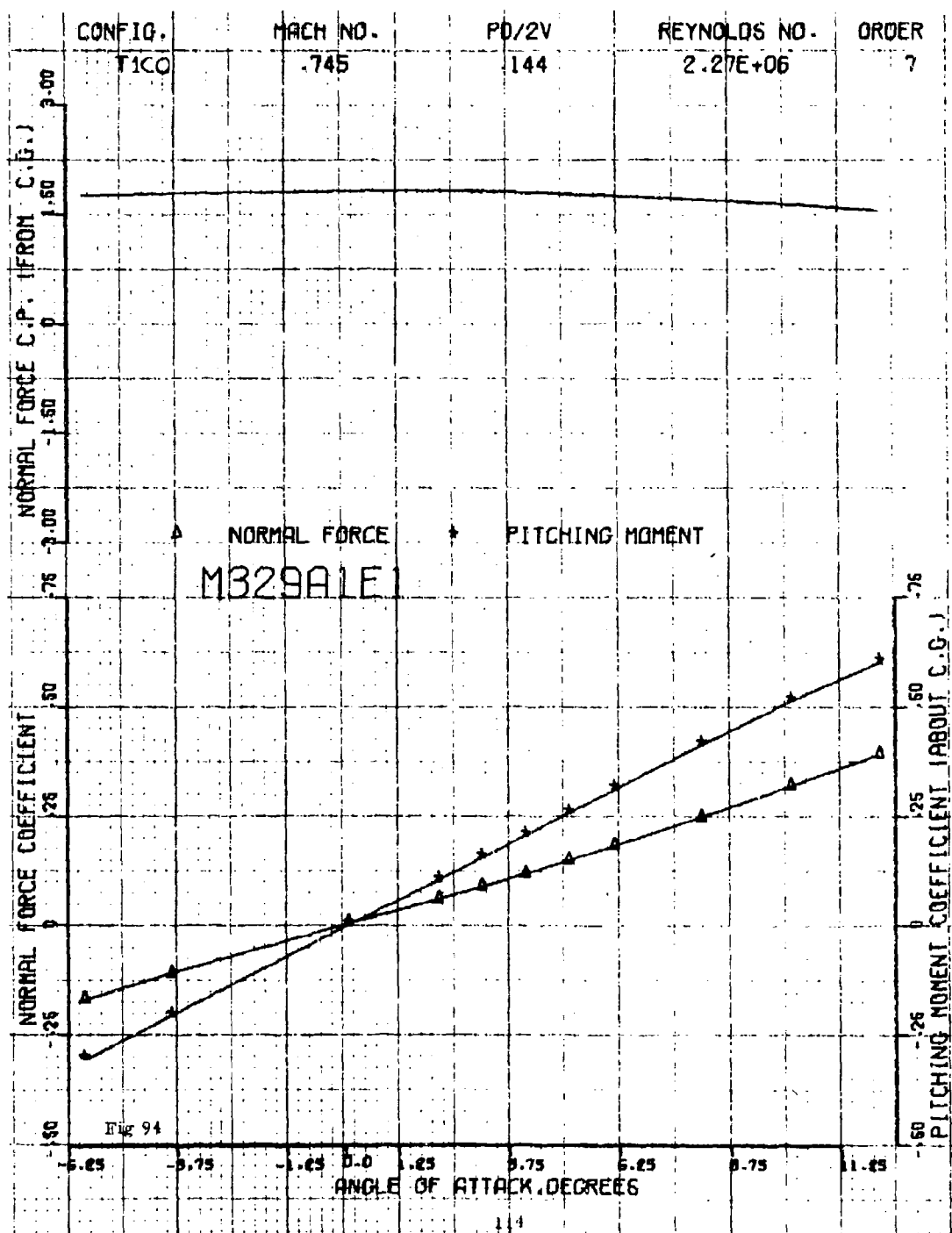


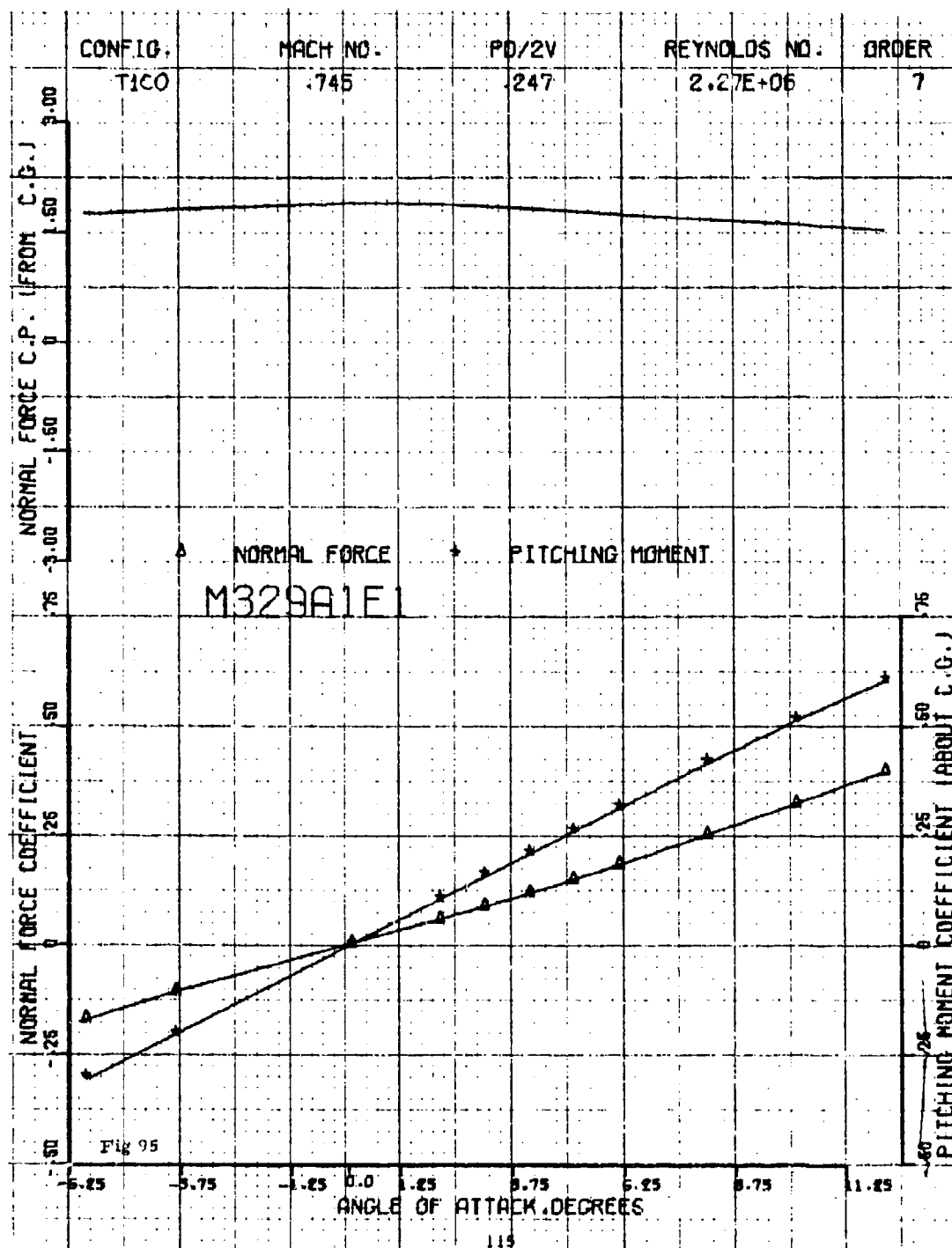


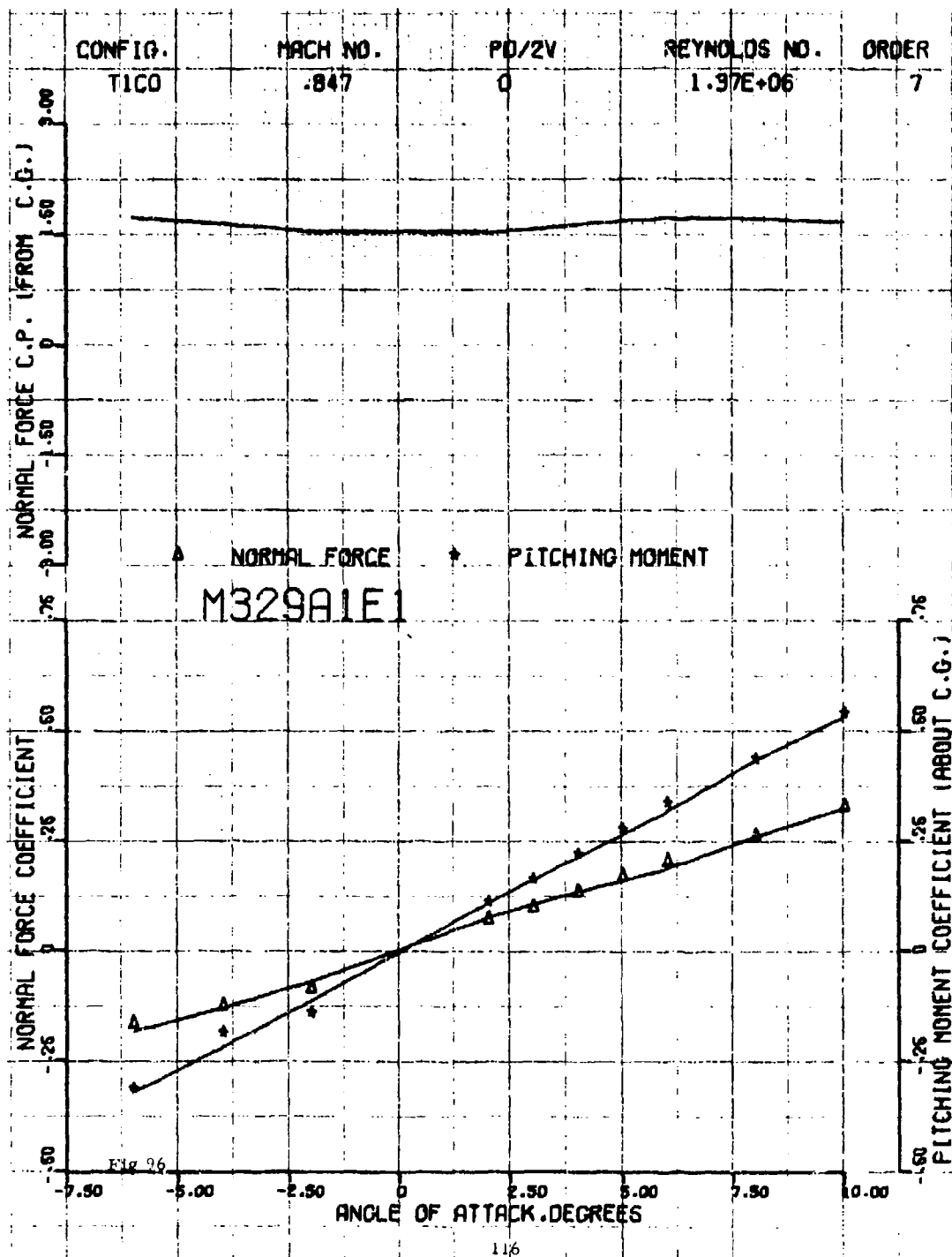


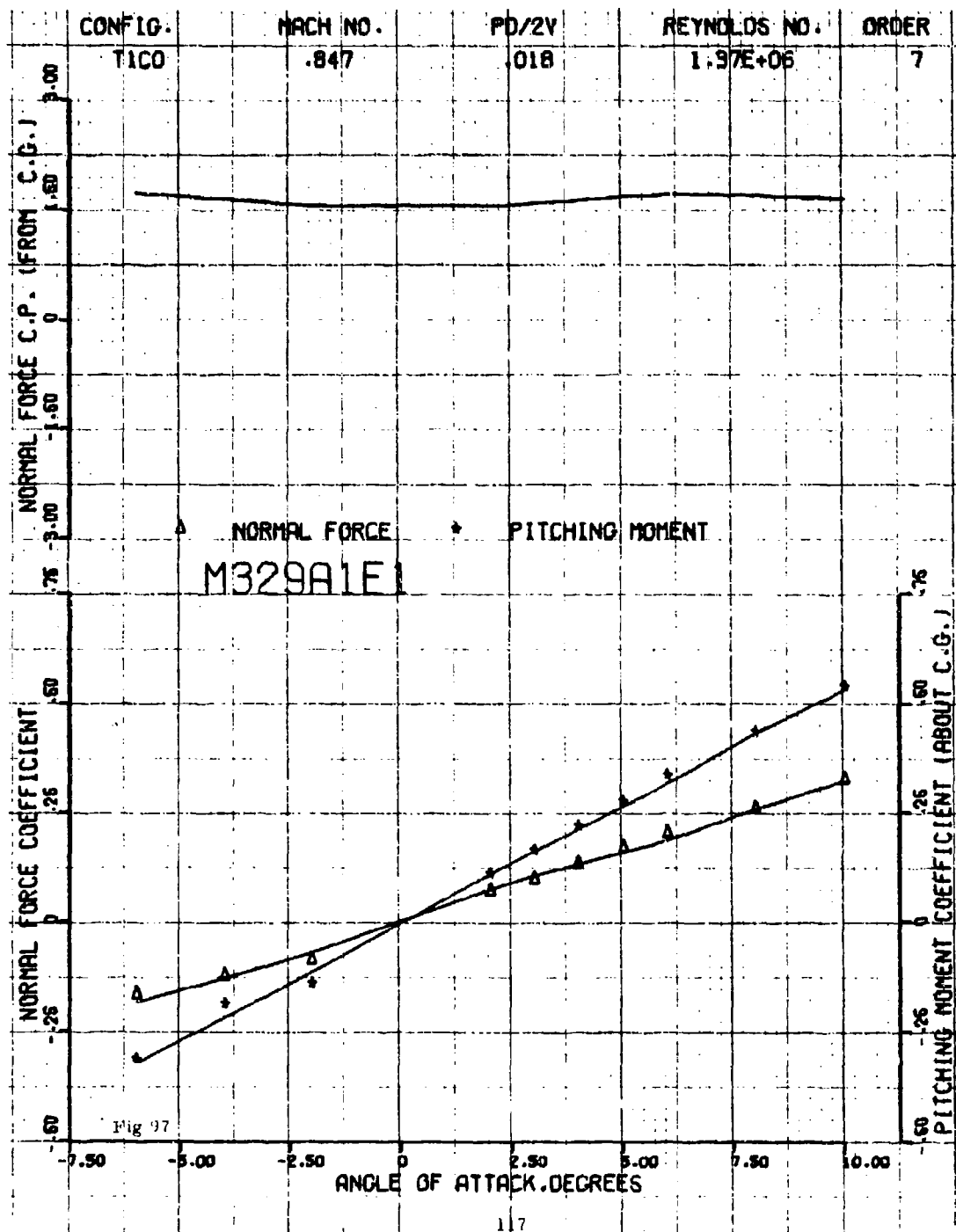












CONFIG.
TICO

MACH NO.
.847

PO/2V
.036

REYNOLDS NO.
1.37E+06

ORDER
7

NORMAL FORCE C.P. (FROM C.G.)

3.00
1.50
0
-1.50
-3.00

▲ NORMAL FORCE

• PITCHING MOMENT

M329A1E1

NORMAL FORCE COEFFICIENT

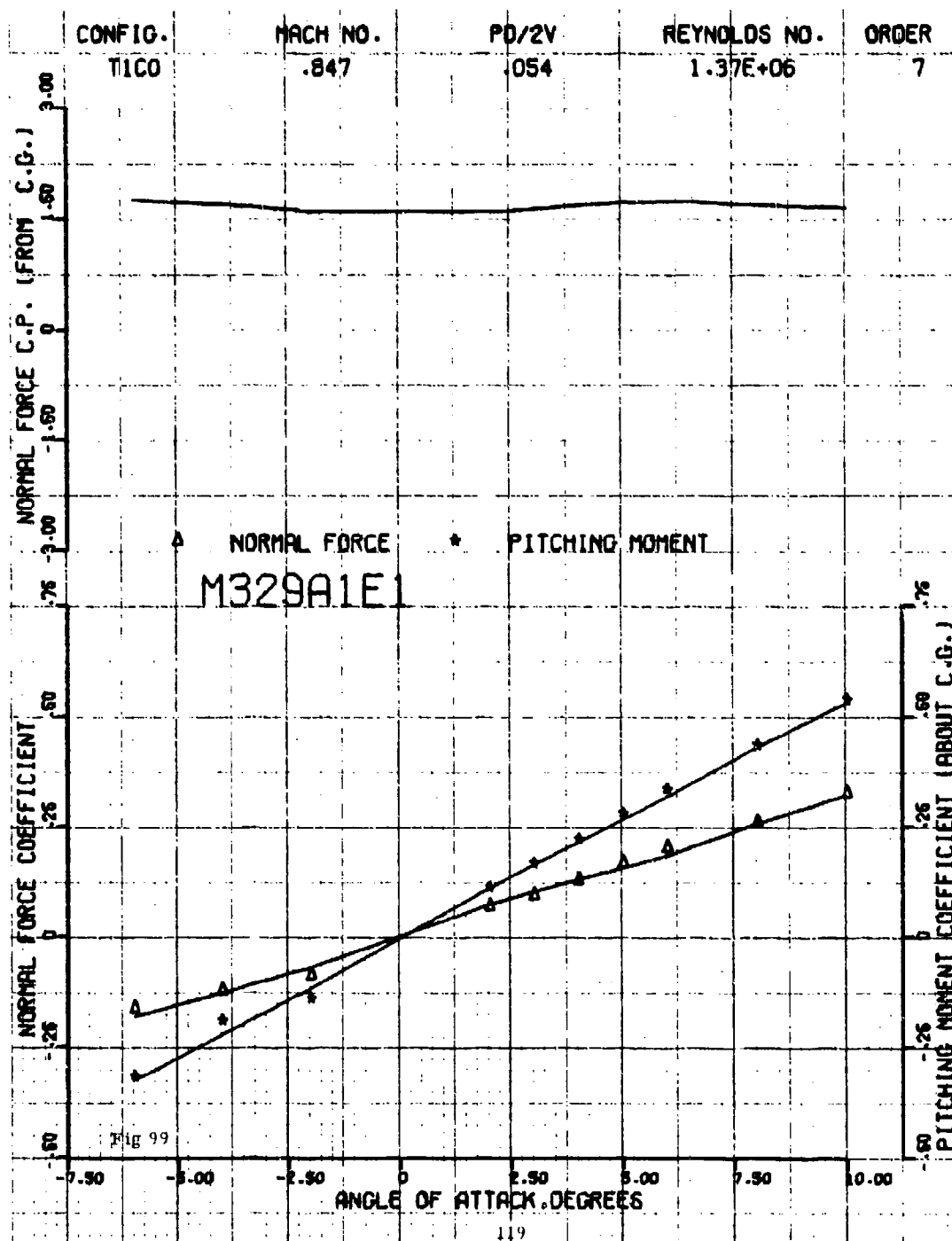
.50
.25
0
-.25
-.50

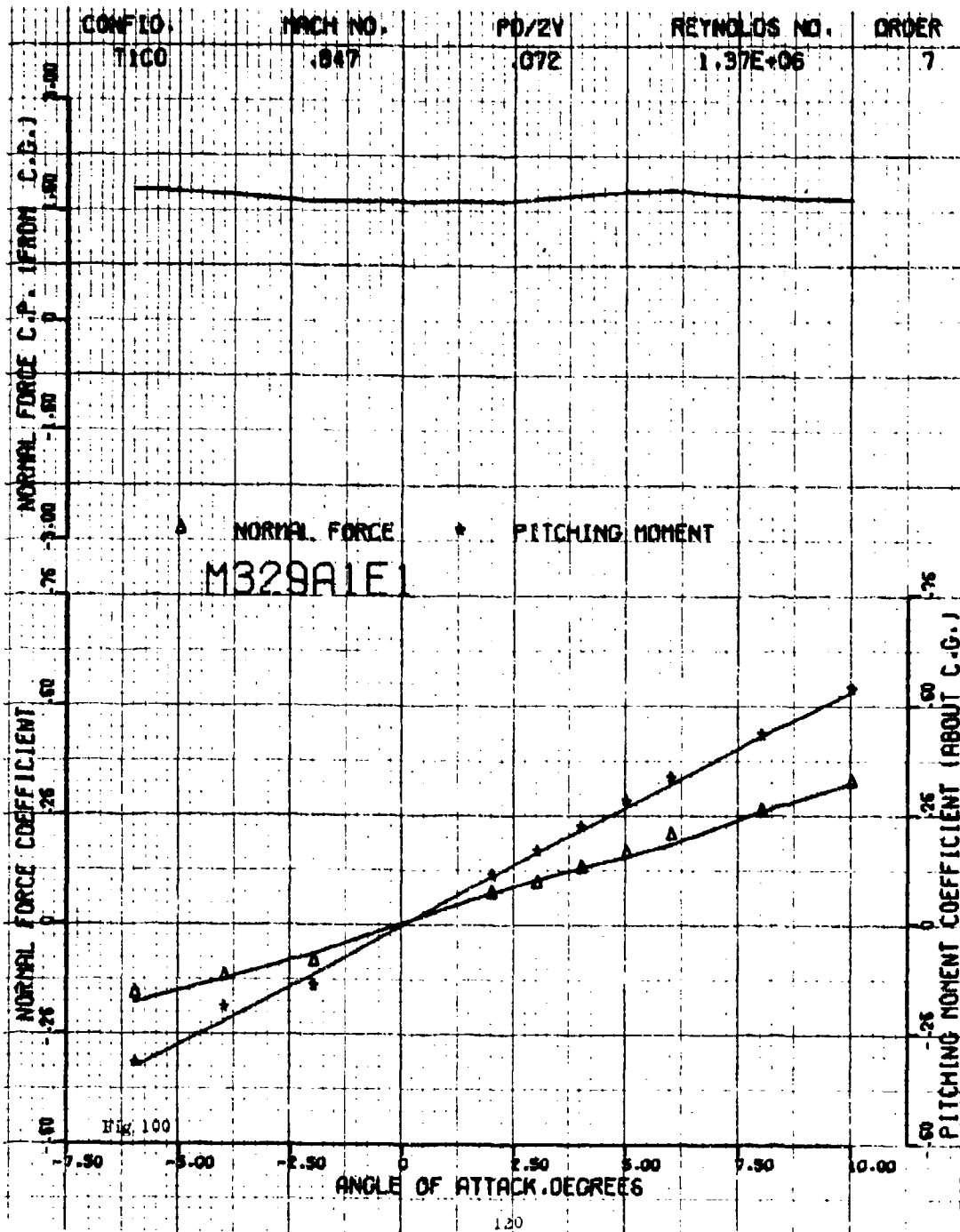
Fig 98

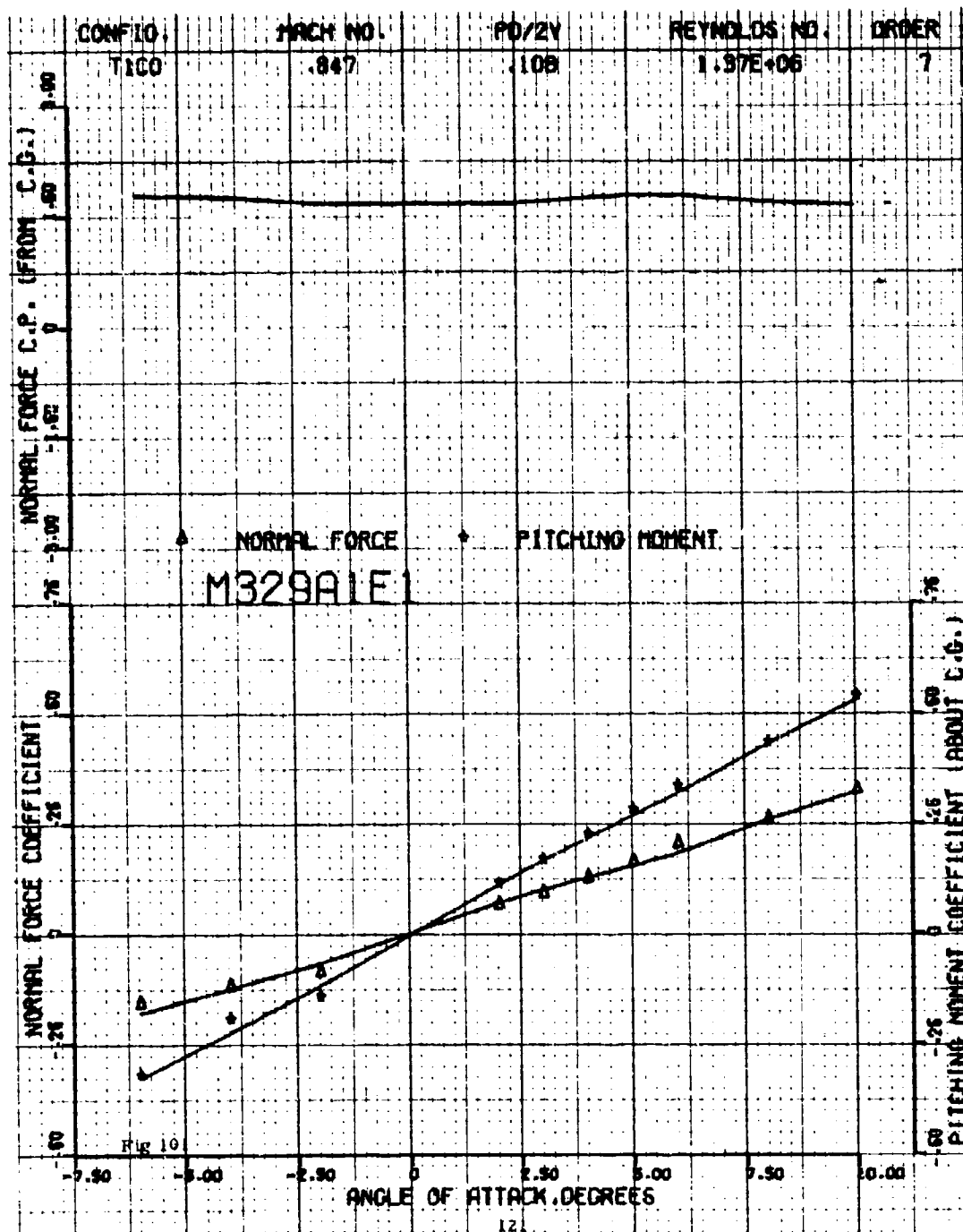
ANGLE OF ATTACK, DEGREES

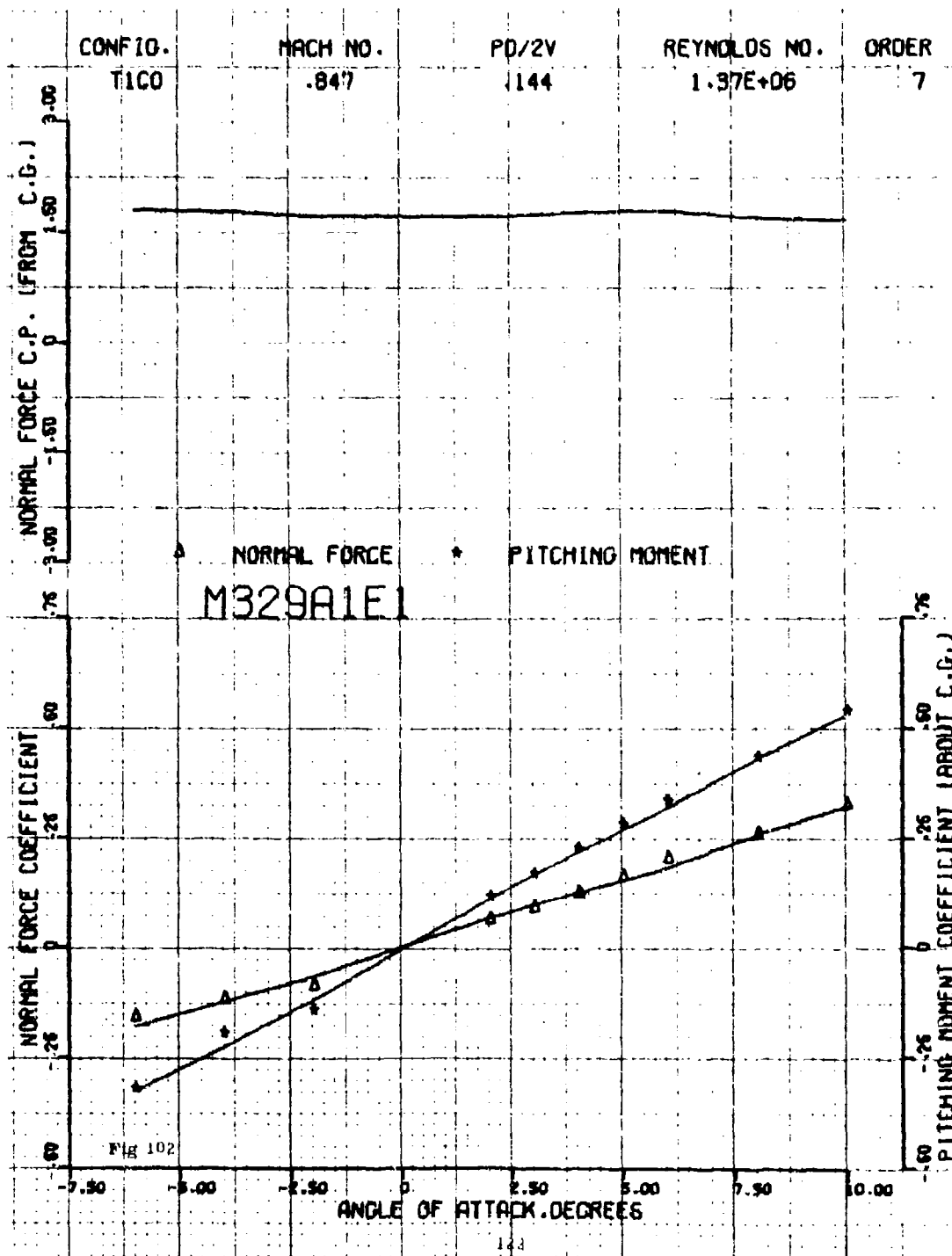
PITCHING MOMENT COEFFICIENT (ABOUT C.G.)

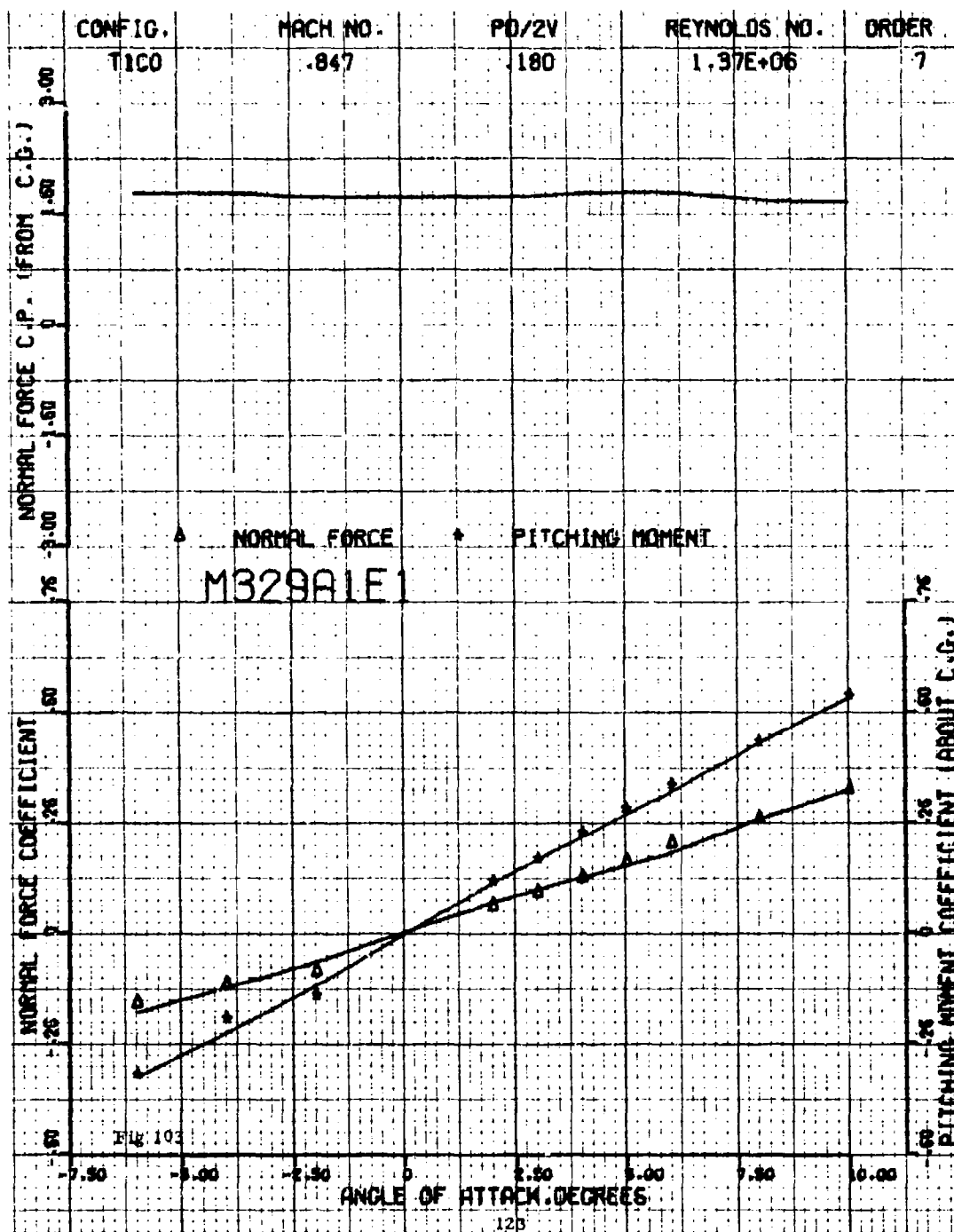
.75
.50
.25
0
-.25
-.50

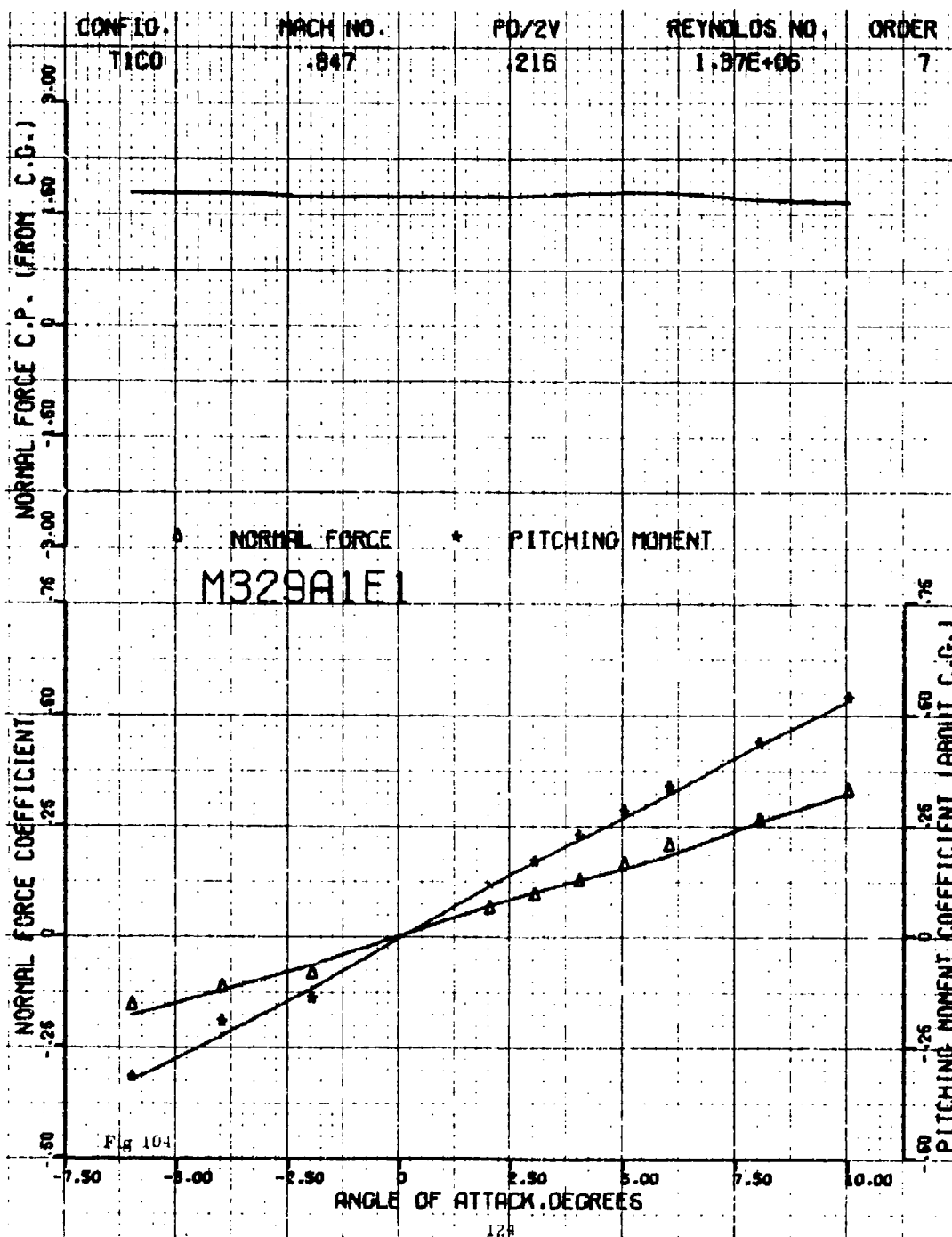


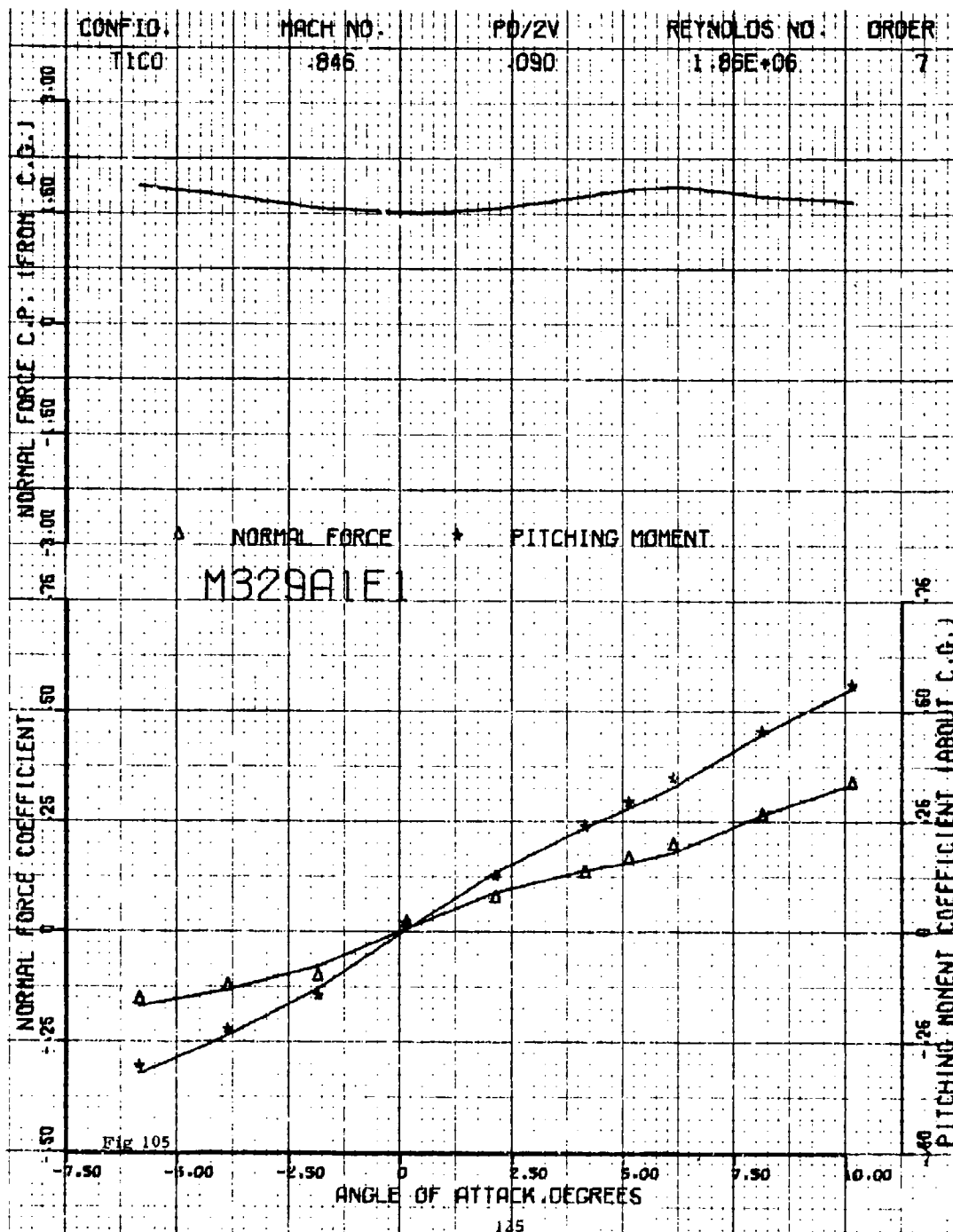


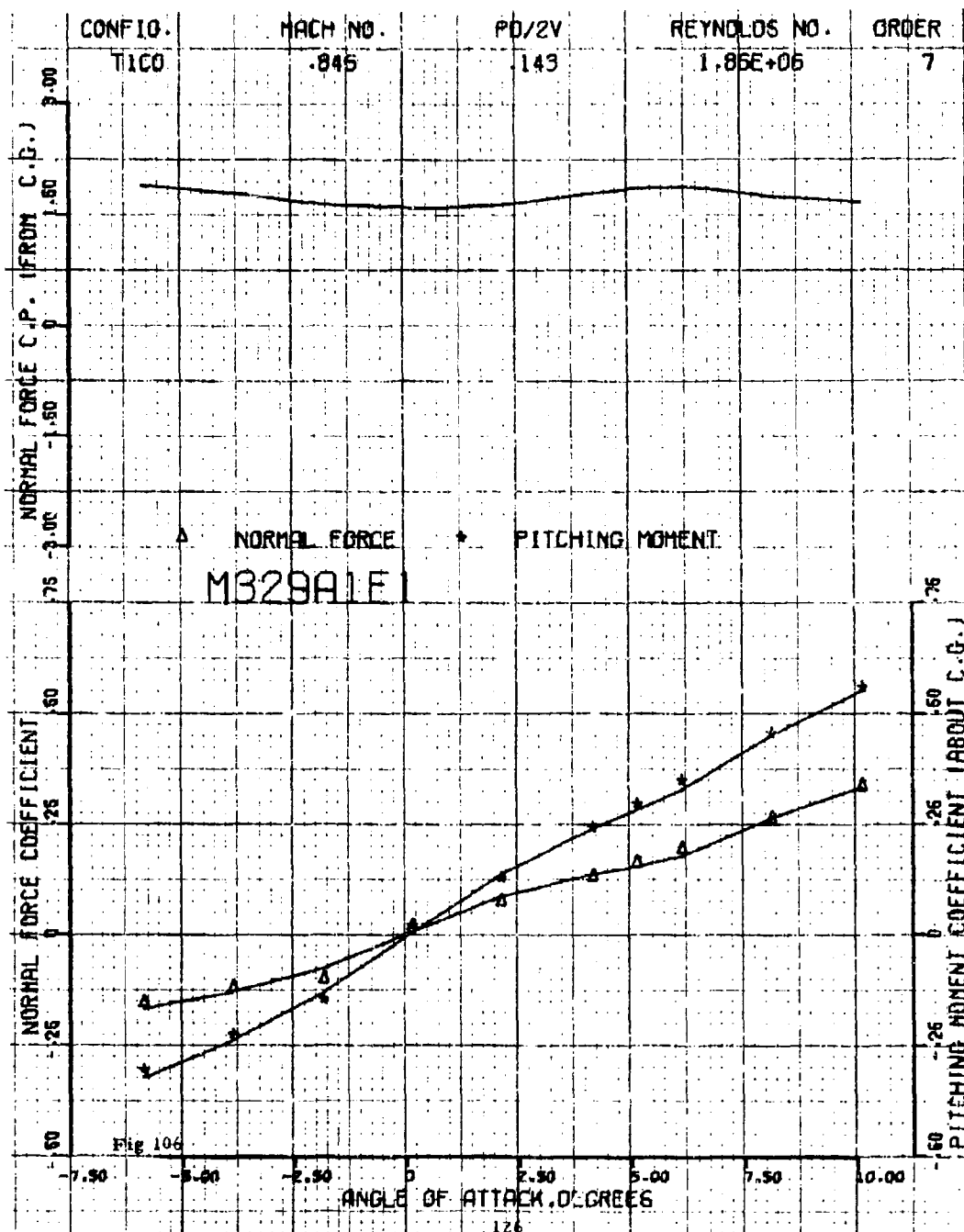


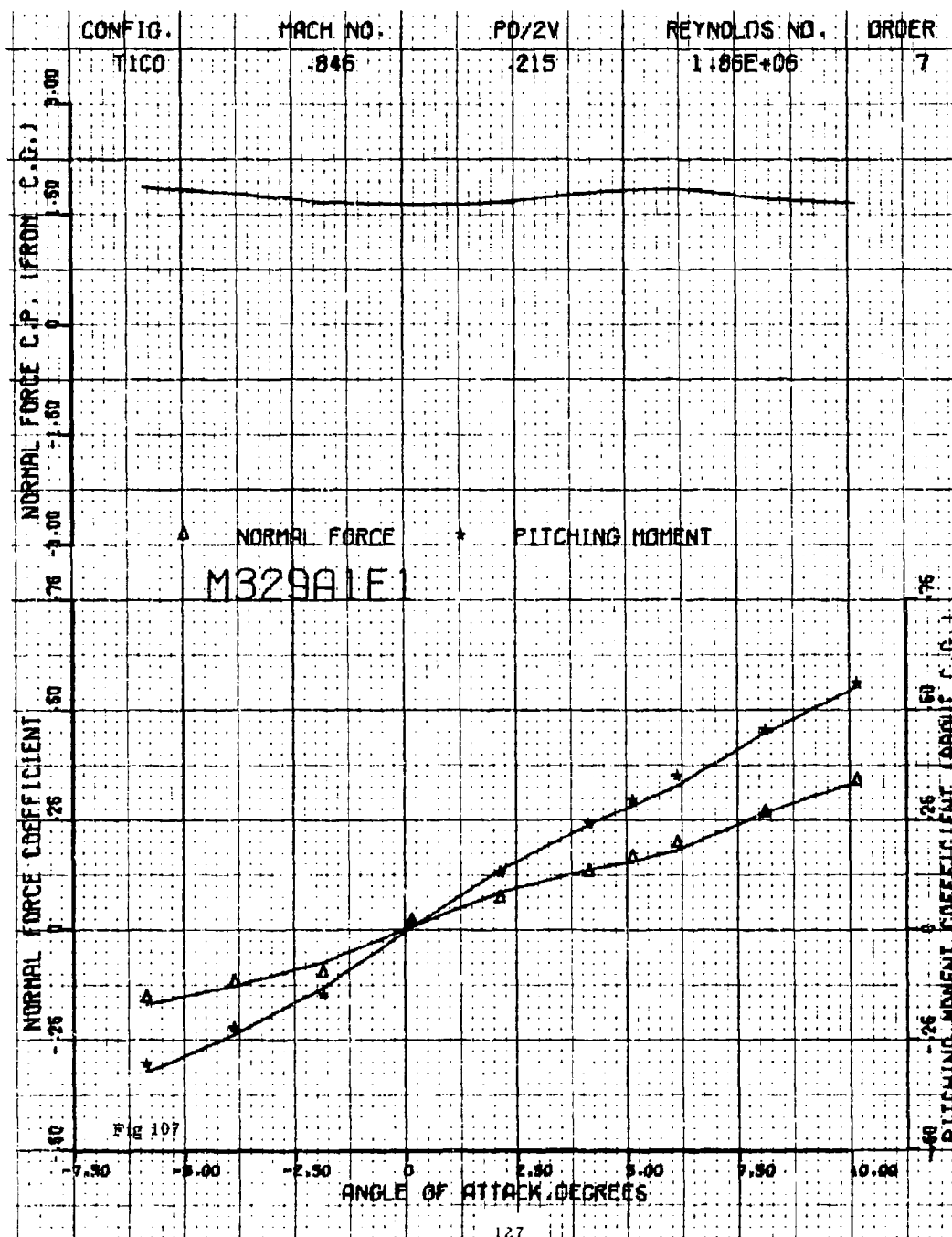


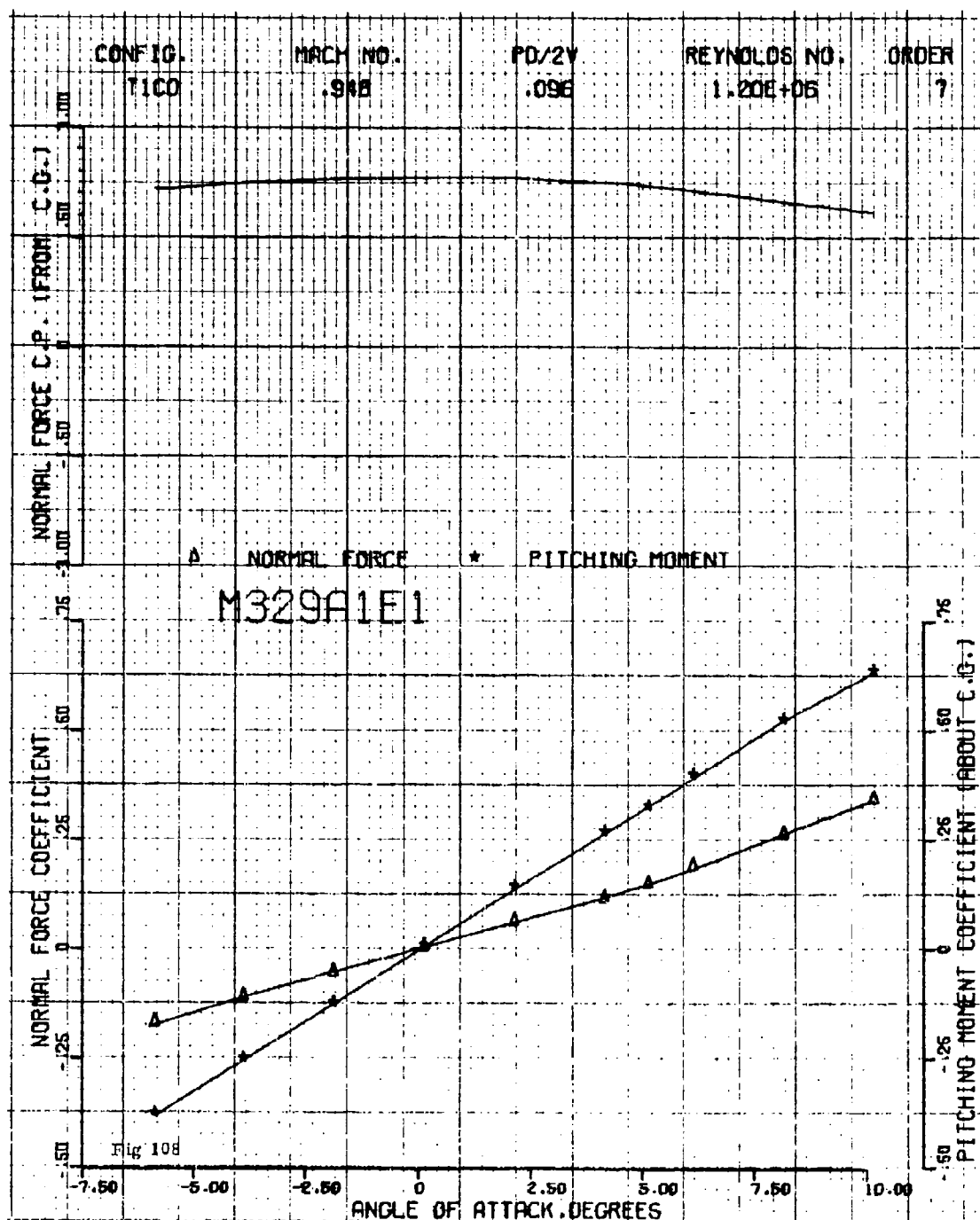


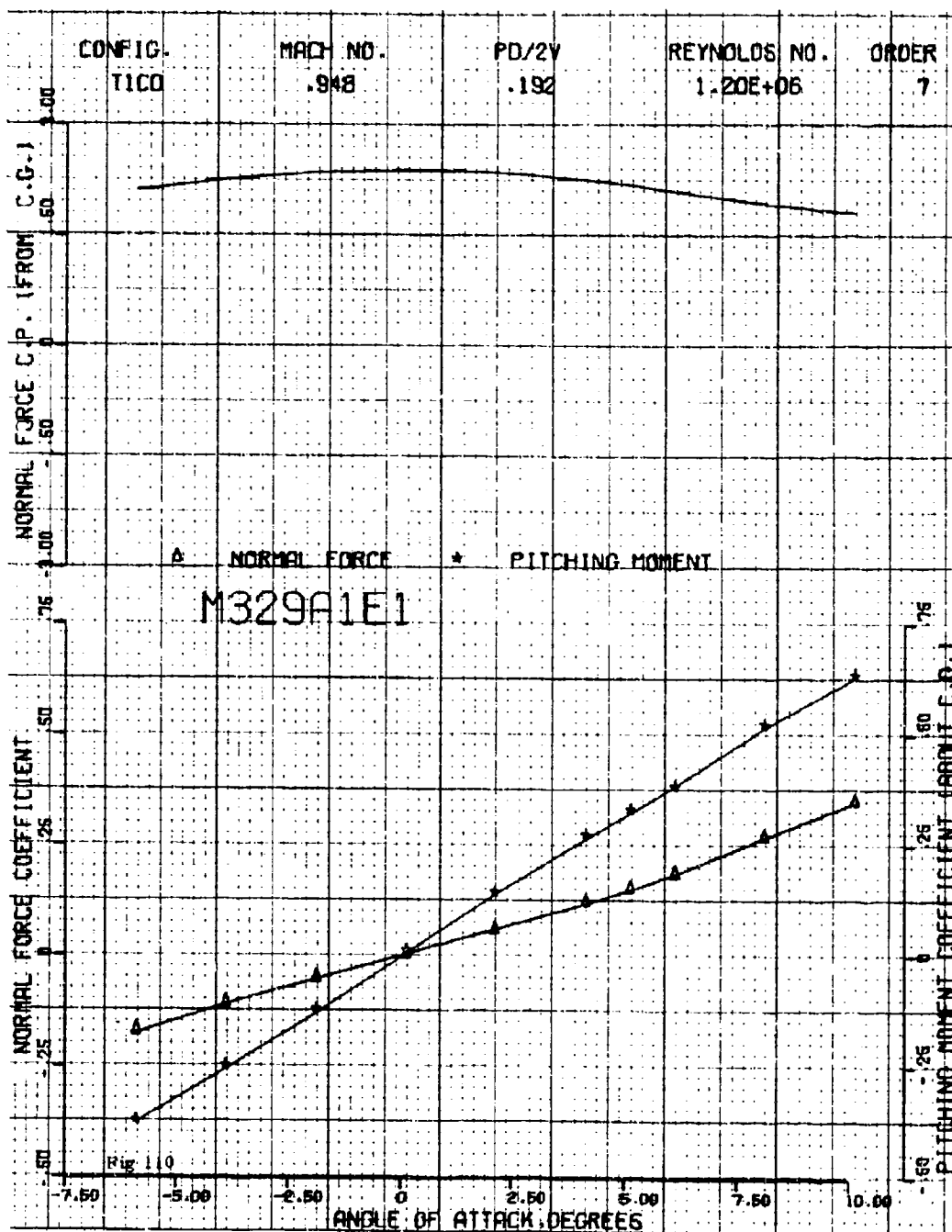


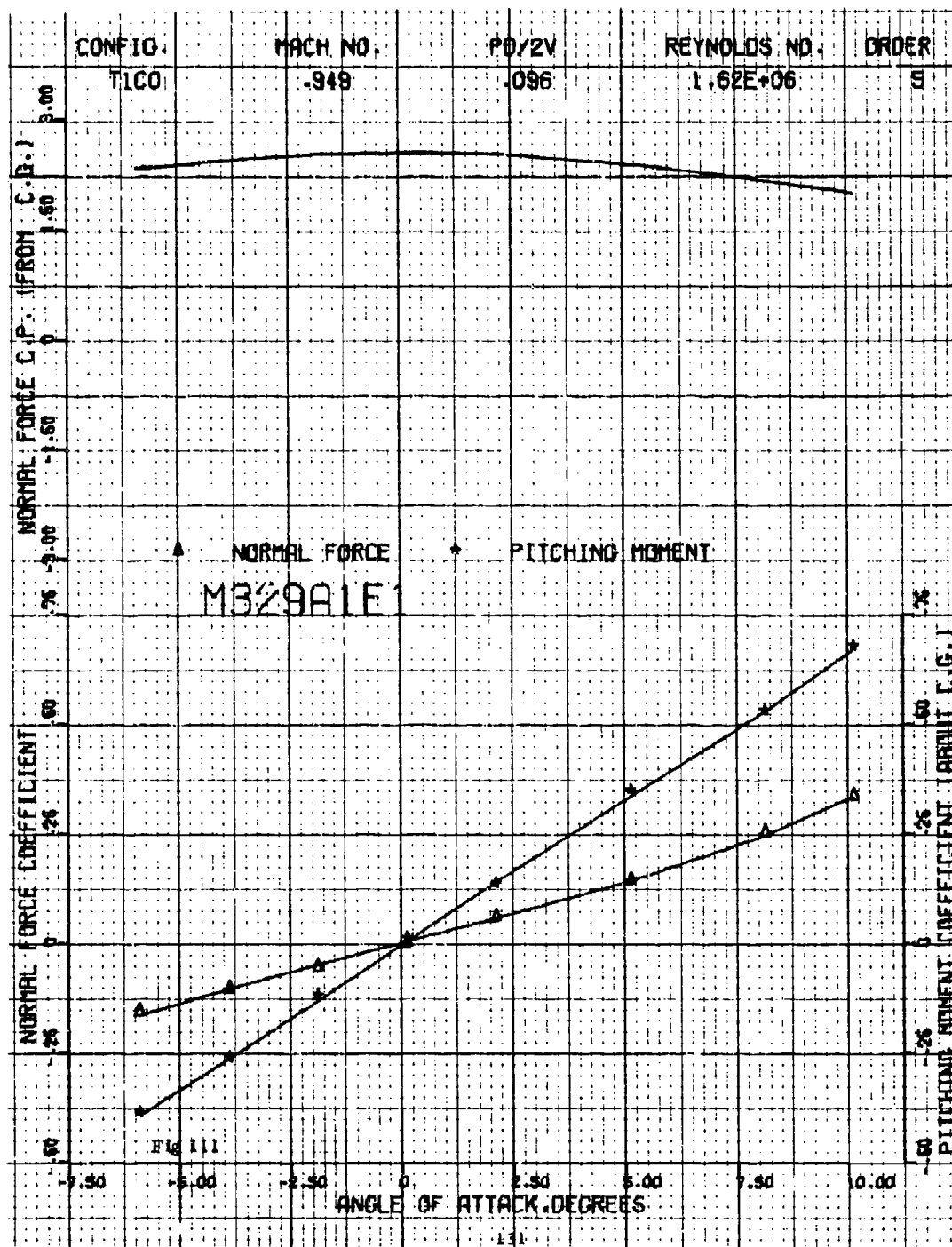


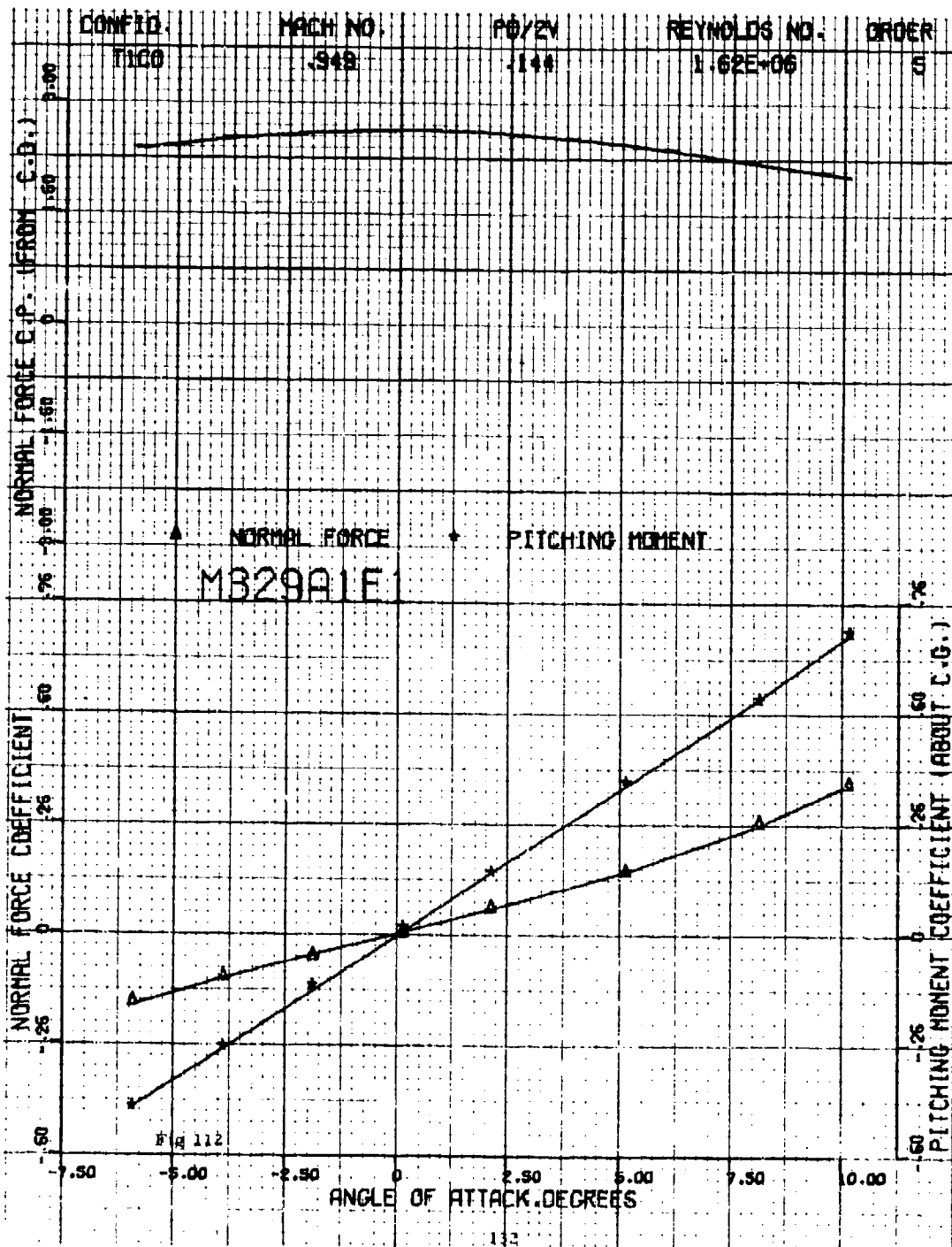


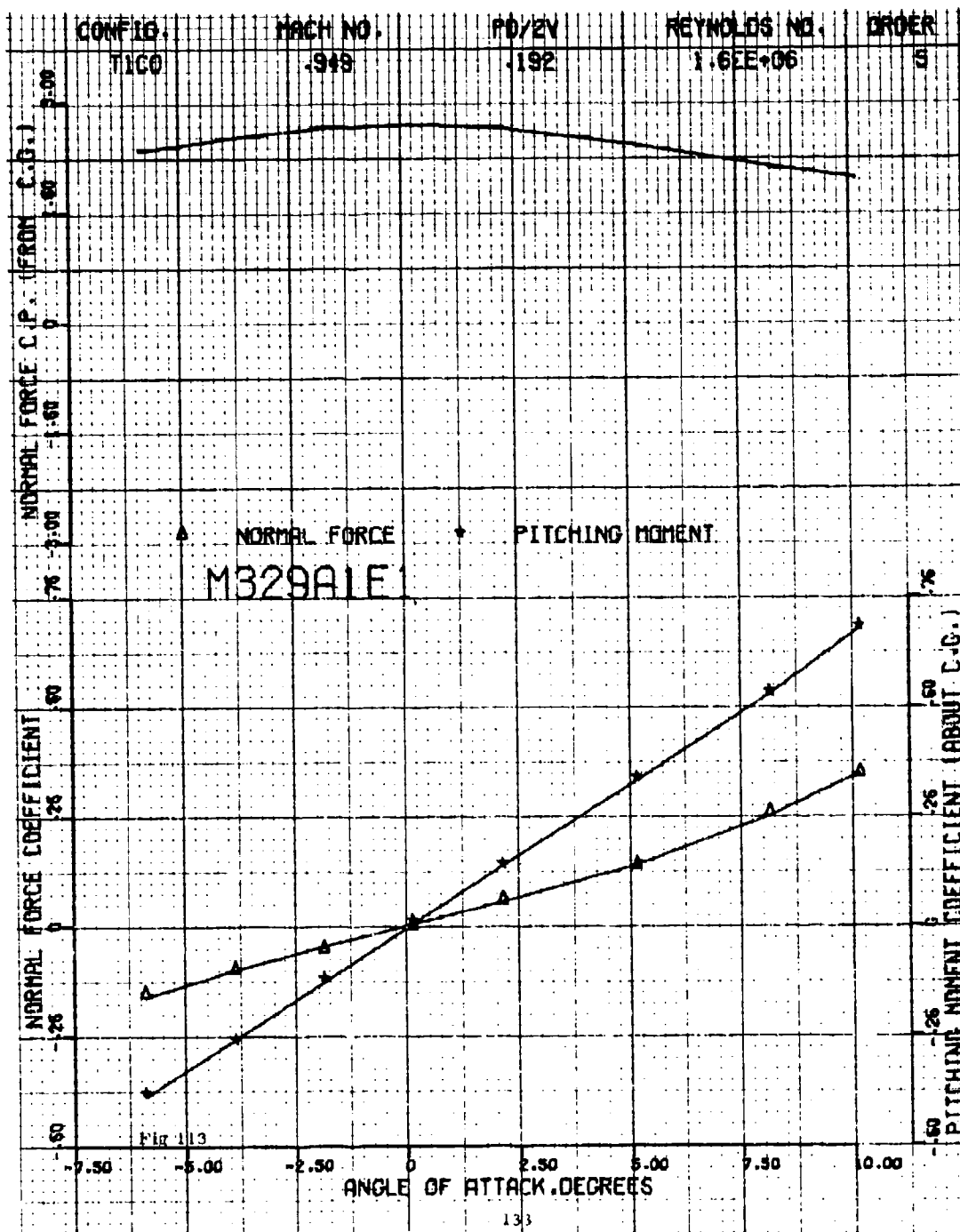


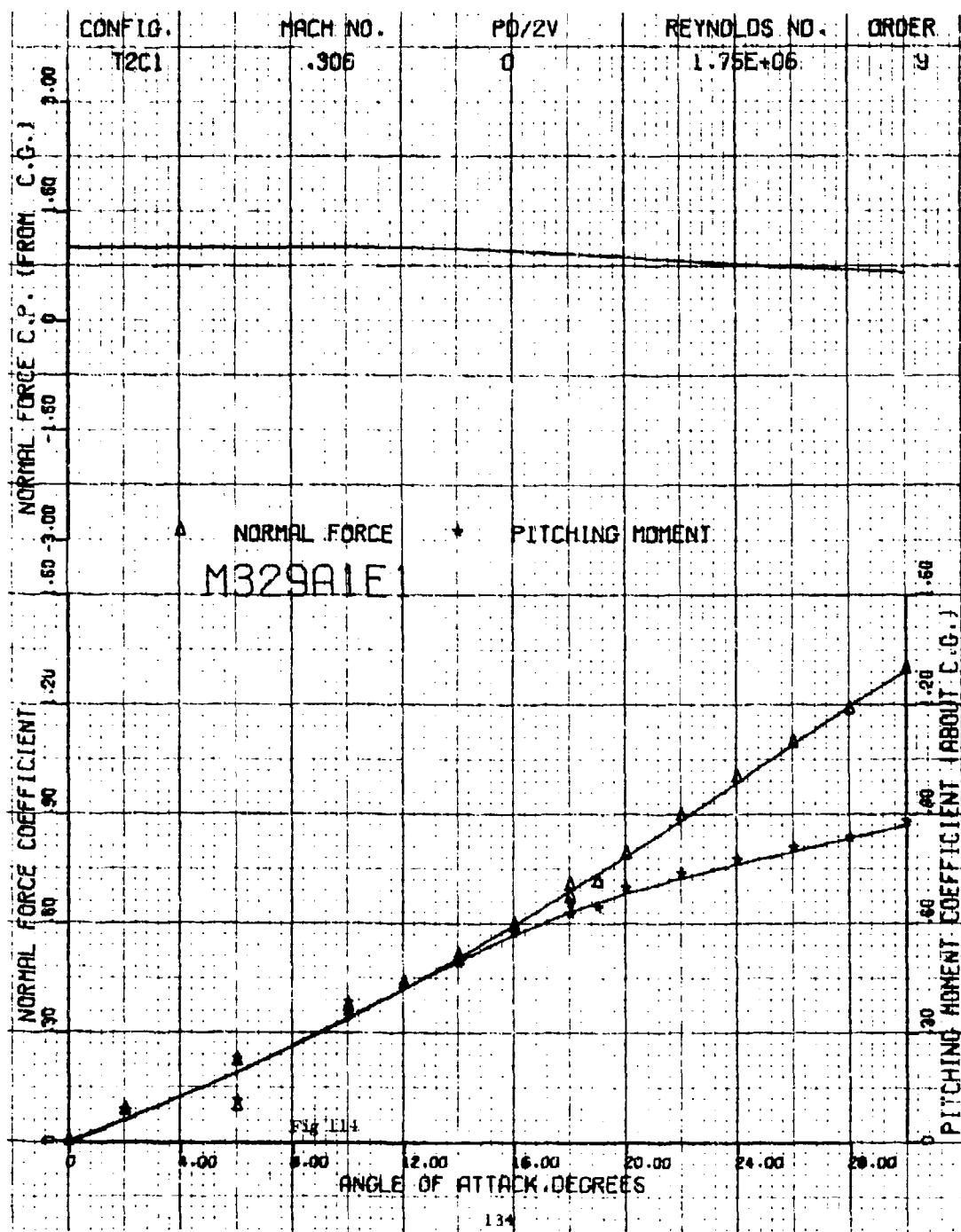


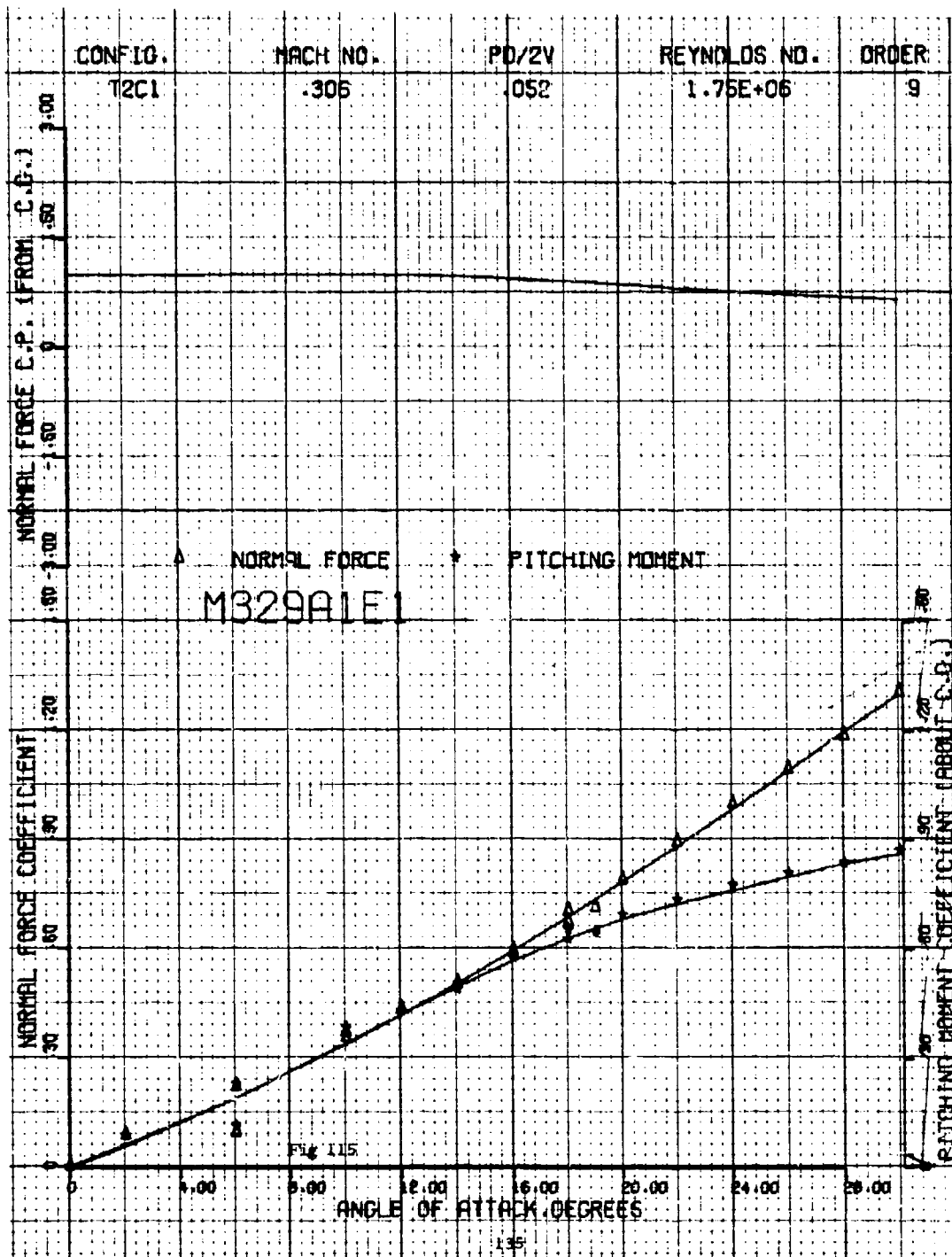


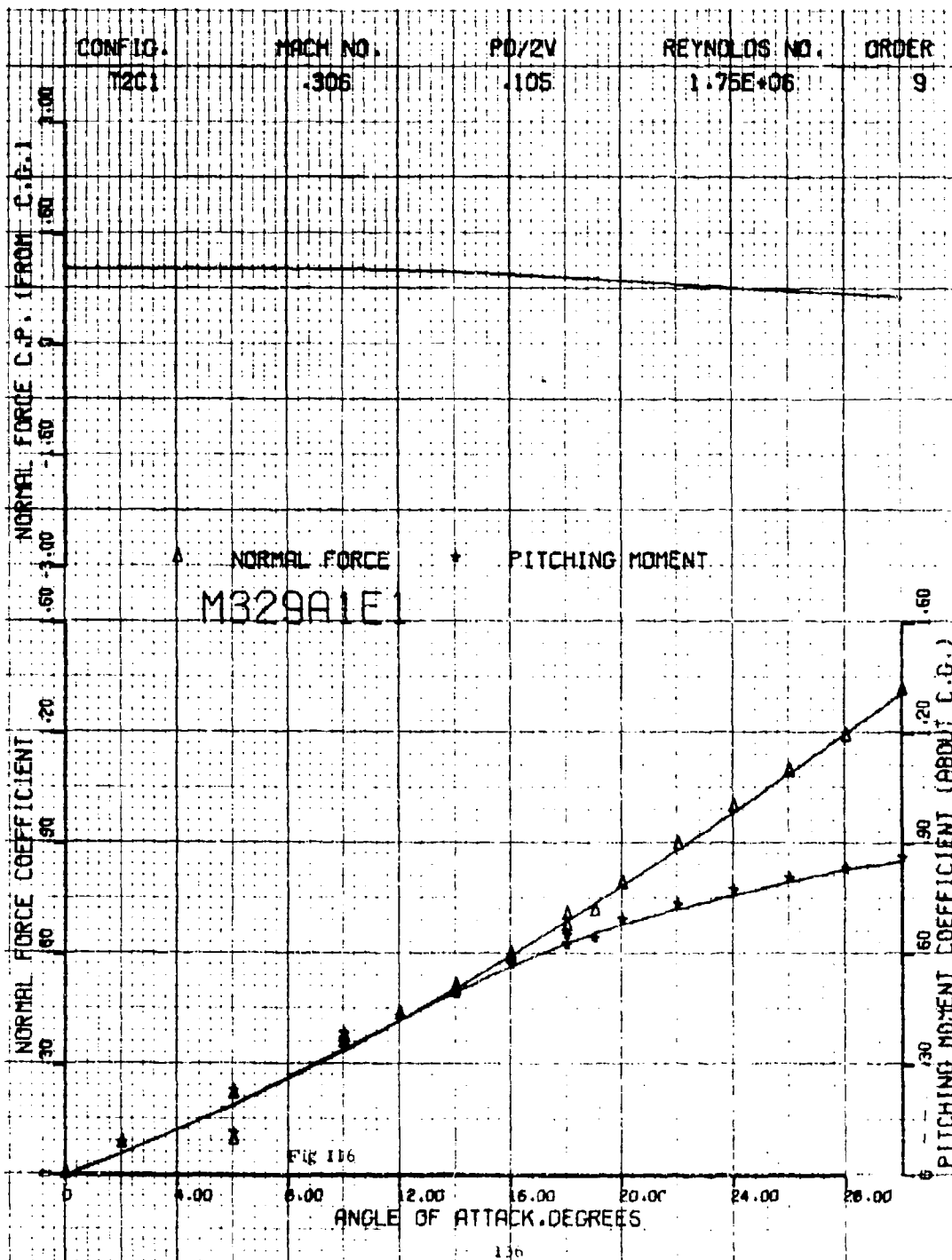


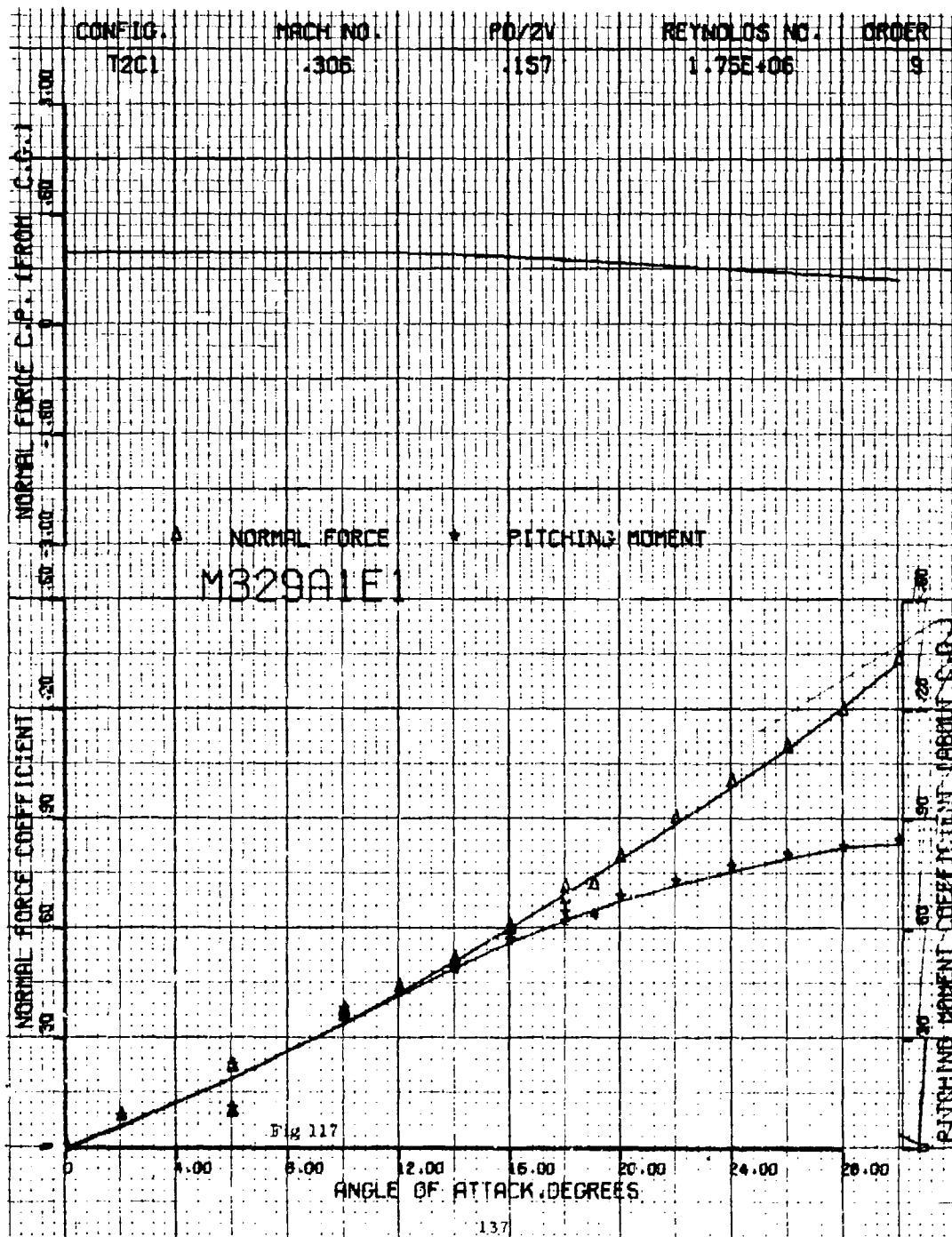


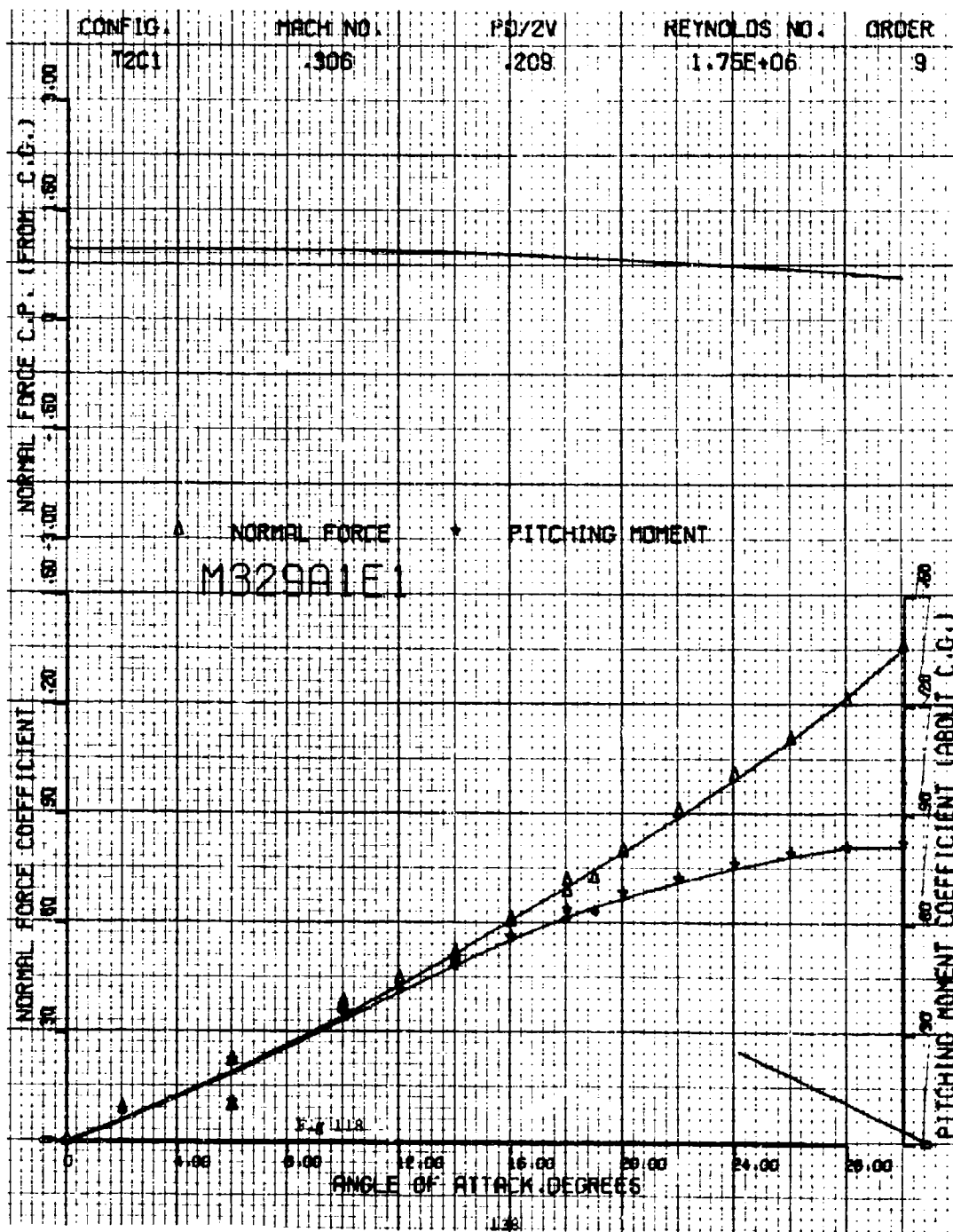


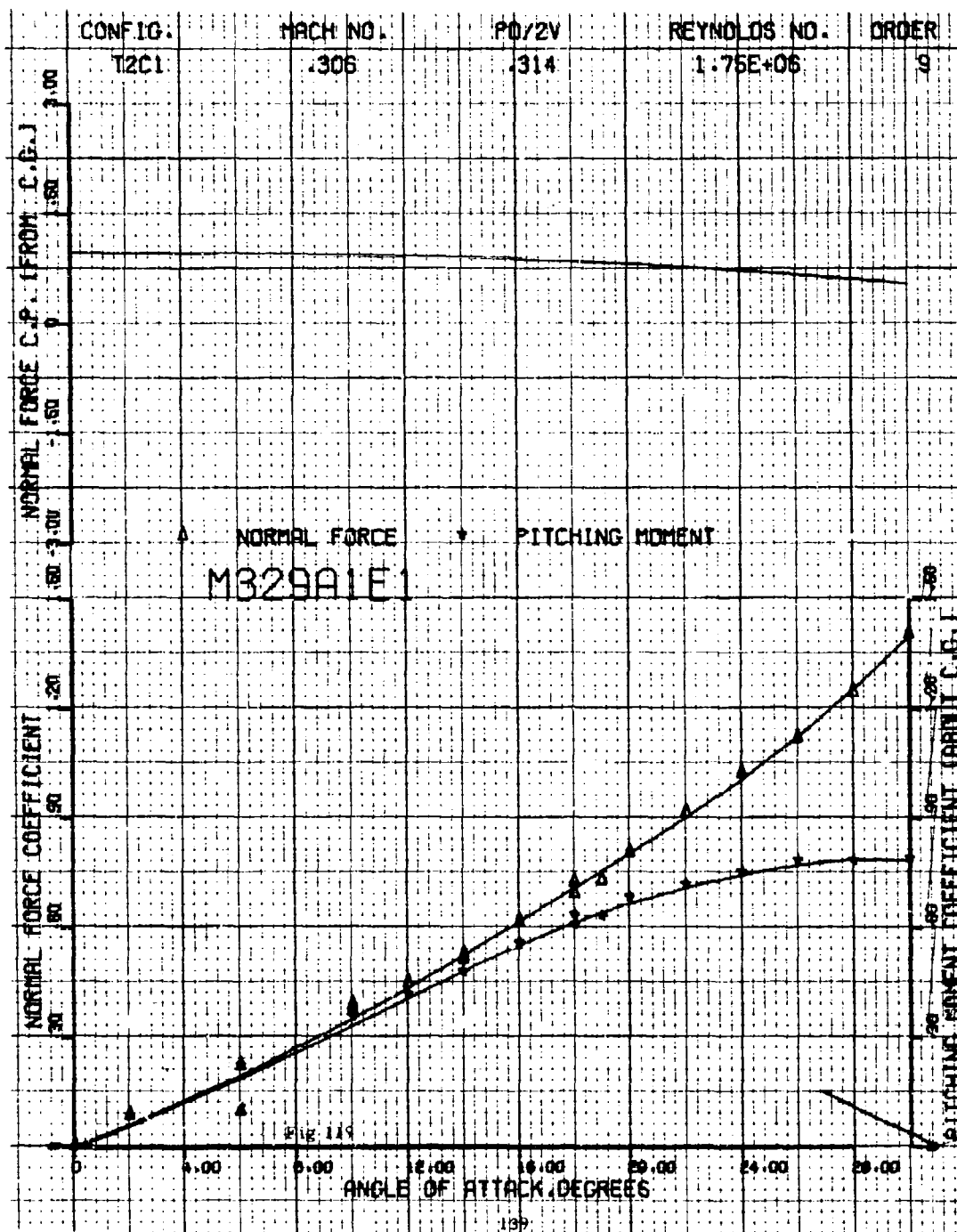


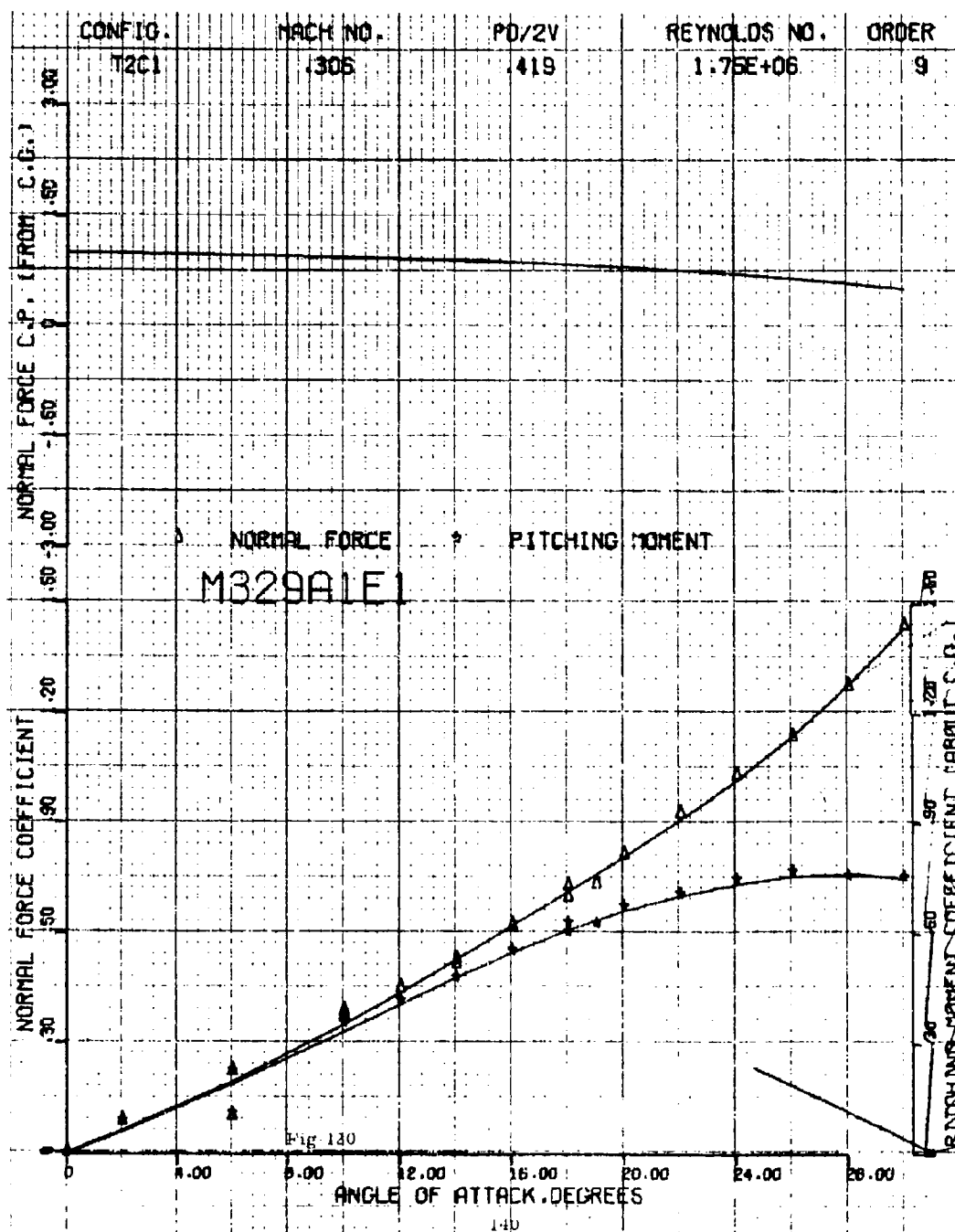


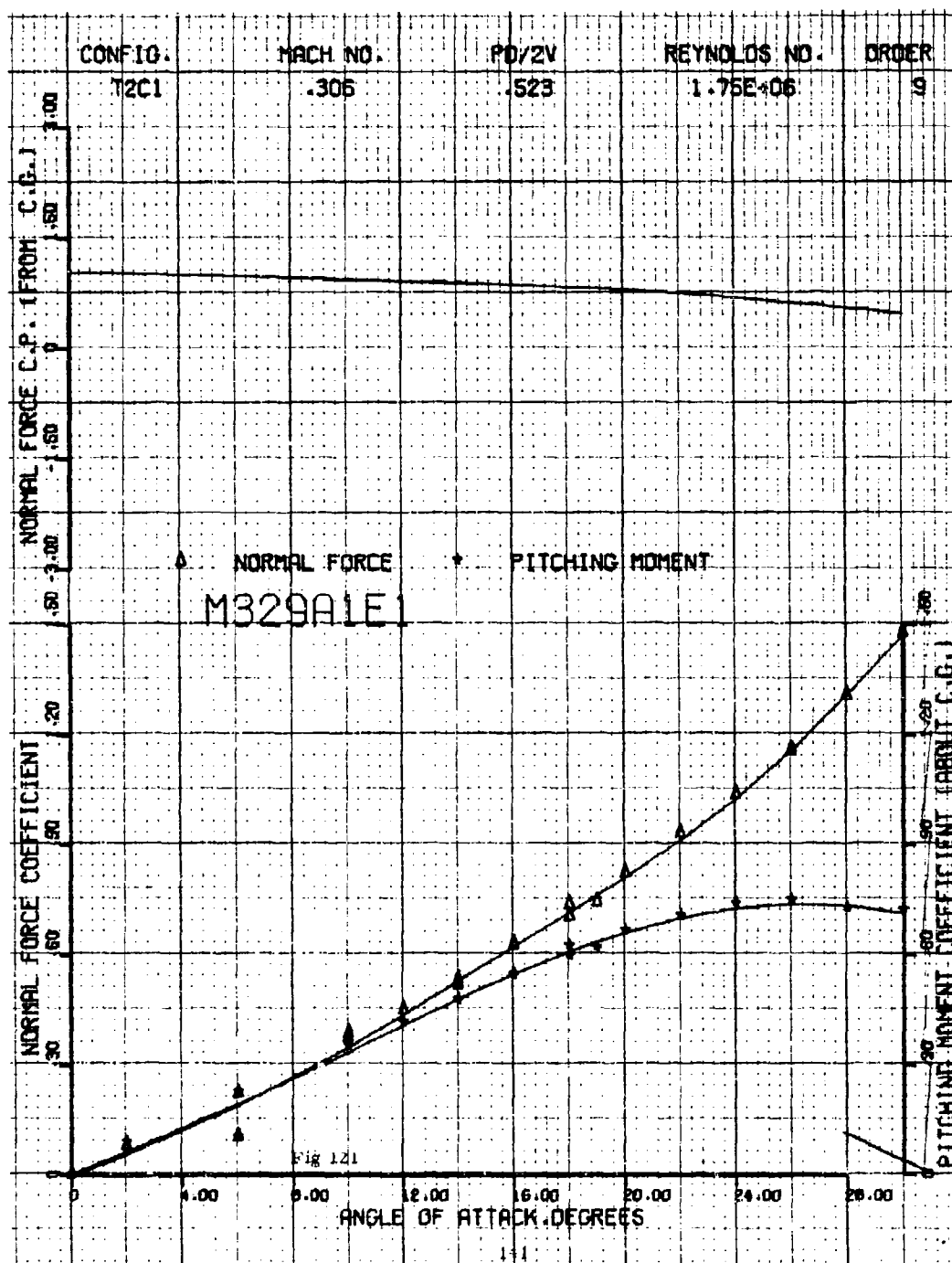


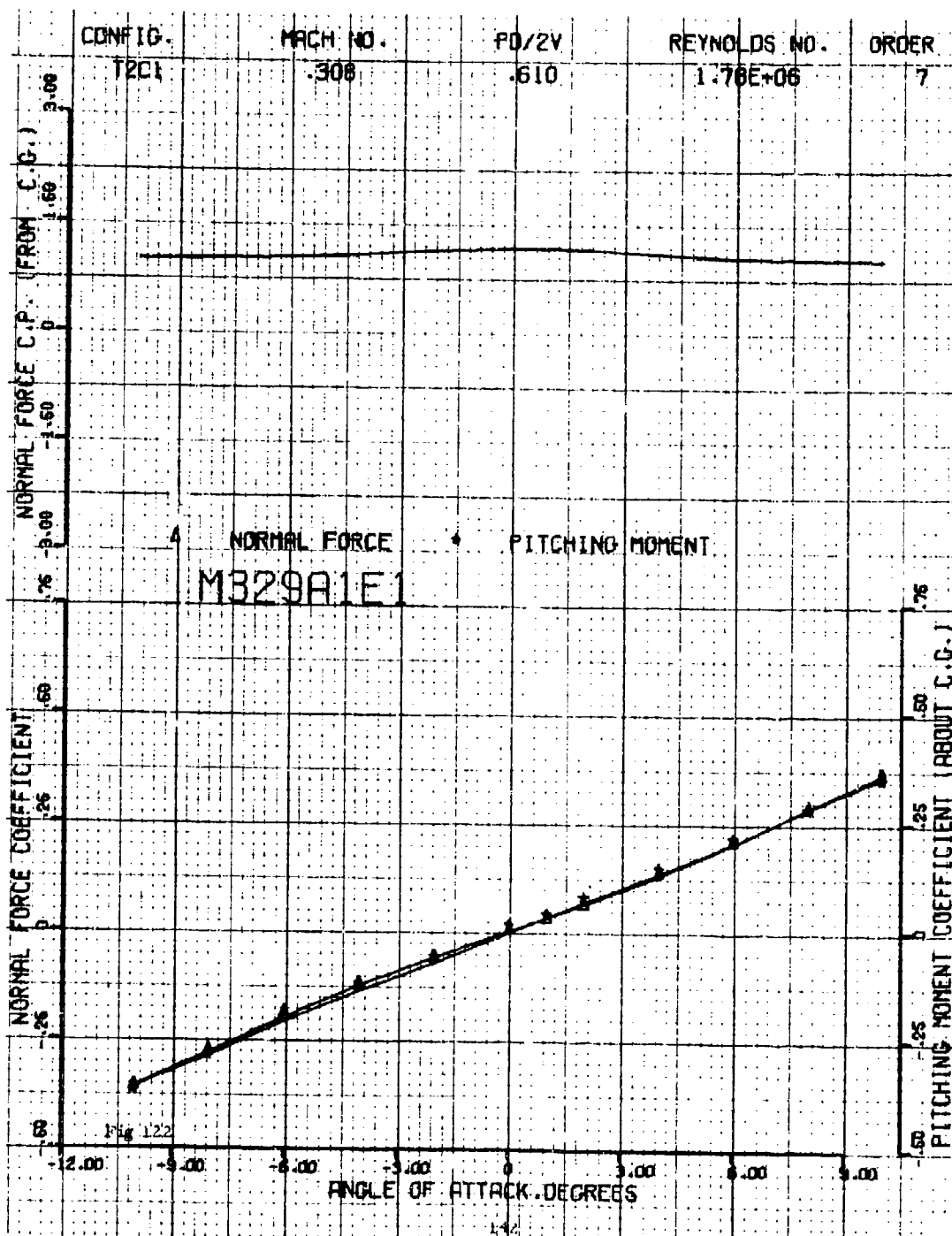


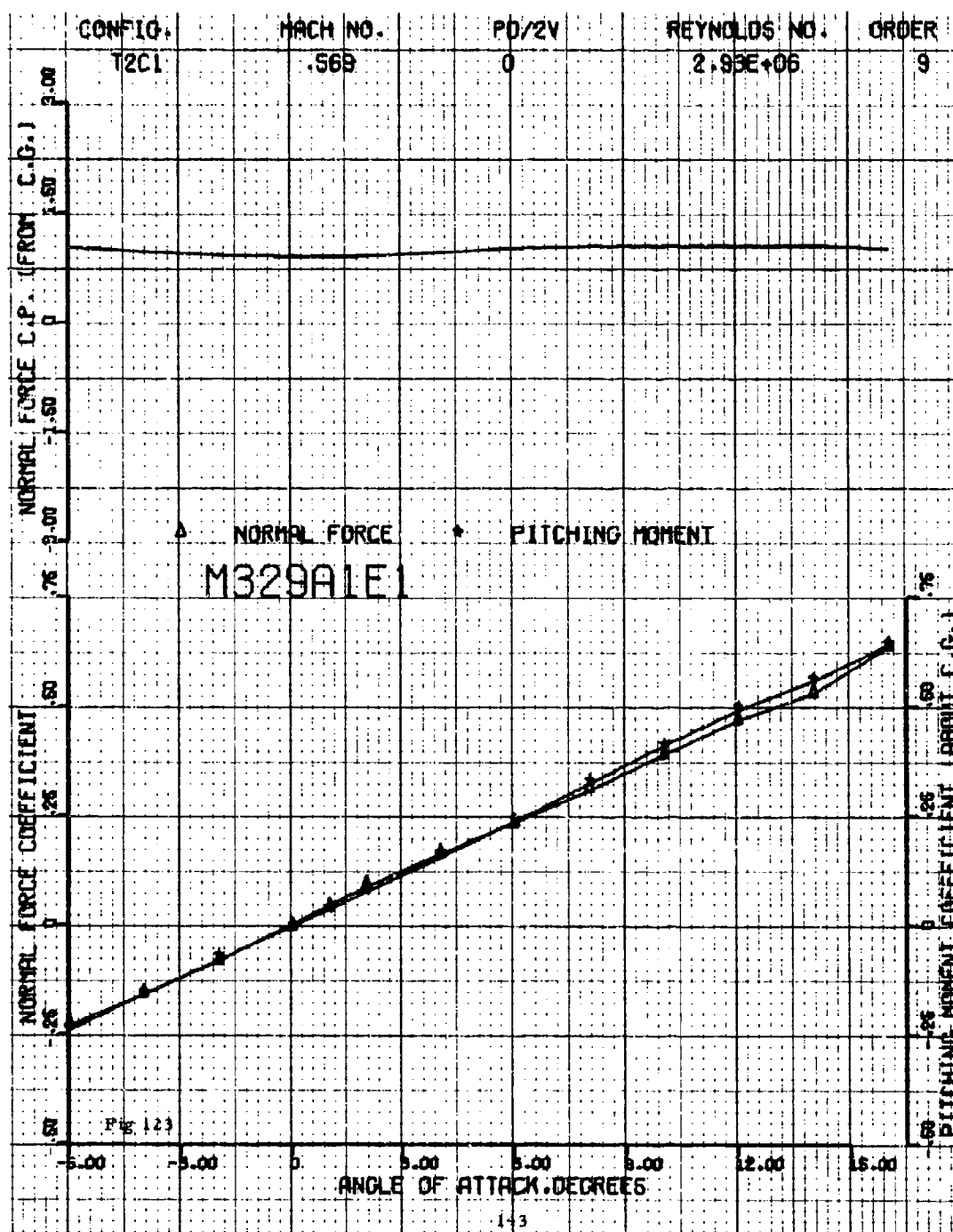


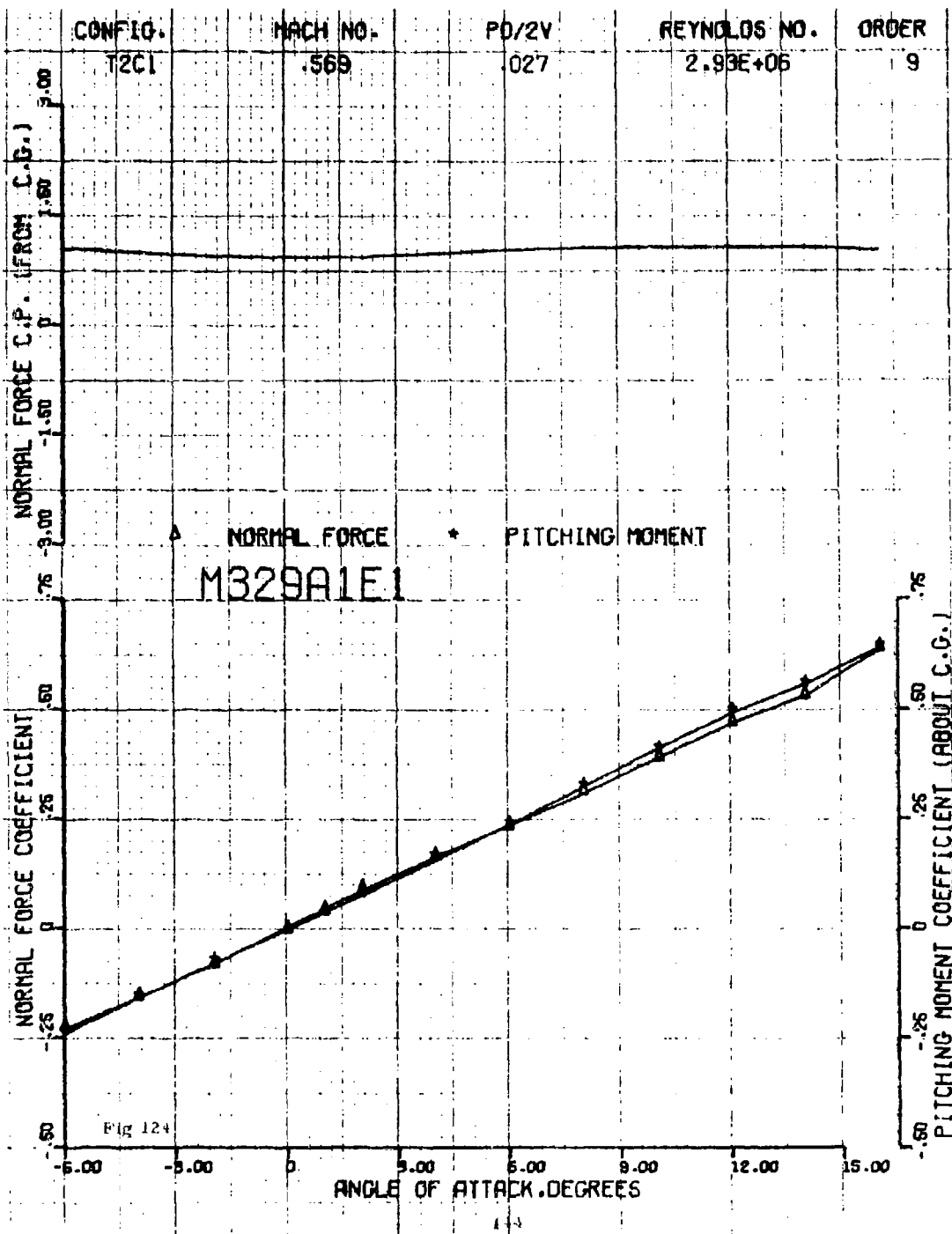


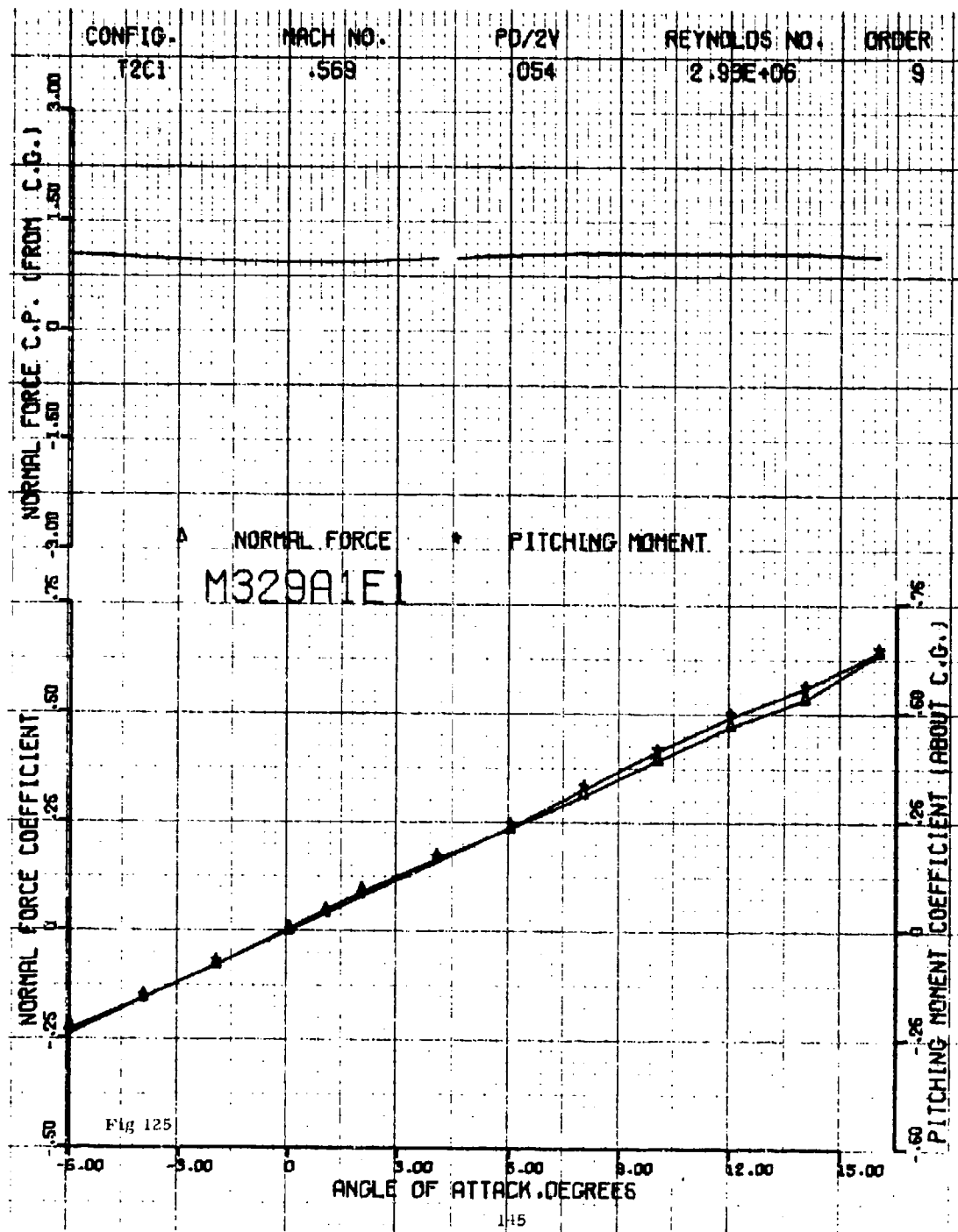


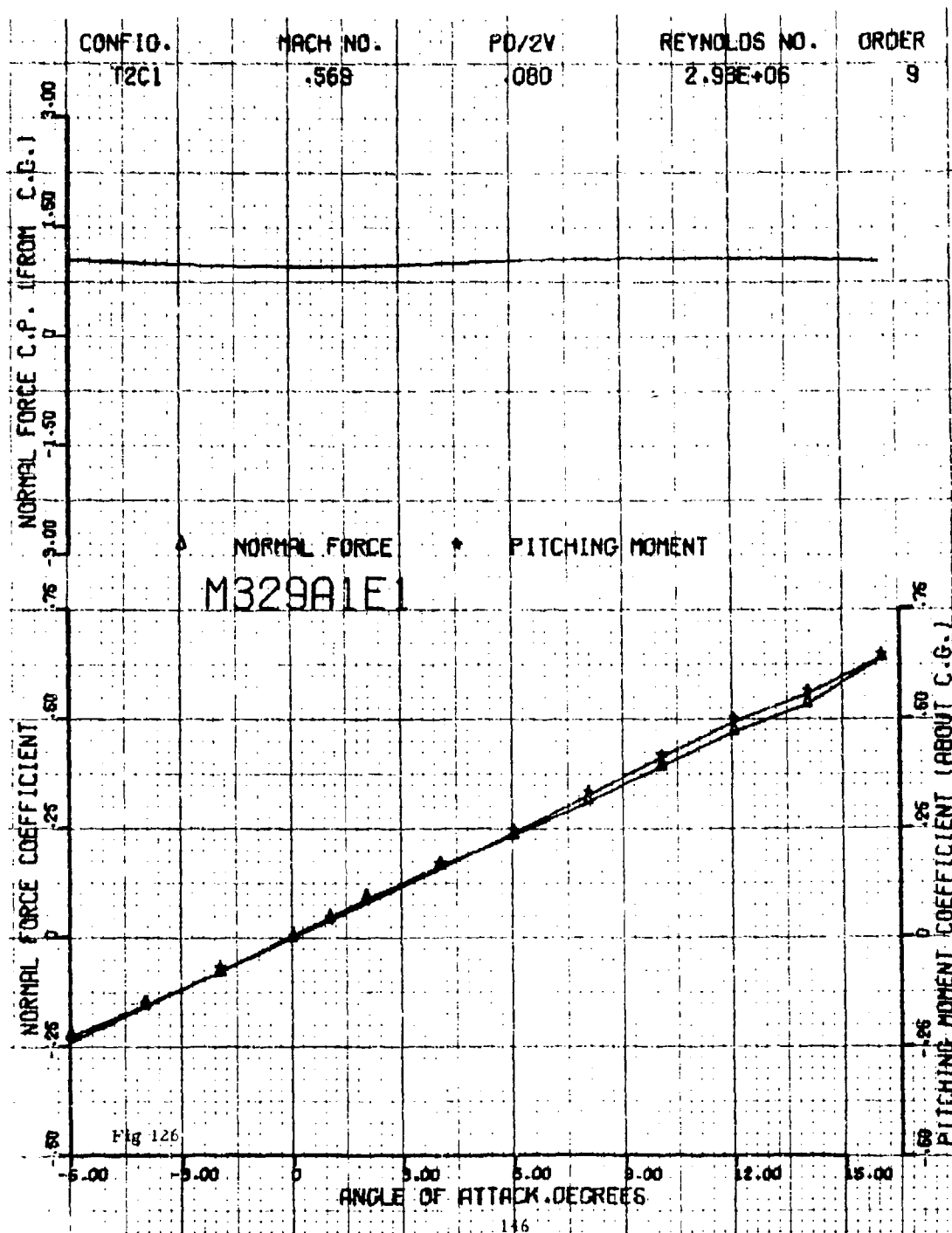


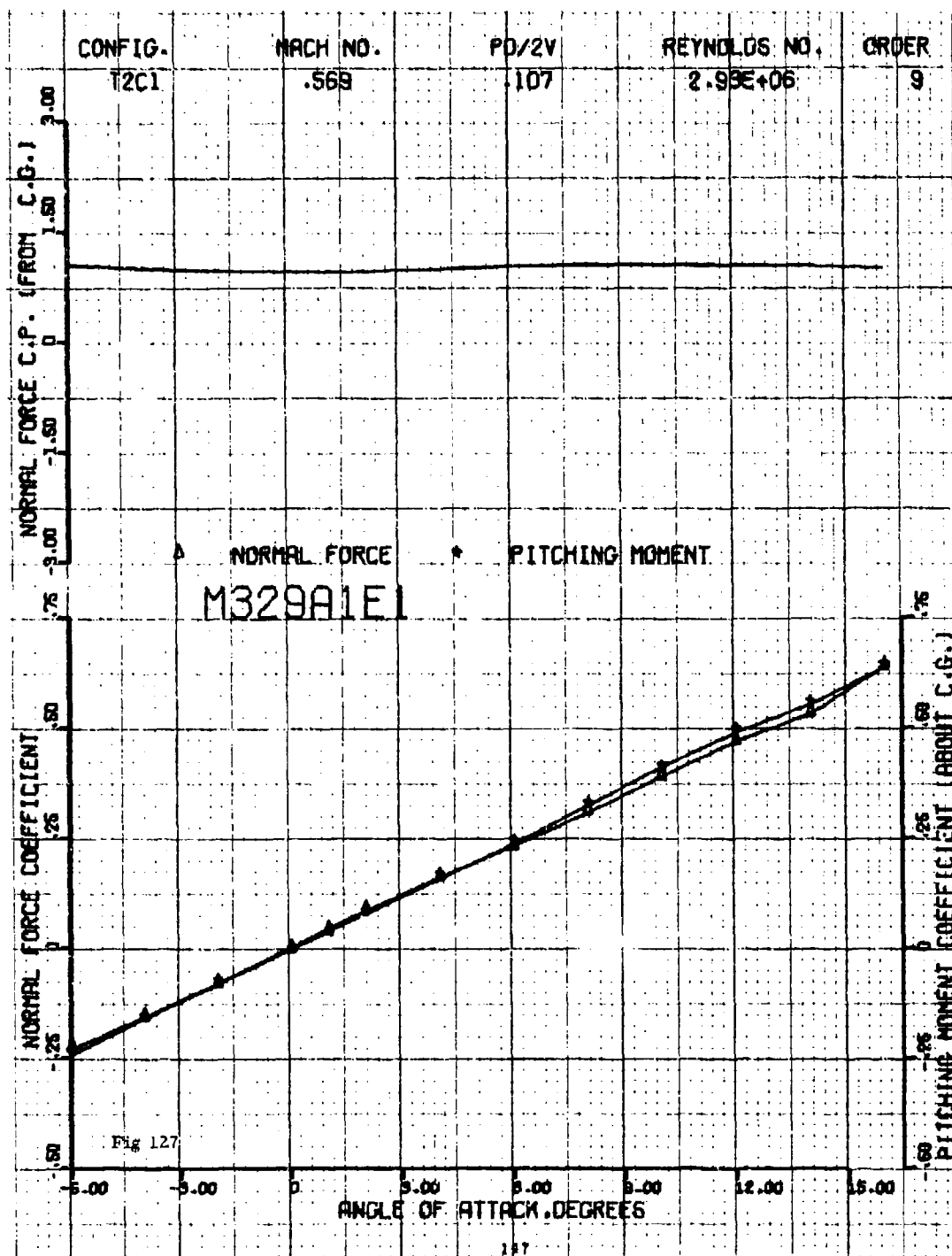


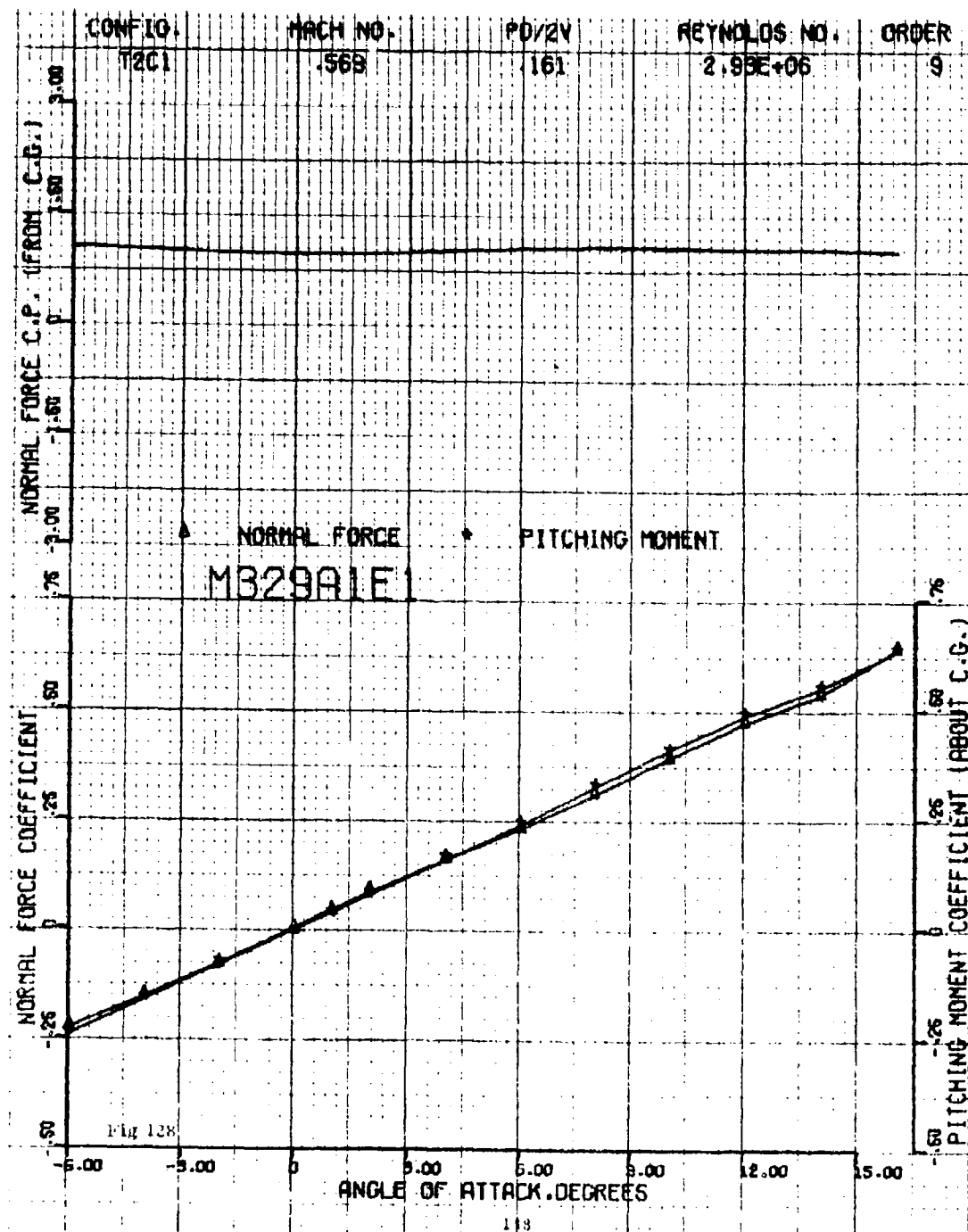


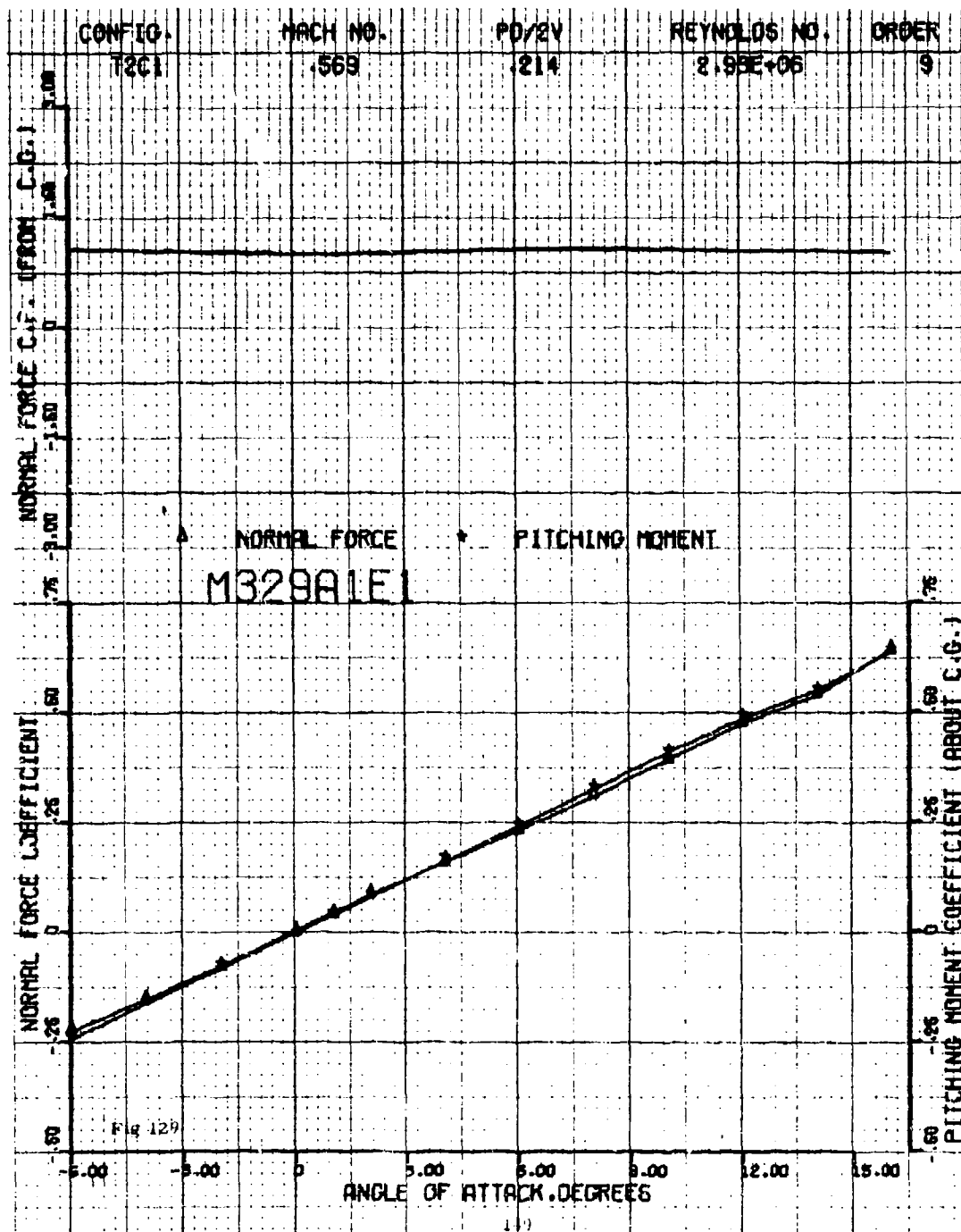


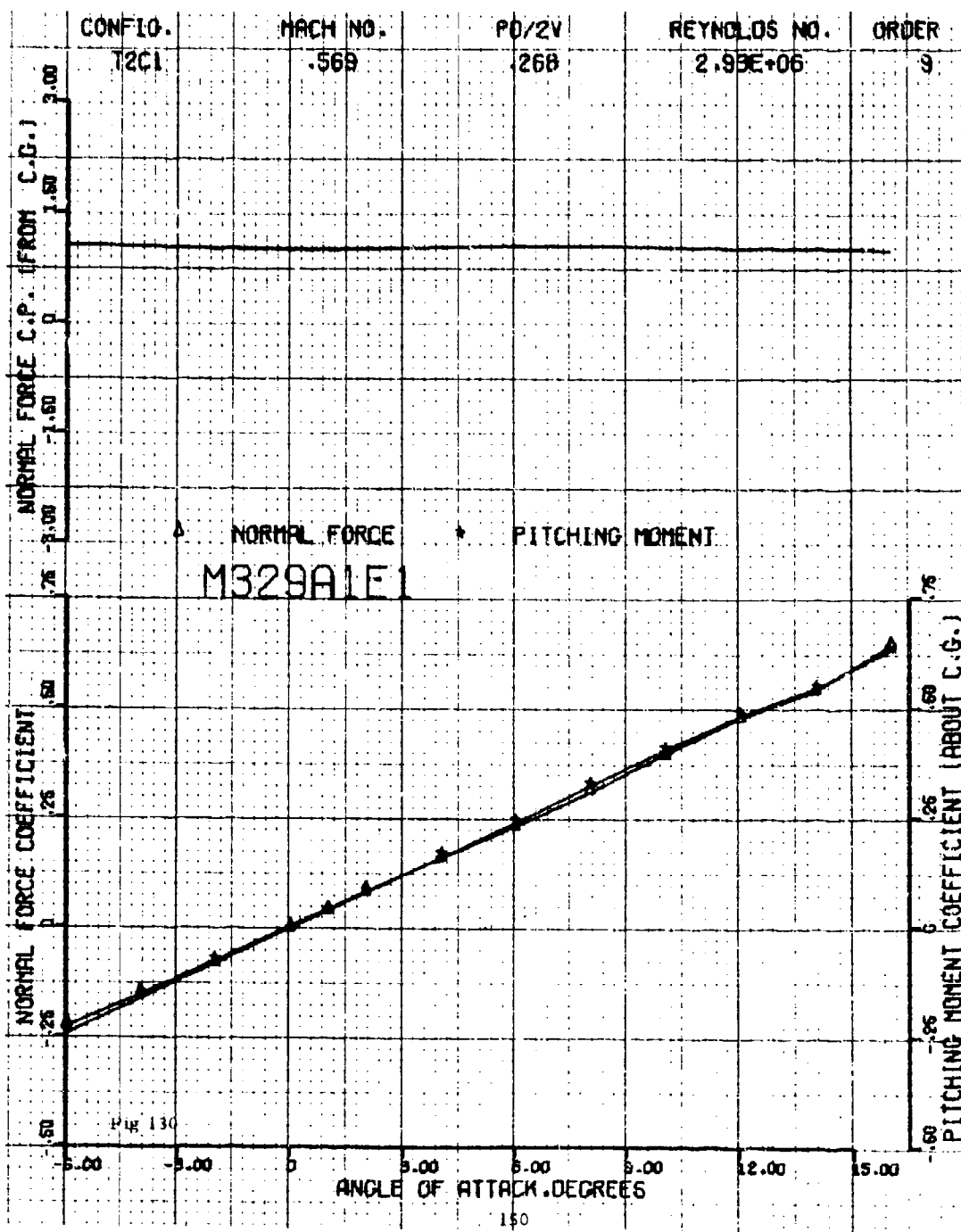


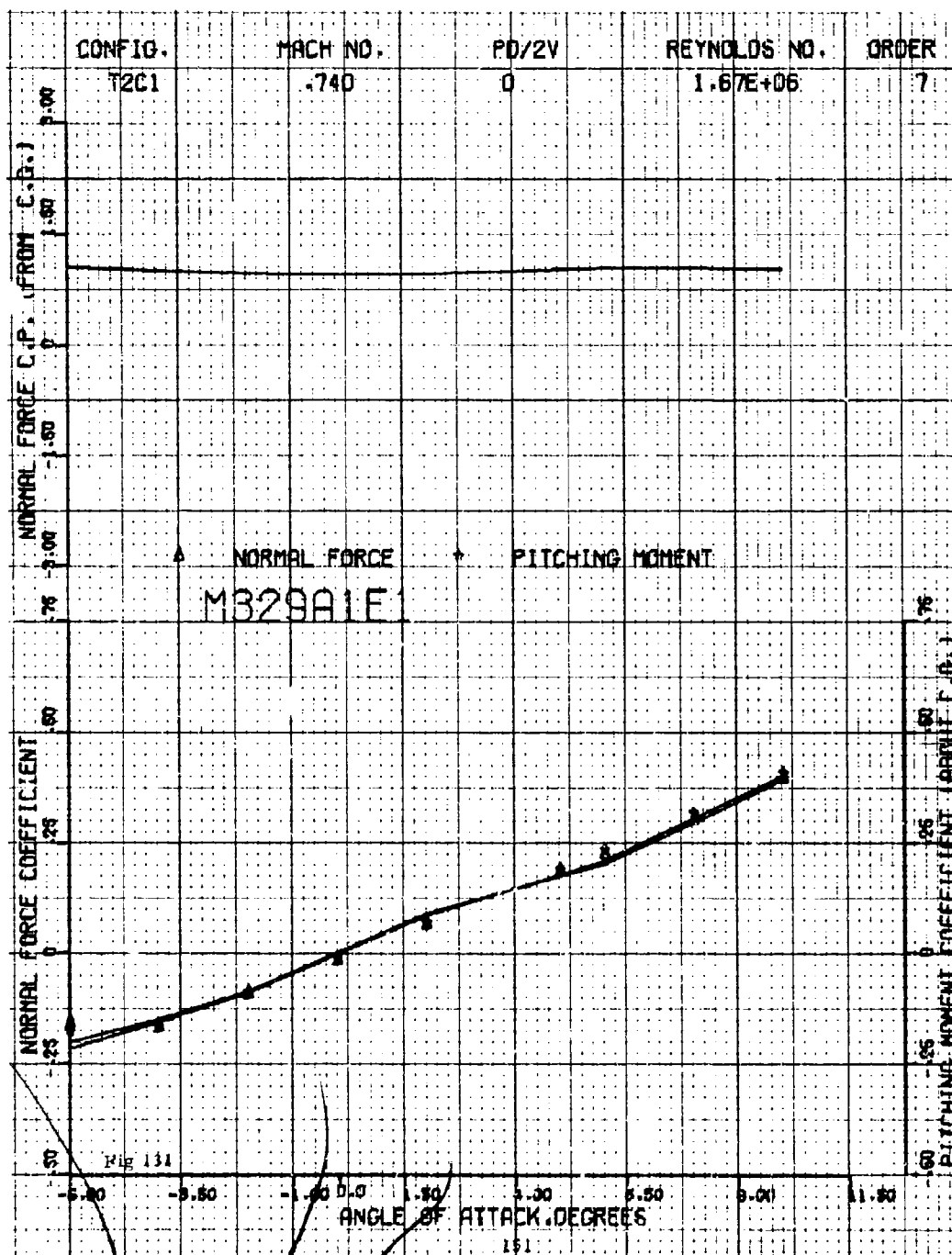


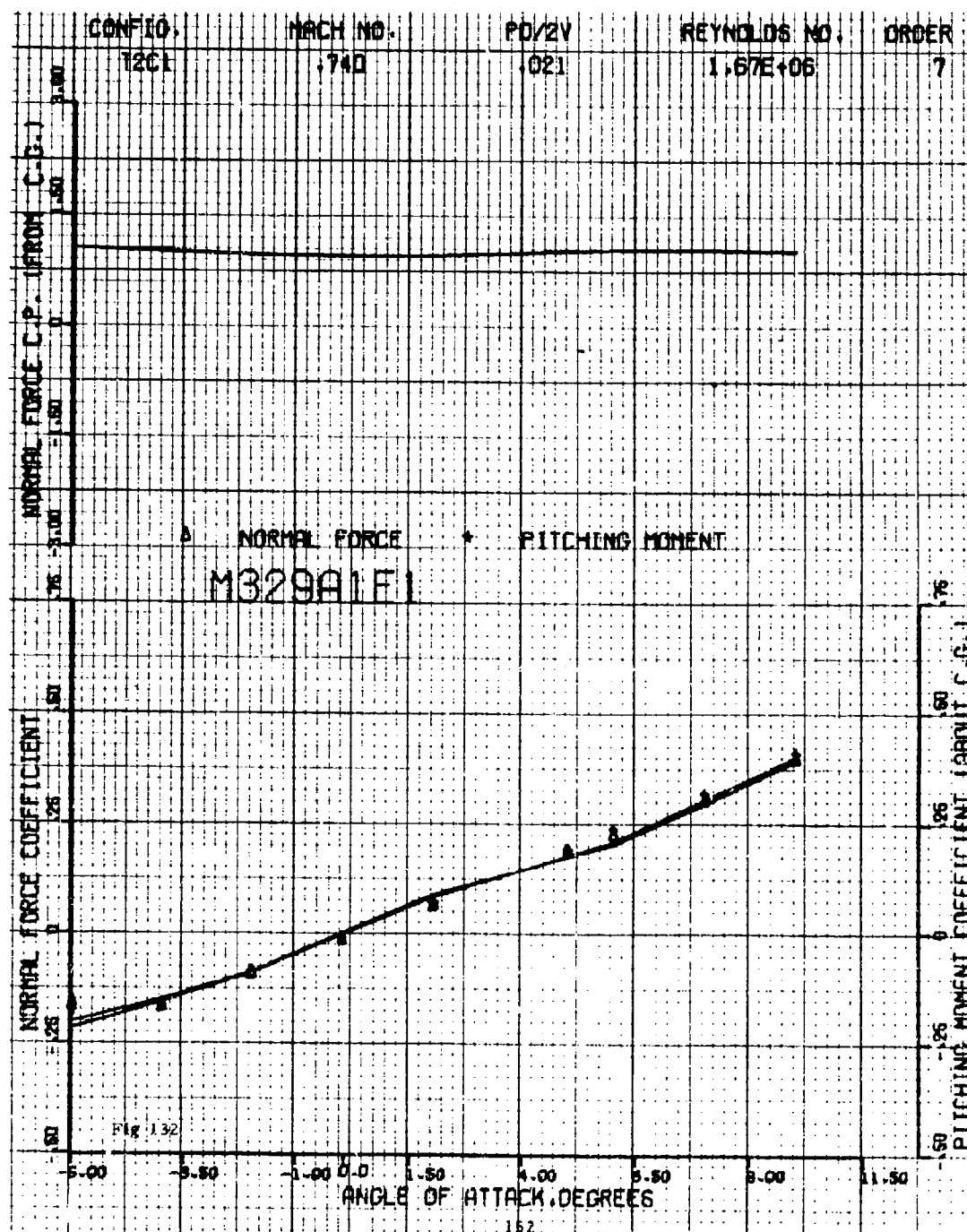


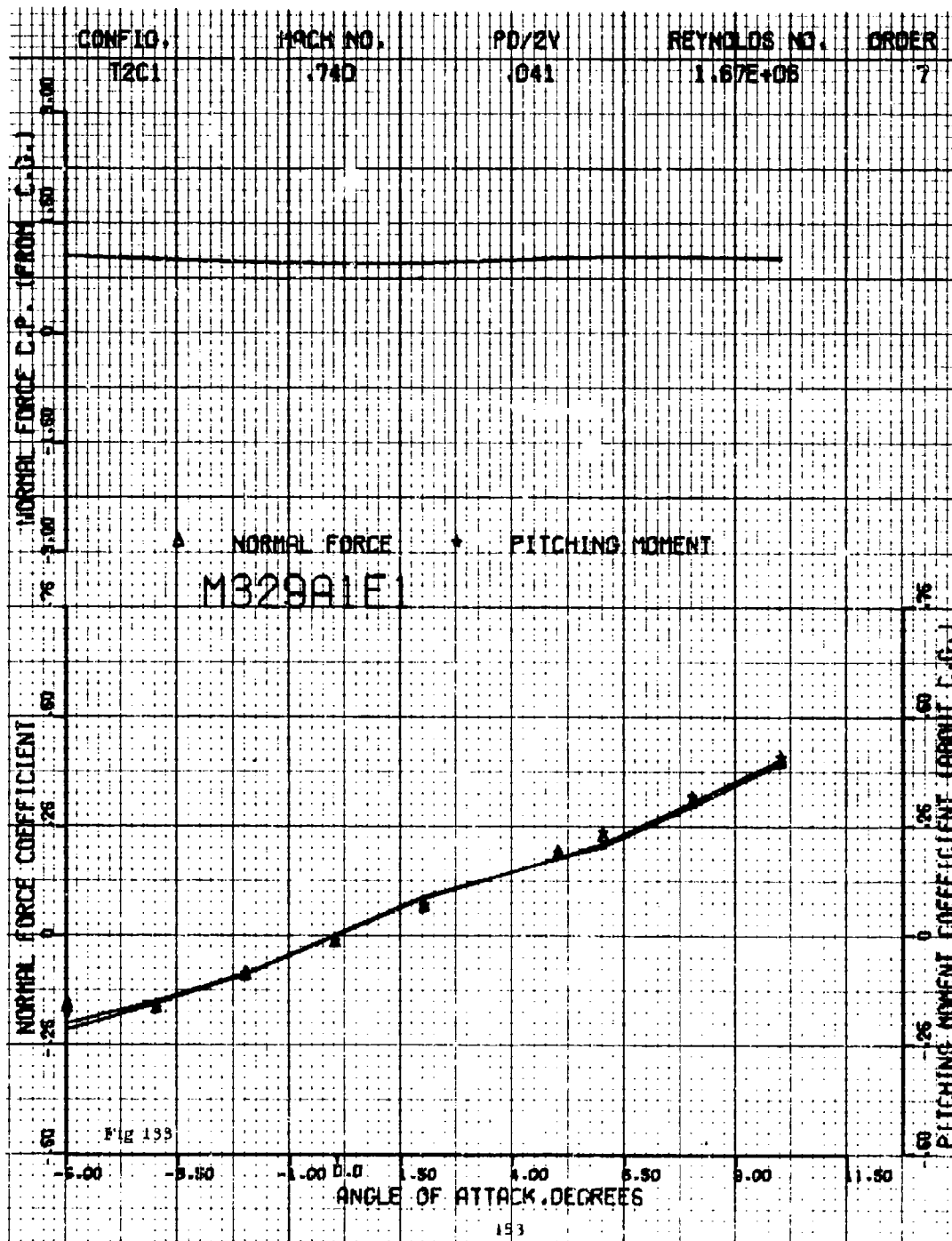


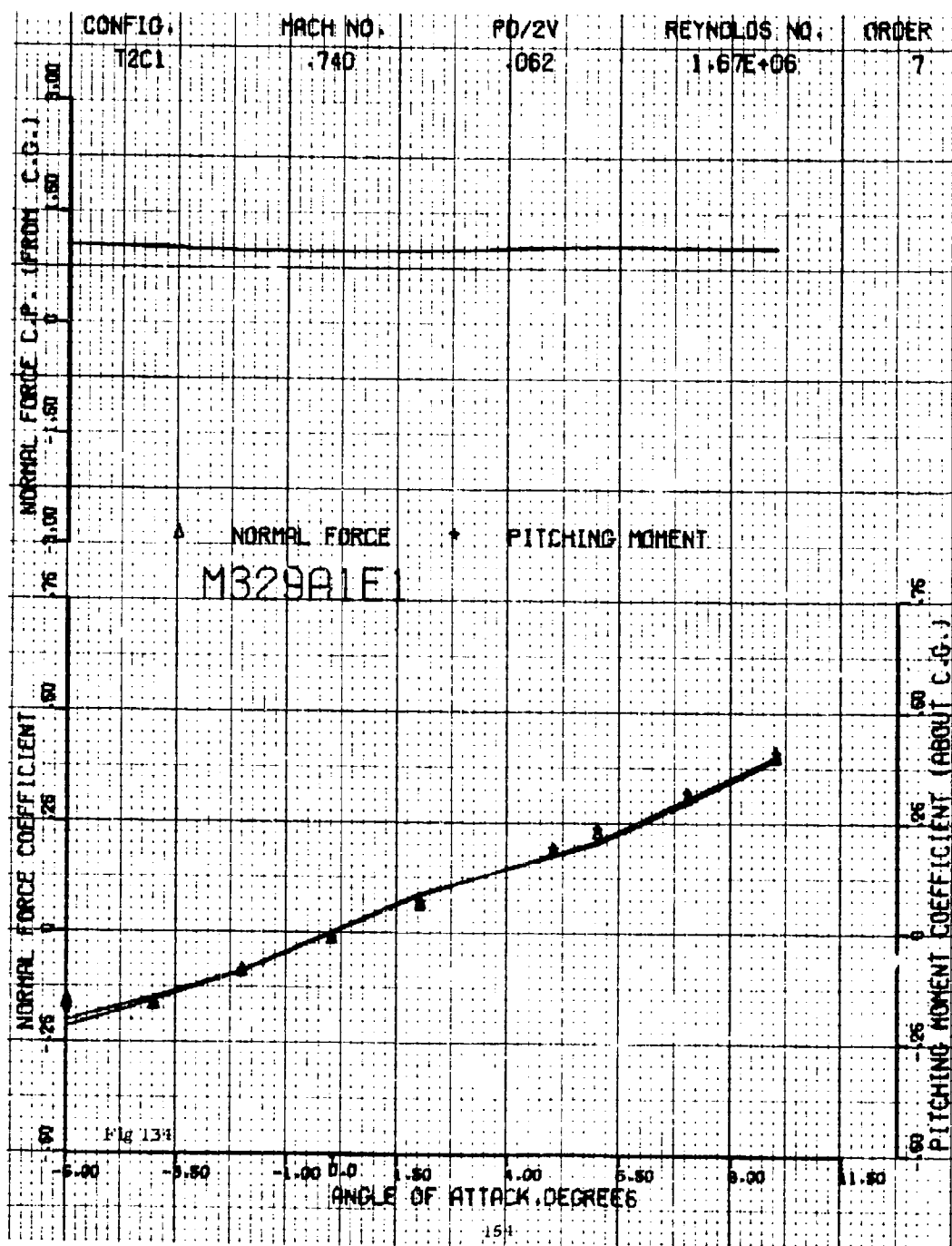


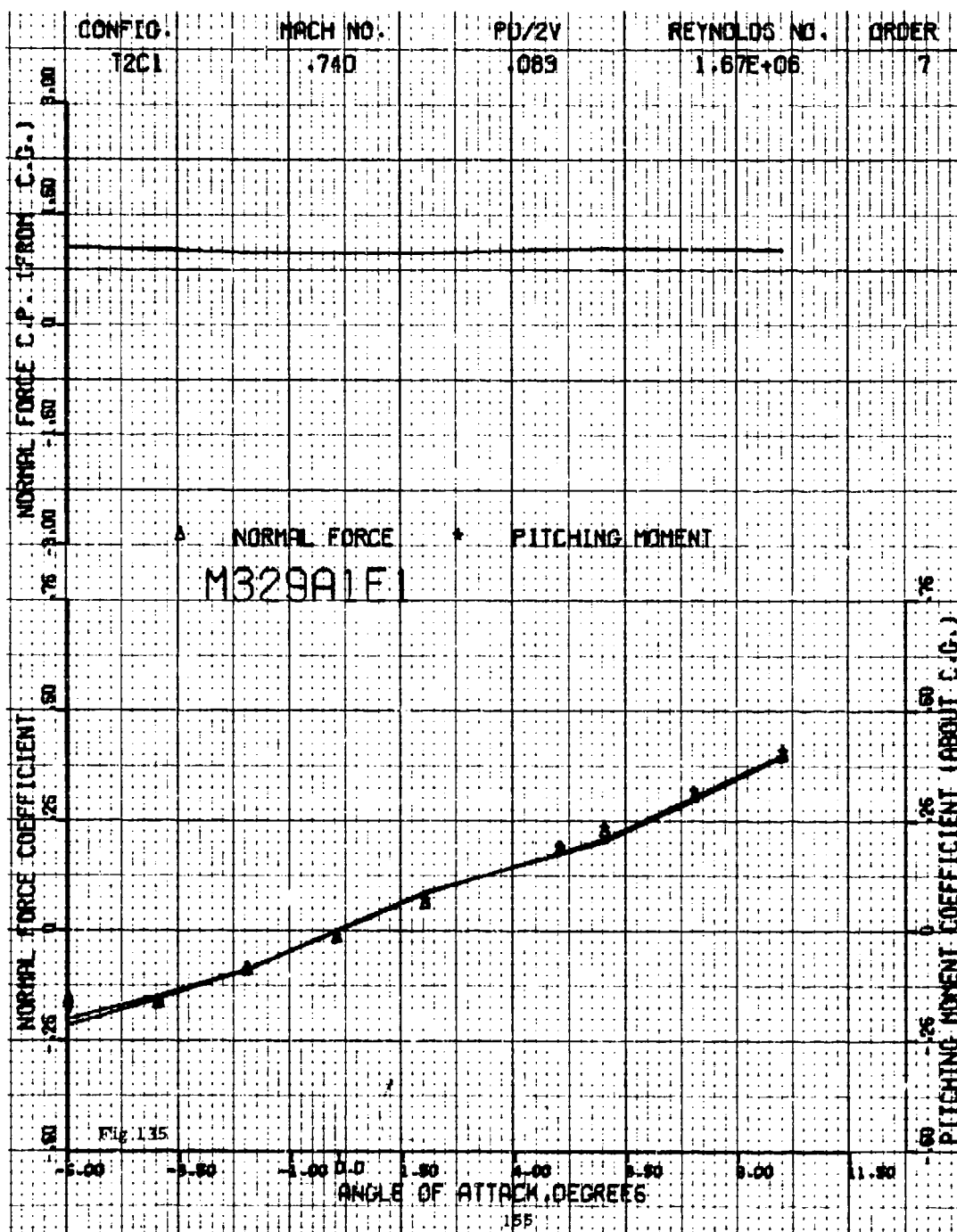


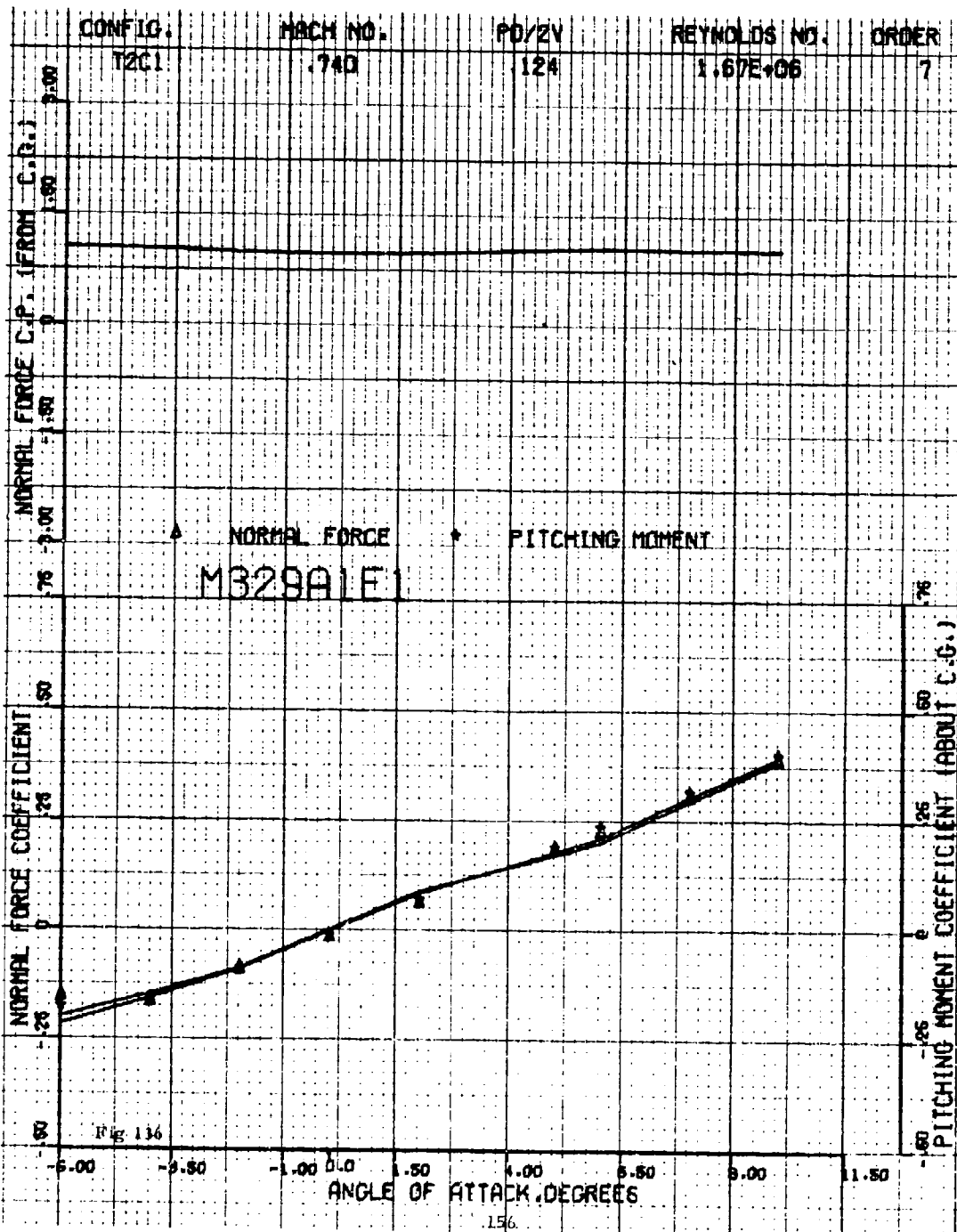


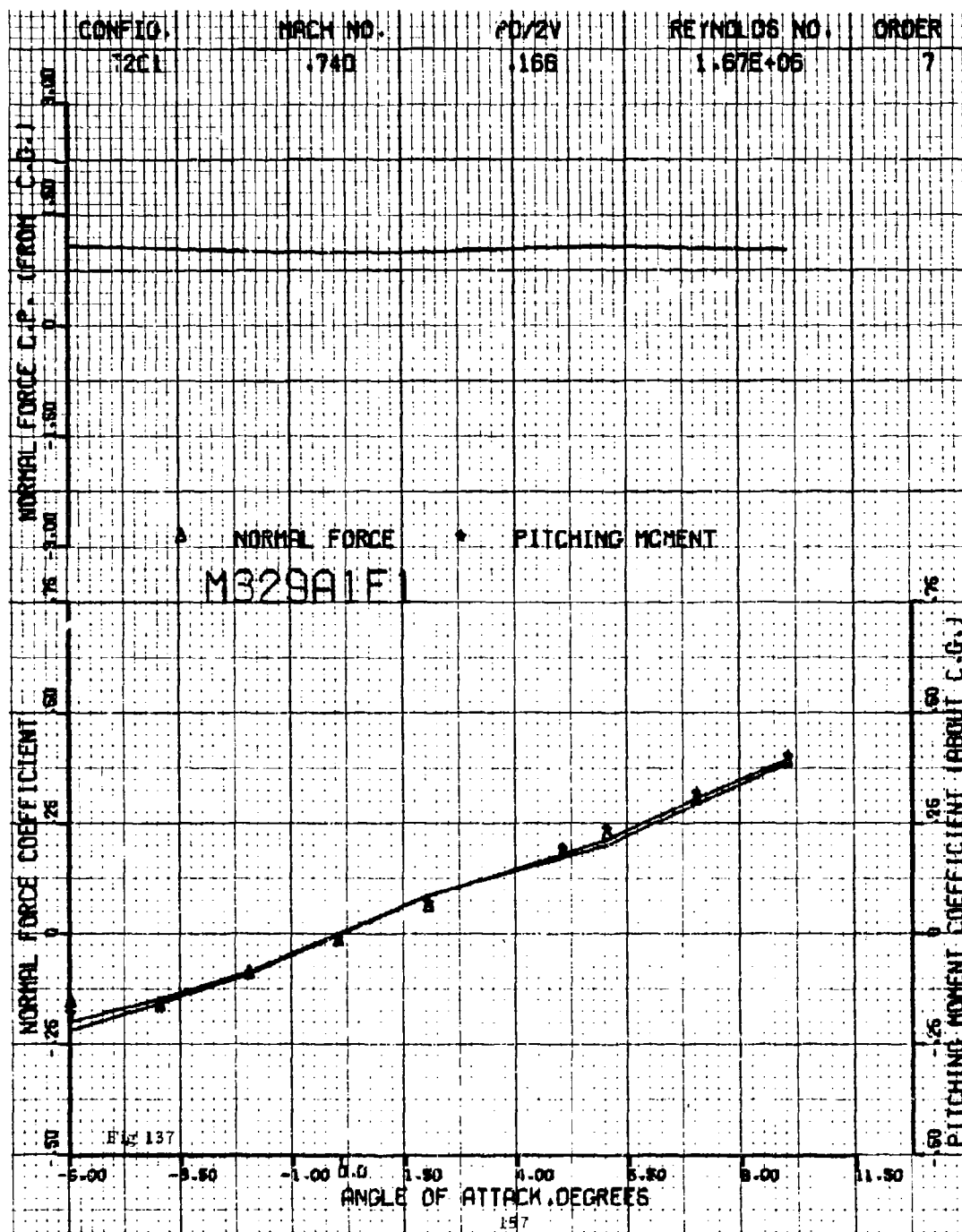


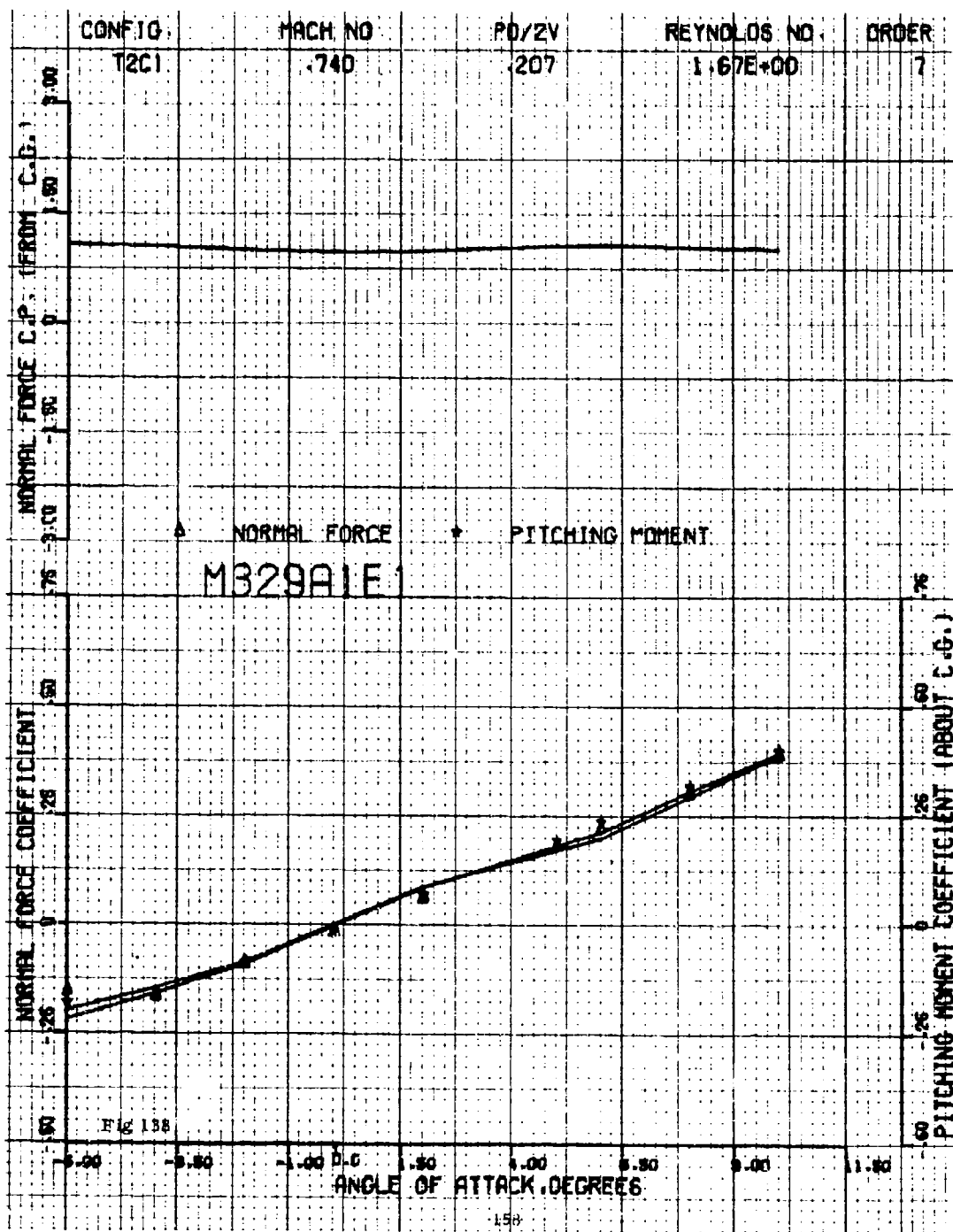


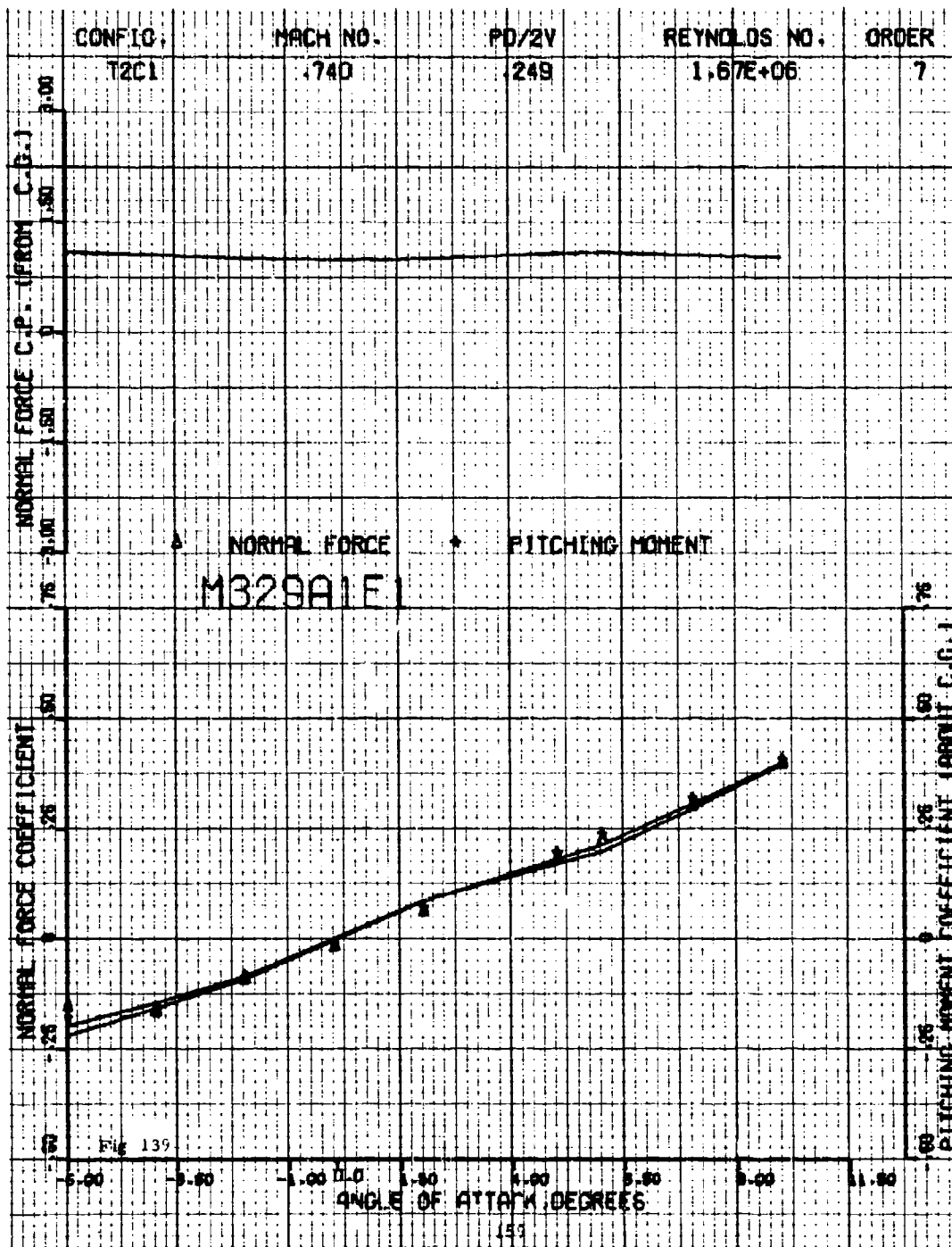


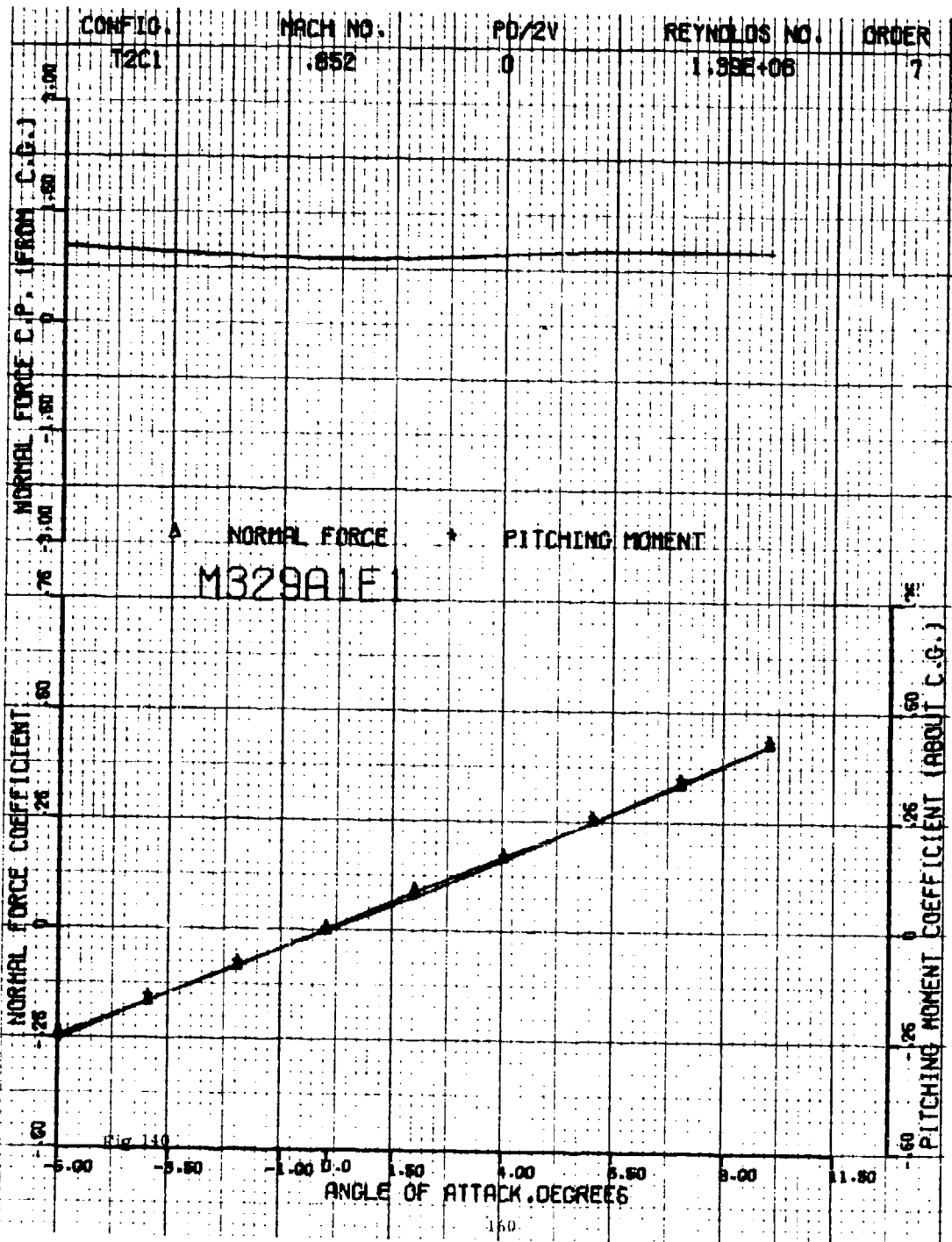


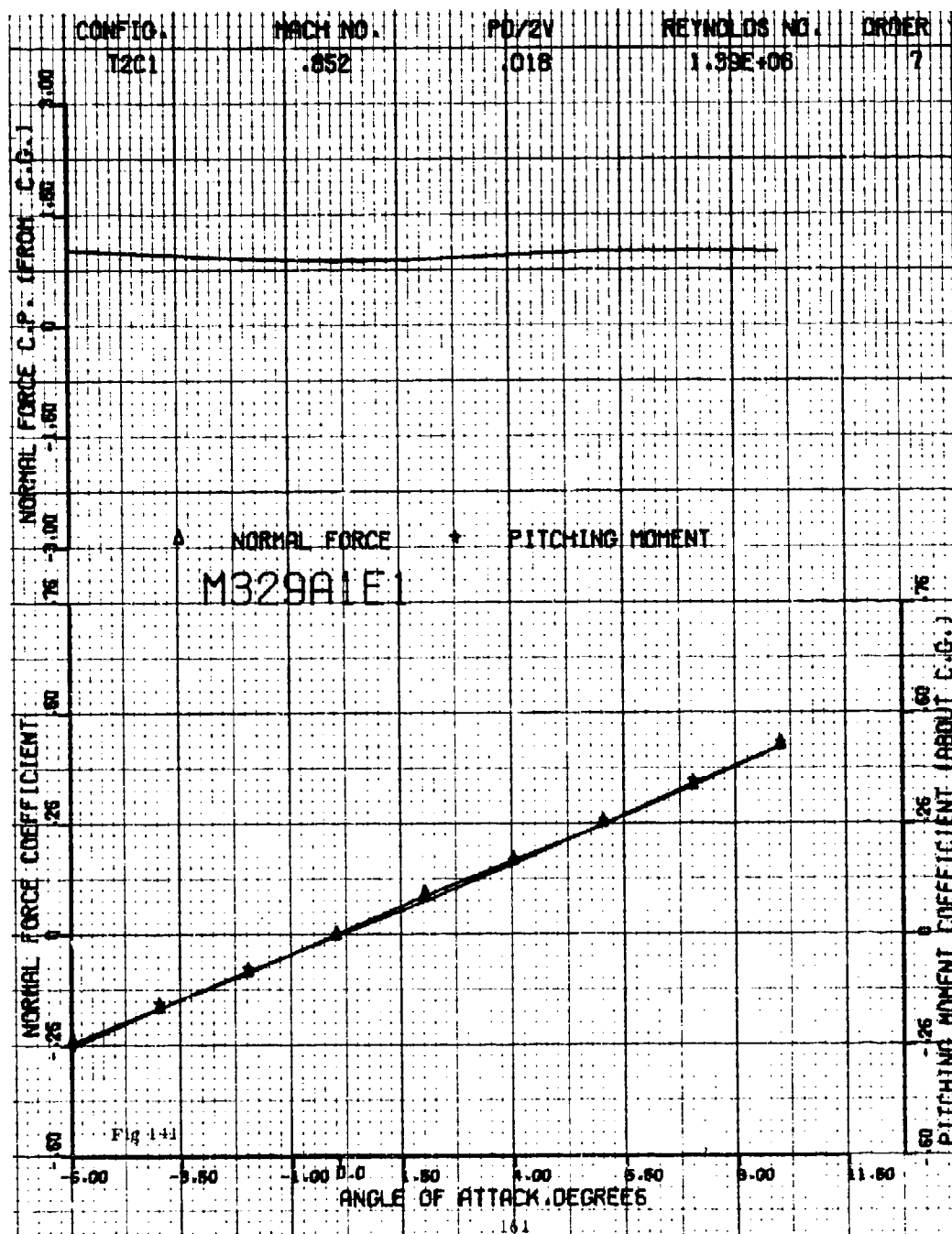


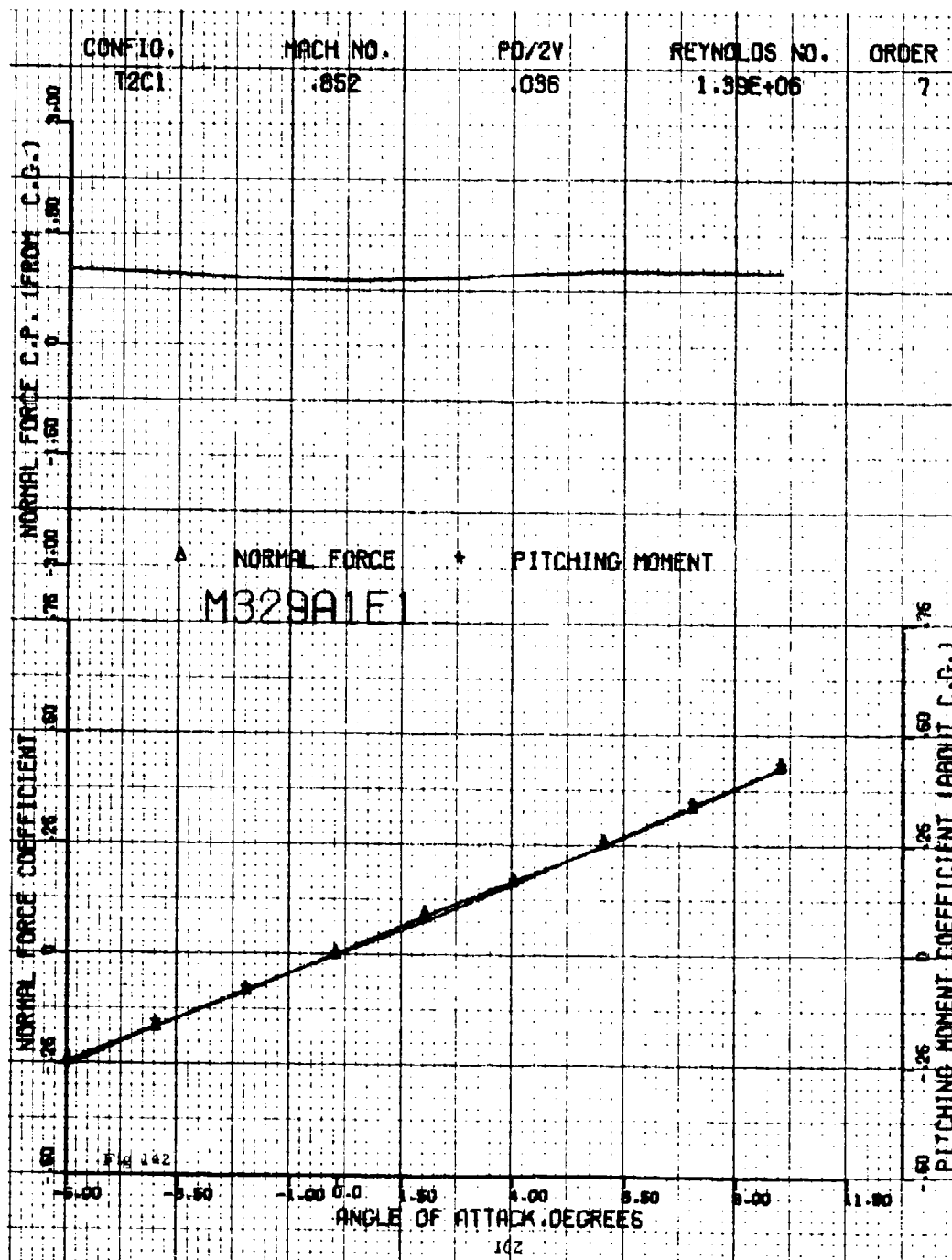


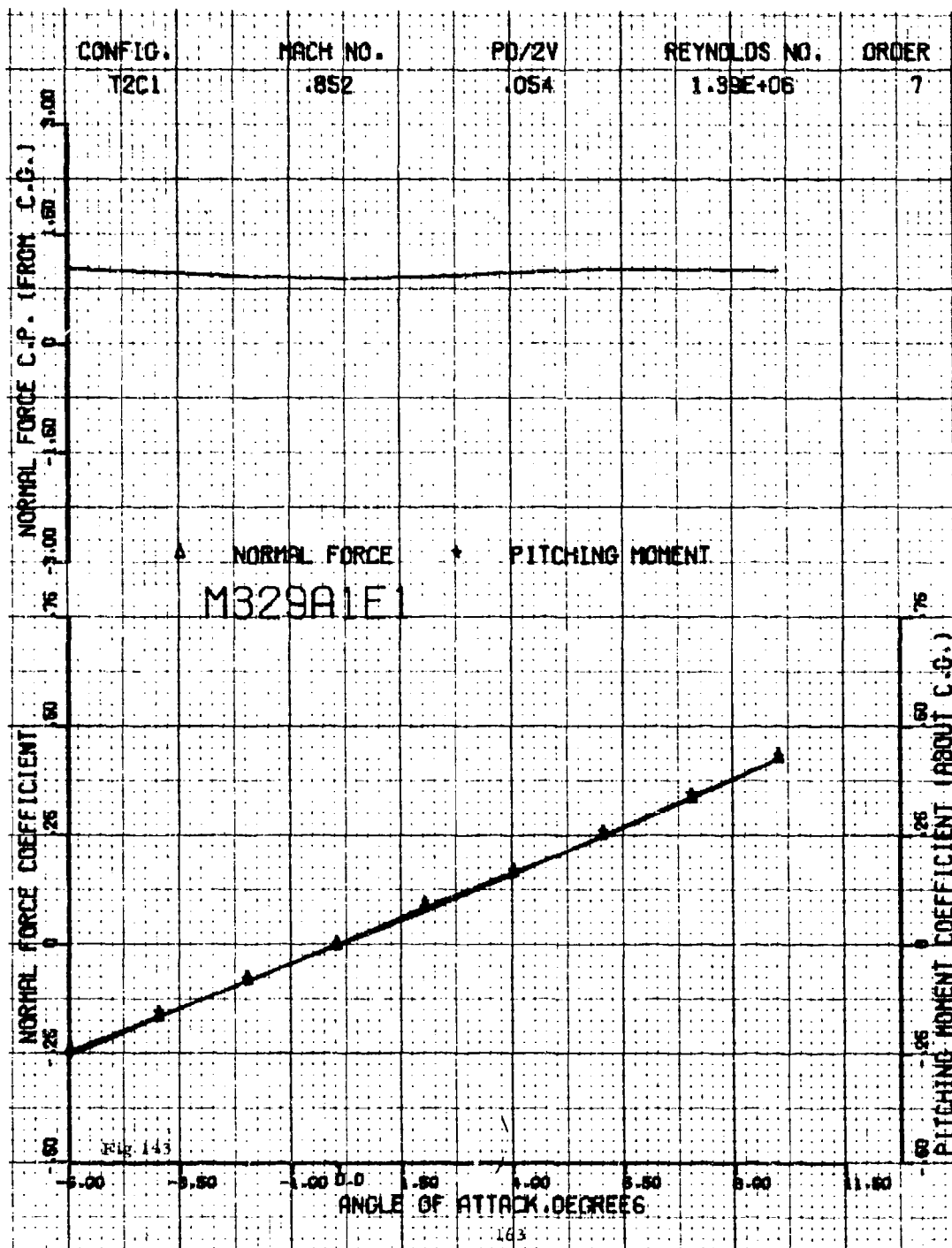


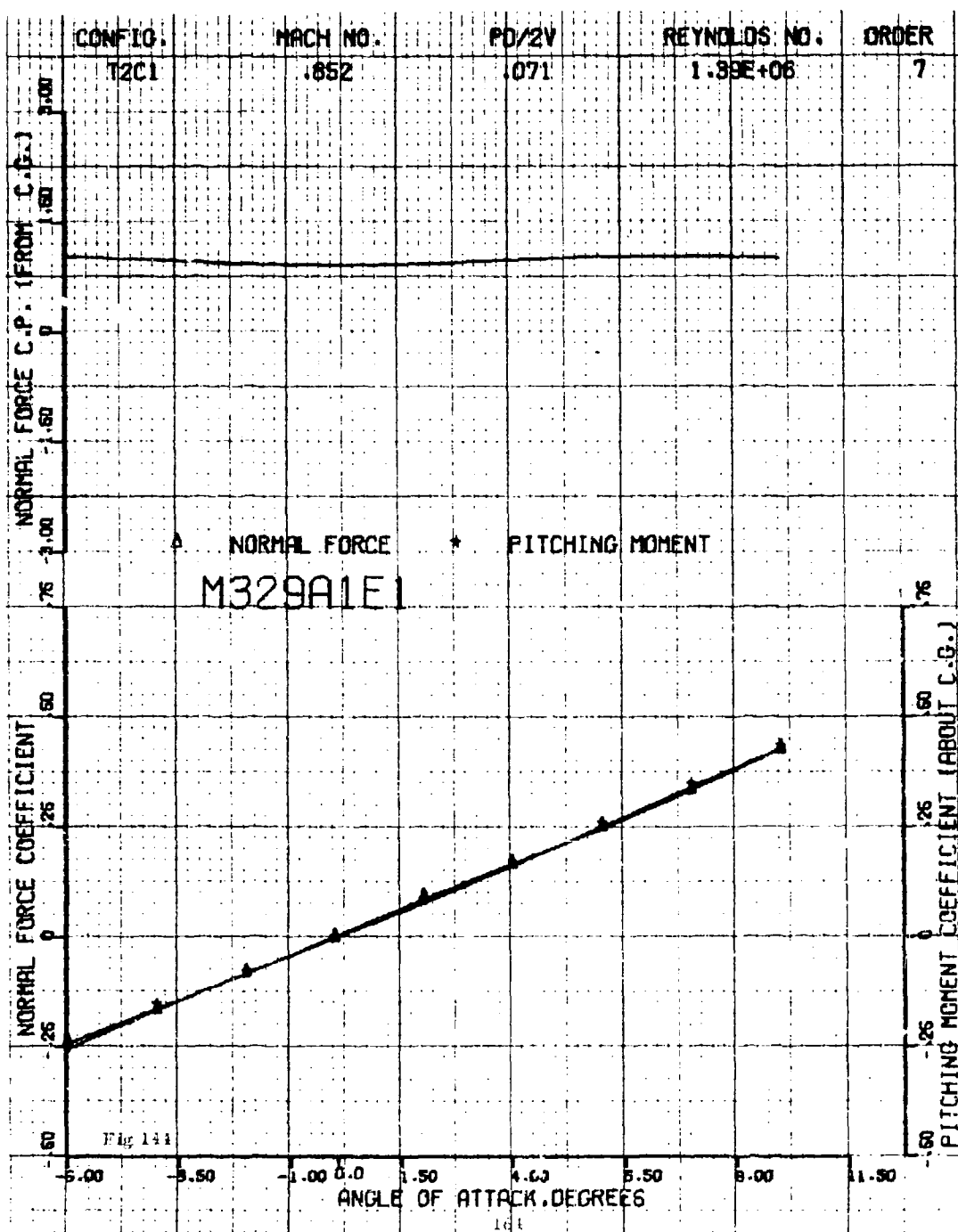


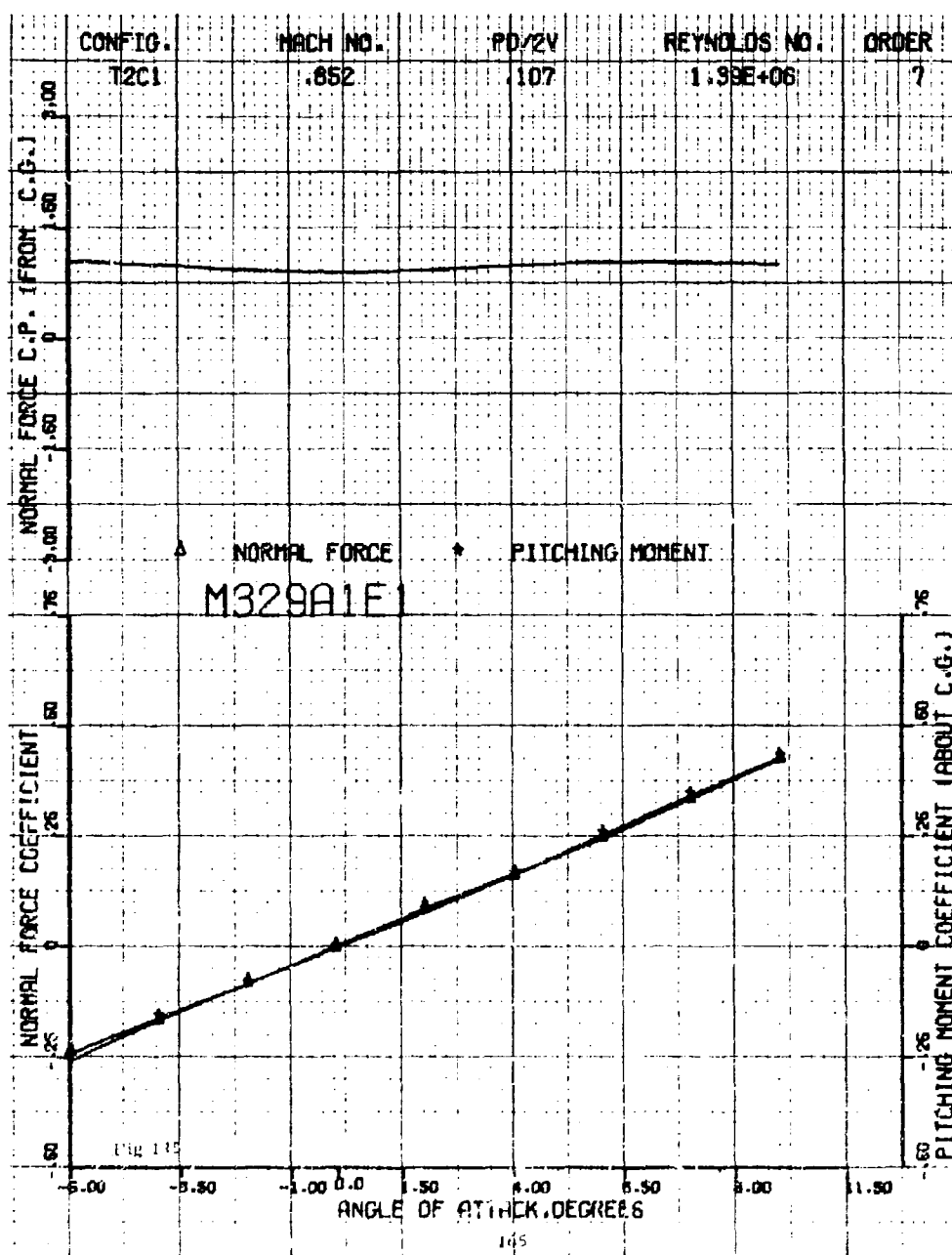


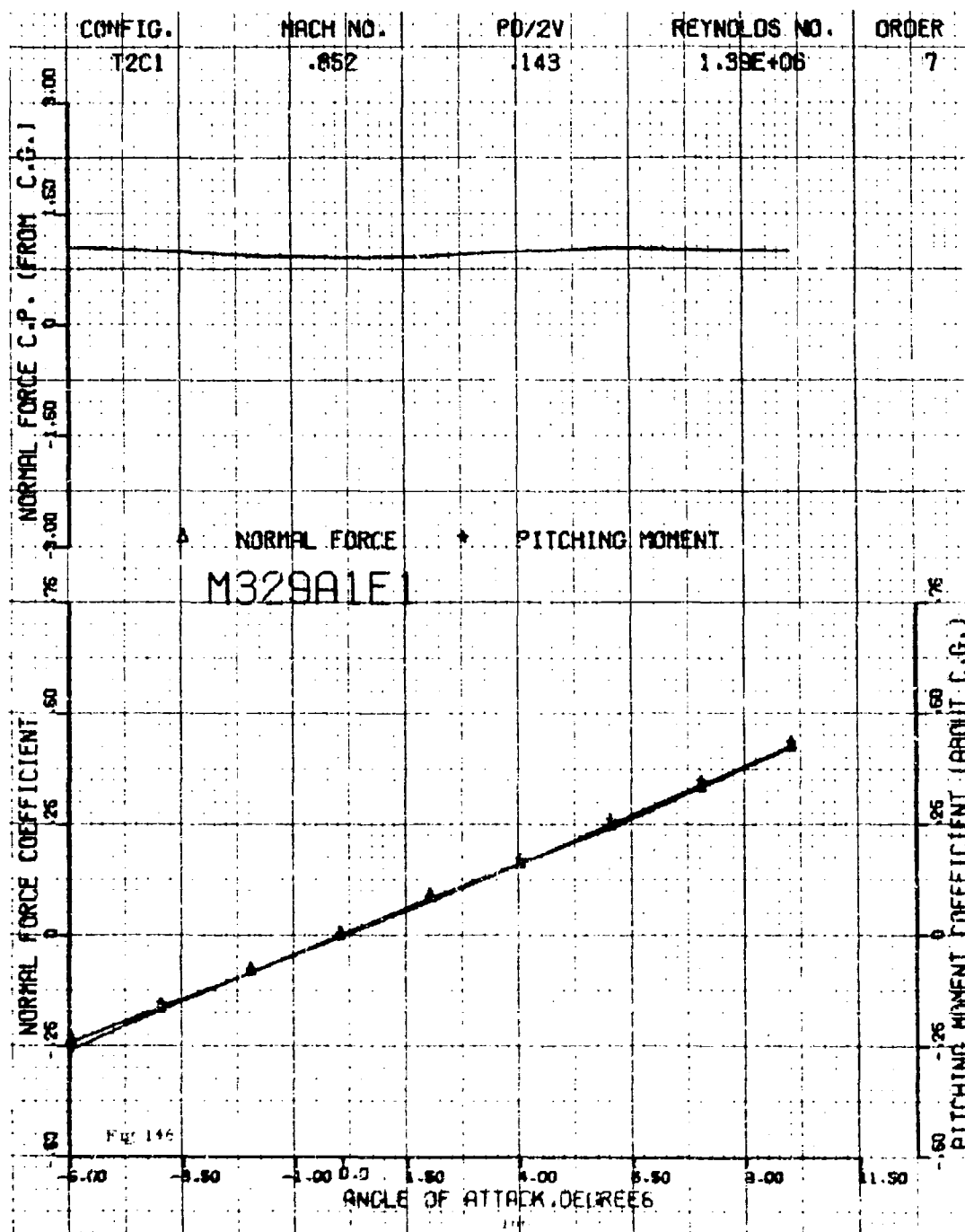


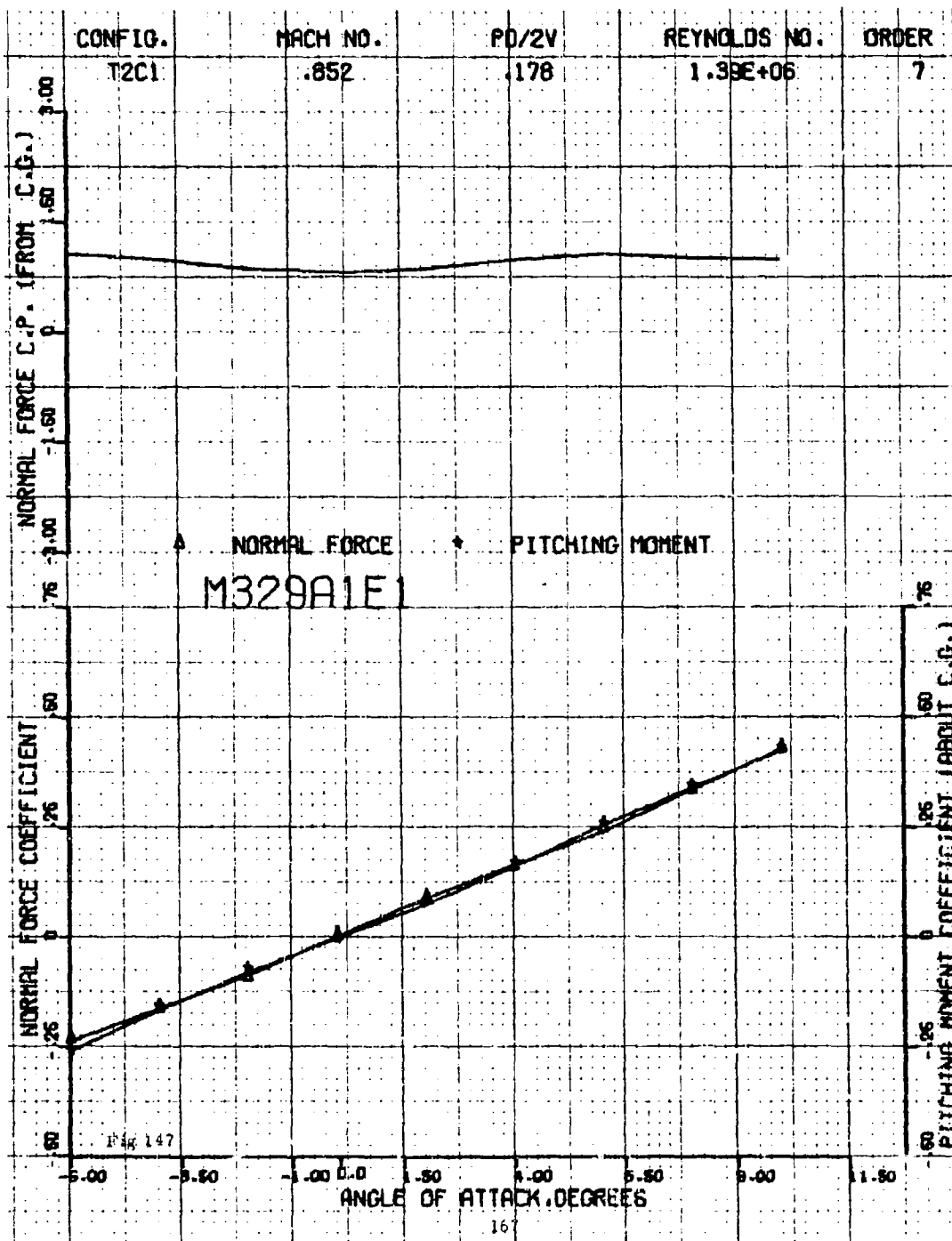


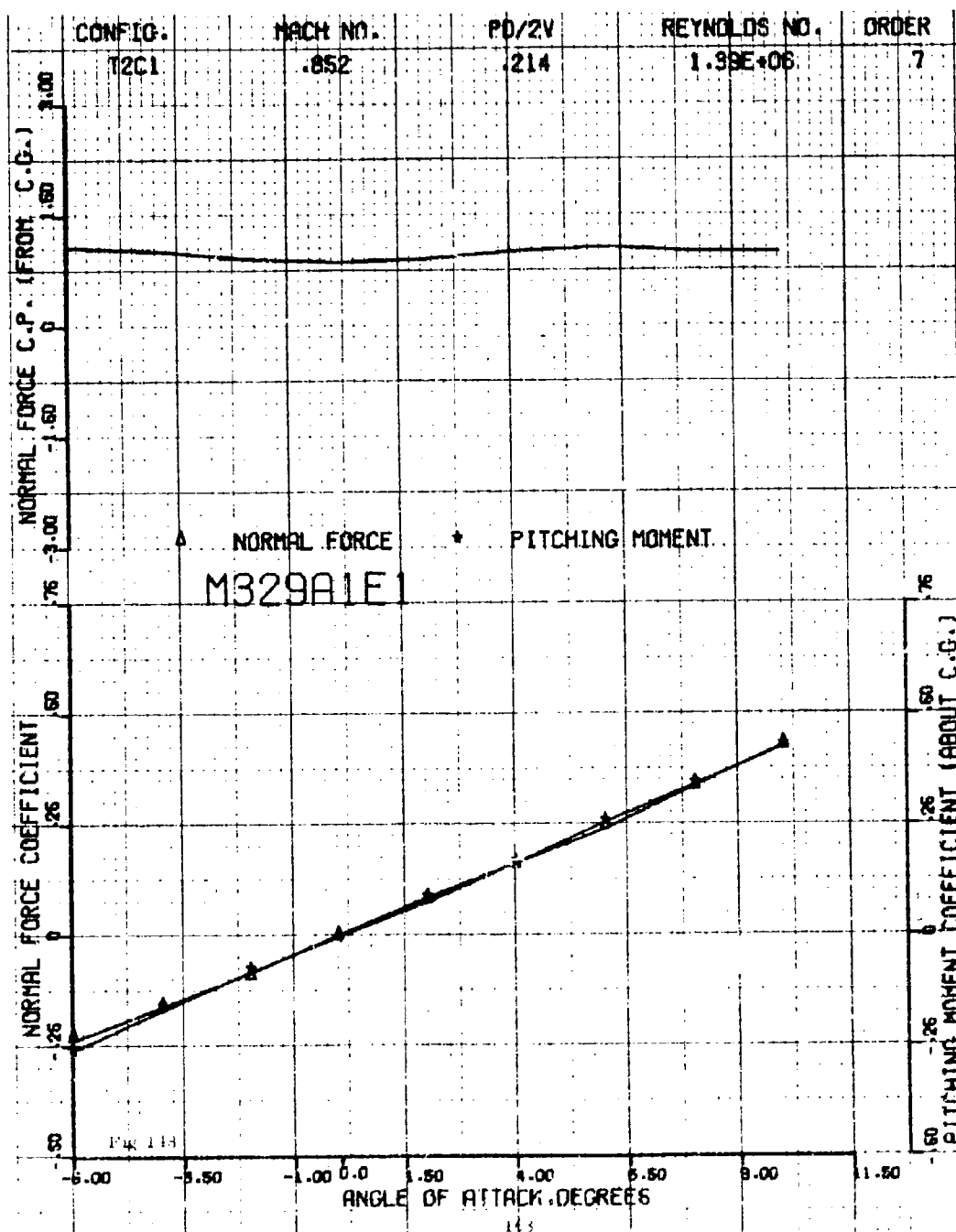


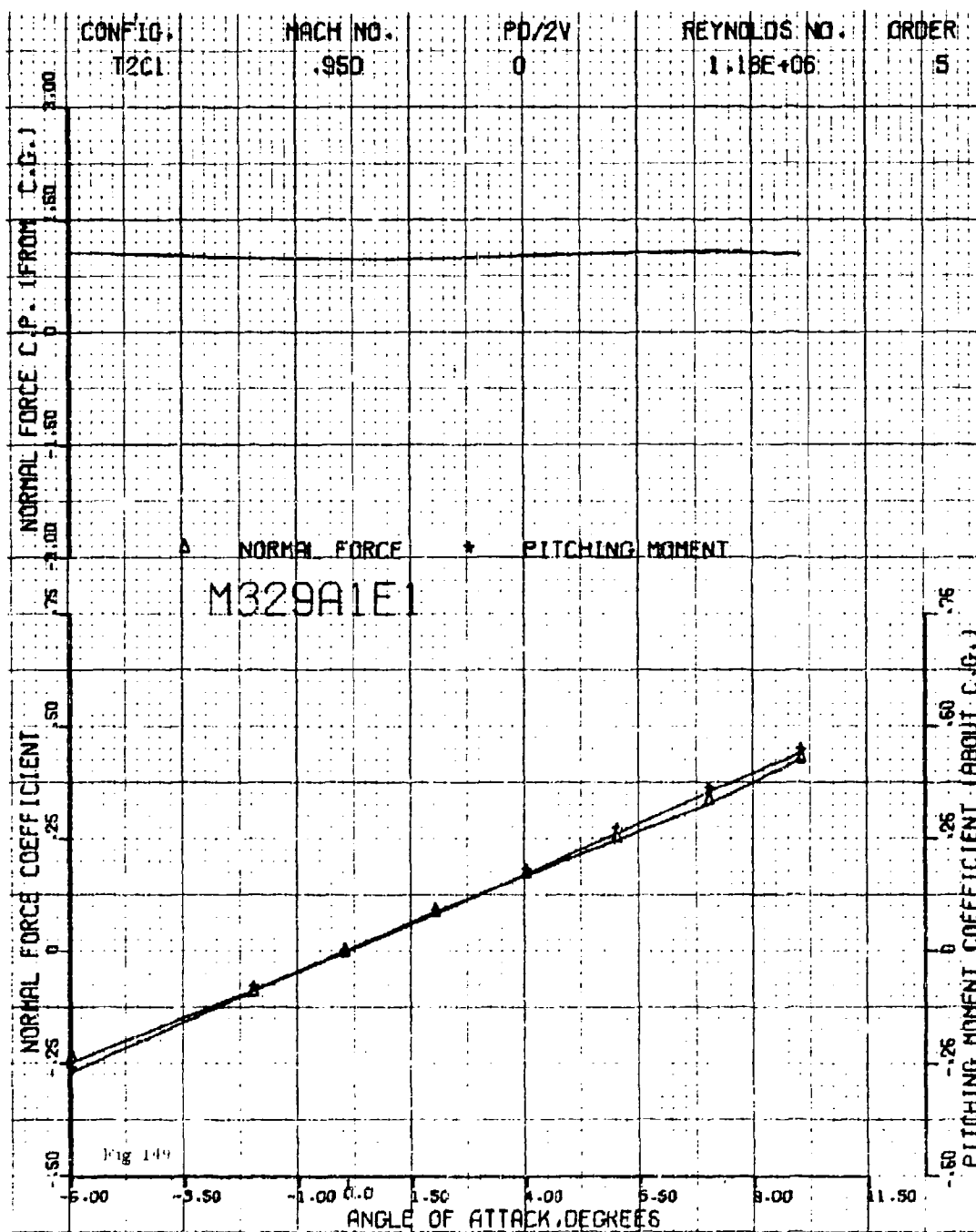


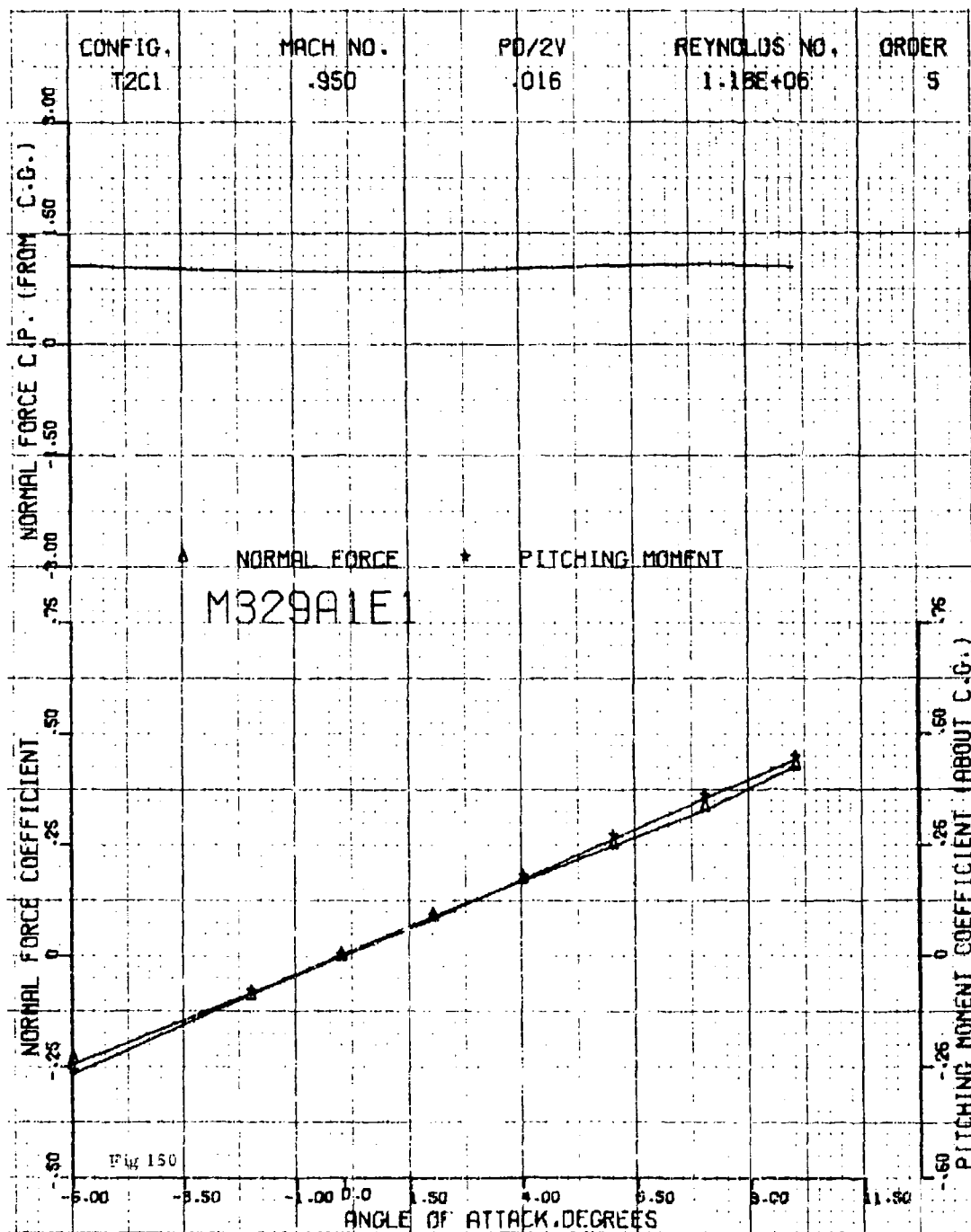


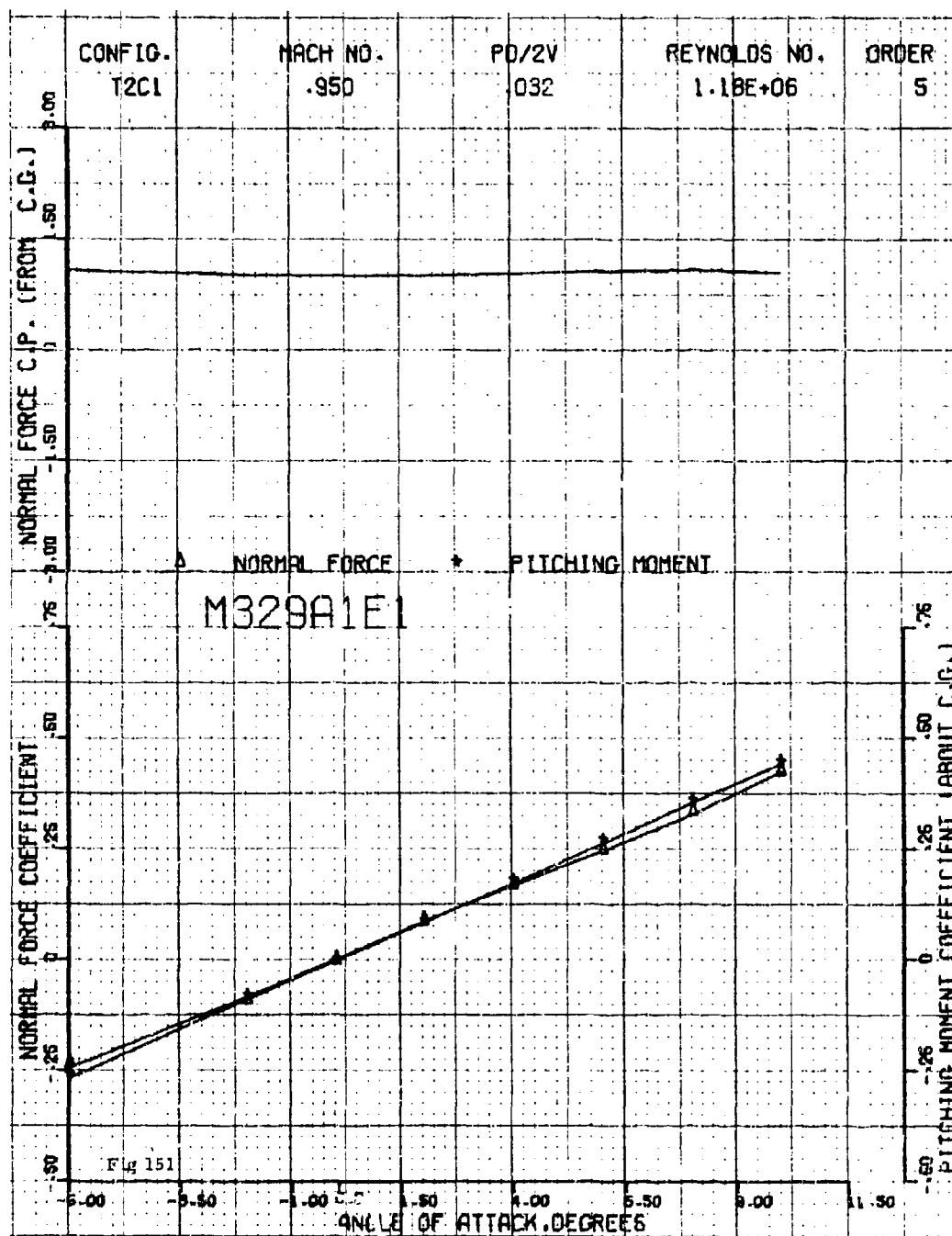


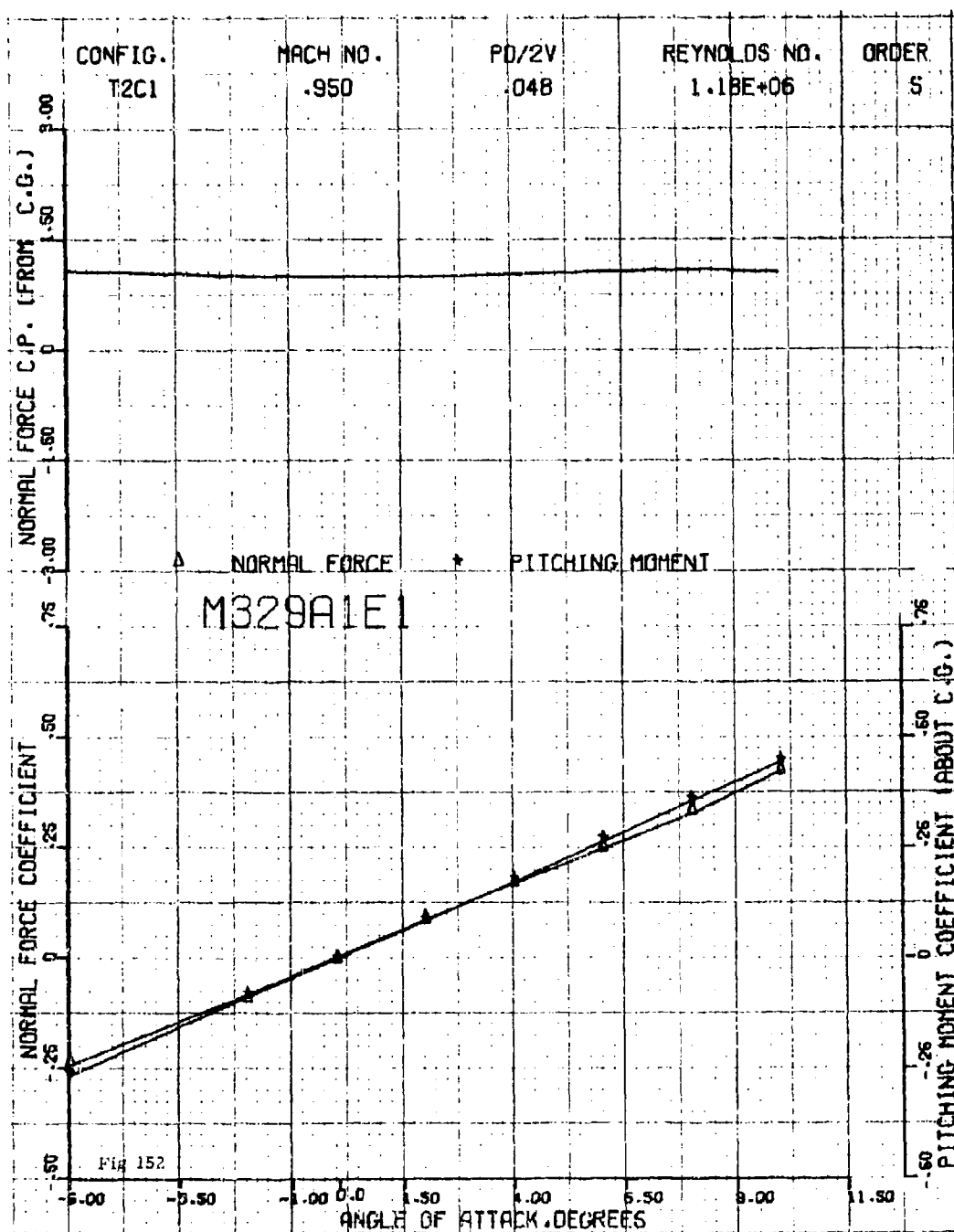


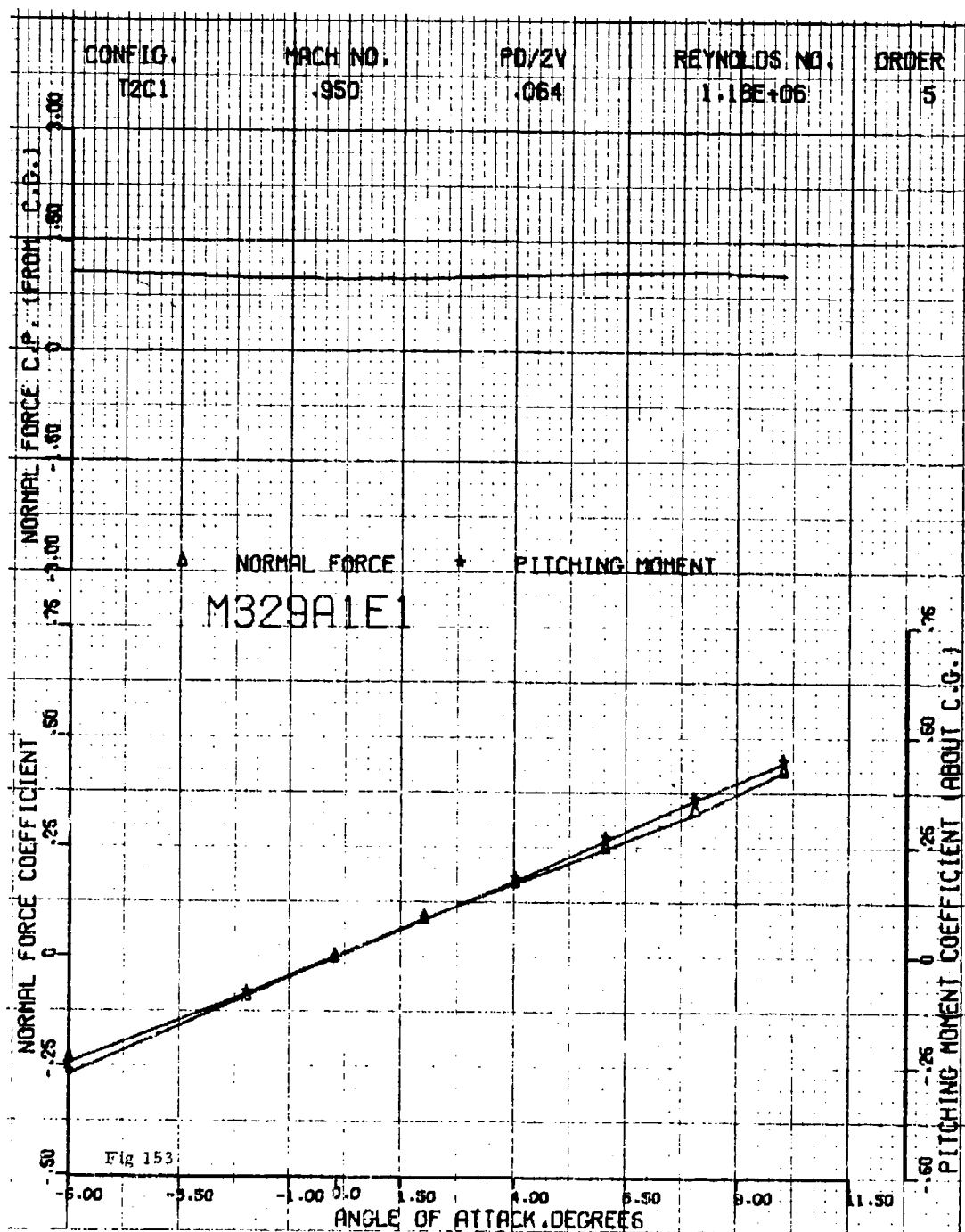


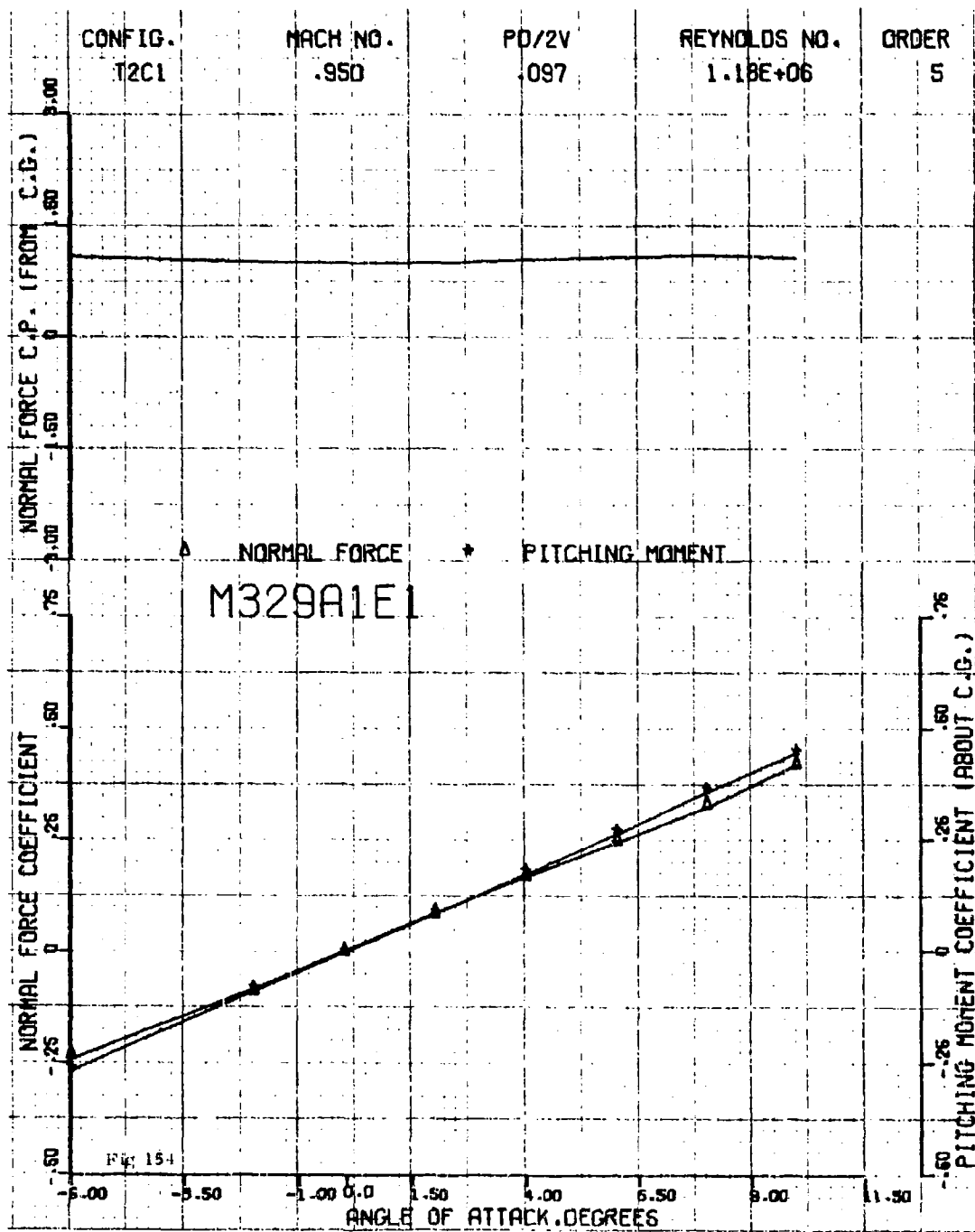


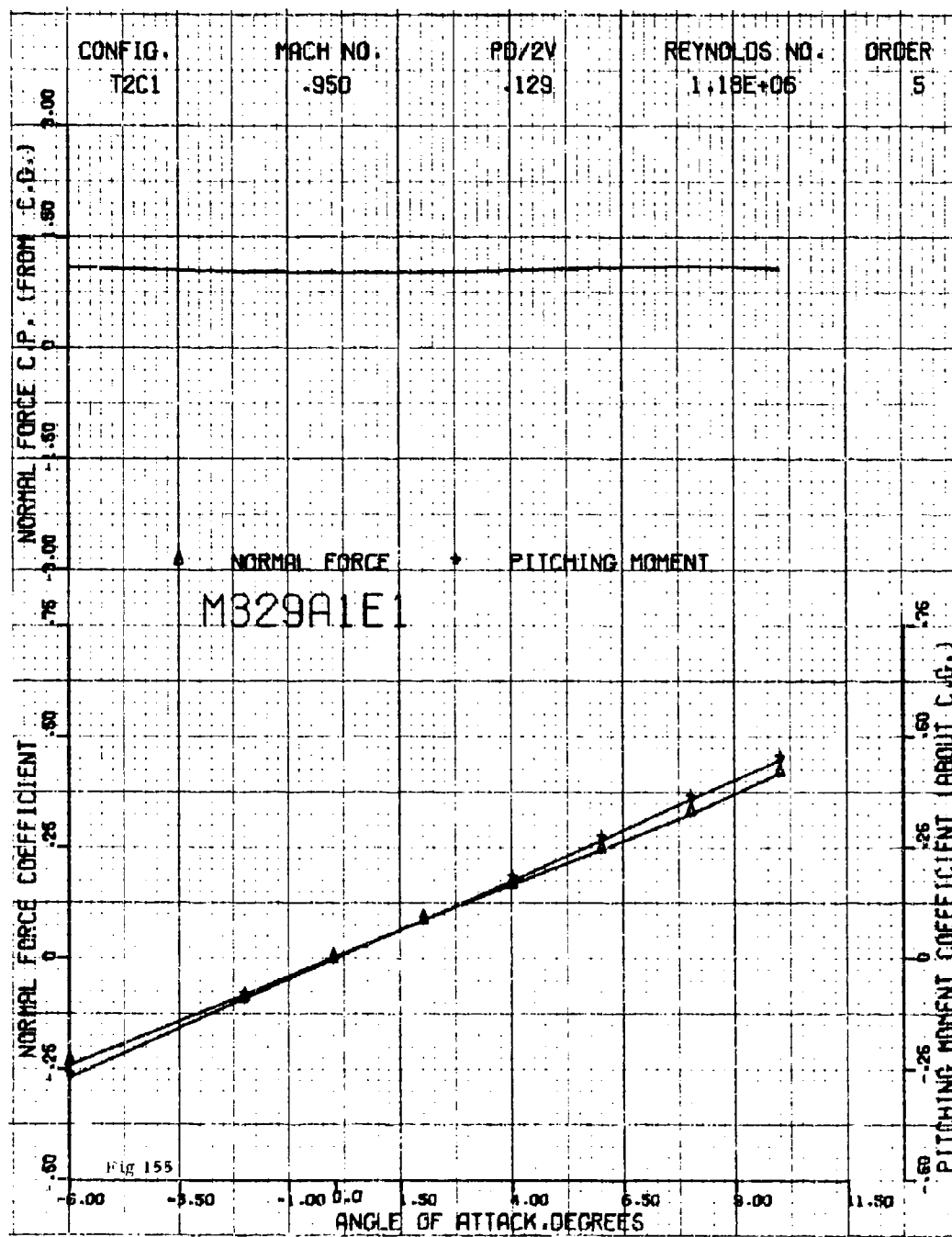


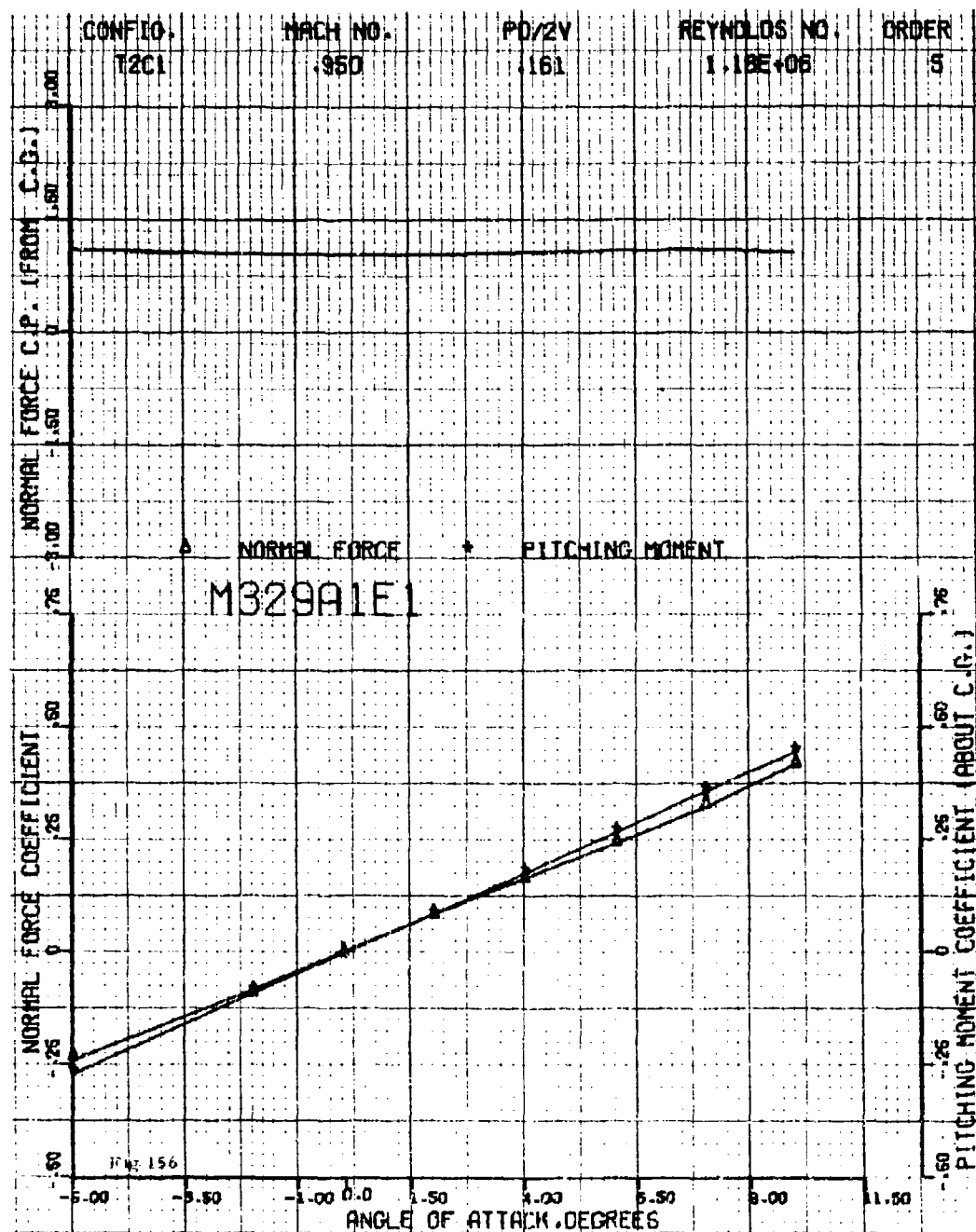


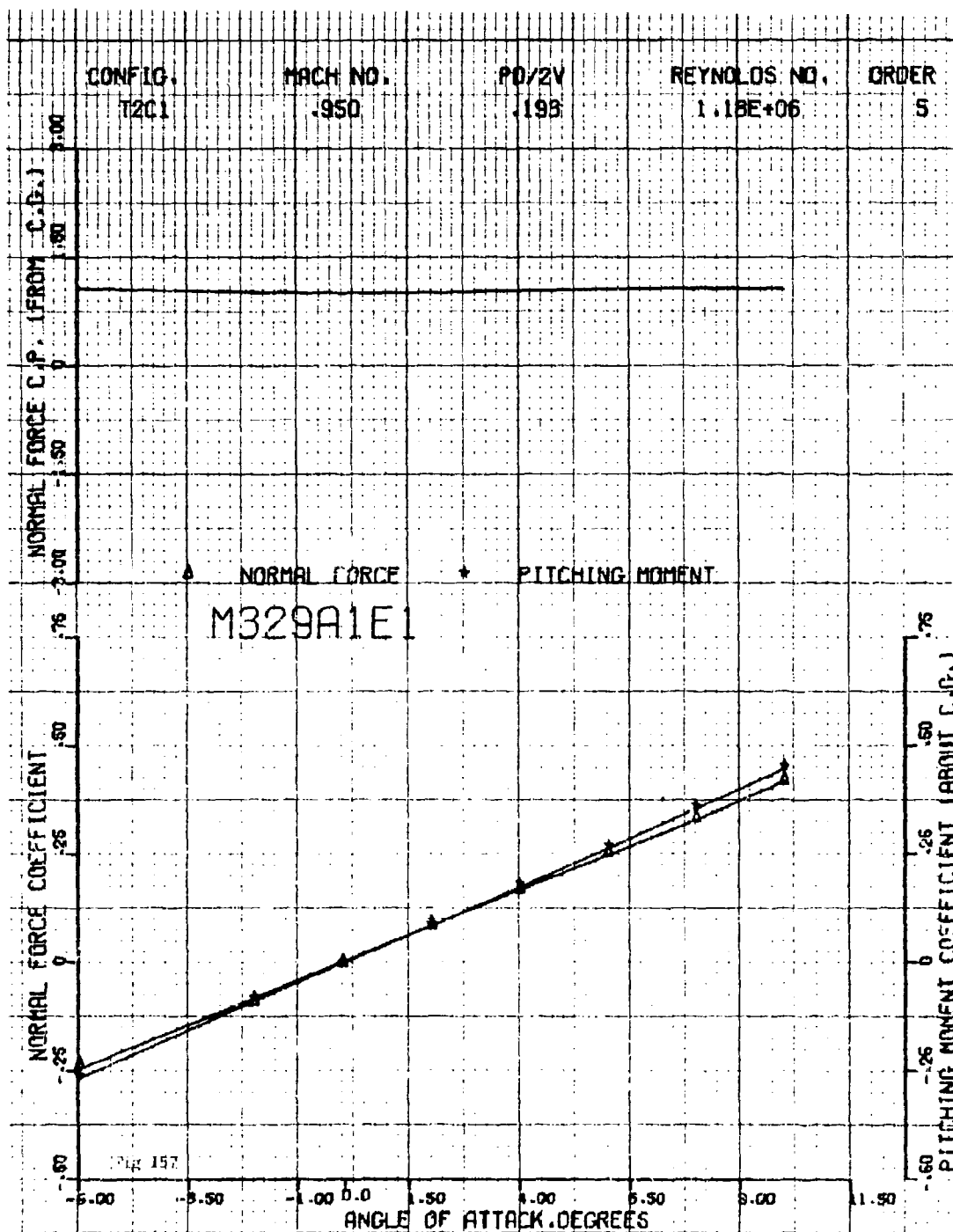










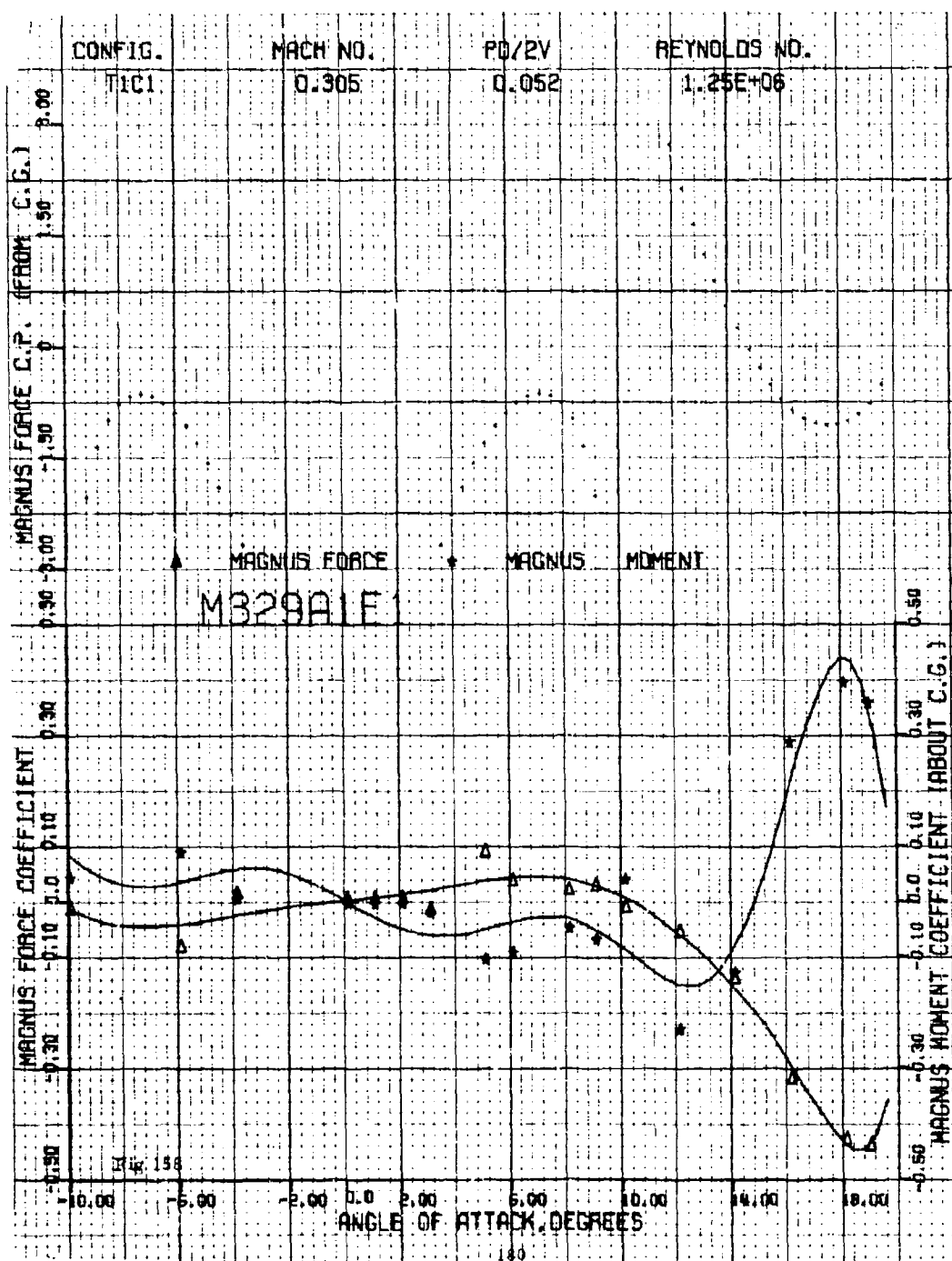


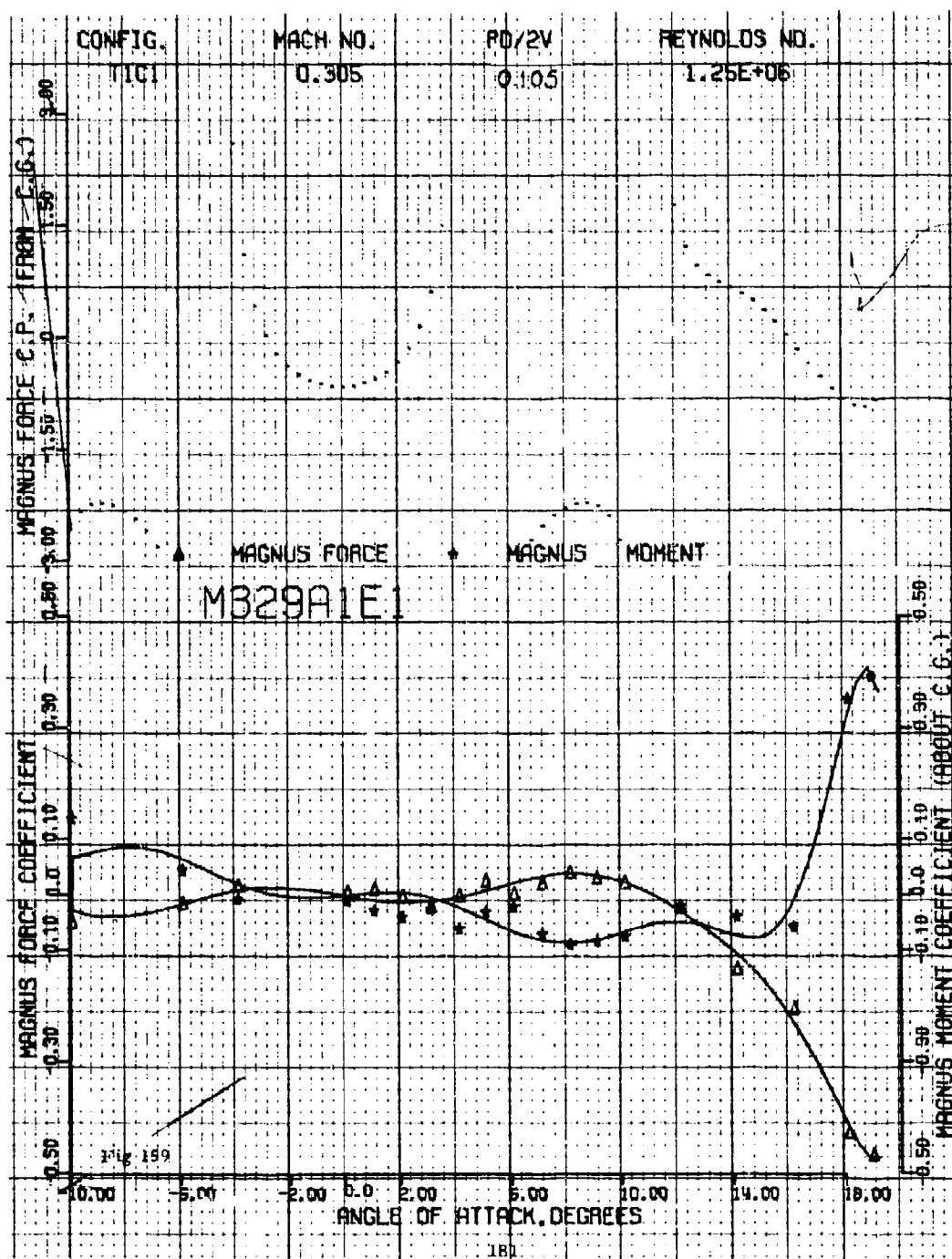
Figures 158 through 333

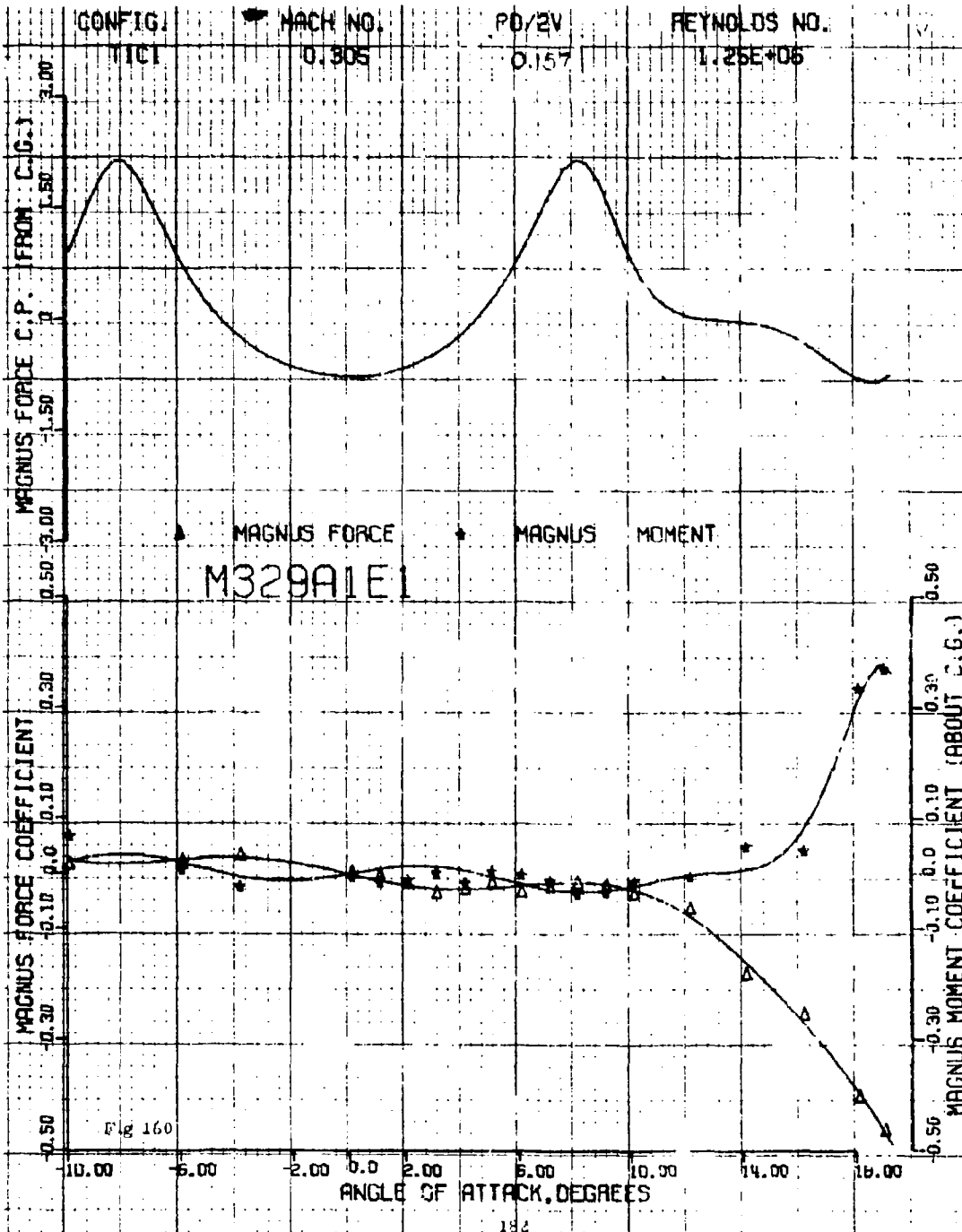
Magnus force coefficient, Magnus moment coefficient,
Magnus force center of pressure vs angle of attack.

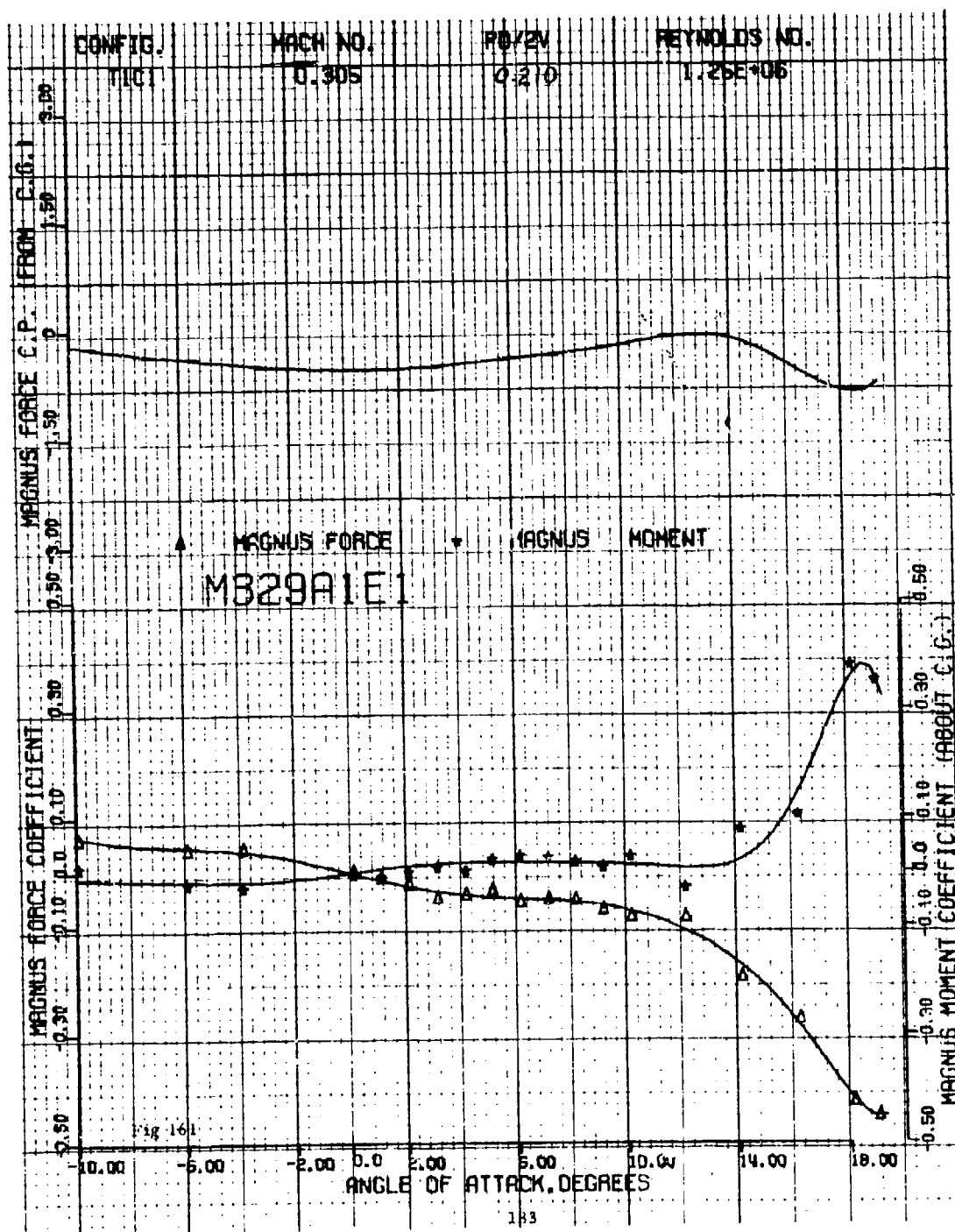
(Includes several configurations, Mach numbers,
 $pd/2V$'s and Reynolds numbers [12' PWT] .)

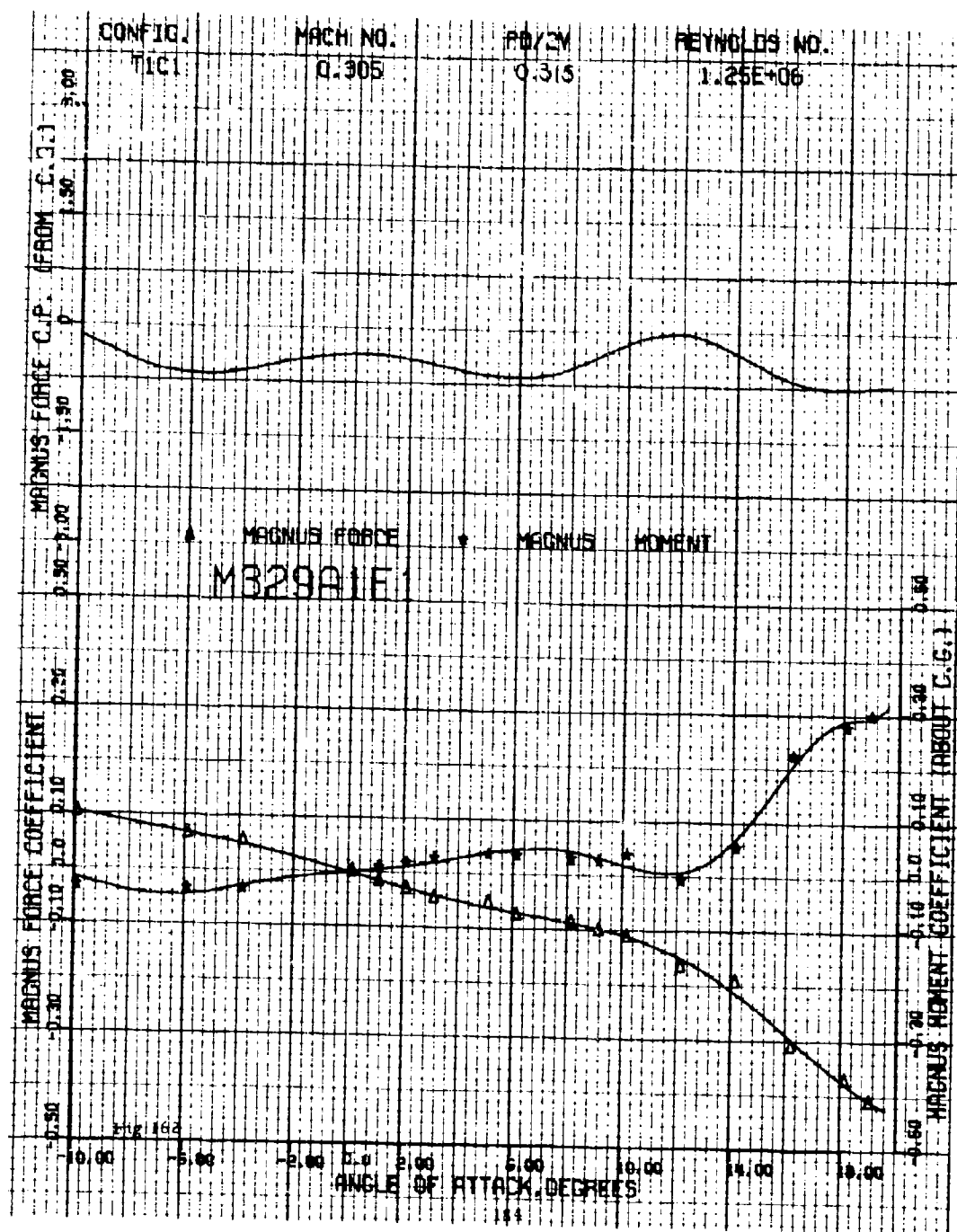
Preceding page blank

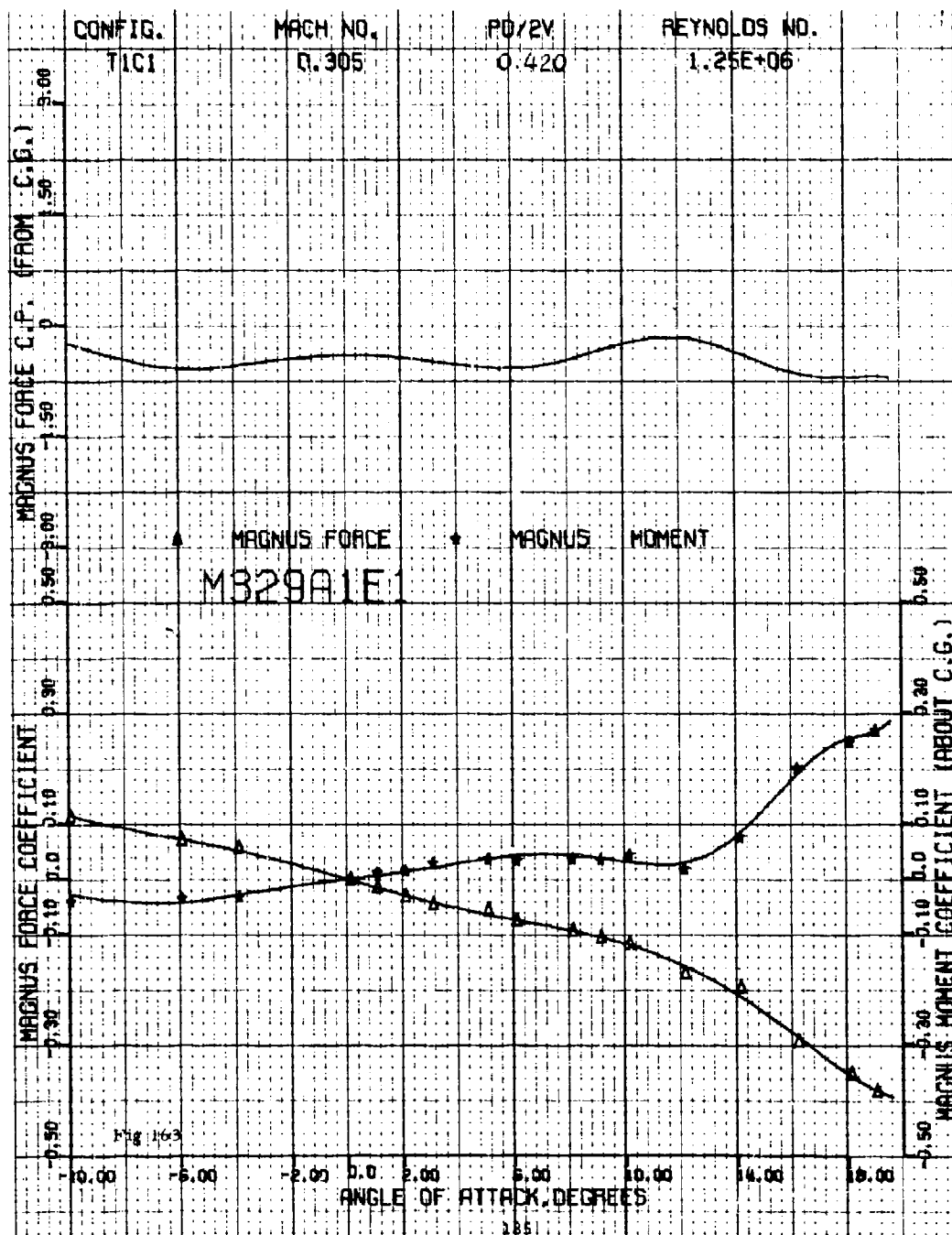


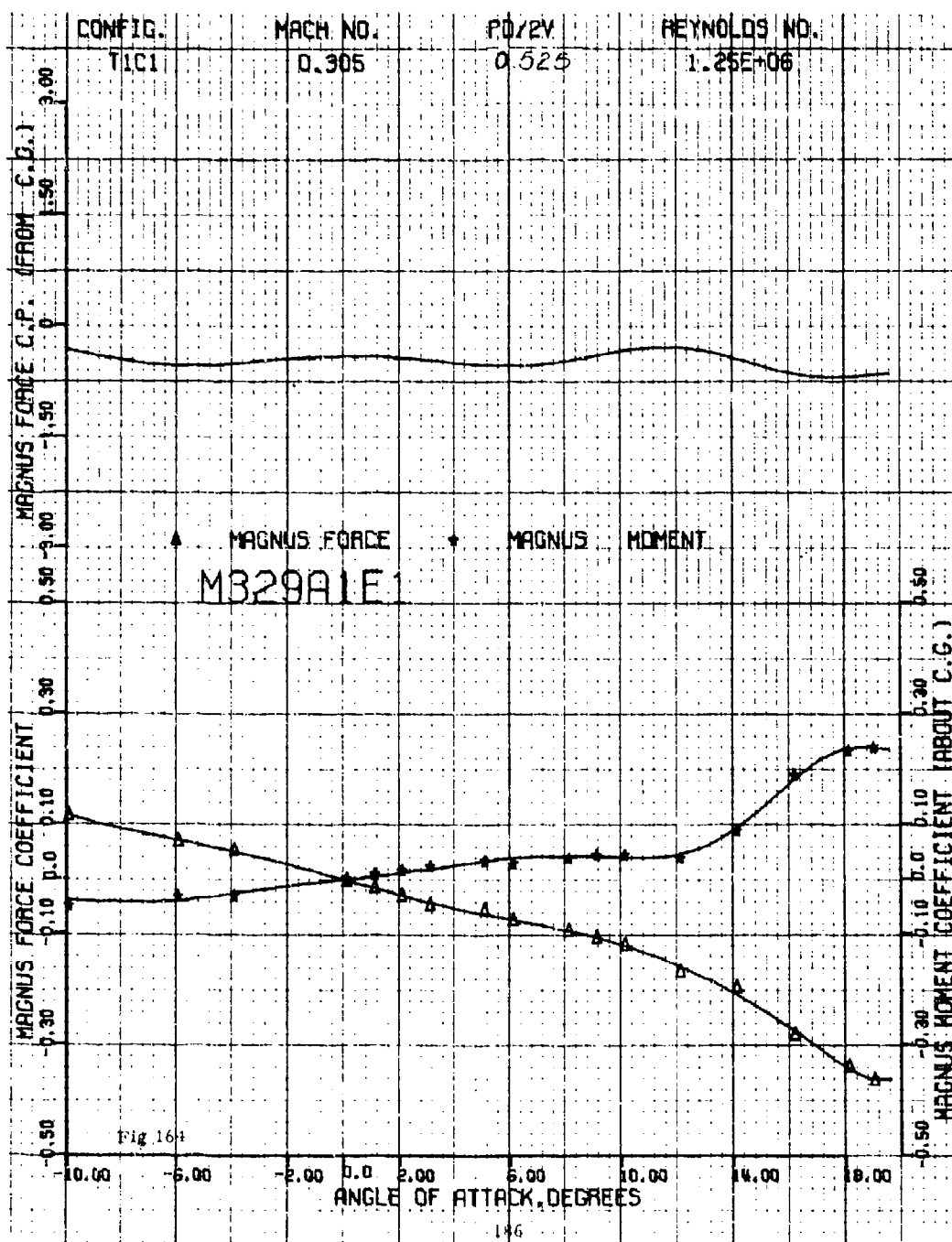


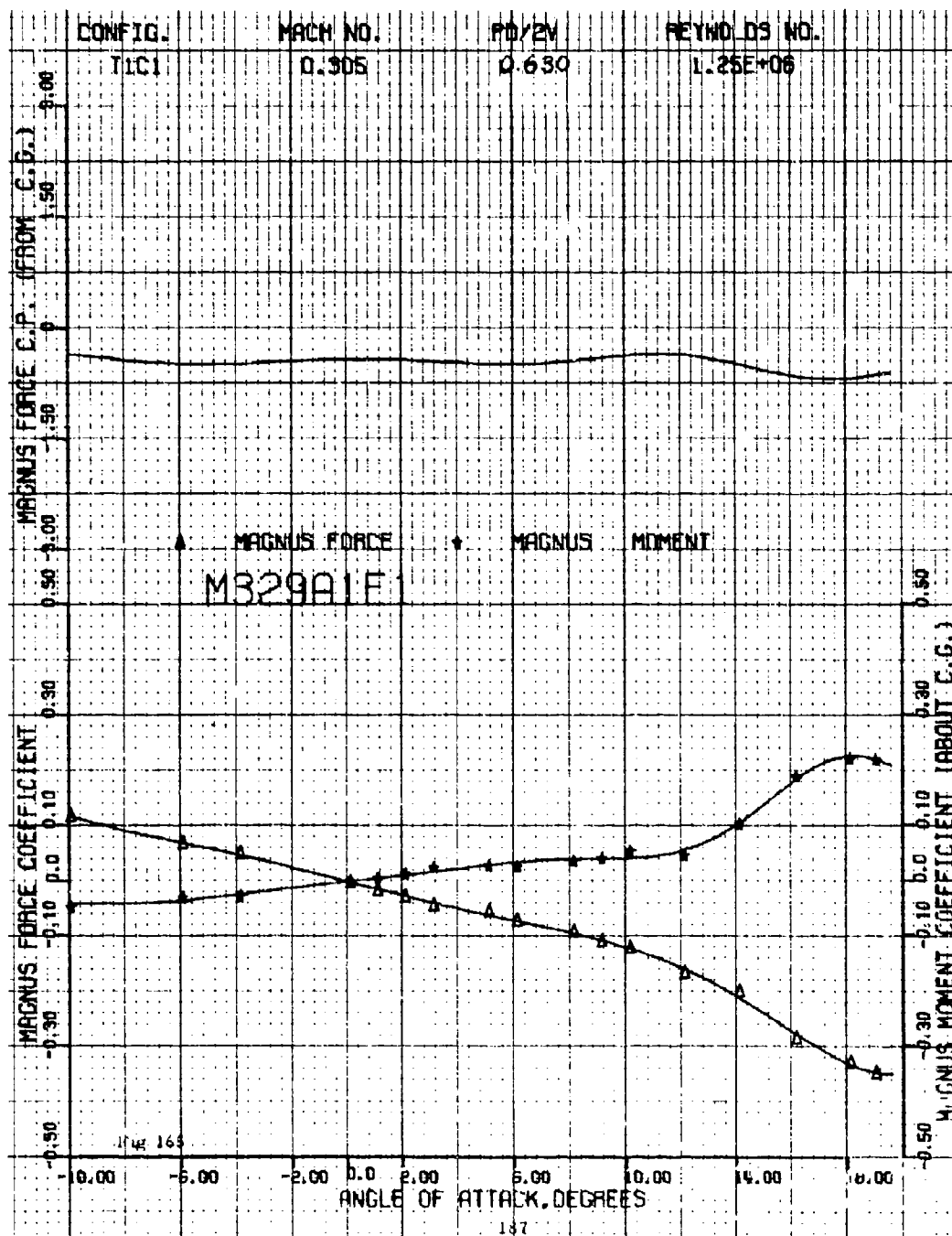


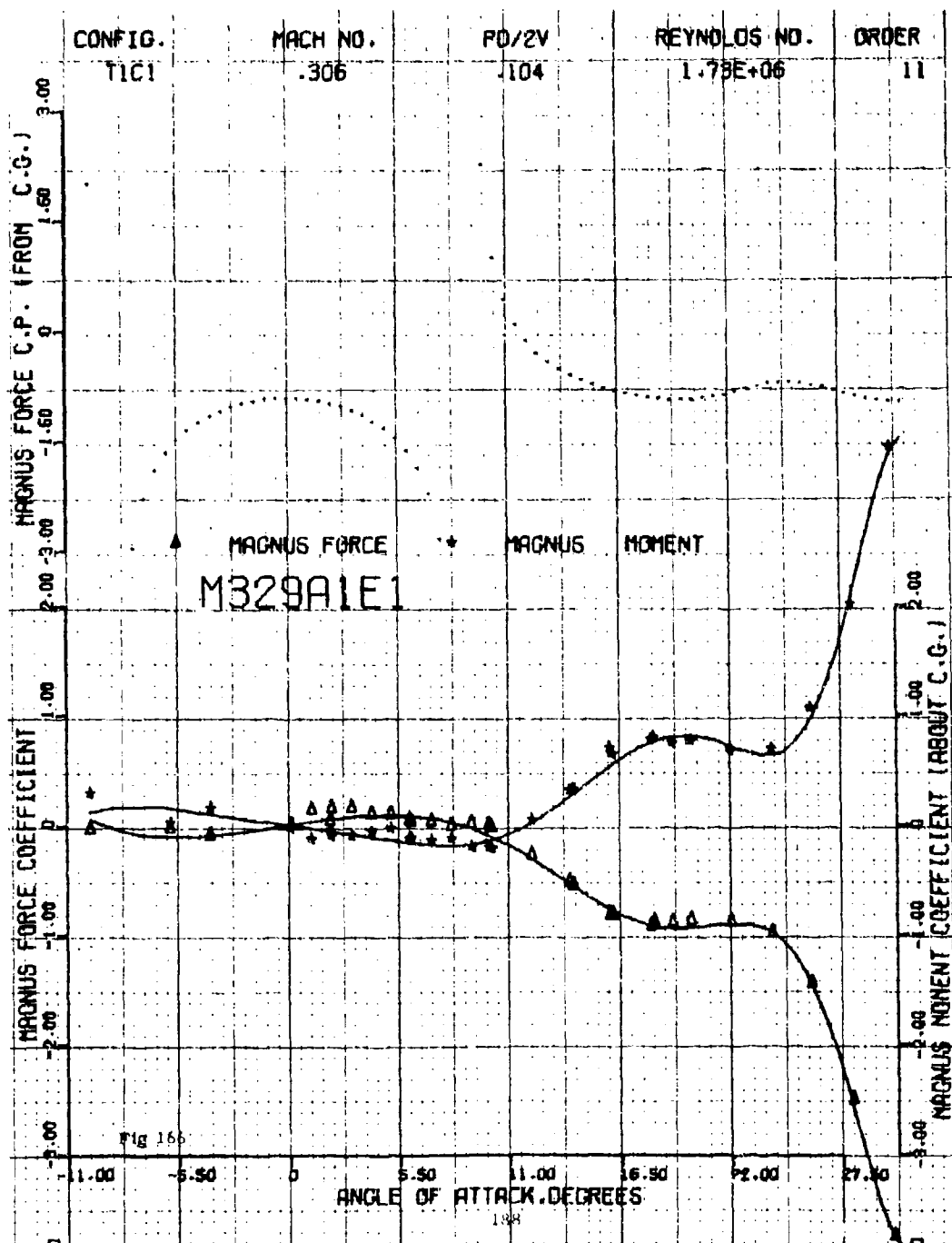


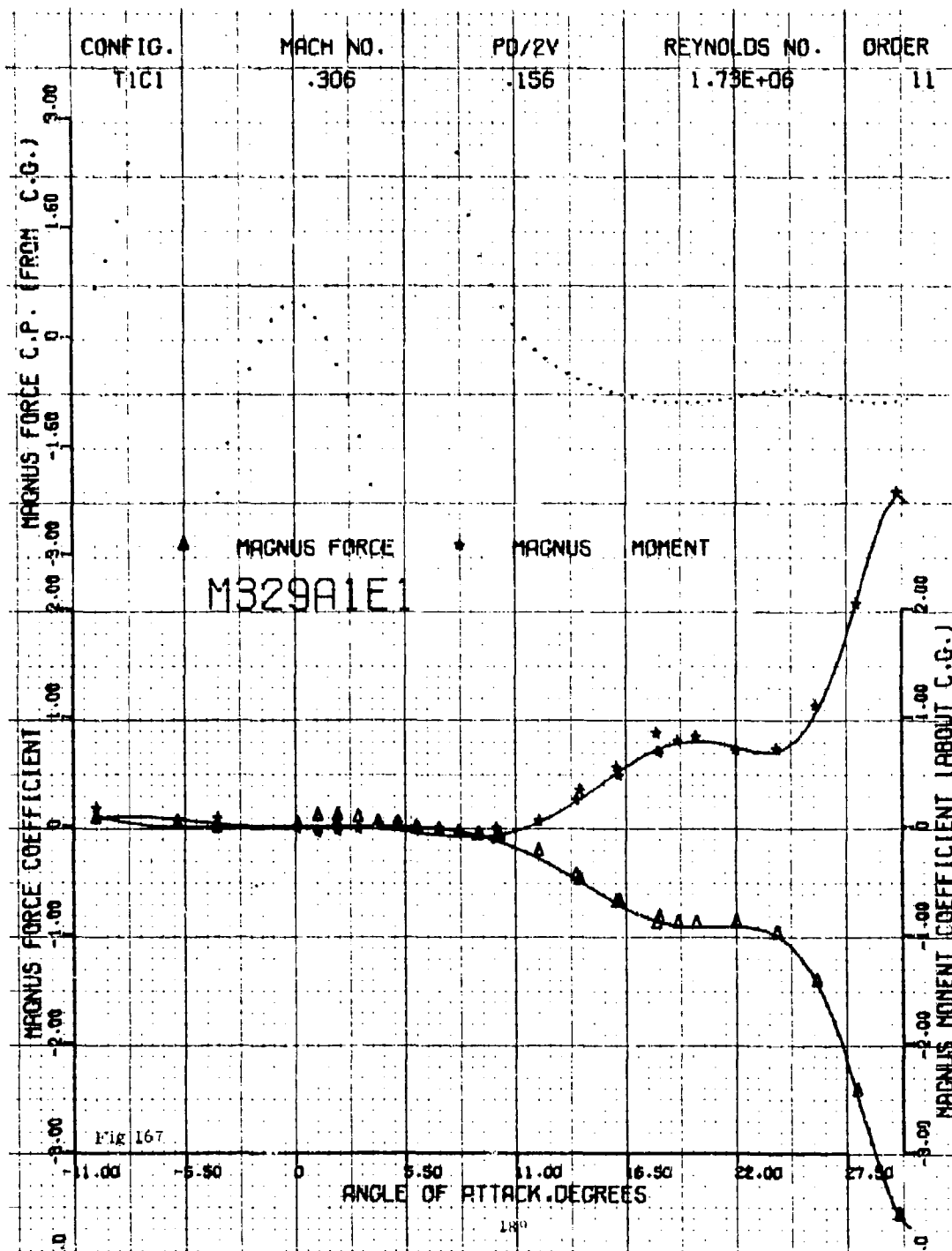


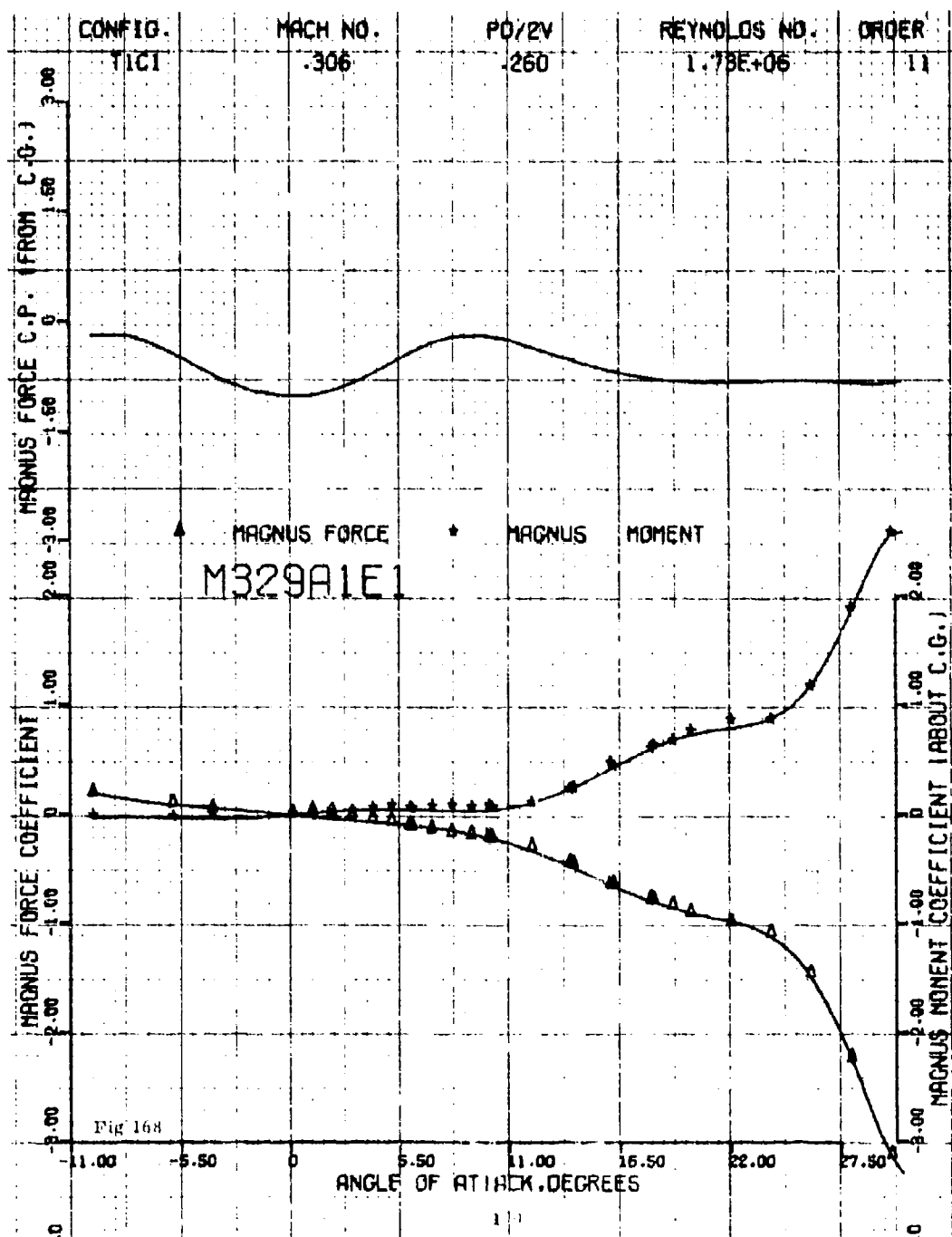


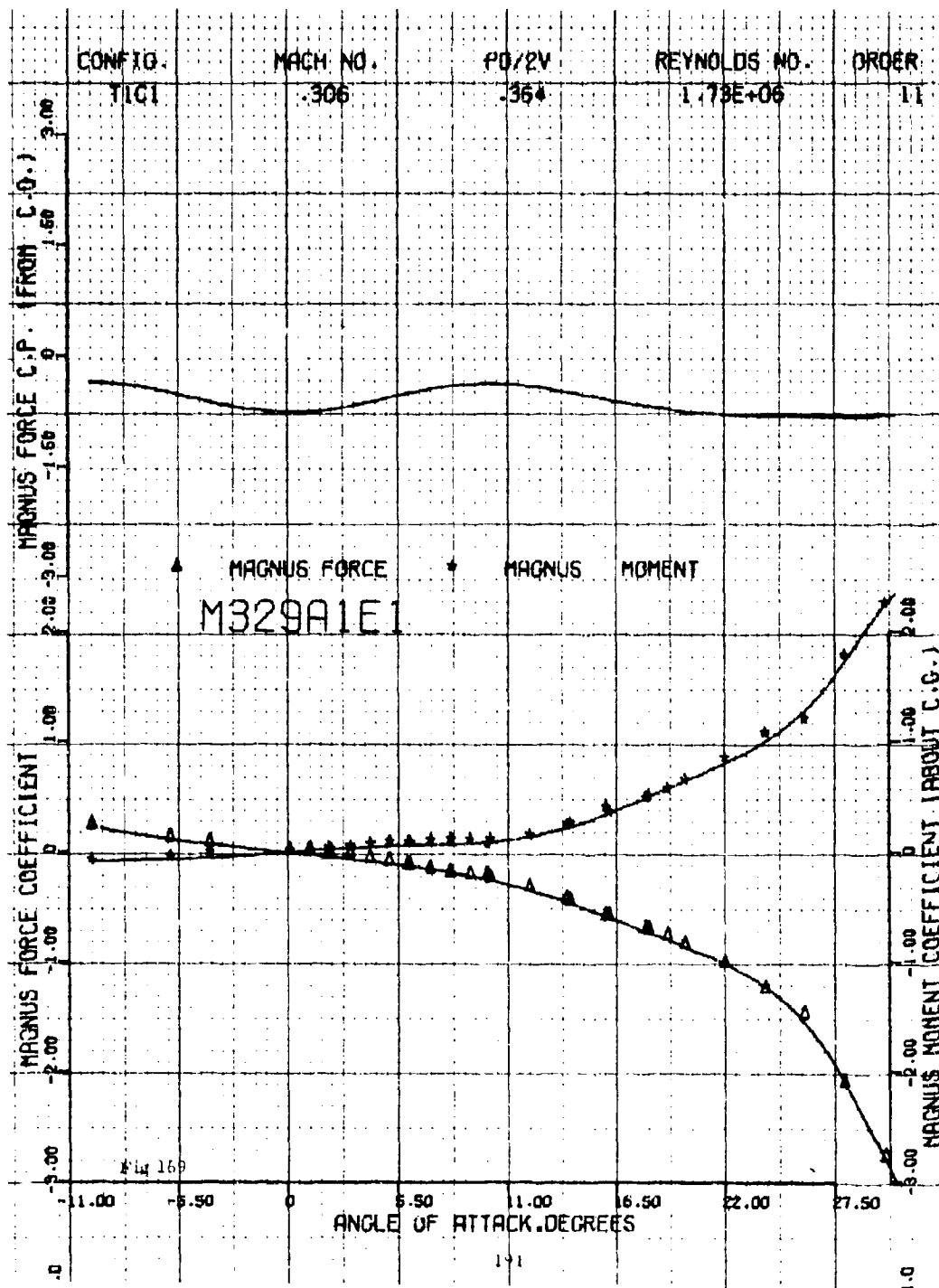


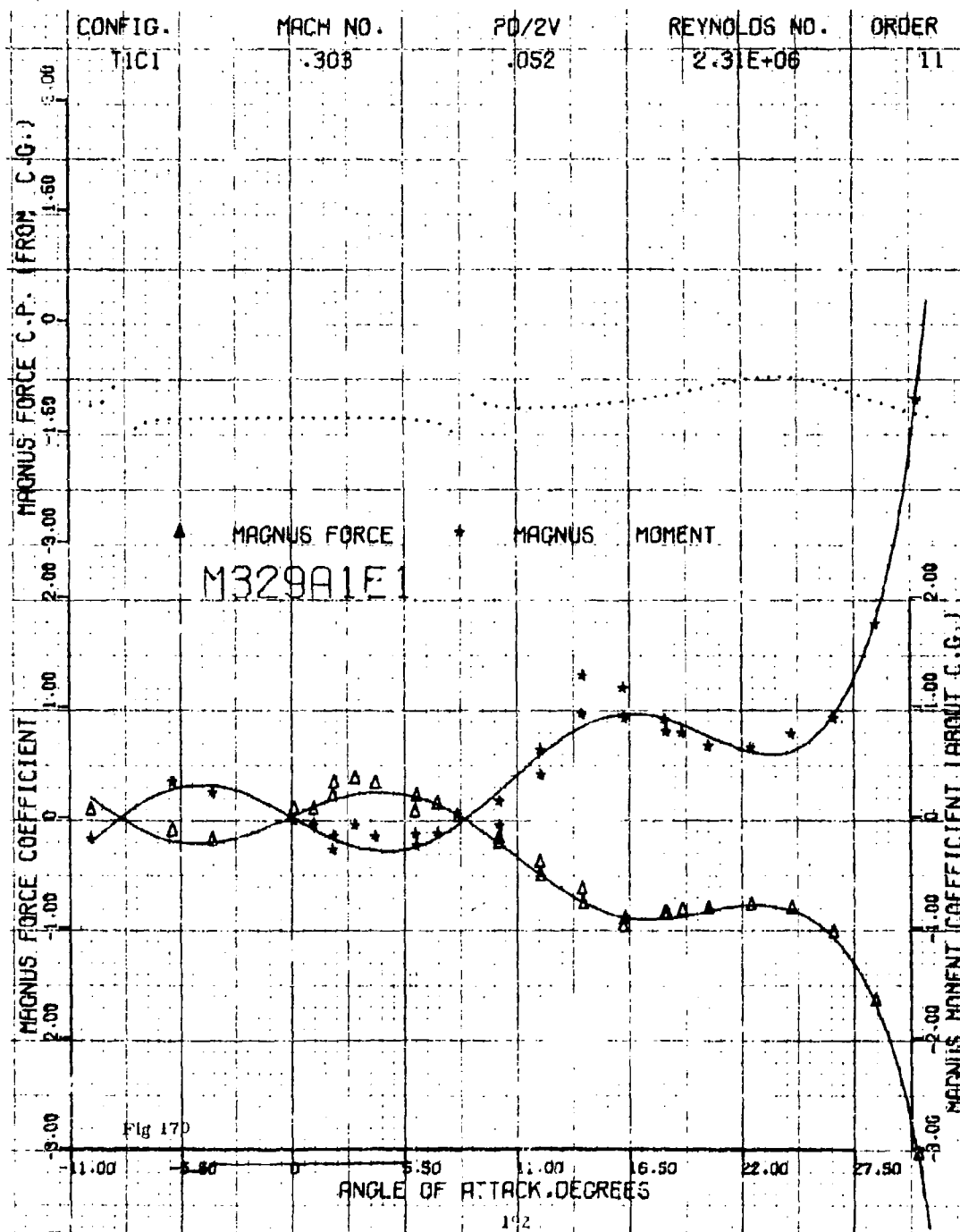


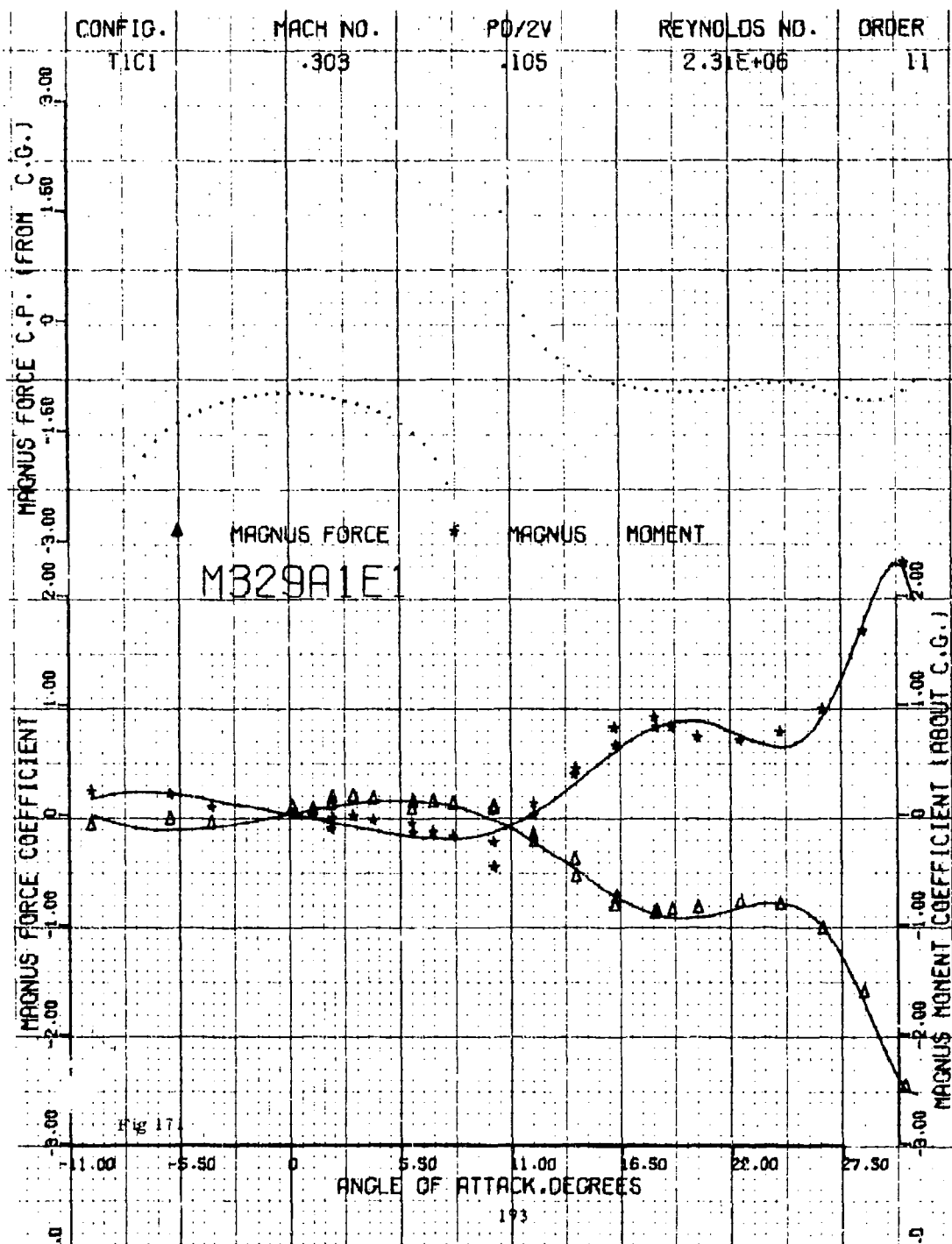


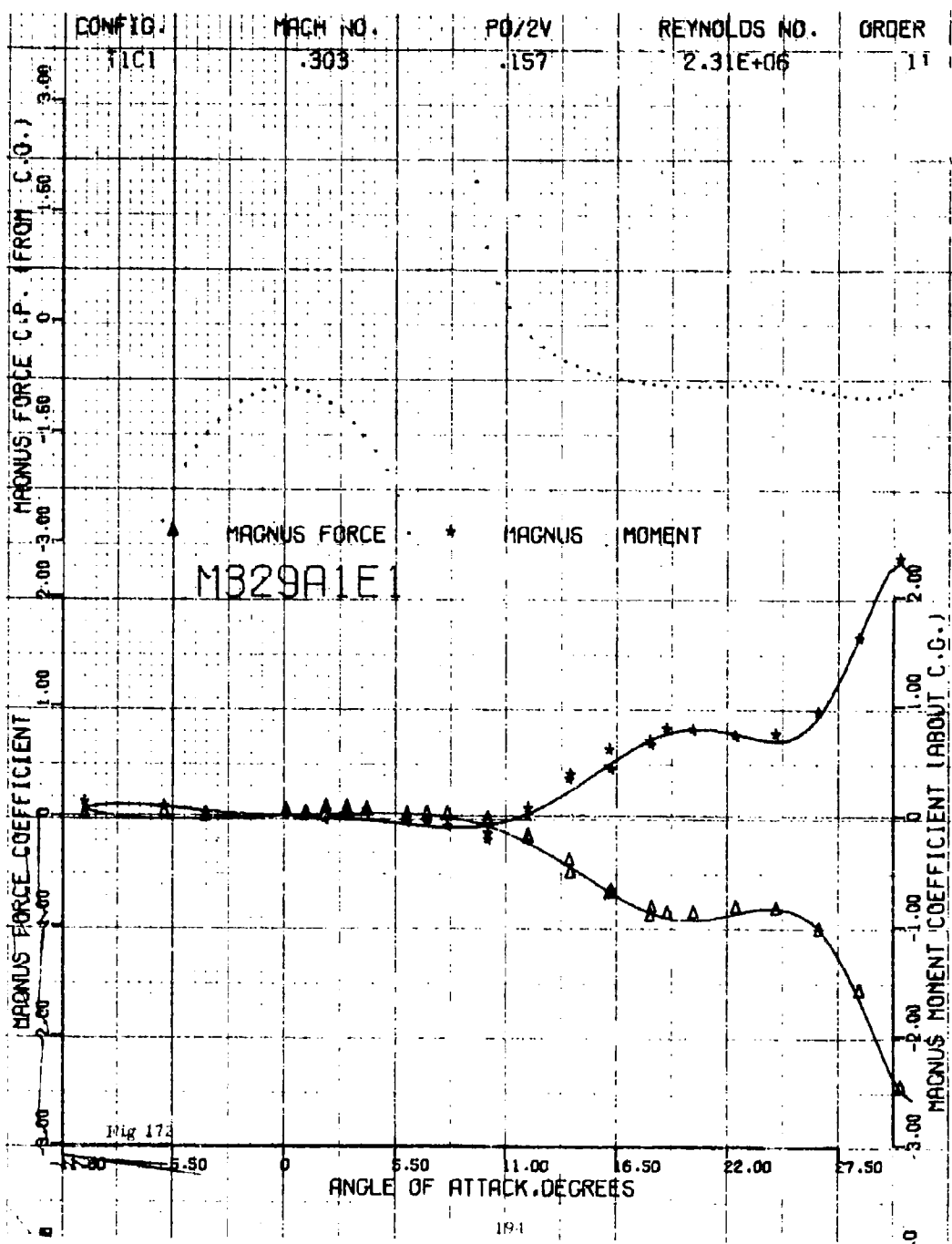


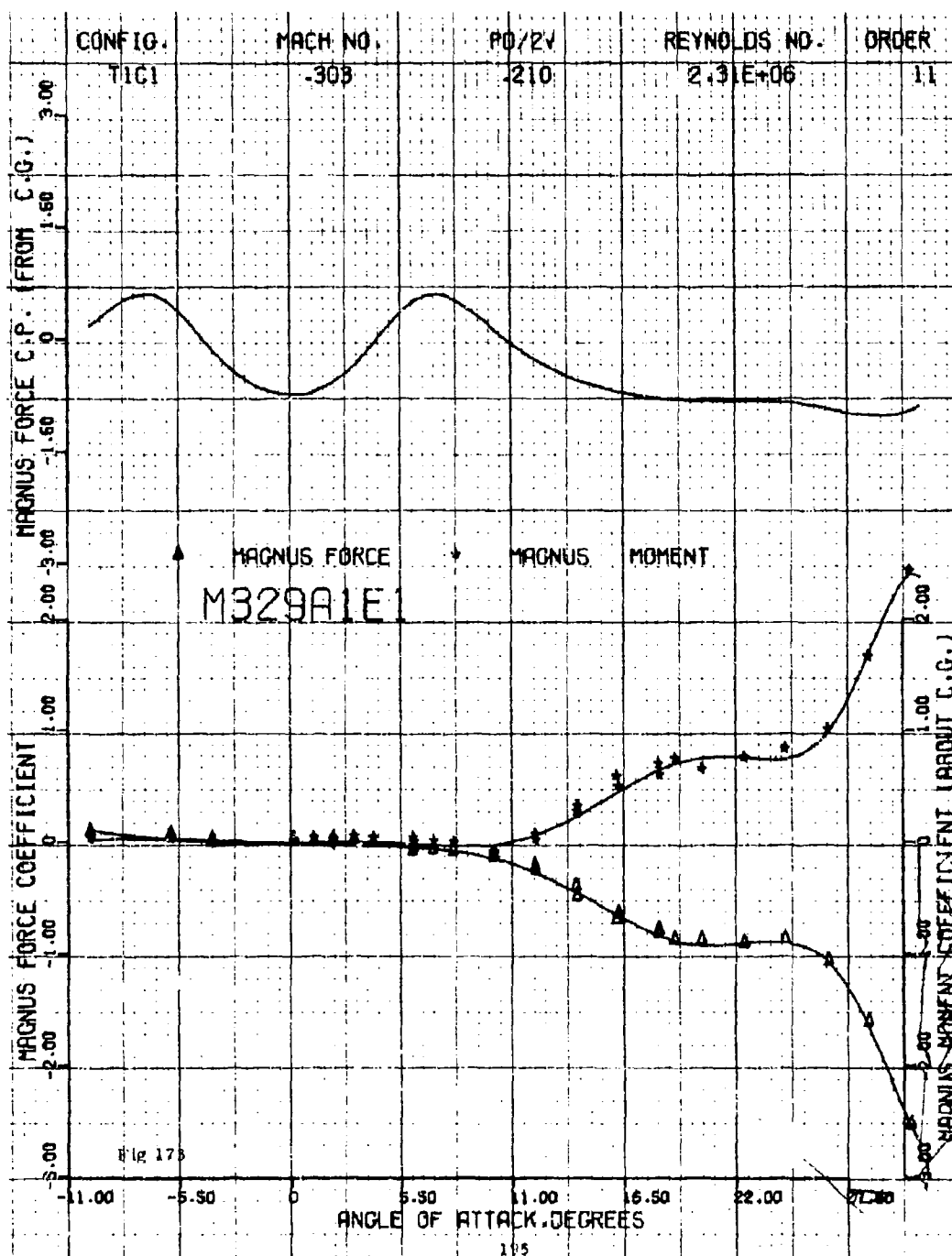


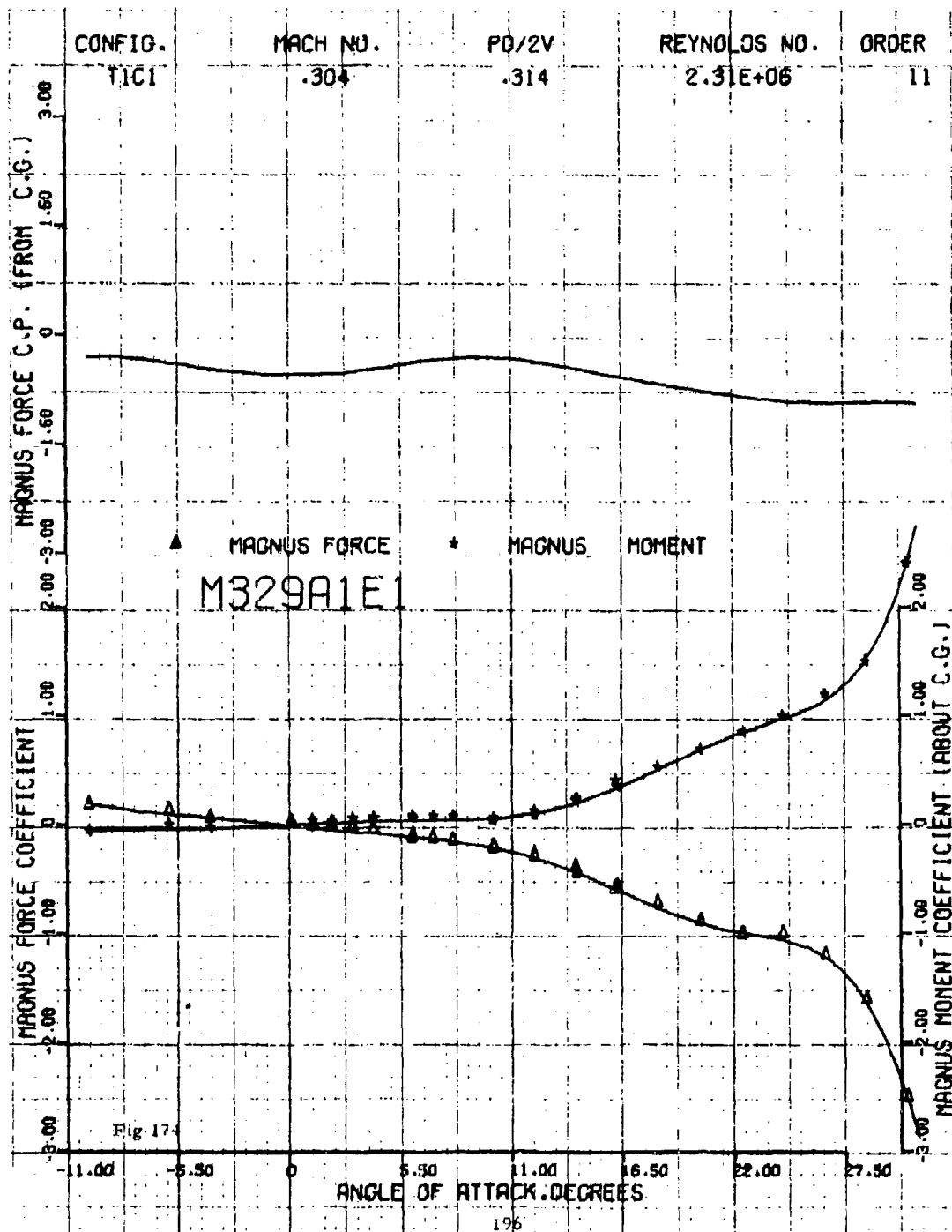


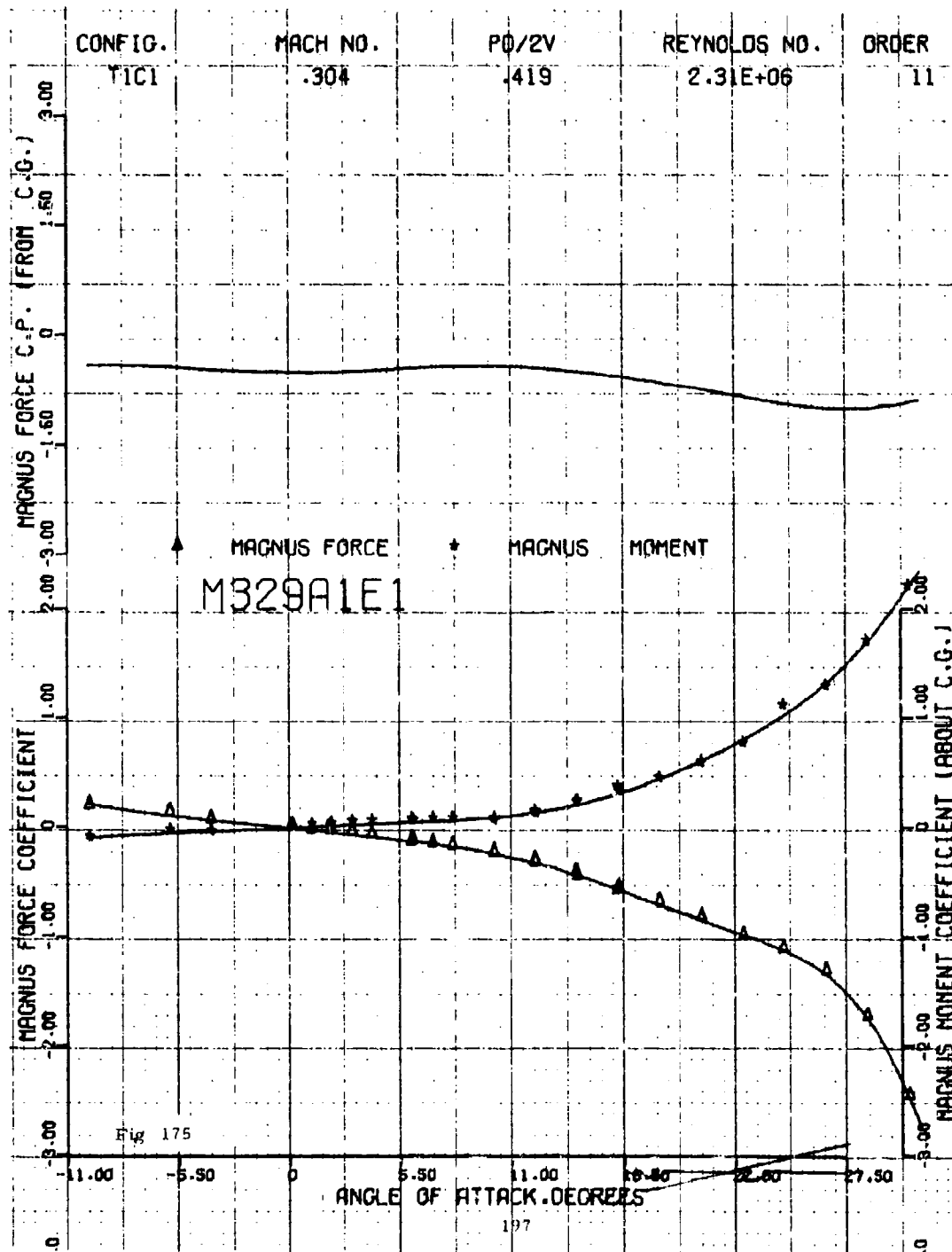


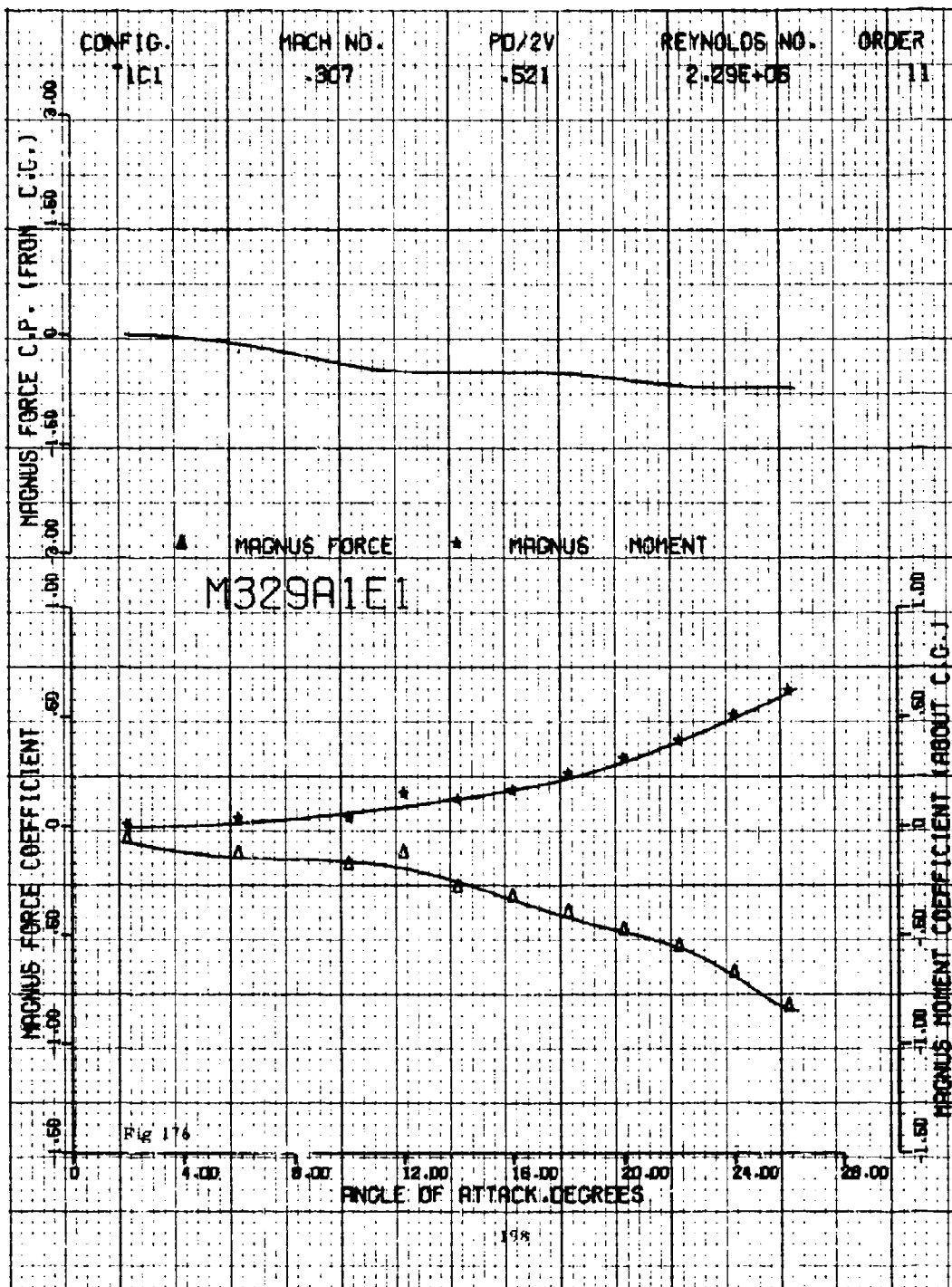


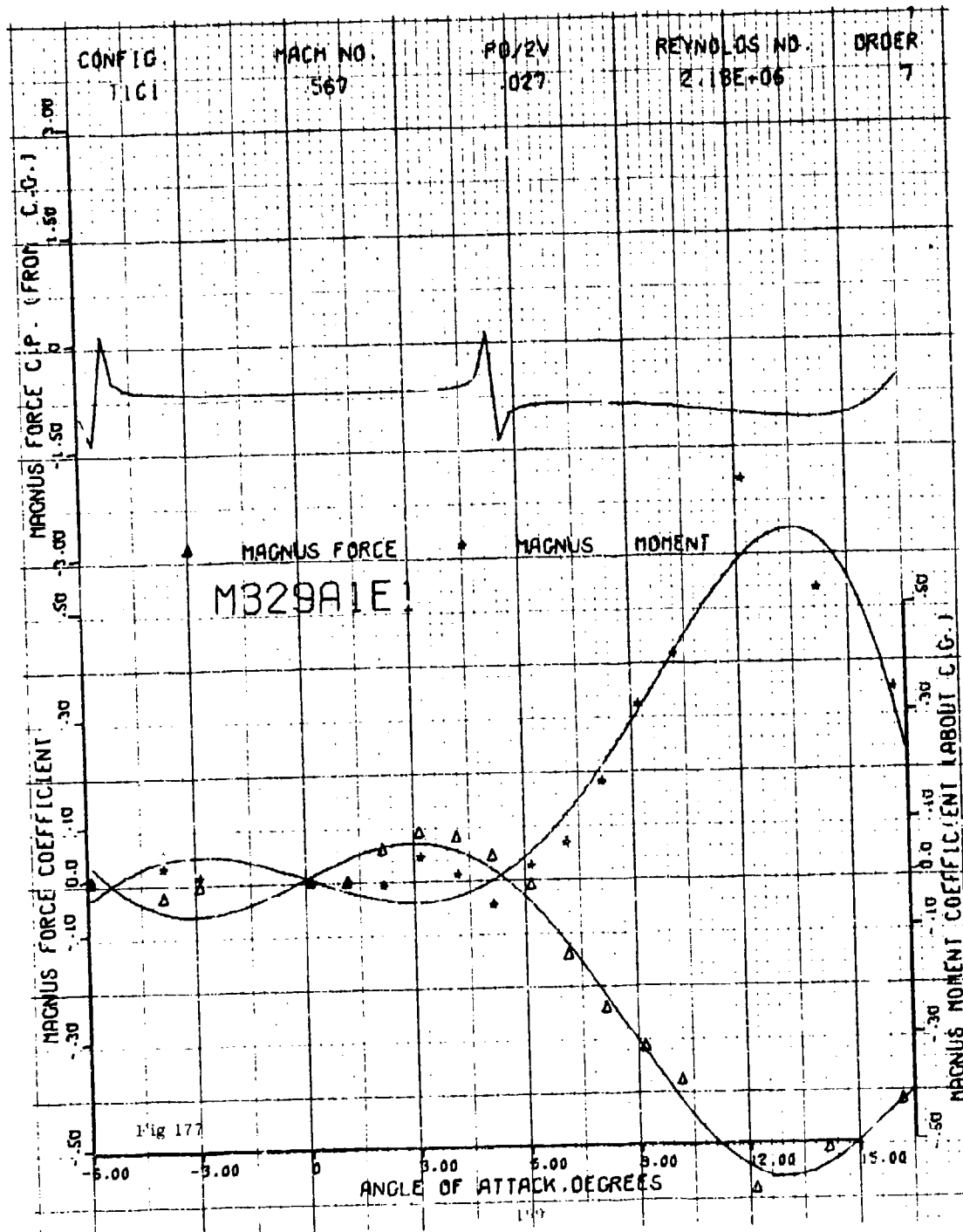


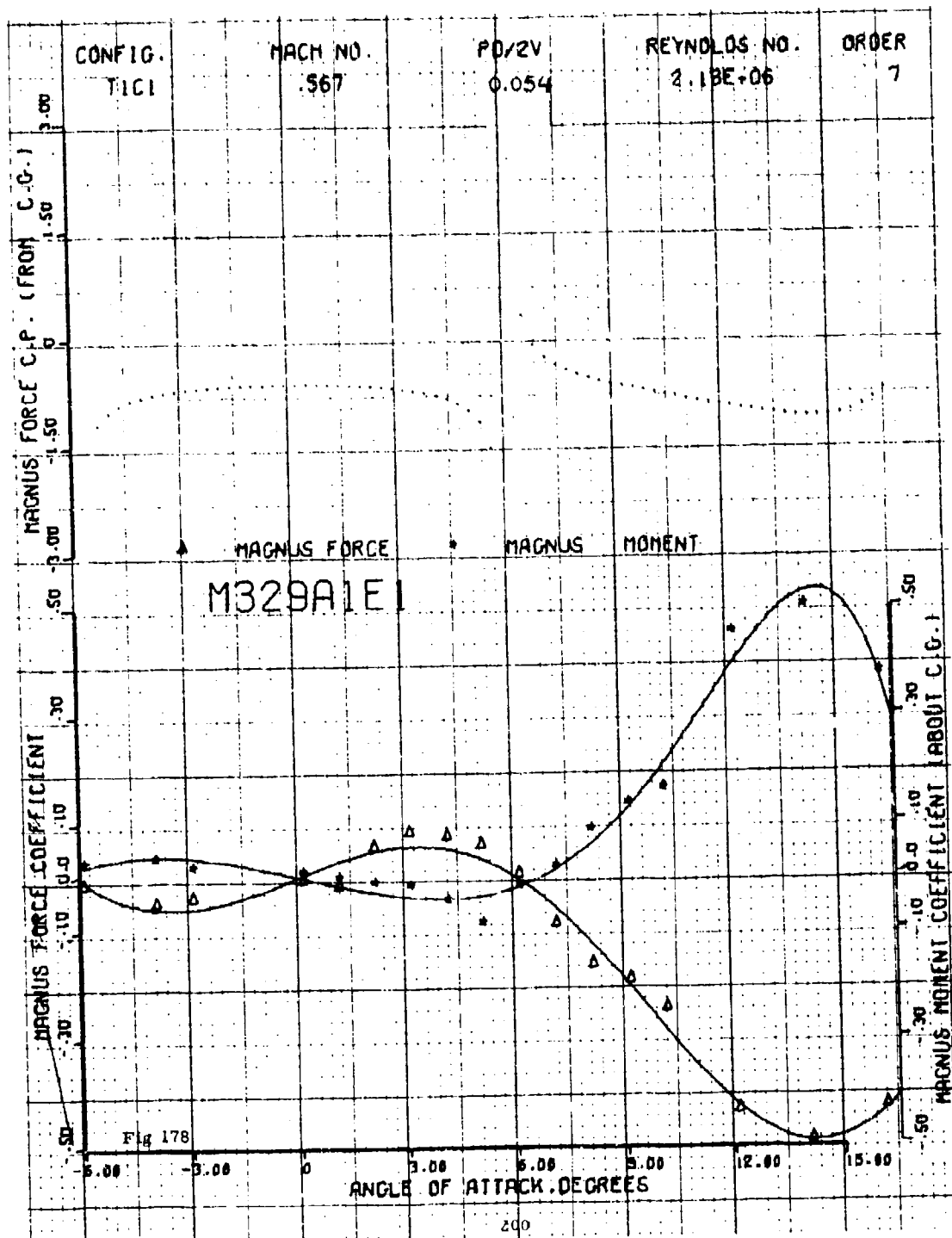


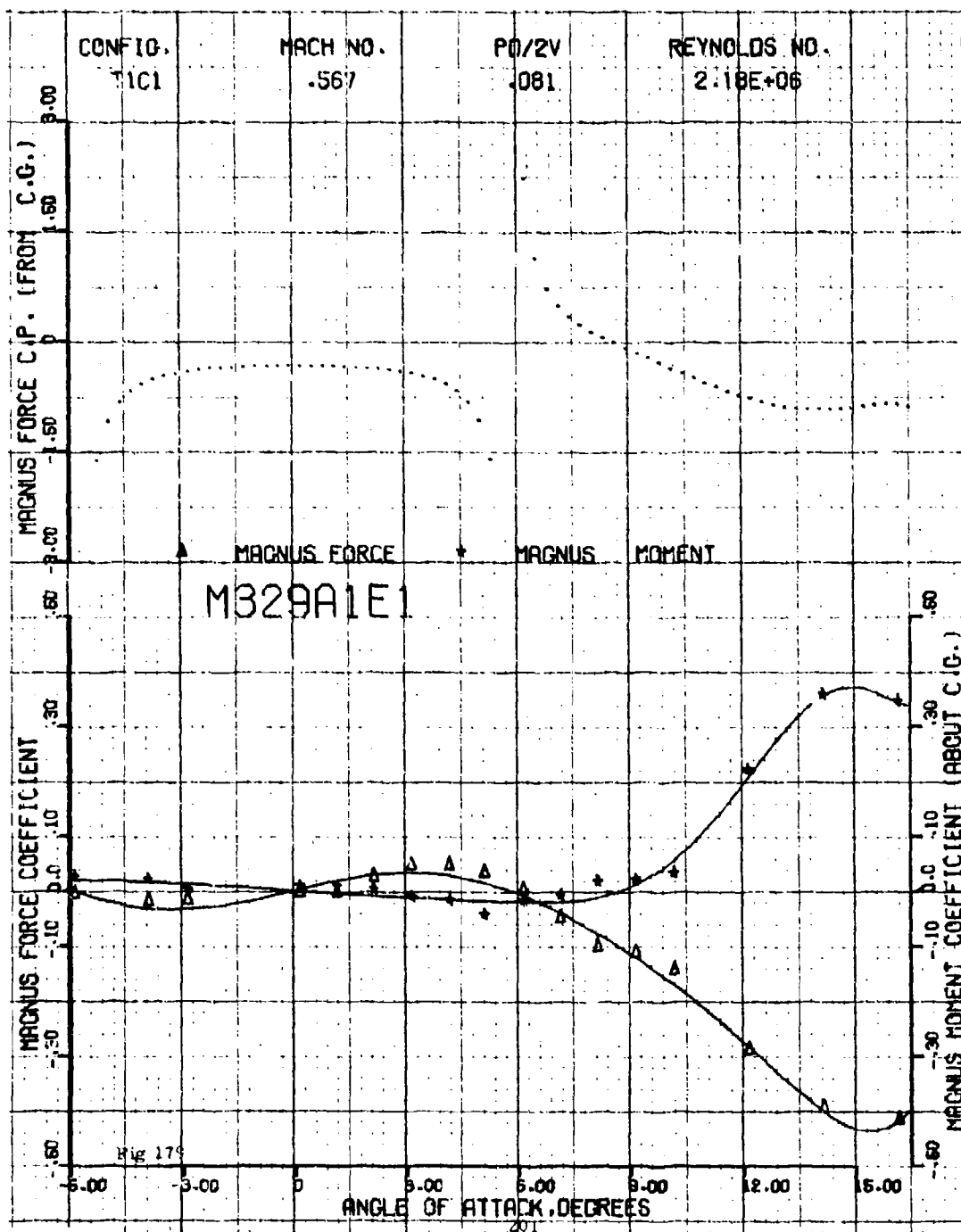


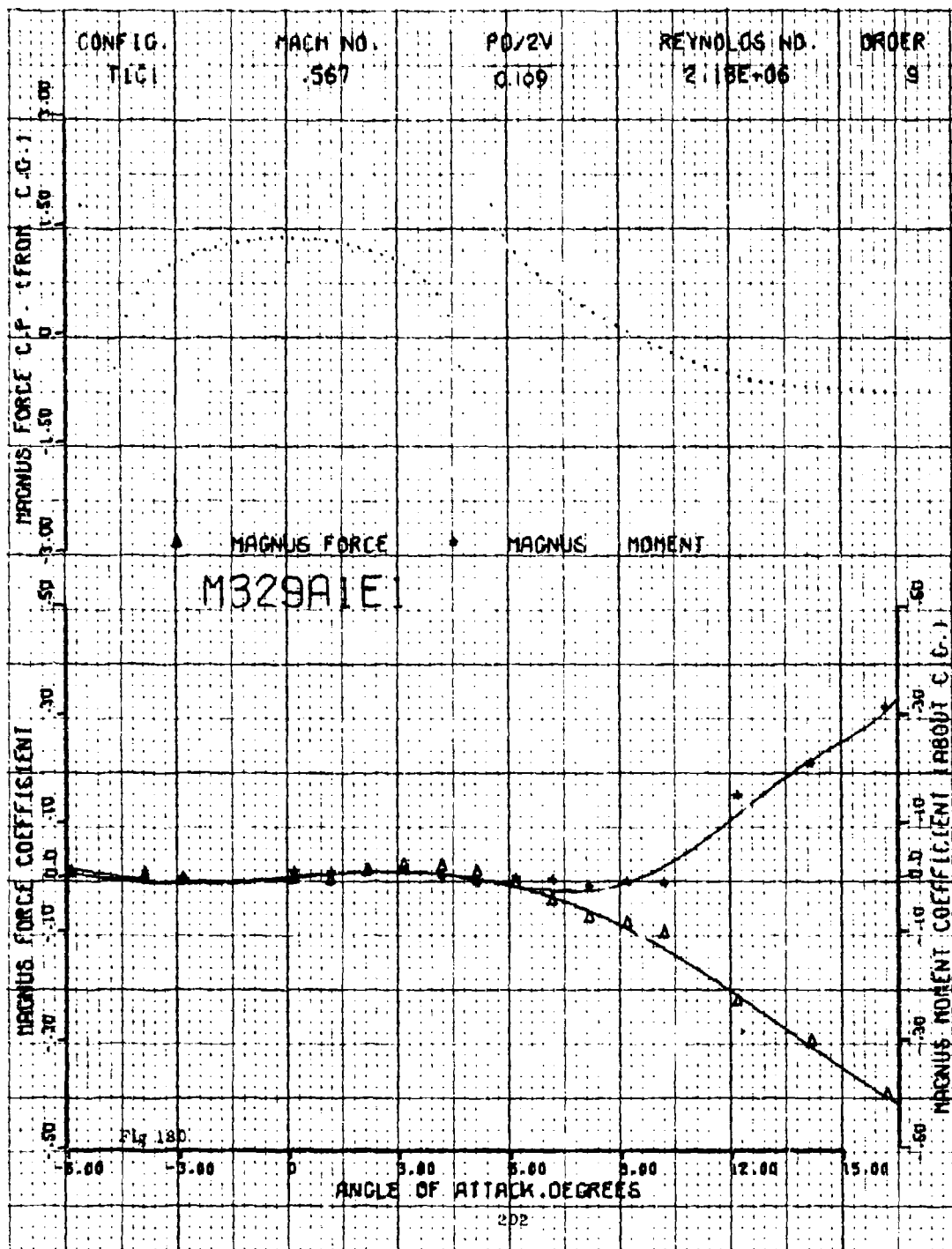


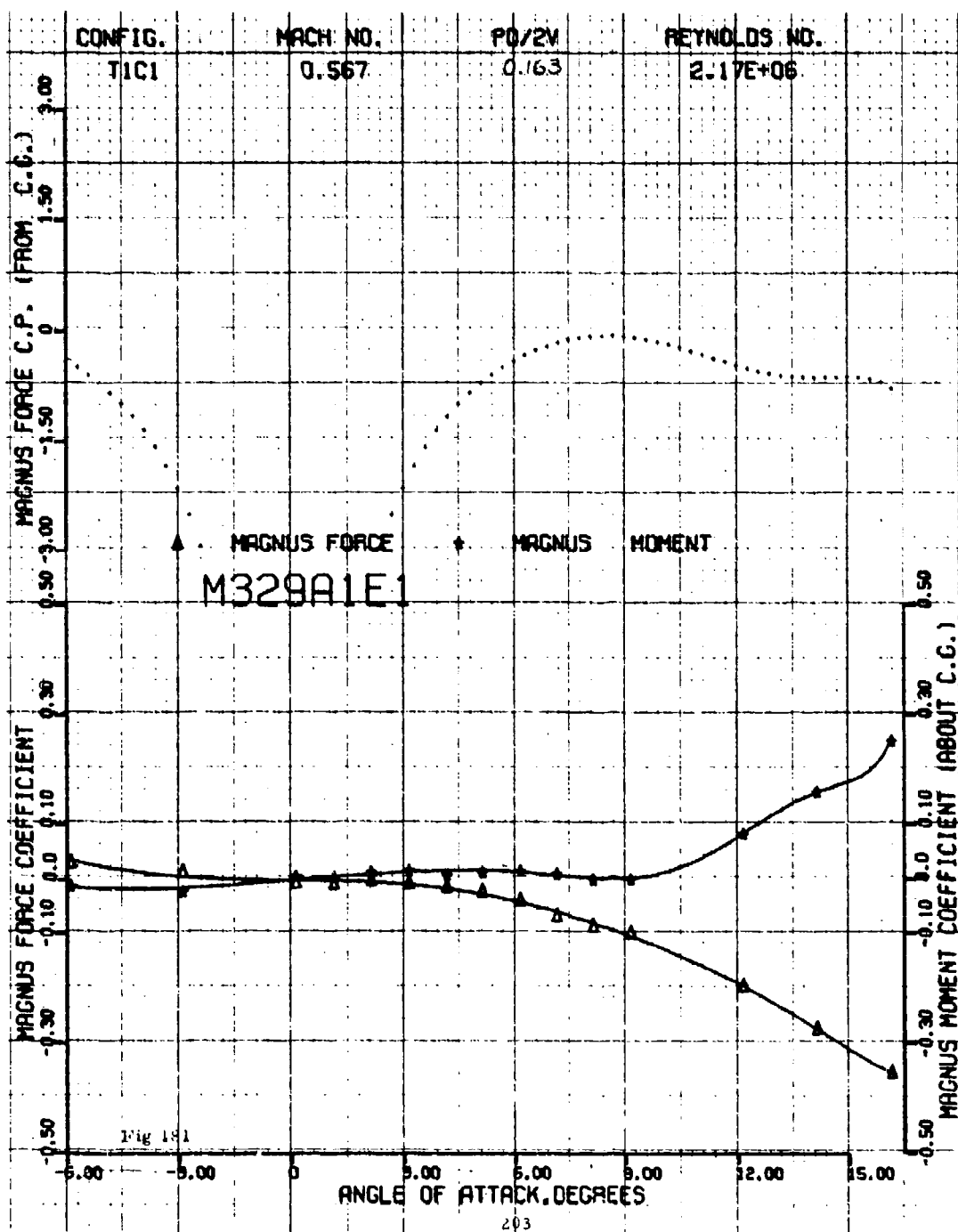


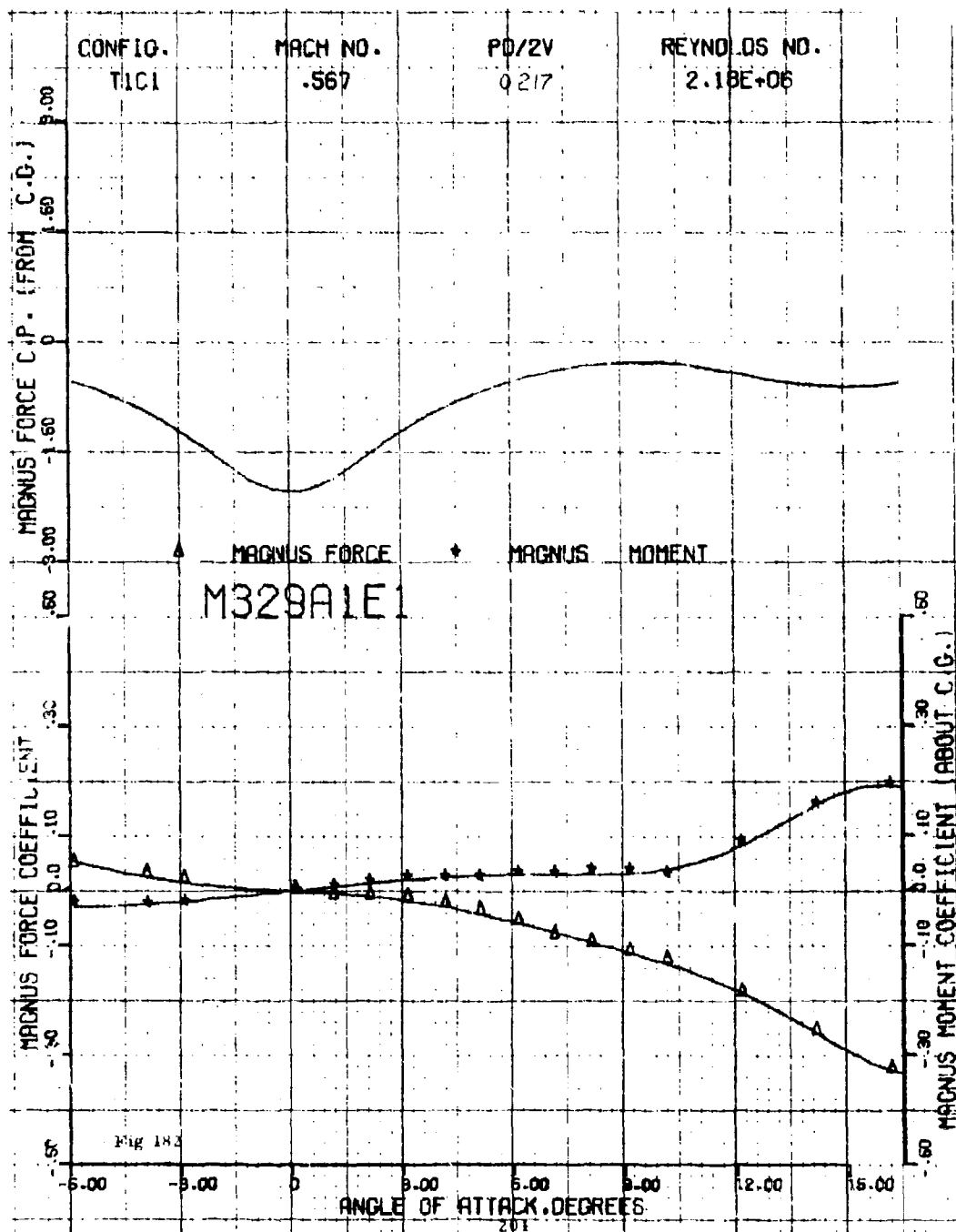


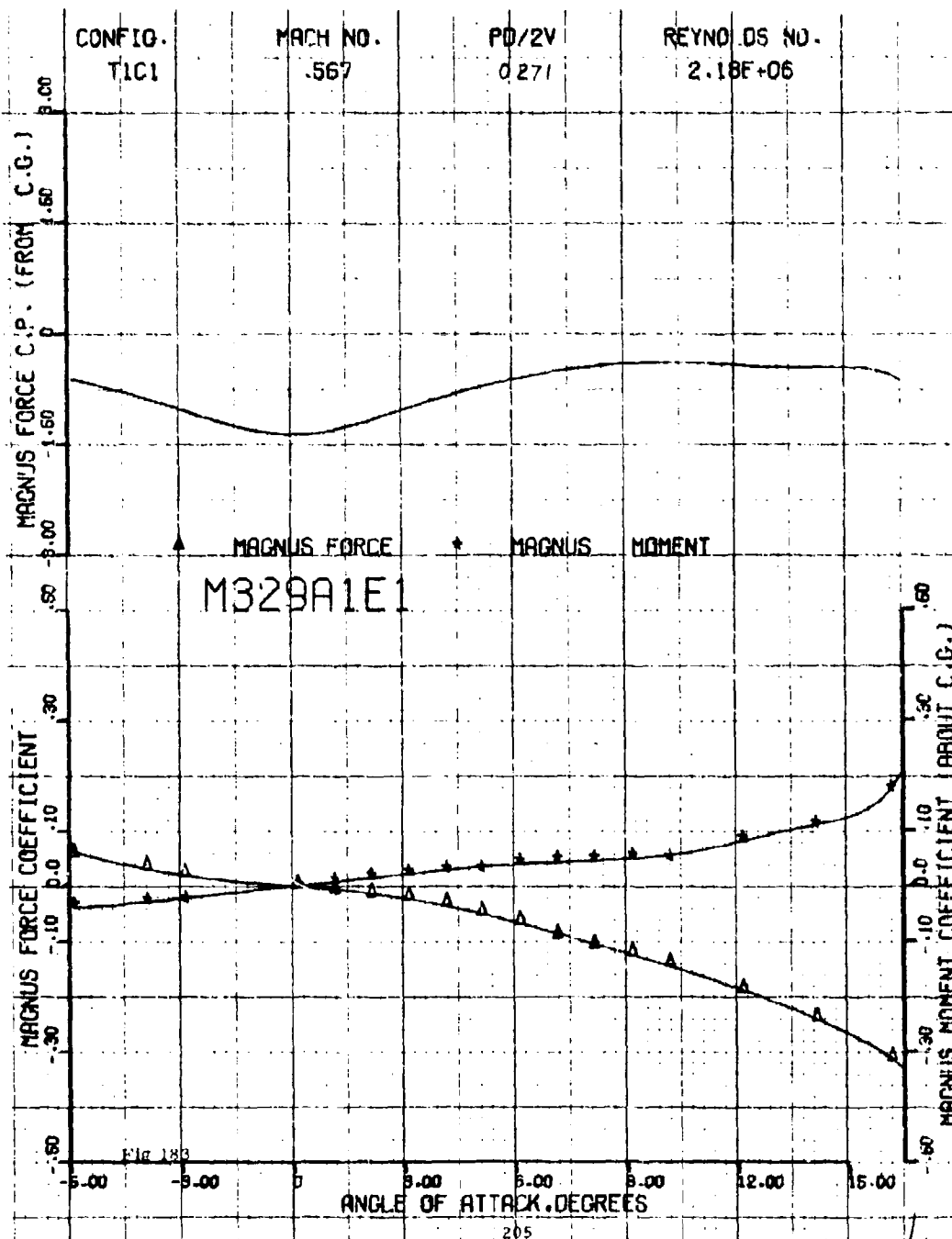


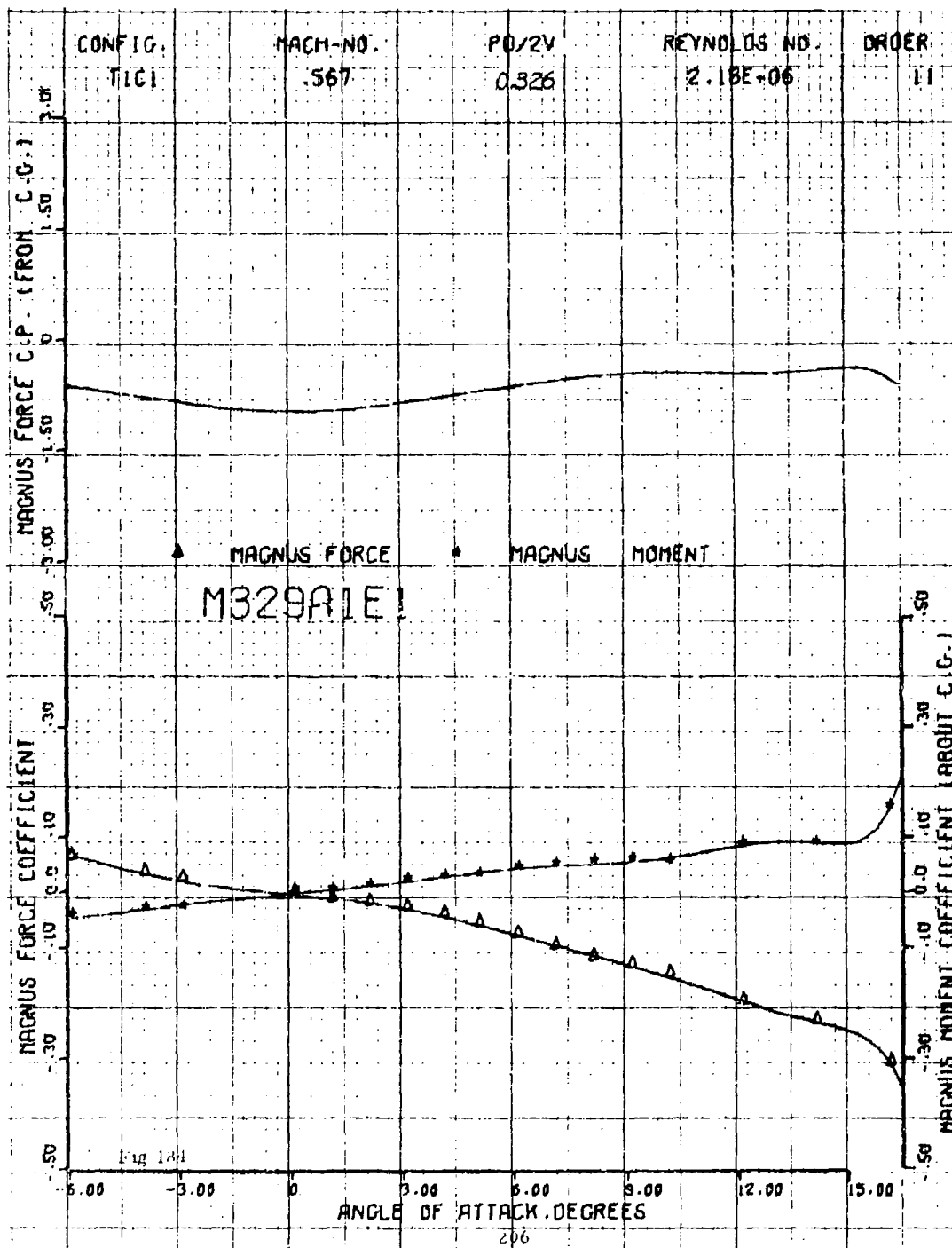


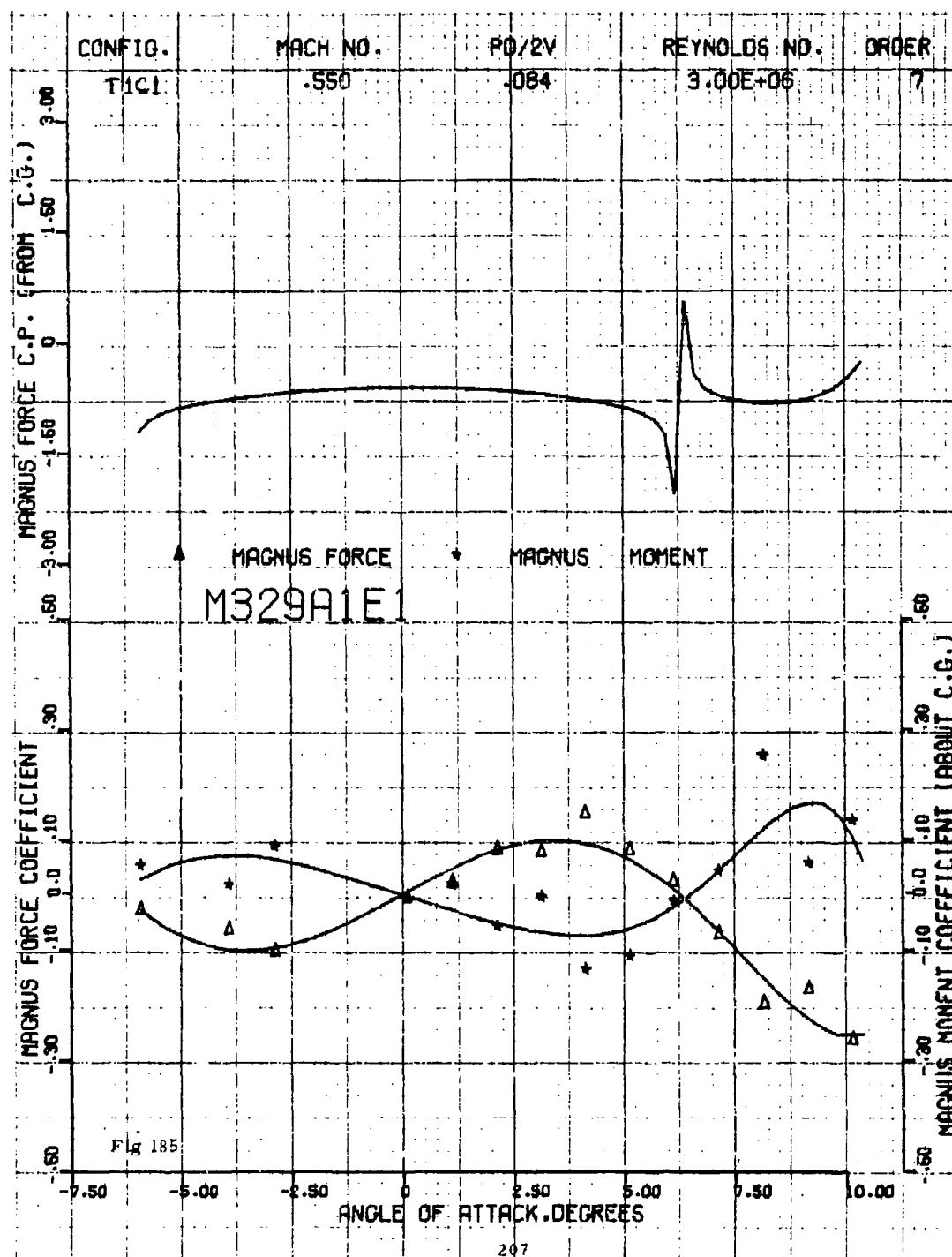


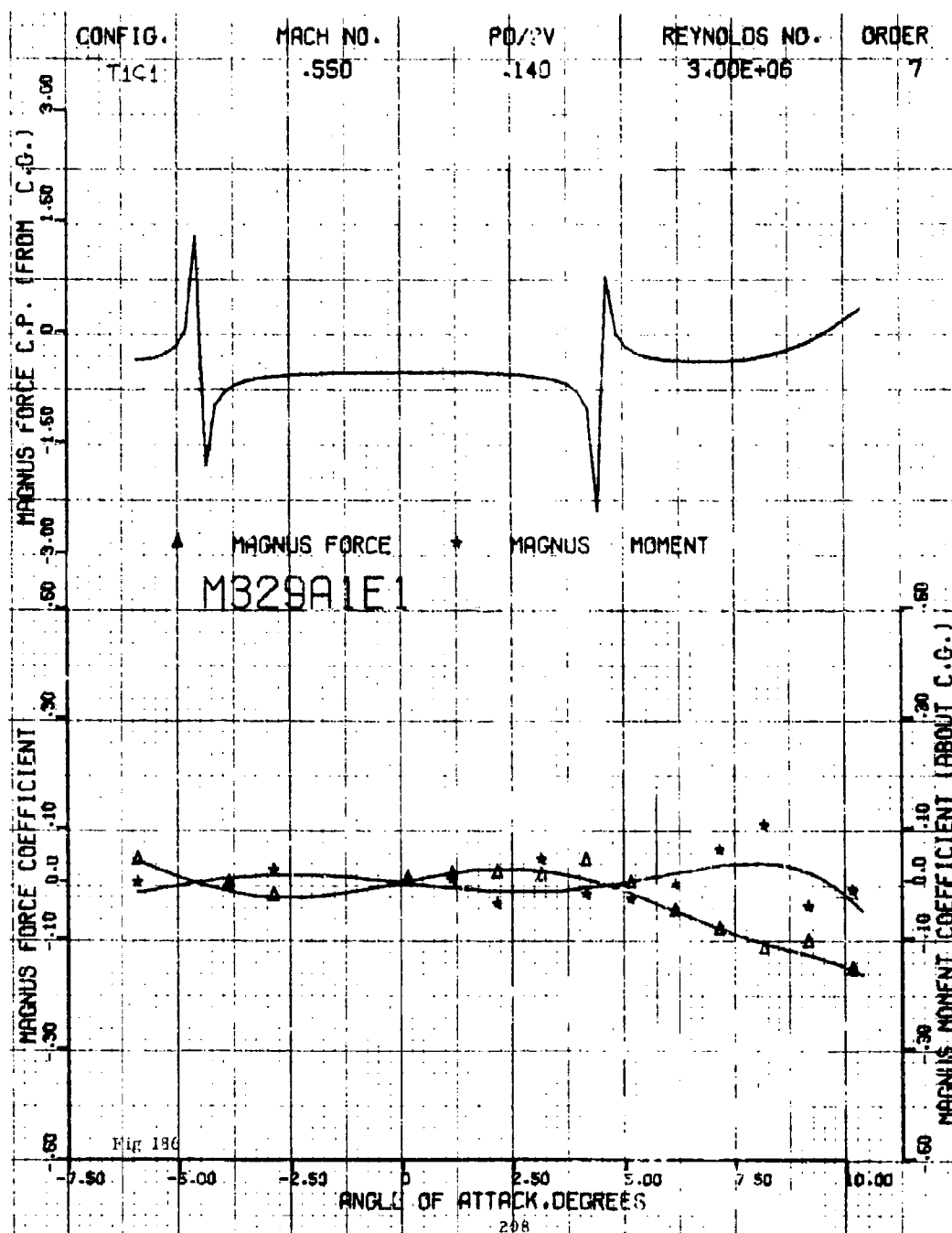


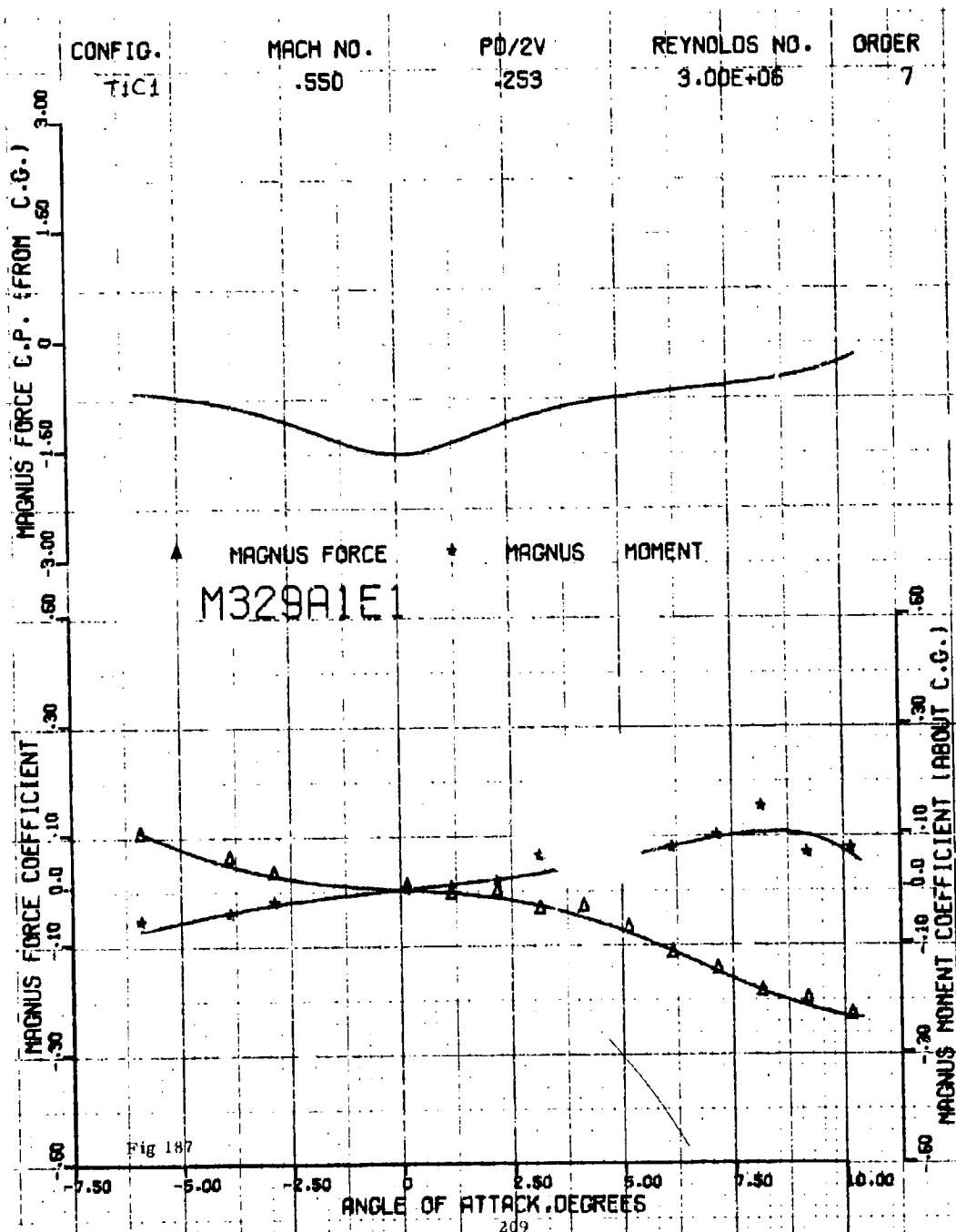


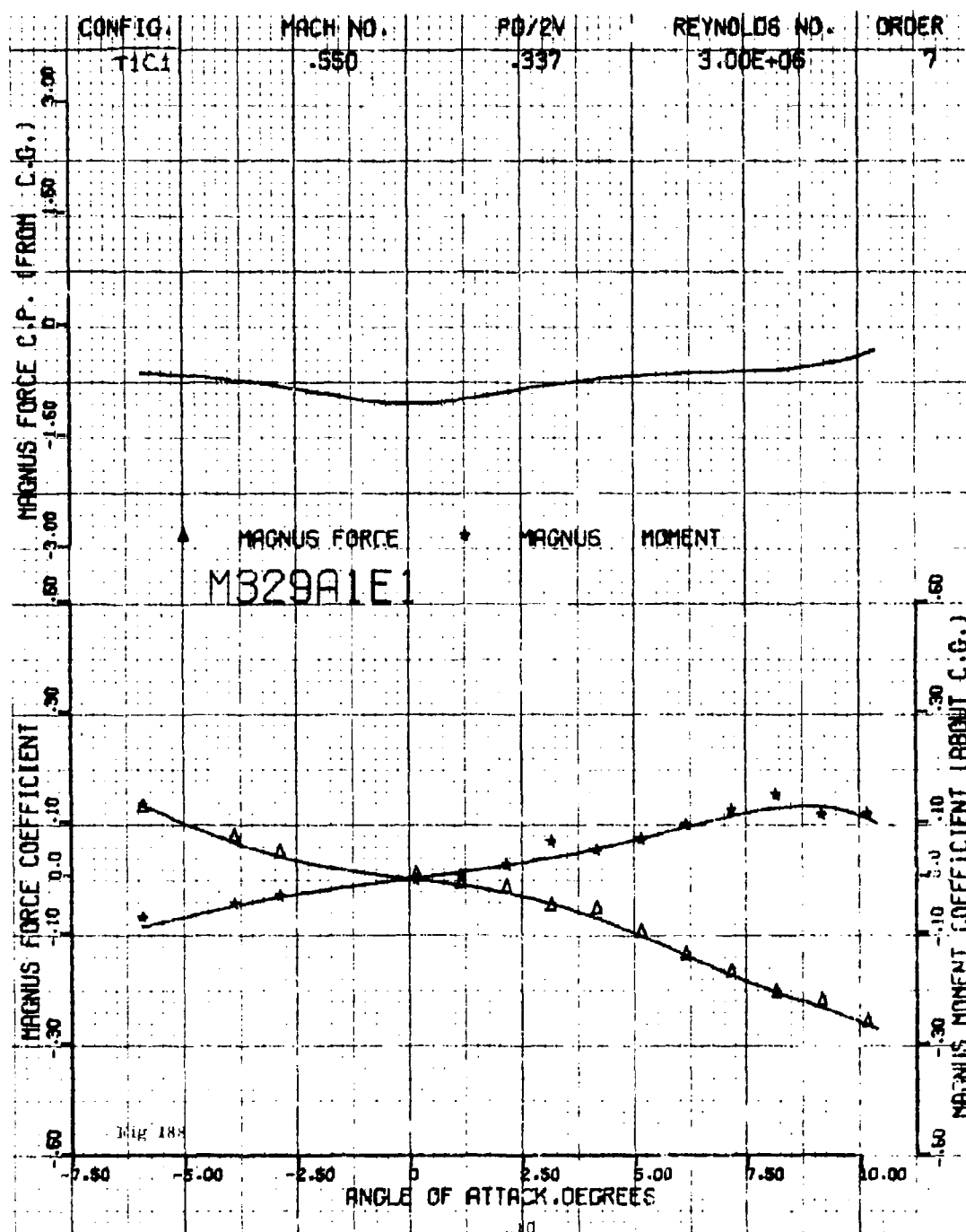


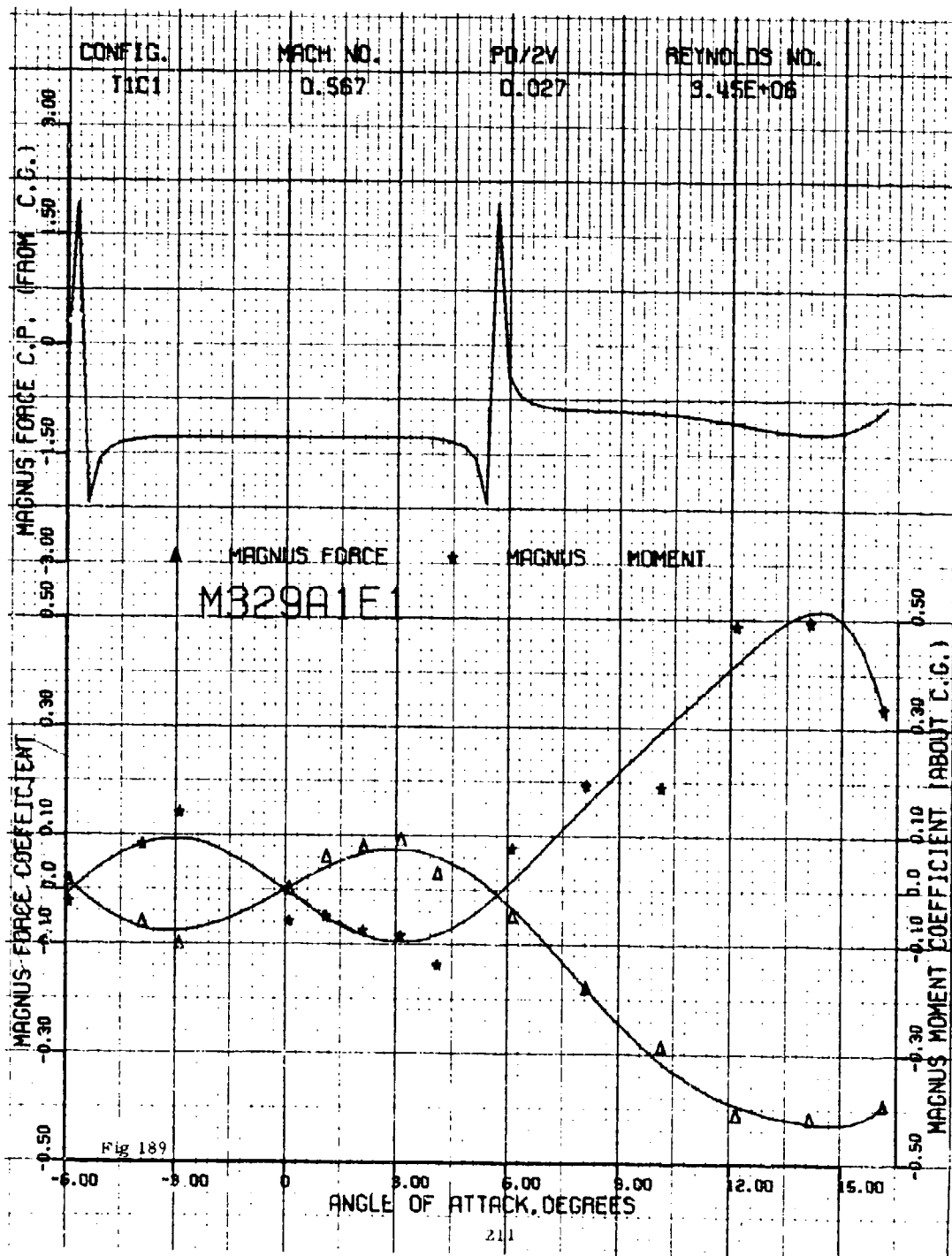


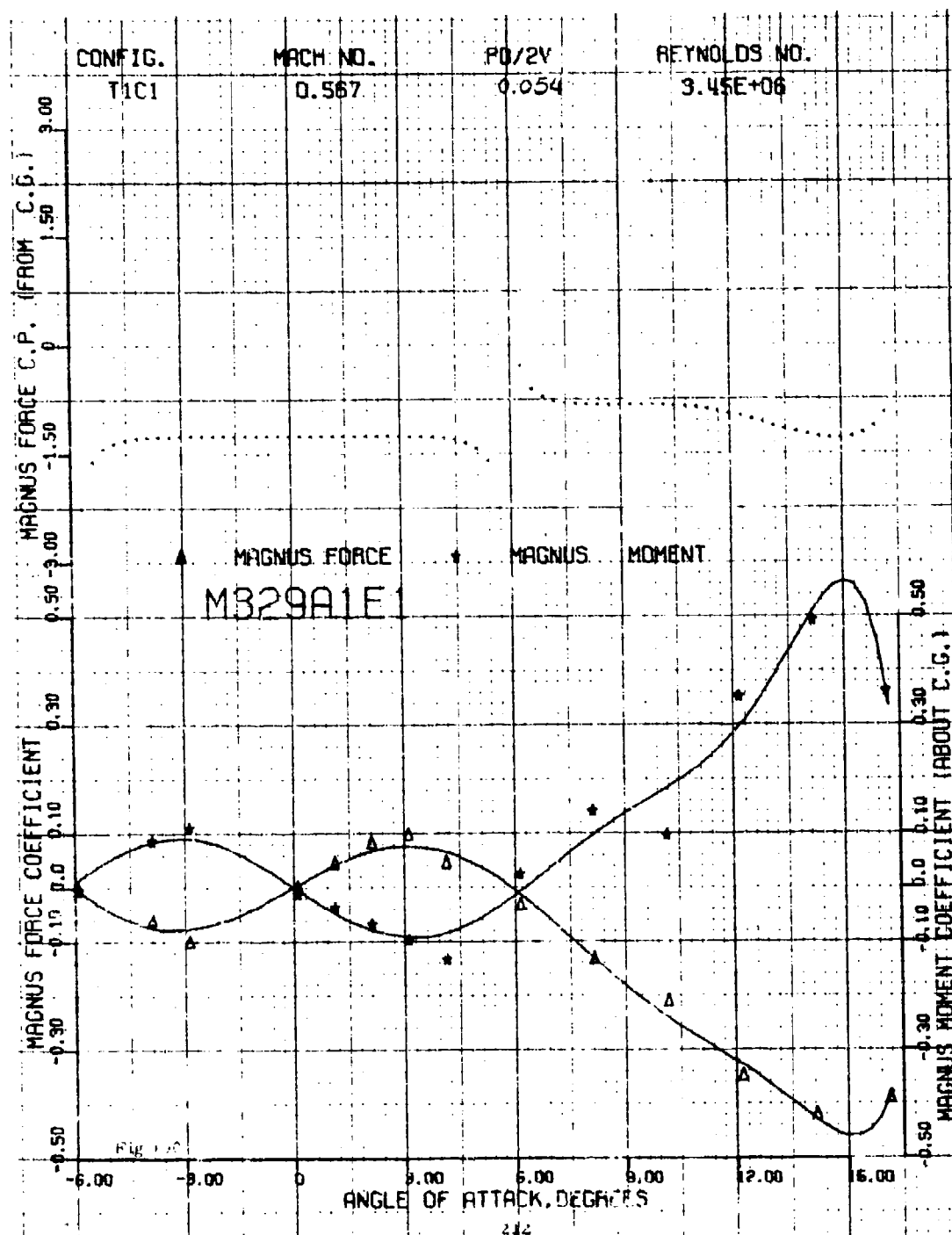


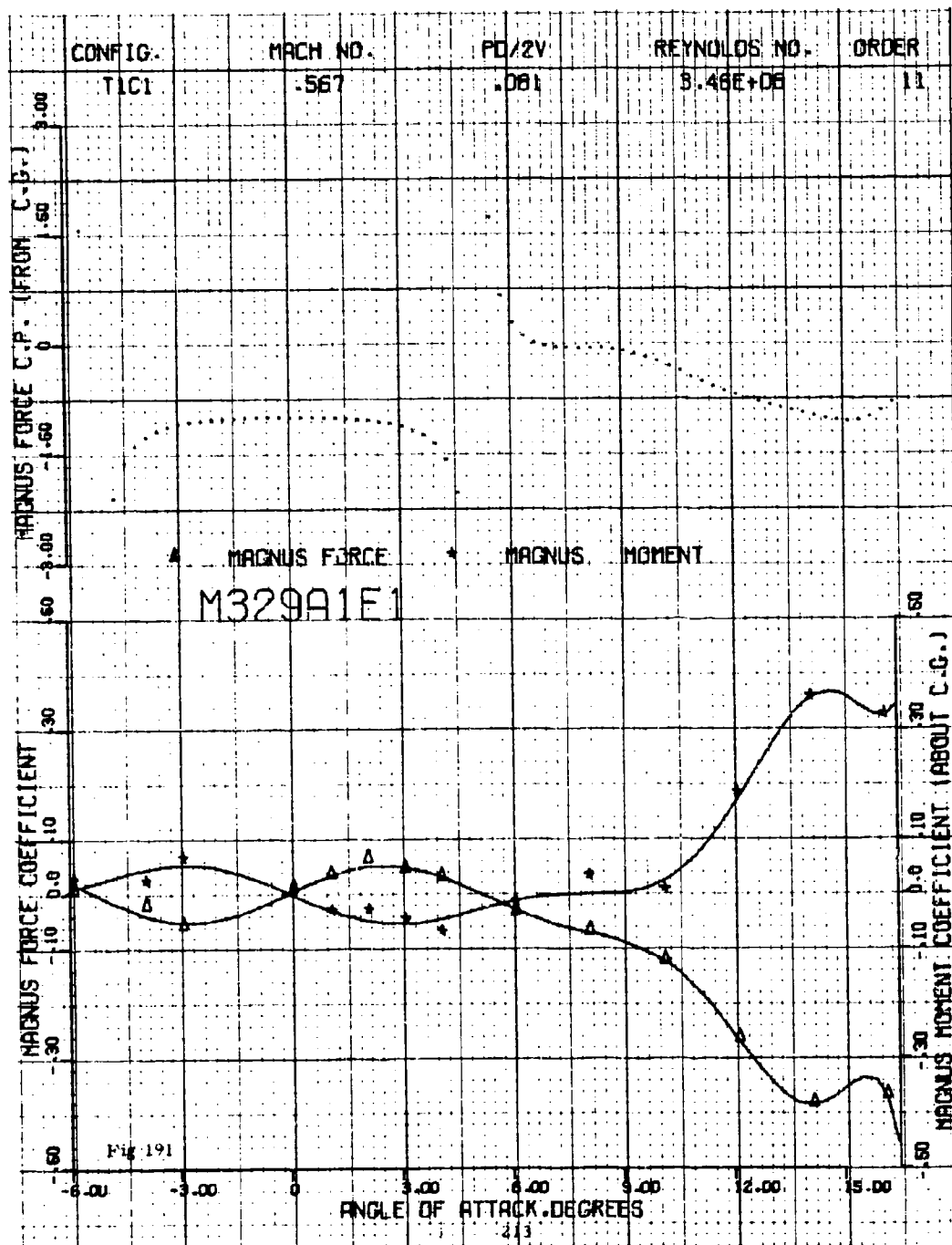


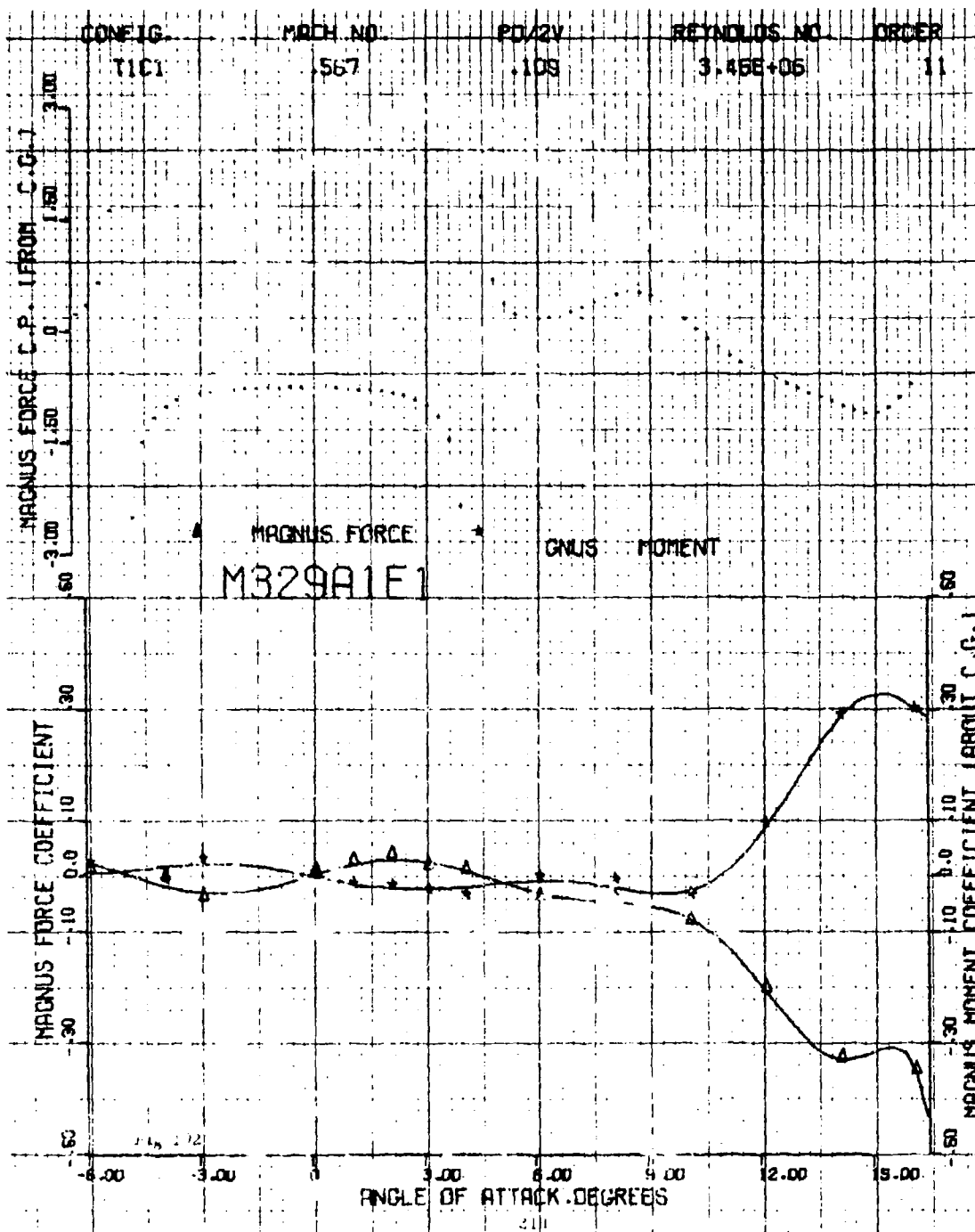


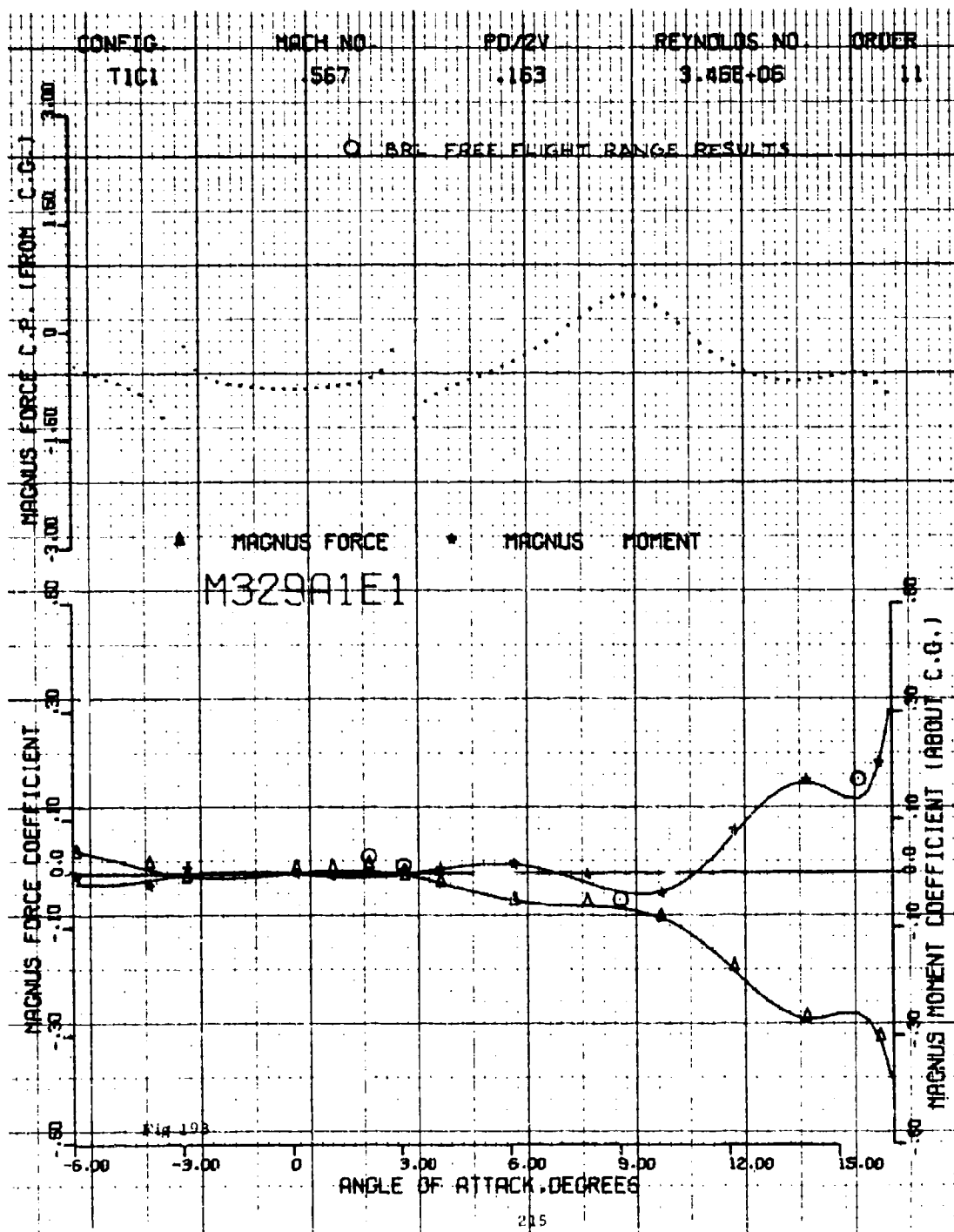


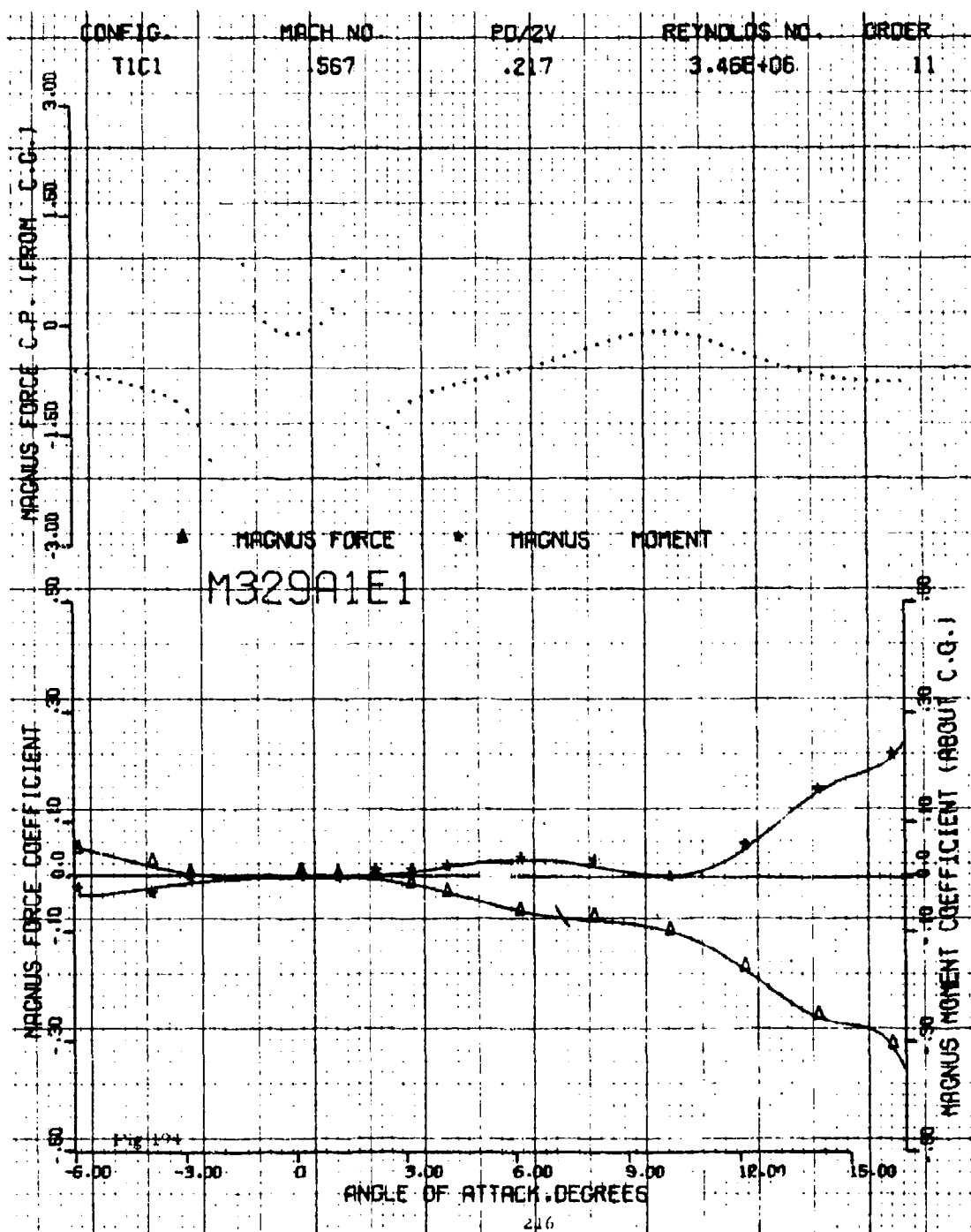












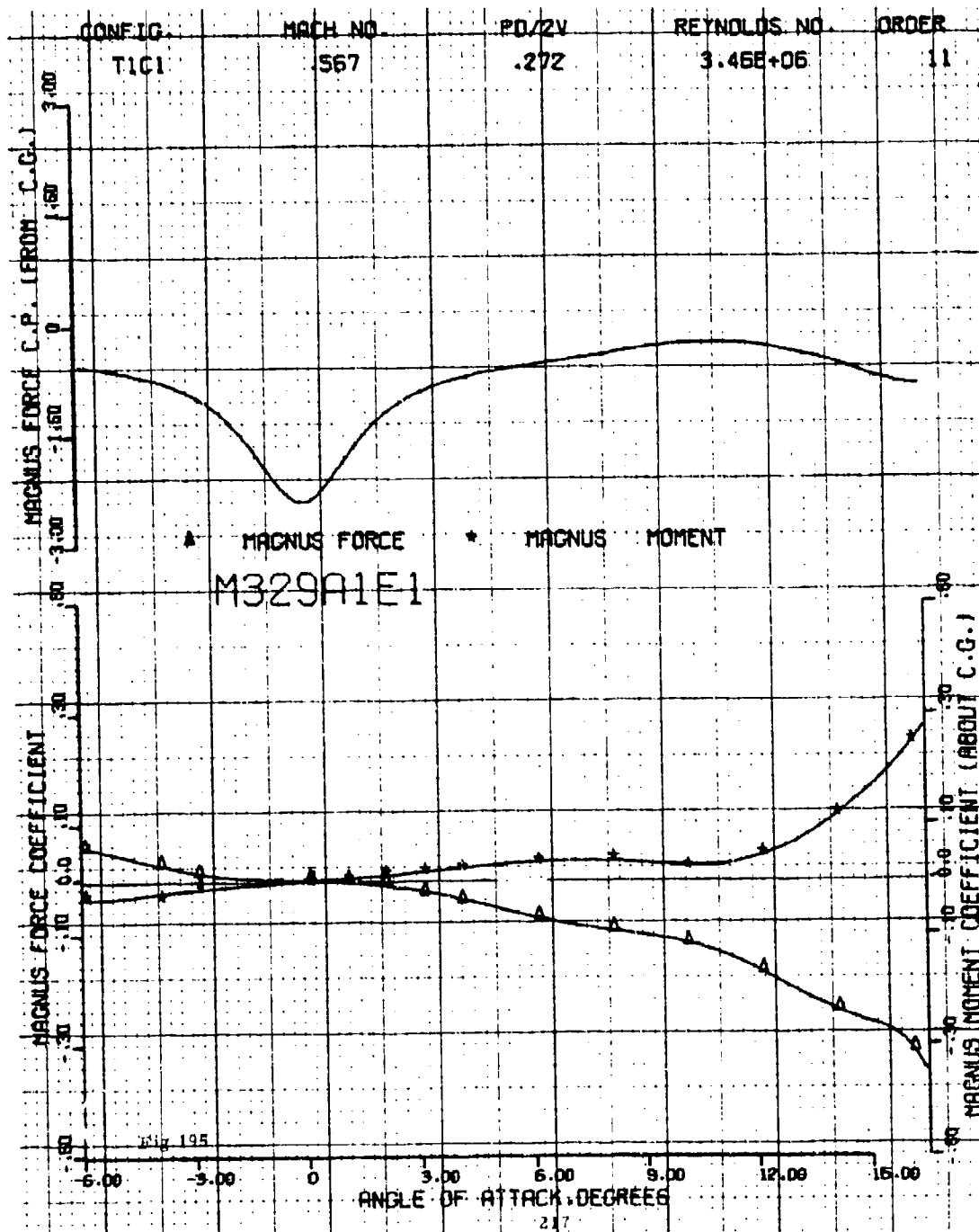
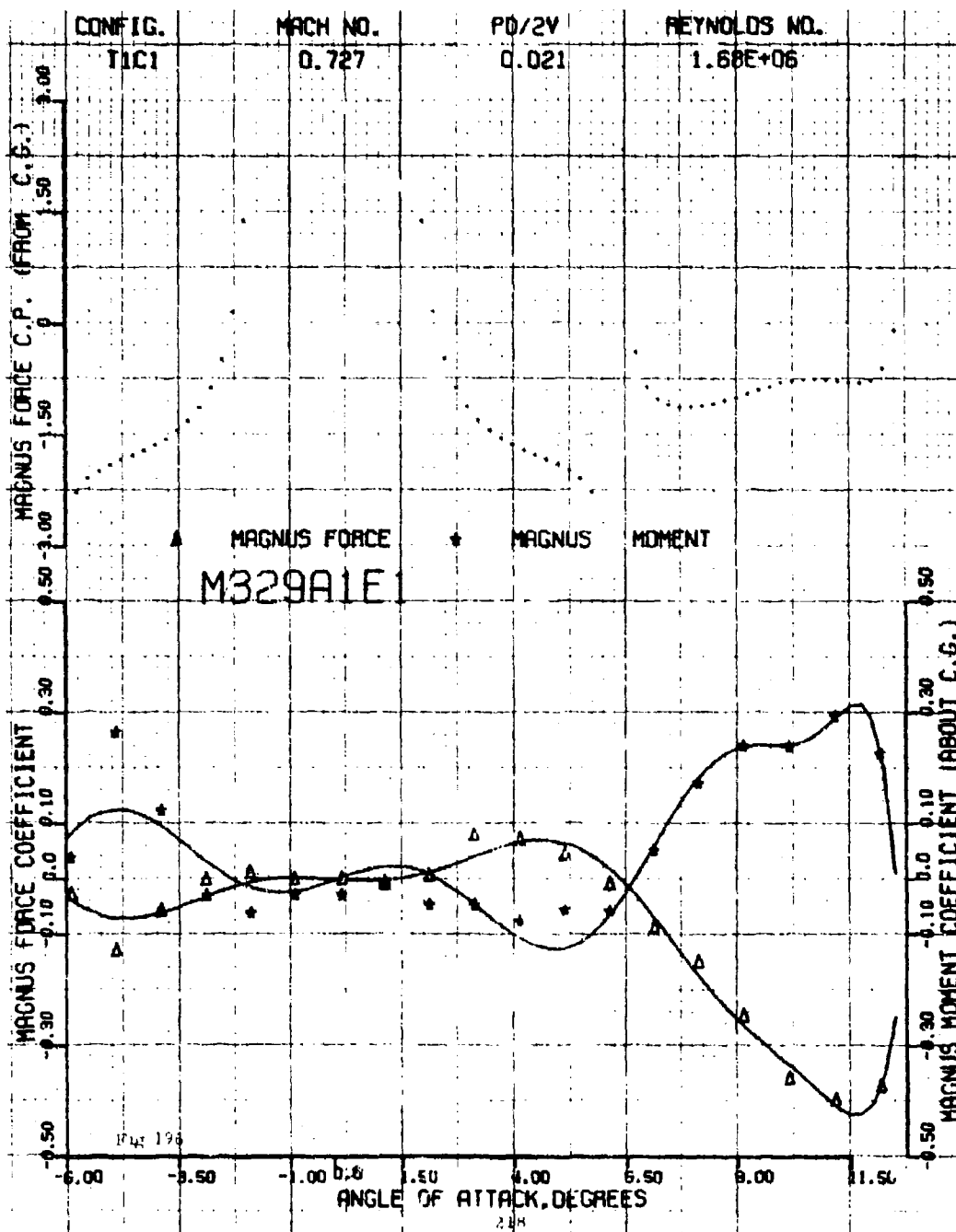
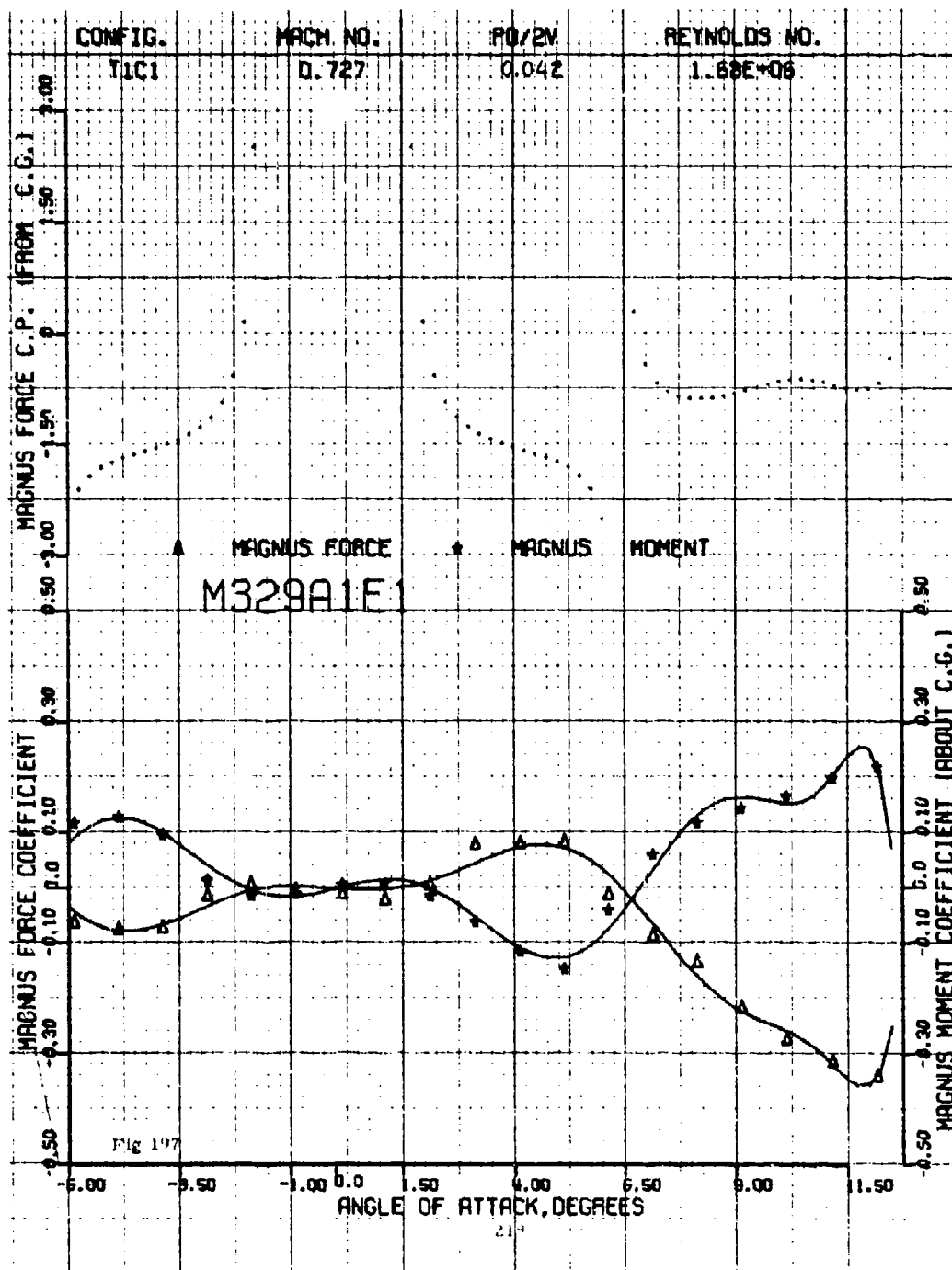
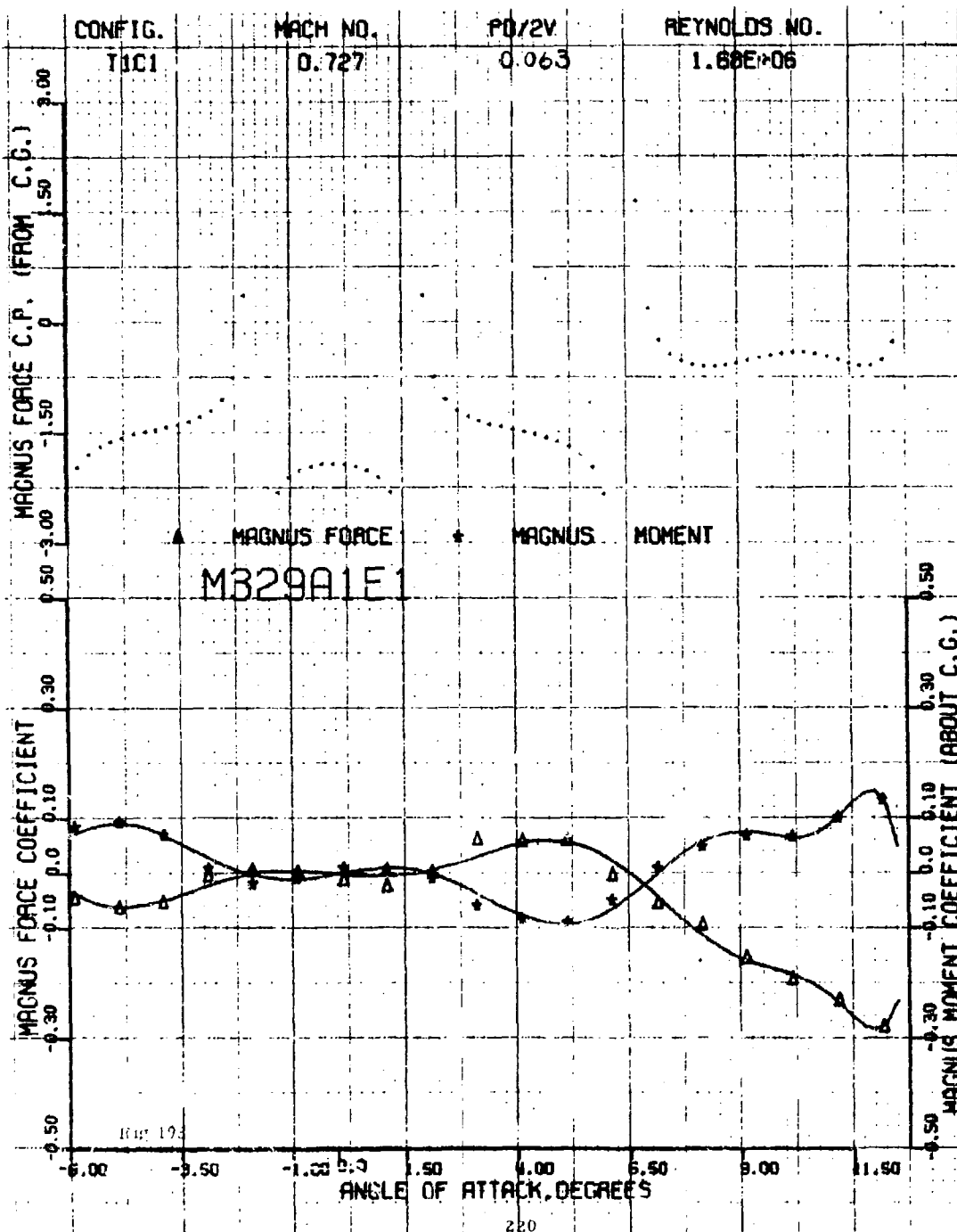
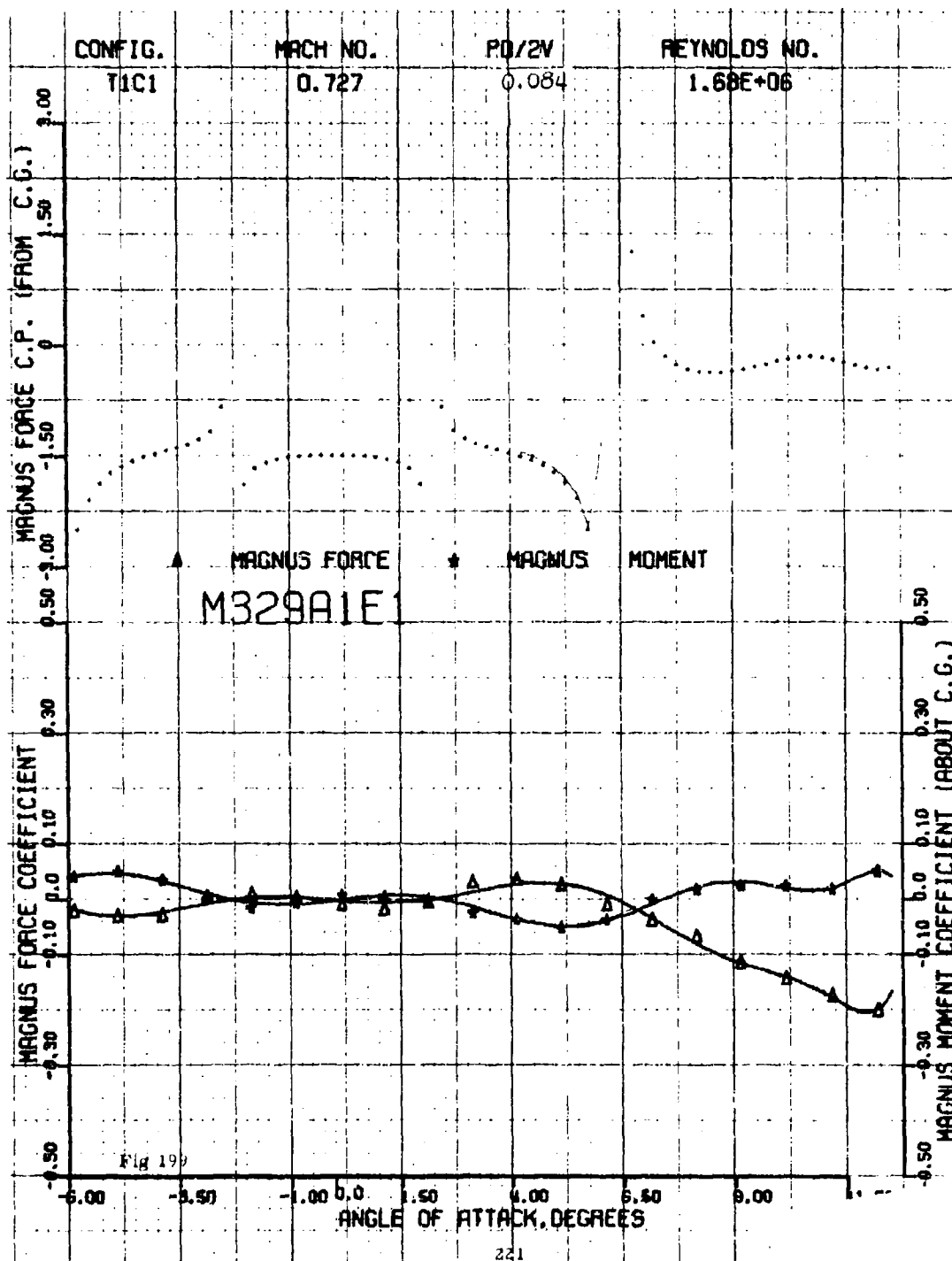


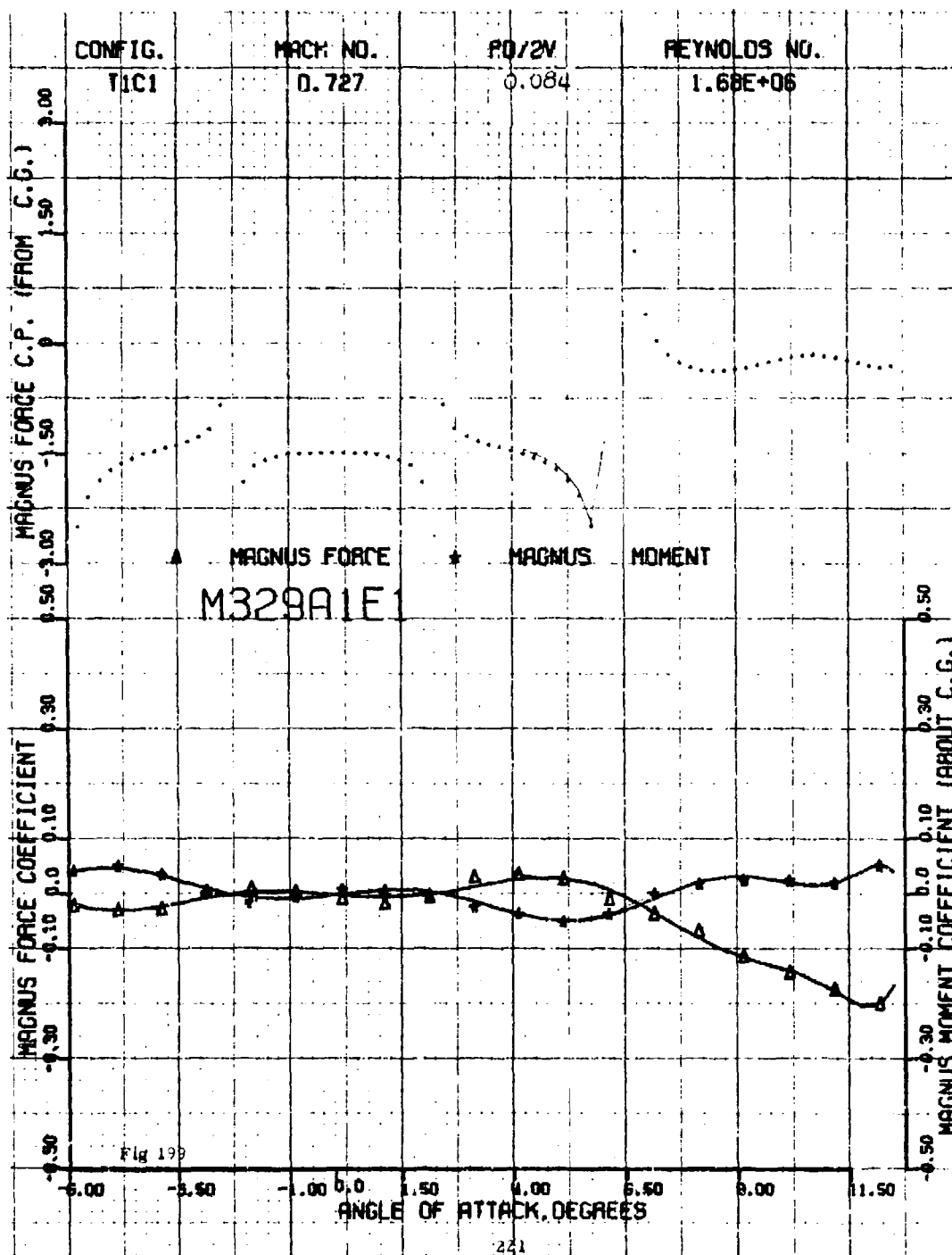
Fig 195

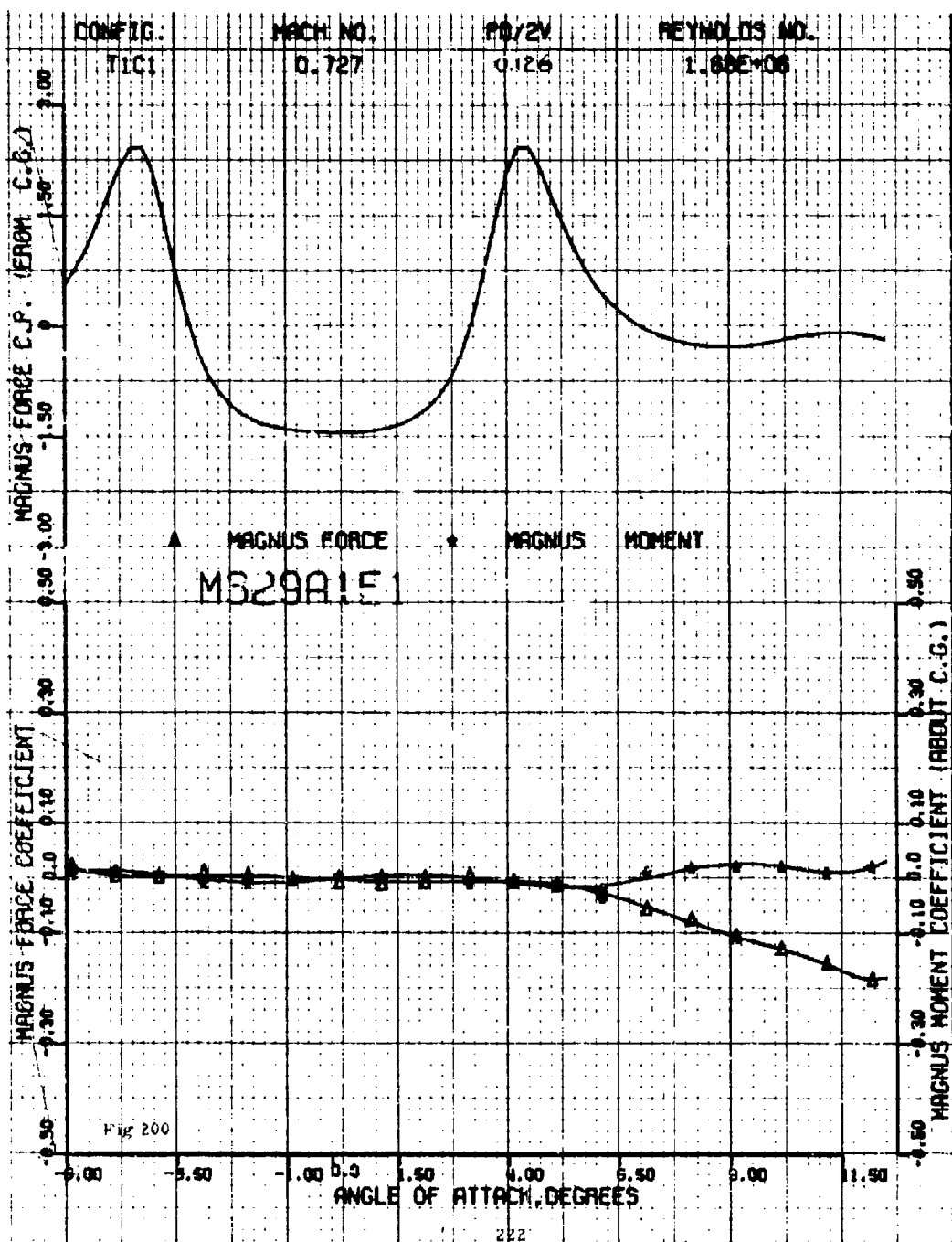


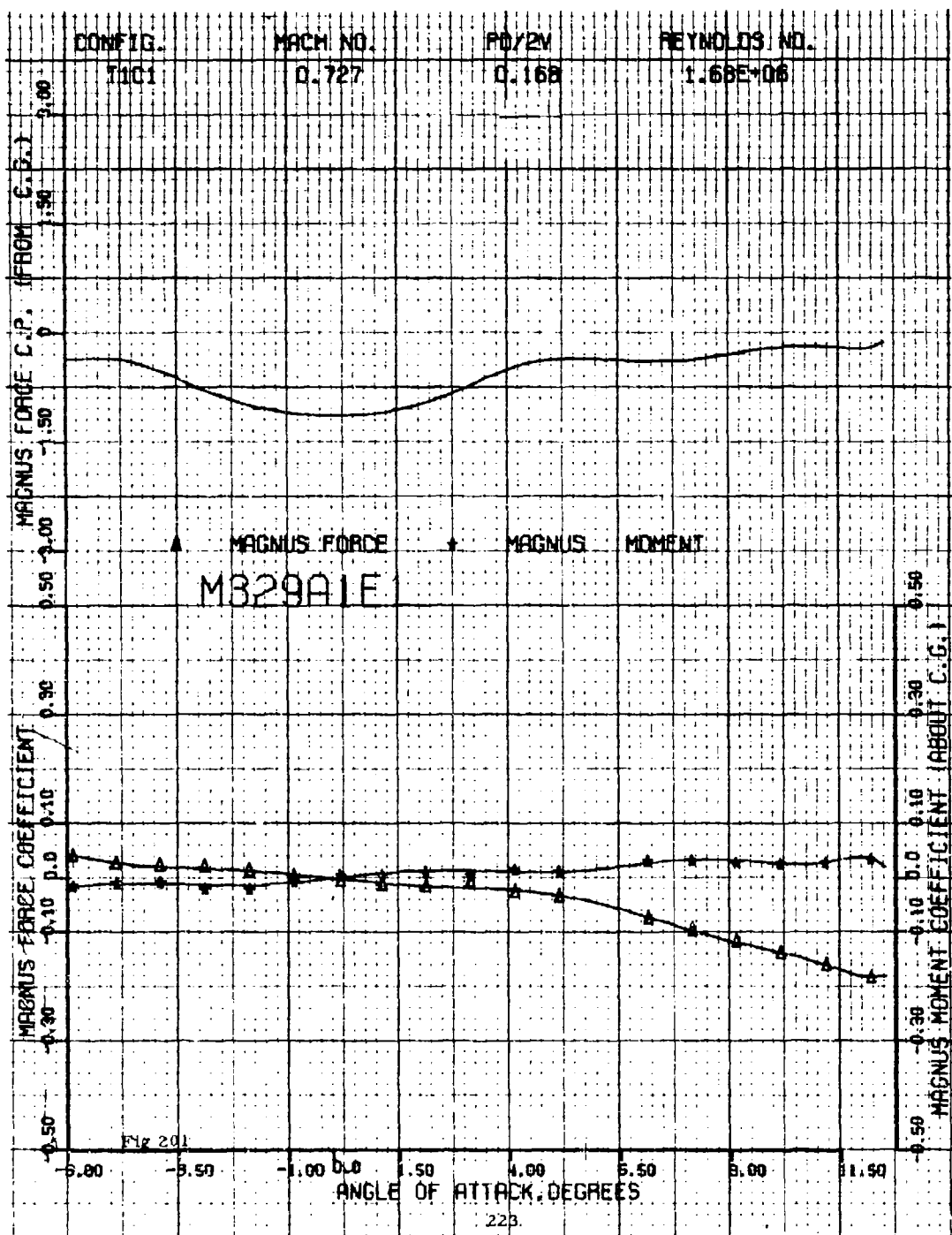


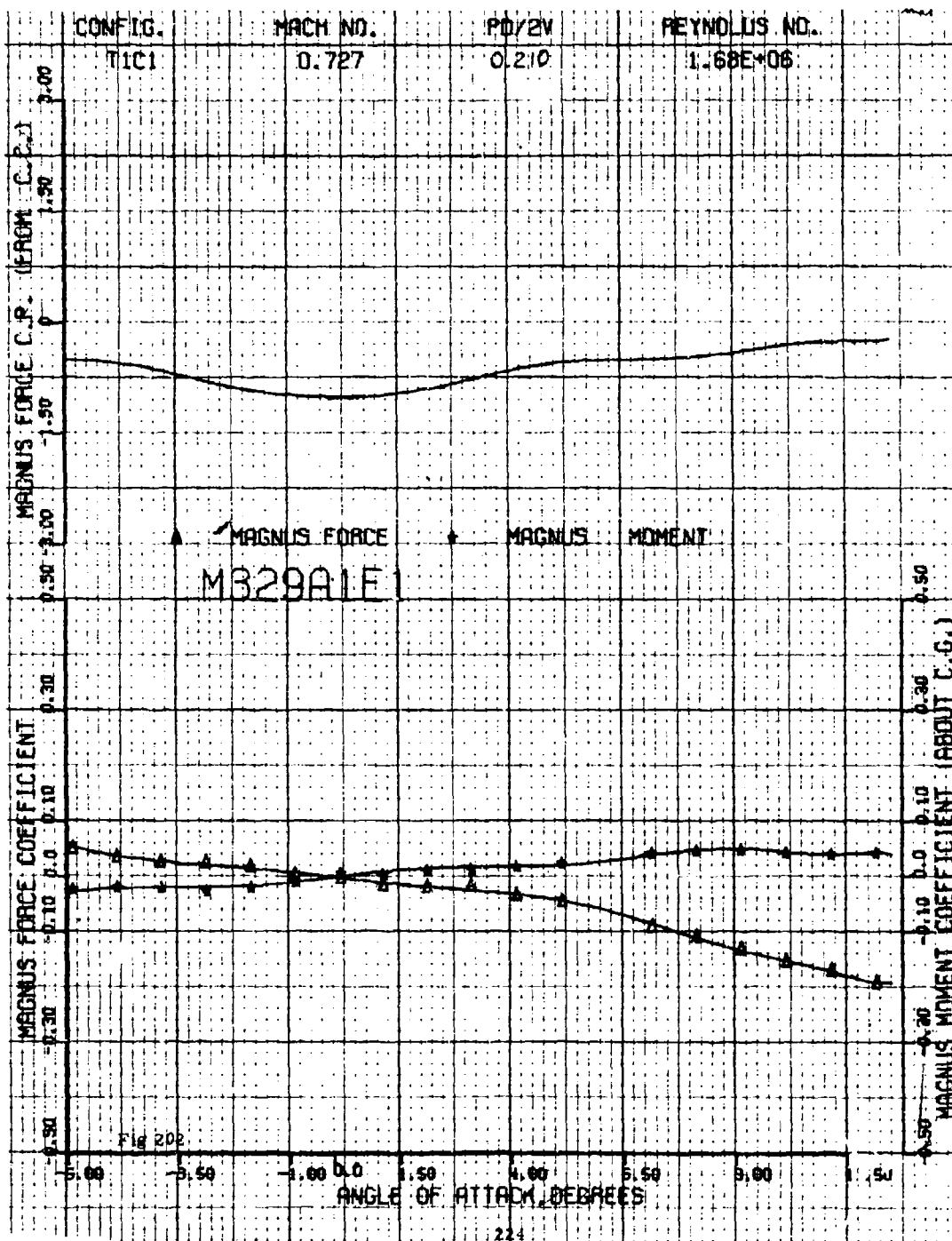


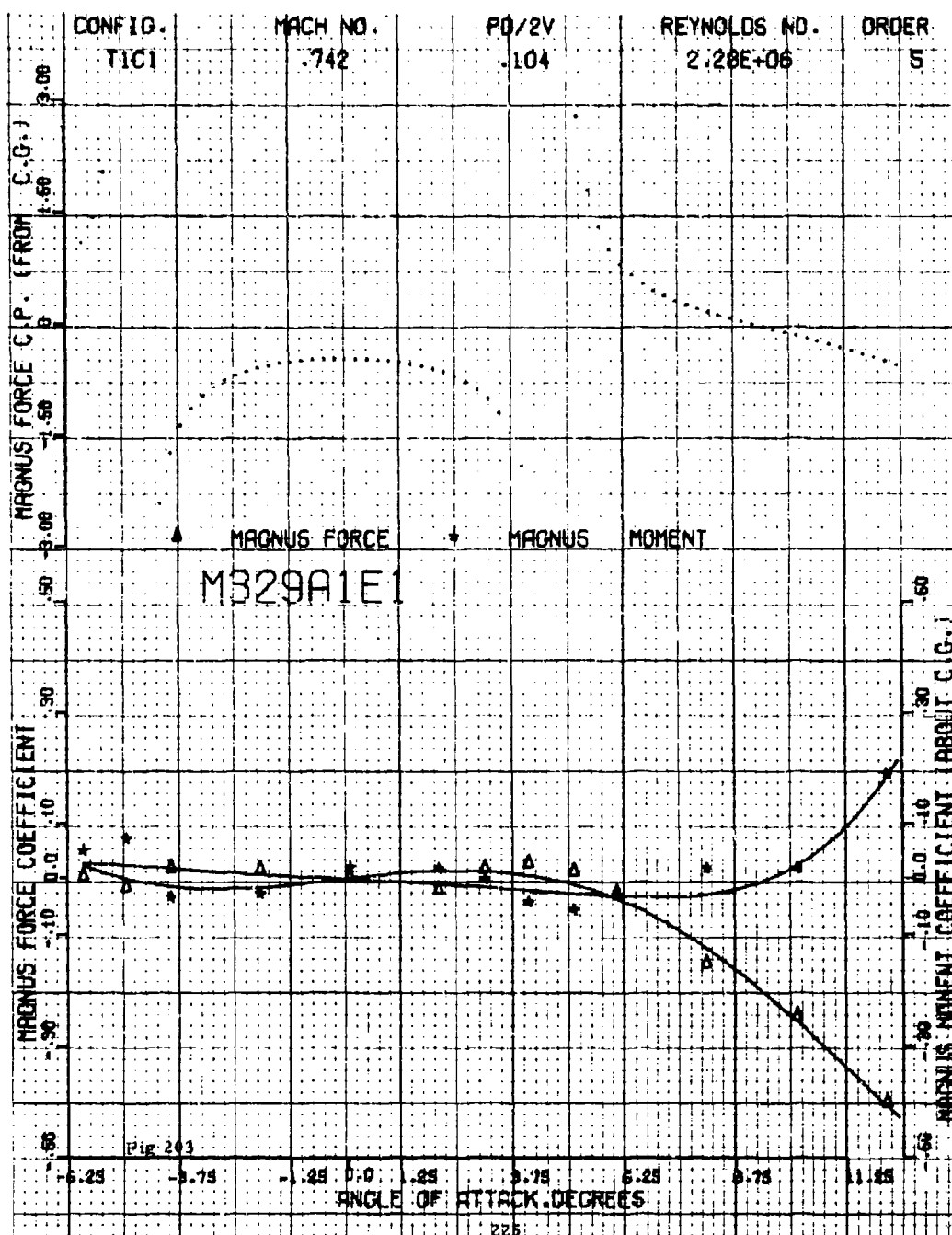


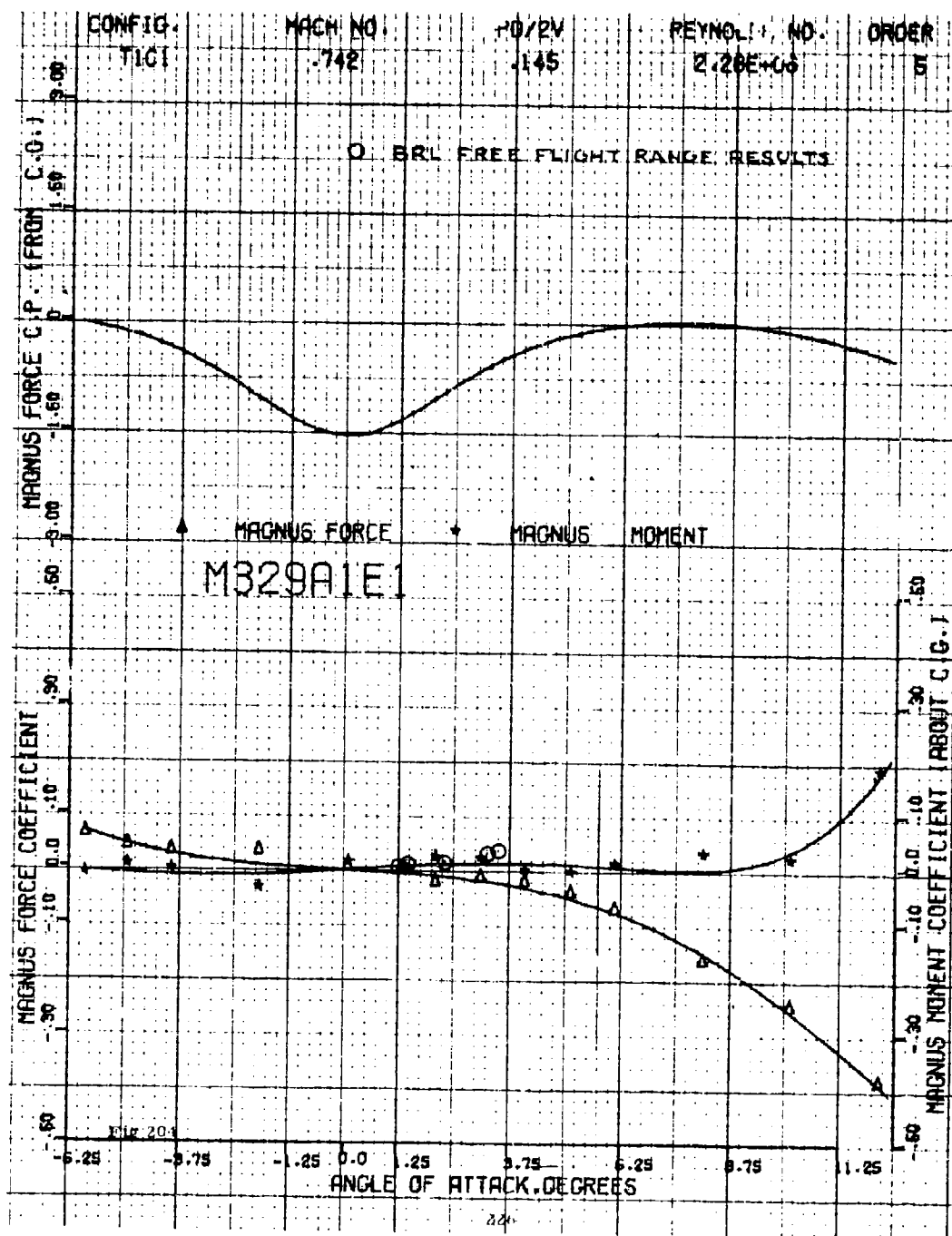


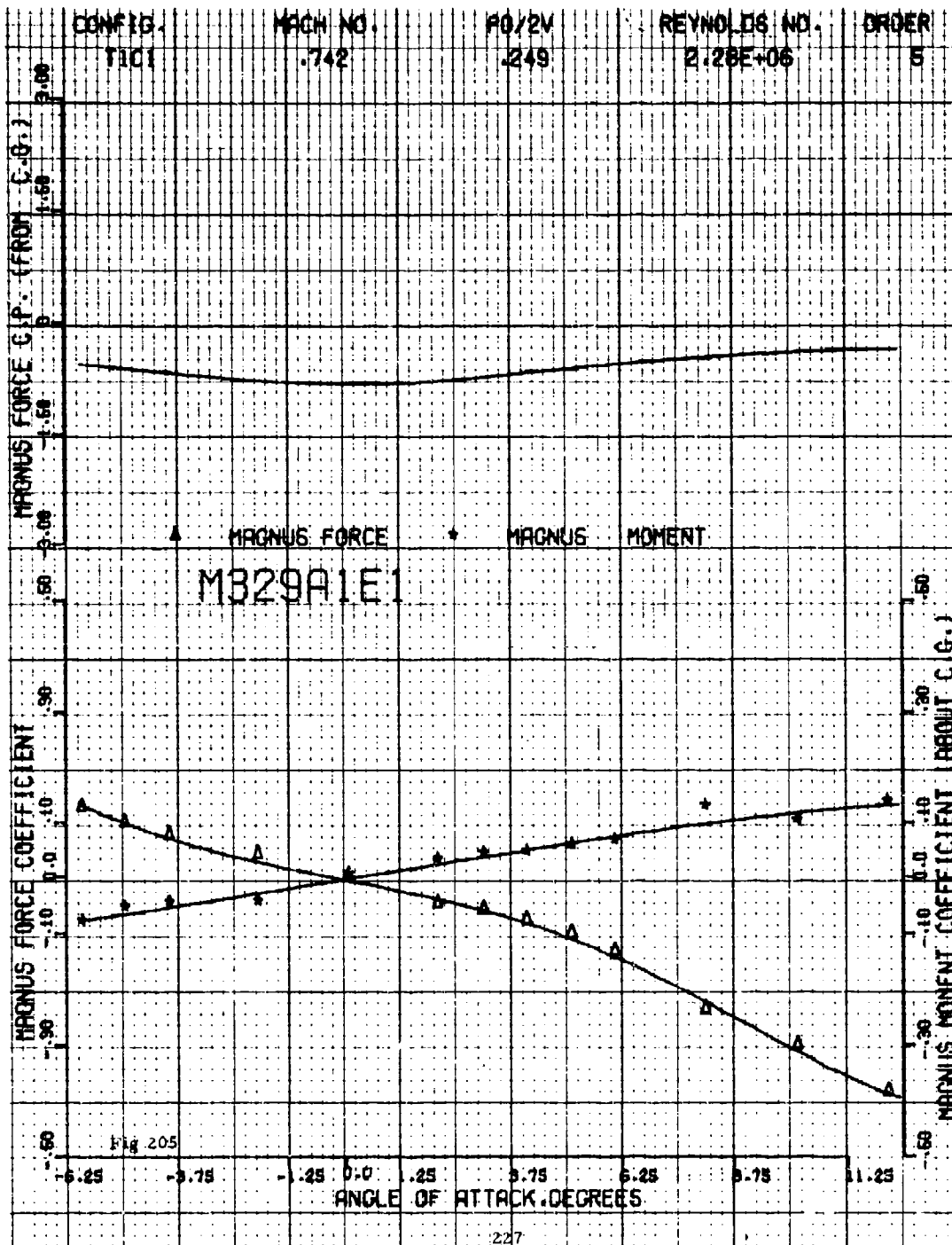


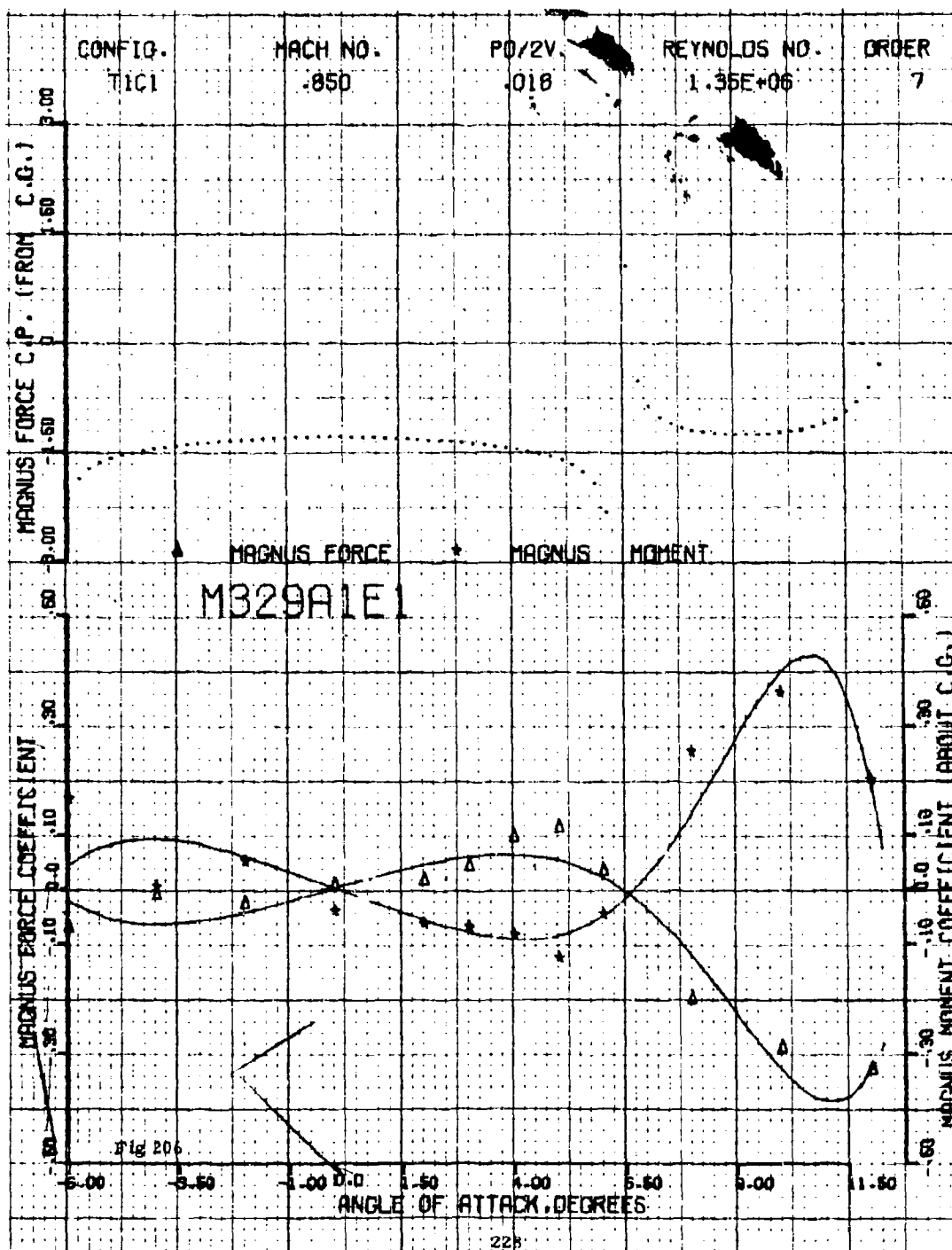


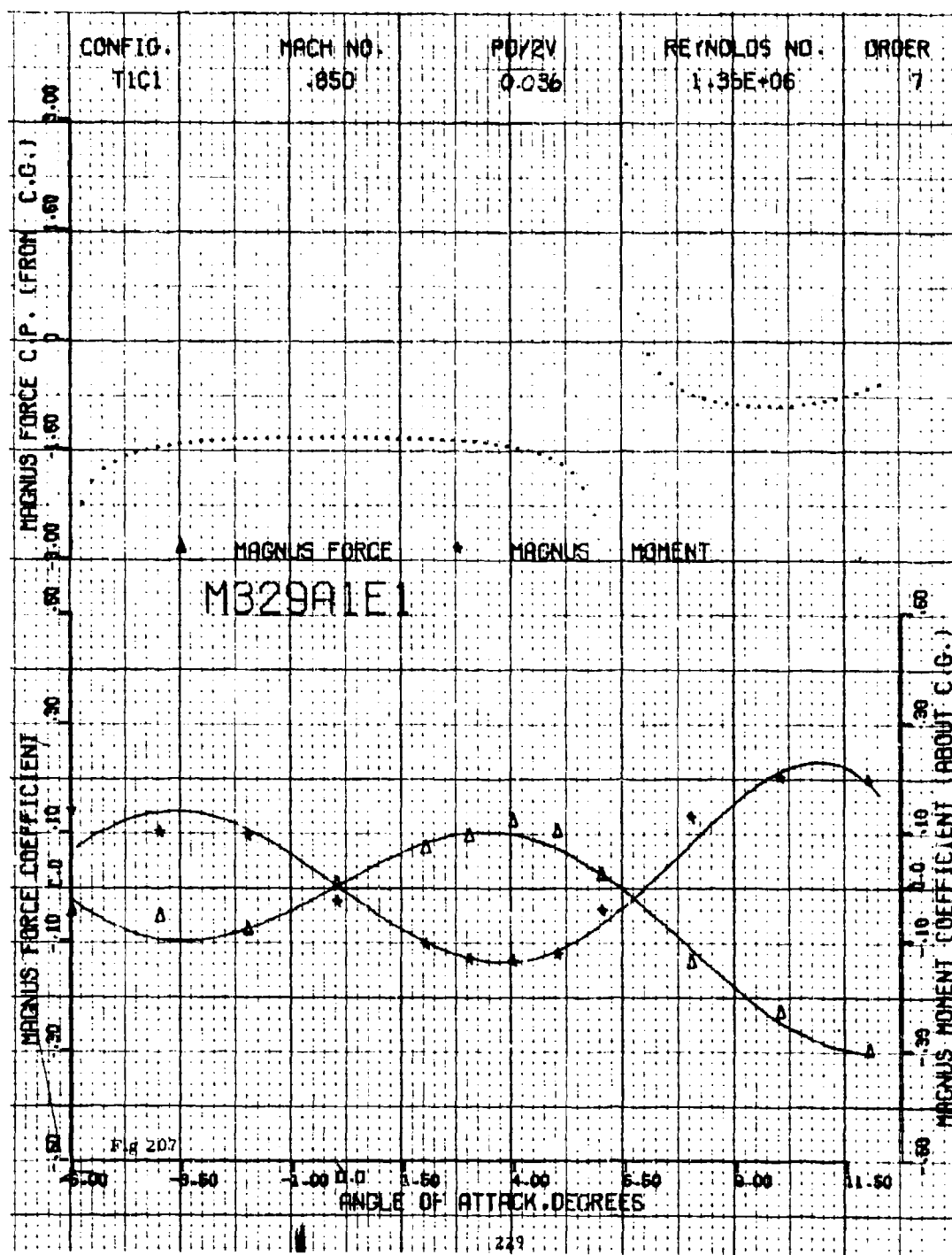


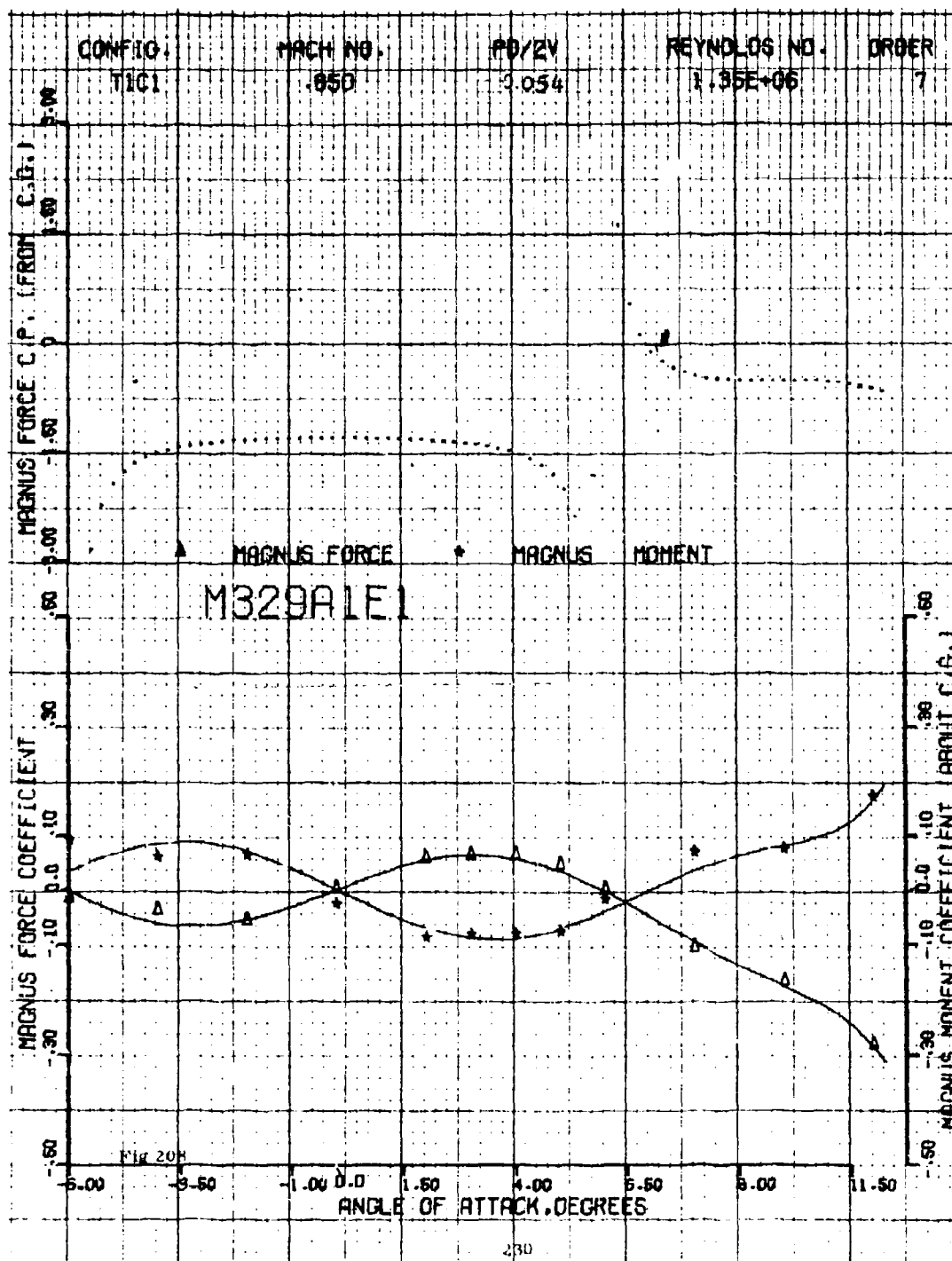


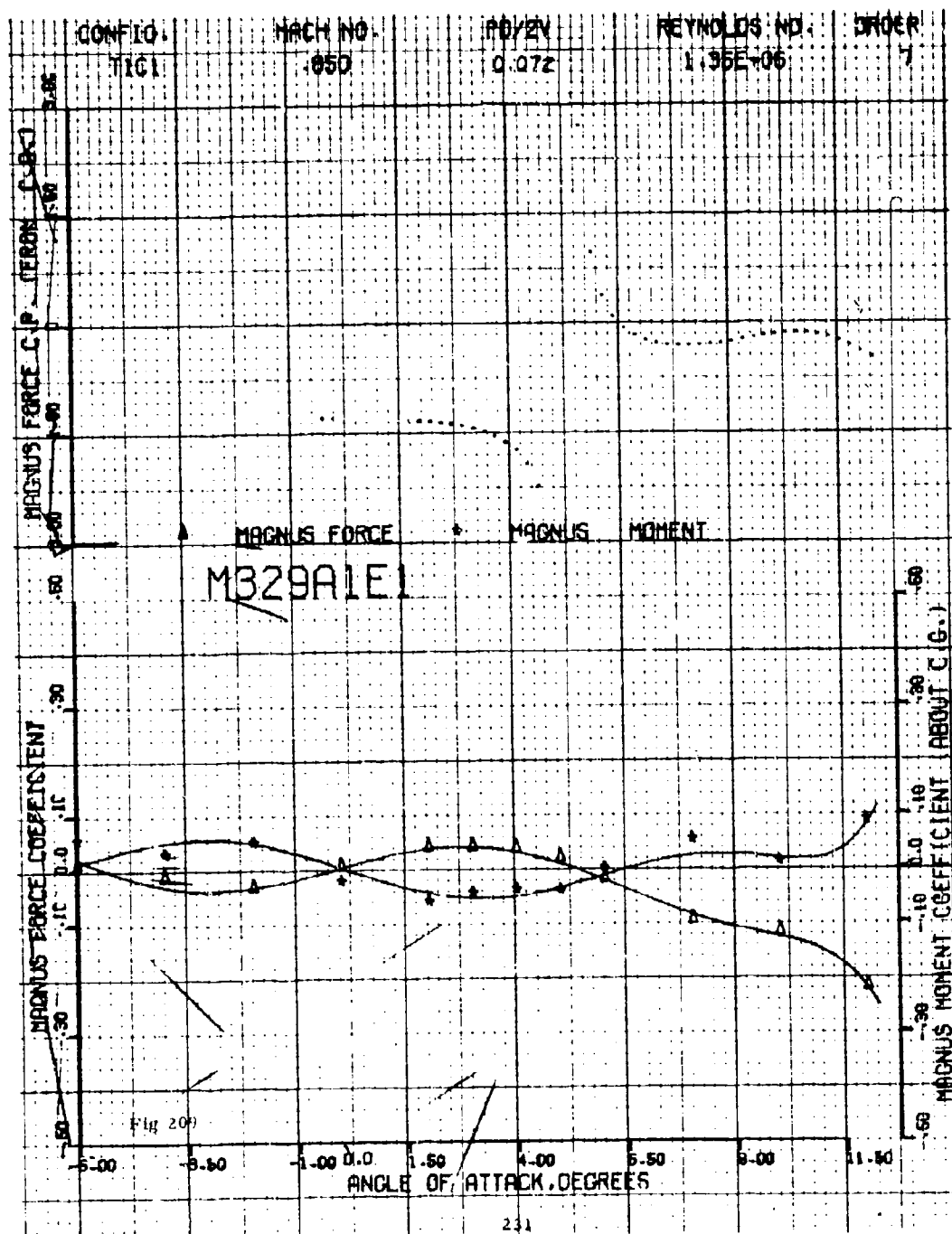


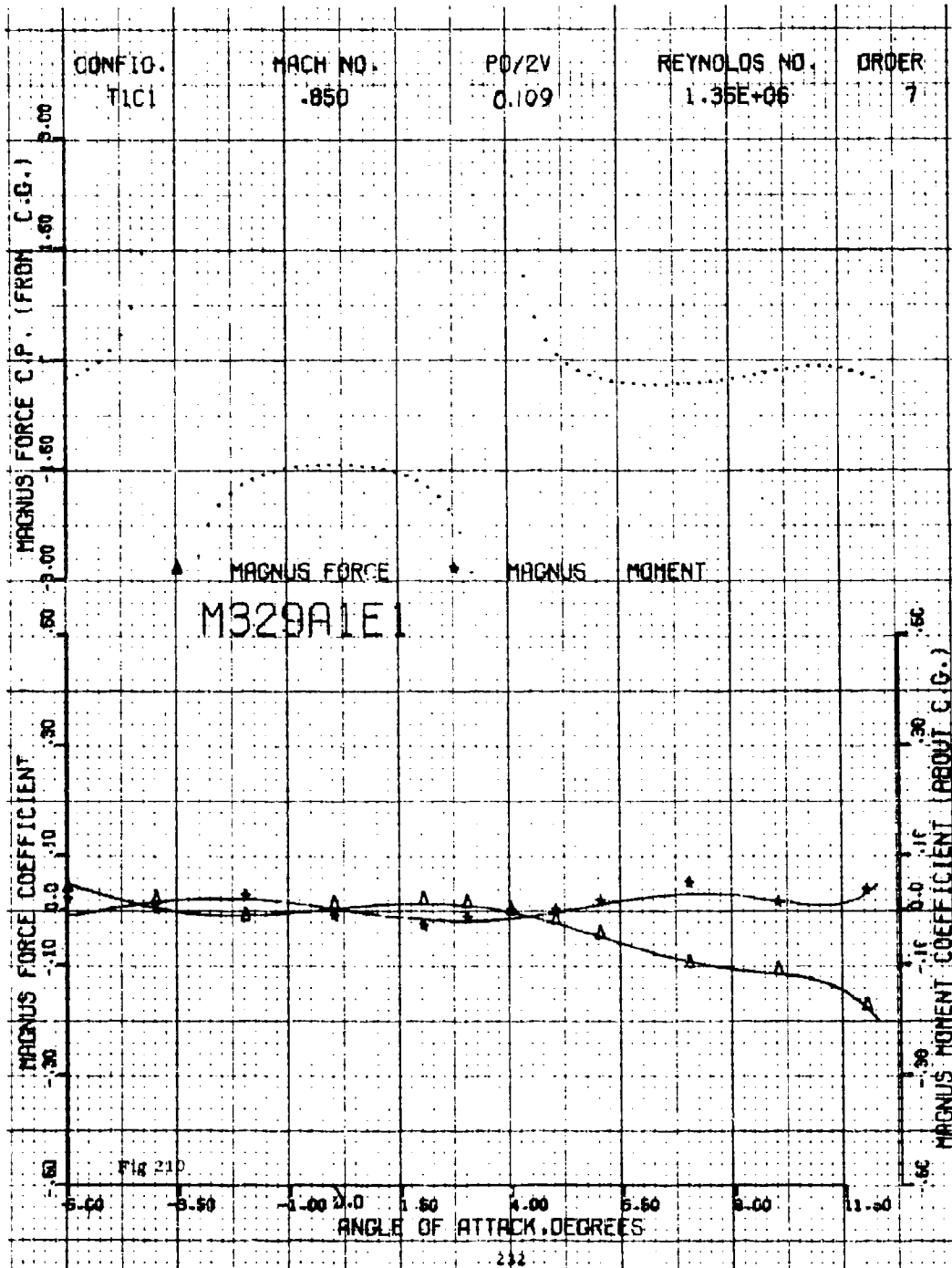


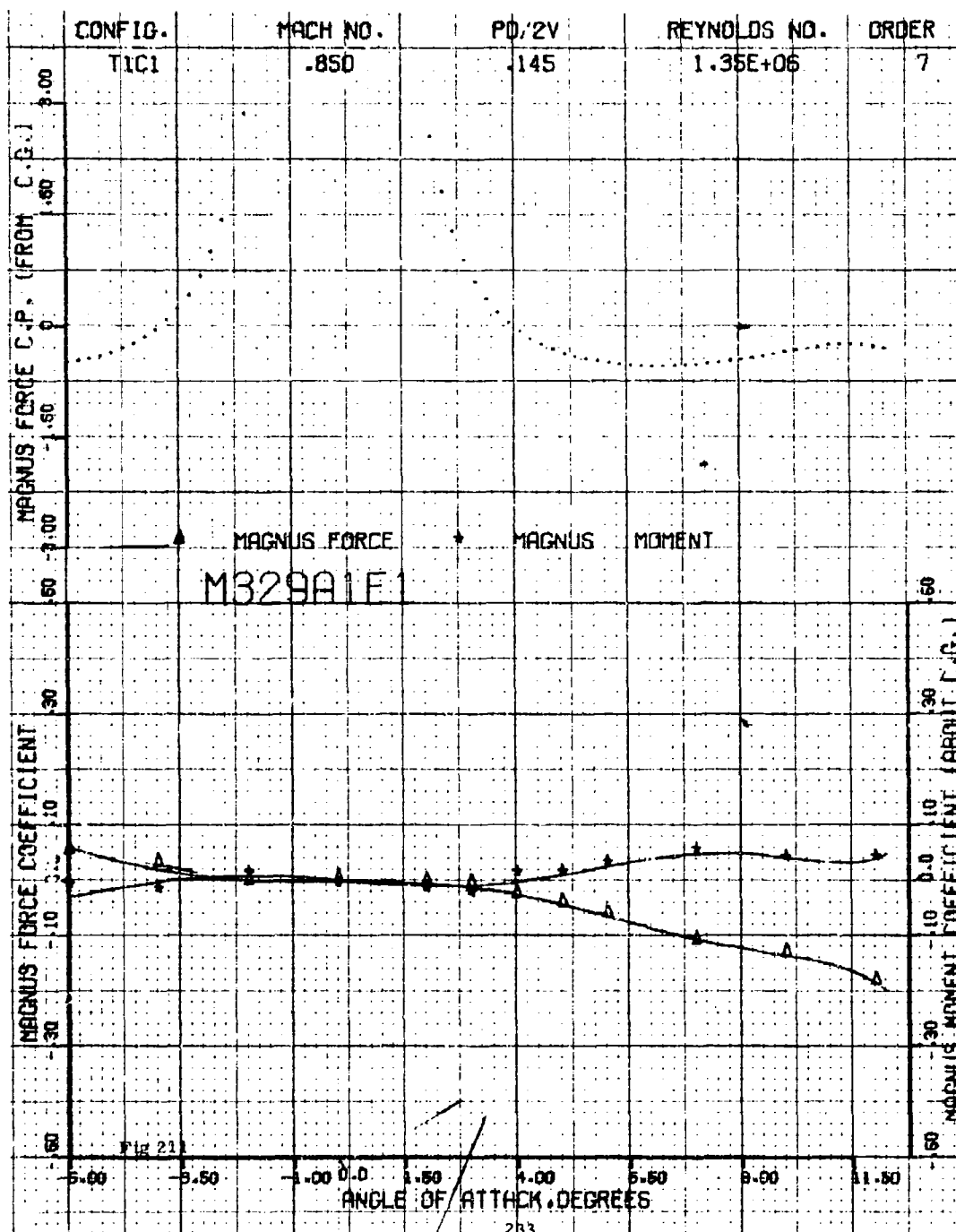


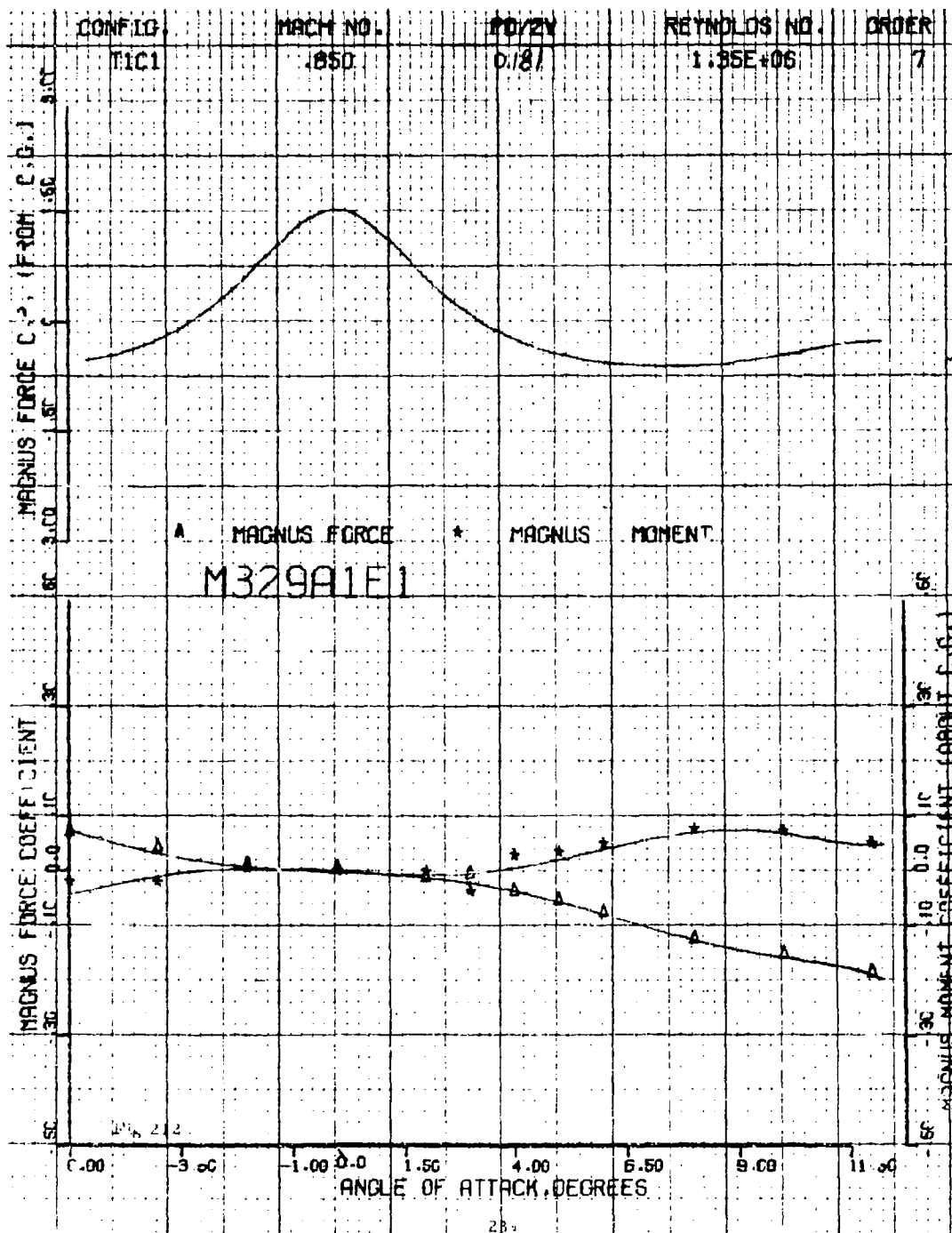


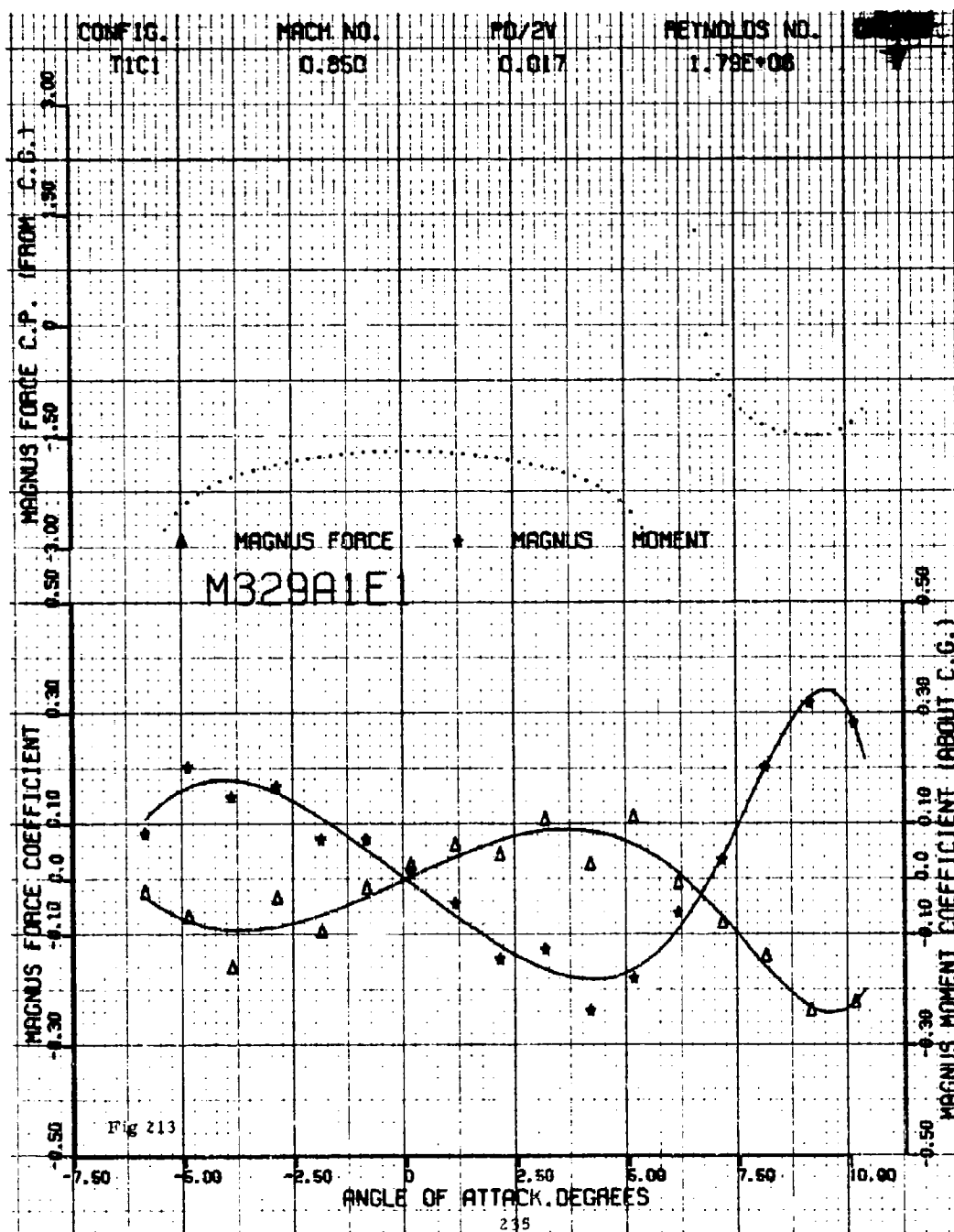












CONFIG. T1C1 MACH NO. 0.850 PD/2V 0.036 REYNOLDS NO. 1.79E+06 ORDER 7

MAGNUS FORCE C.P. (FROM C.G.)

MAGNUS FORCE

MAGNUS MOMENT

M329A1E1

MAGNUS FORCE COEFFICIENT

MAGNUS MOMENT COEFFICIENT (ABOUT C.G.)

ANGLE OF ATTACK, DEGREES

Fig 214

236

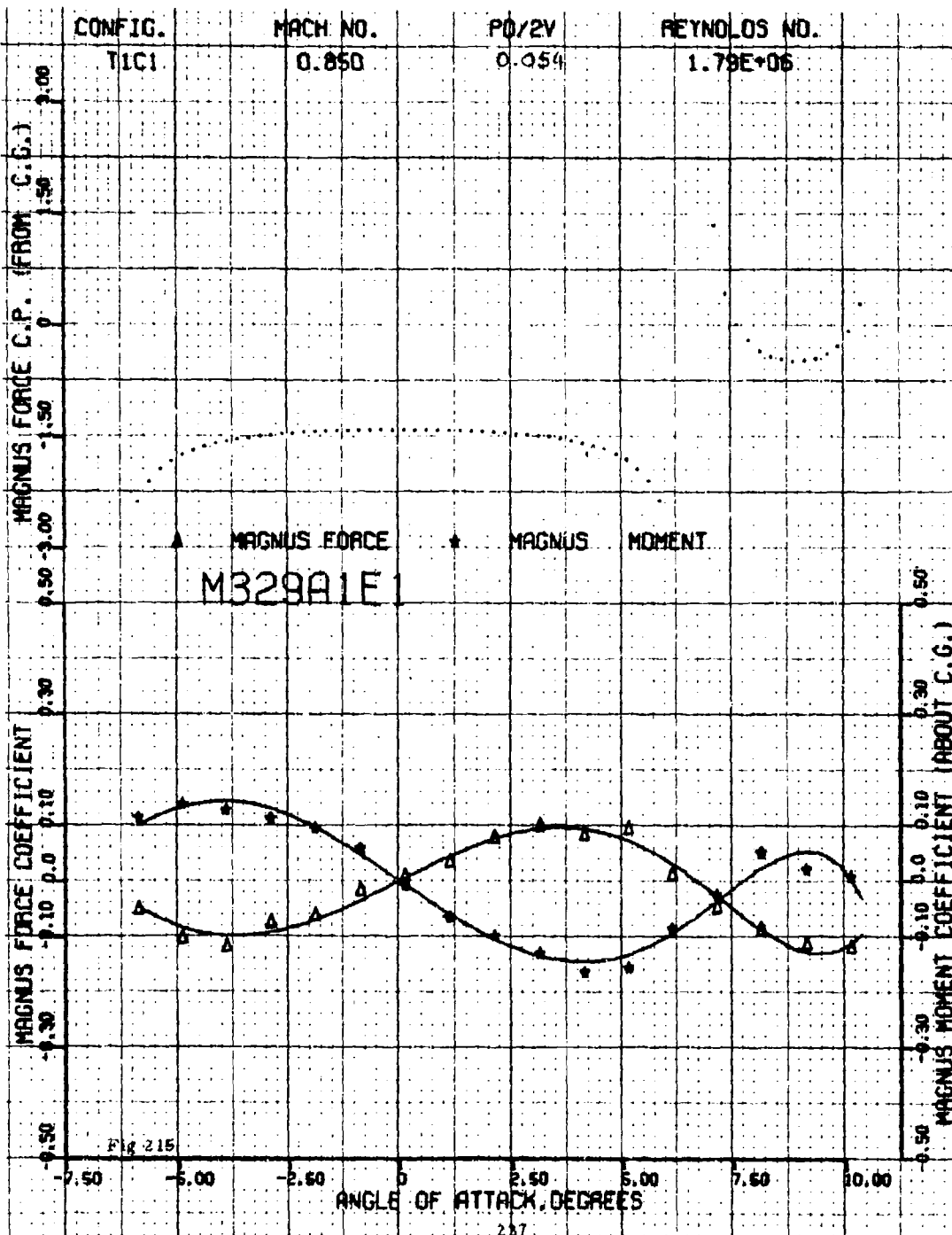
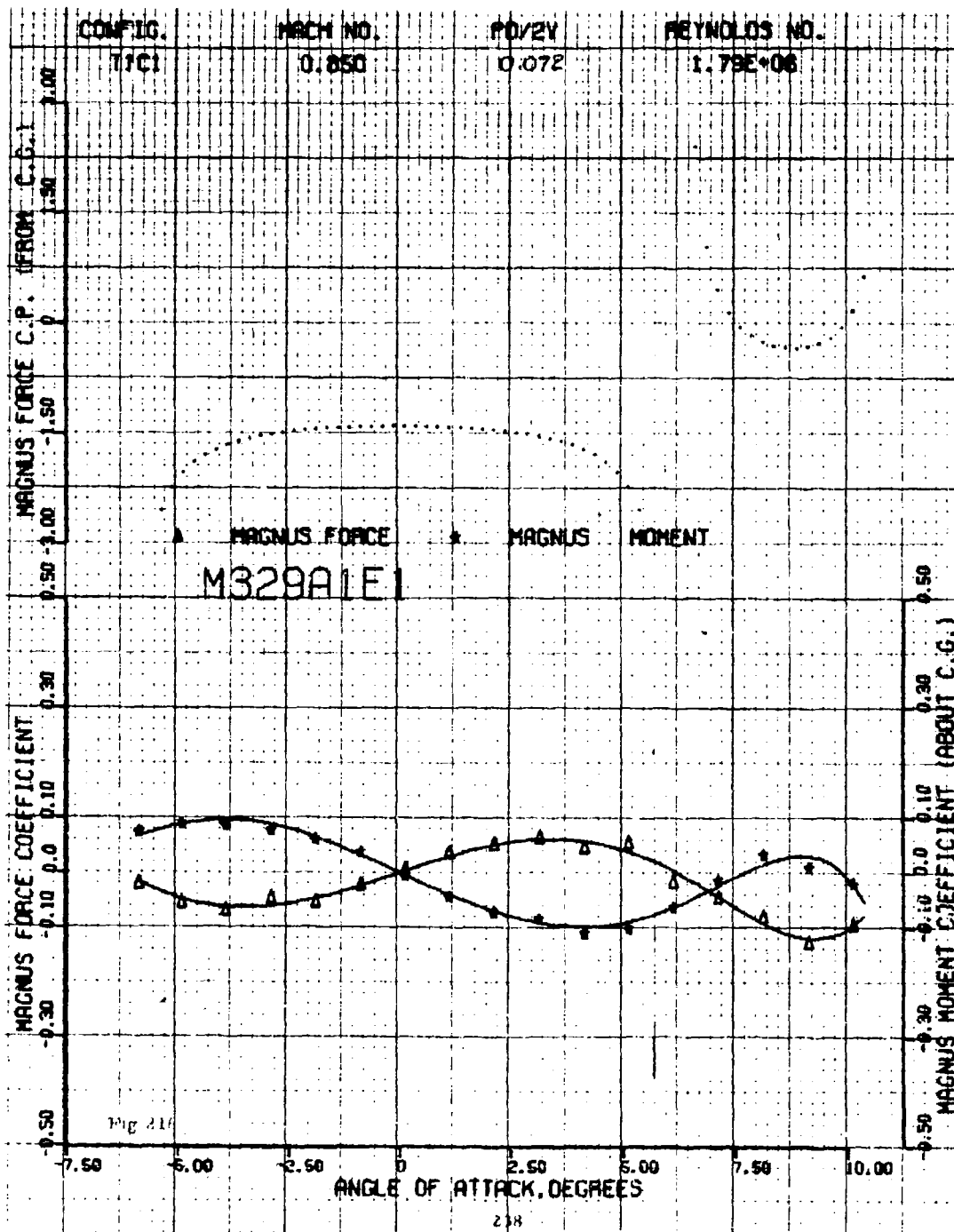
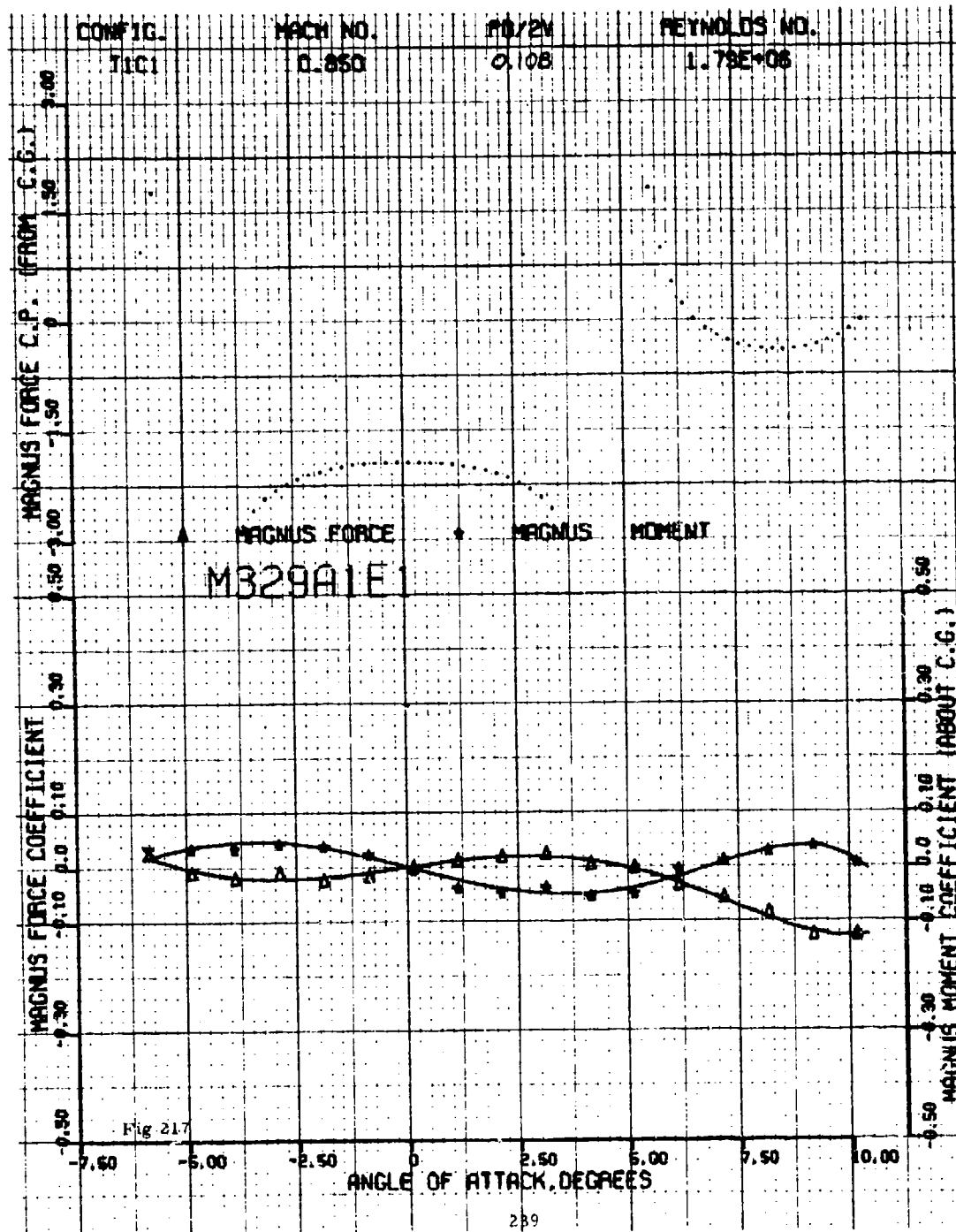
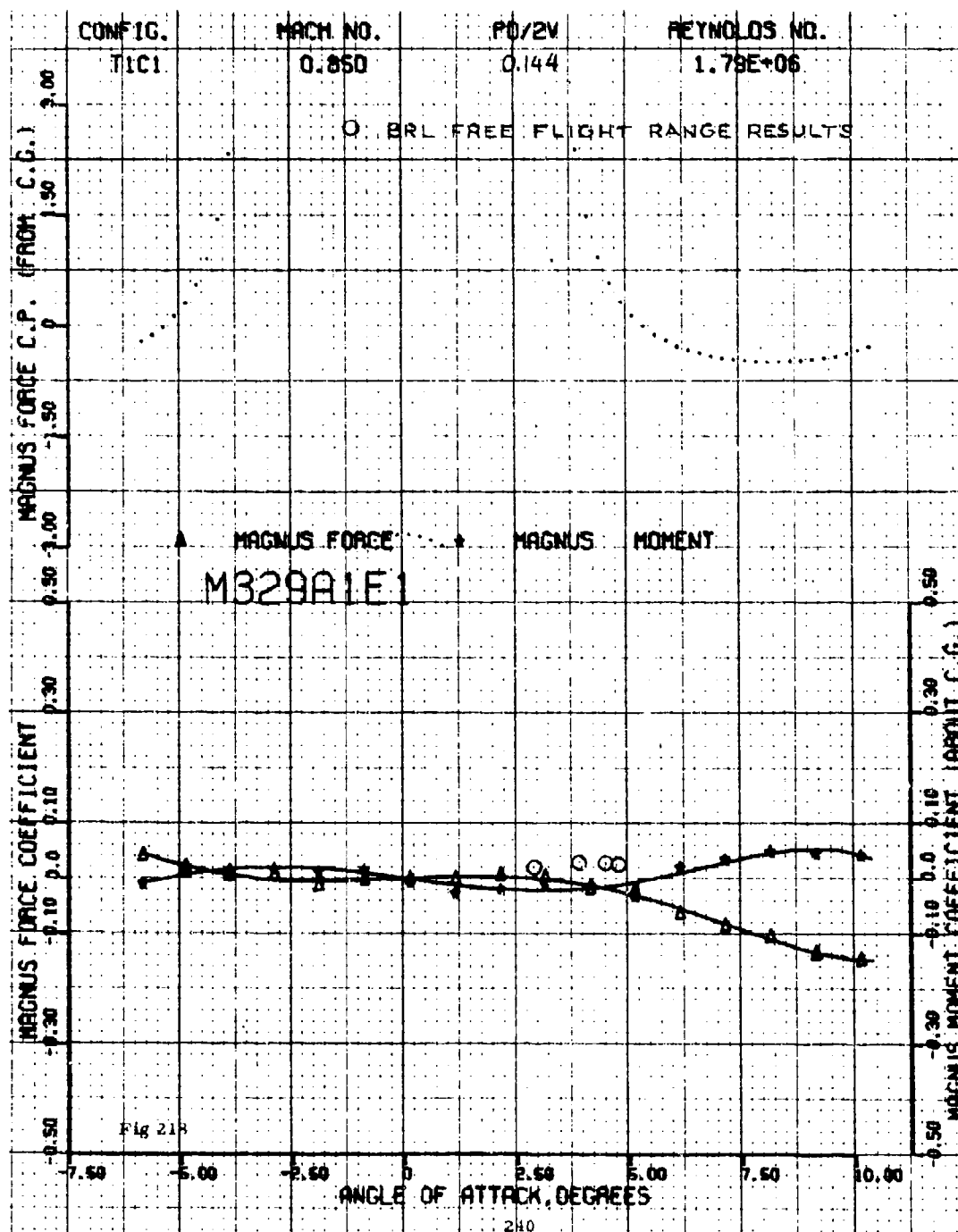
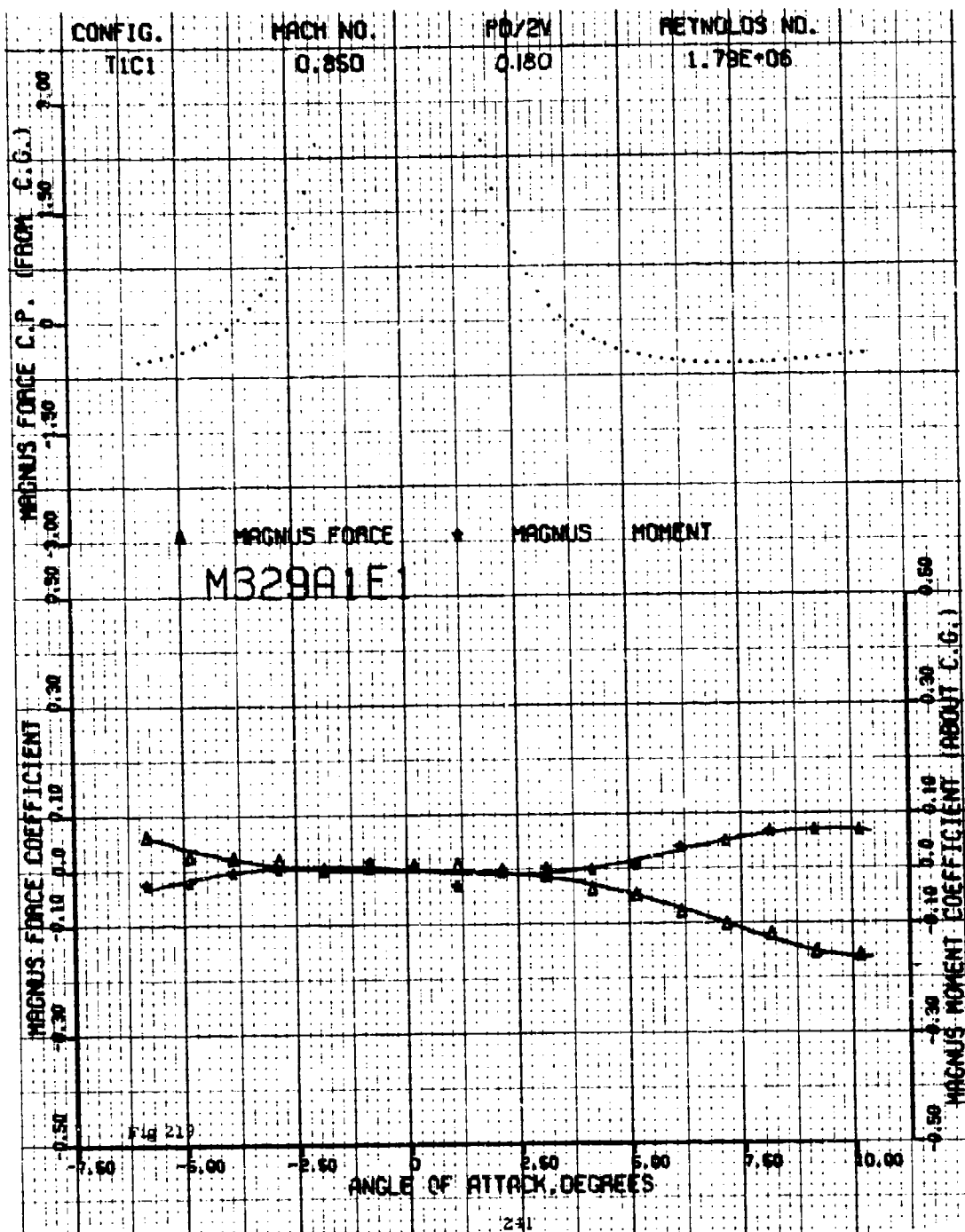


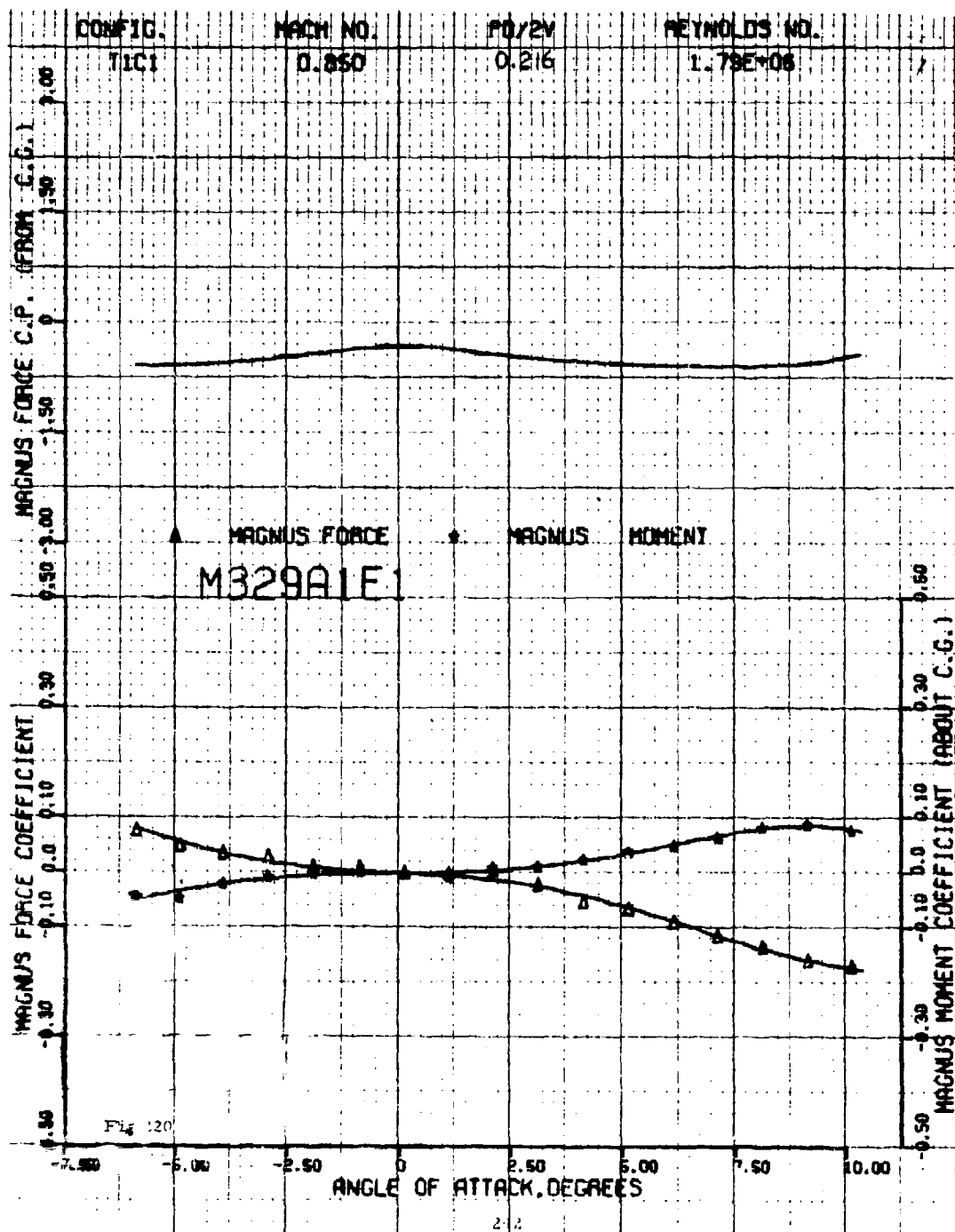
Fig 215

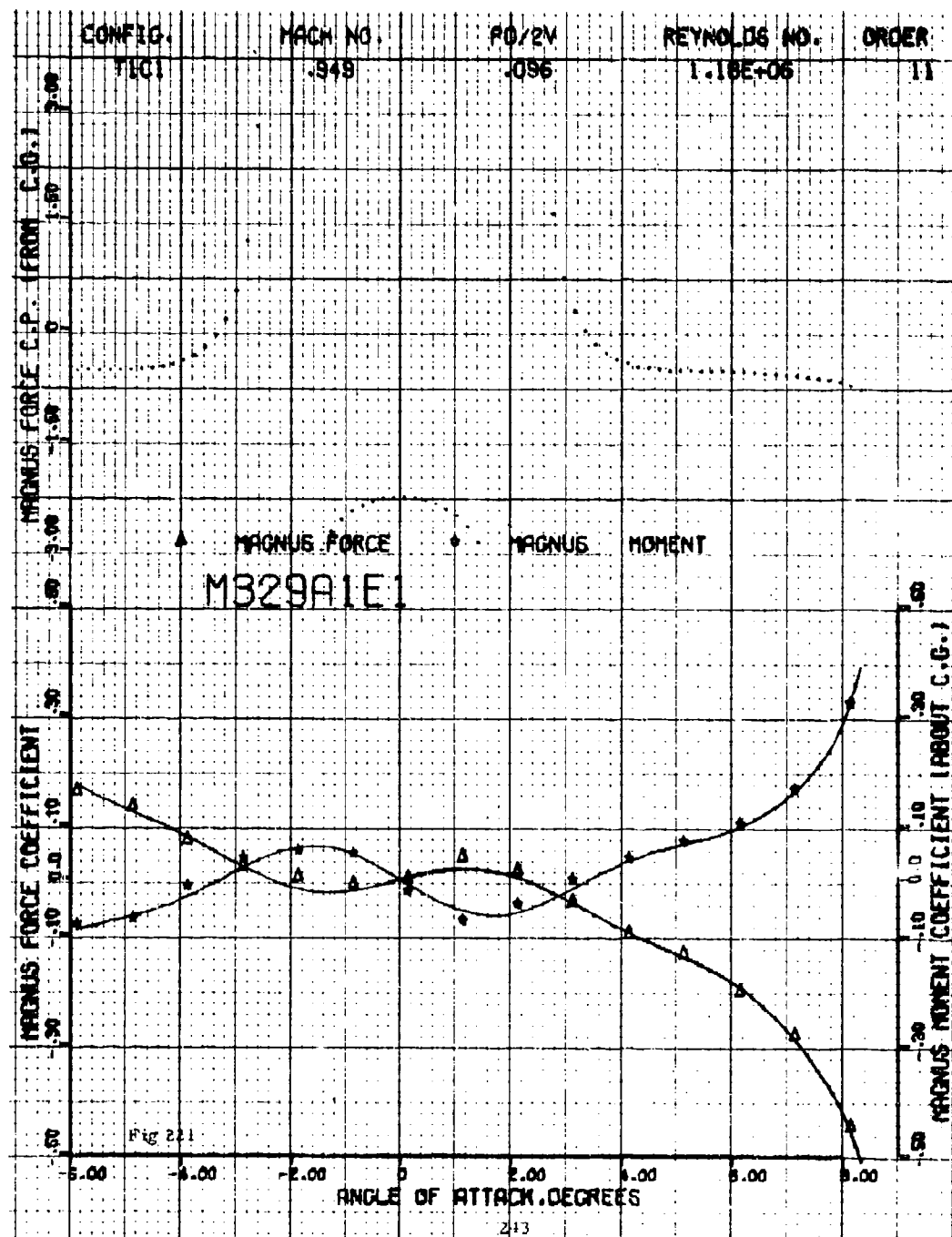


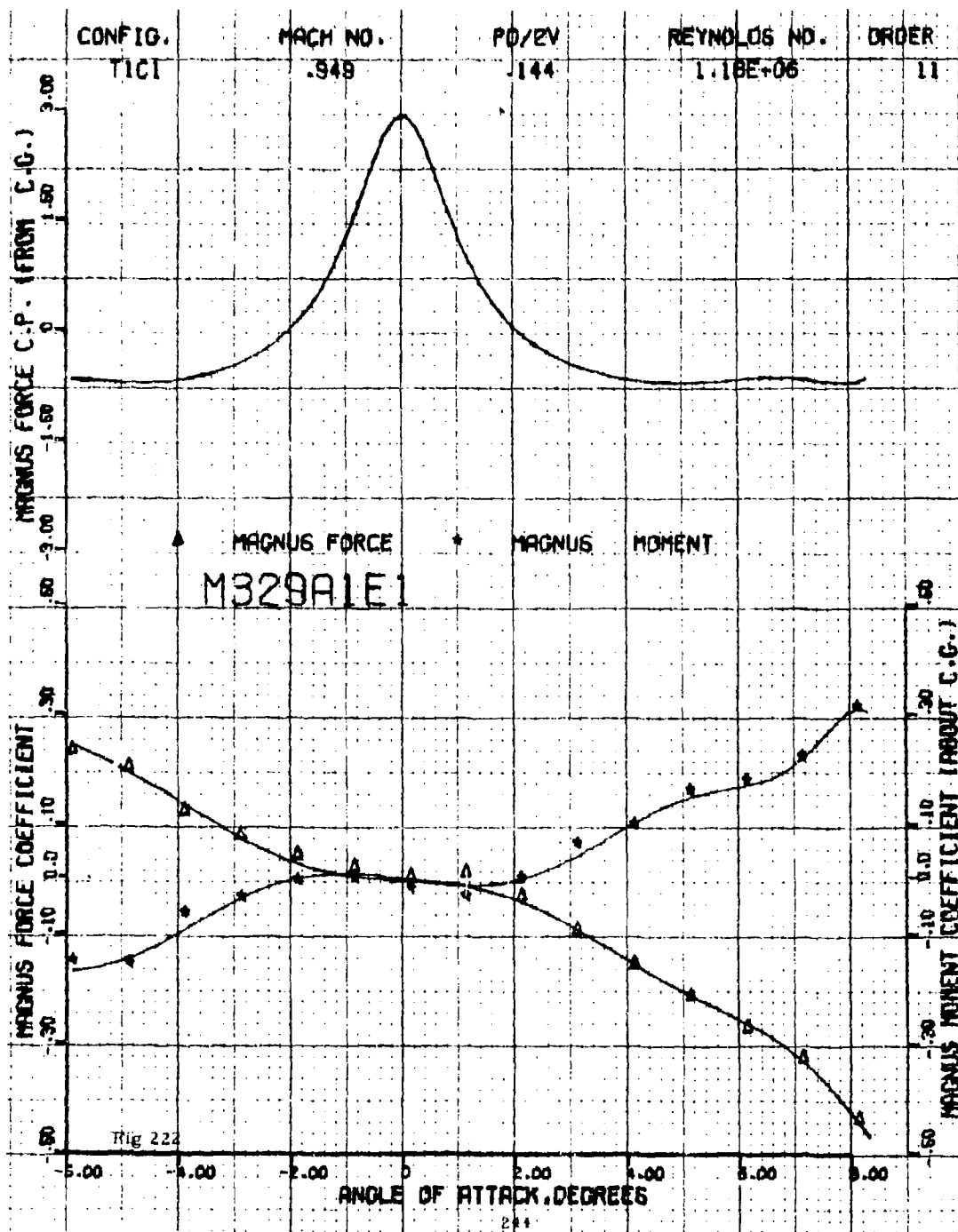


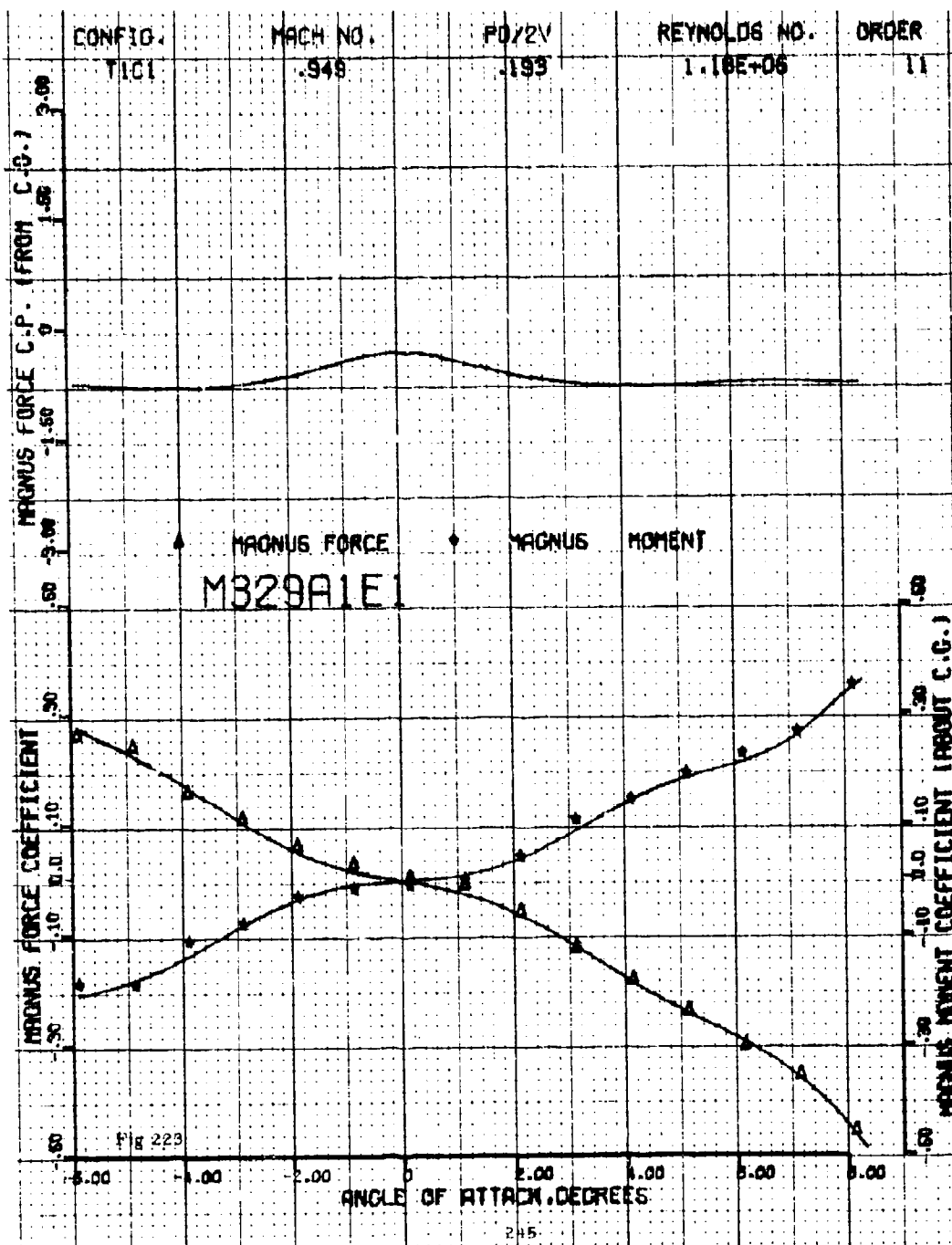


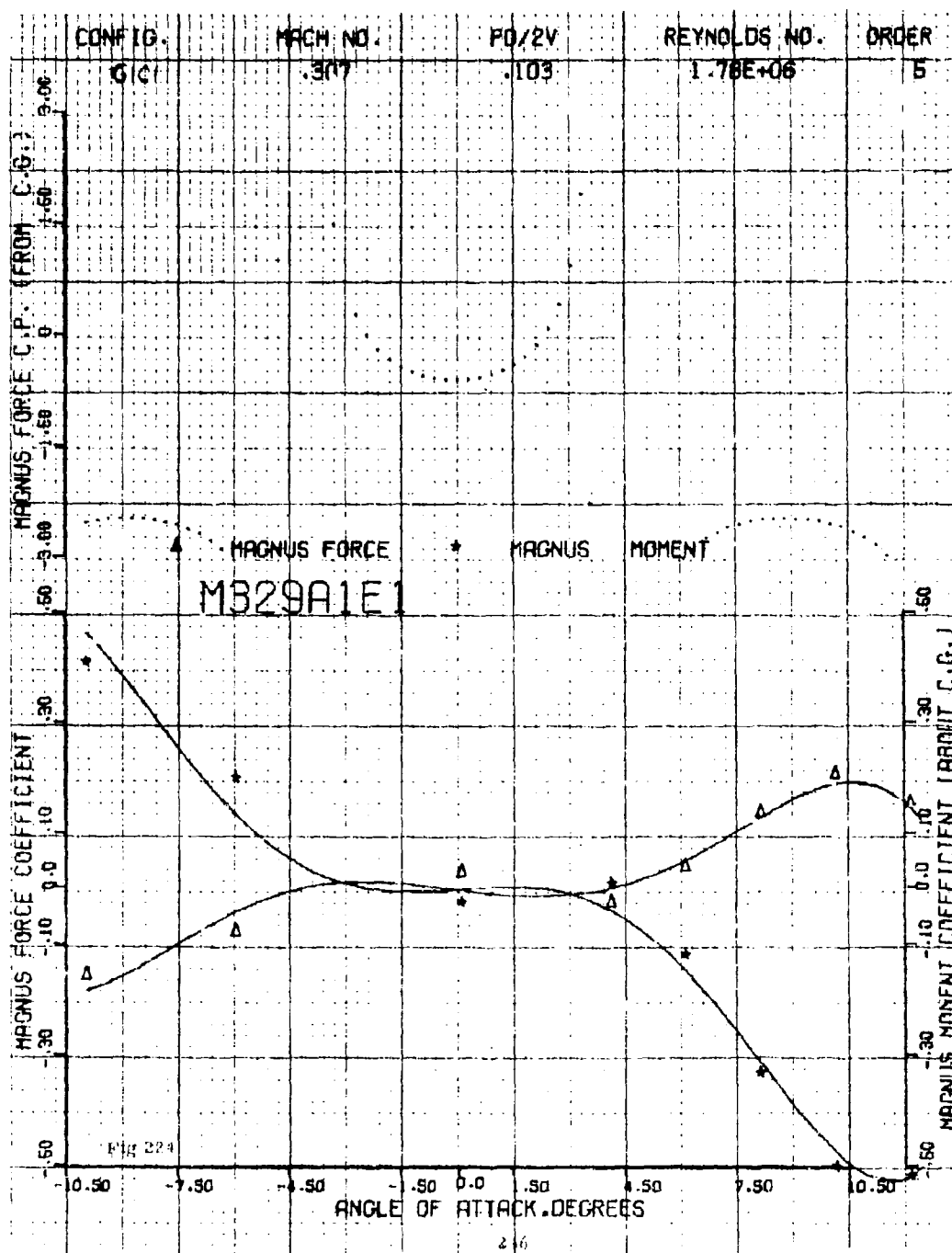


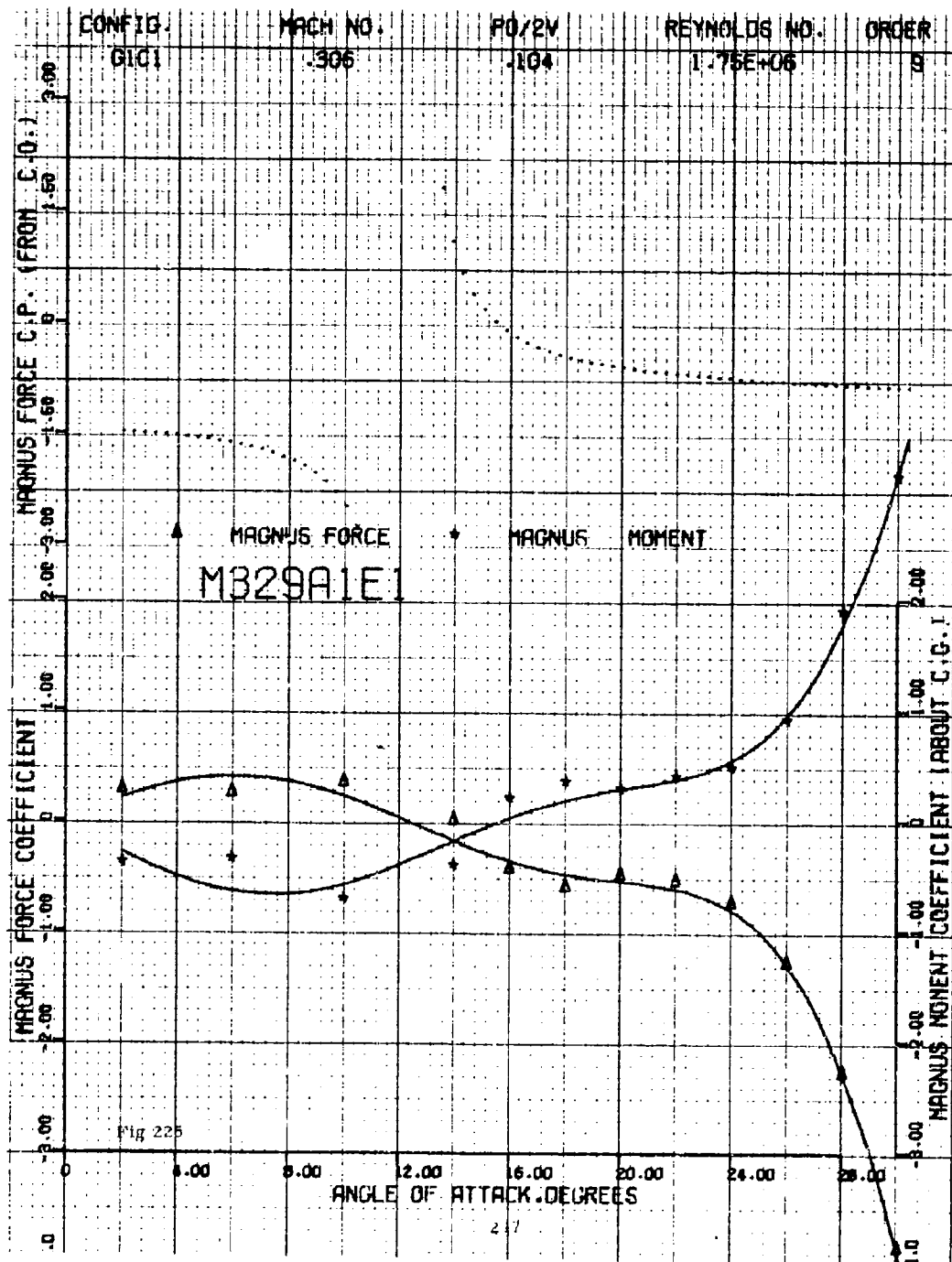


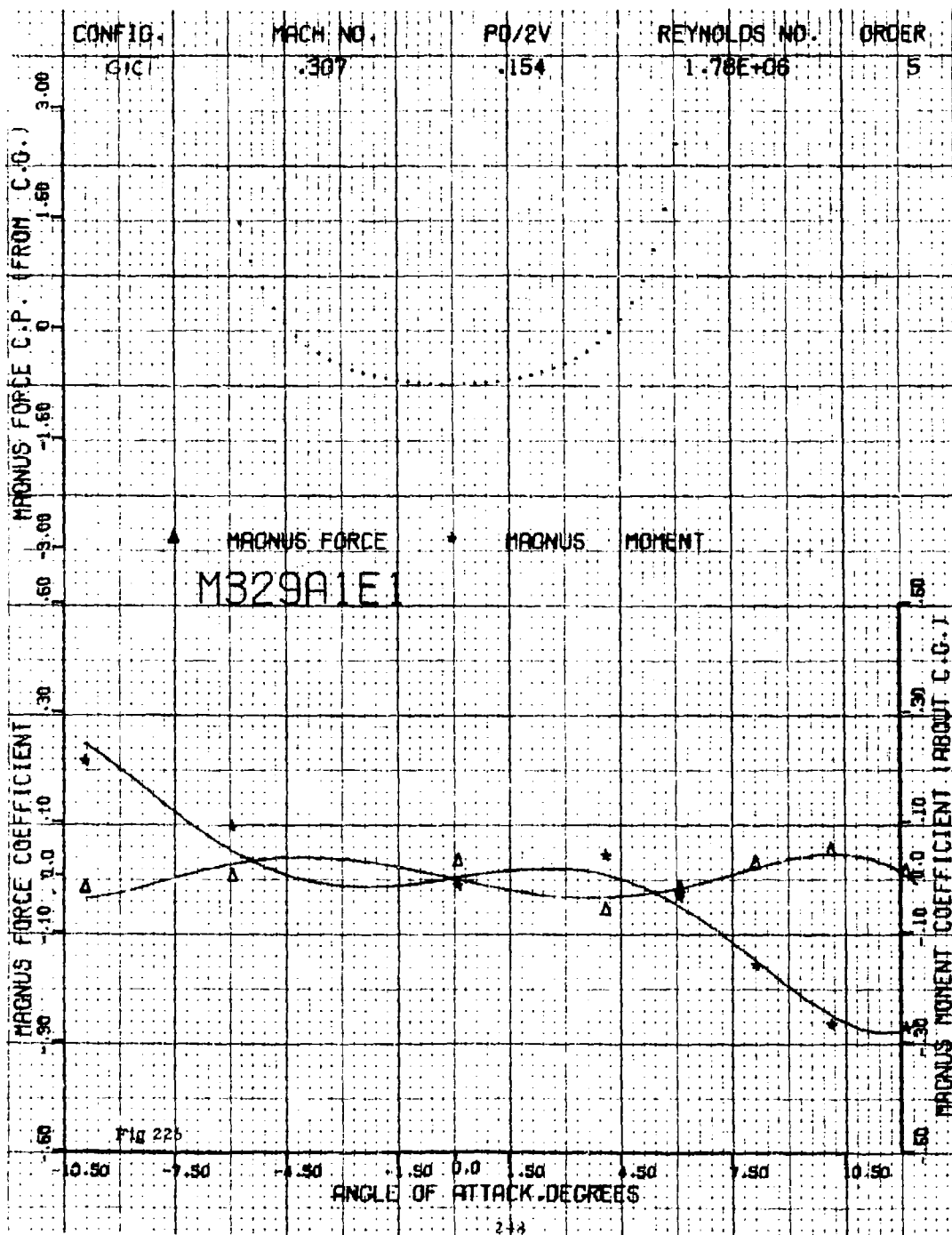




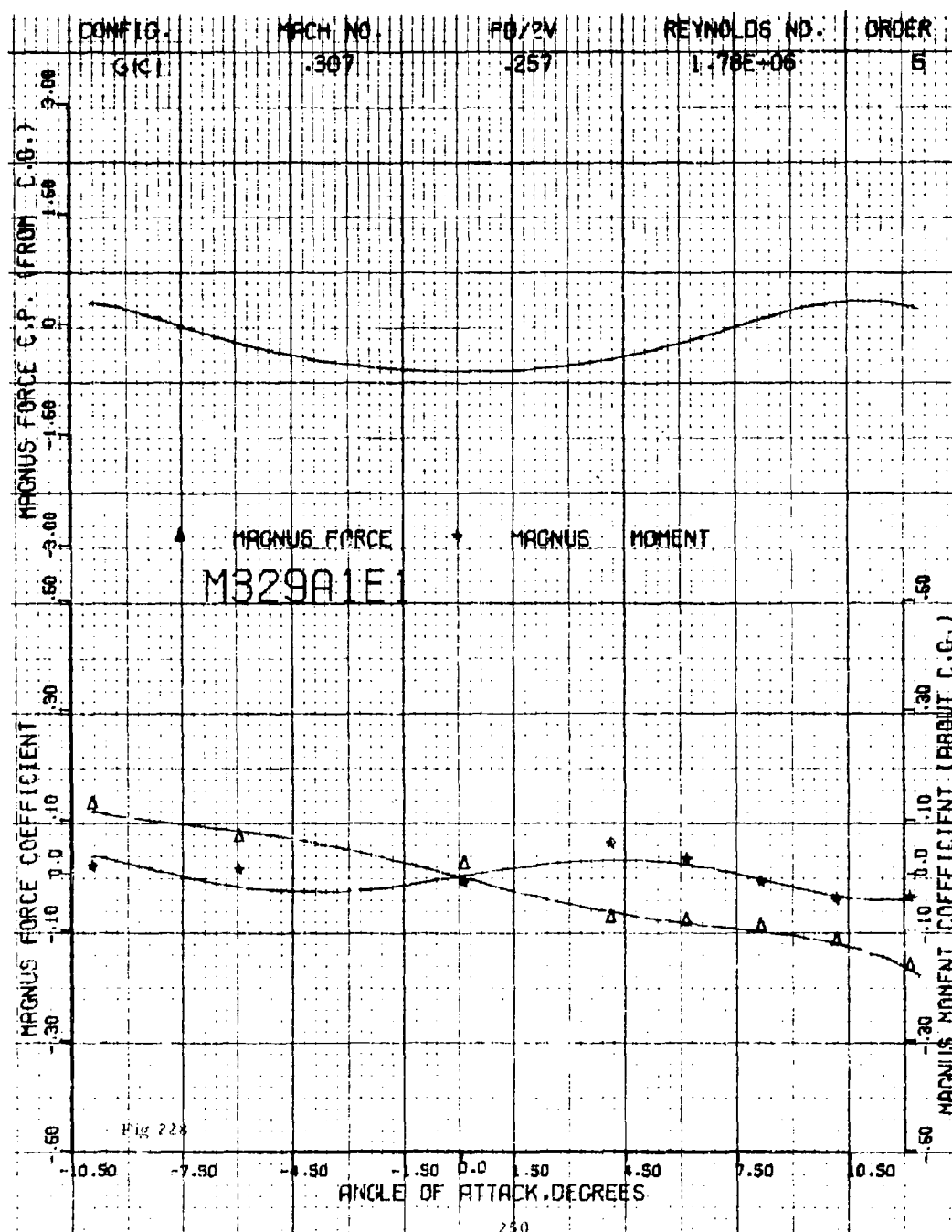


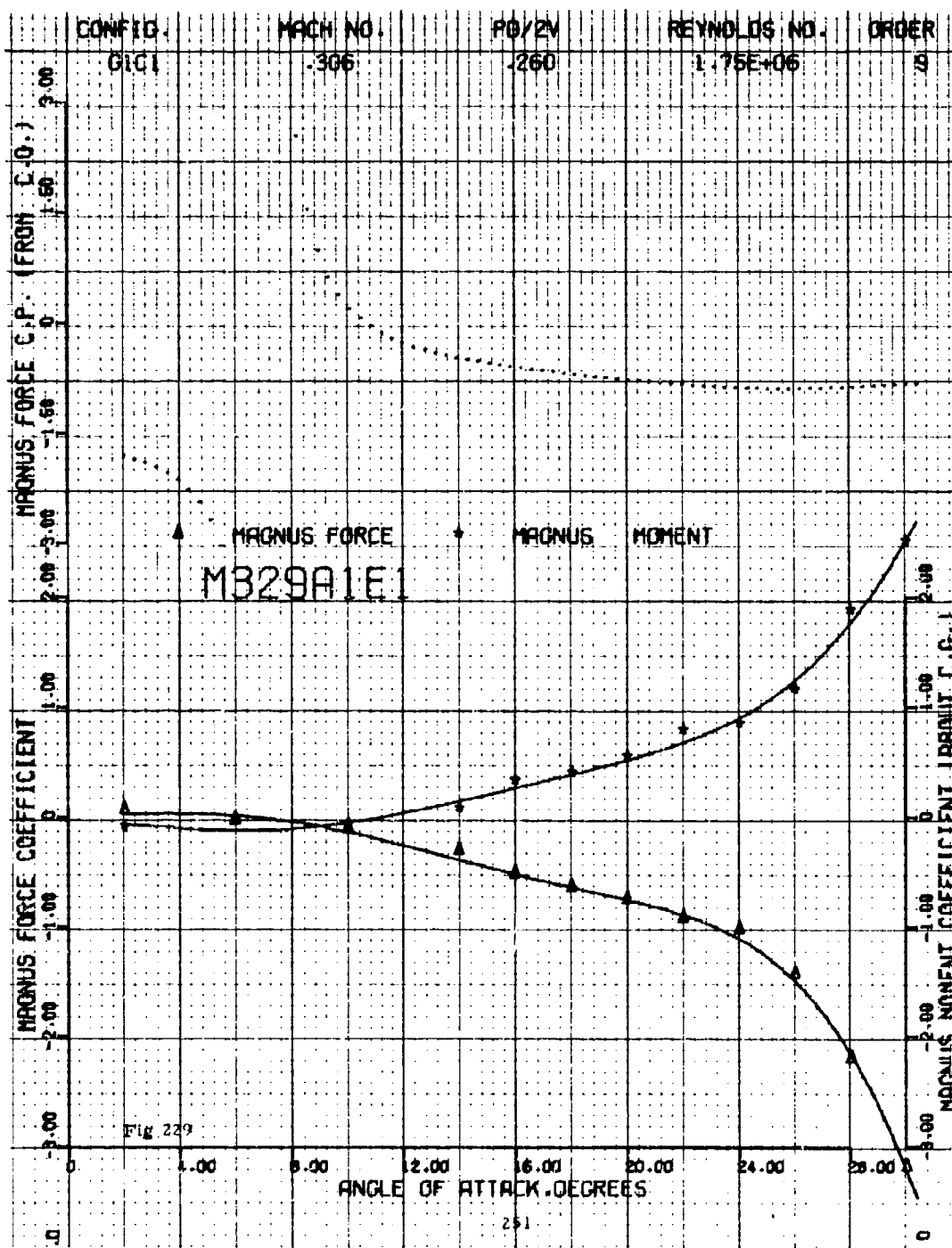


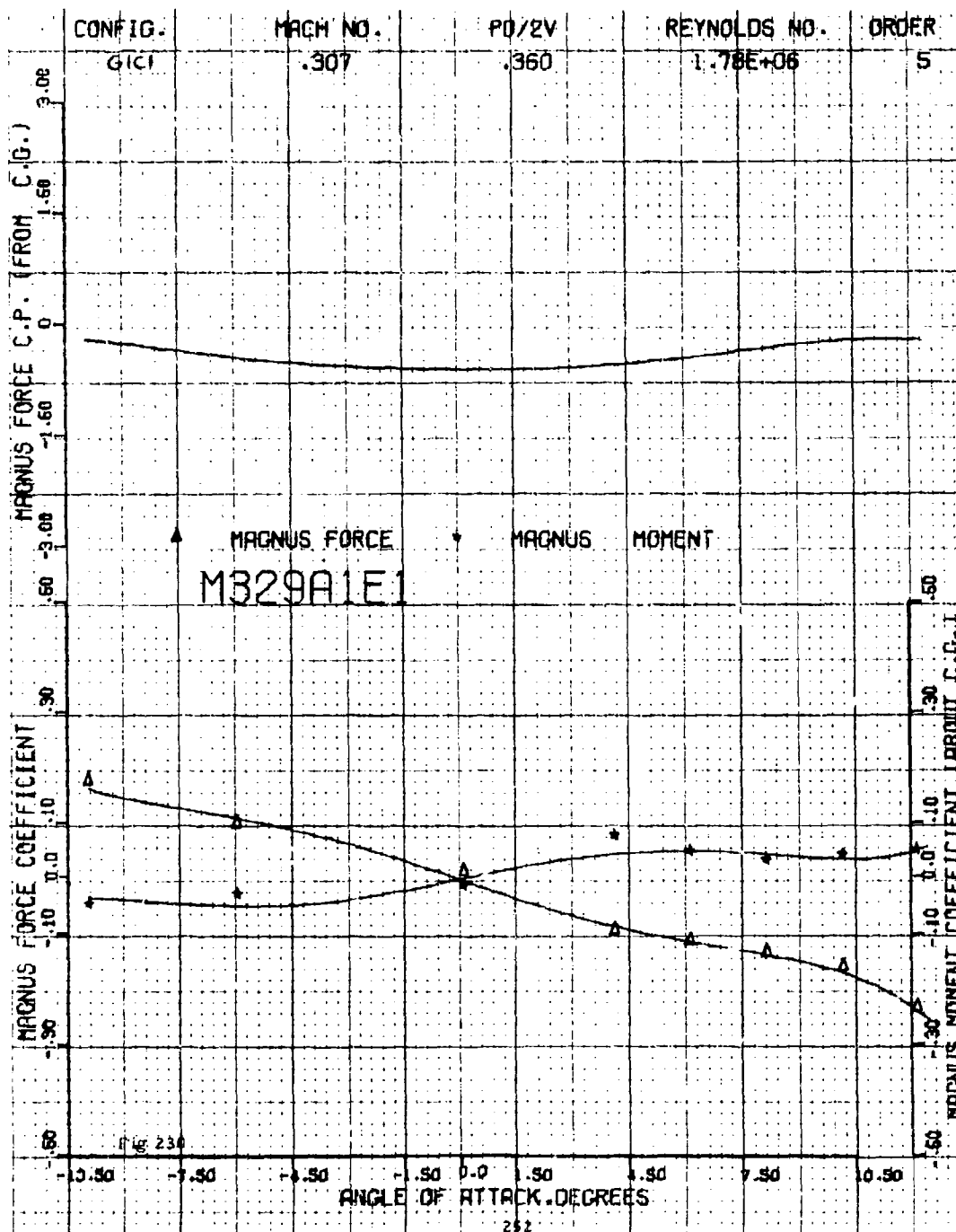


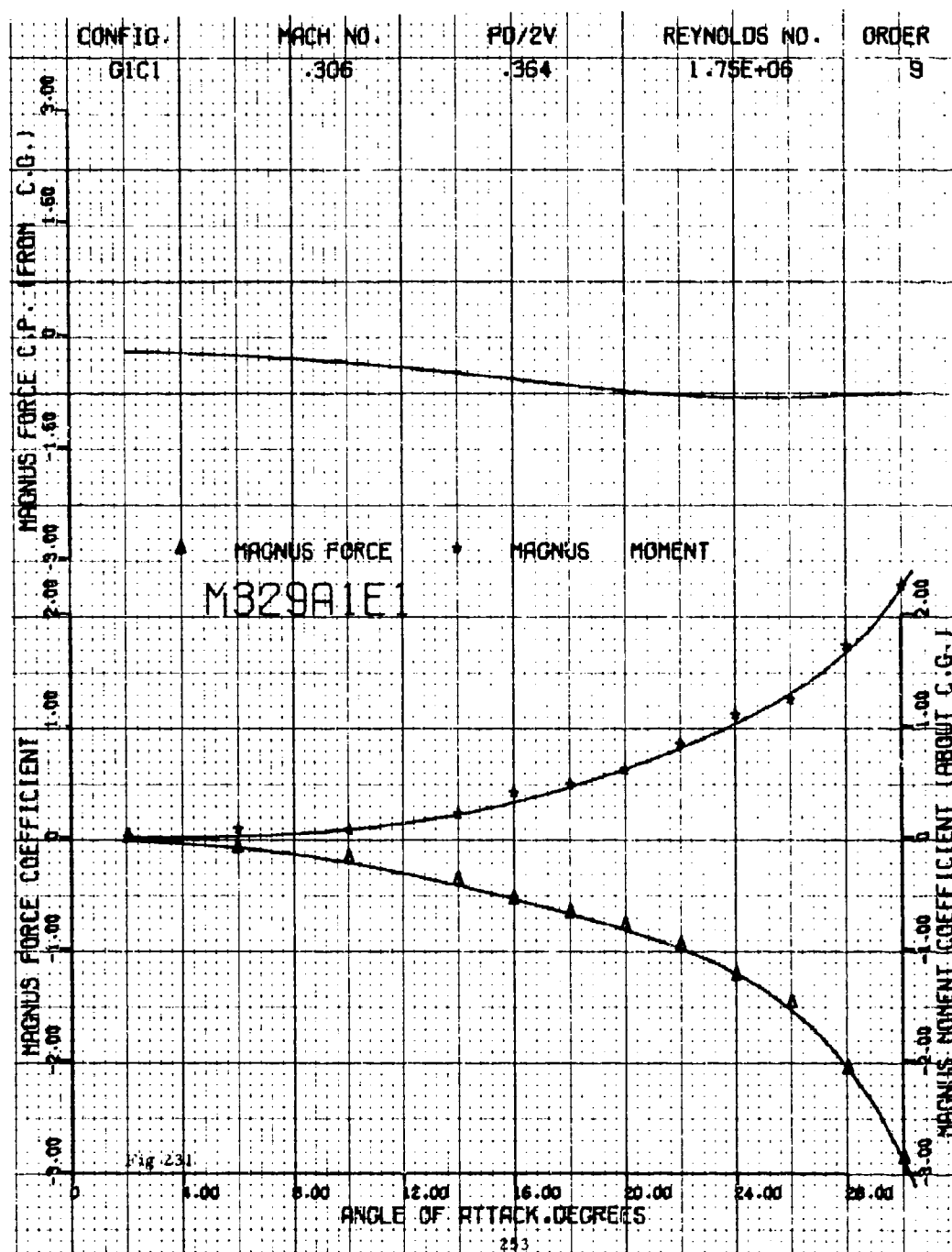


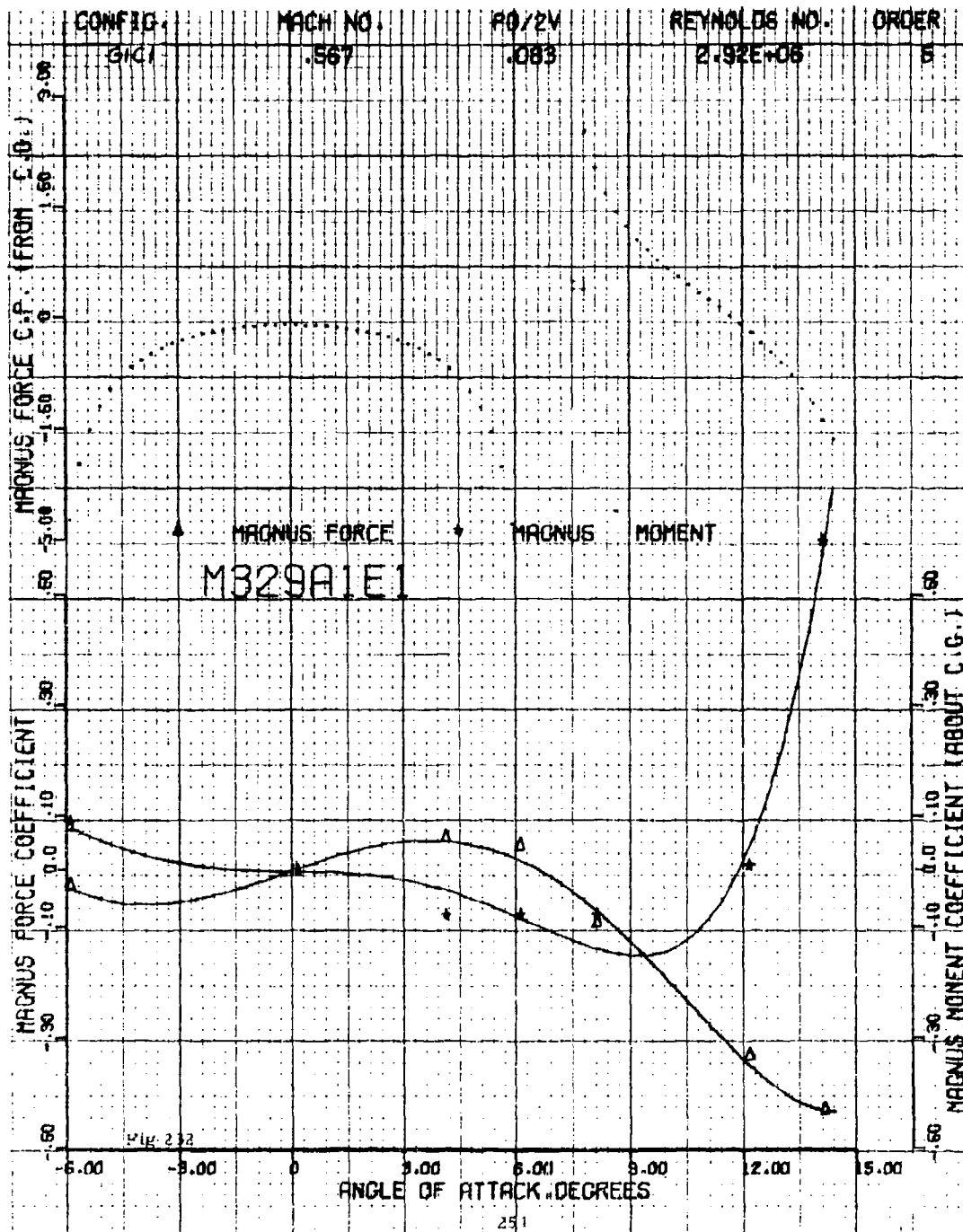
[illegible]

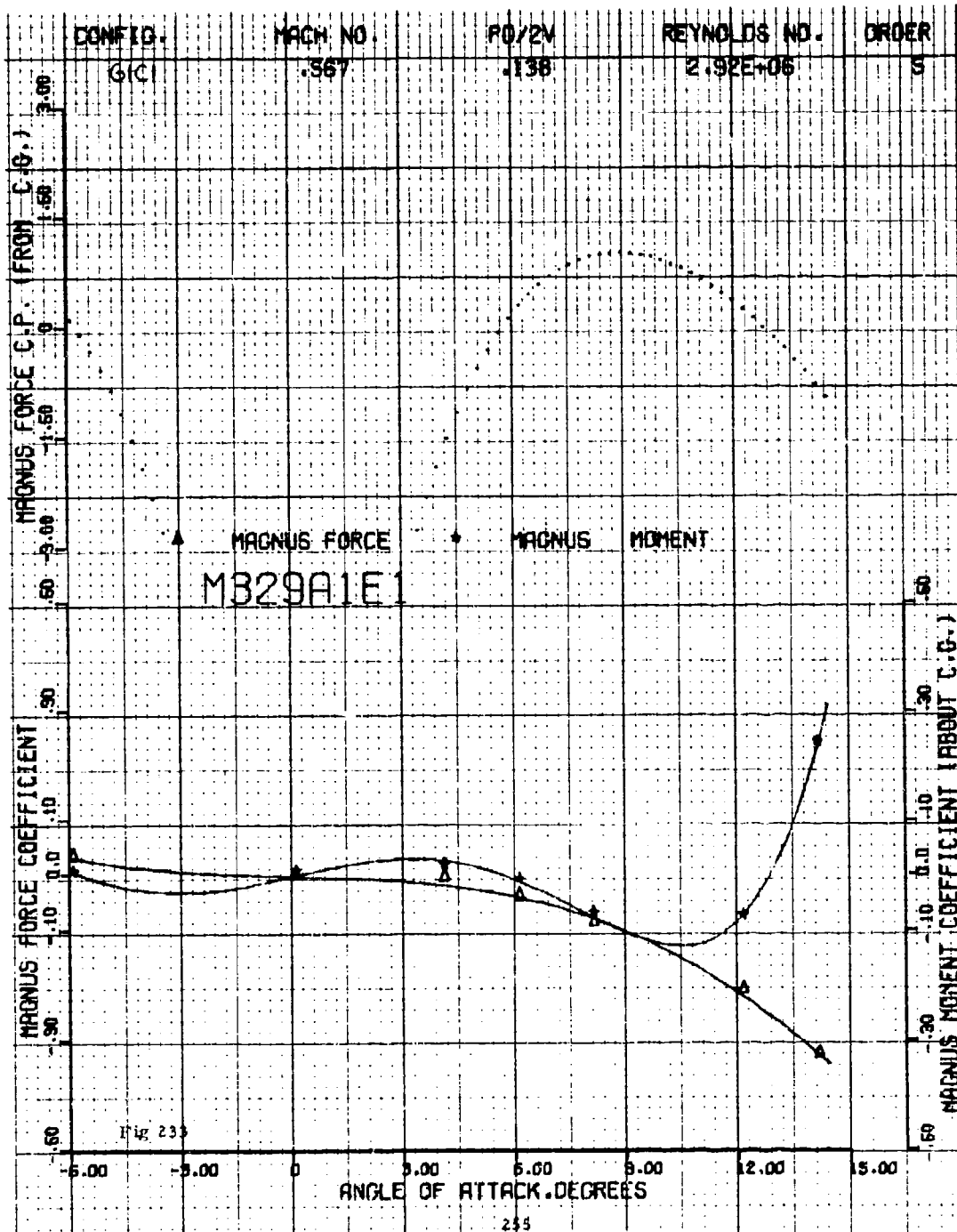


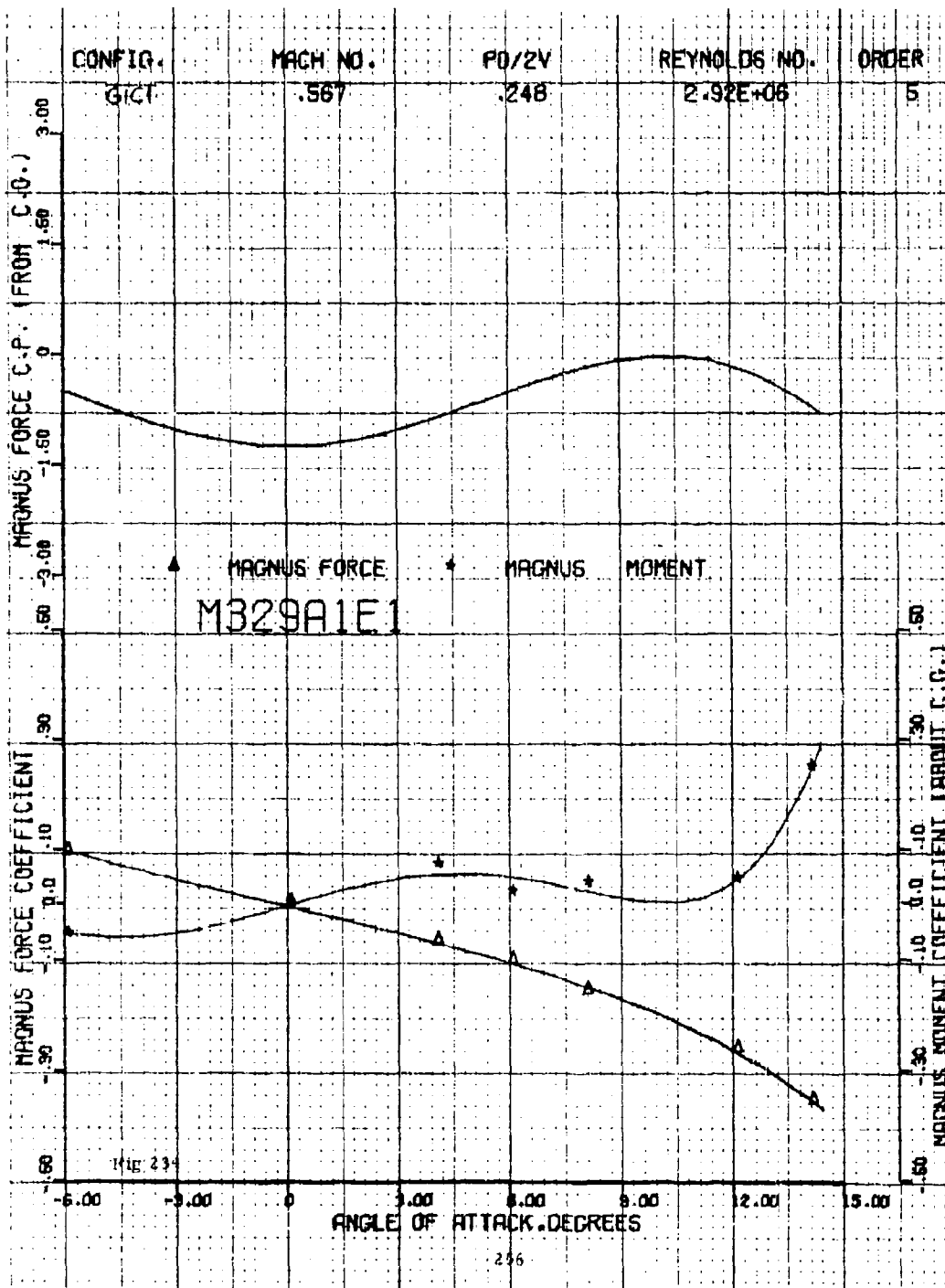


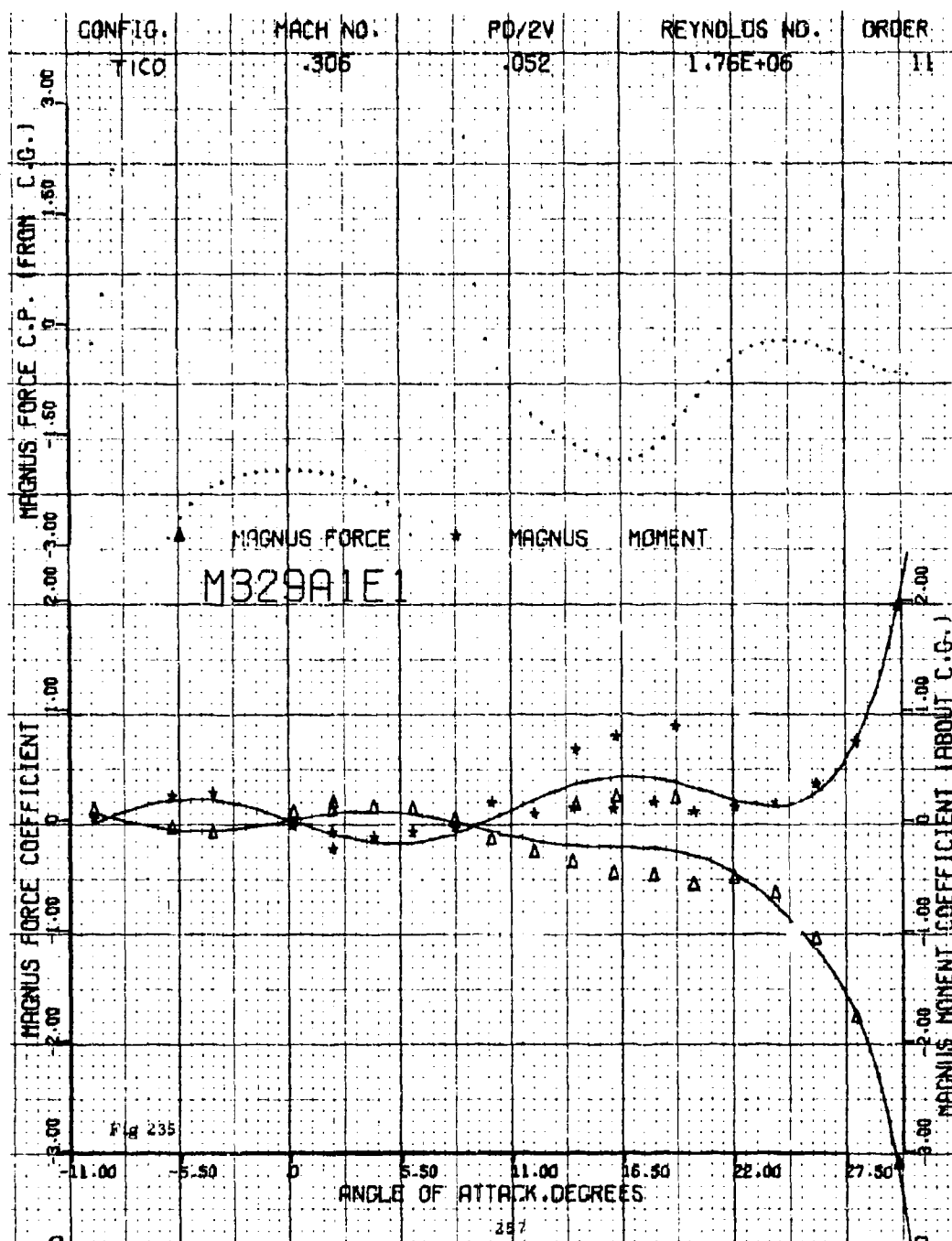


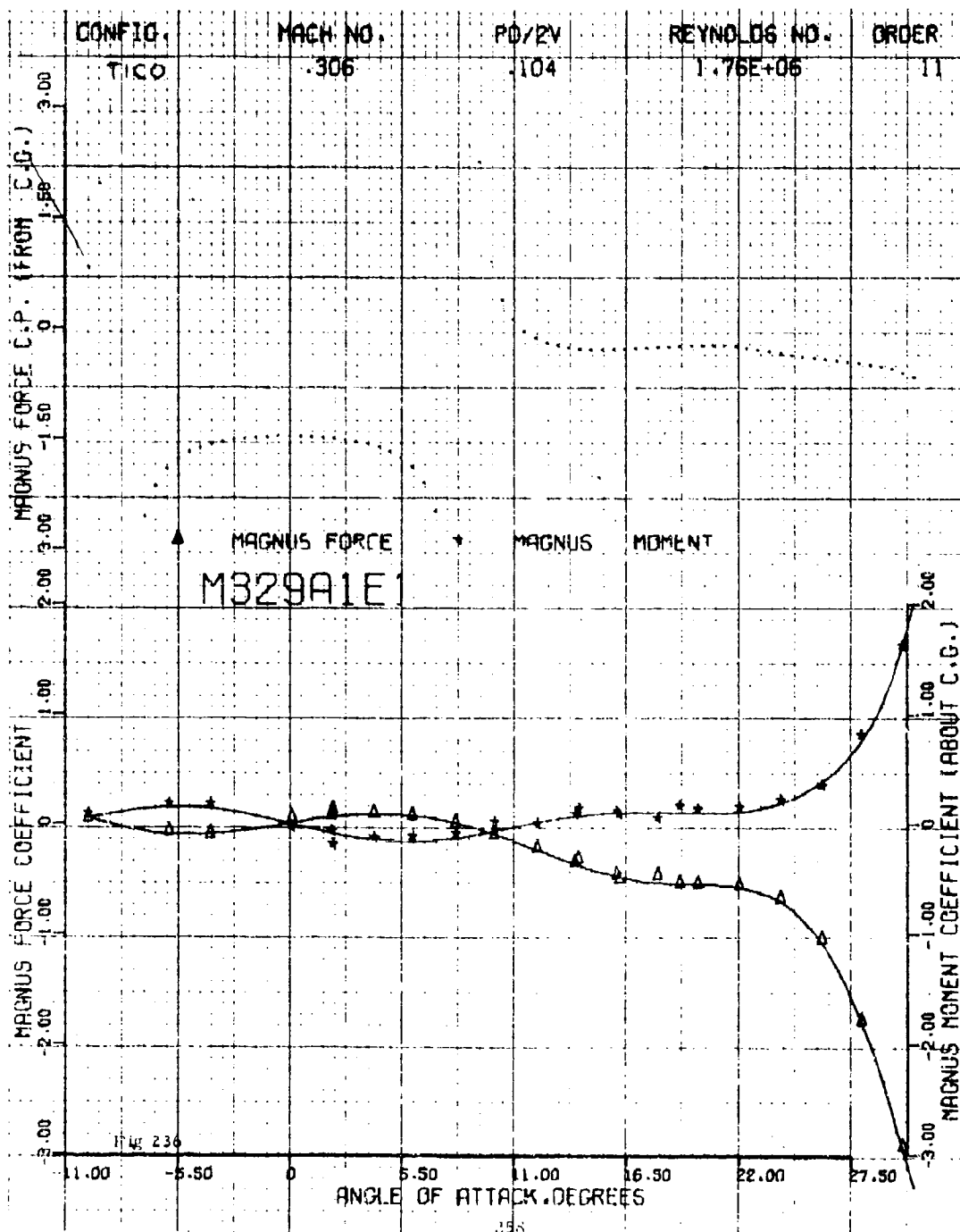


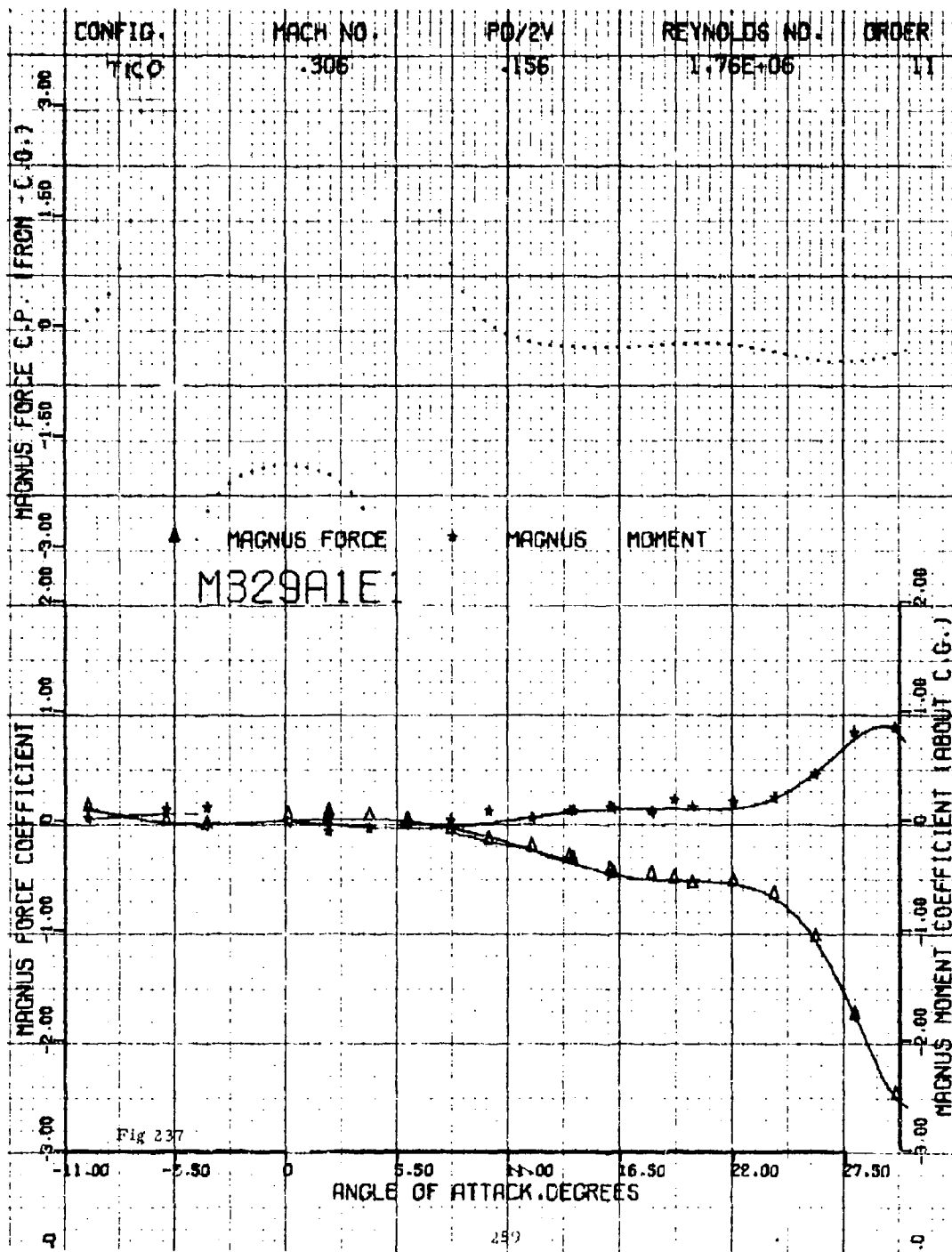


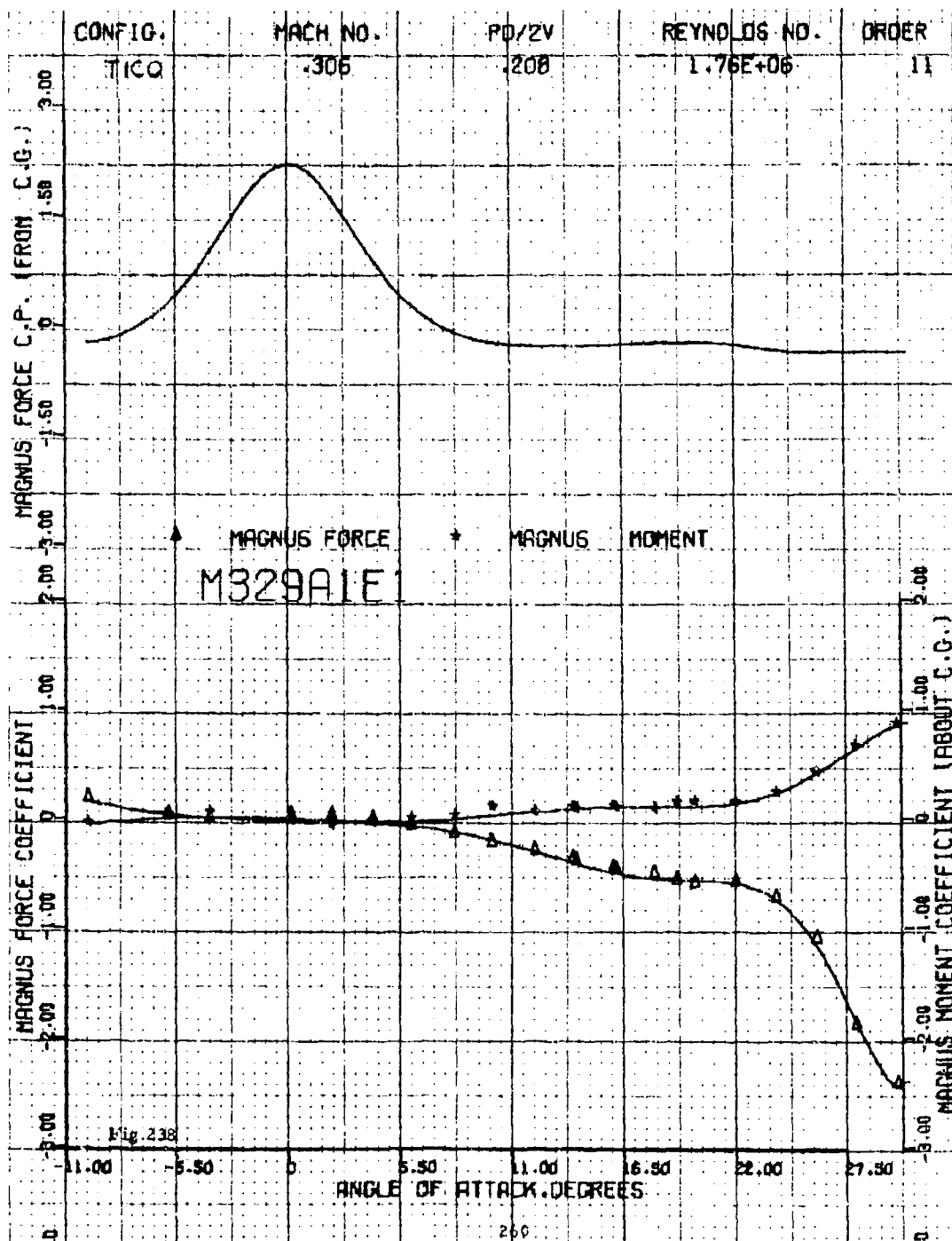


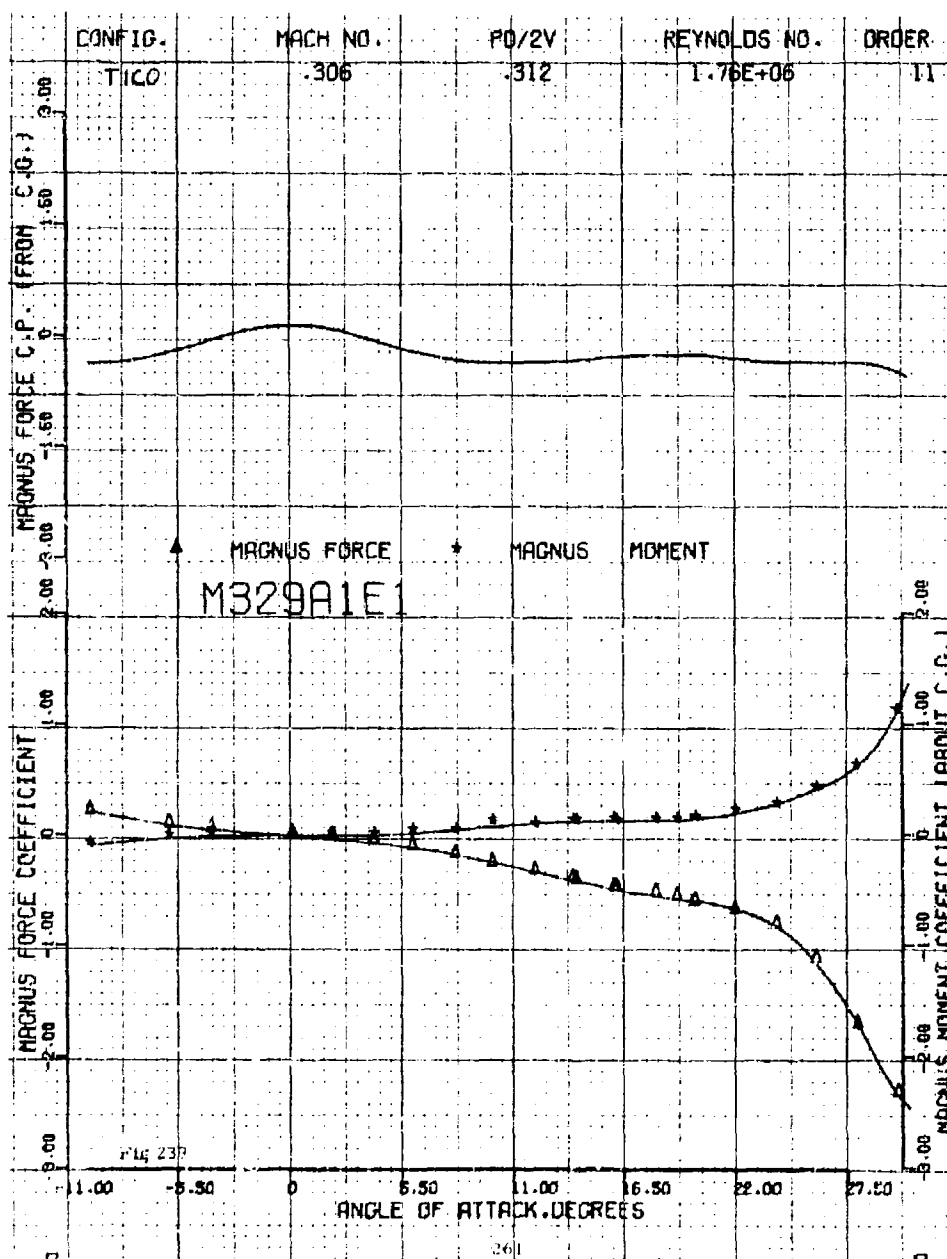


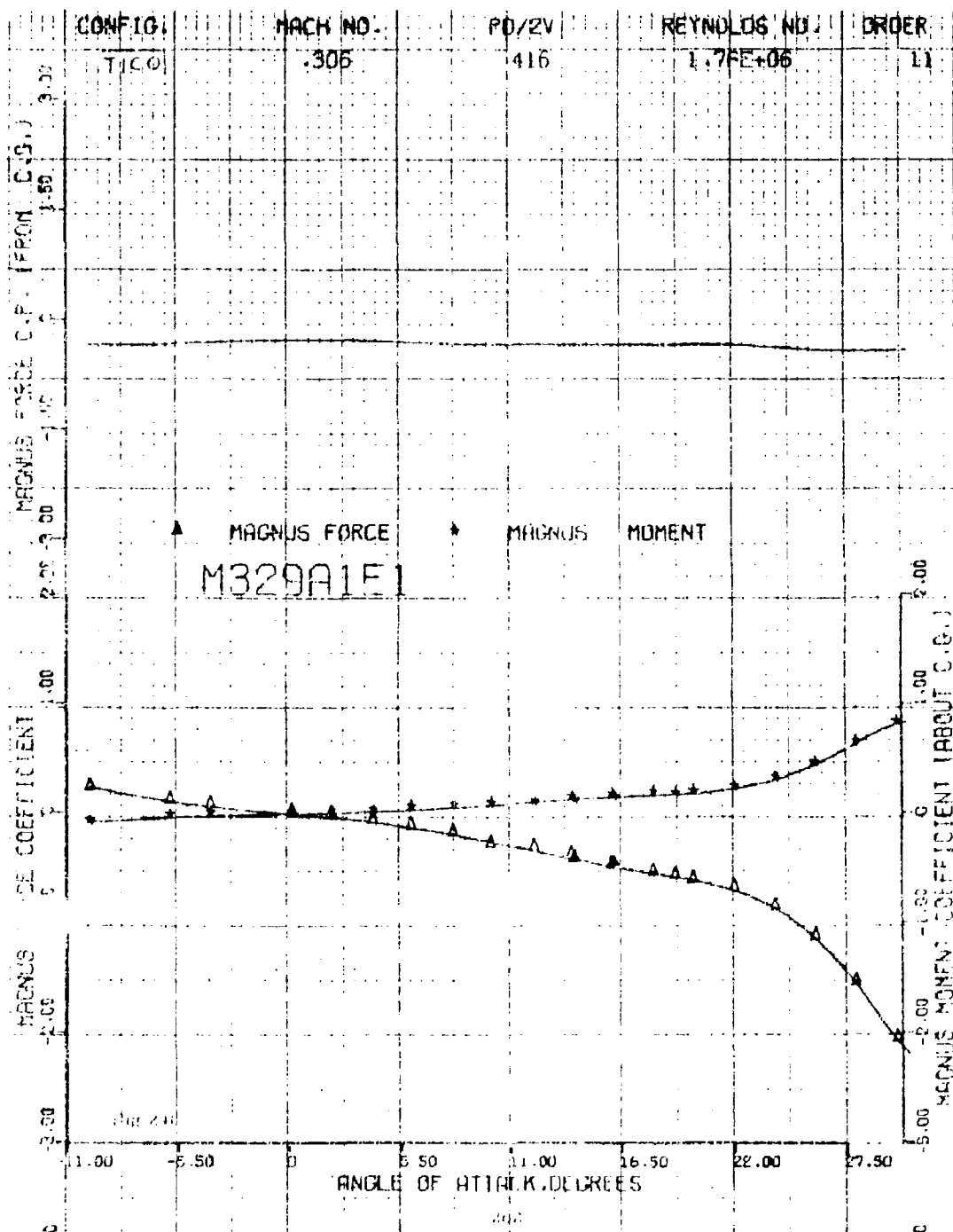


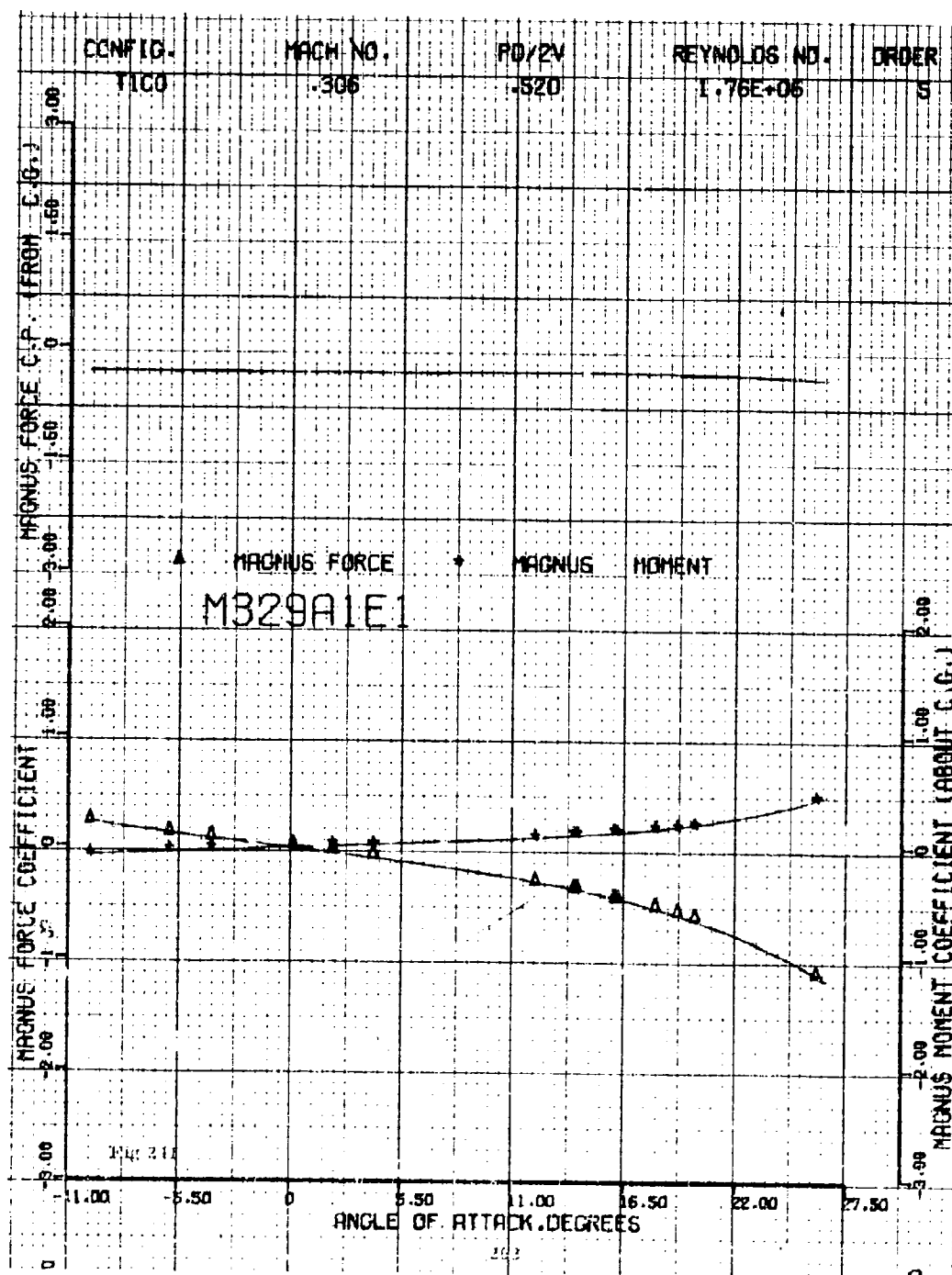


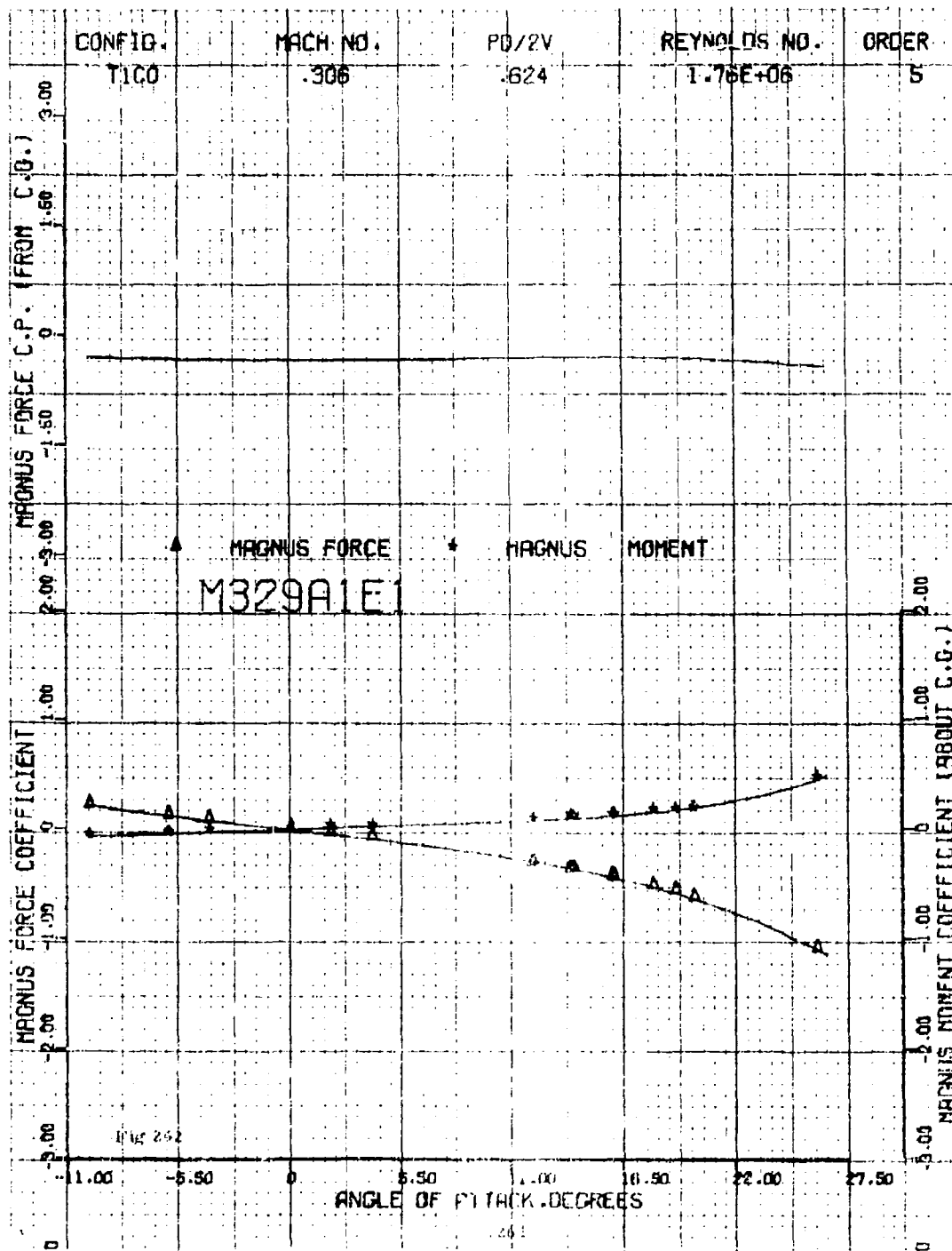


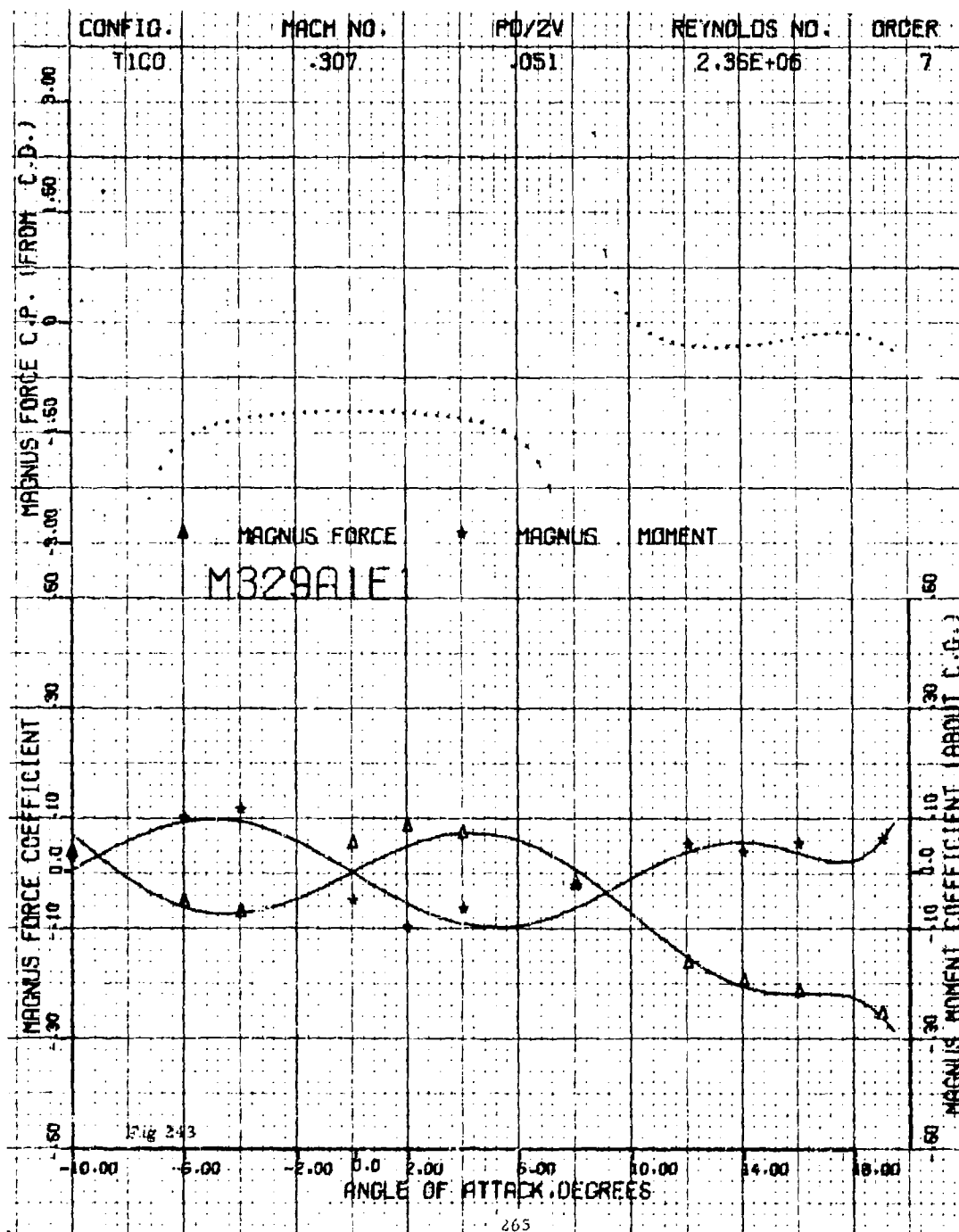


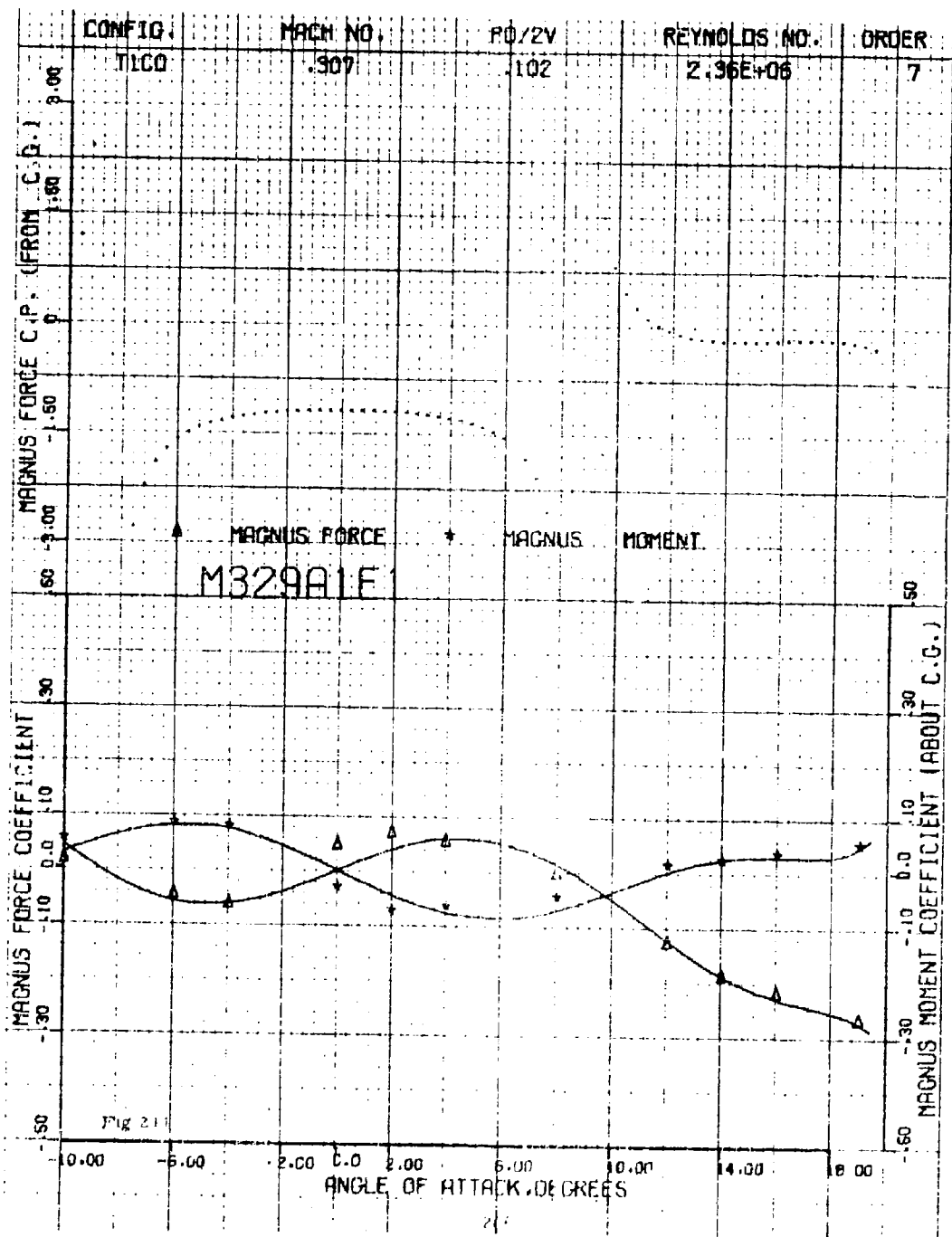


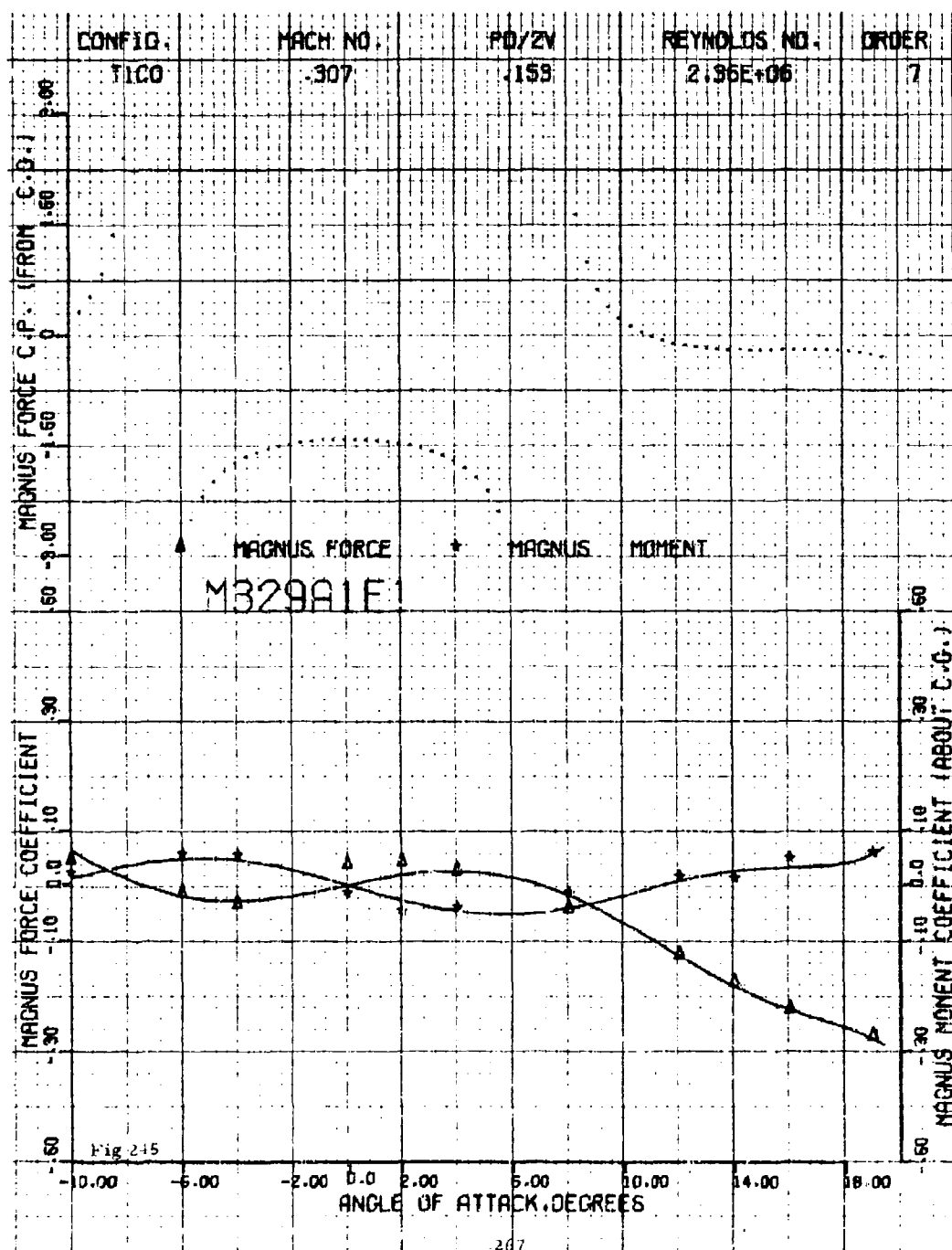


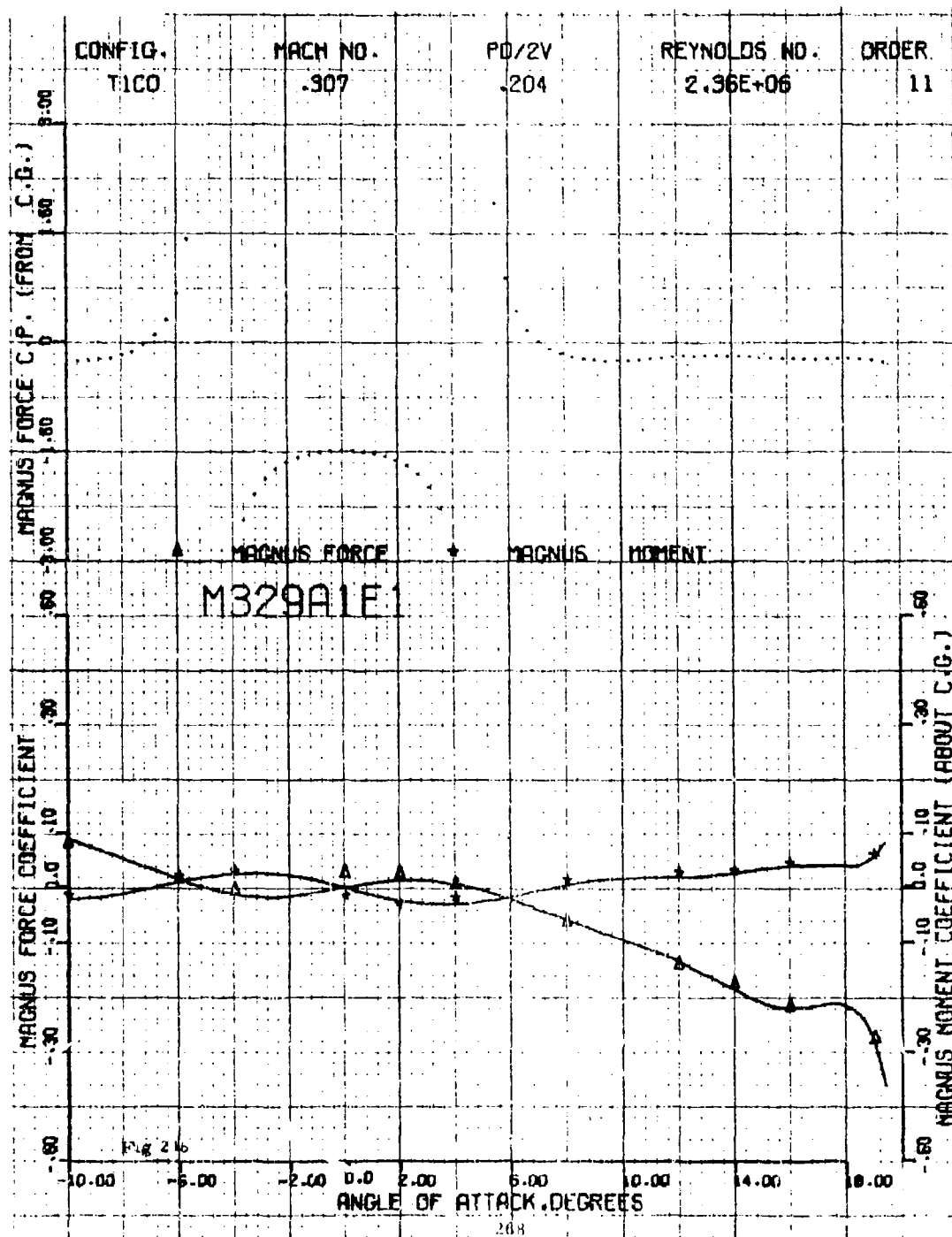


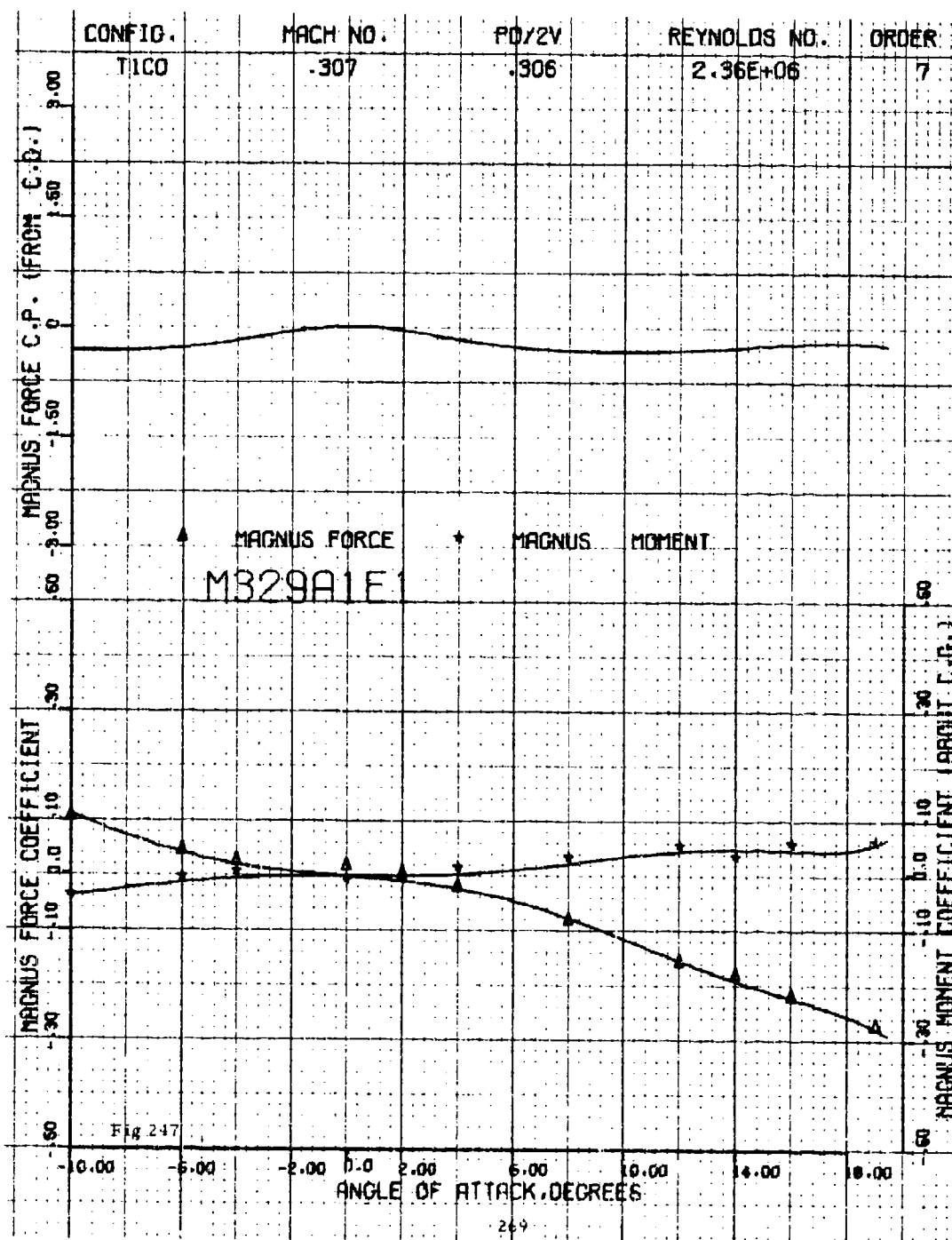


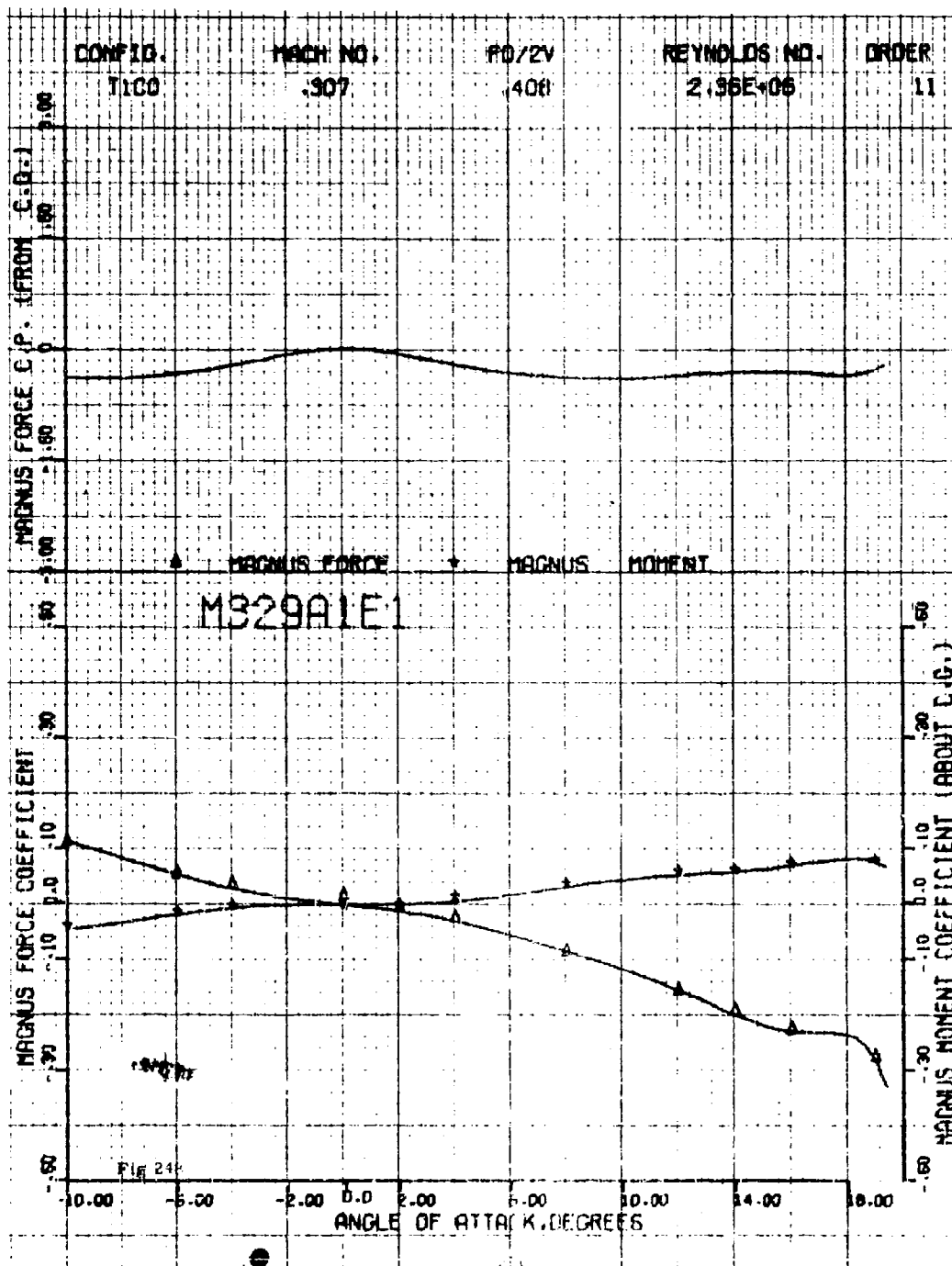












CONFIG. TICO

MACH NO..307

PQ/ZV.510

REYNOLDS NO. 2.96E+06

ORDER 11

MAGNUS FORCE C.P. (FROM C.D.)

MAGNUS FORCE

MAGNUS MOMENT

M328ALE1

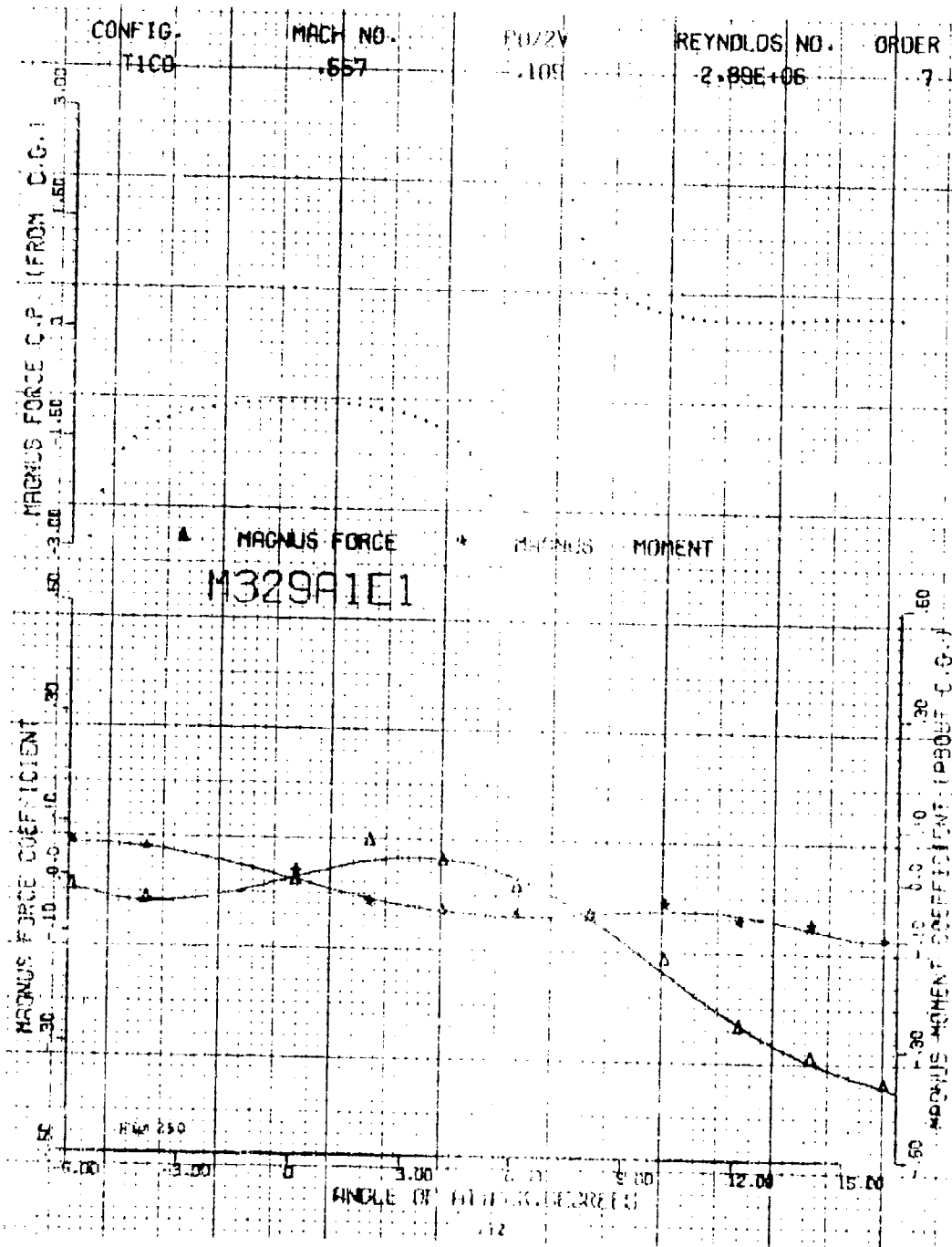
MAGNUS FORCE COEFFICIENT

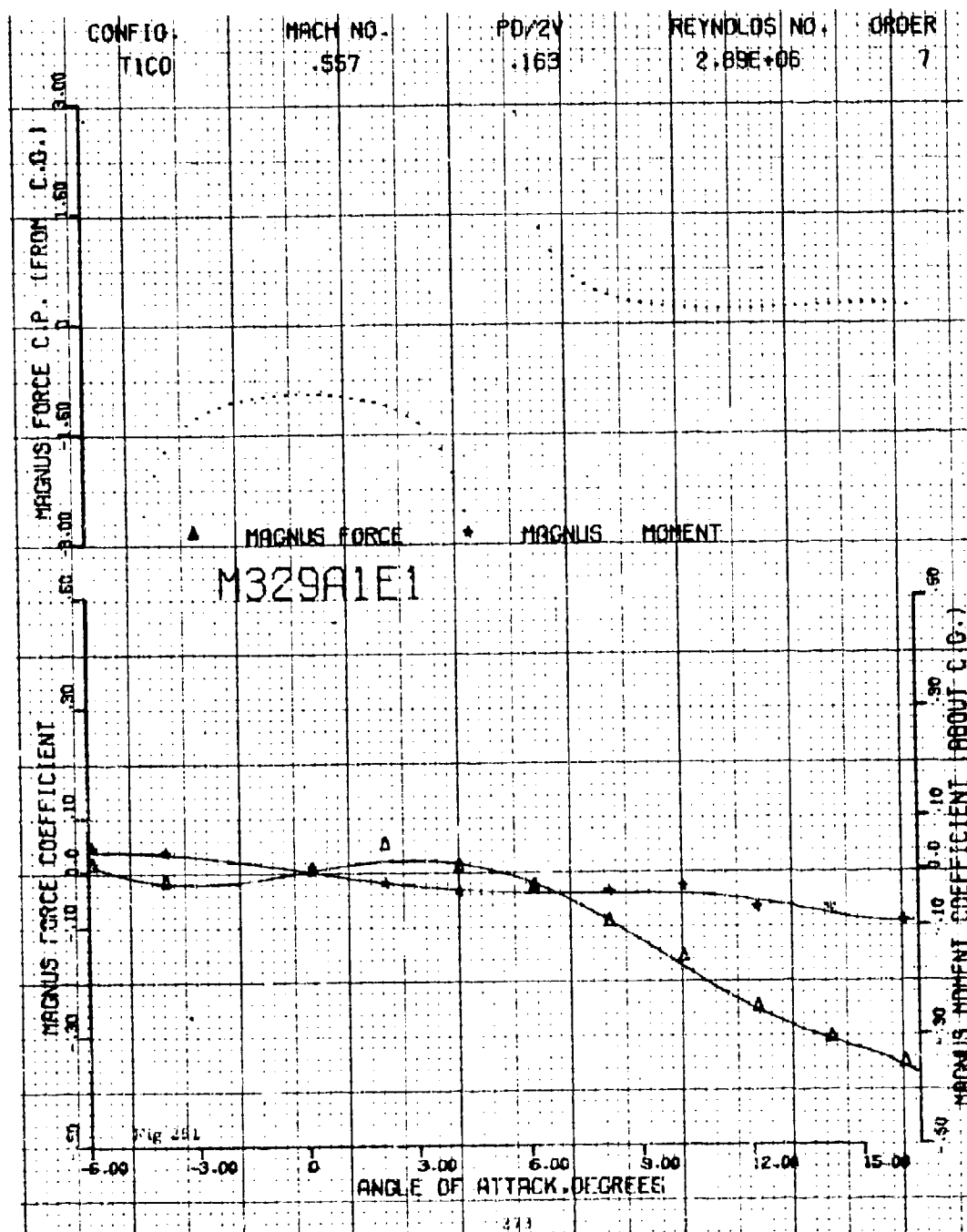
MAGNUS MOMENT COEFFICIENT ABOUT C.G.

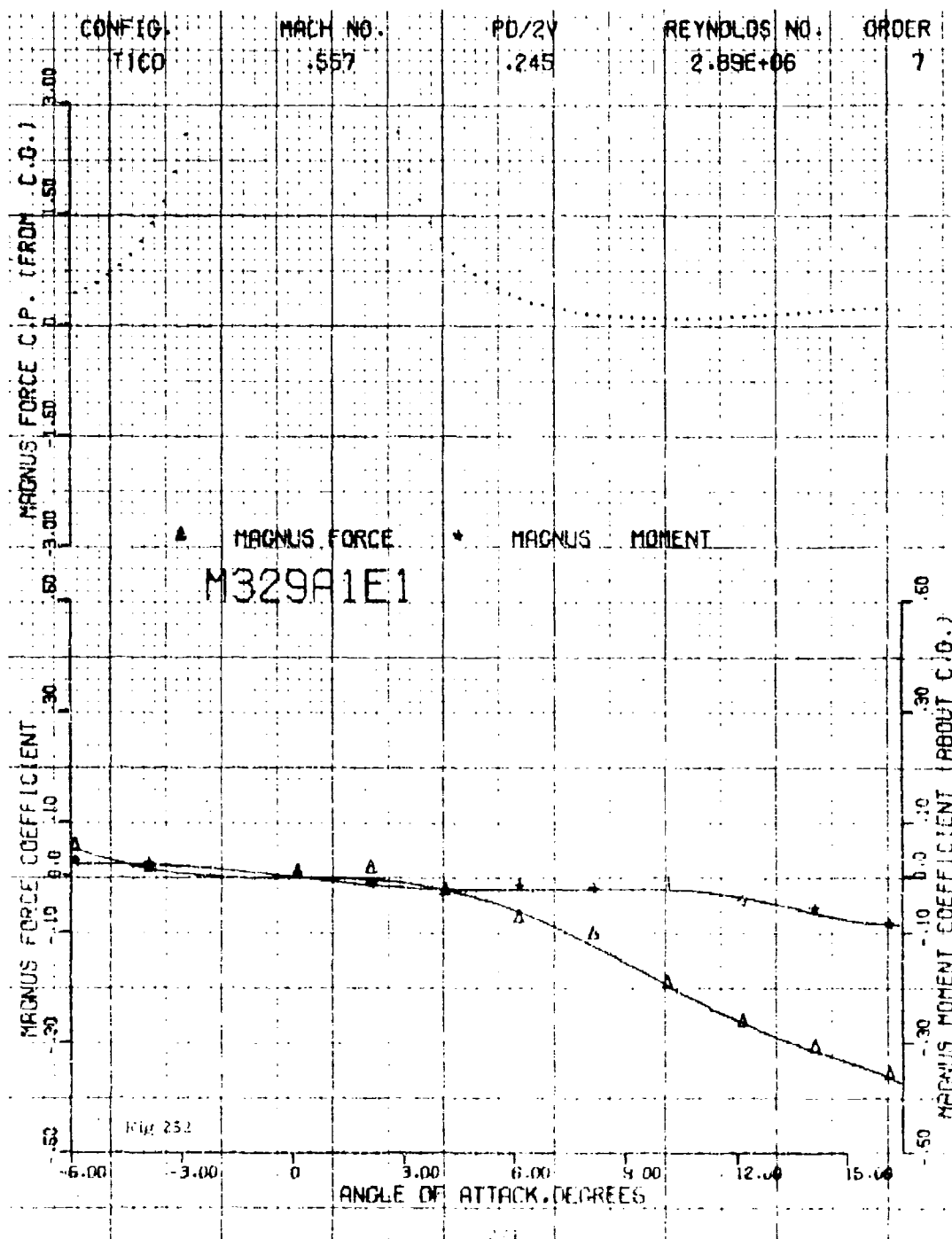
ANGLE OF ATTACK DEGREES

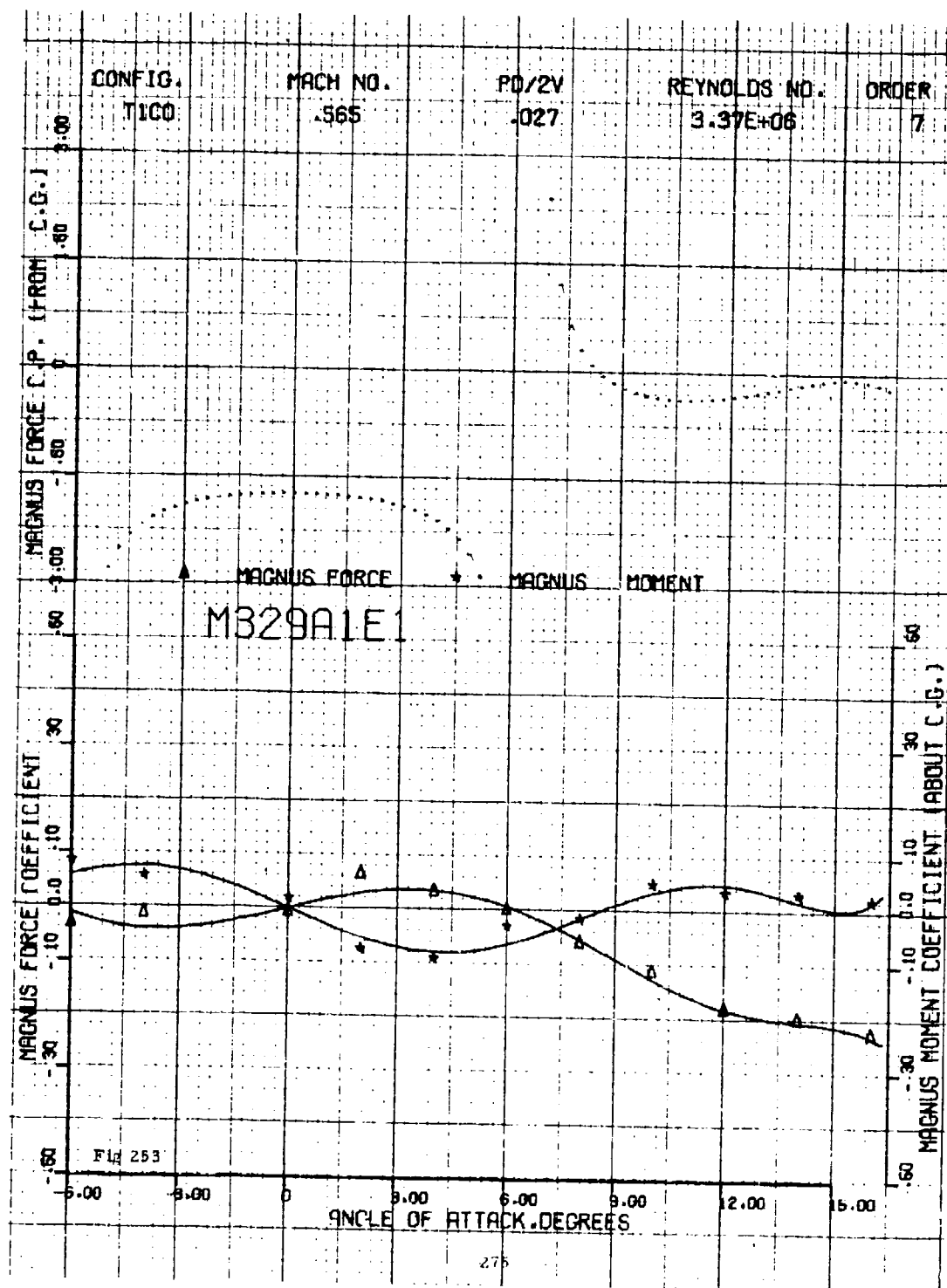
Fig 317

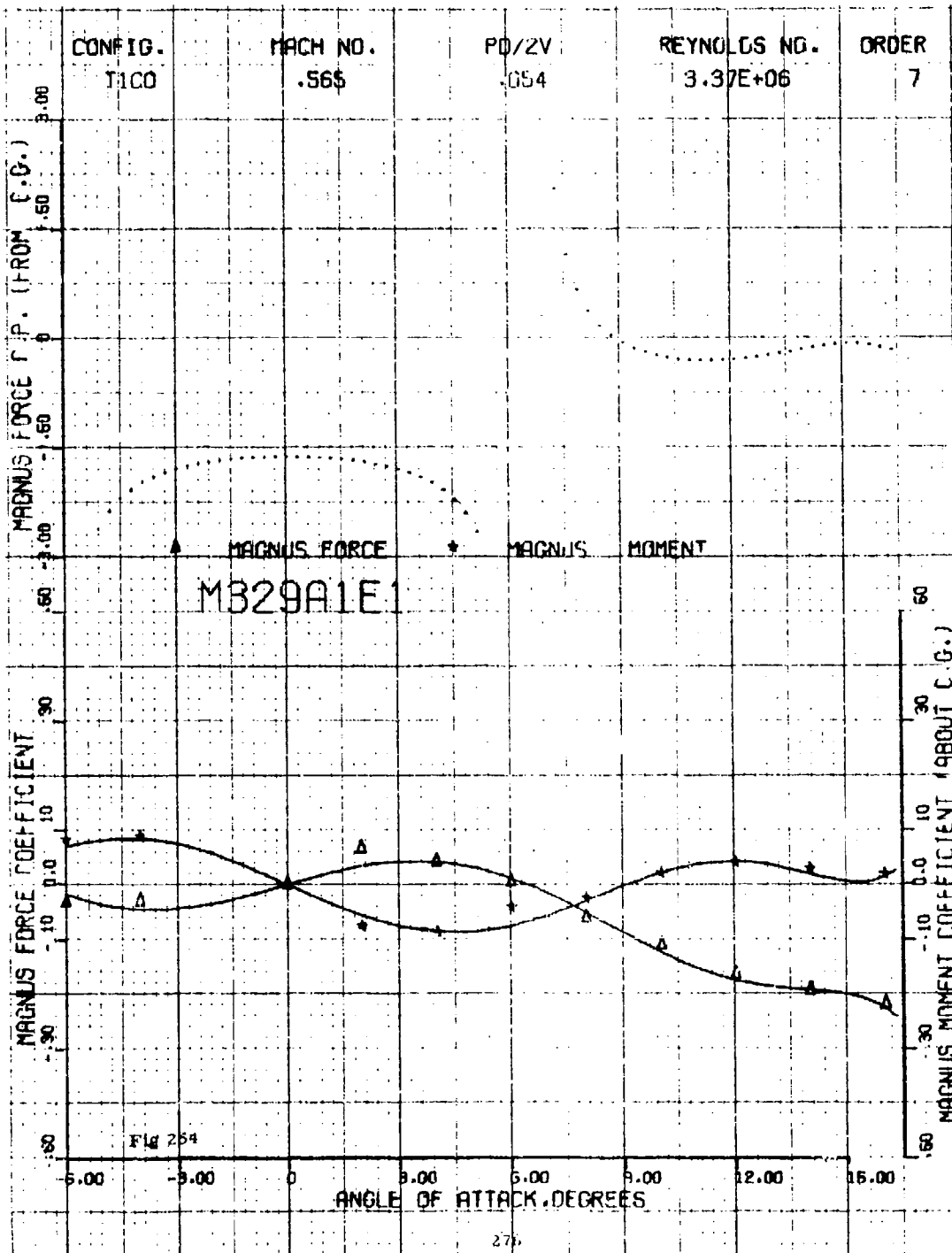
291

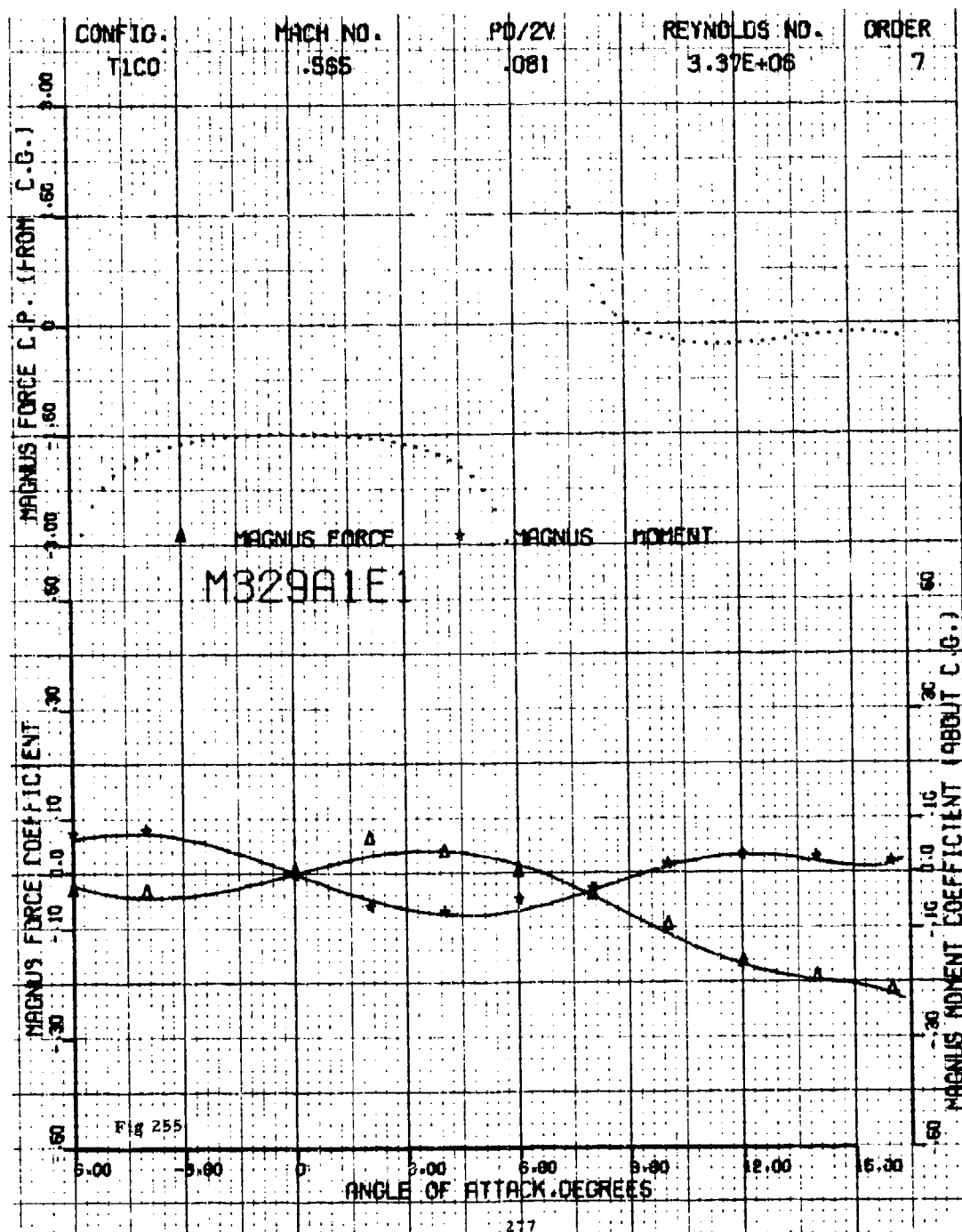


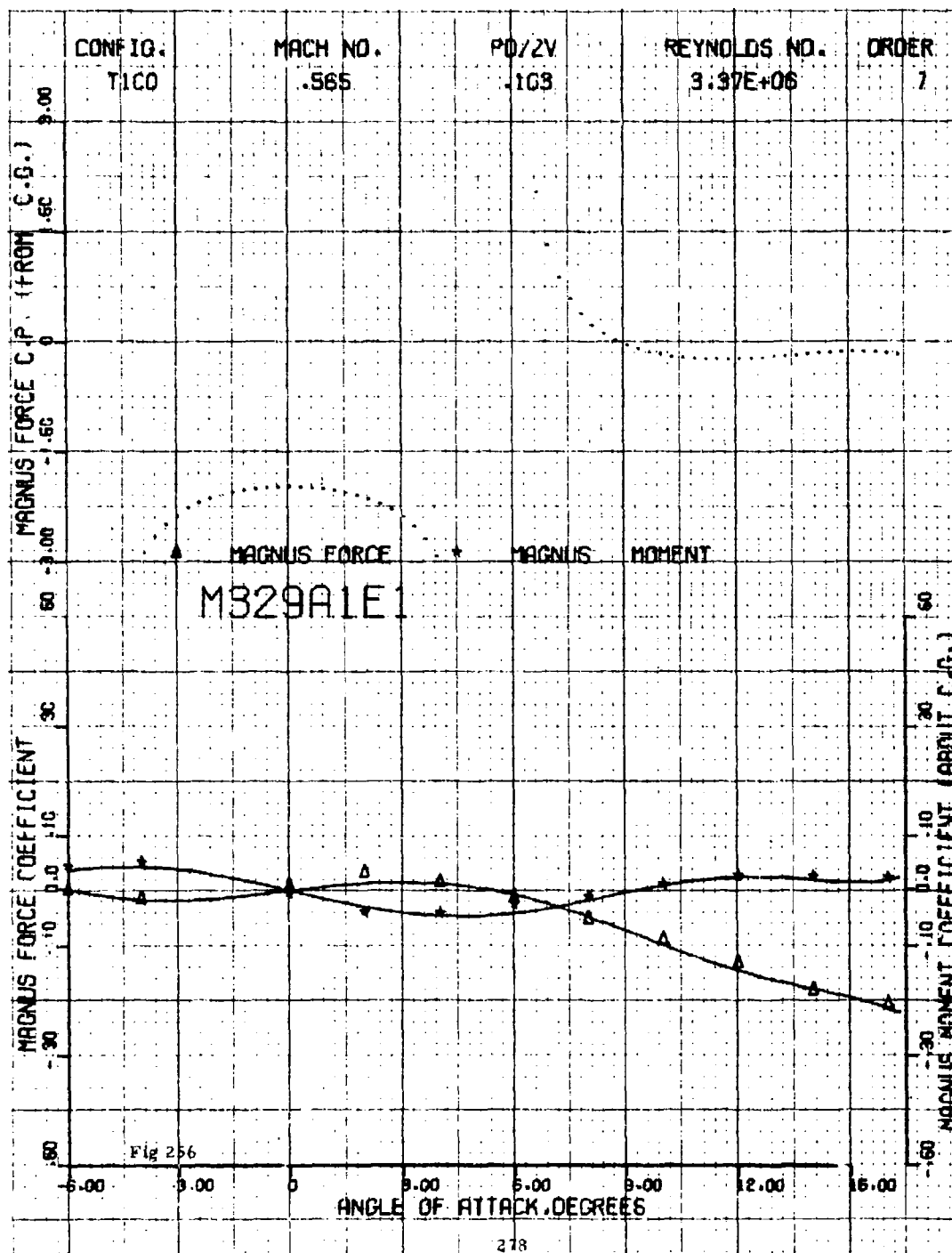












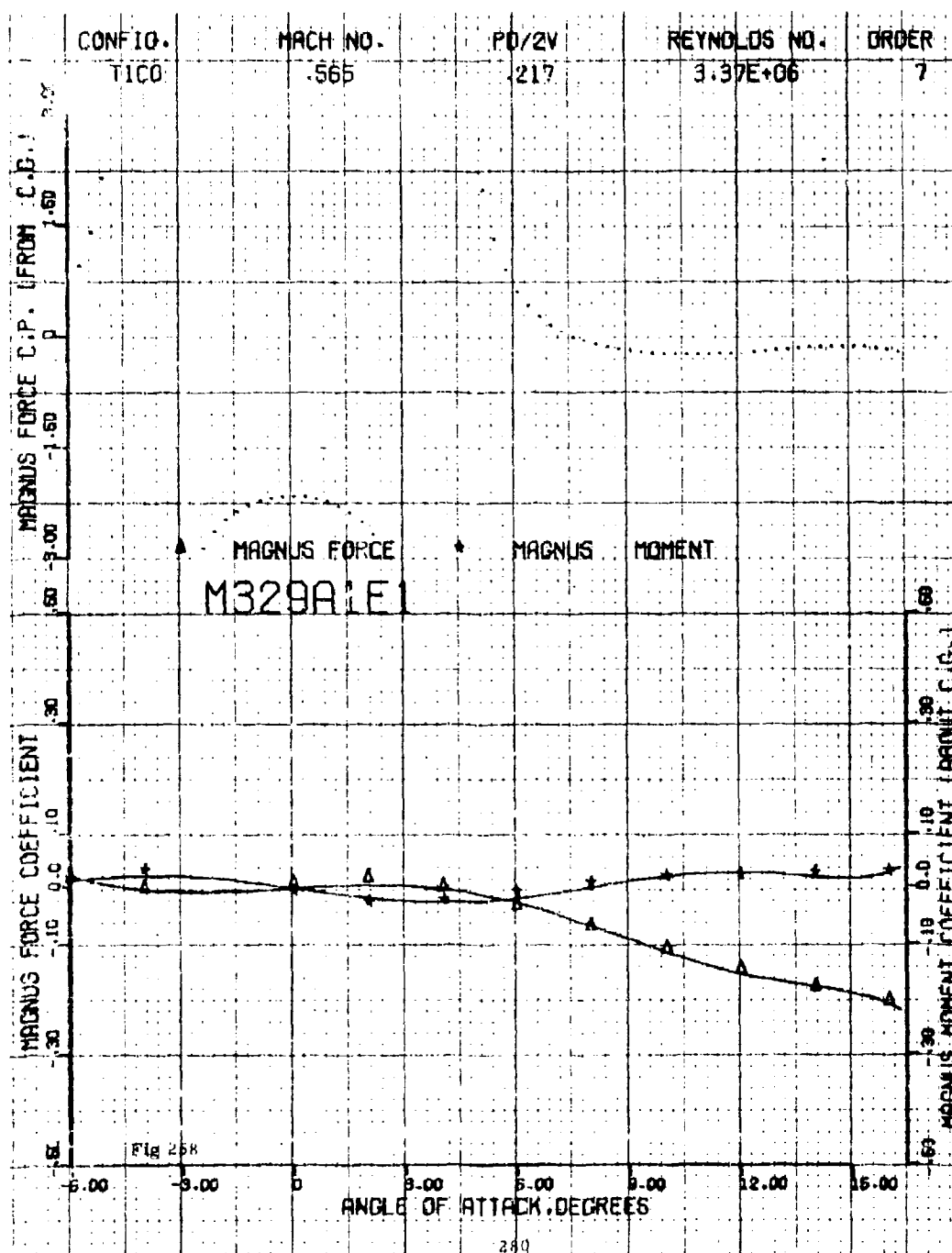
CONFIG.	MACH NO.	RD/ZV	REYNOLDS NO.	ORDER
T100	.565	.108	3.37E+06	7

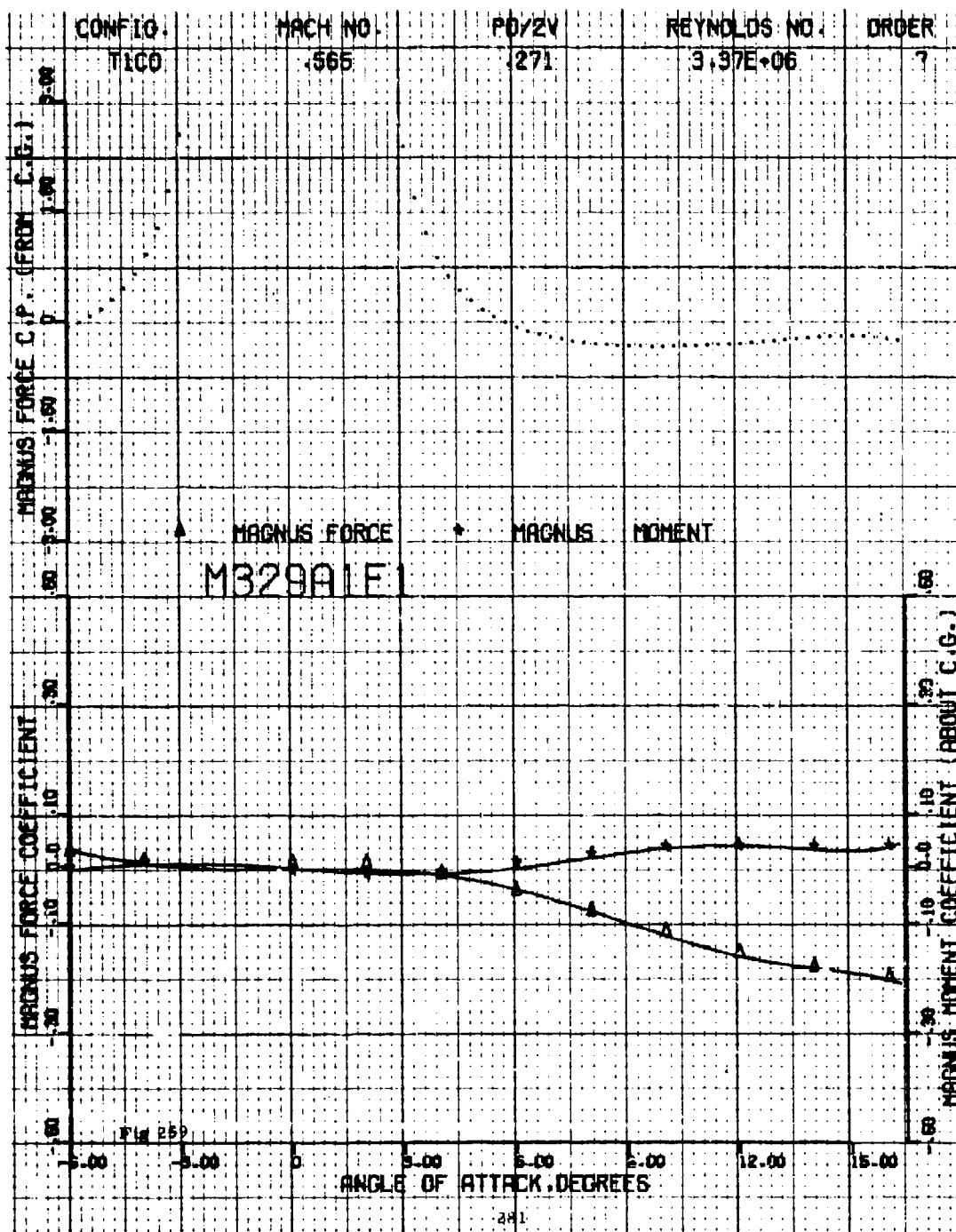
MB29A1E1

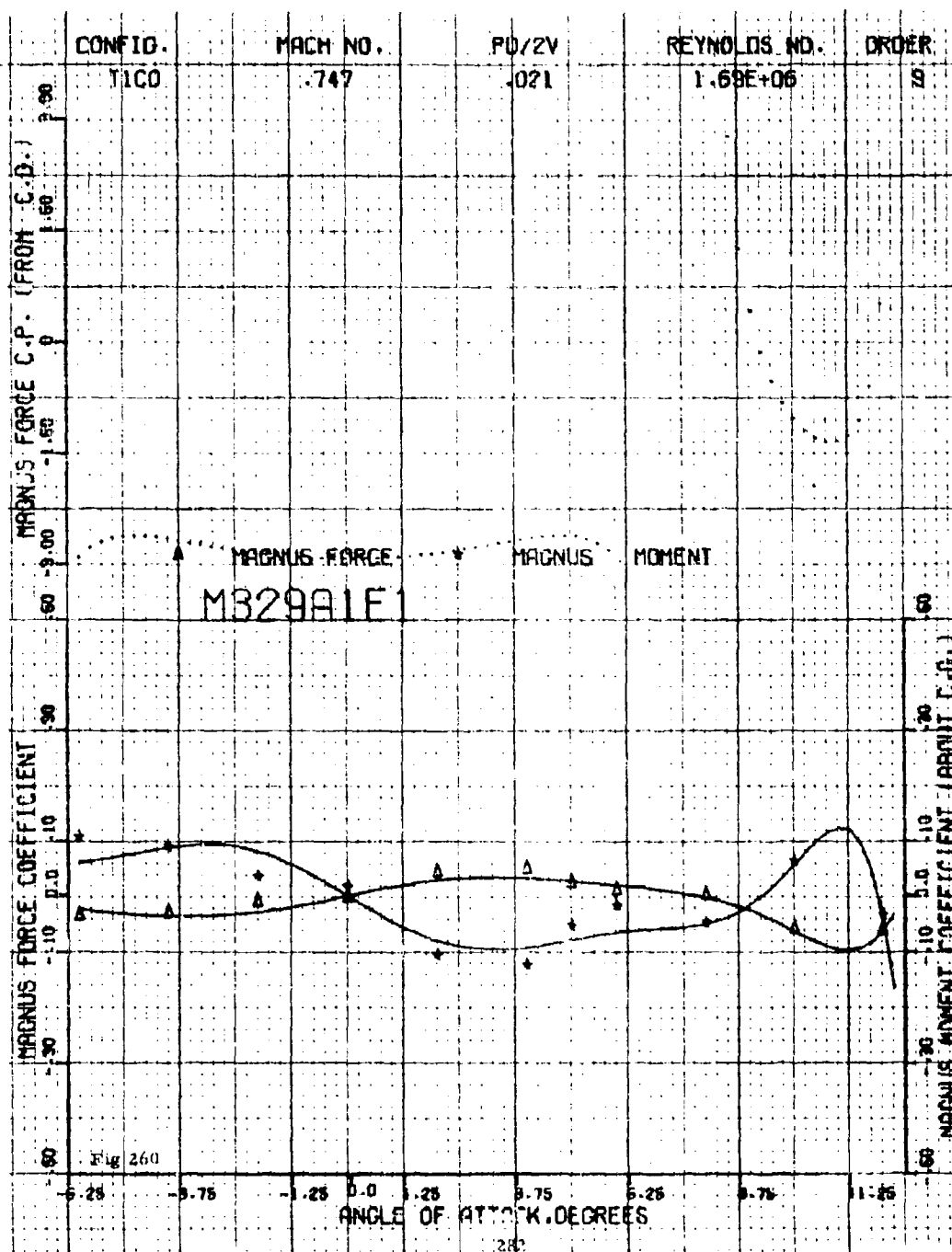
Angle of Attack (Degrees)	Magnus Force Coefficient (C _l)	Magnus Moment Coefficient (C _m)
0.00	0.05	0.05
0.50	0.10	0.10
1.00	0.10	0.10
1.50	0.05	0.05
2.00	0.00	0.00
2.50	-0.05	-0.05
3.00	-0.10	-0.10

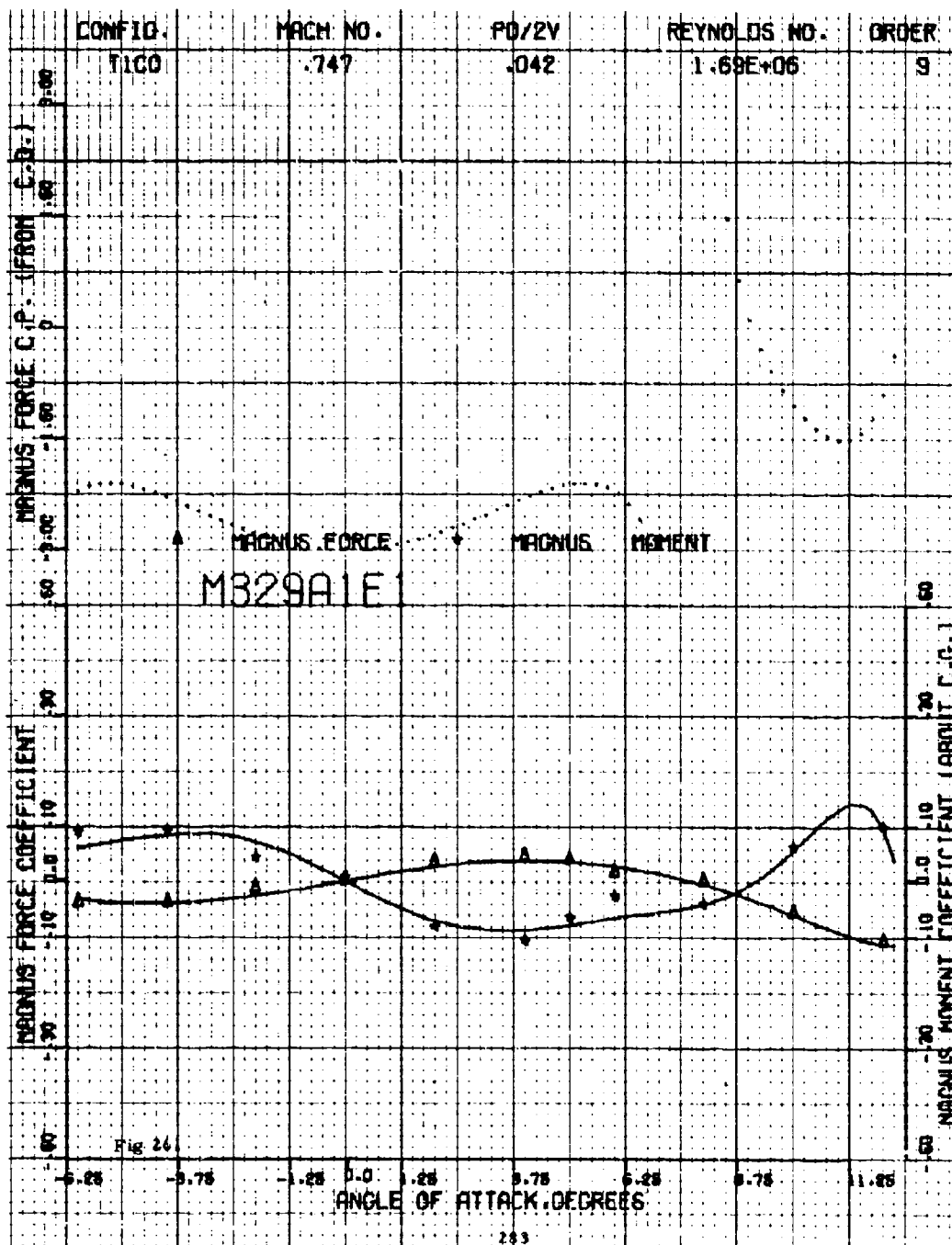
Fig 257

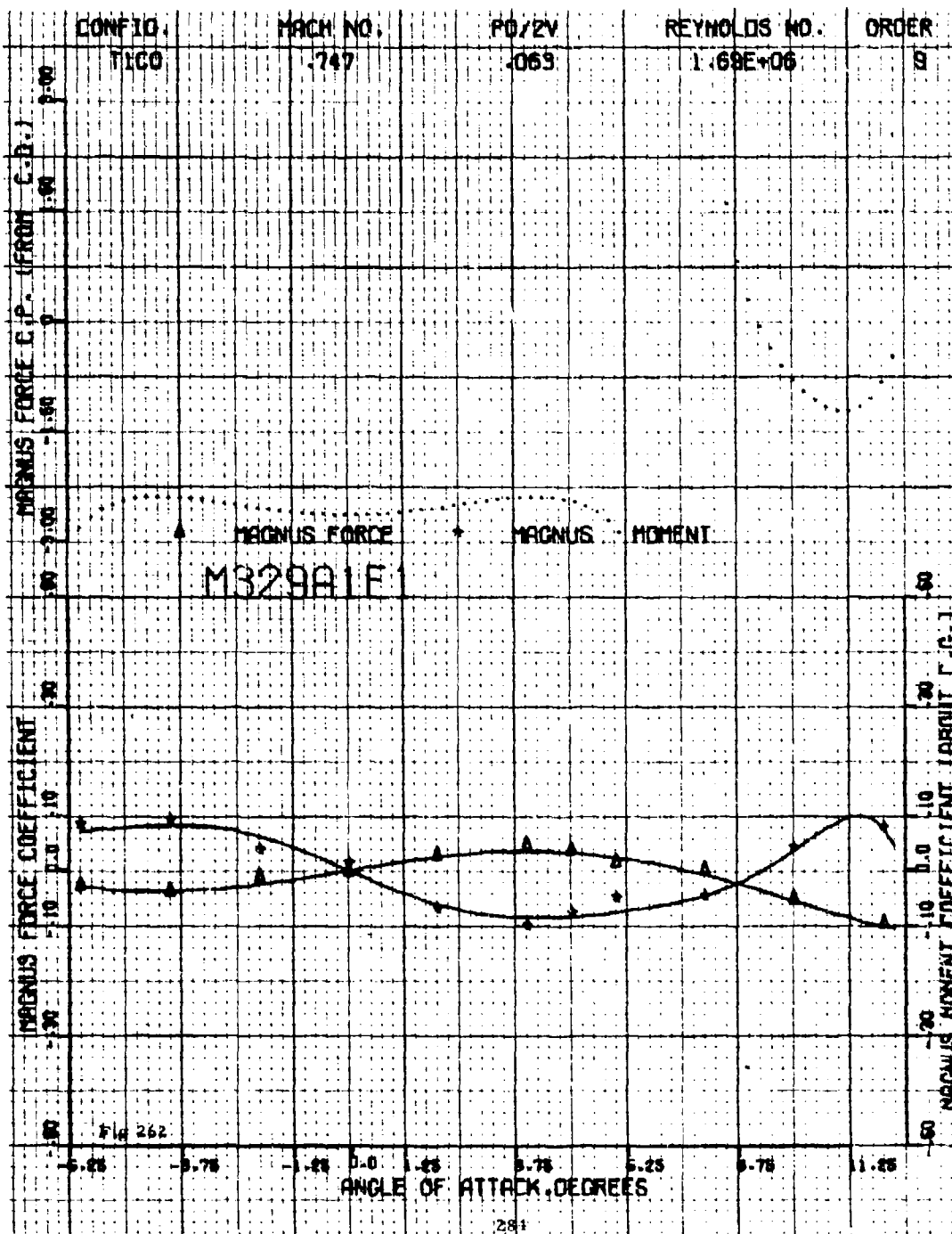
279

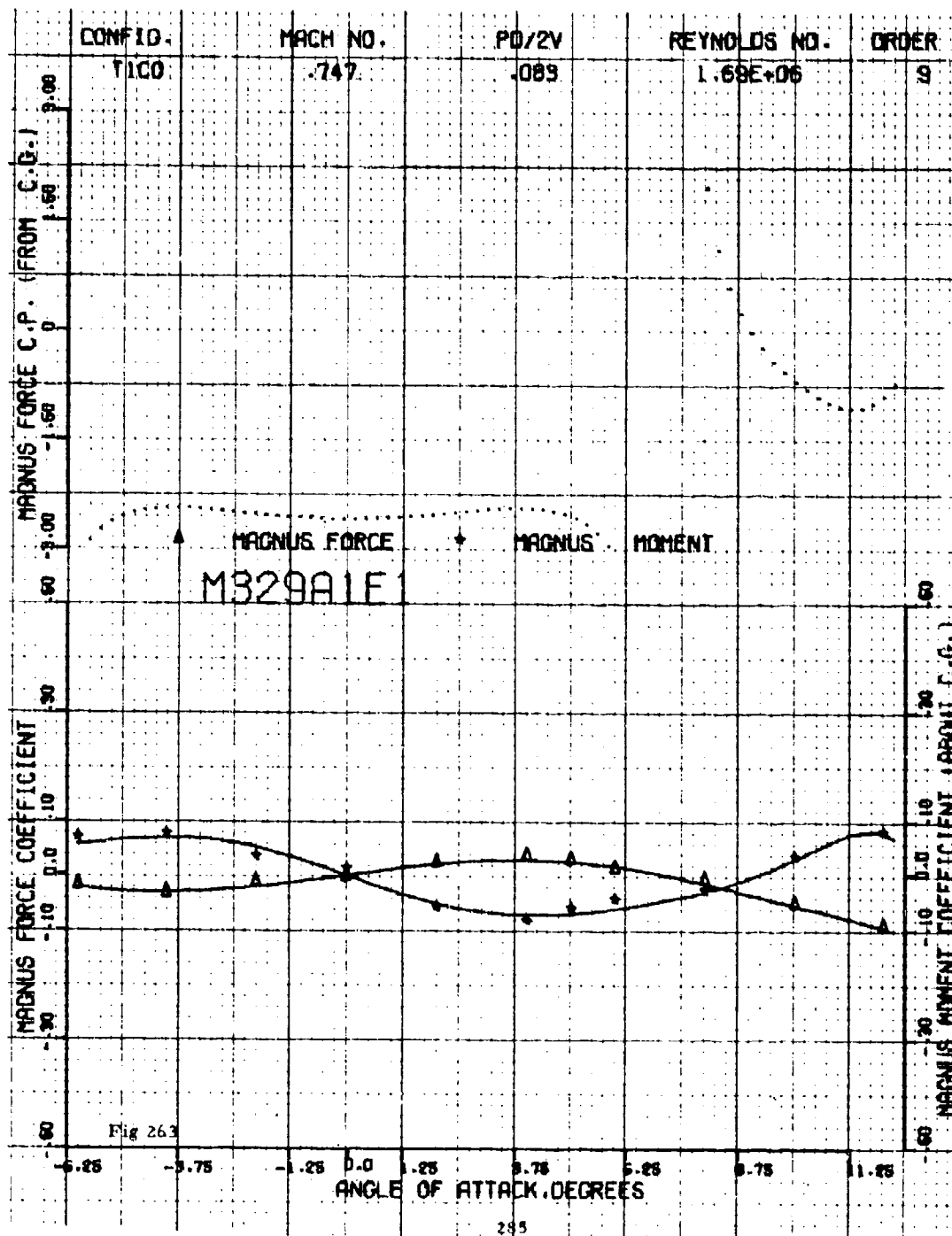


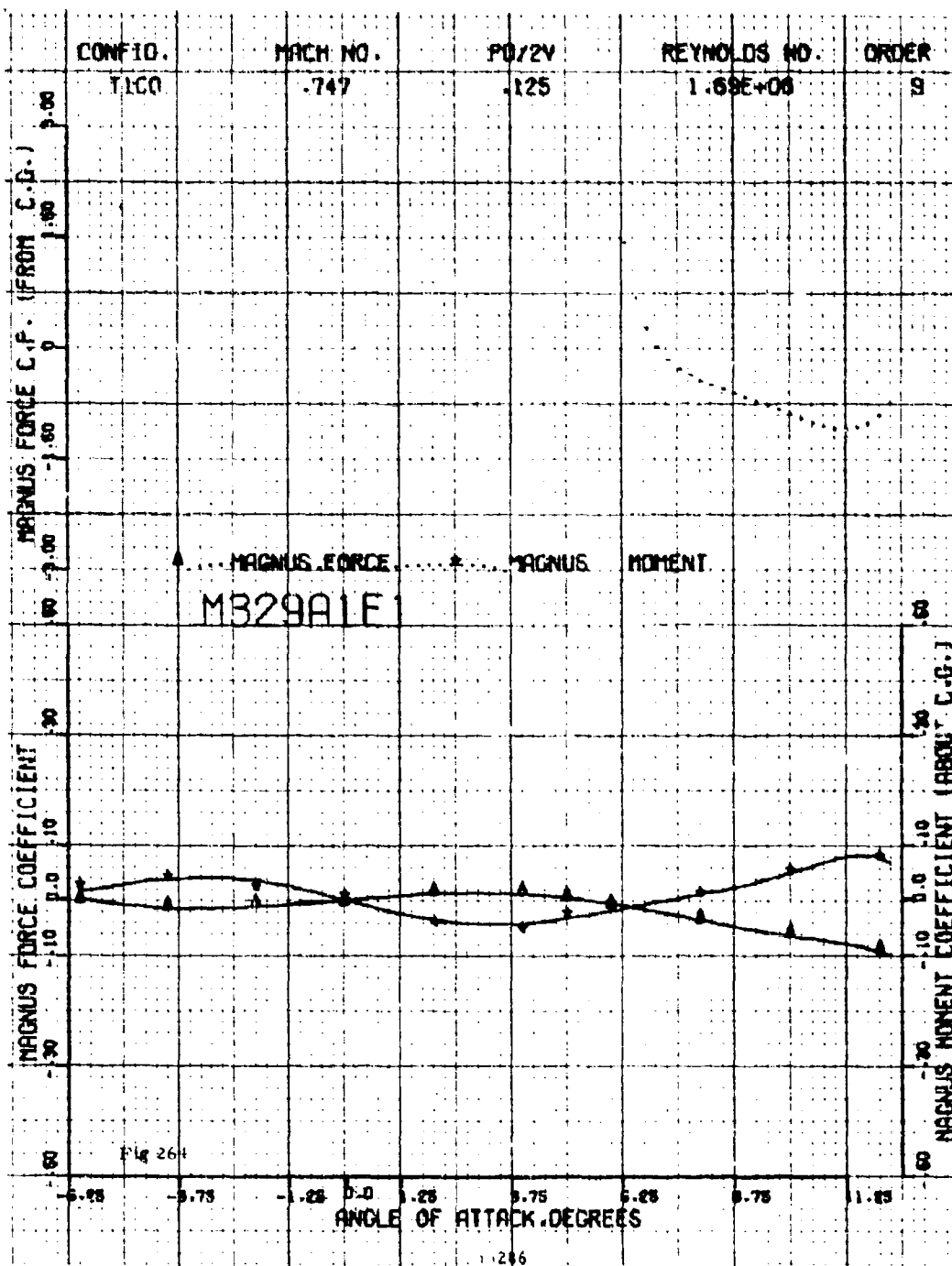


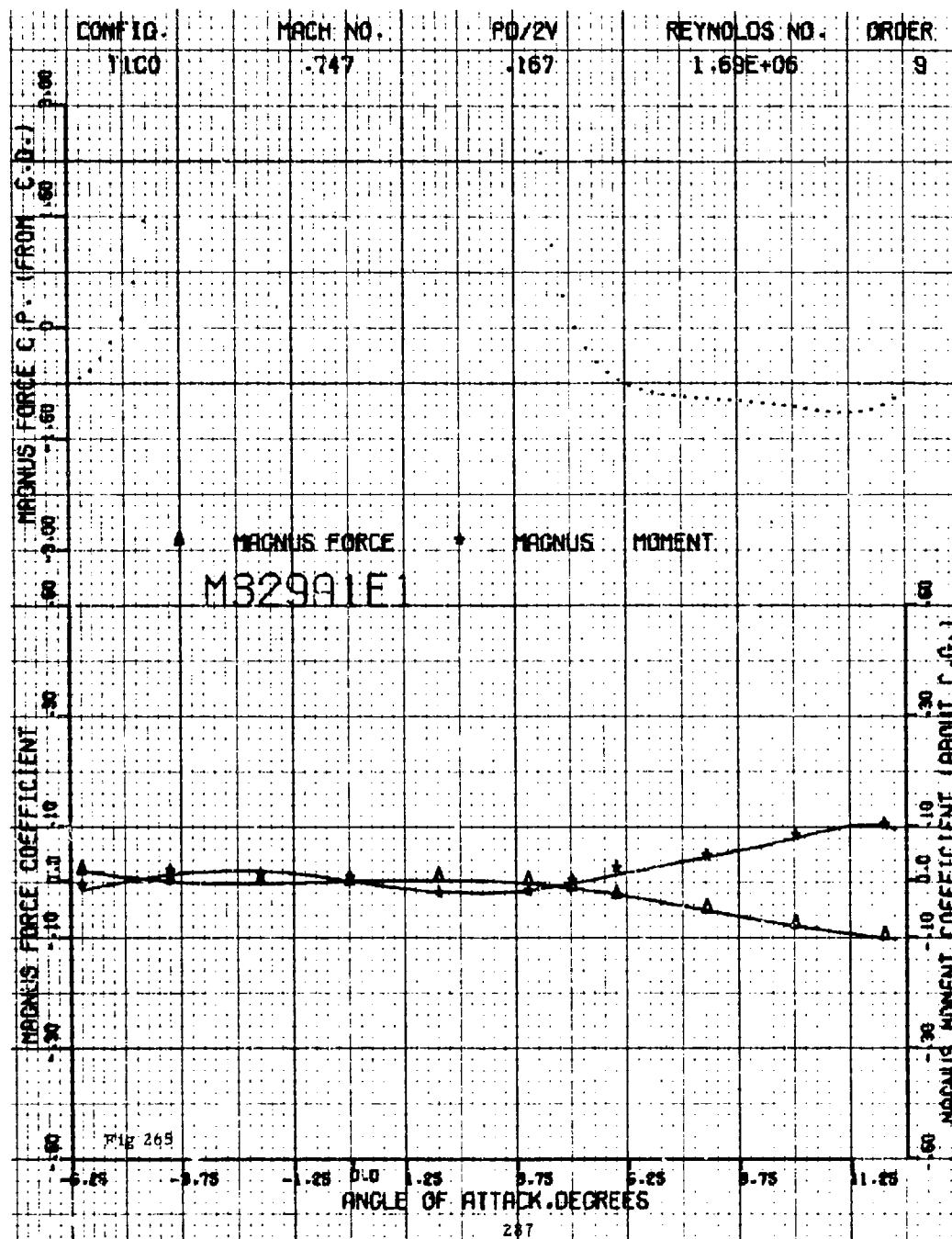


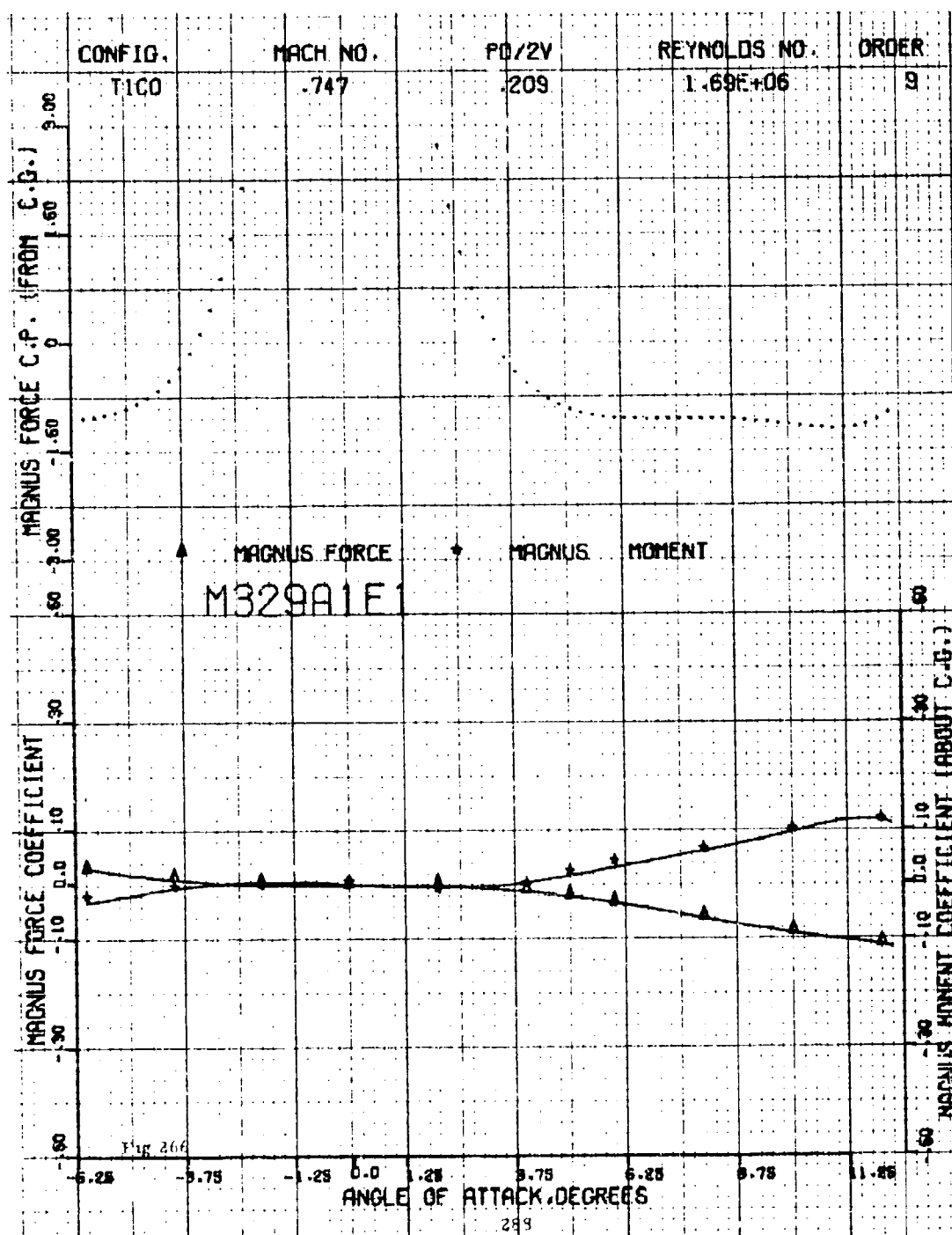


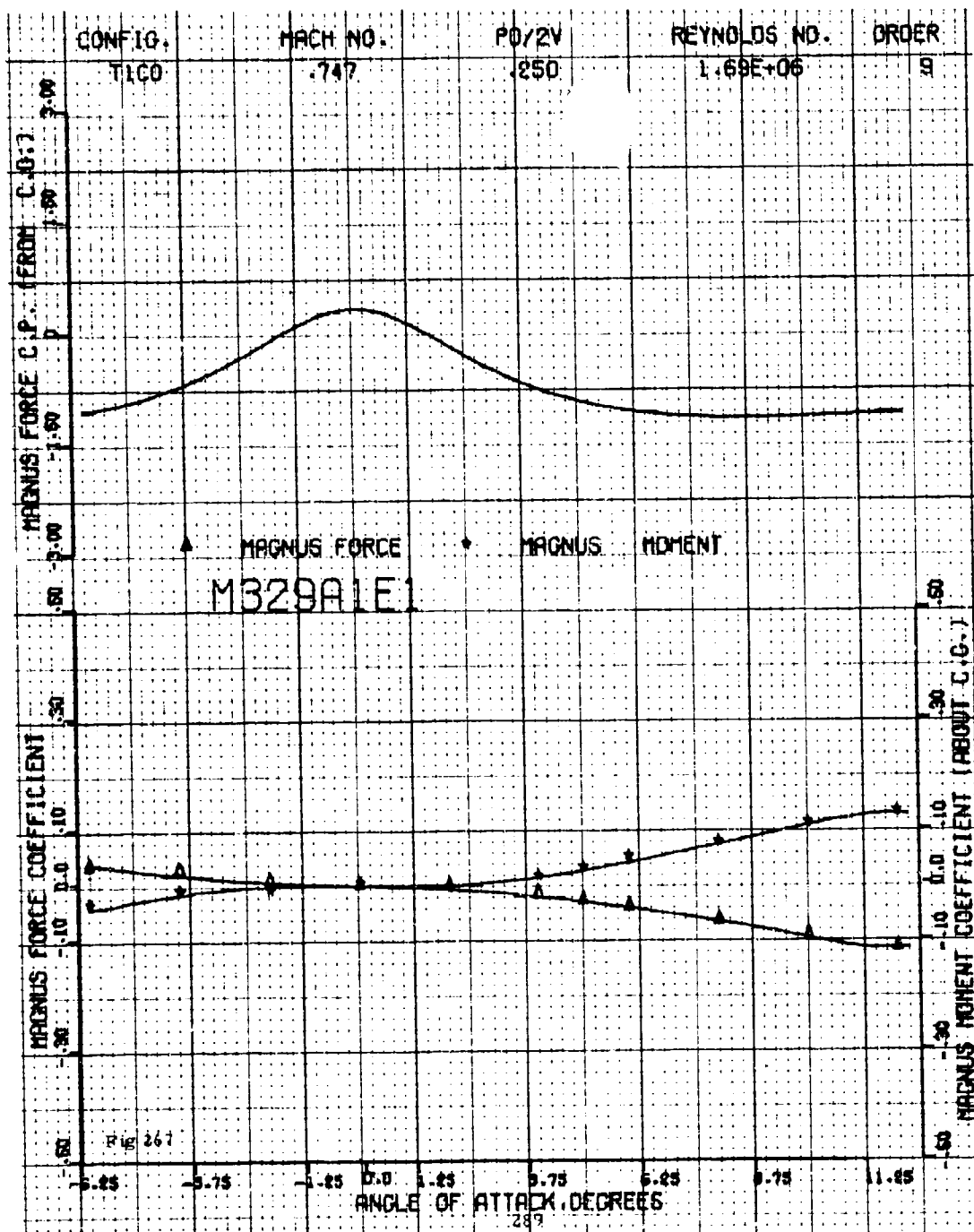


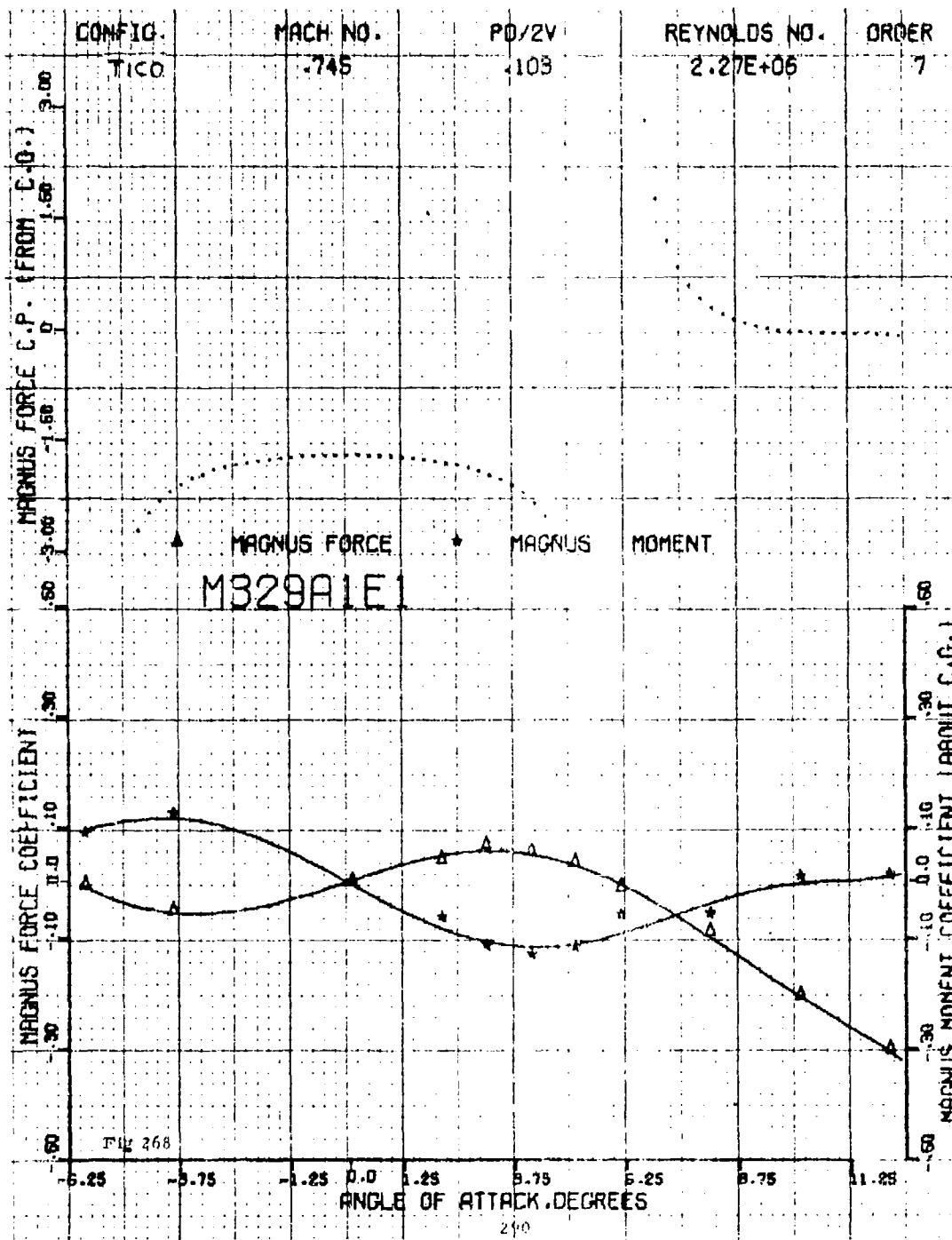


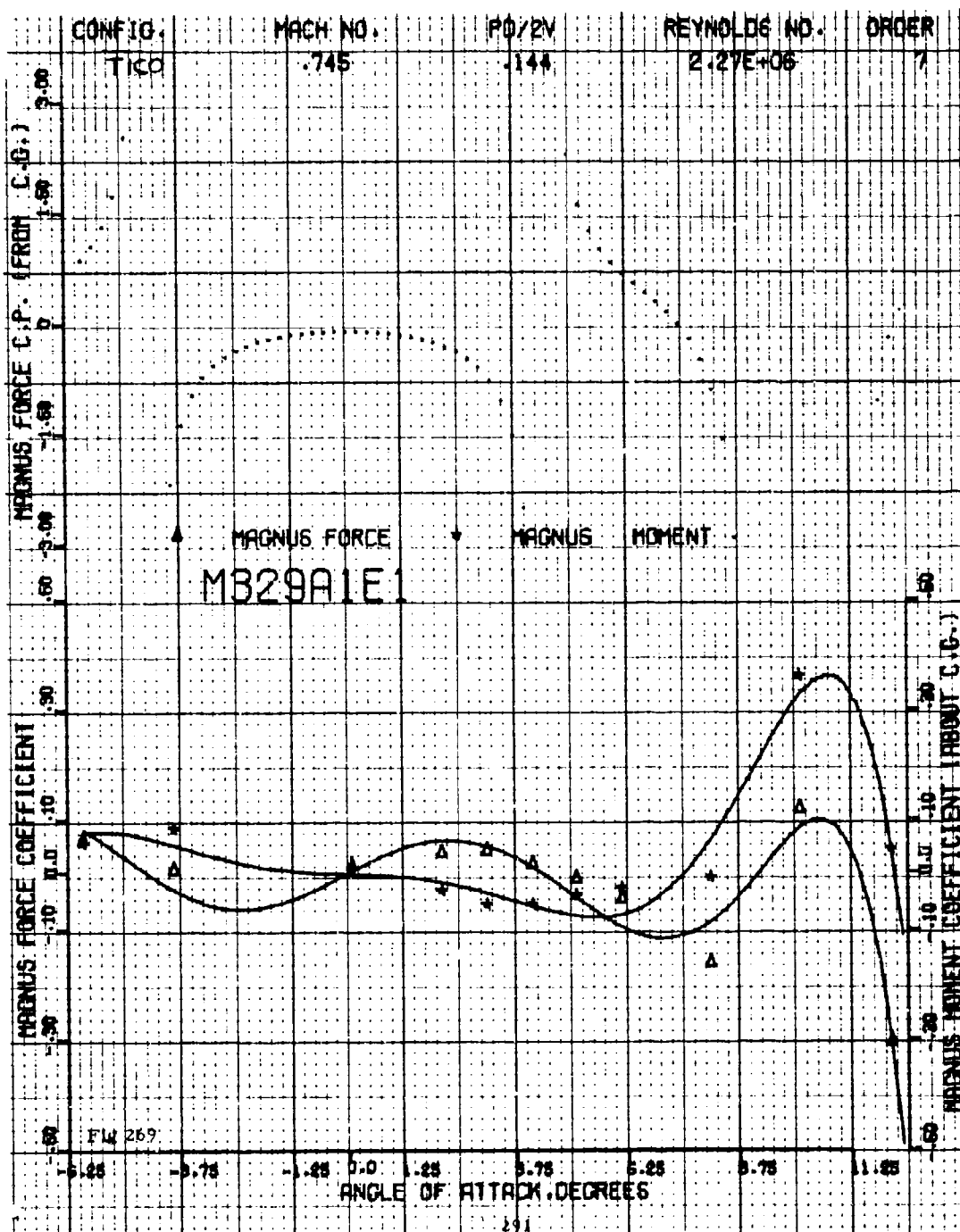


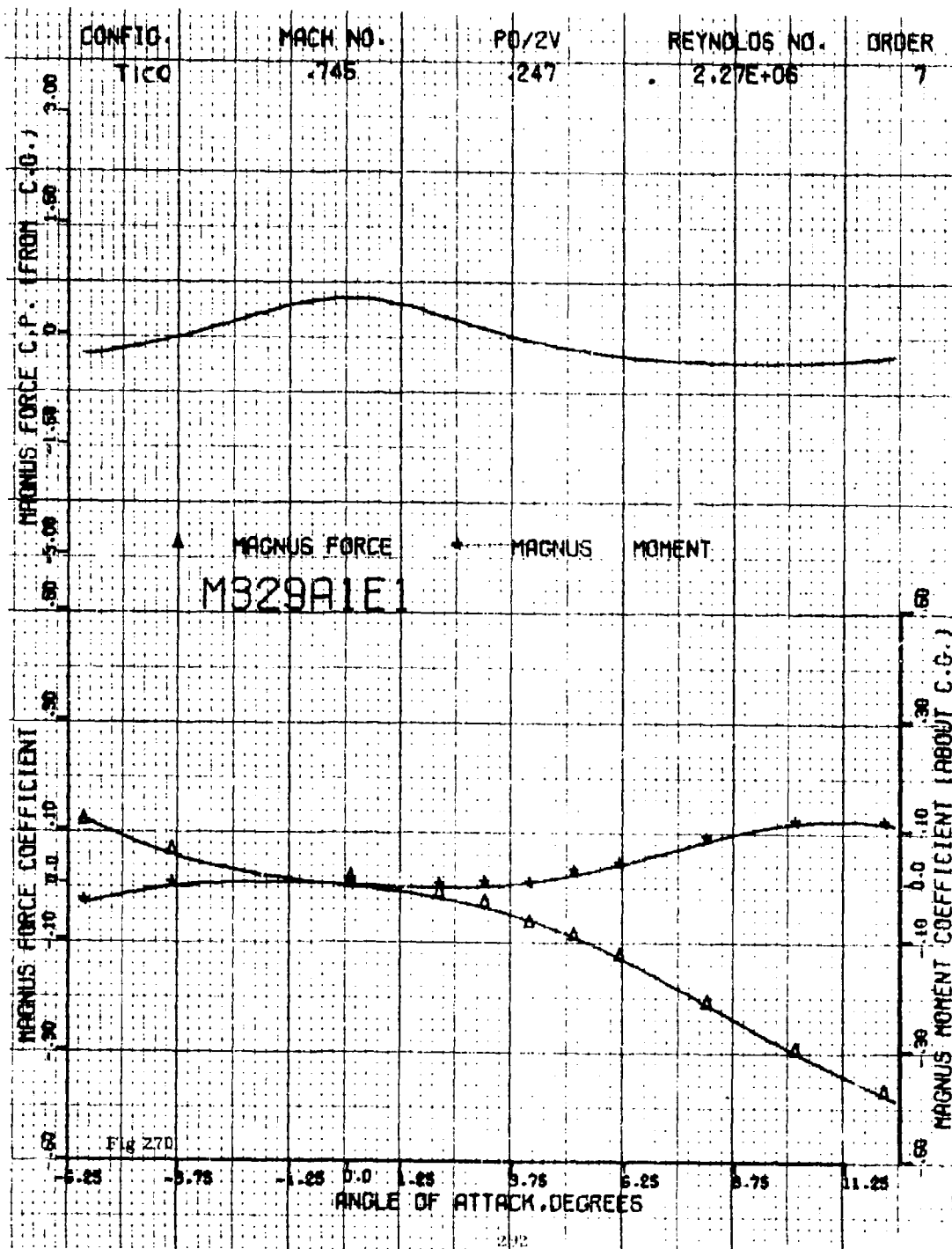


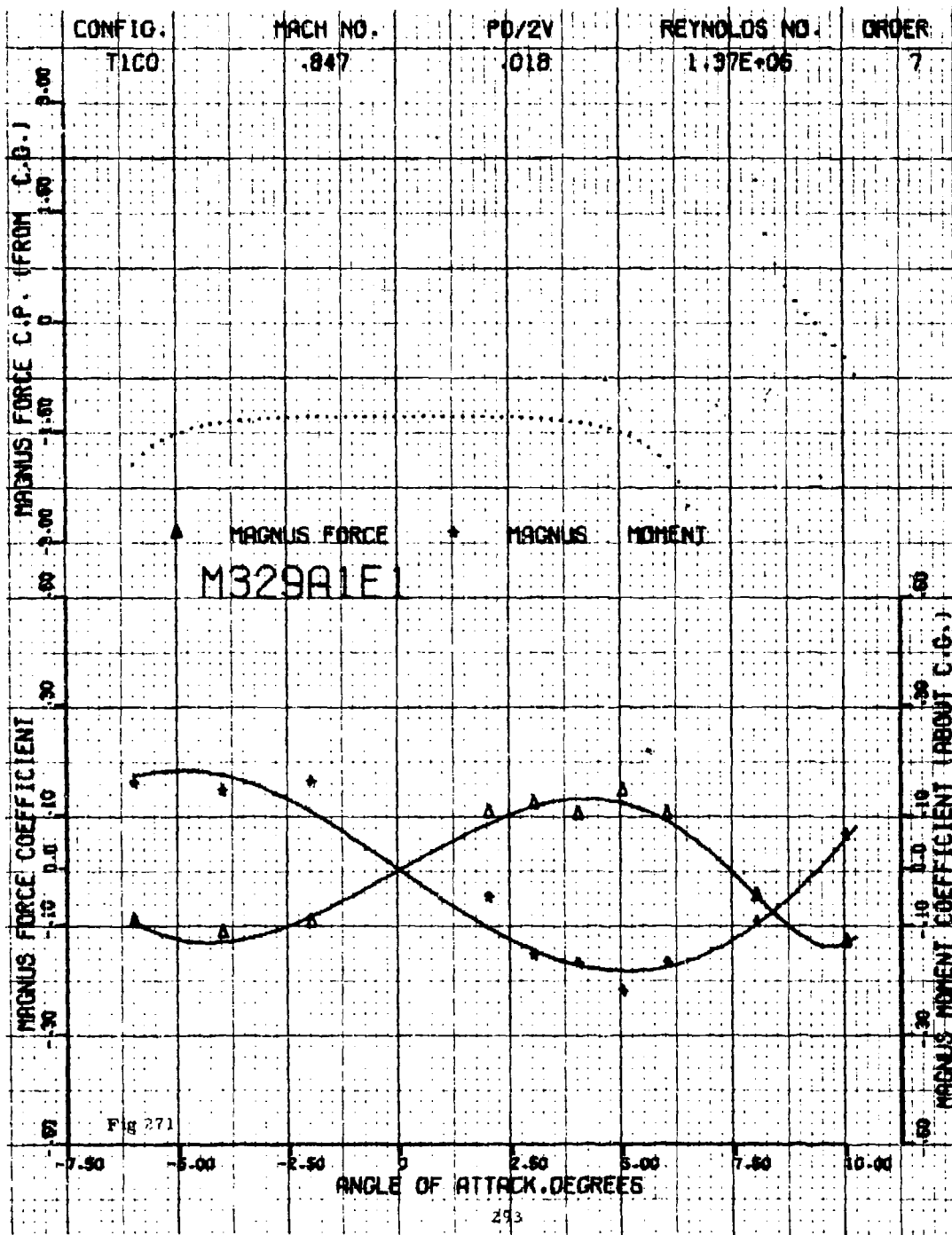


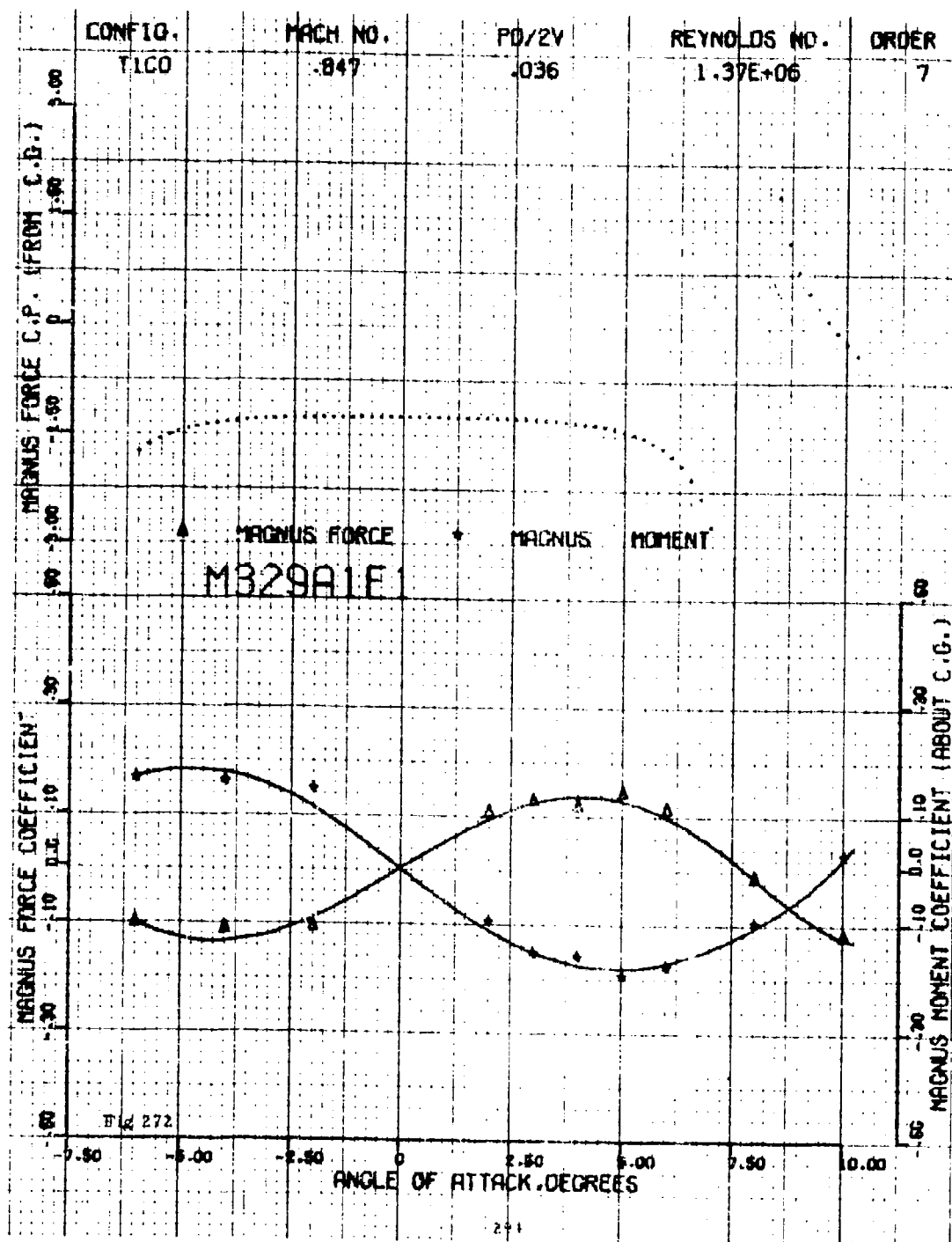


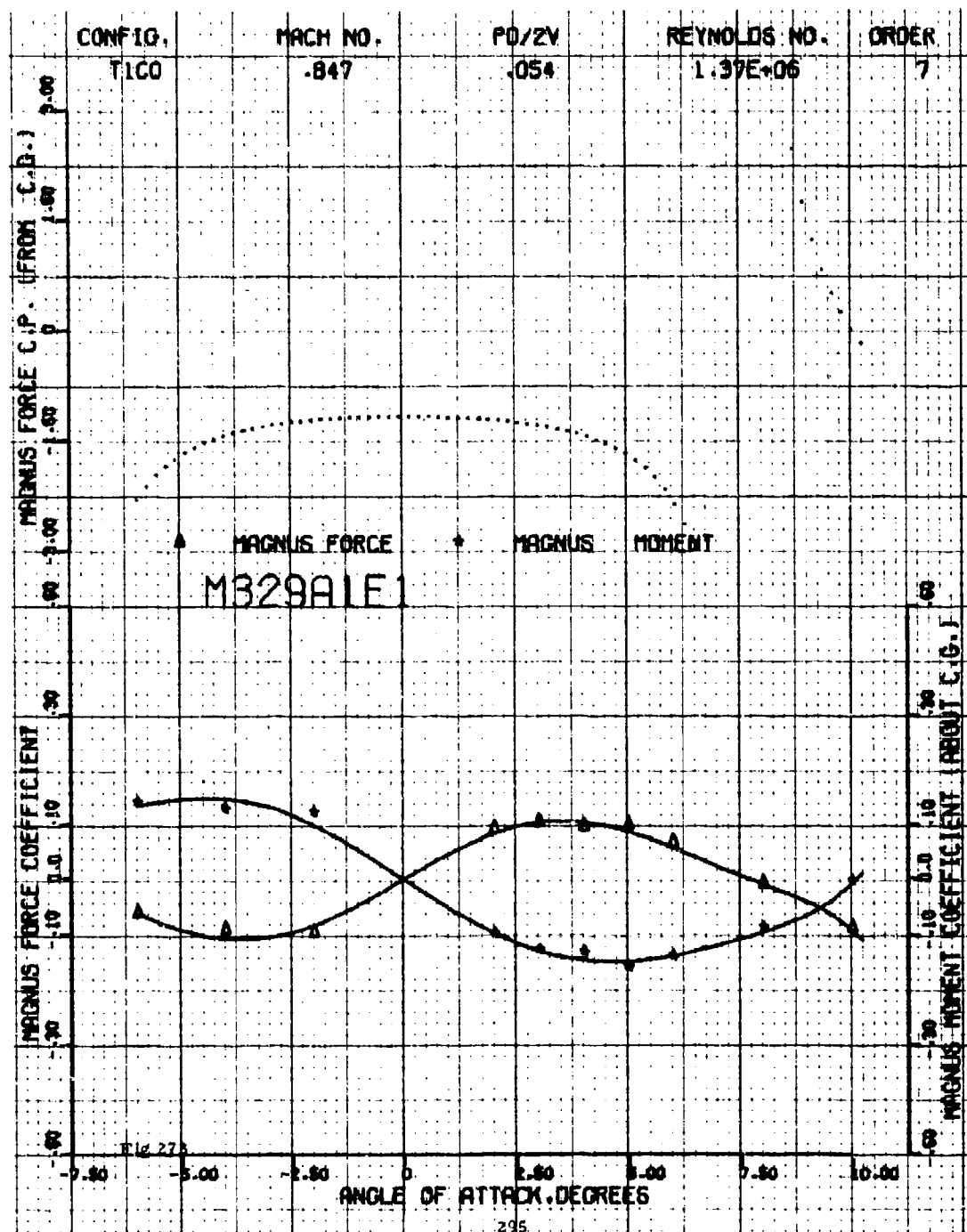


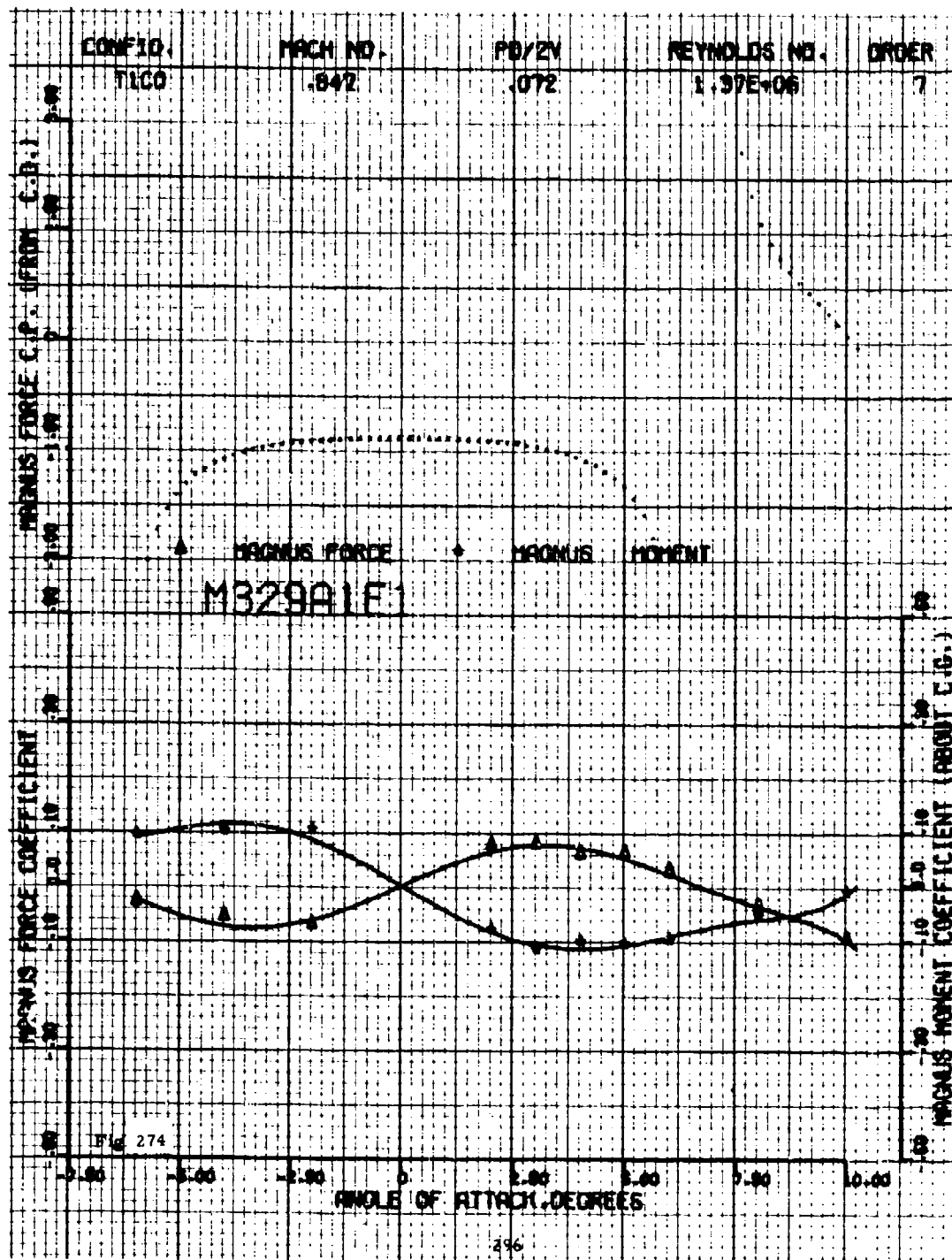


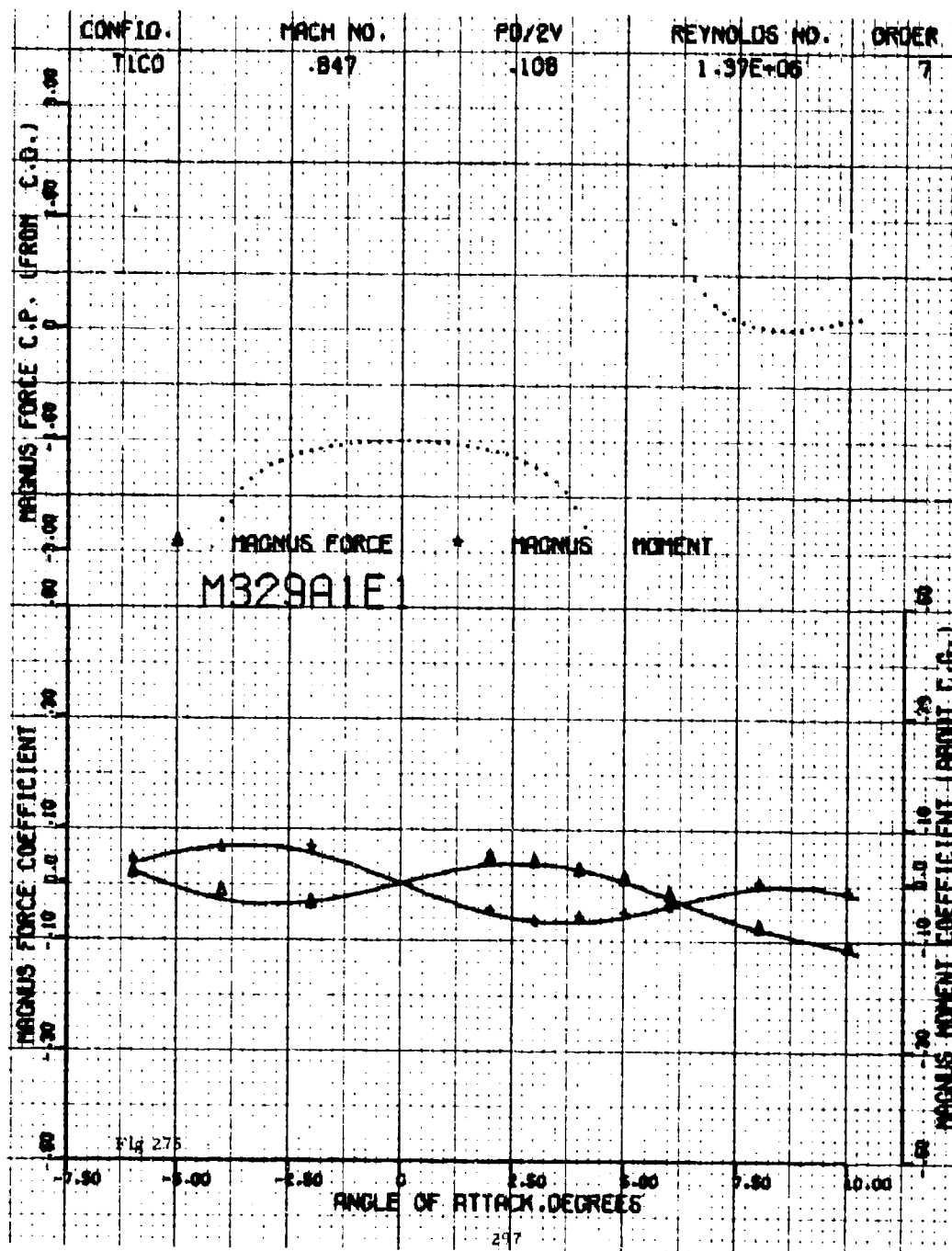


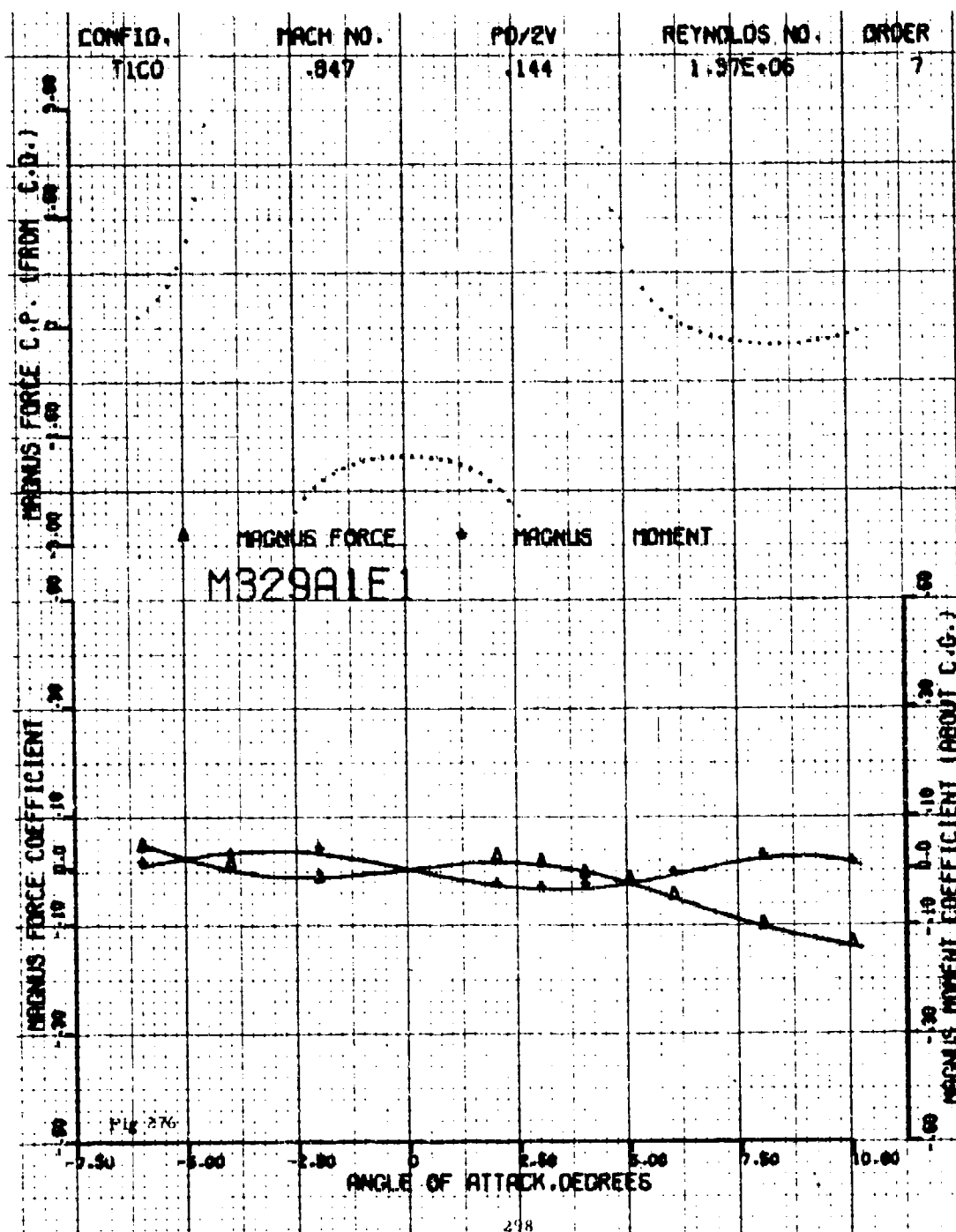


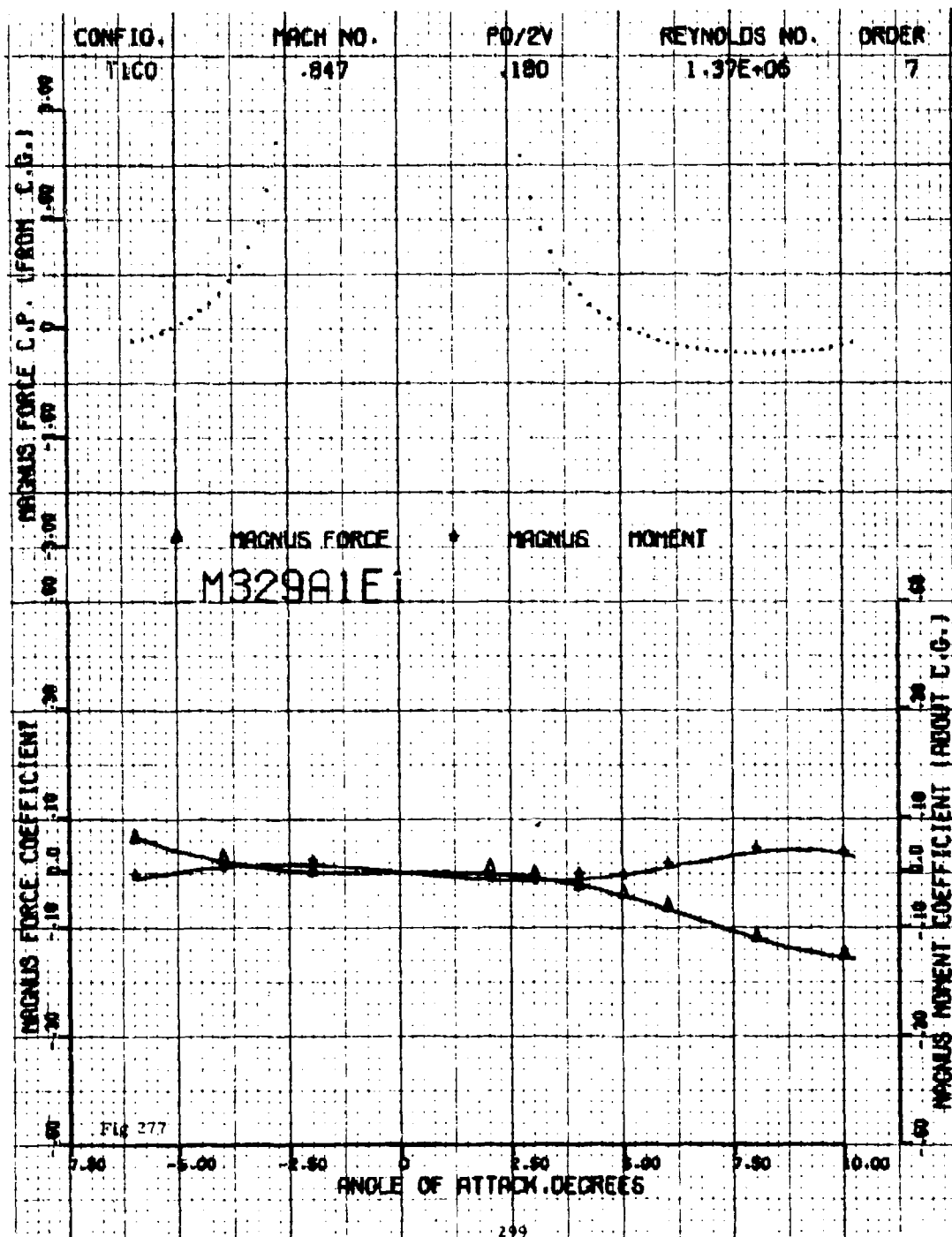


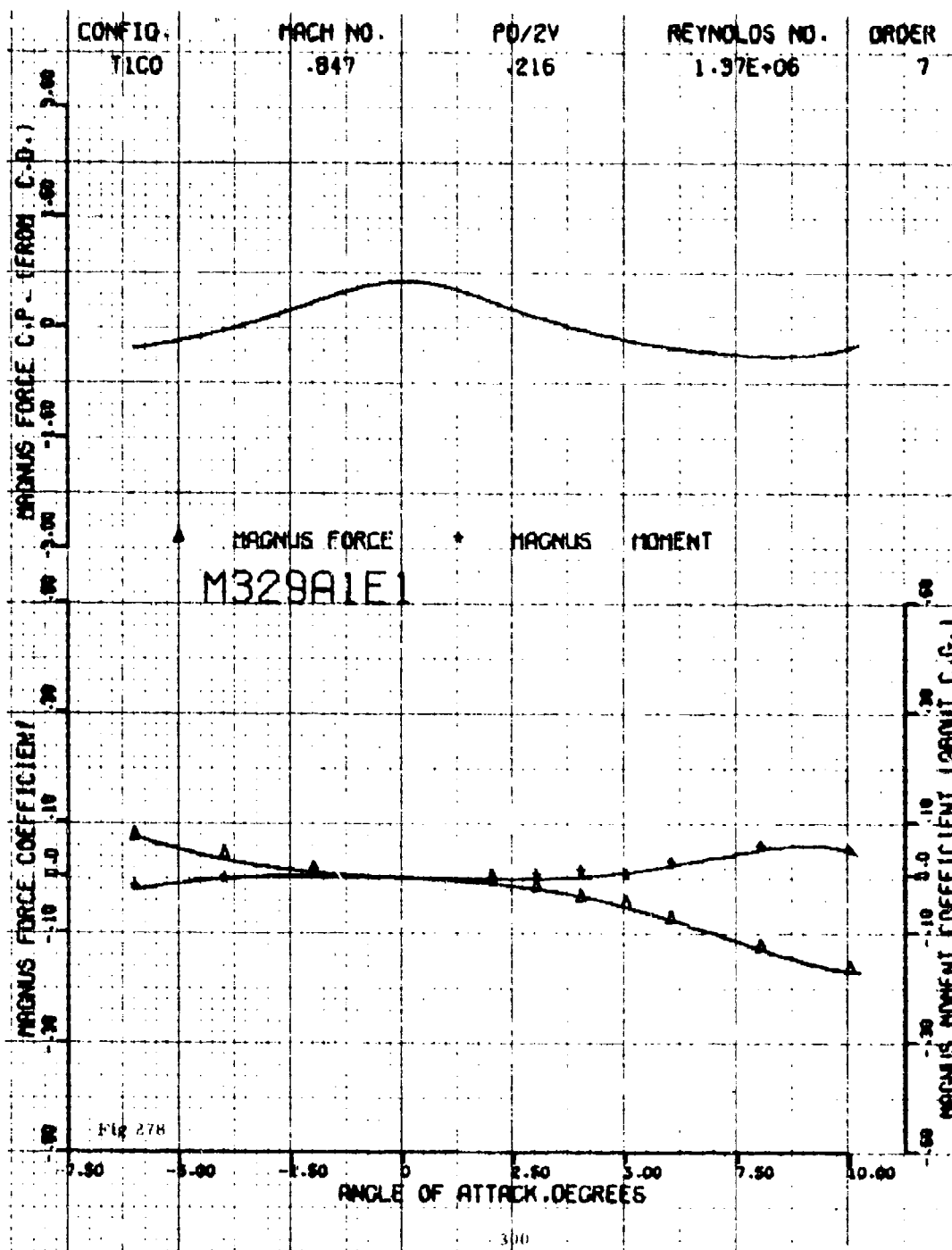


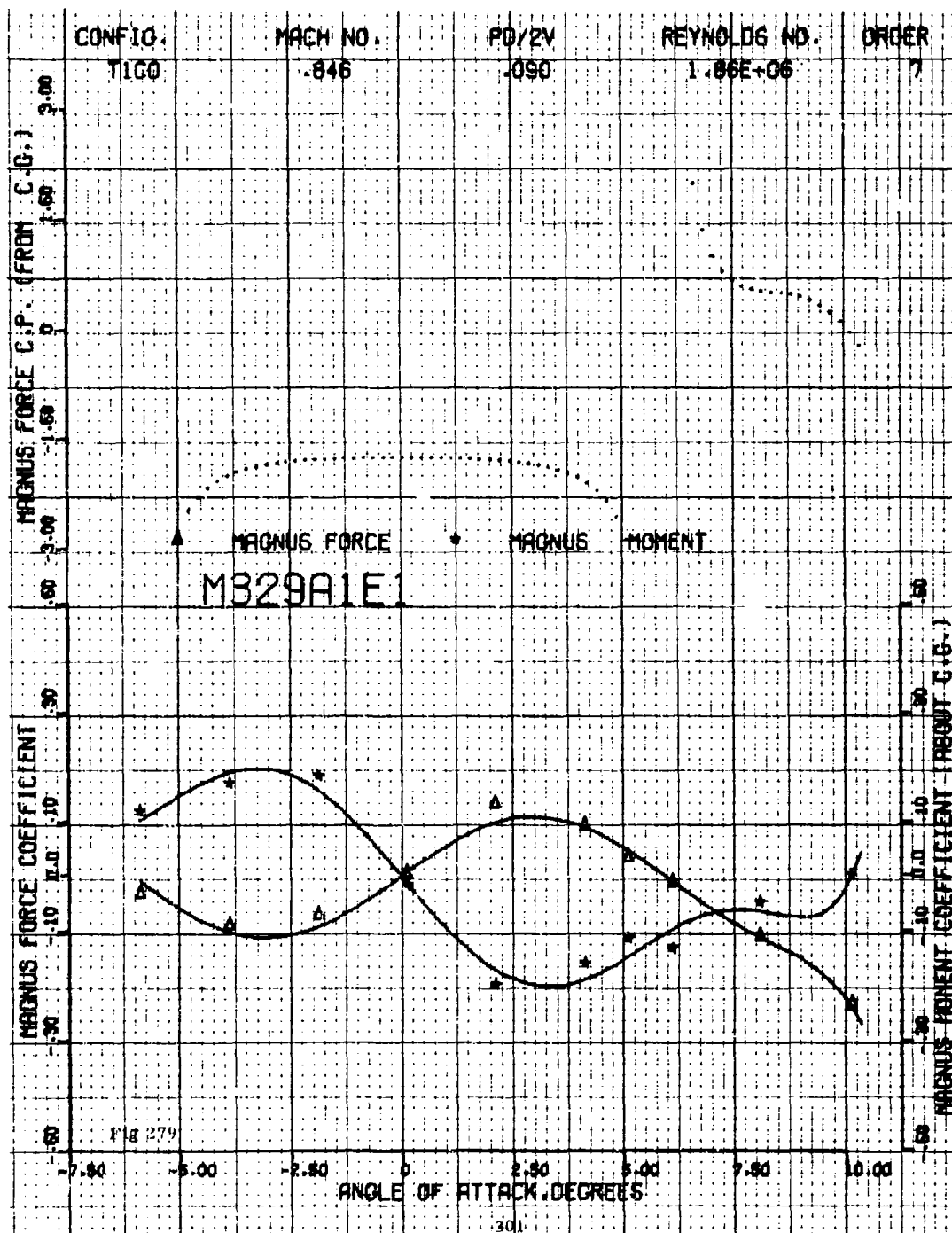


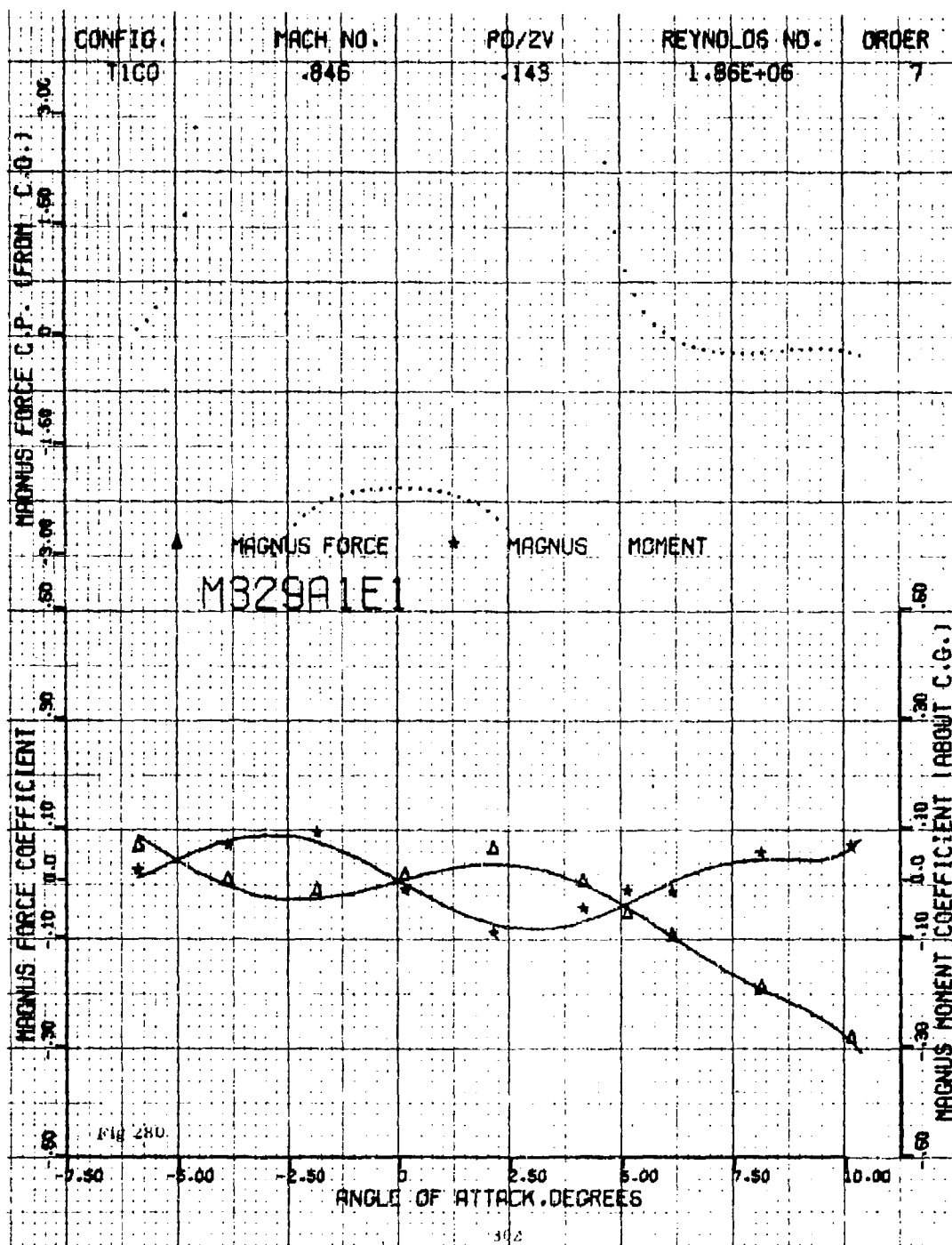


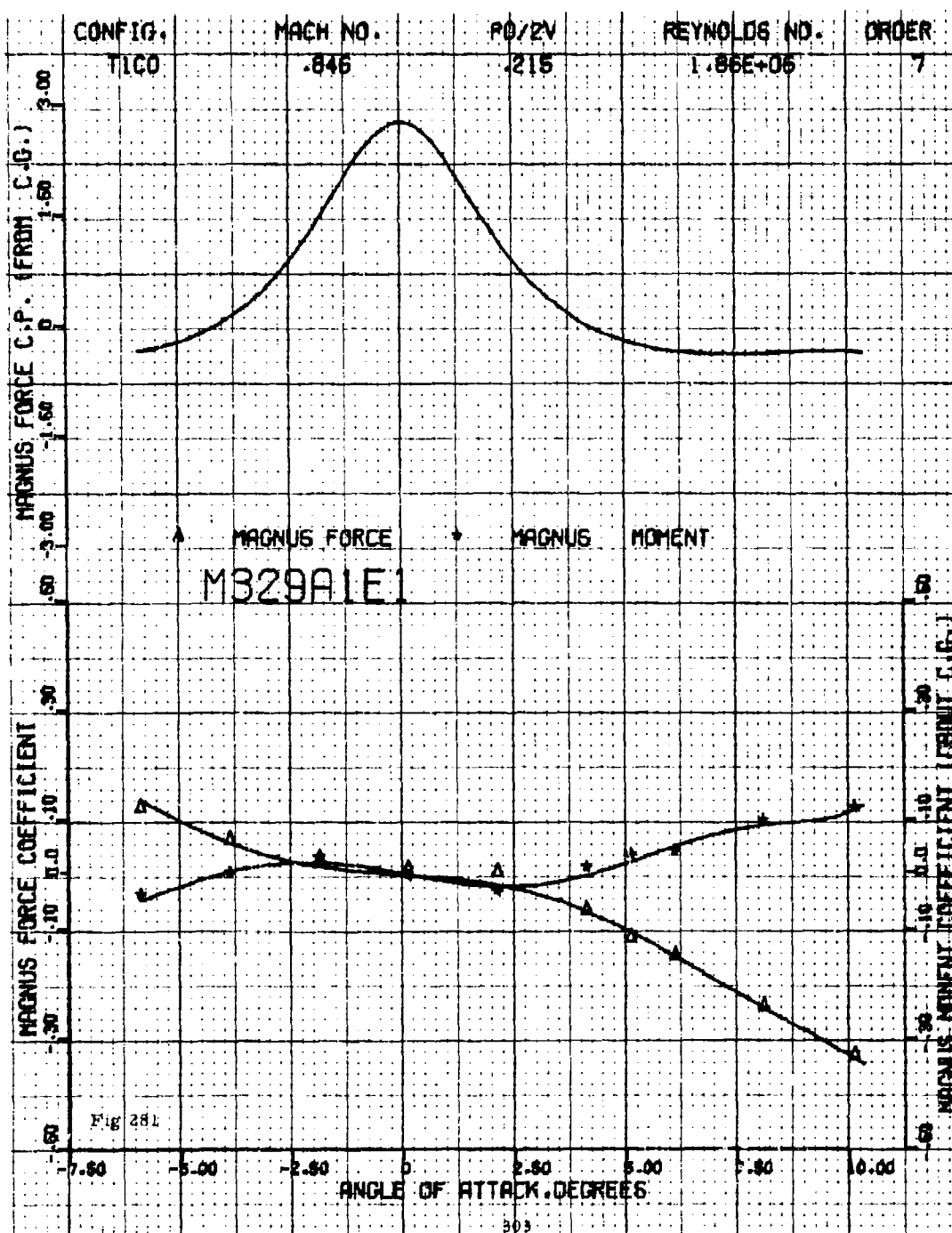


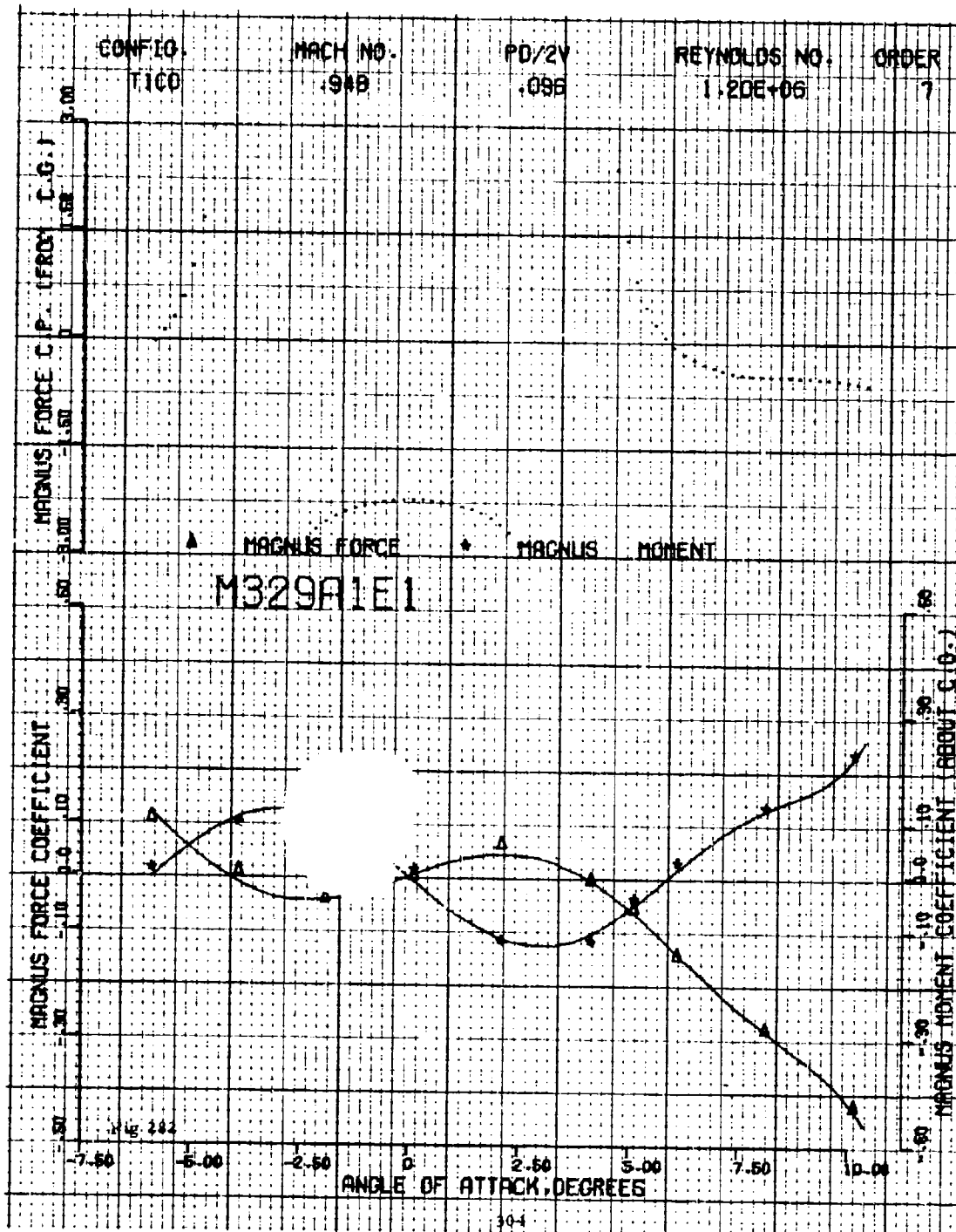




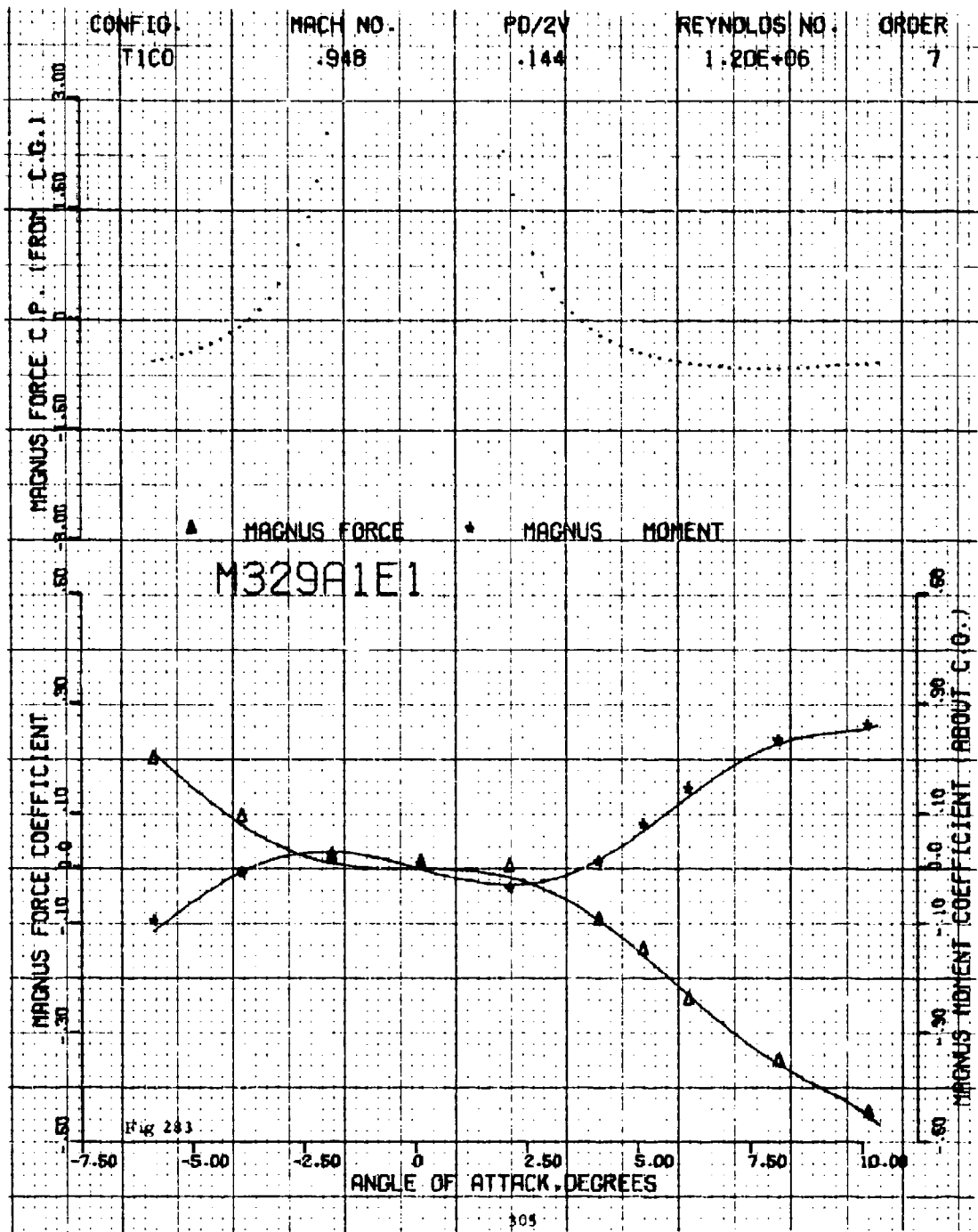


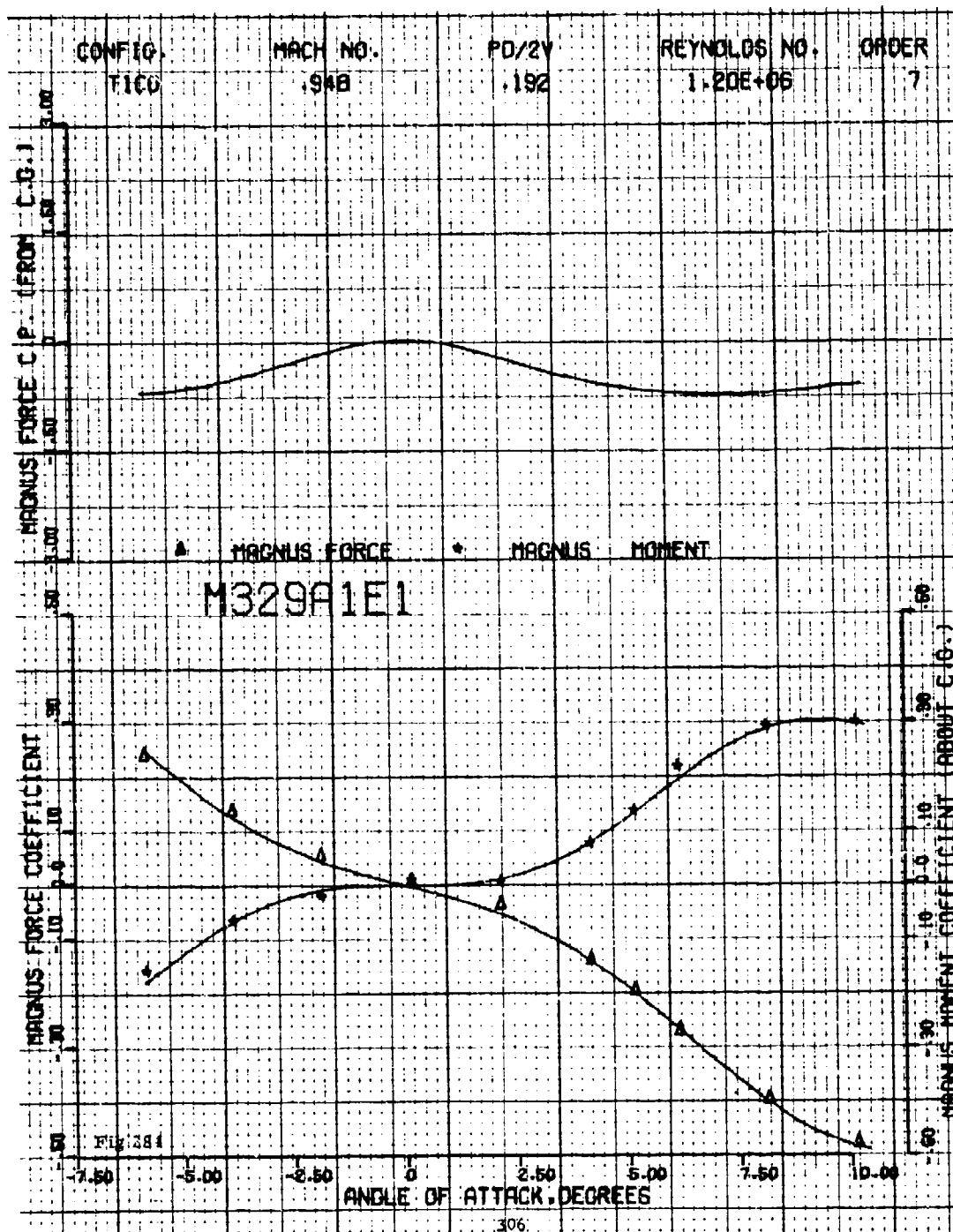


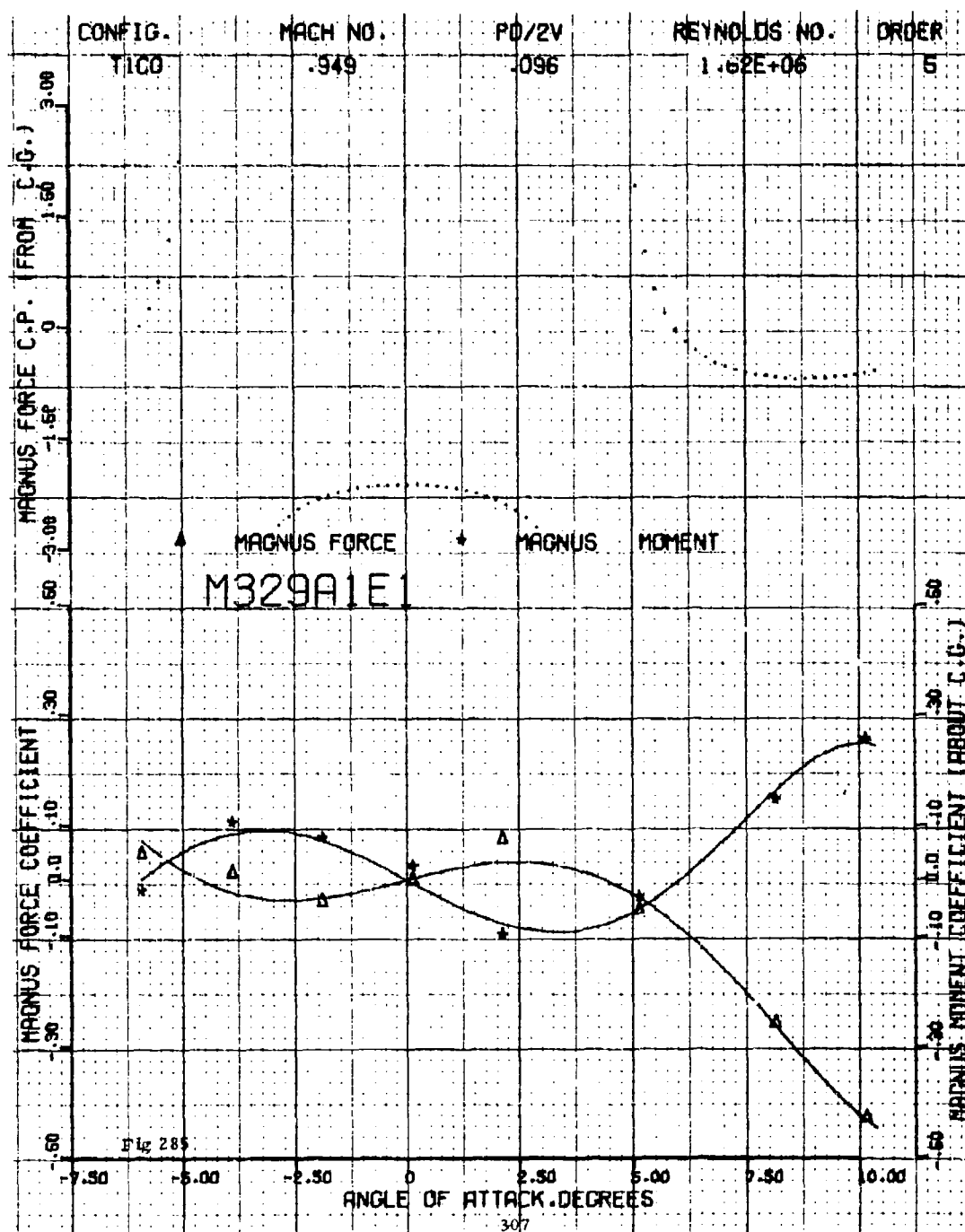


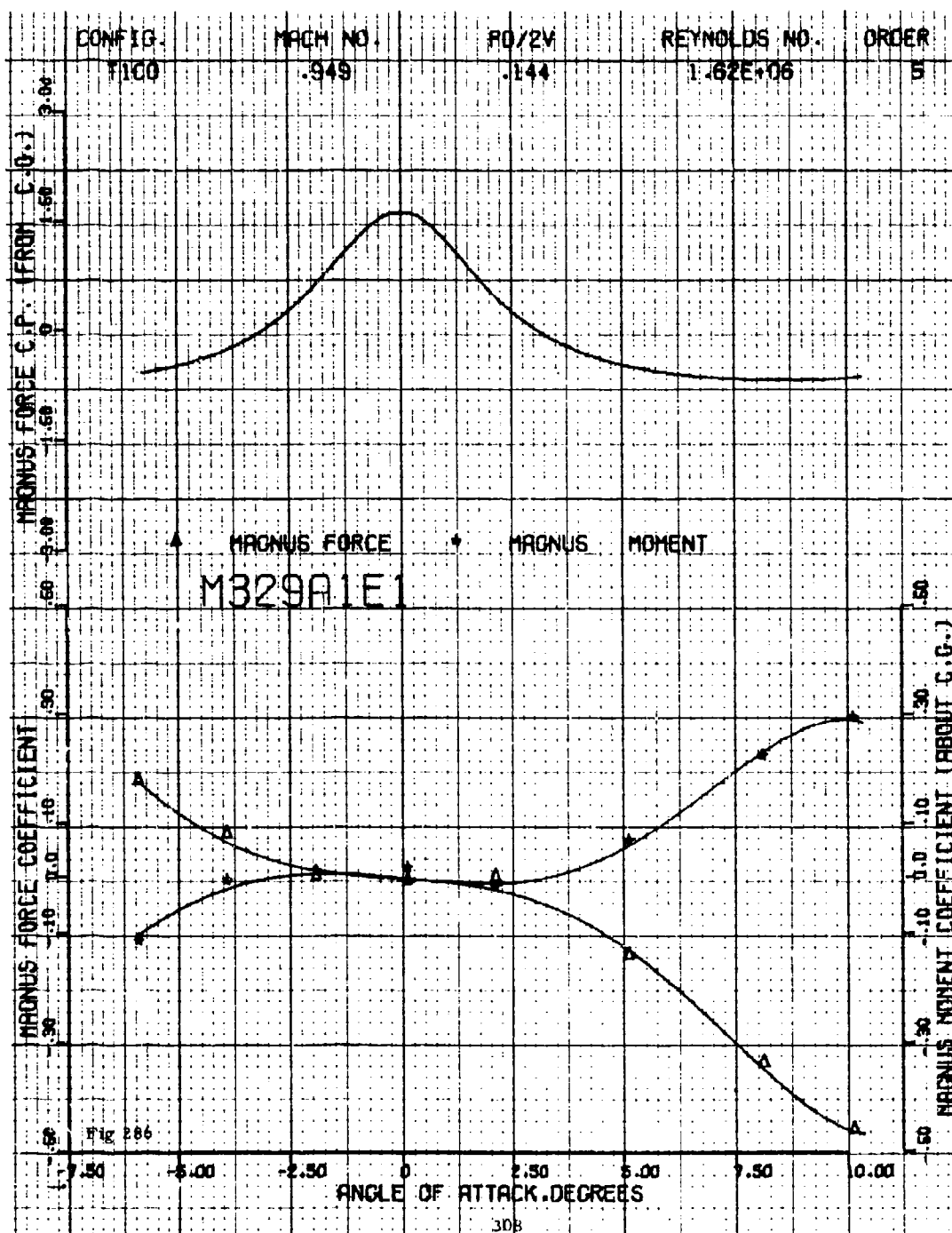


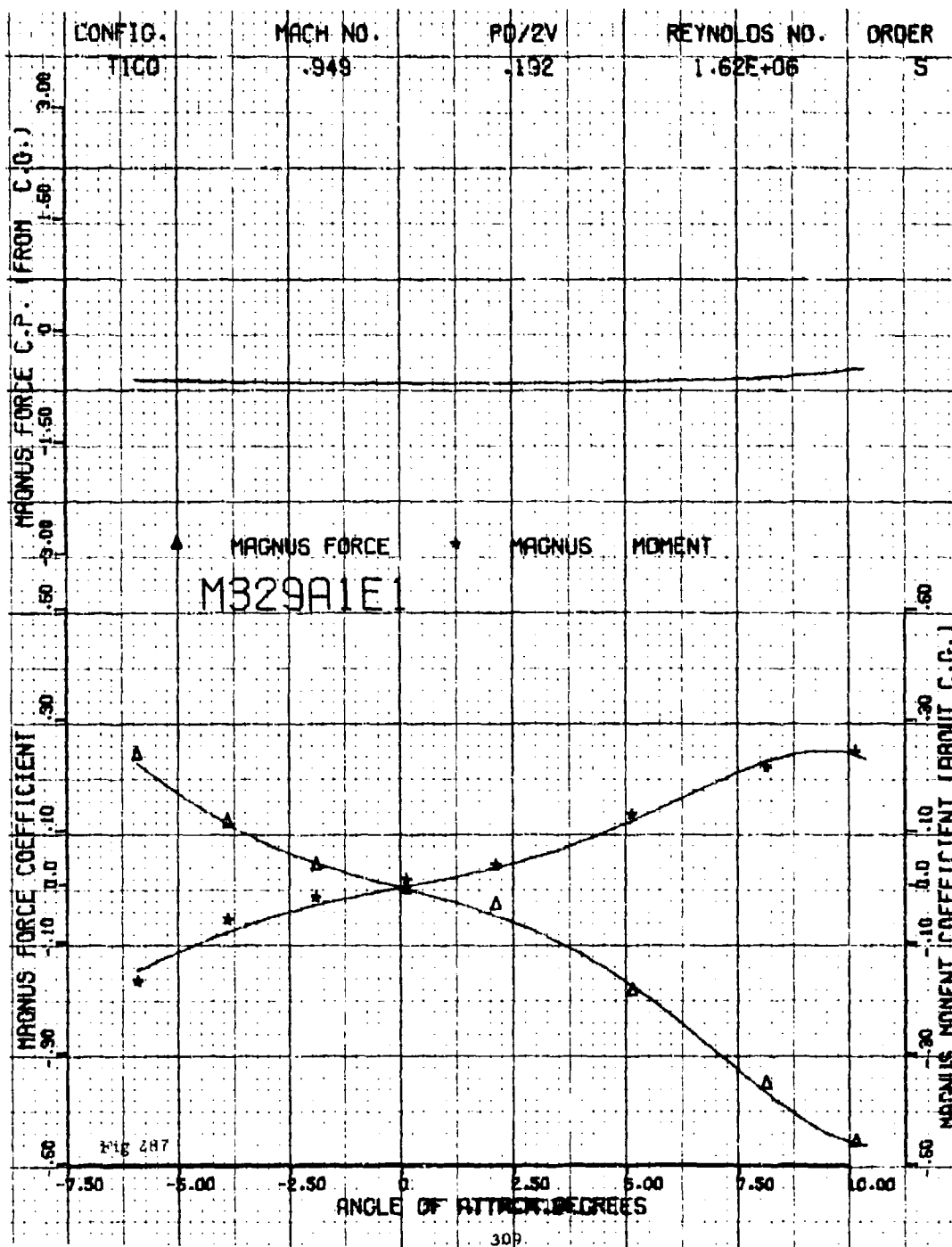
44

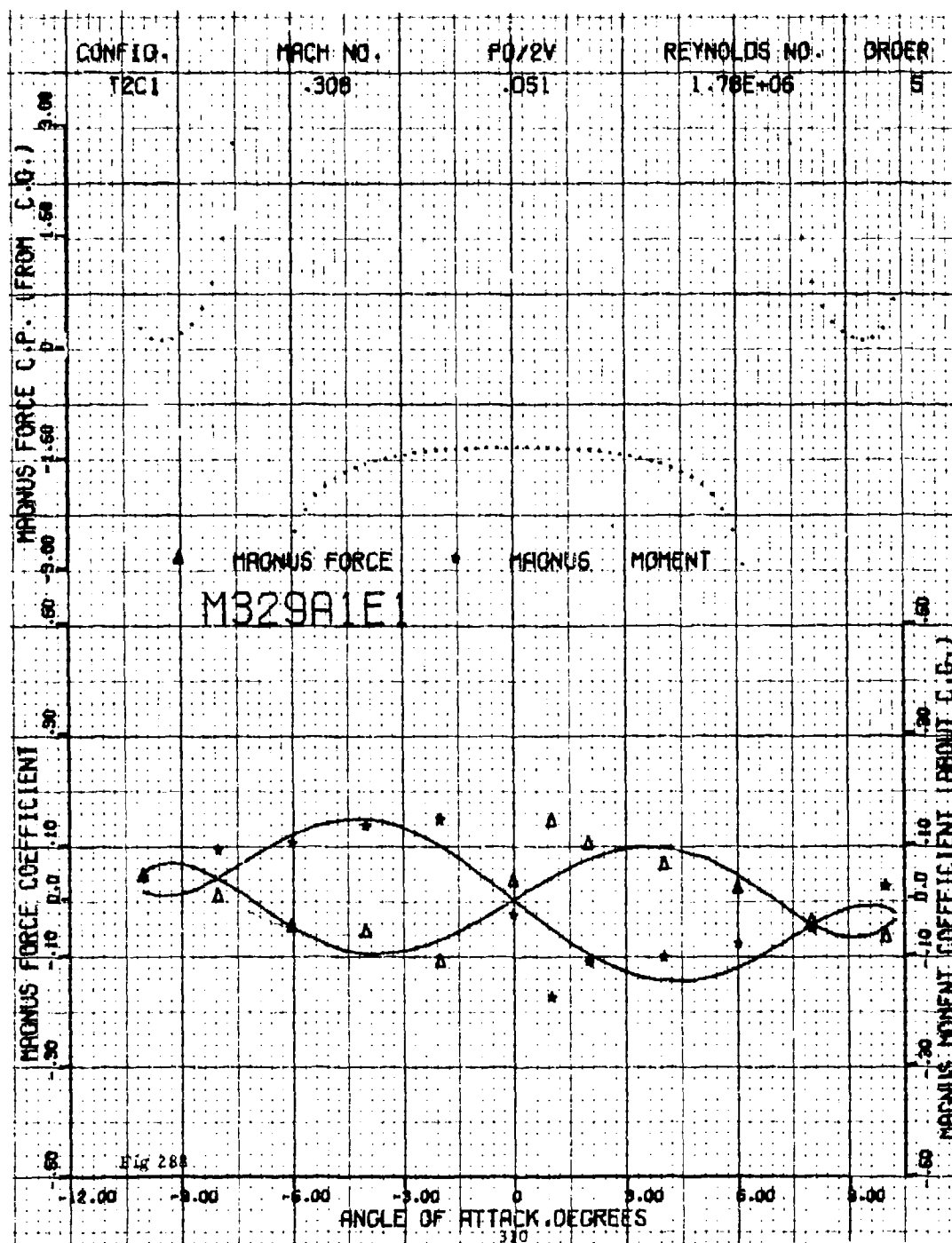


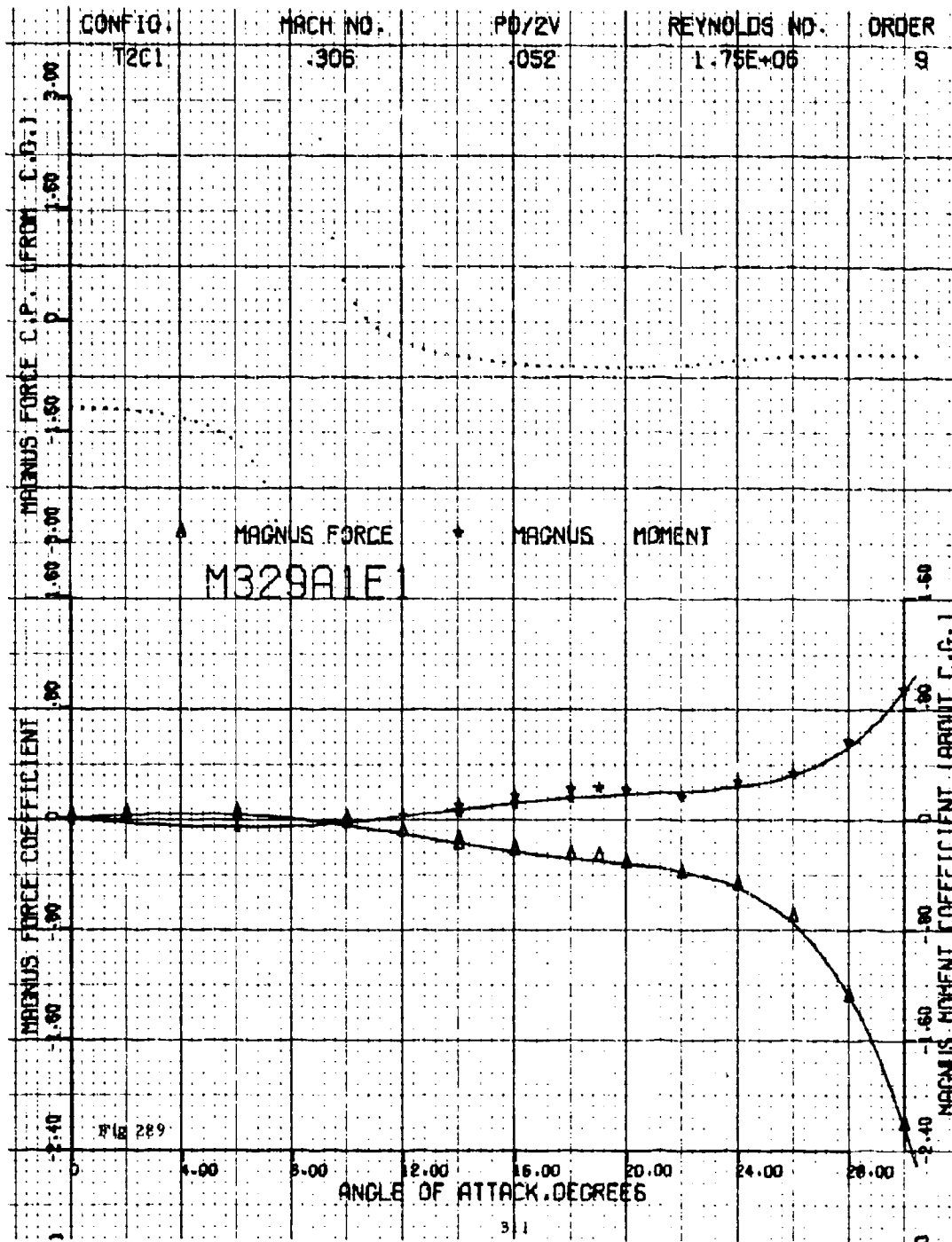












CONFIG. T2C1 MACH NO. .308 PD/2V .102 REYNOLDS NO. 1.78E+06 ORDER 5

MAGNUS FORCE C.P. PERON C.O.C.

MAGNUS FORCE COEFFICIENT

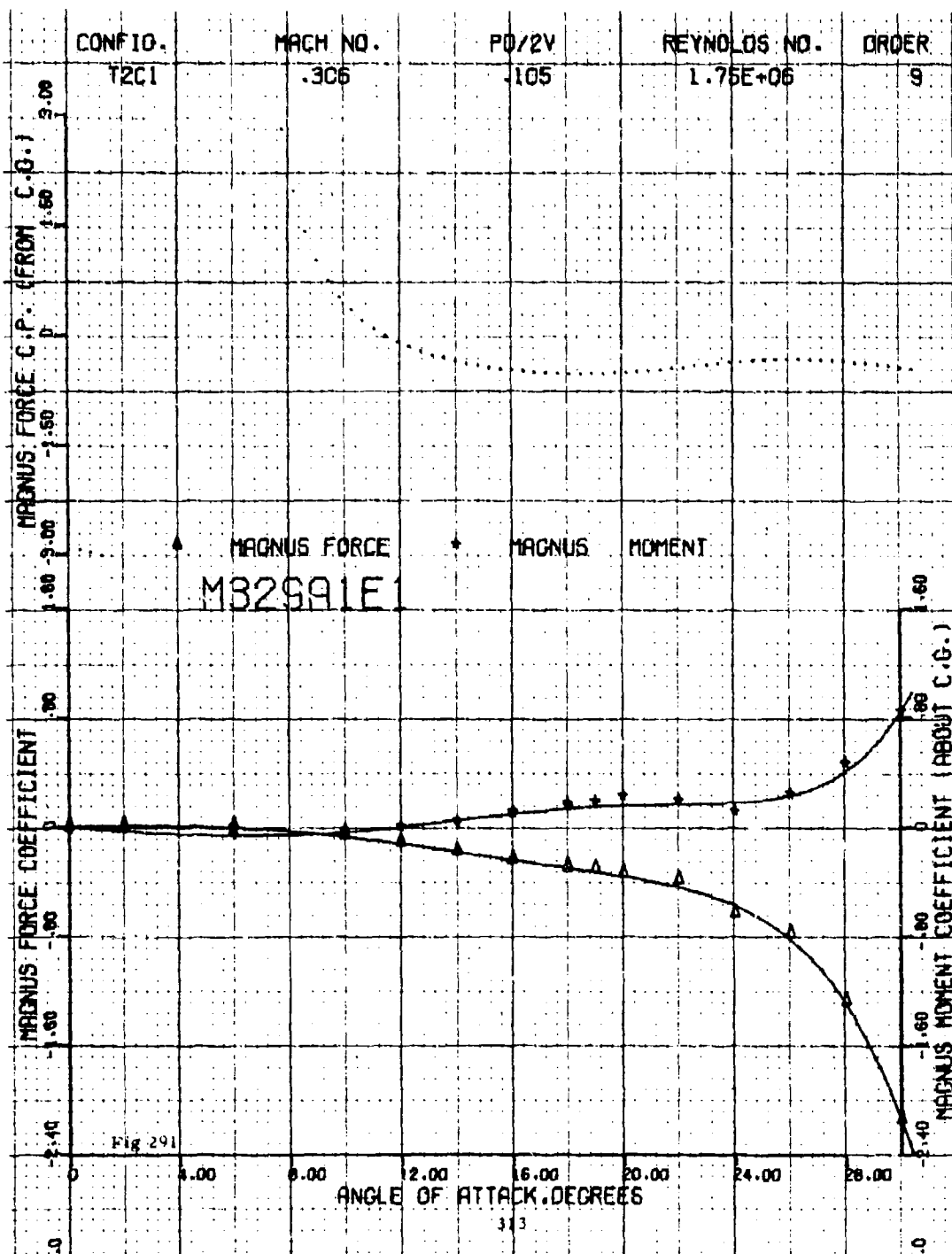
MAGNUS MOMENT COEFFICIENT (ABOUT C.G.)

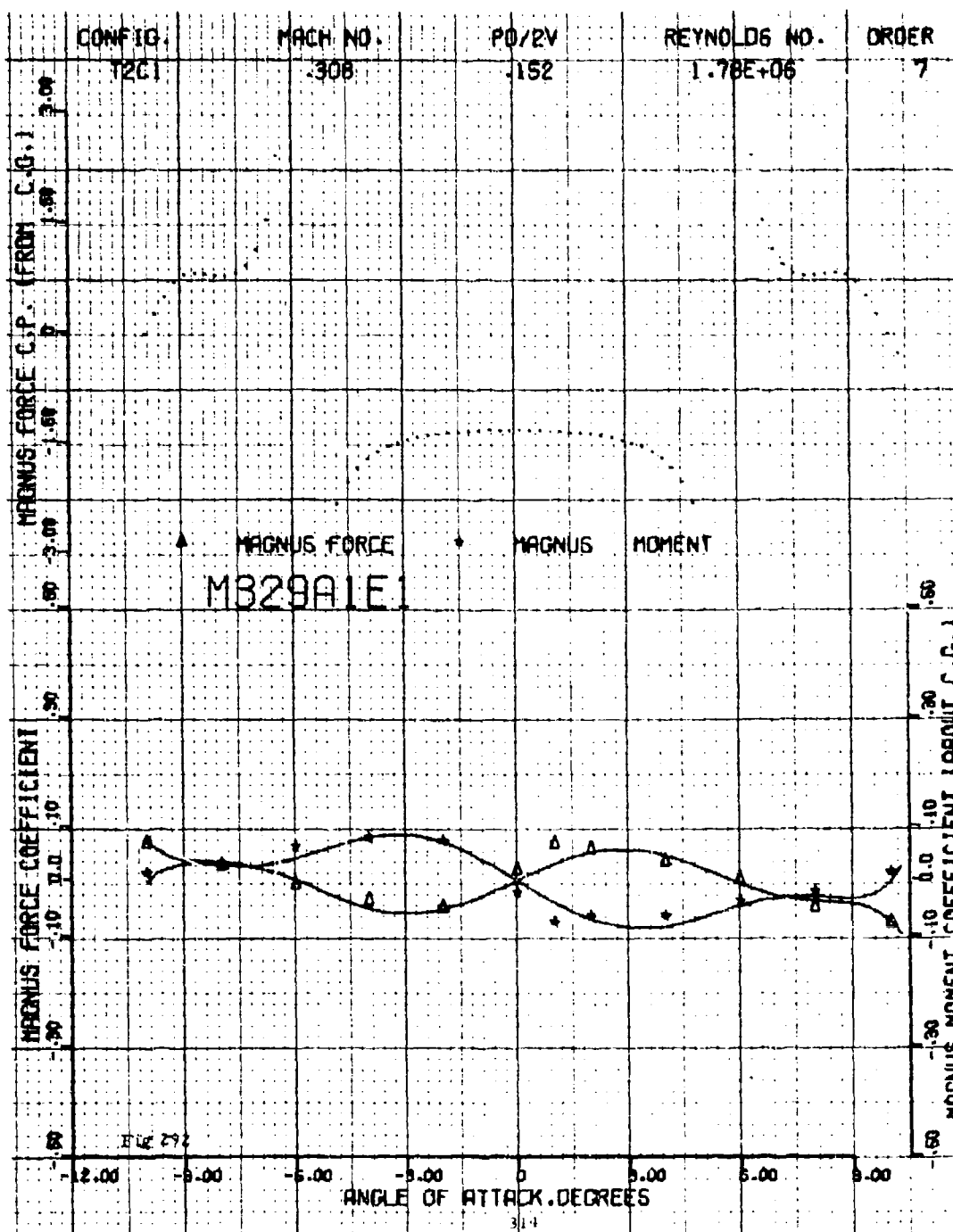
ANGLE OF ATTACK DEGREES

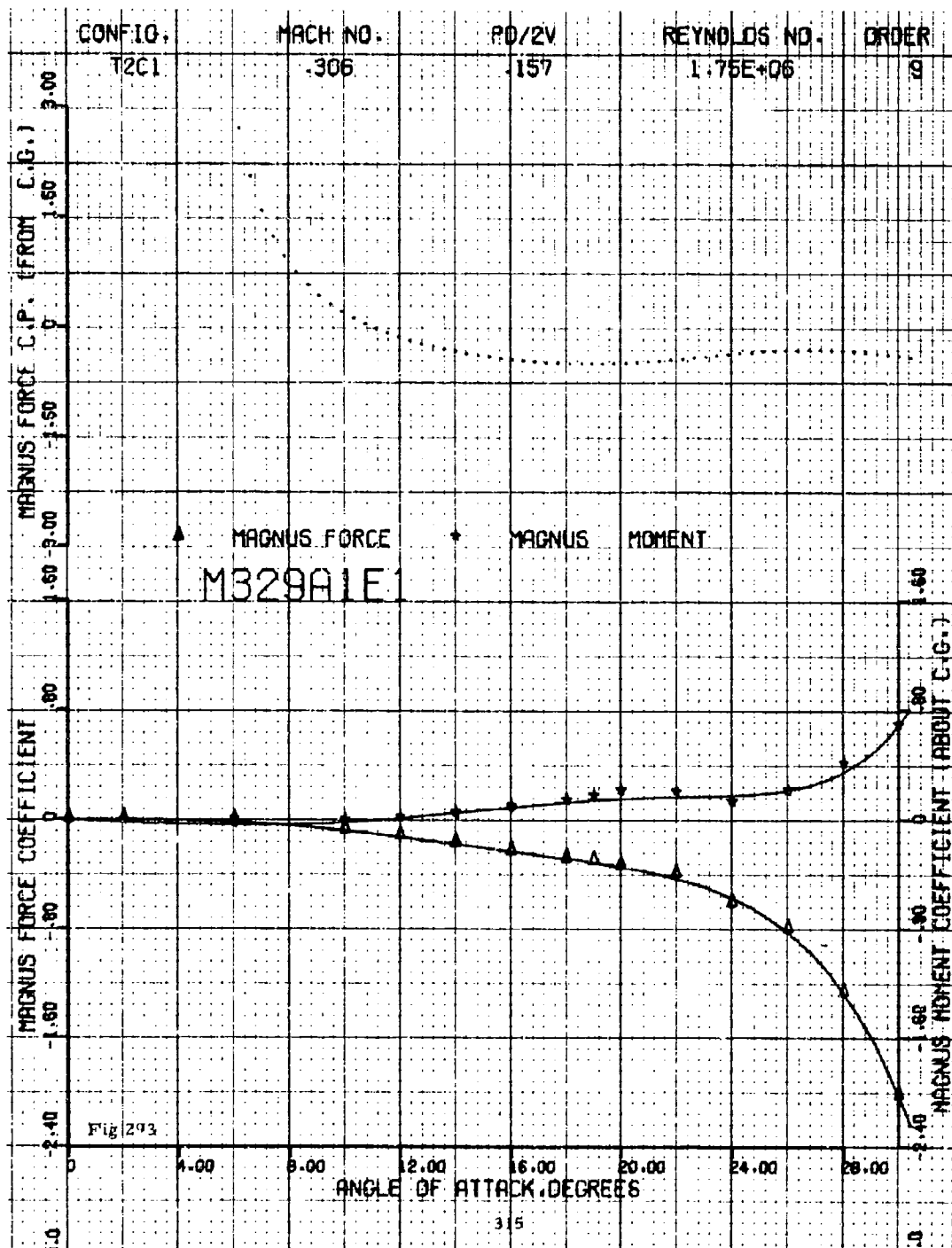
M329A1E1

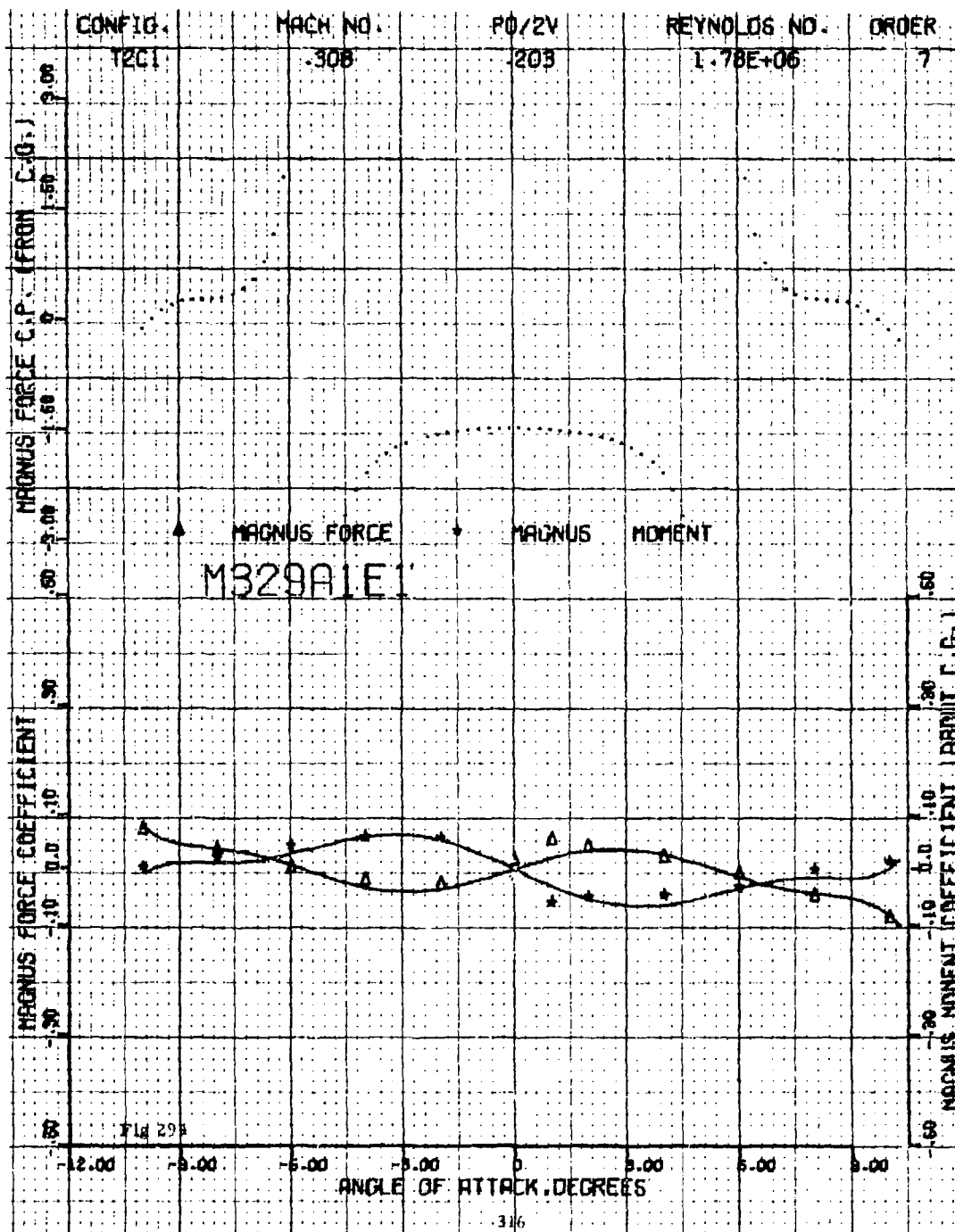
Fig 290

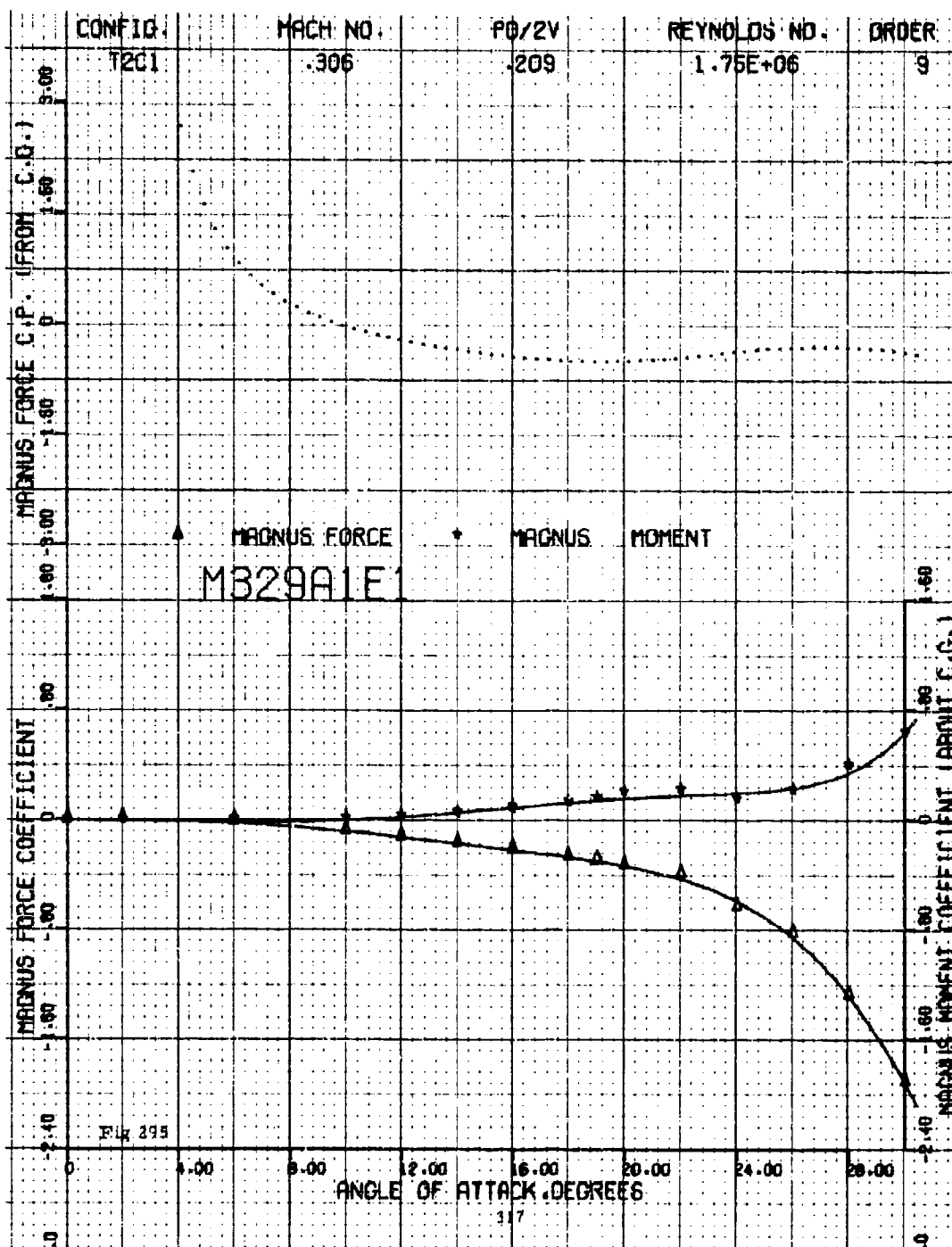
312

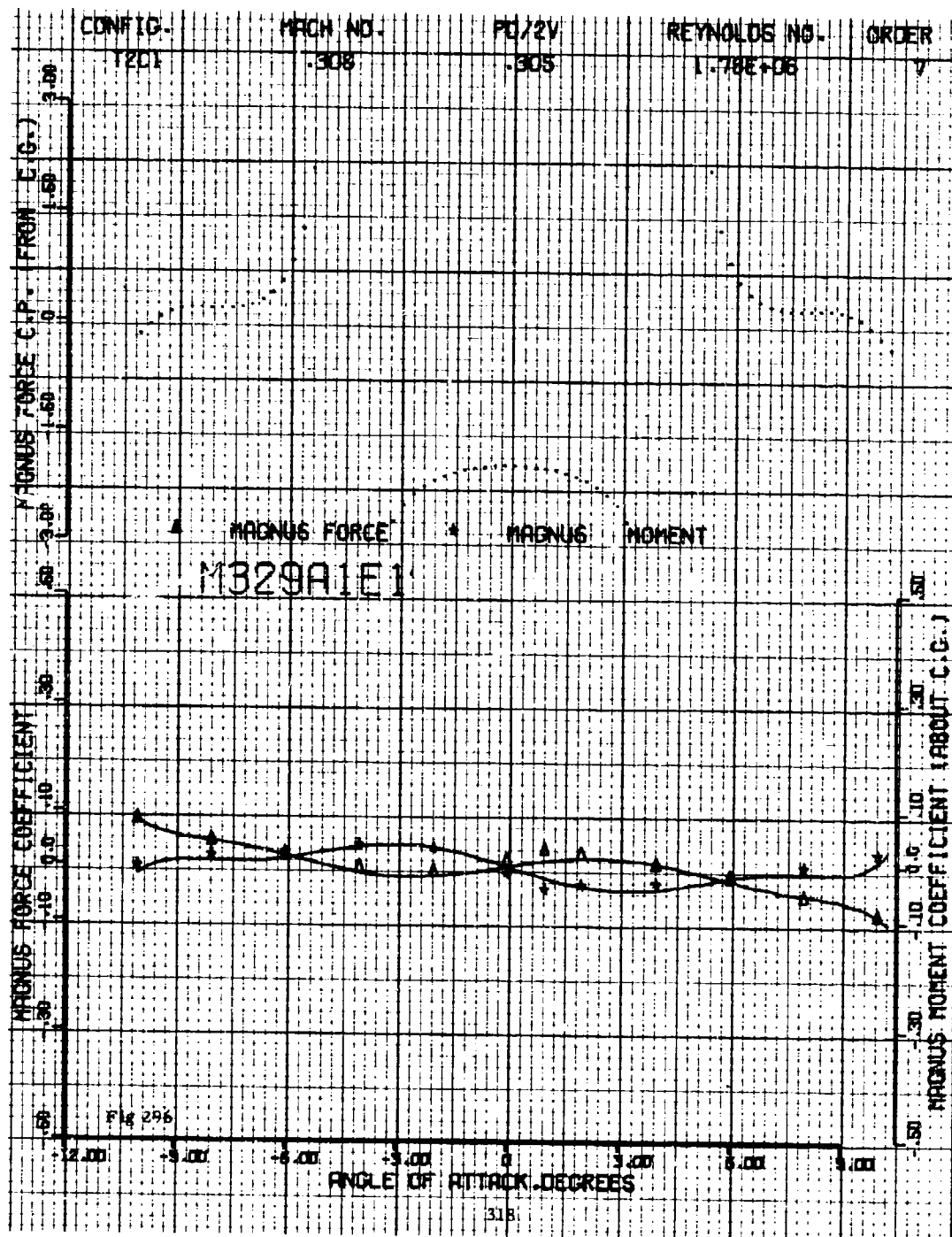


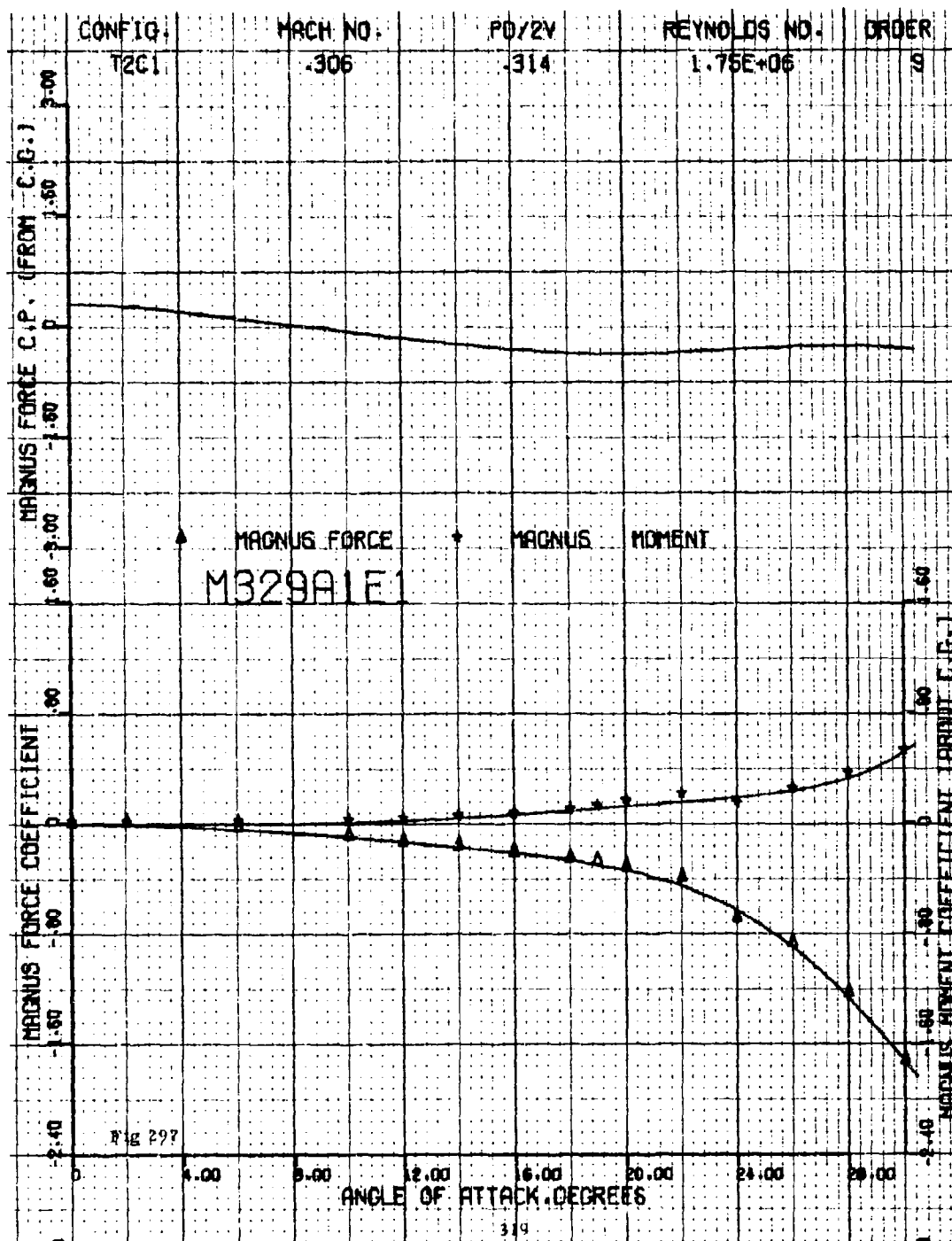


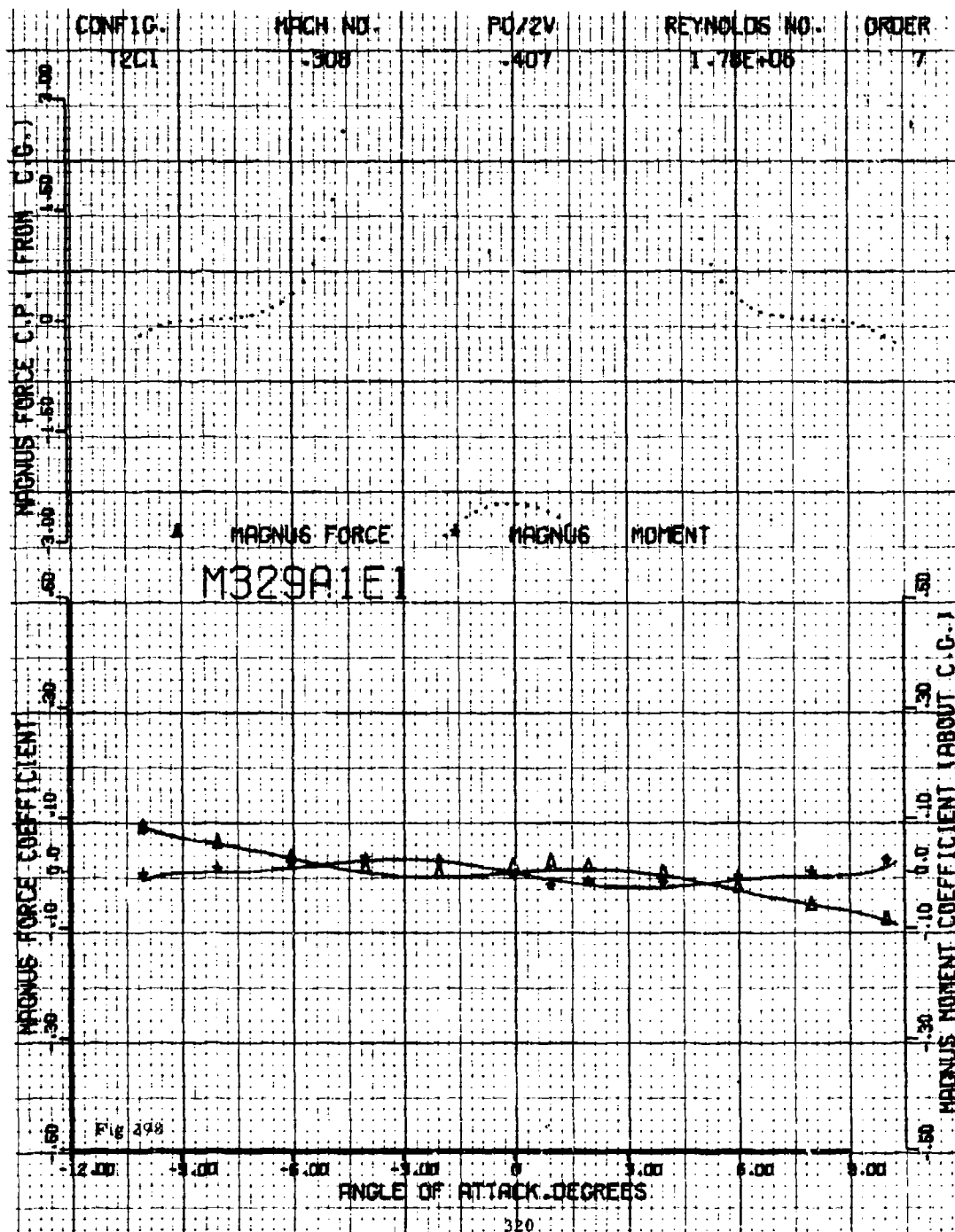


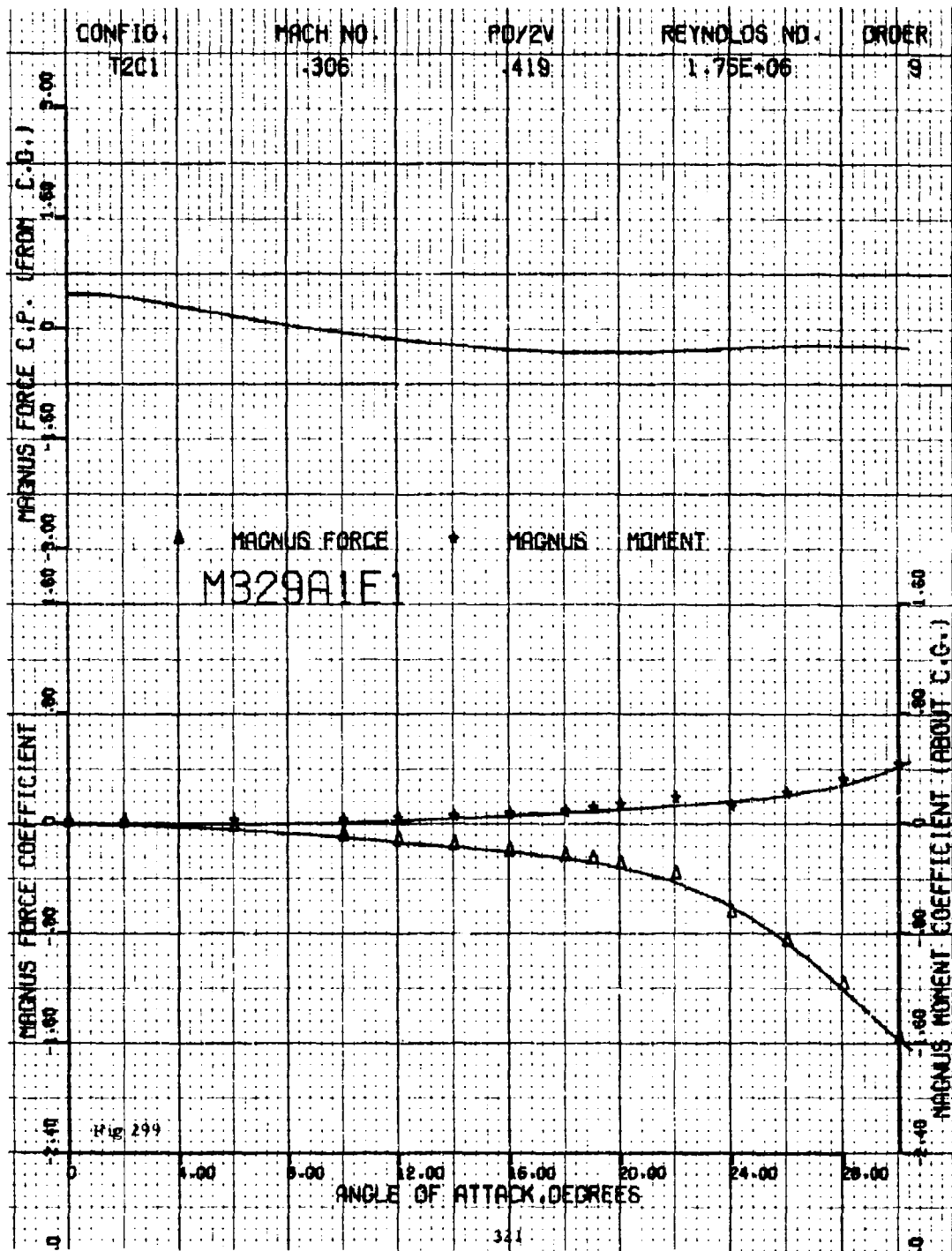


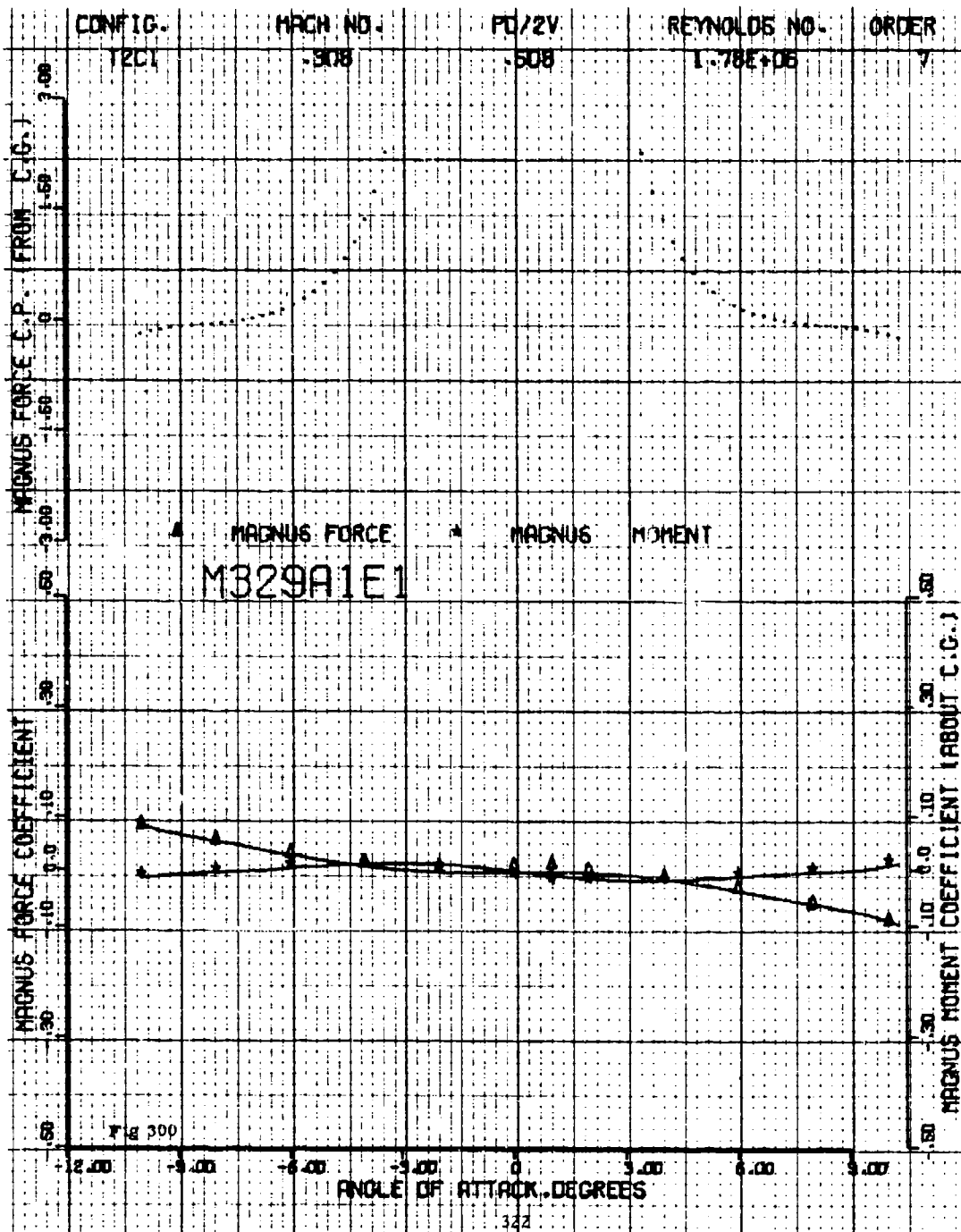


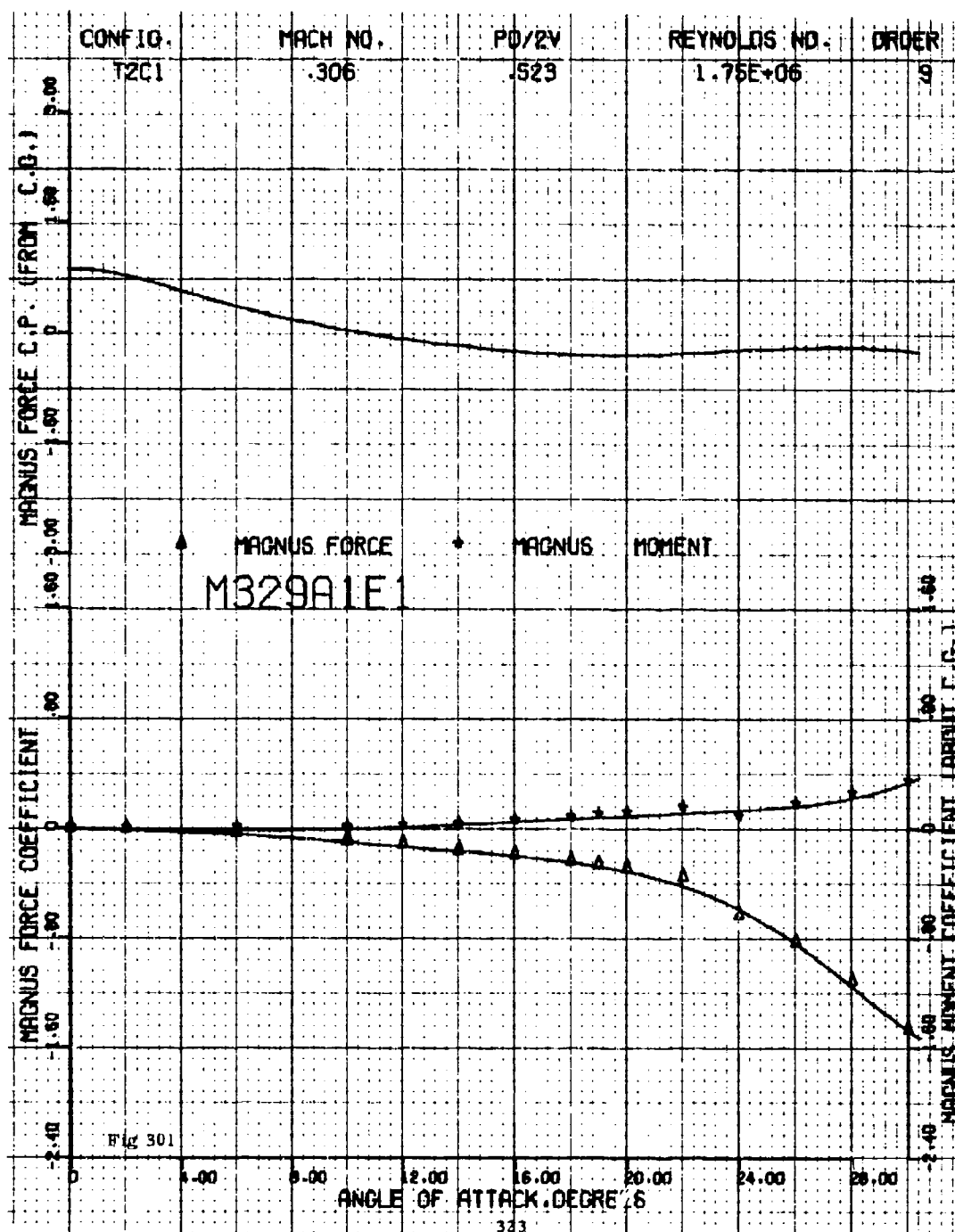


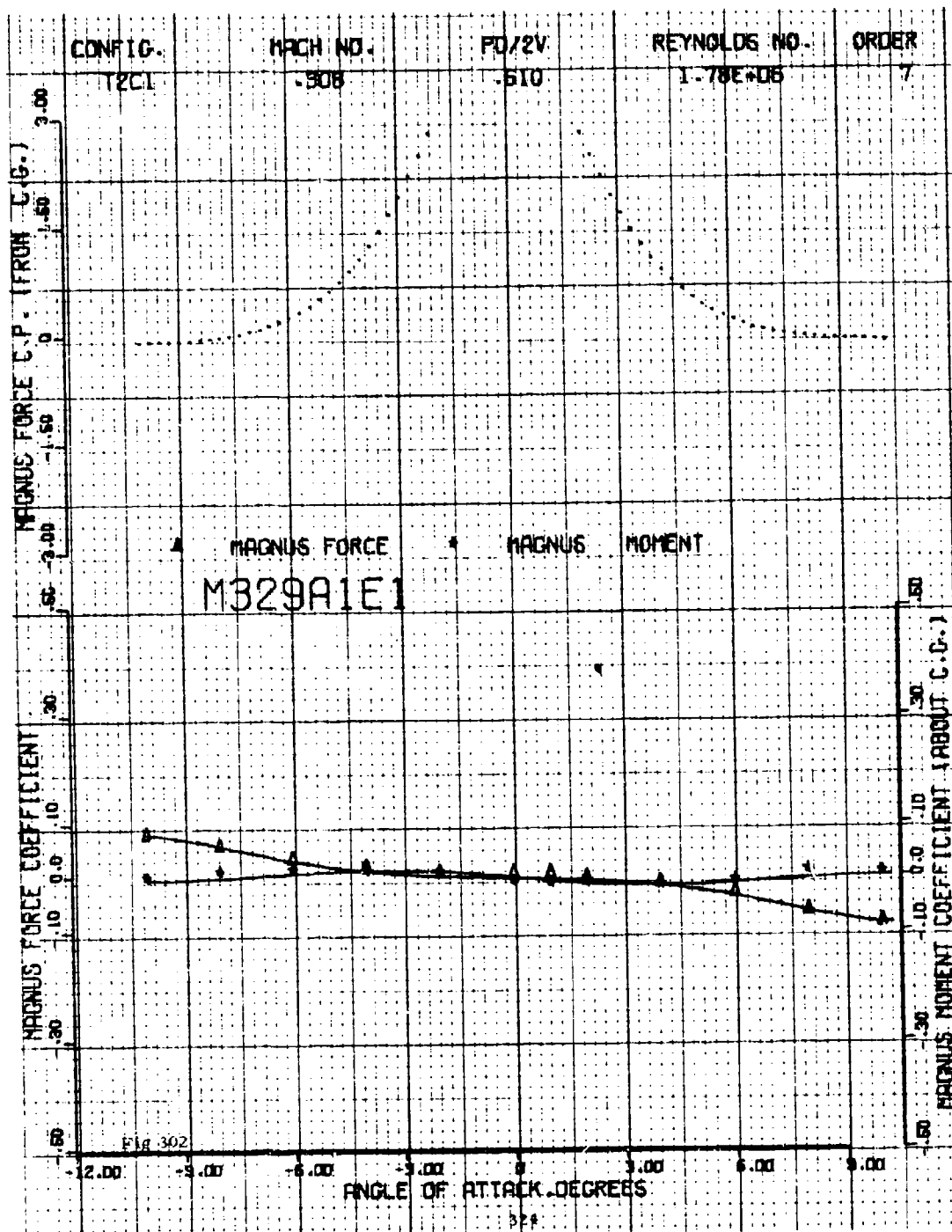












CONFIG. 1201 MACH NO. .569 PO/2V .027 REYNOLDS NO. 2.98E+06 ORDER 9

MAGNUS FORCE C.P. (FROM C.G.)

MAGNUS FORCE MAGNUS MOMENT

M329A1E1

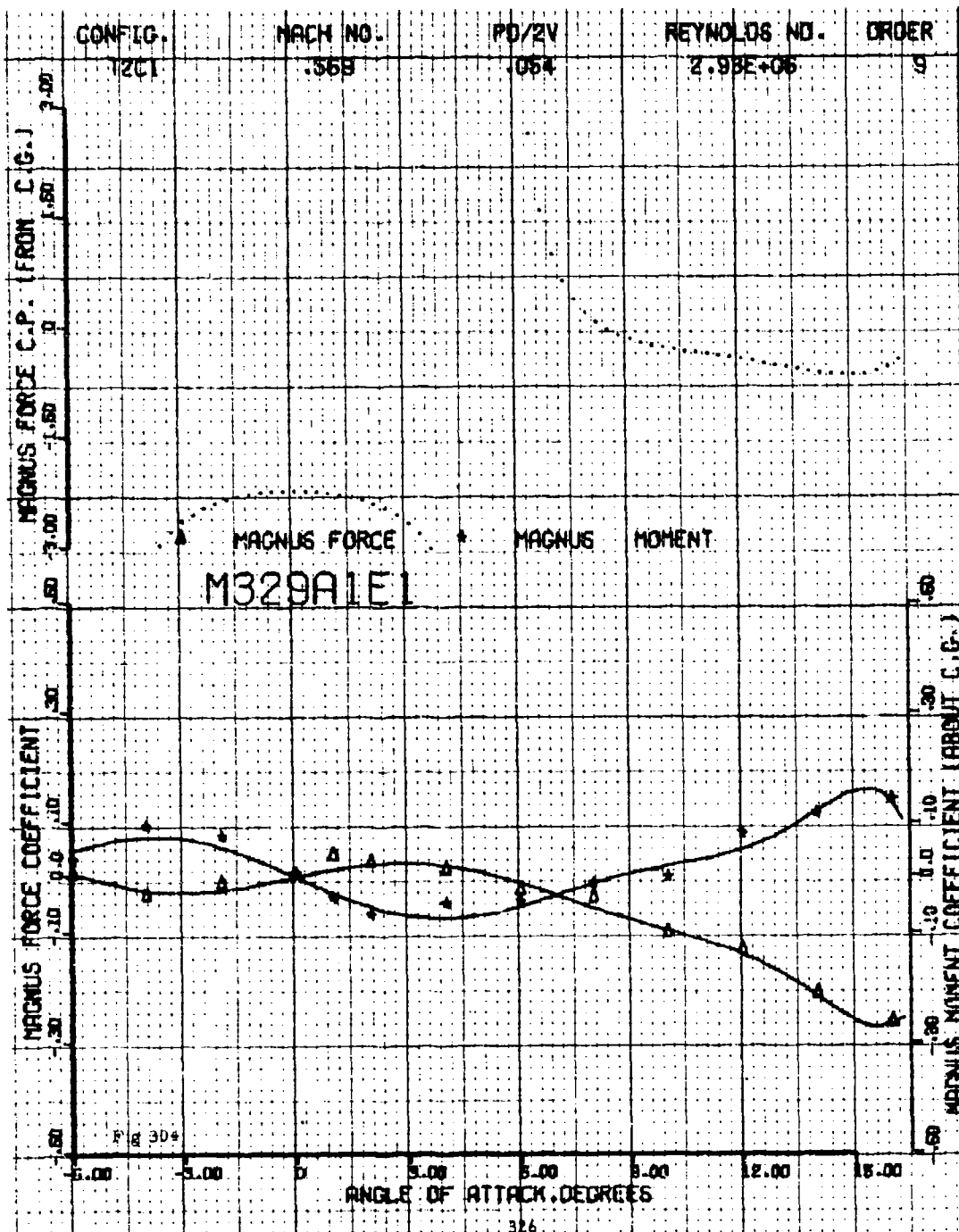
MAGNUS FORCE COEFFICIENT

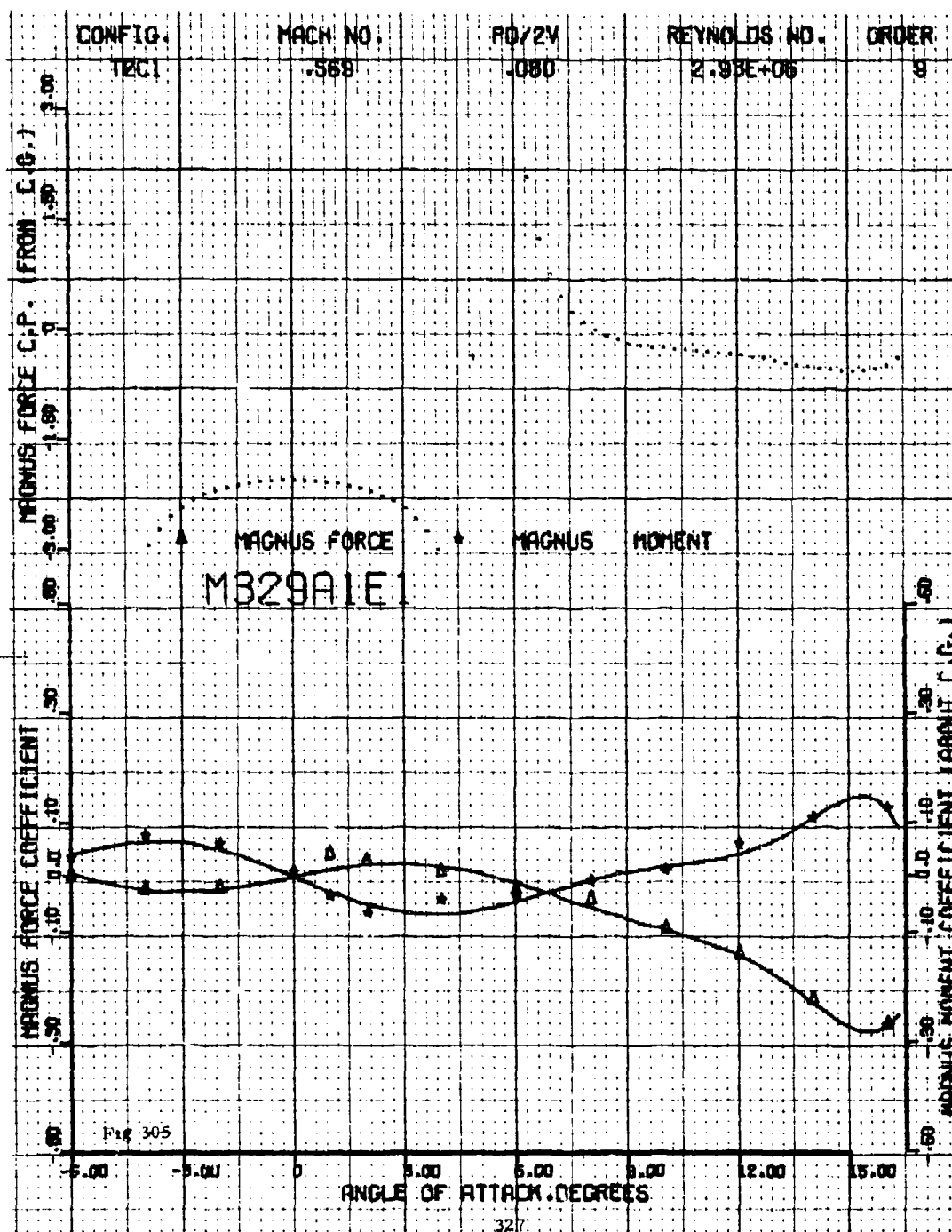
MAGNUS MOMENT COEFFICIENT (C.G.)

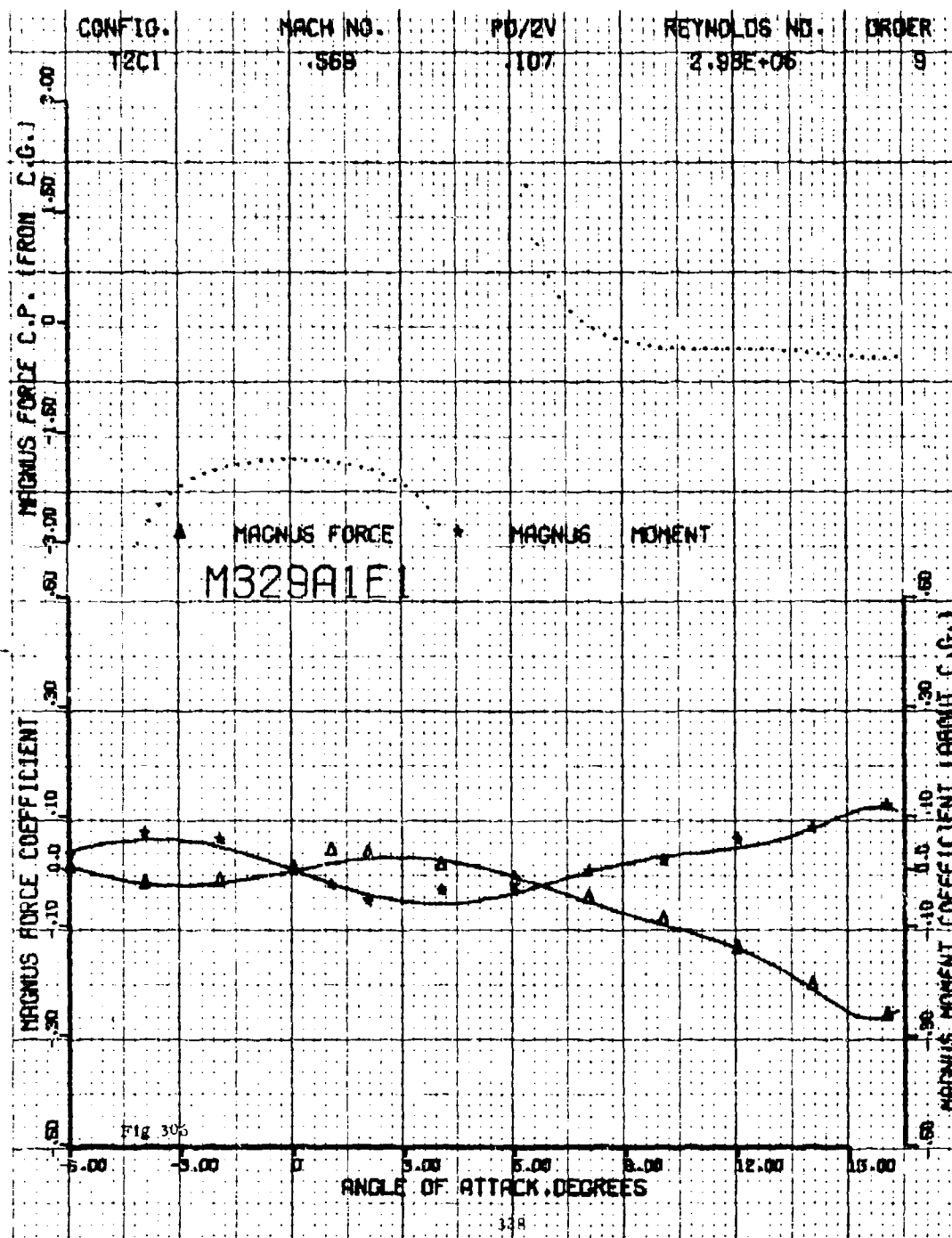
ANGLE OF ATTACK, DEGREES

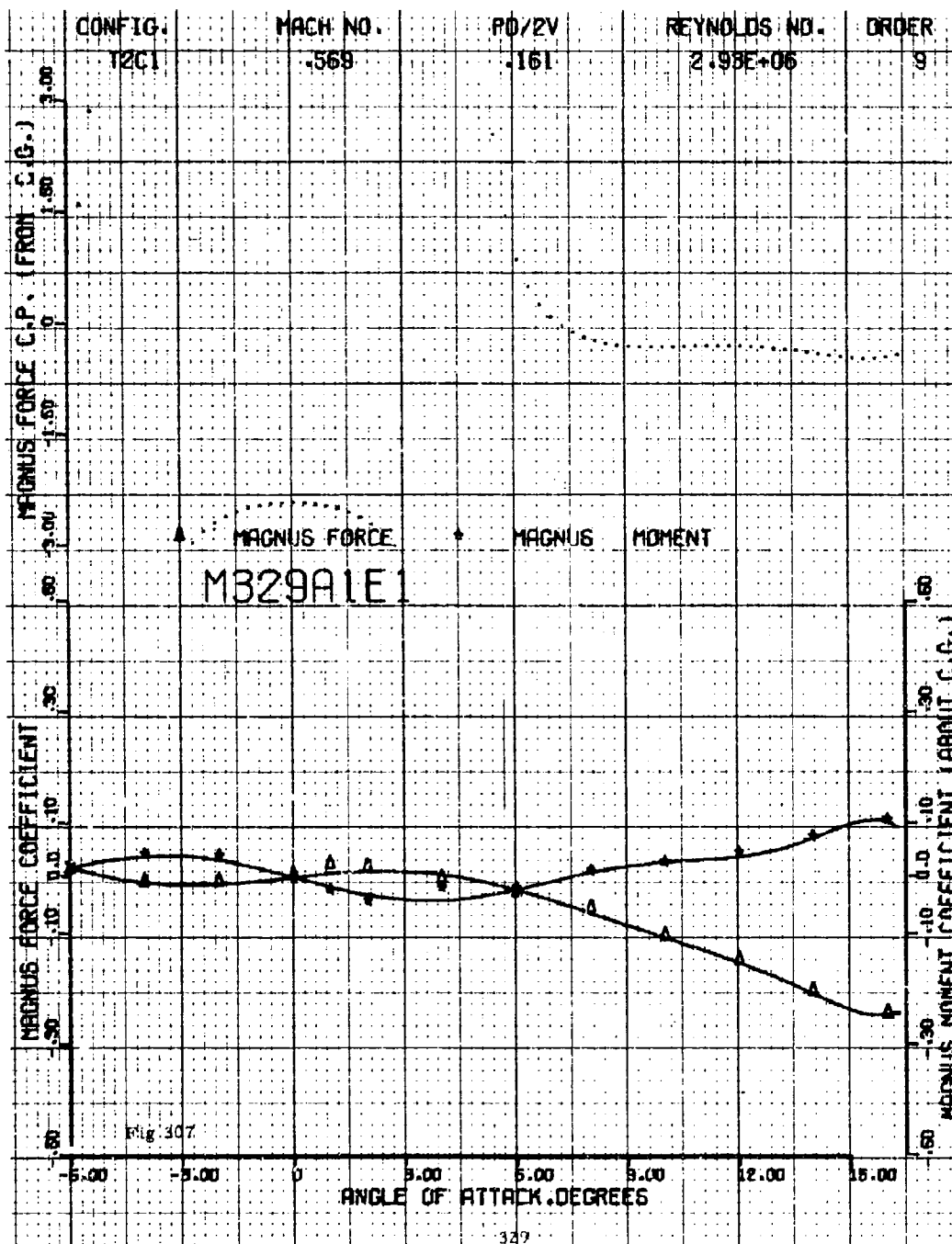
Fig 303

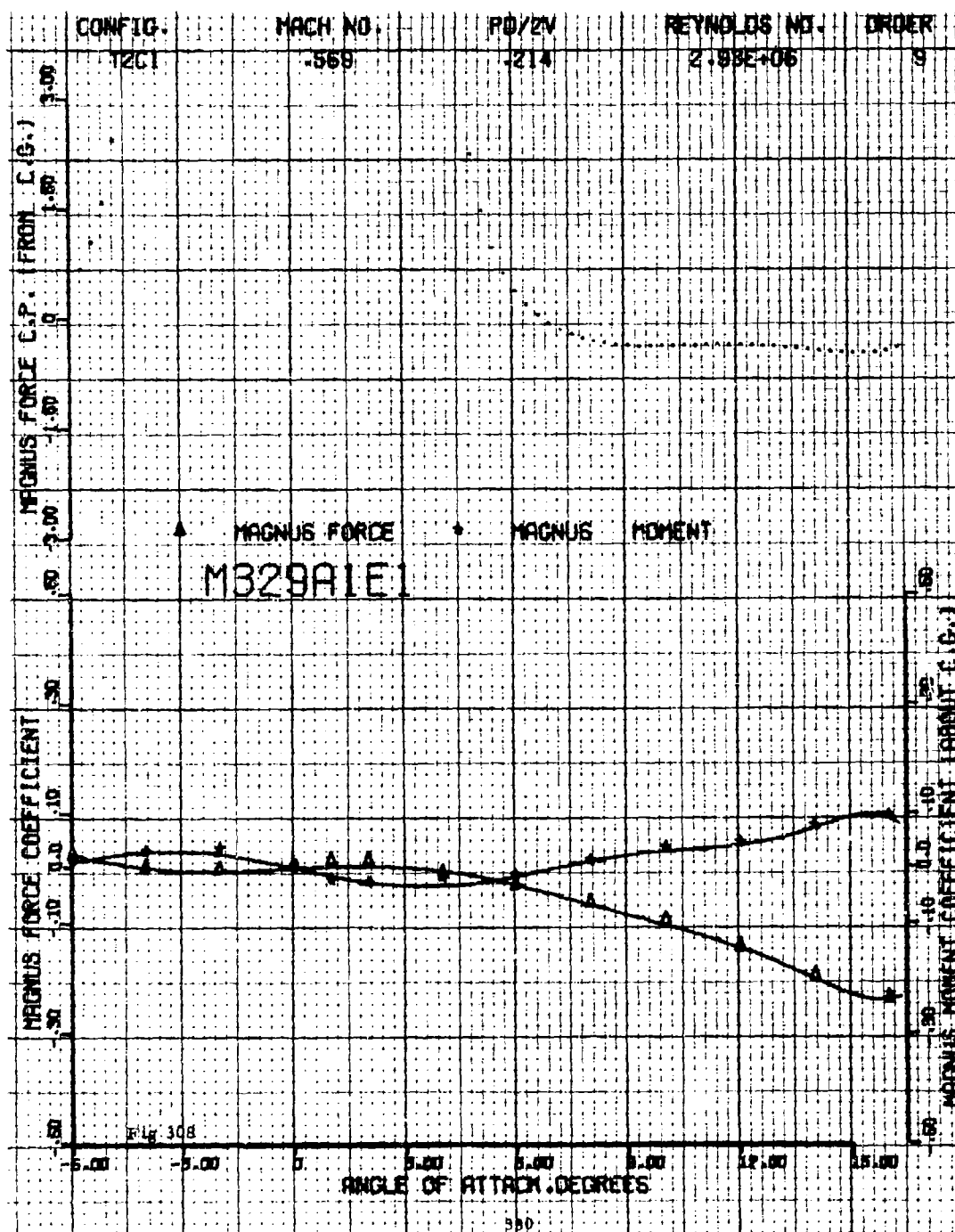
325

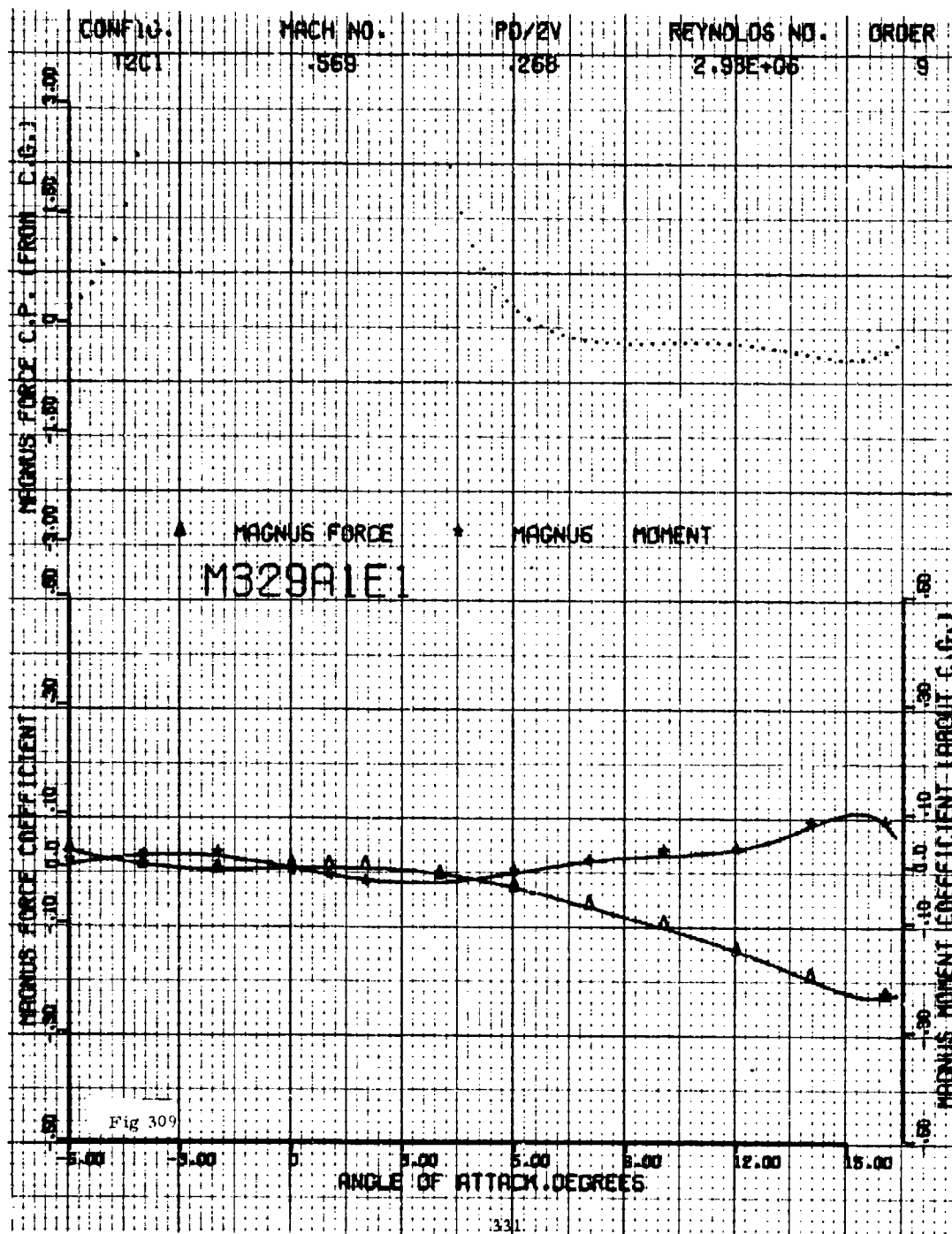


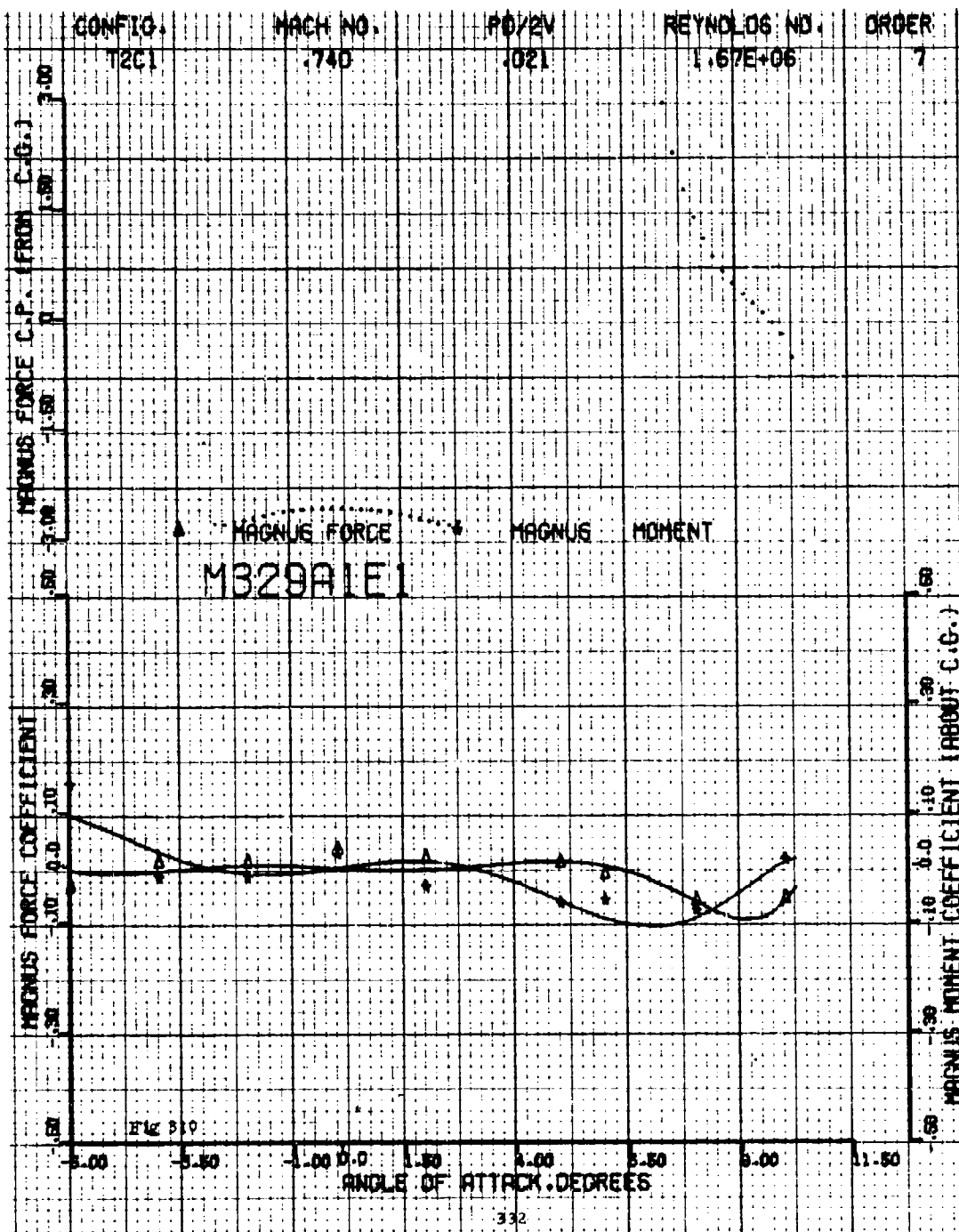


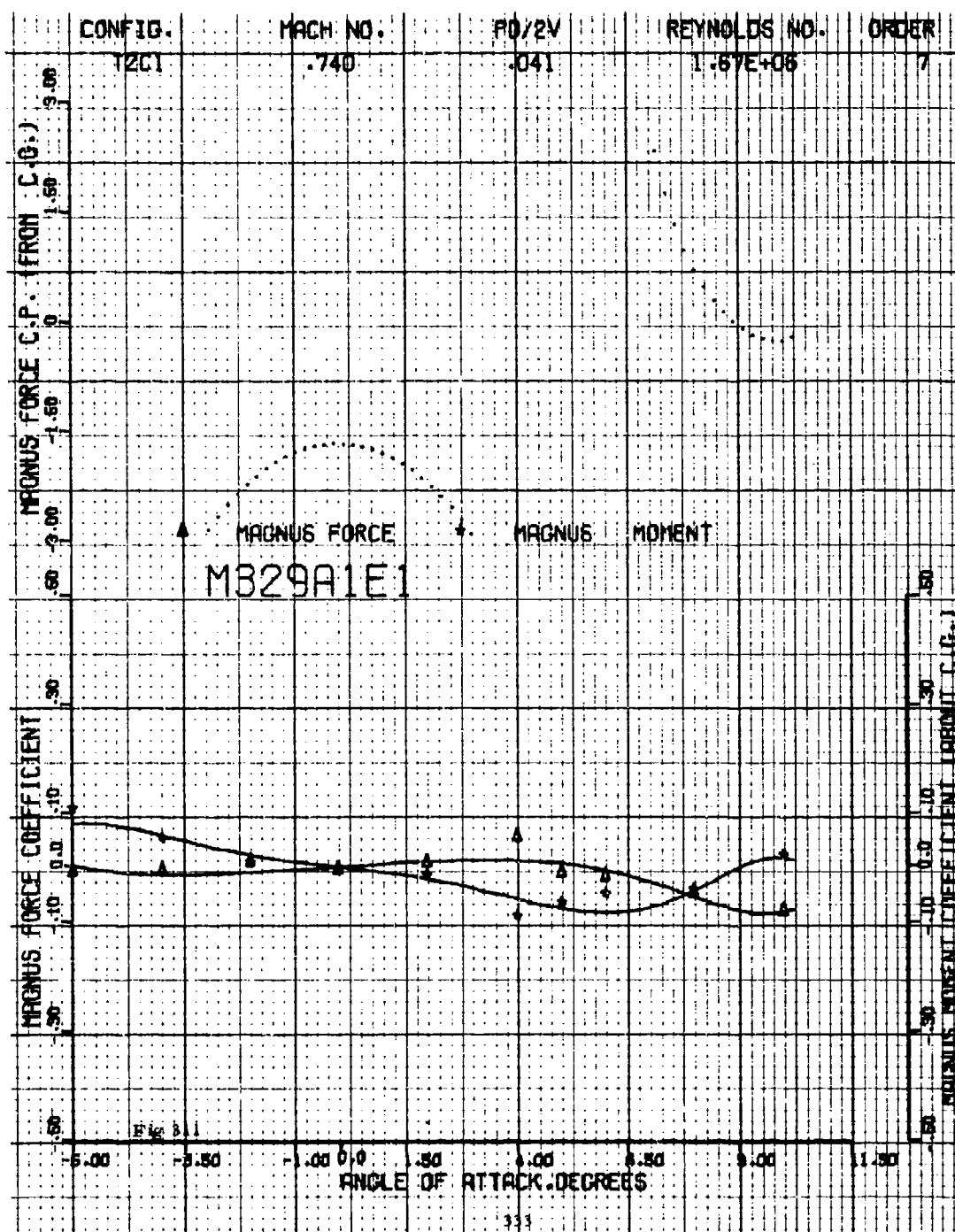


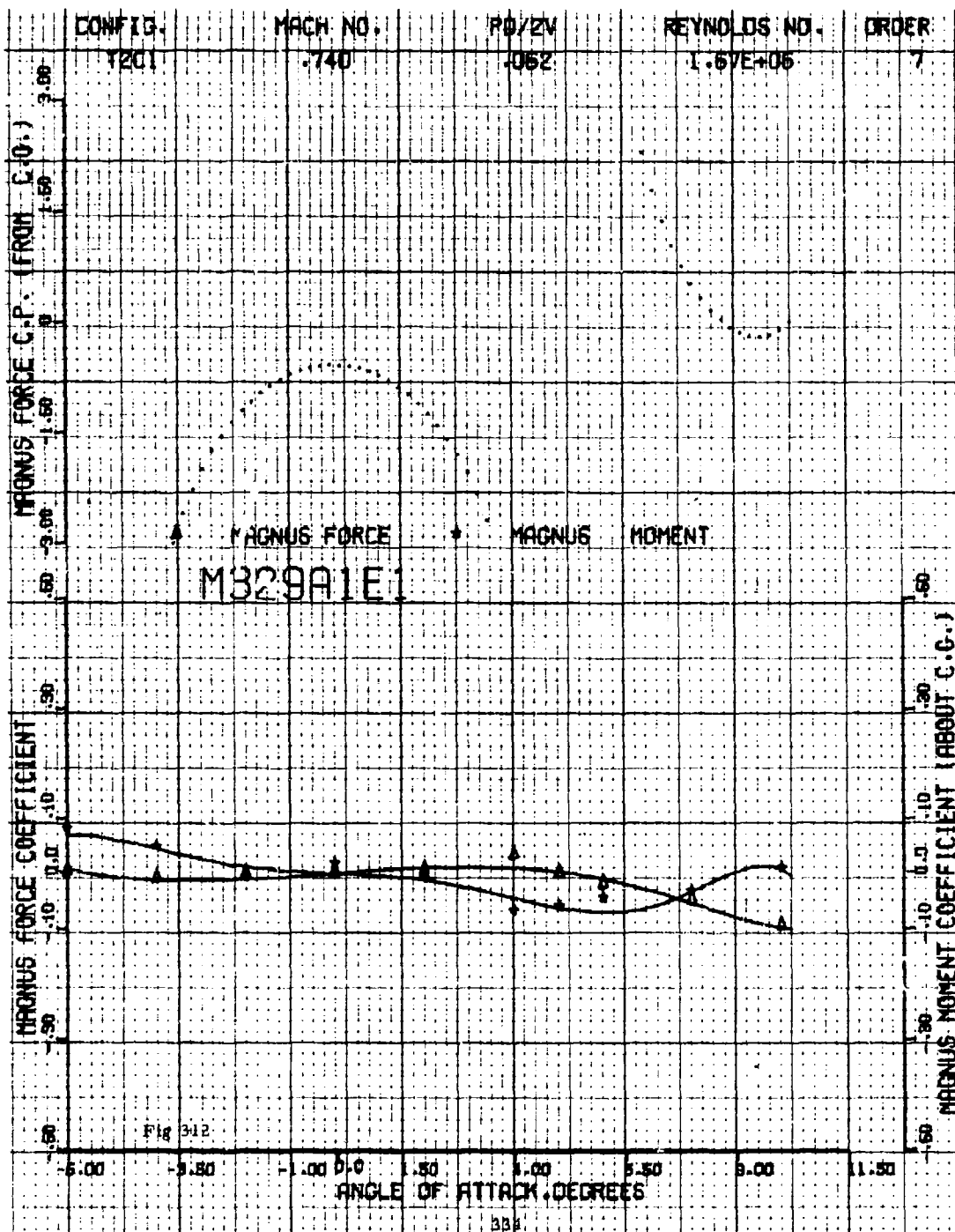


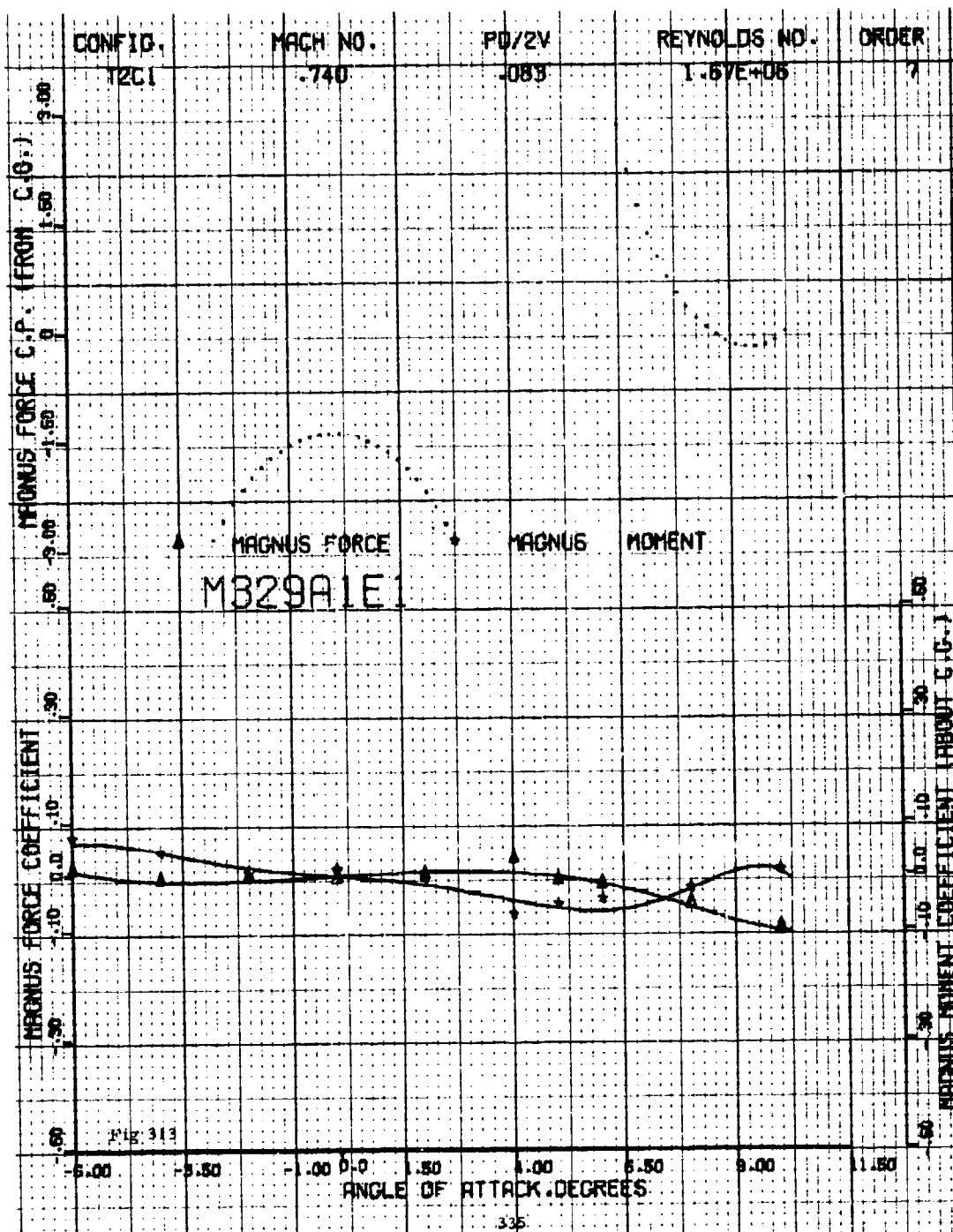


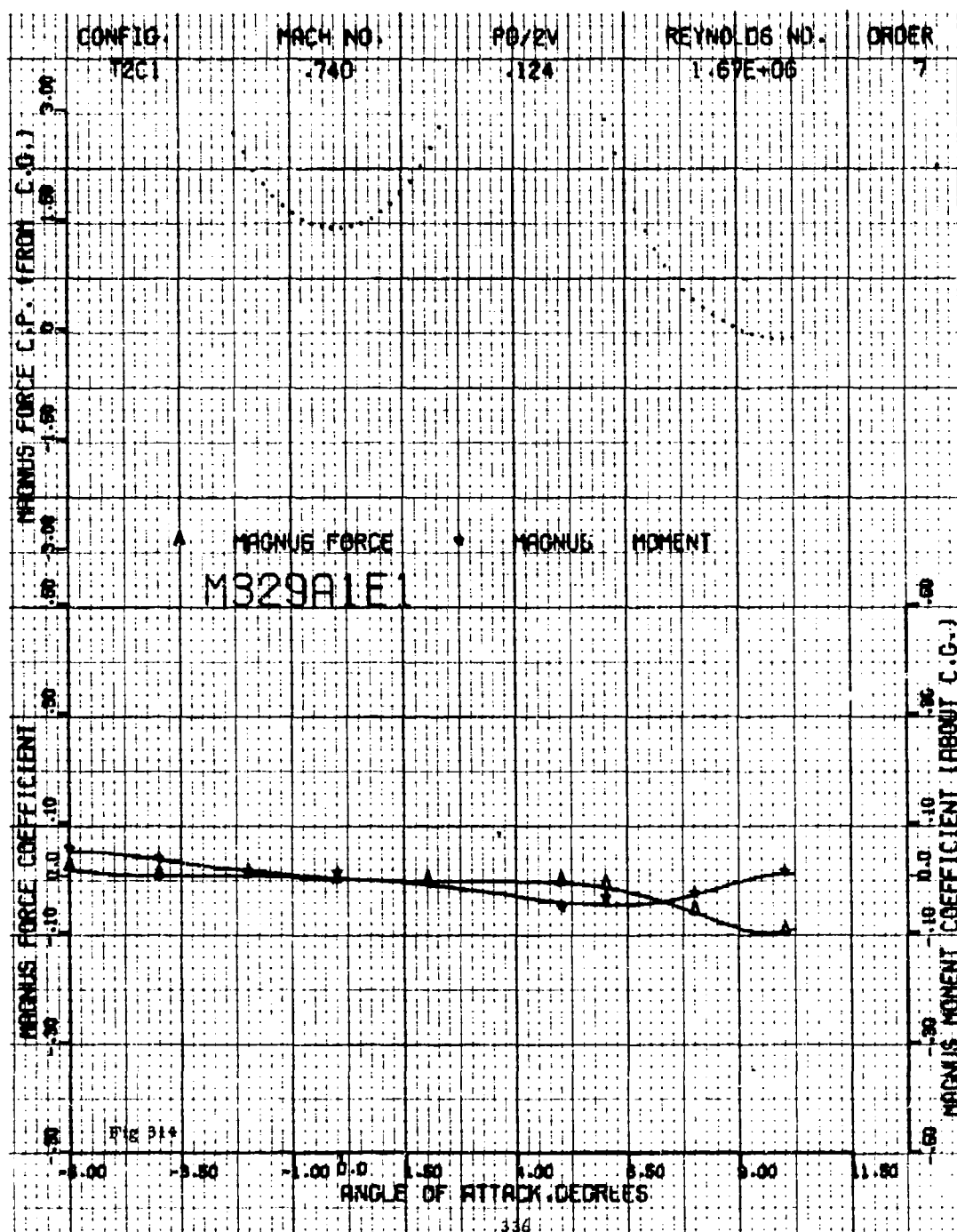


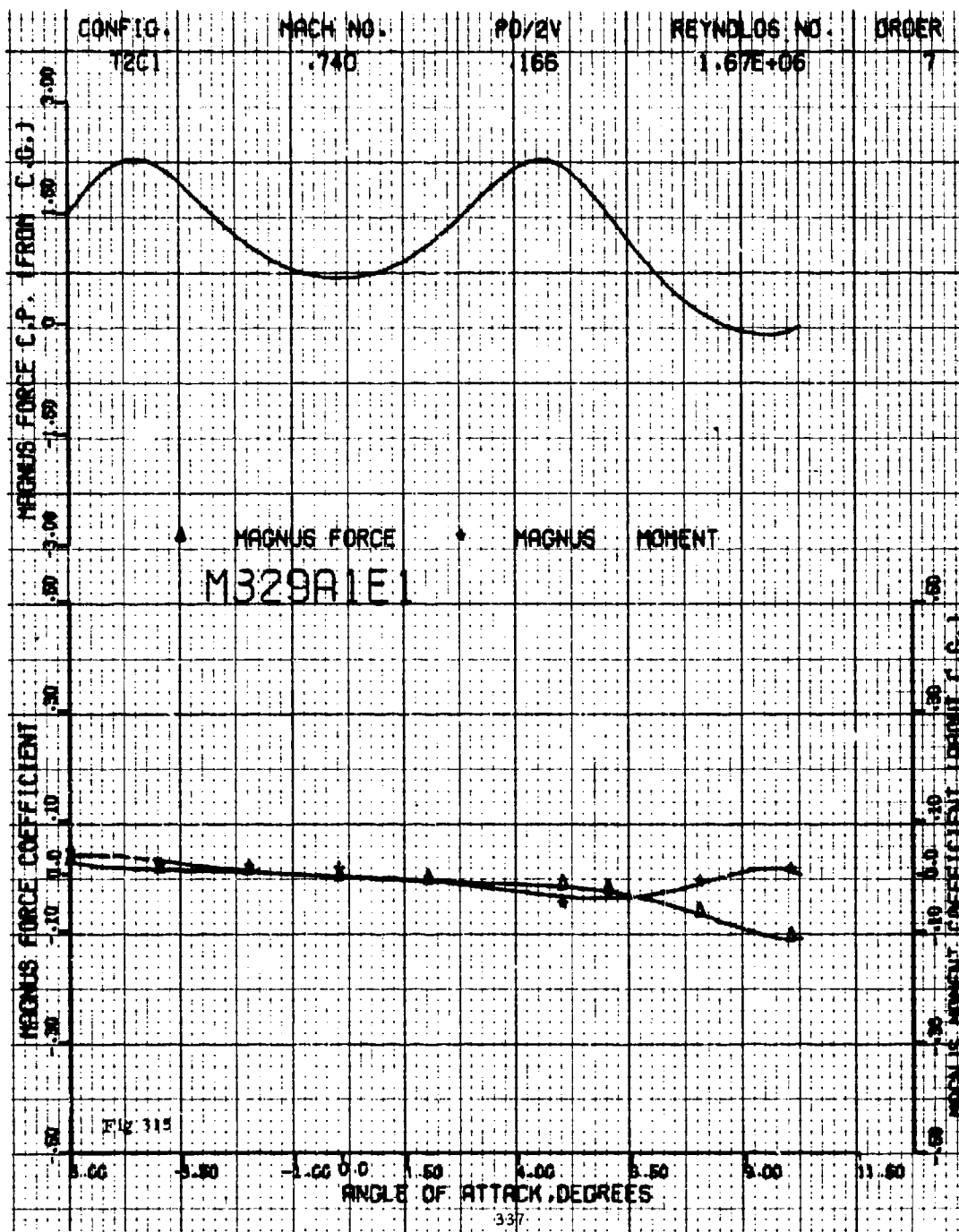


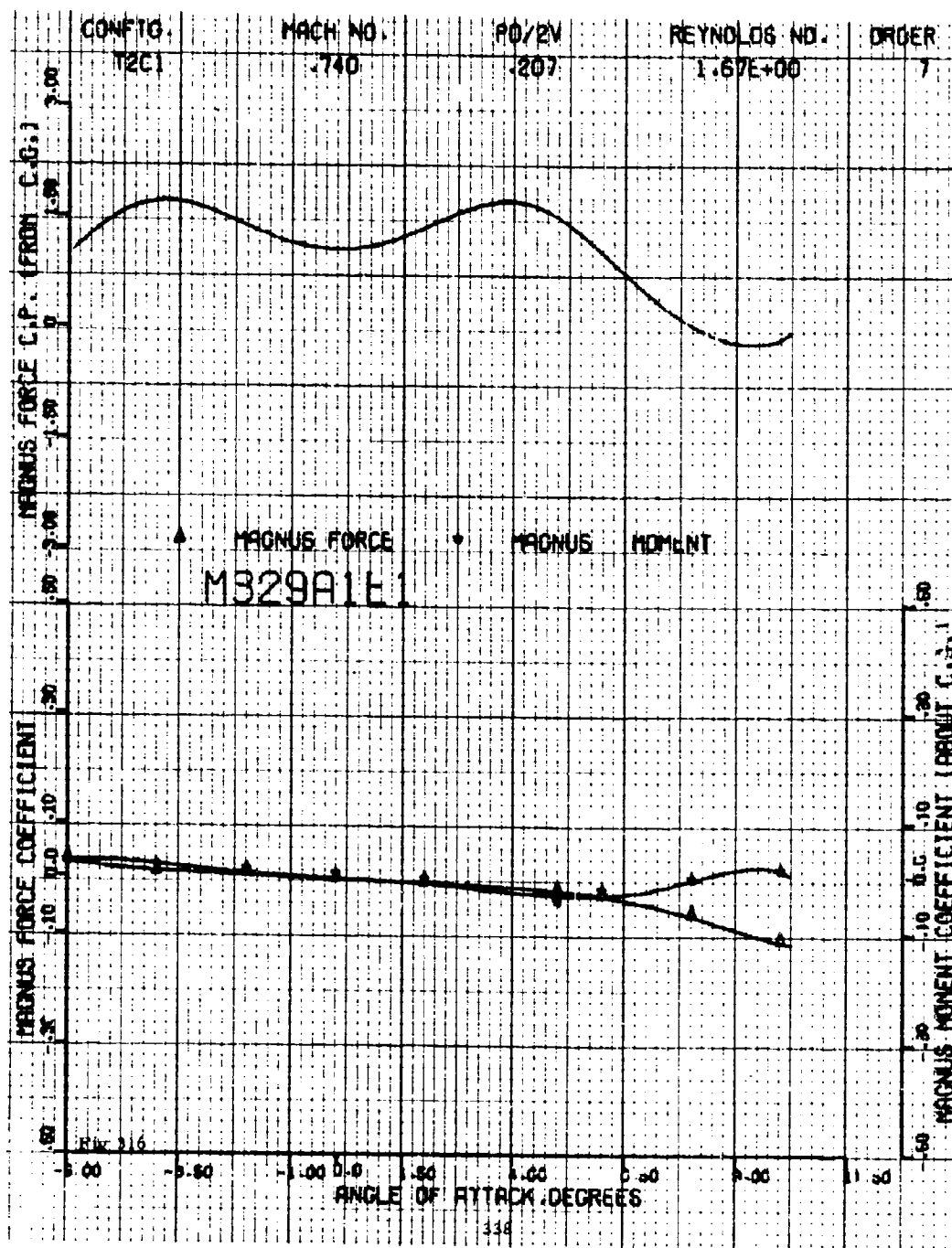


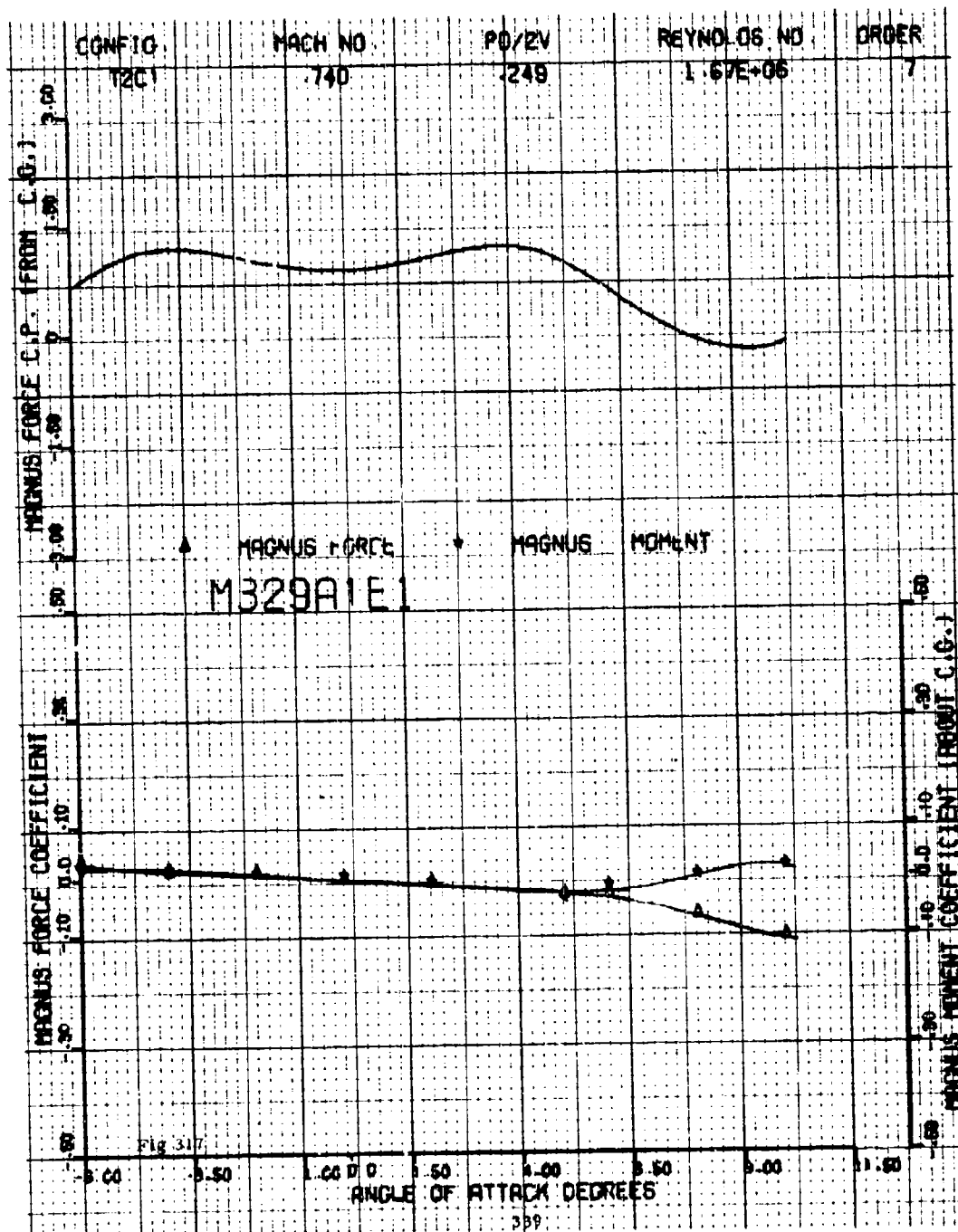


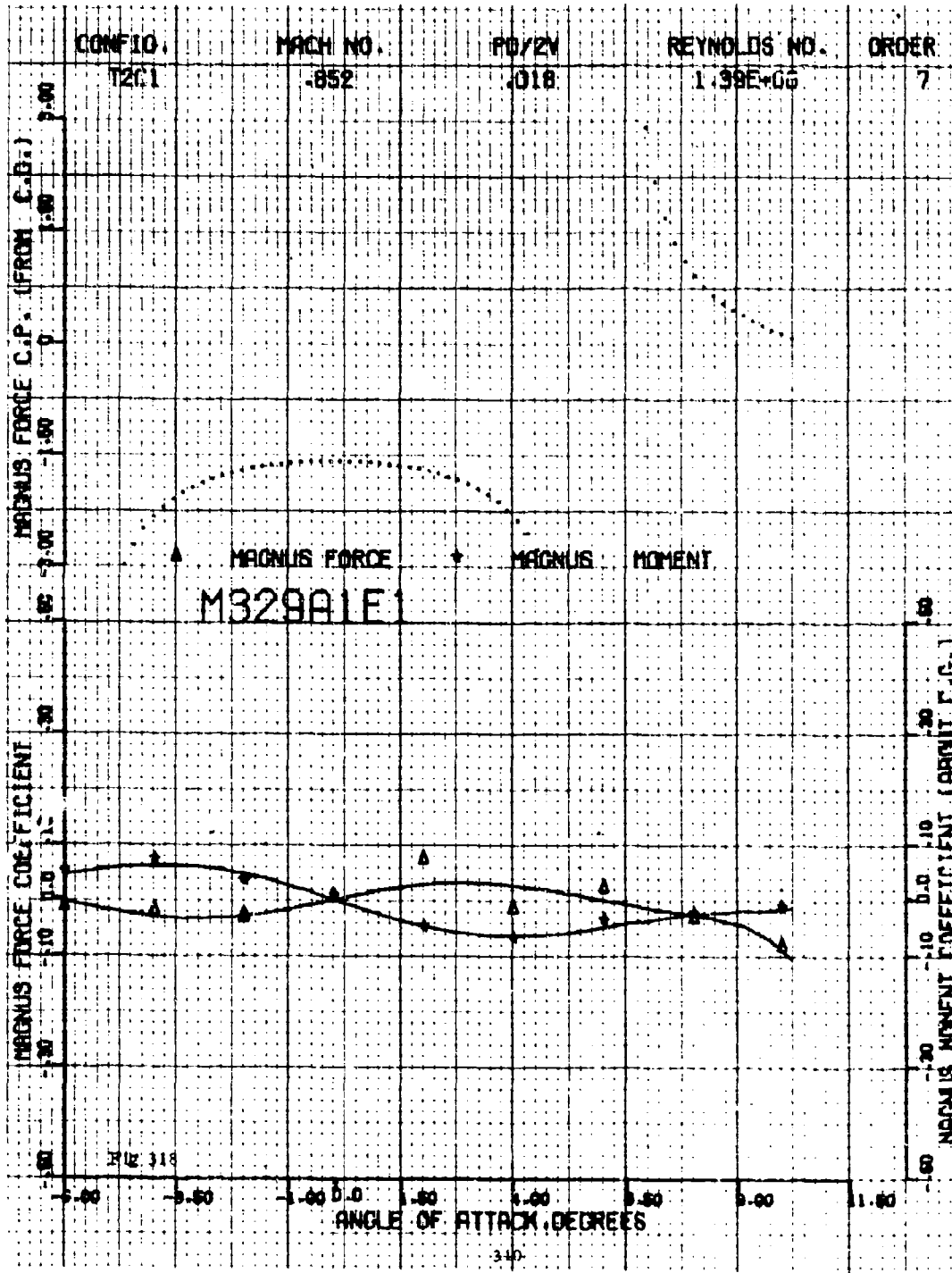


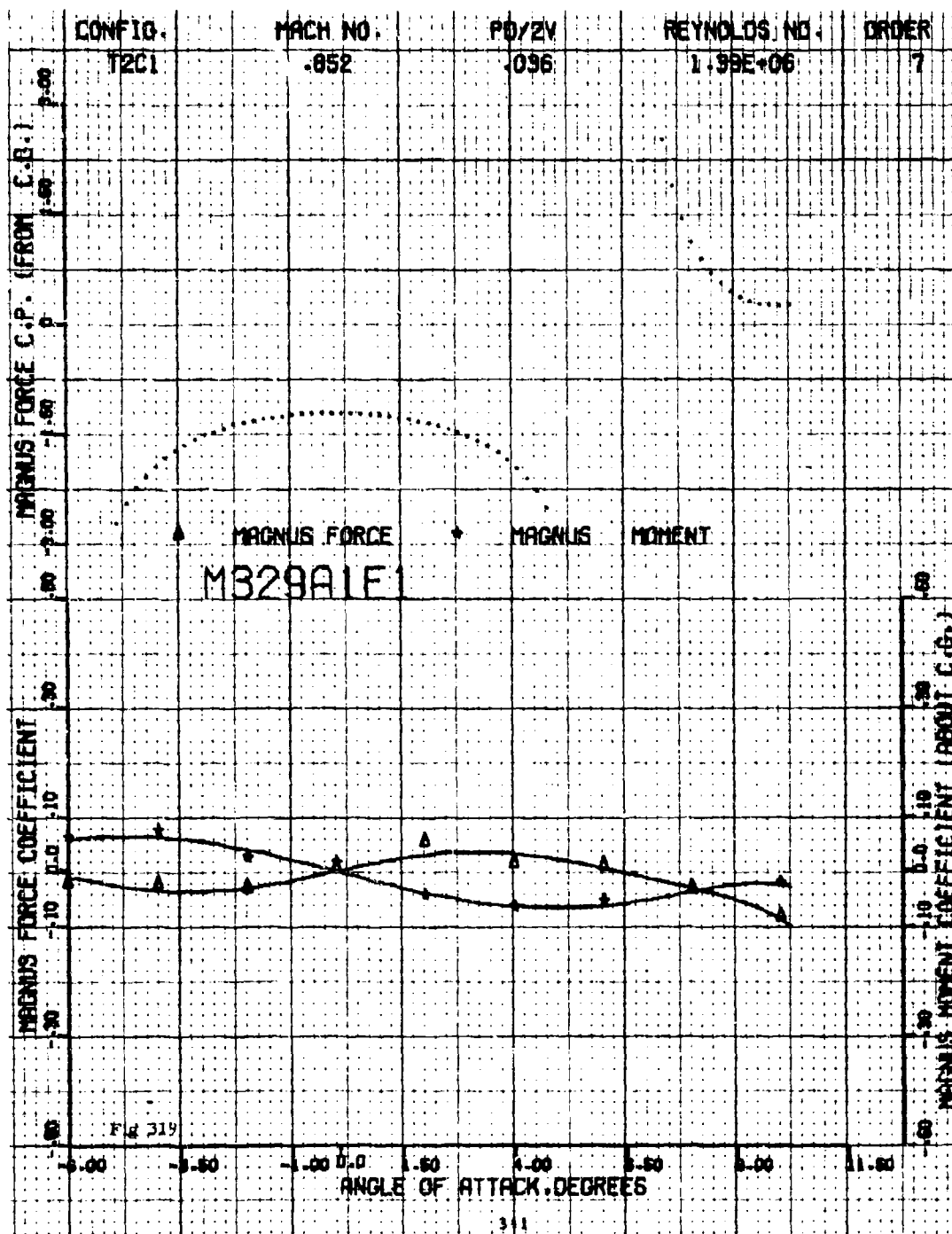


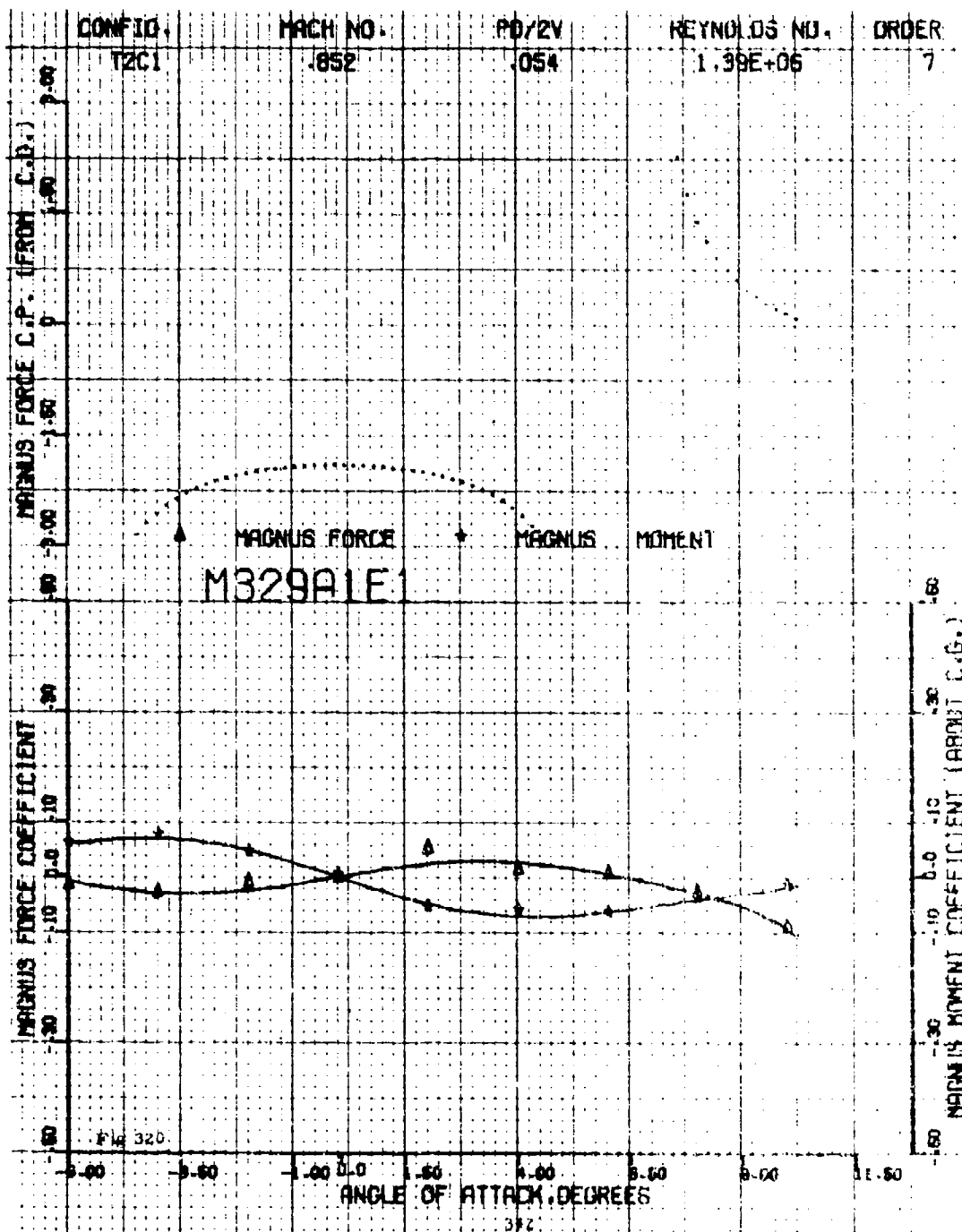


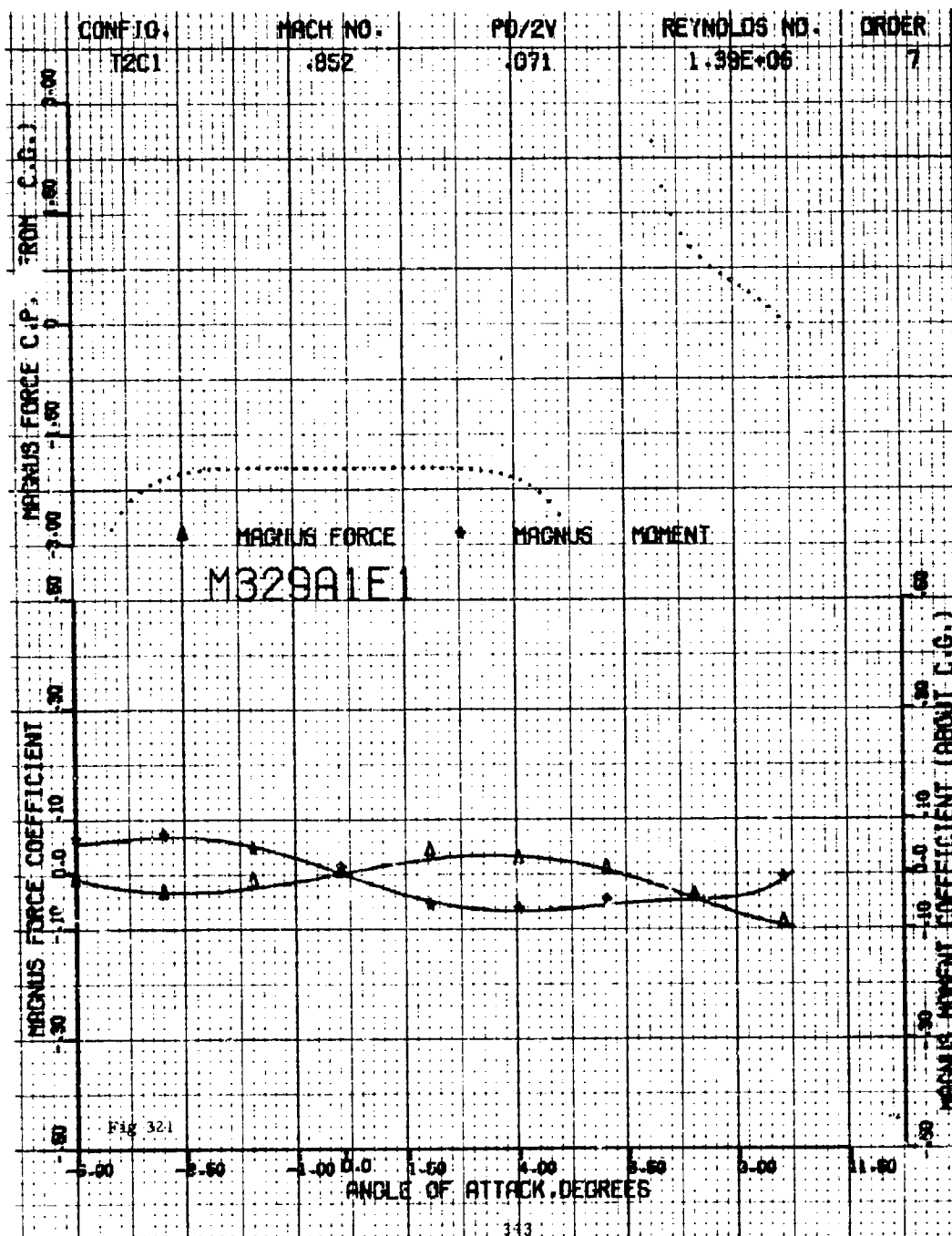


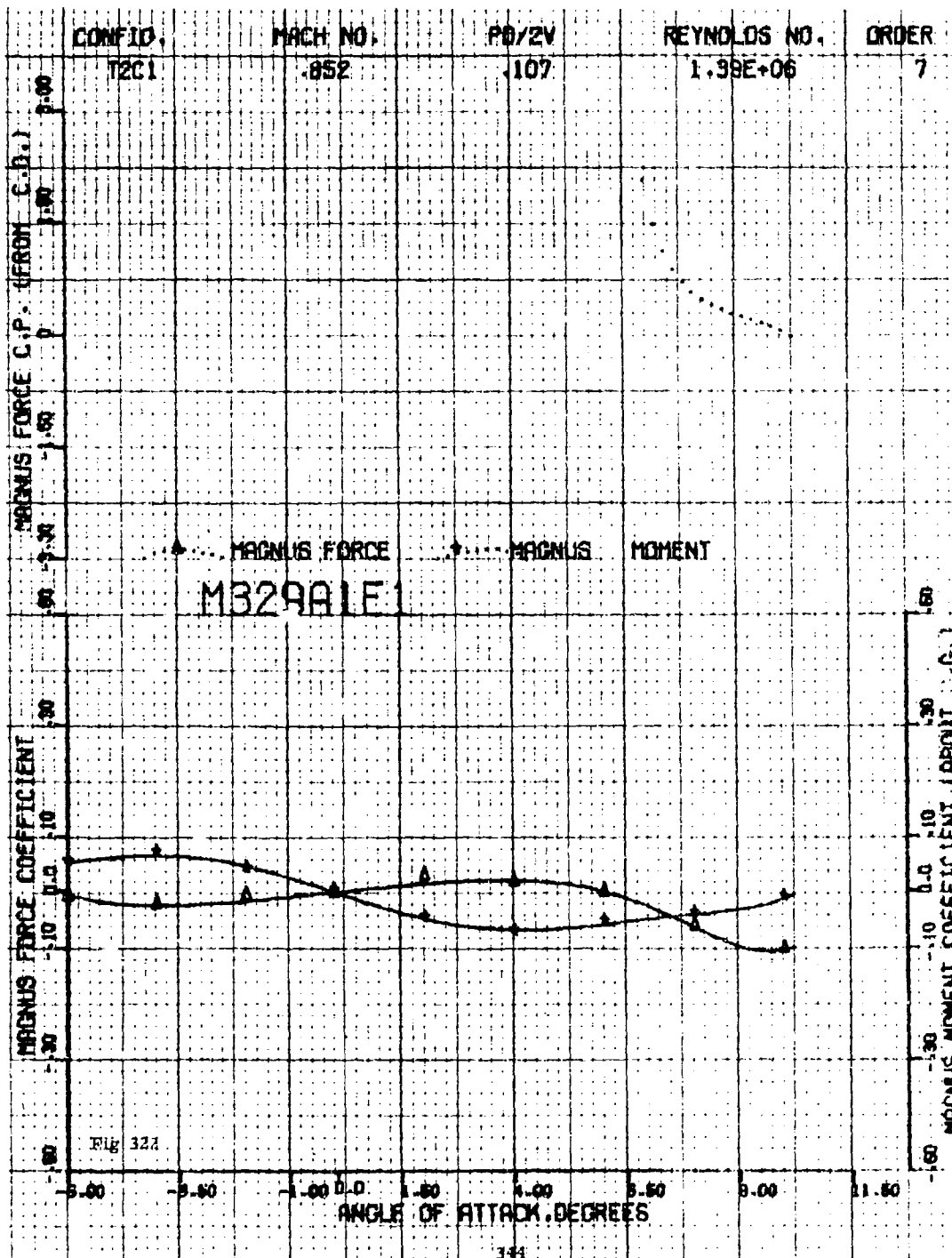


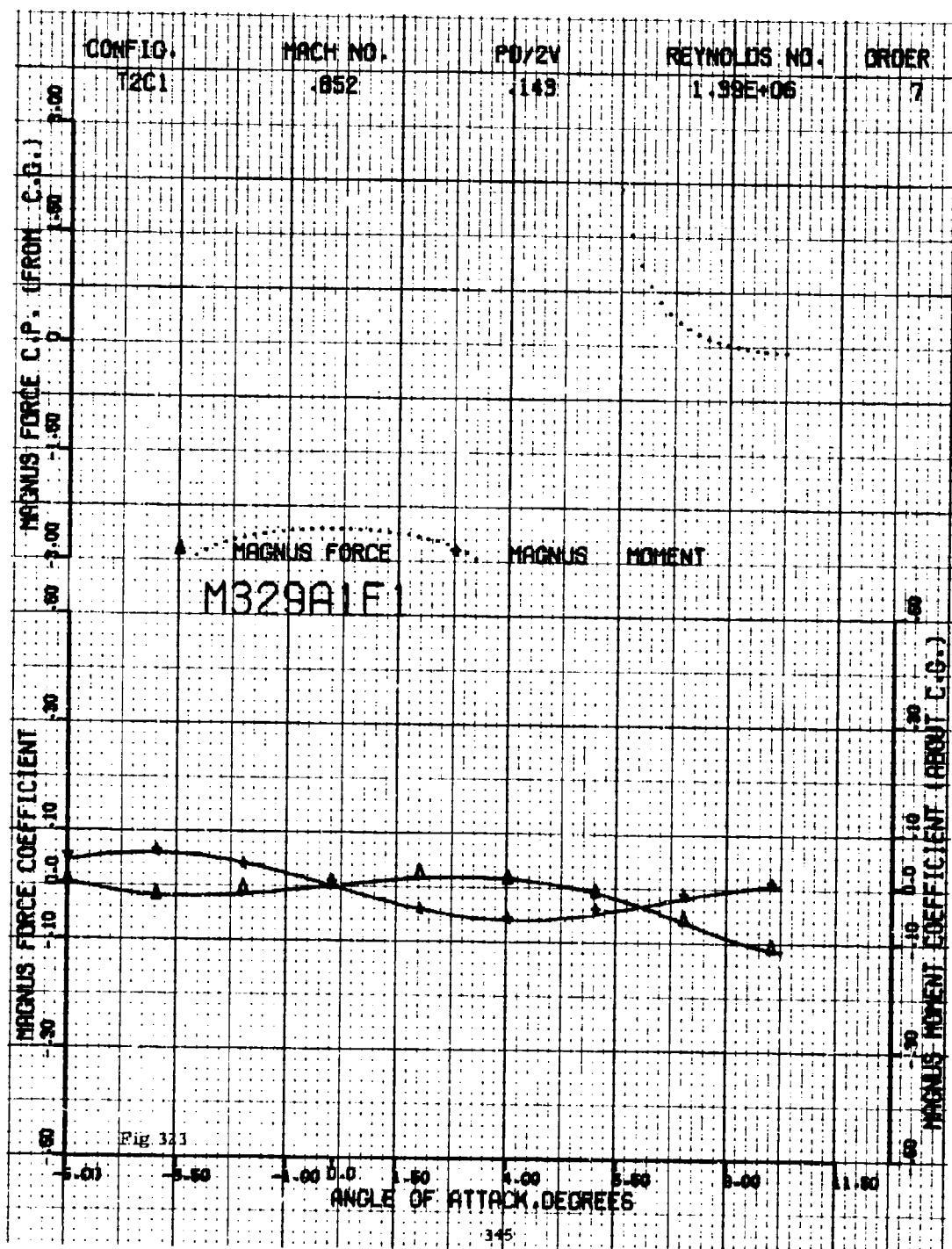


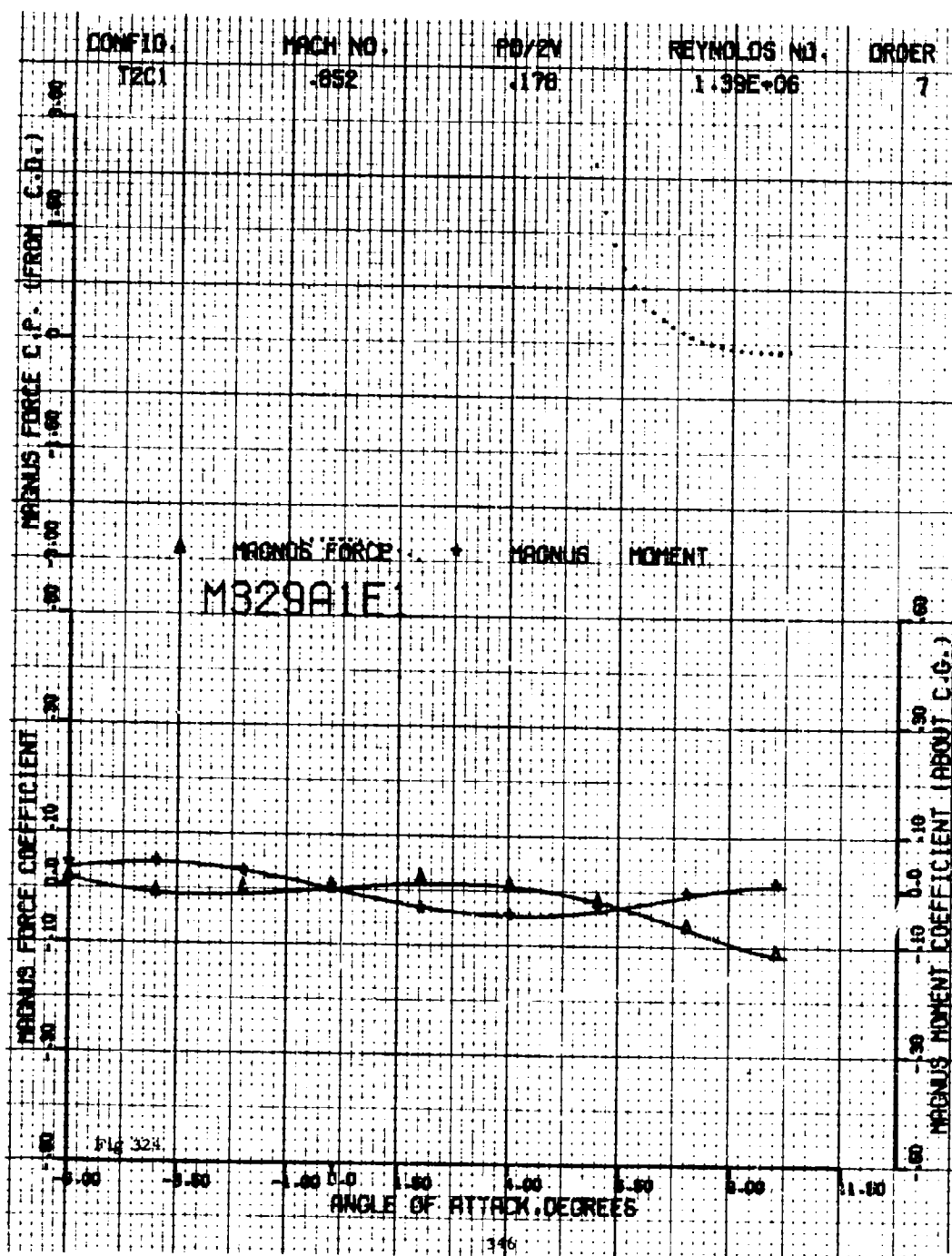


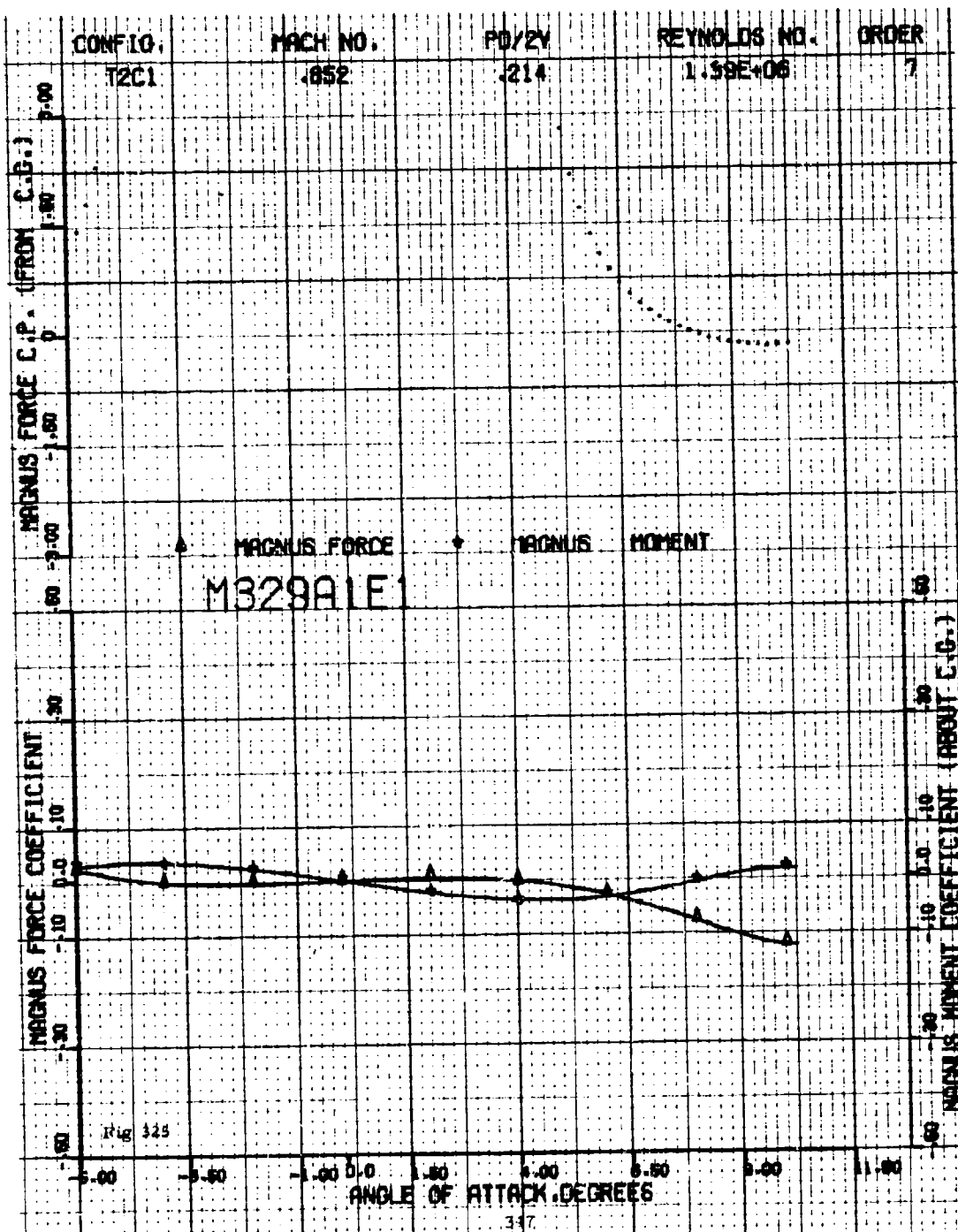


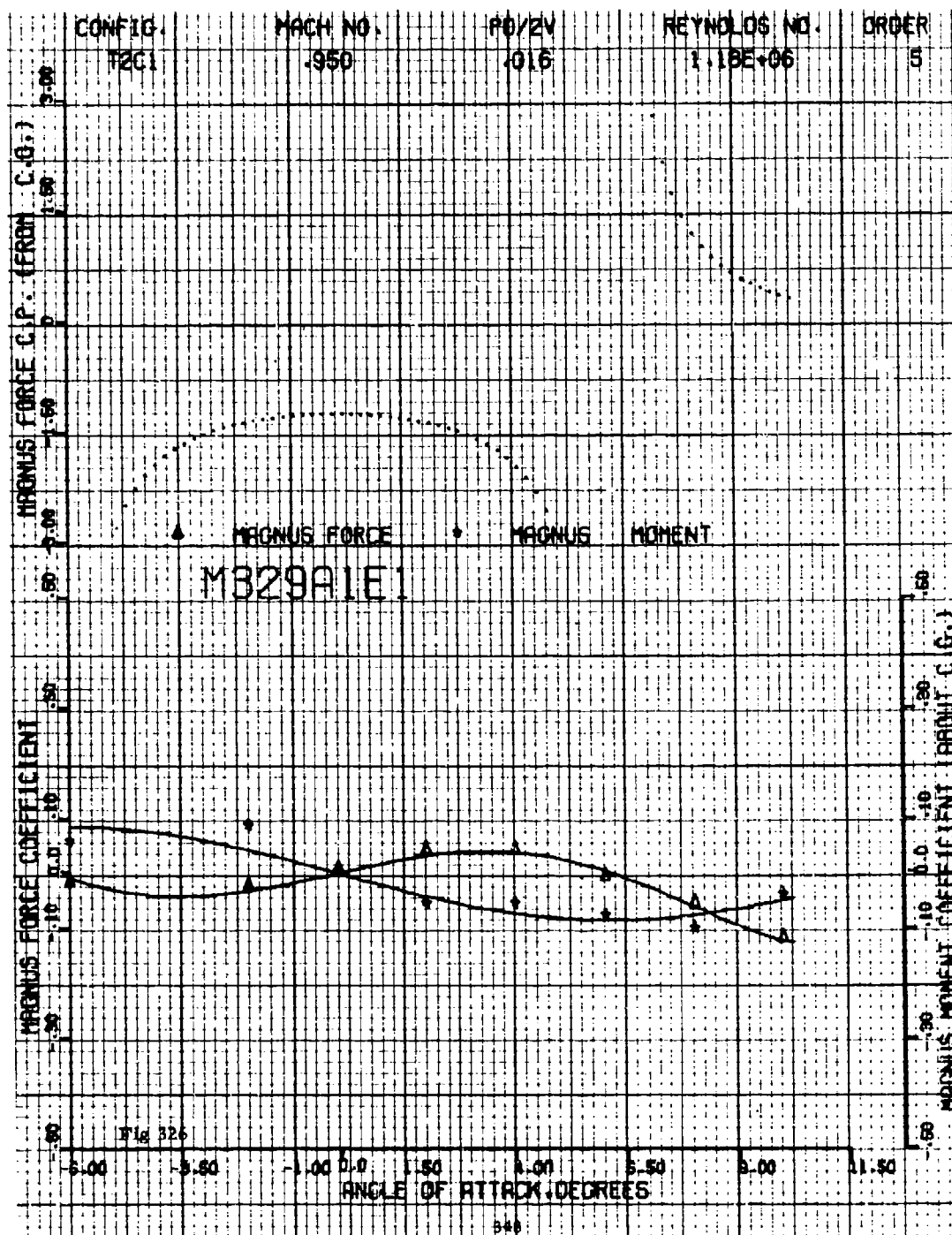


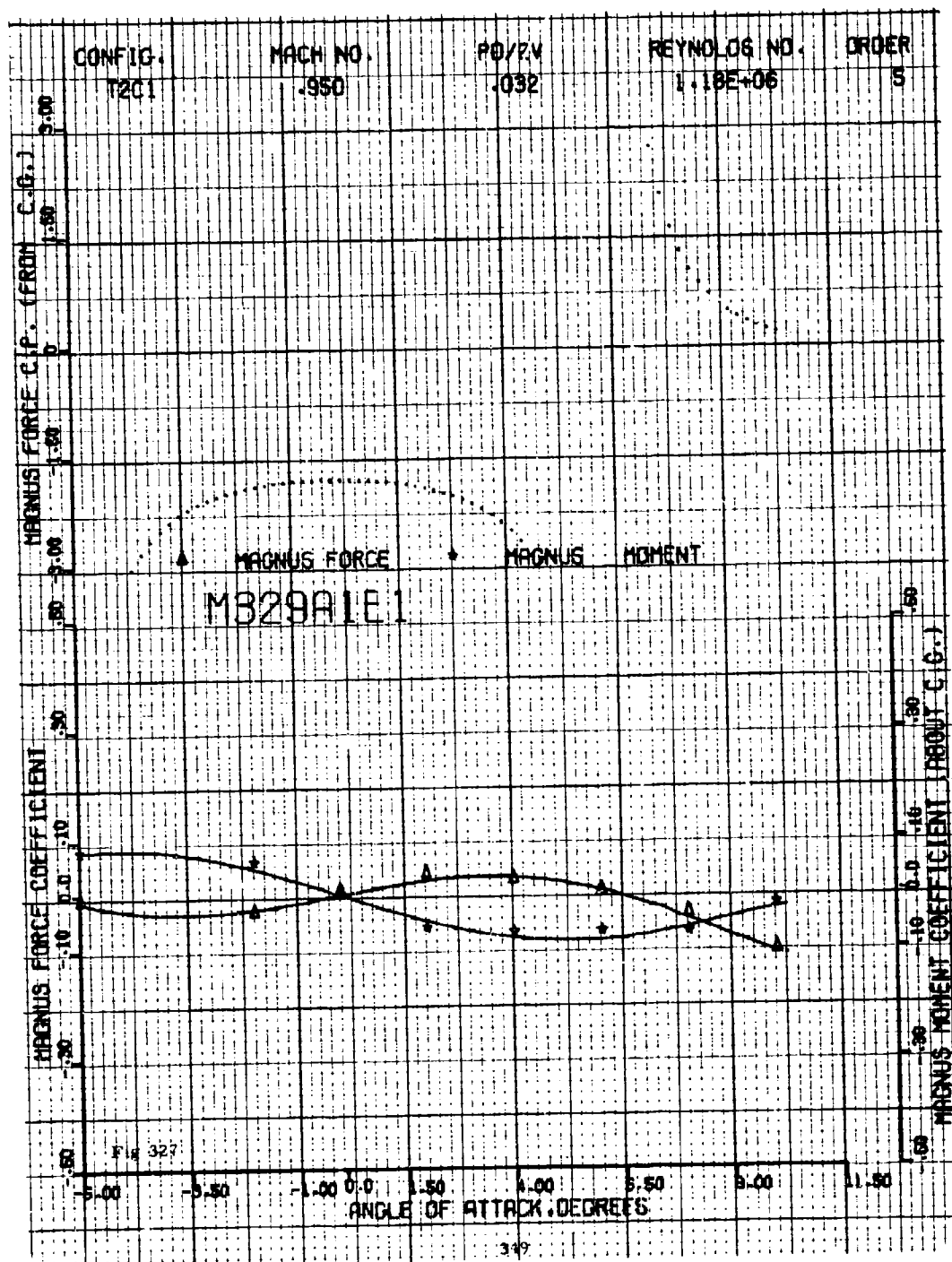


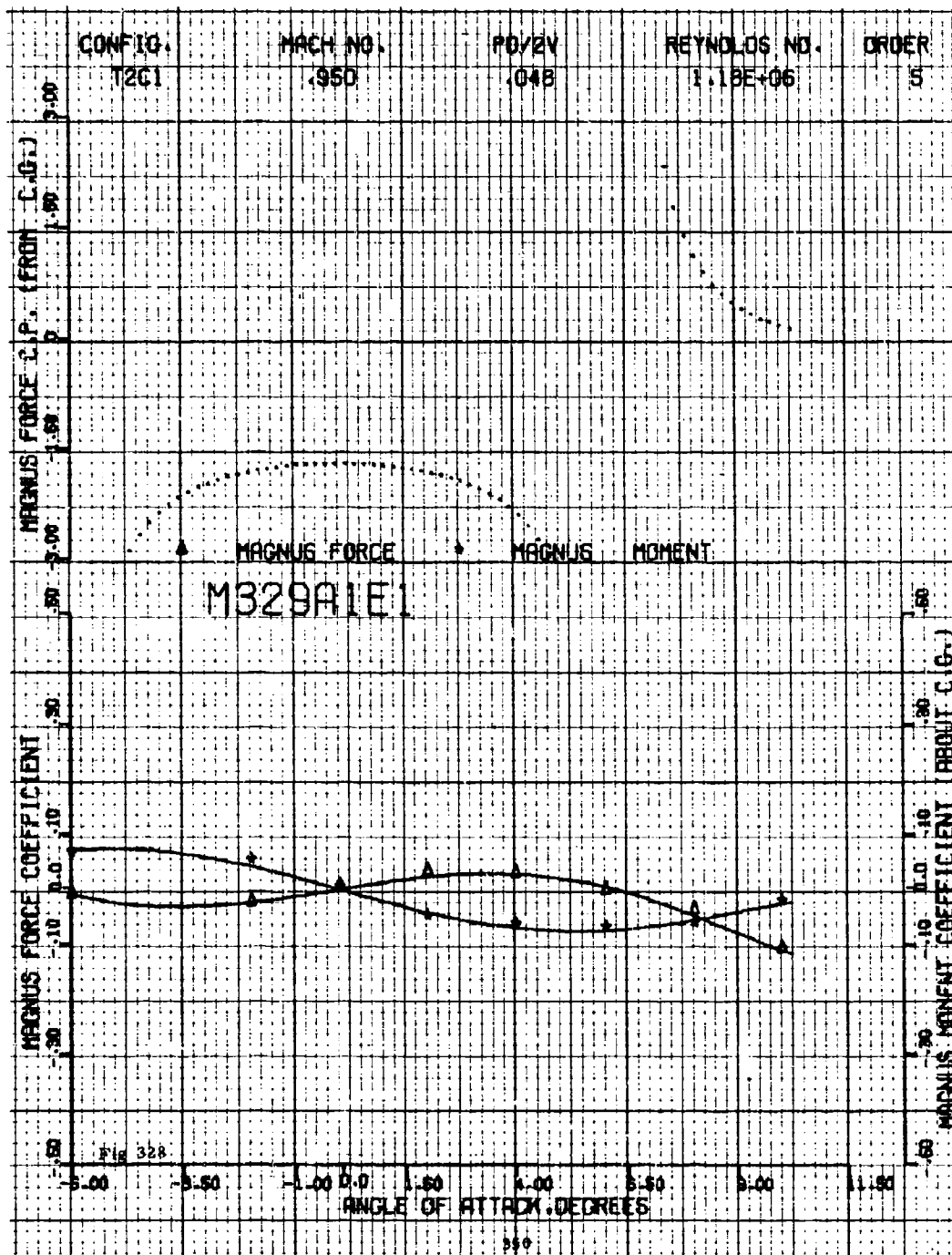


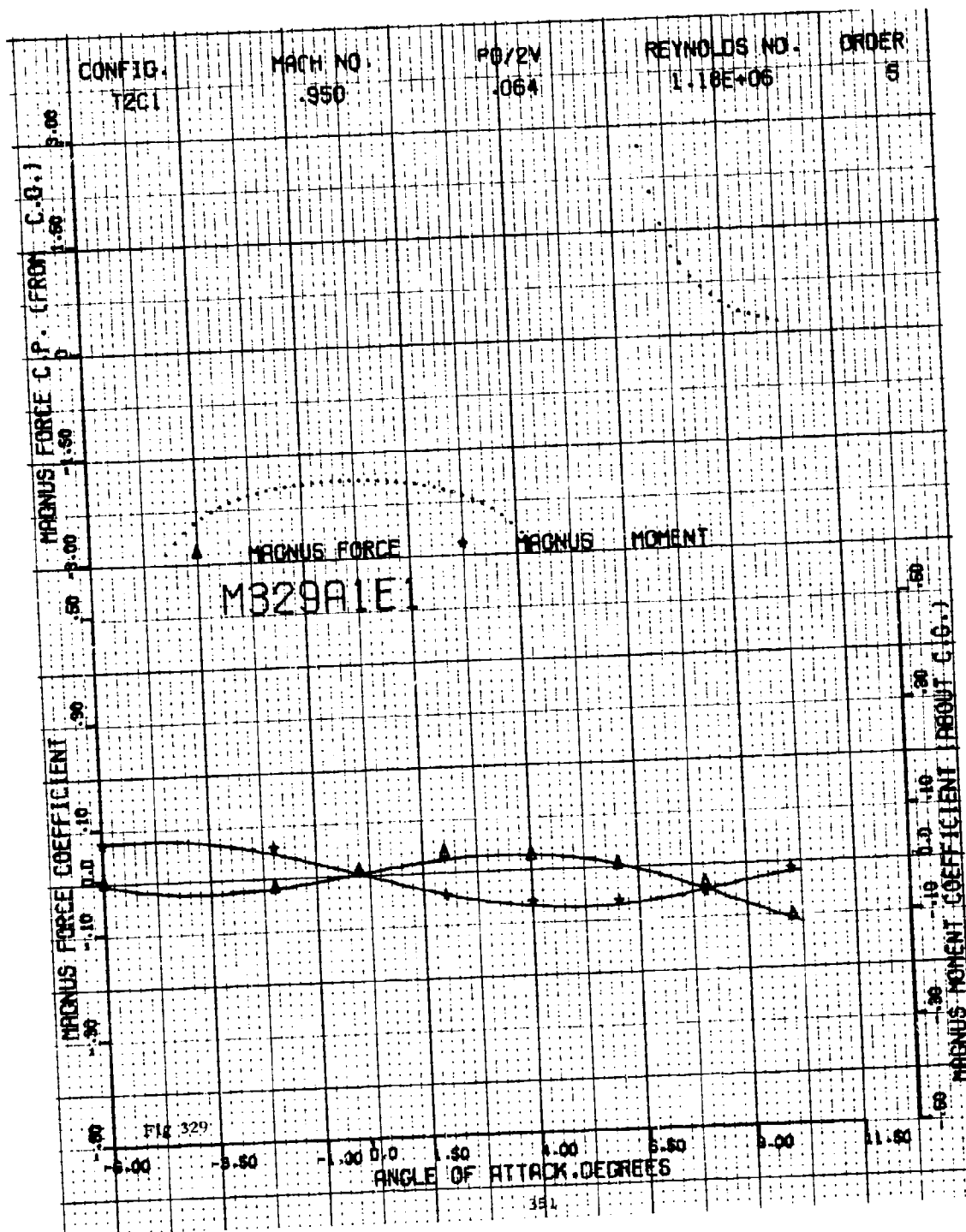


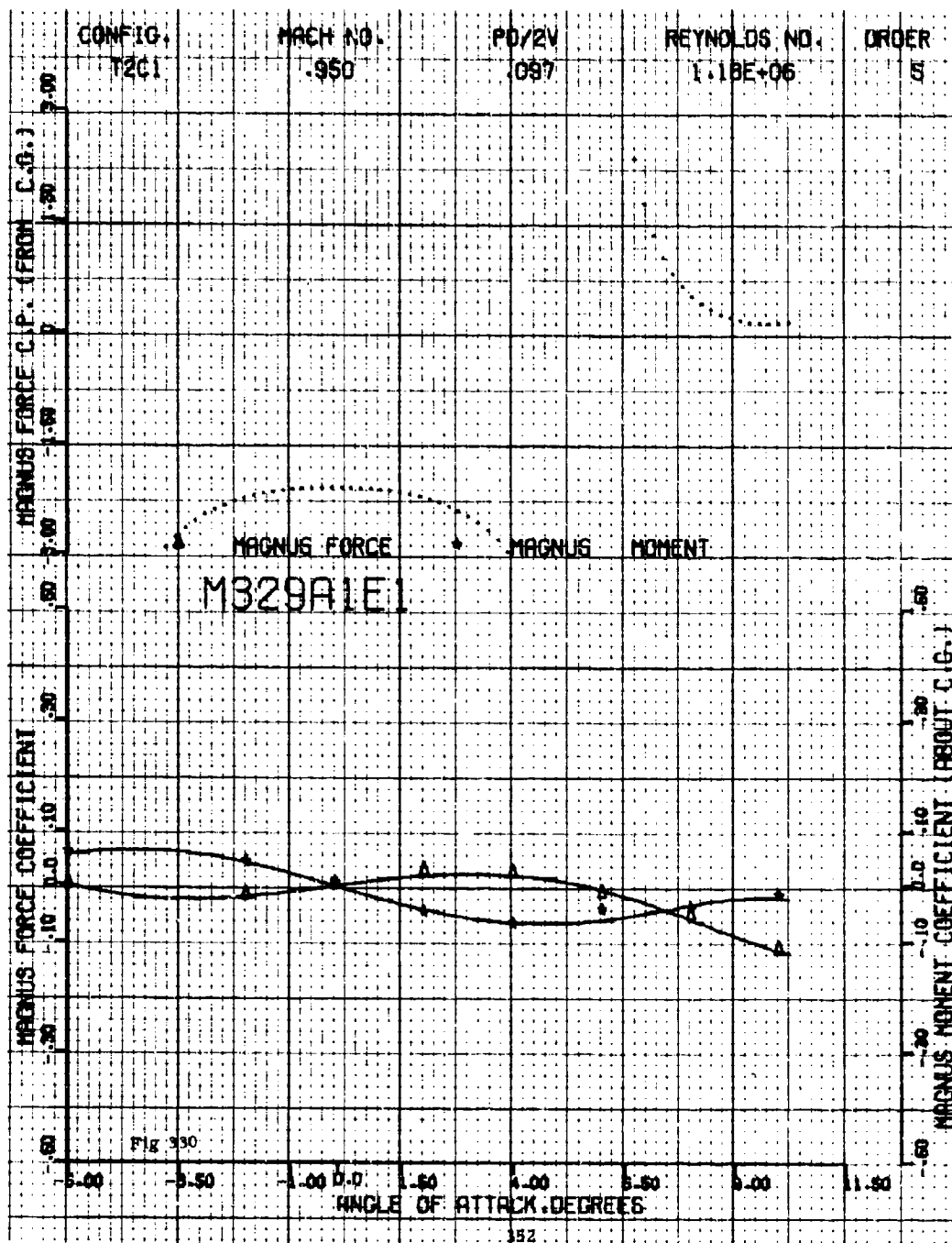












ORDER
5

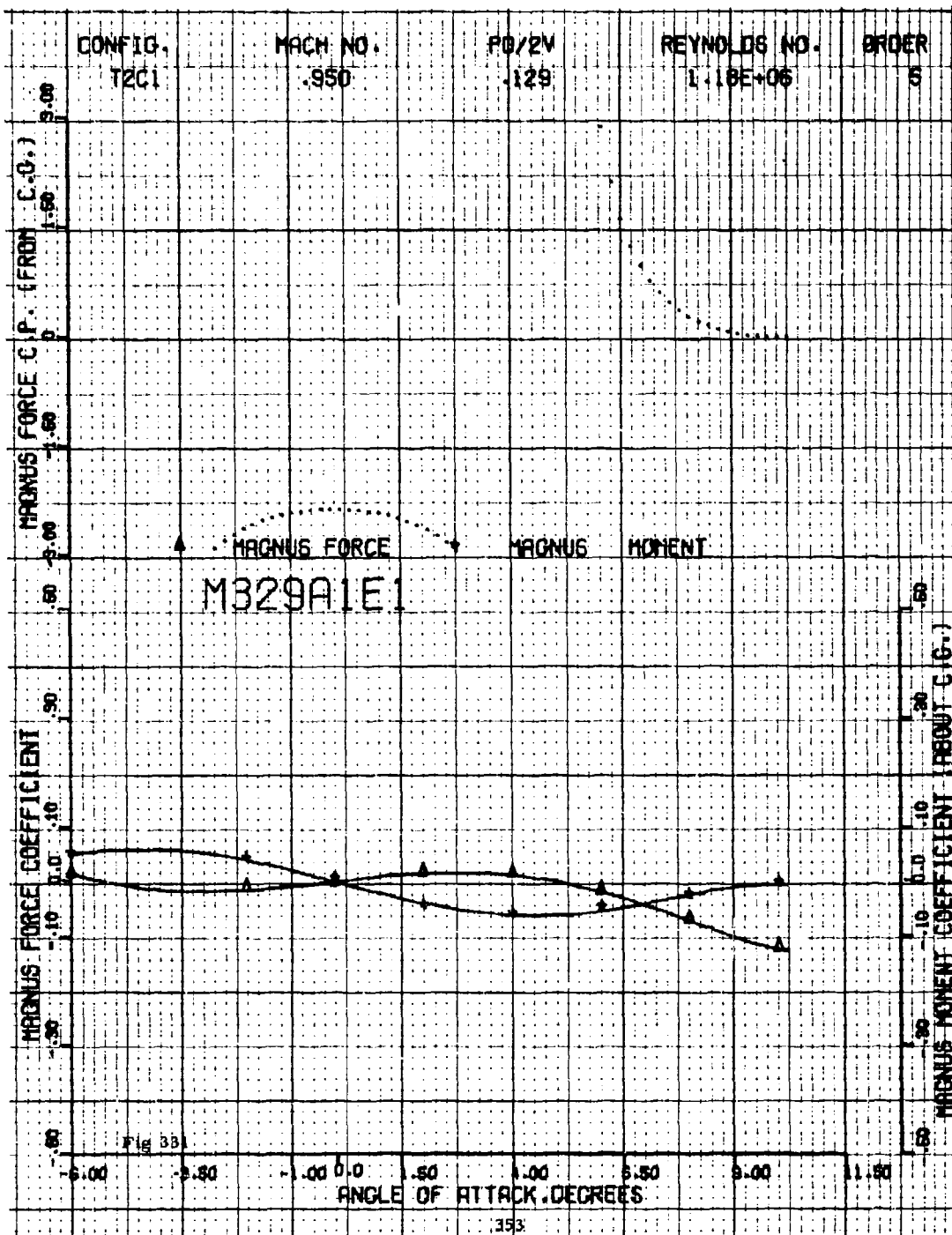
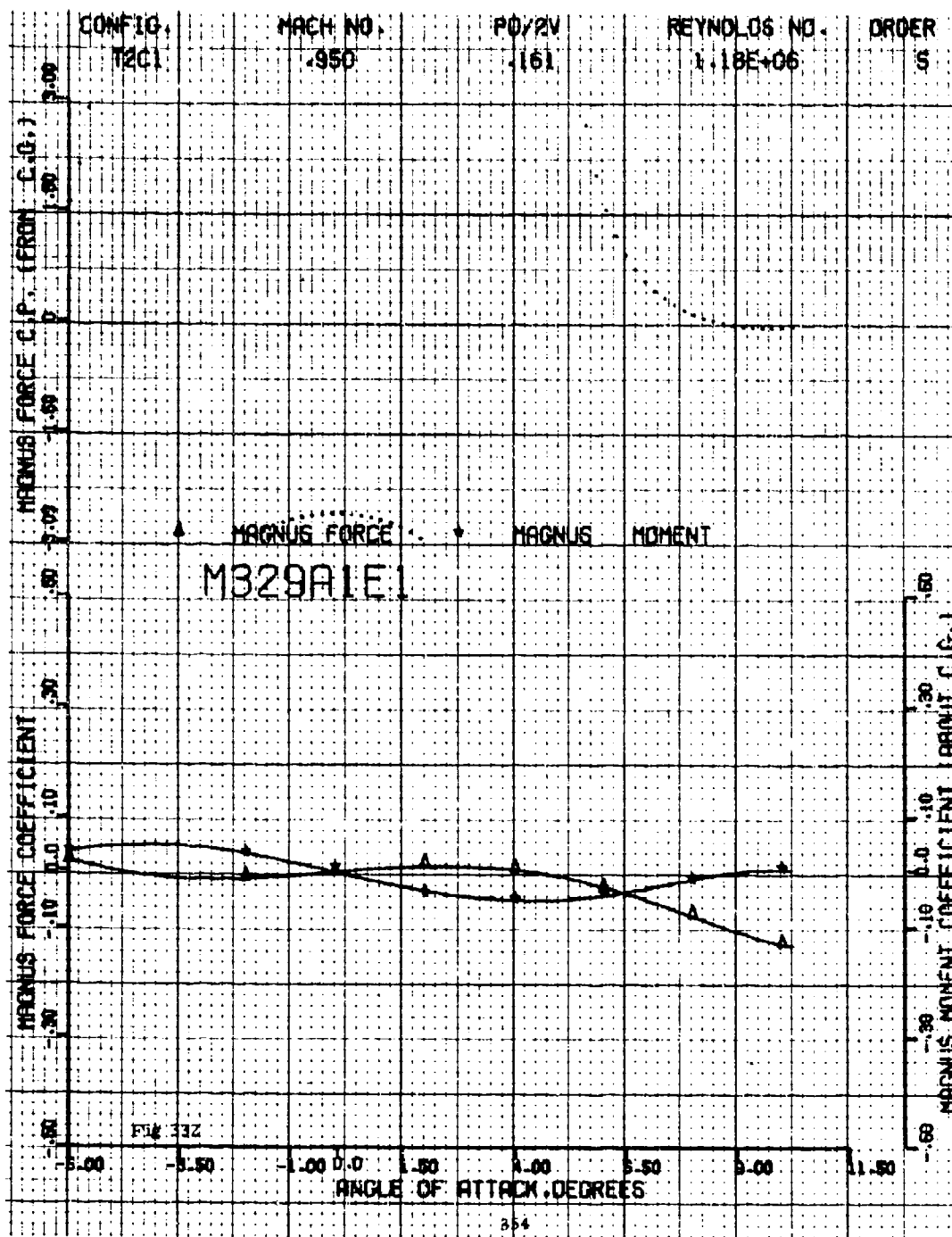
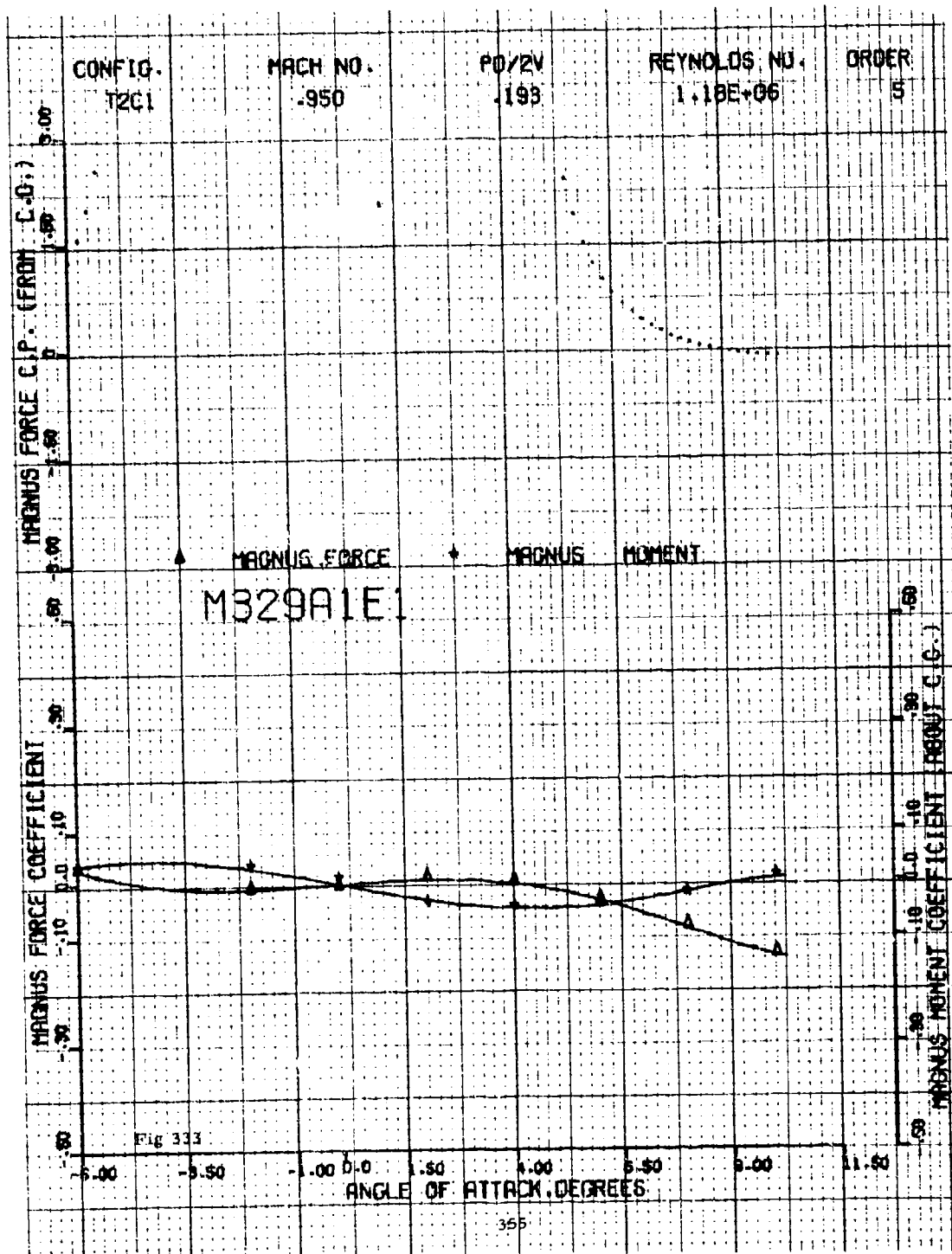


Fig 33

ANGLE OF ATTACK, DEGREES

353

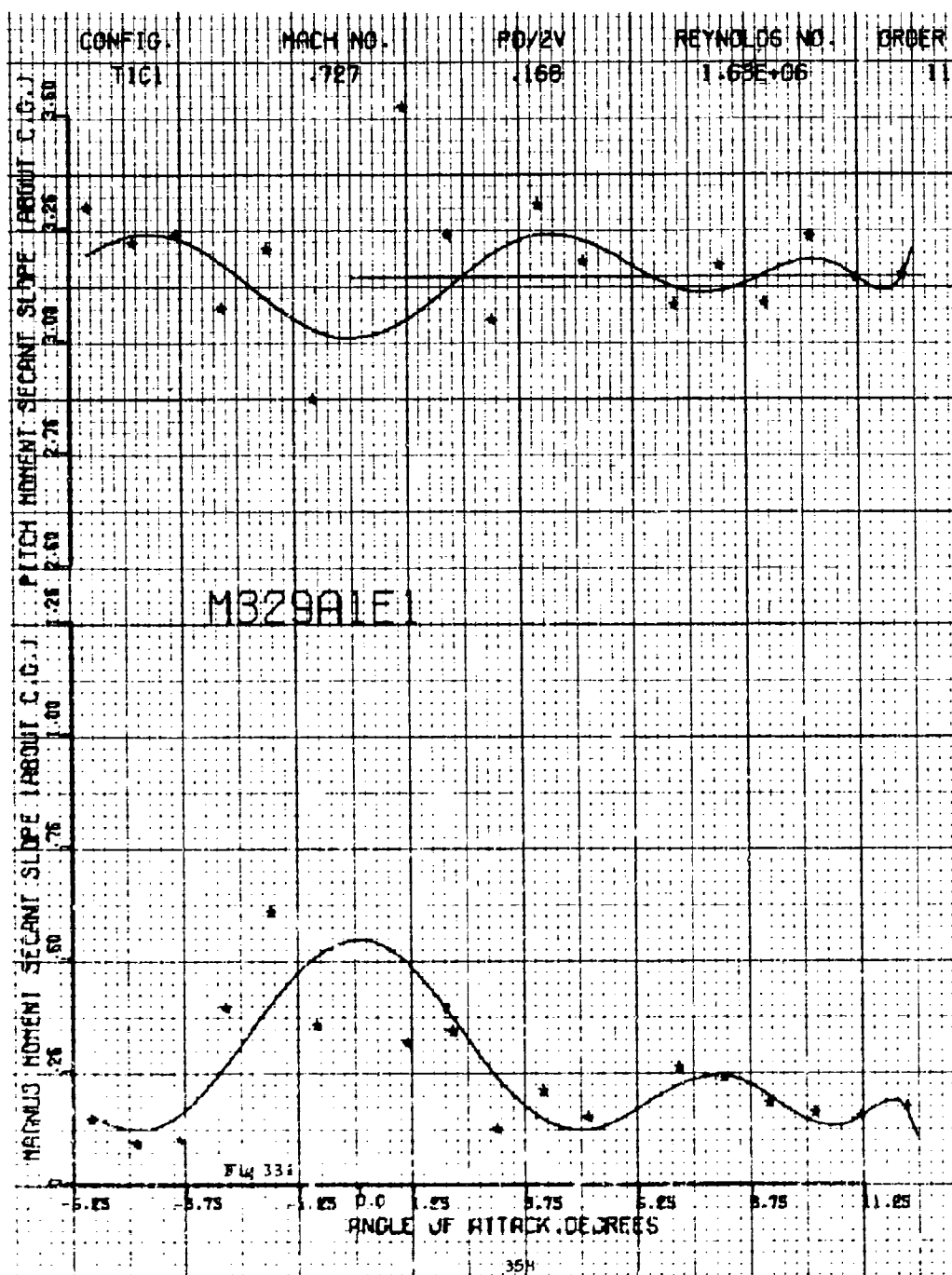


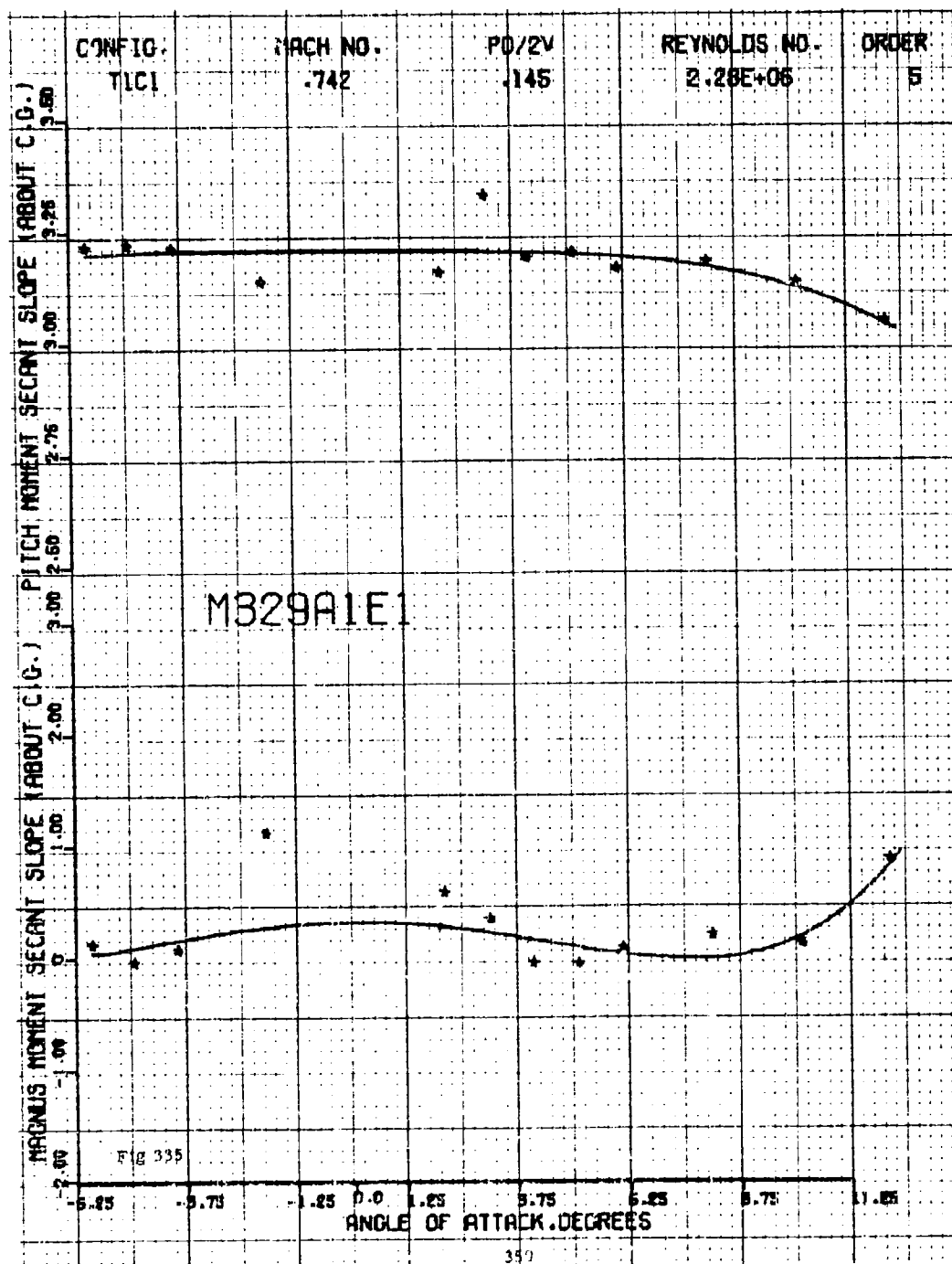


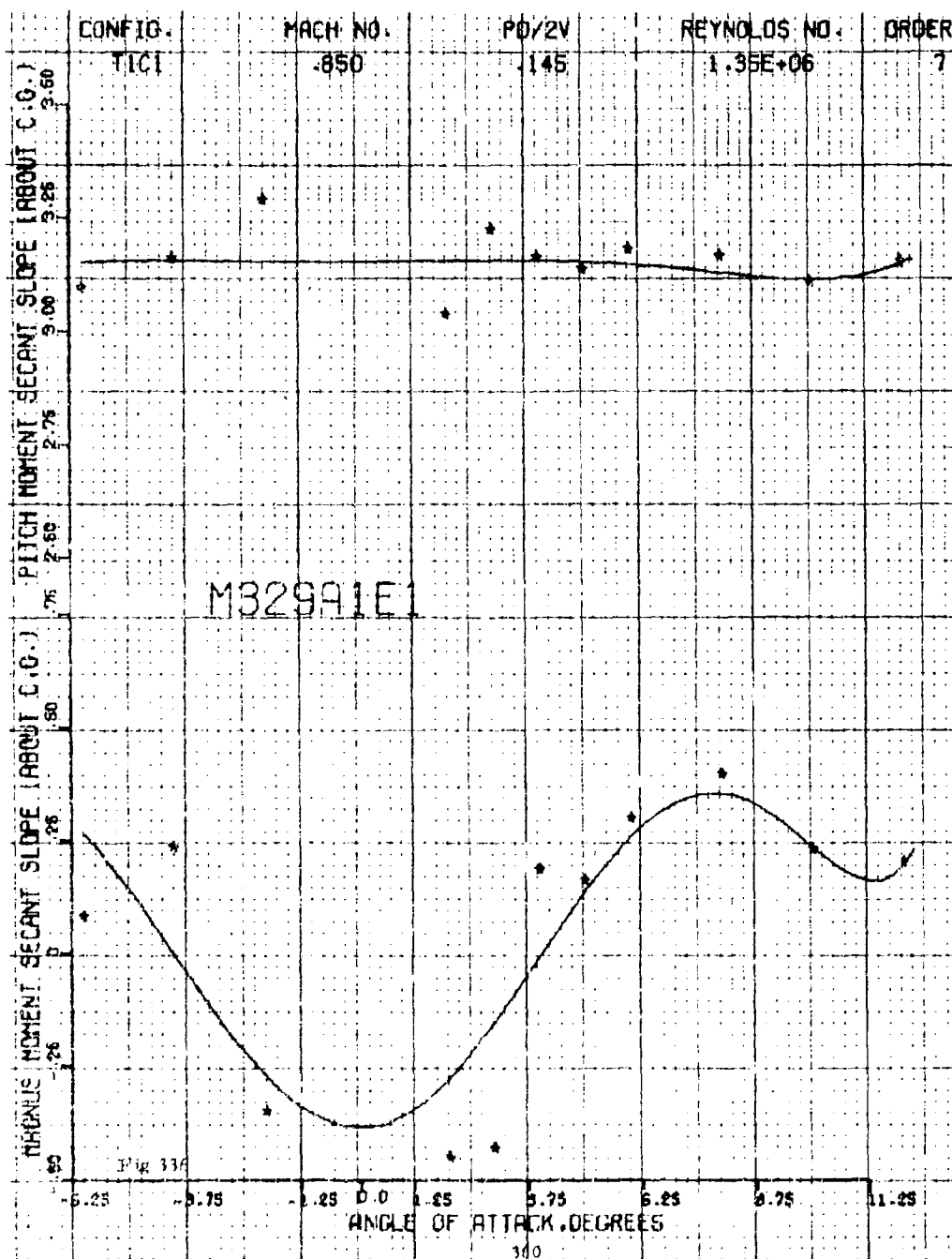
Figures 334 through 357

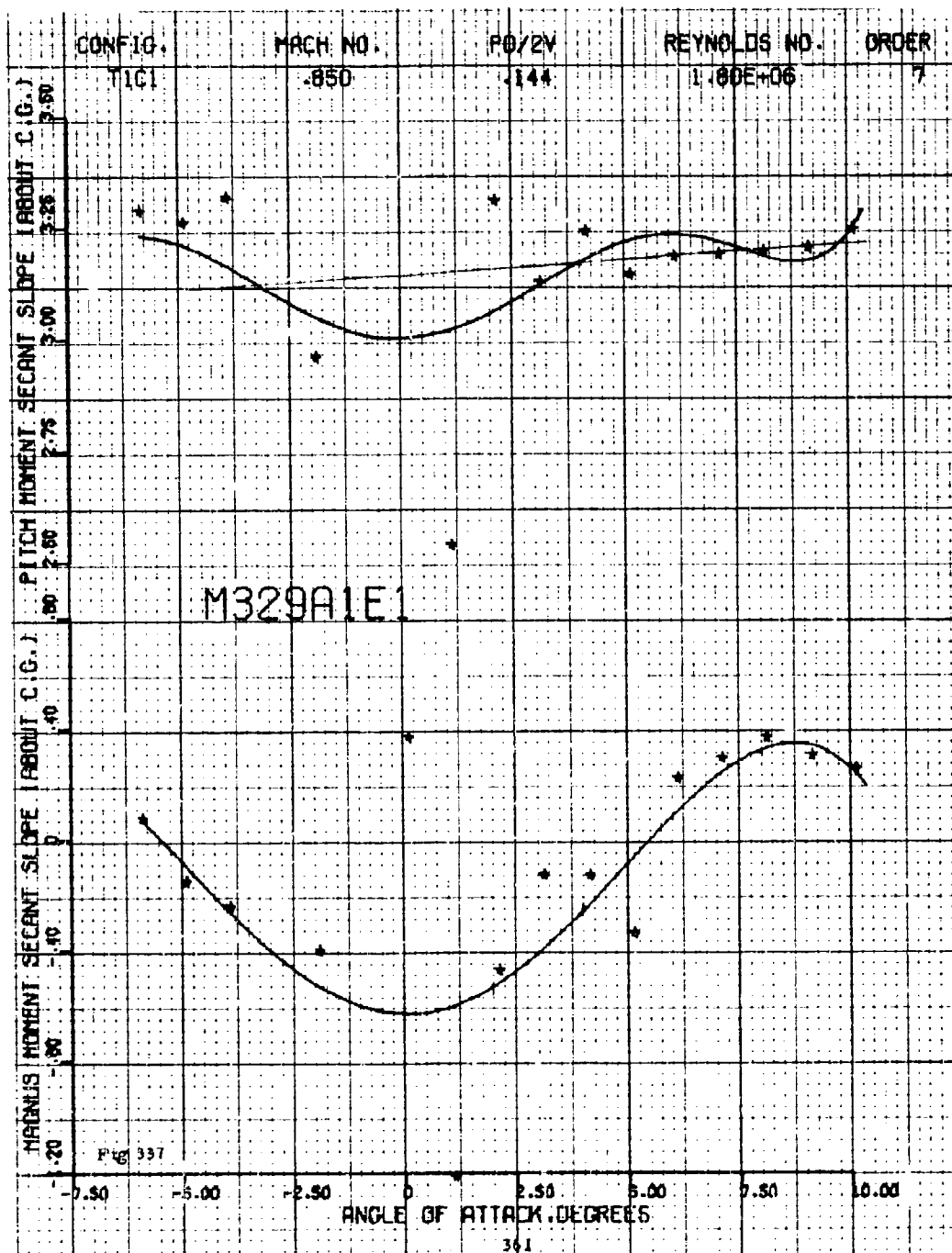
Pitching moment secant slope, Magnus moment secant slope
vs angle of attack

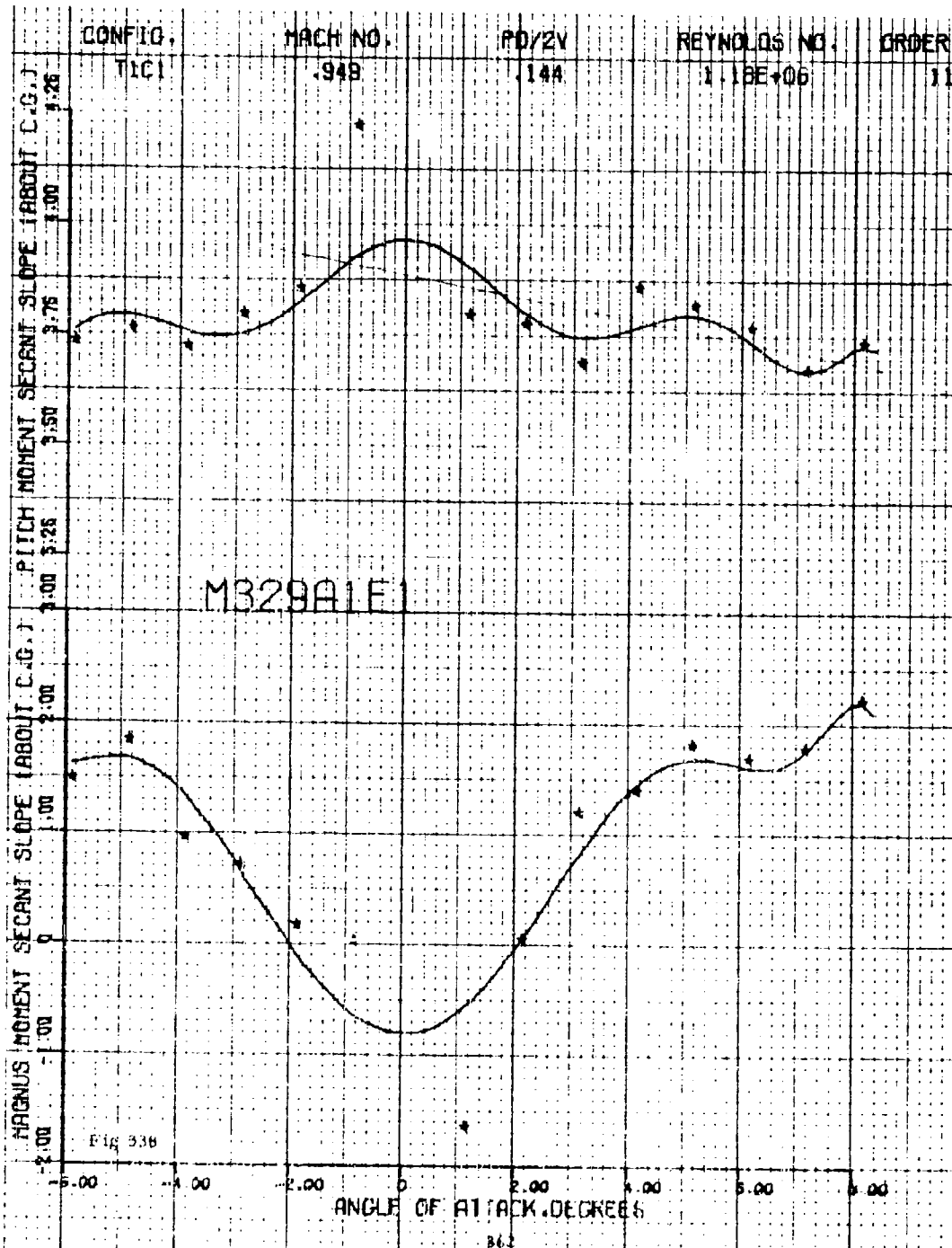
Preceding page blank

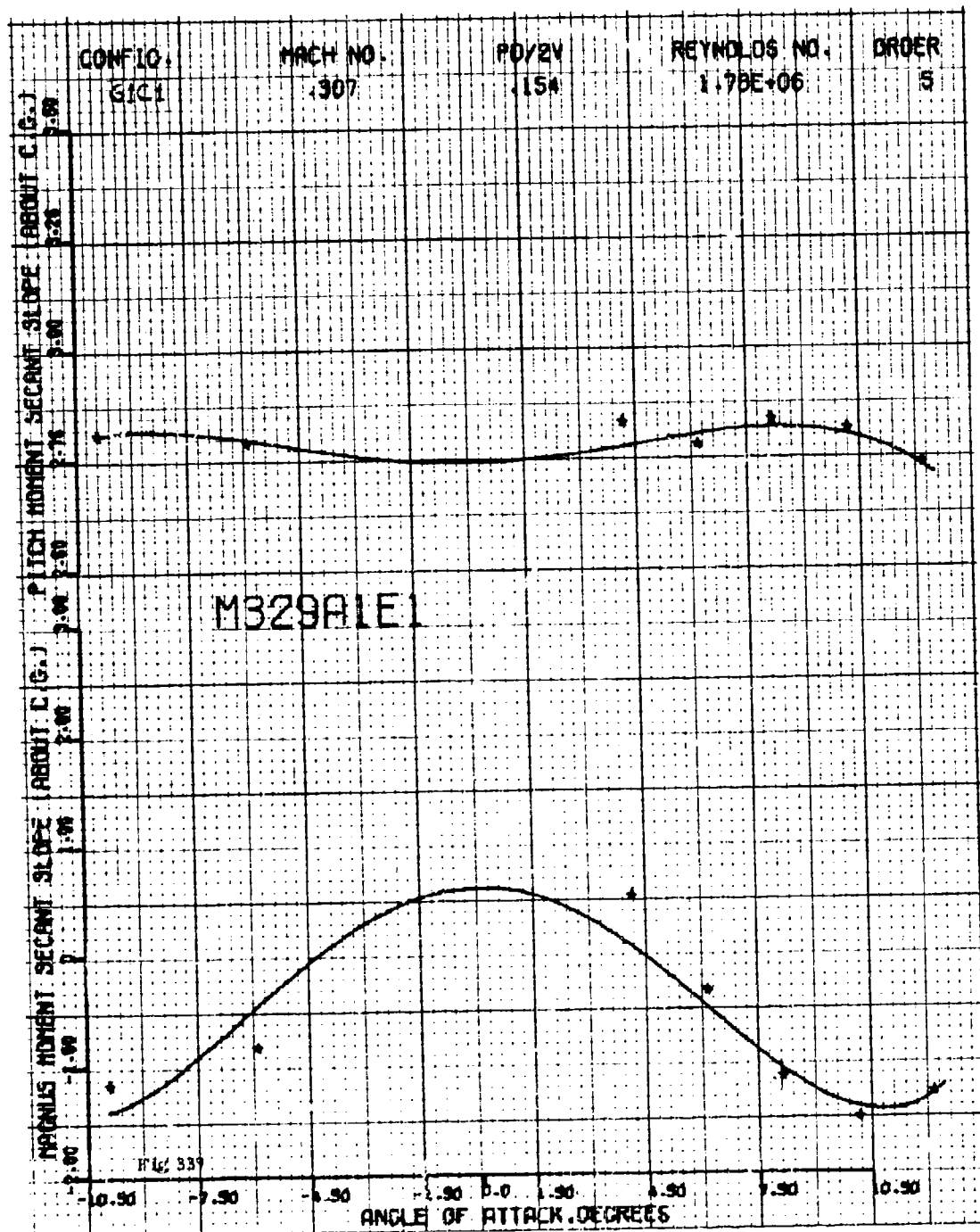




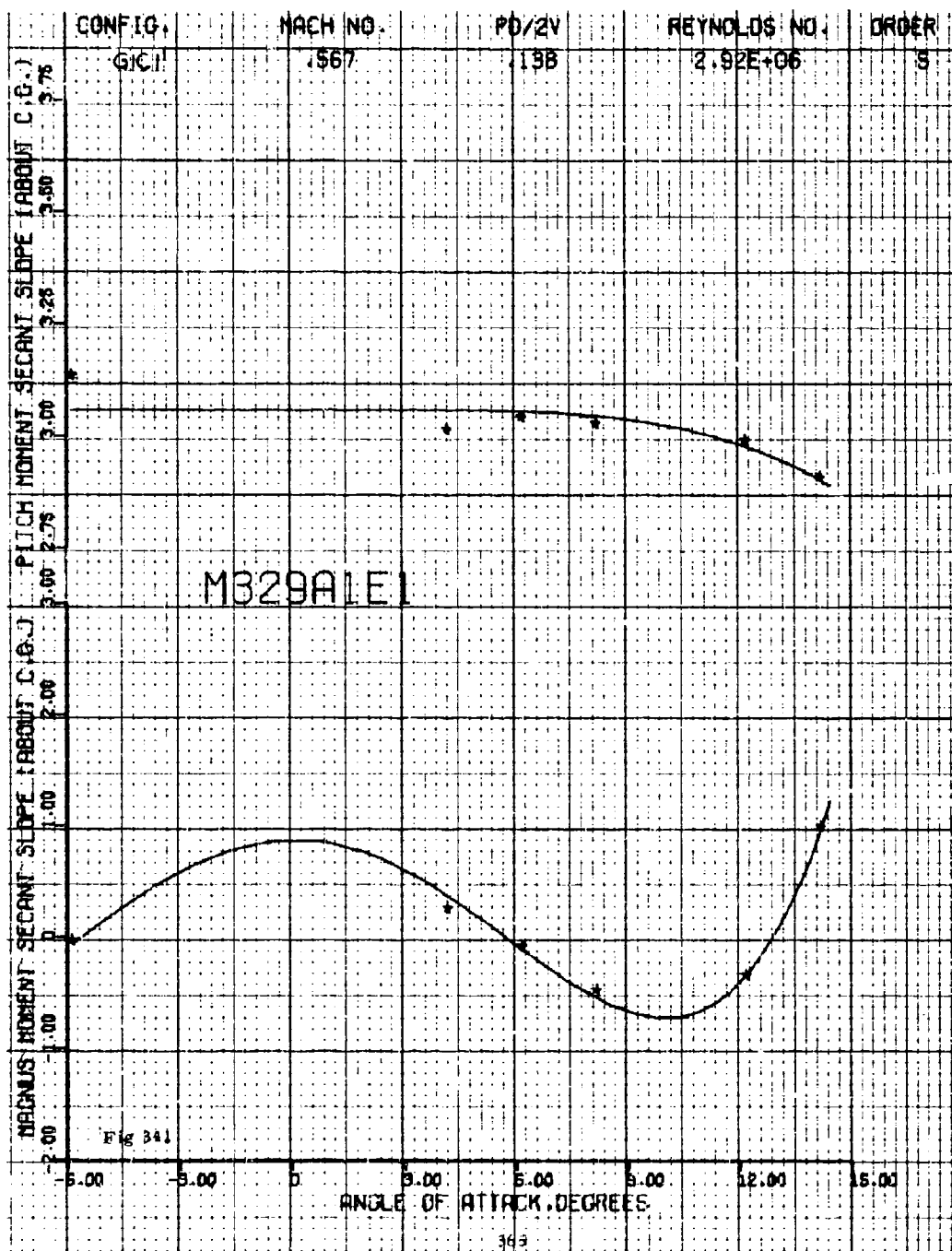


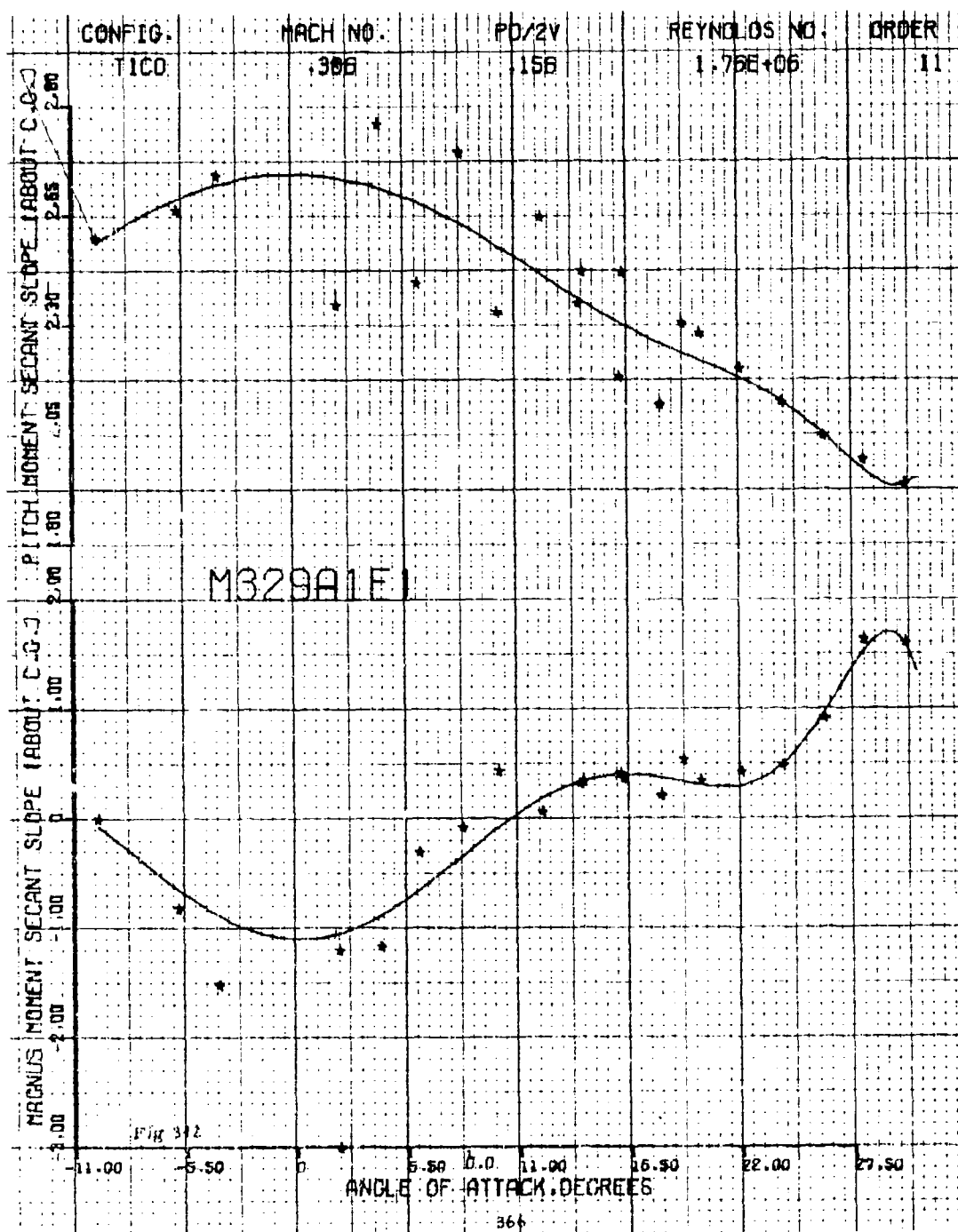


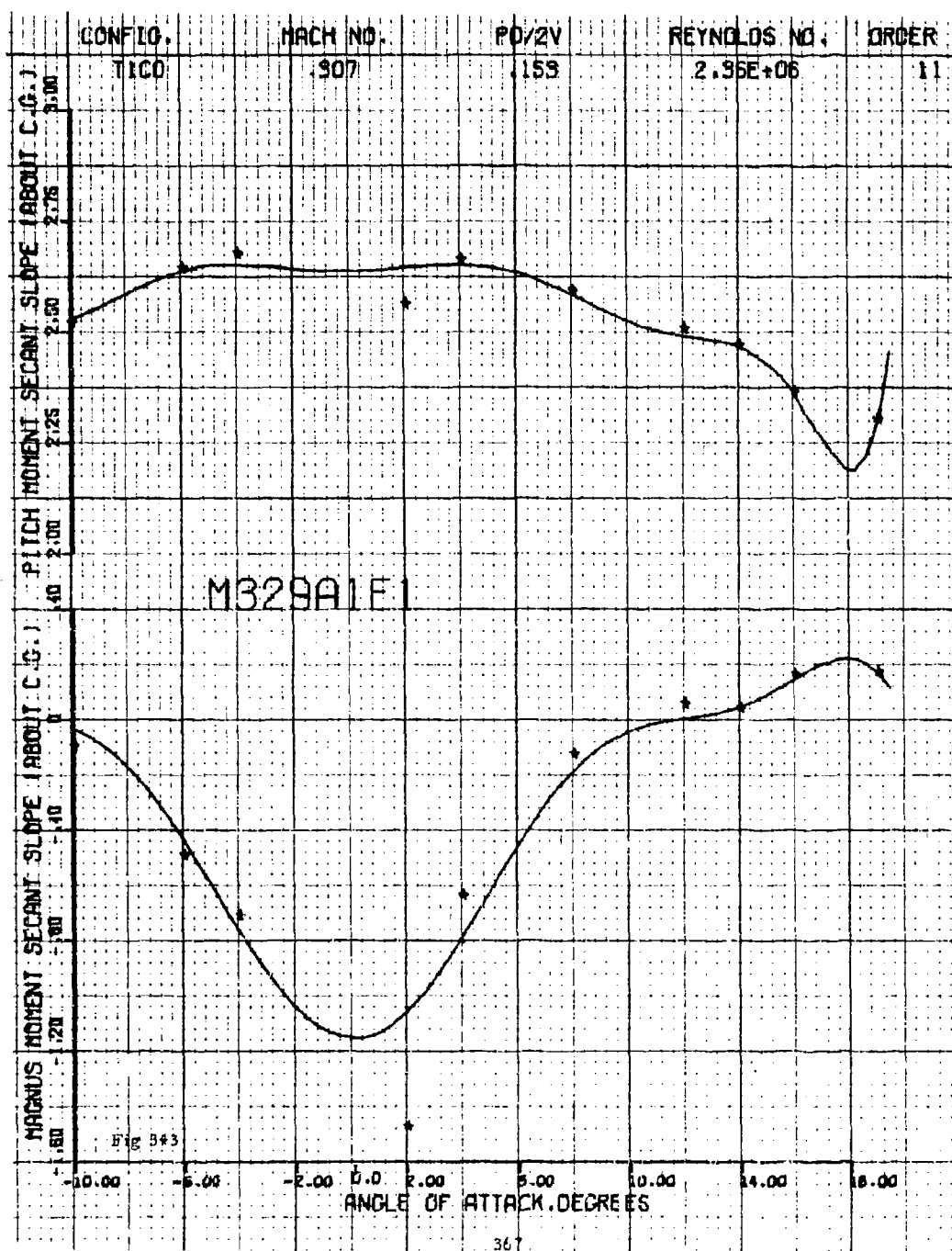


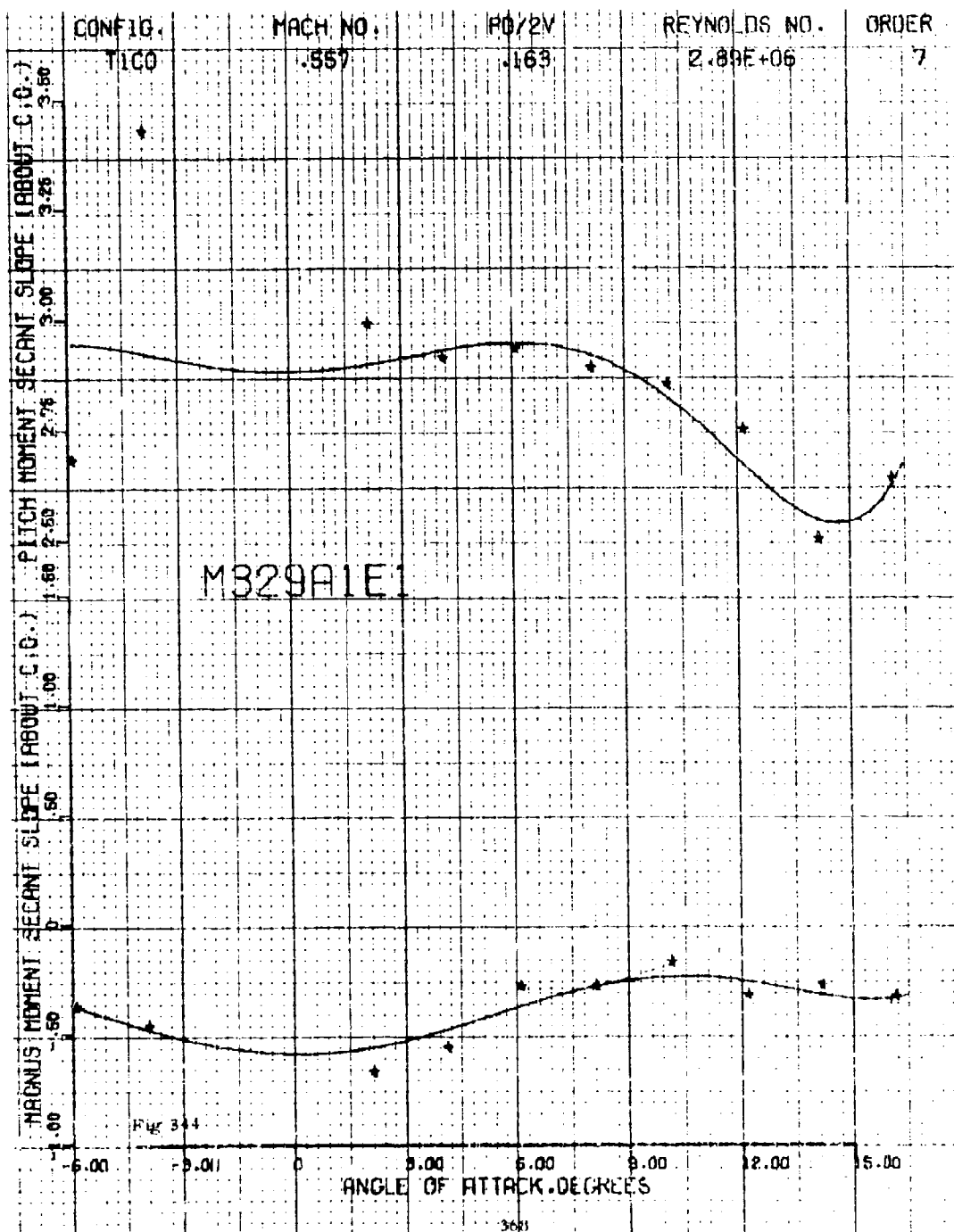


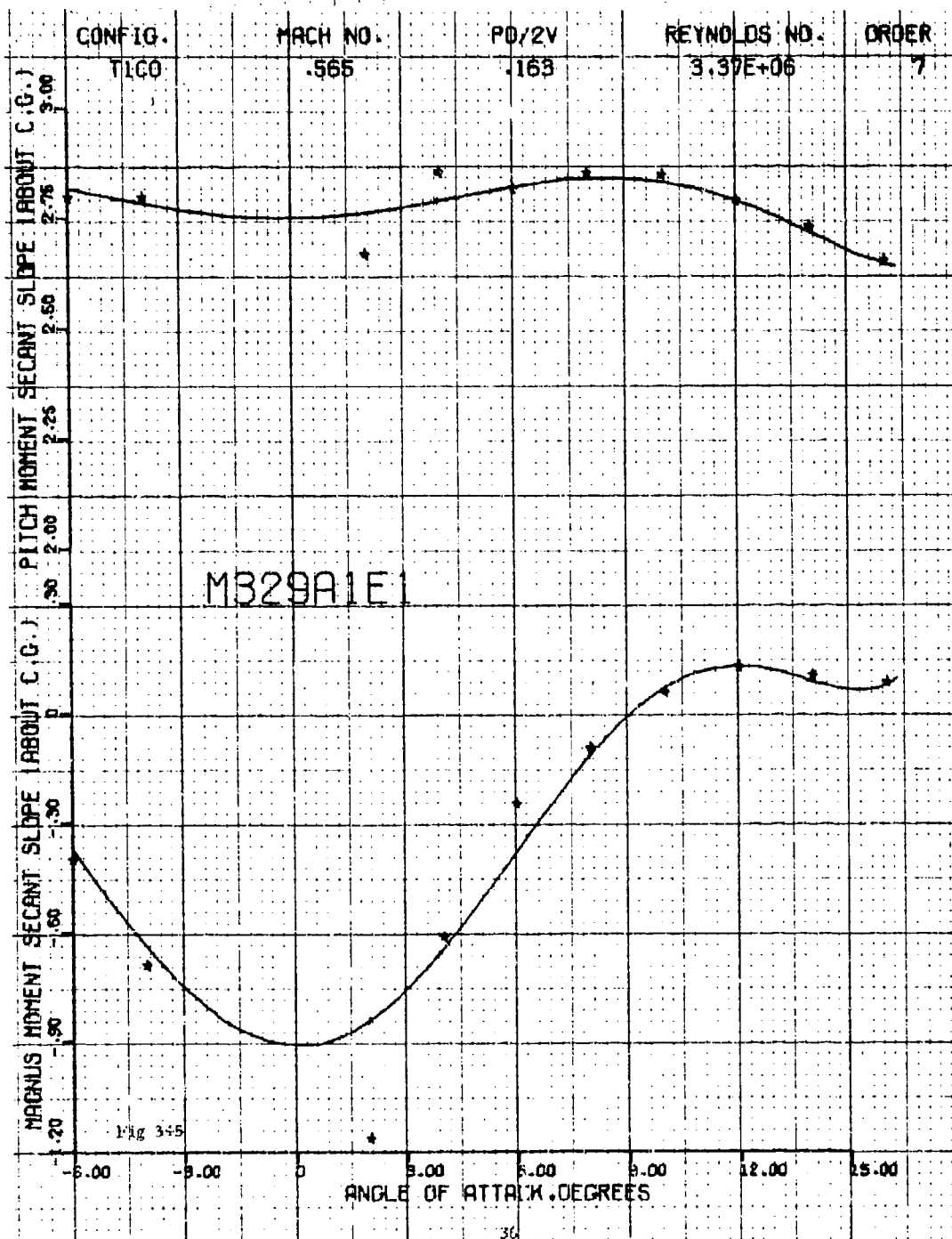


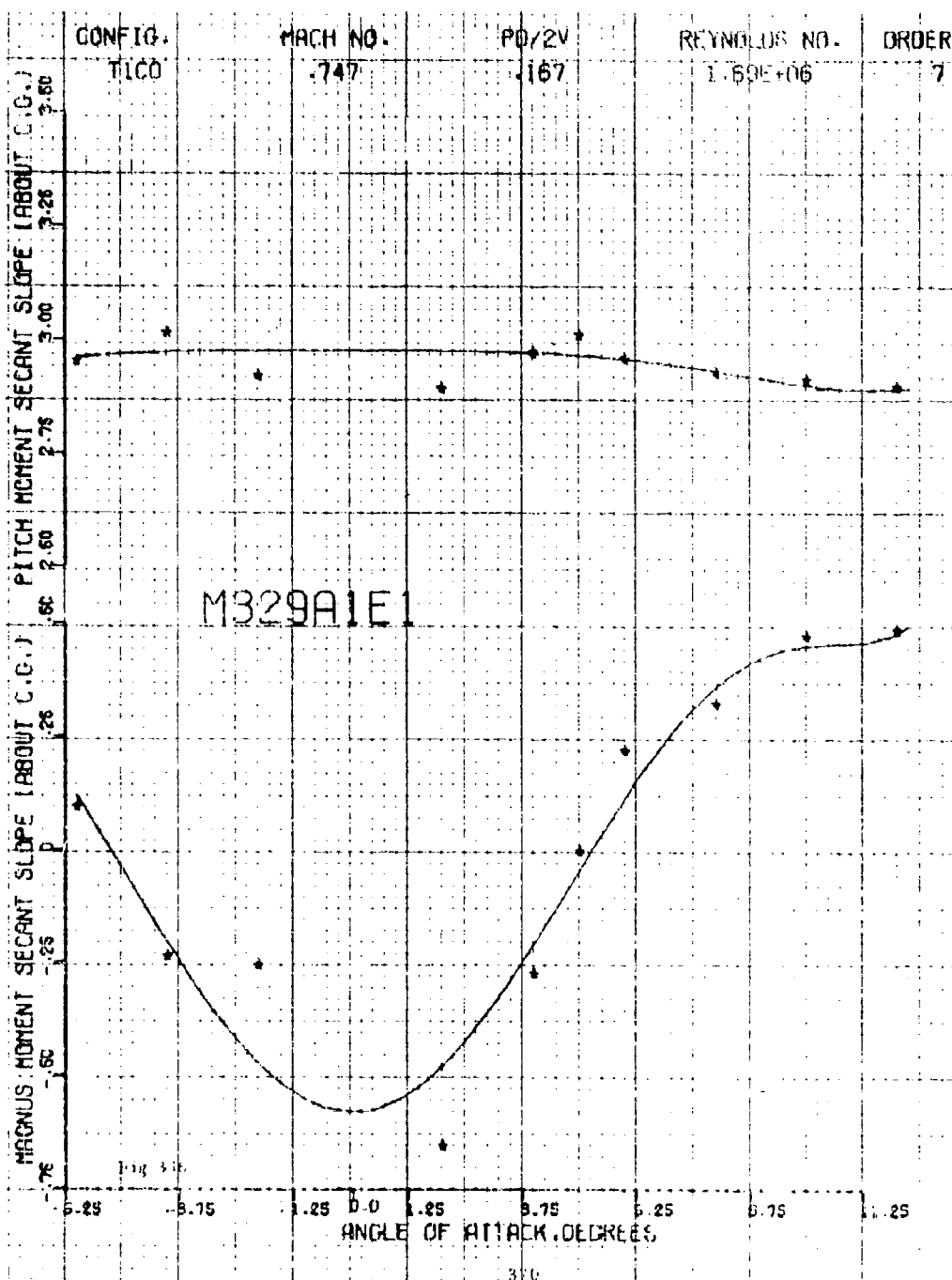


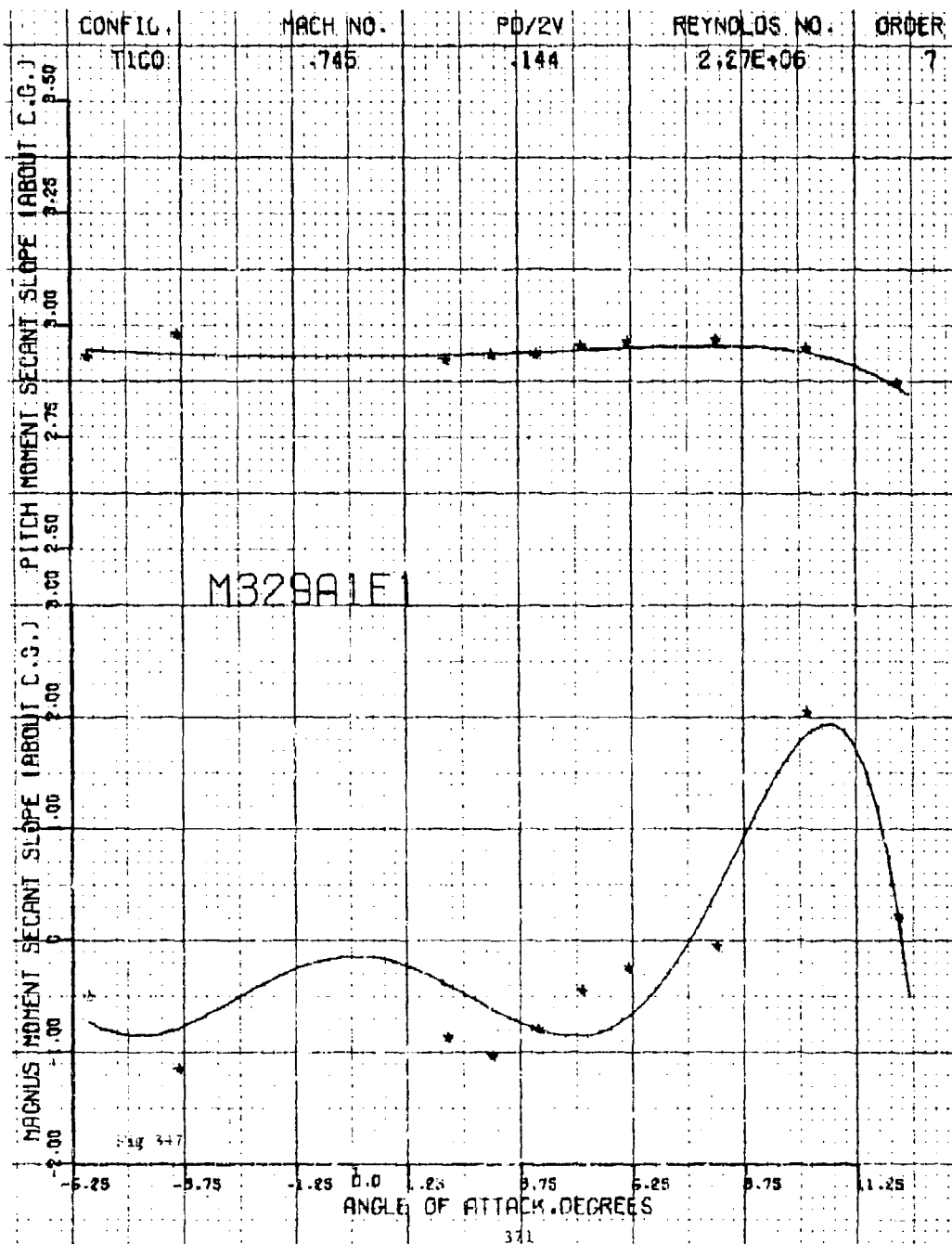


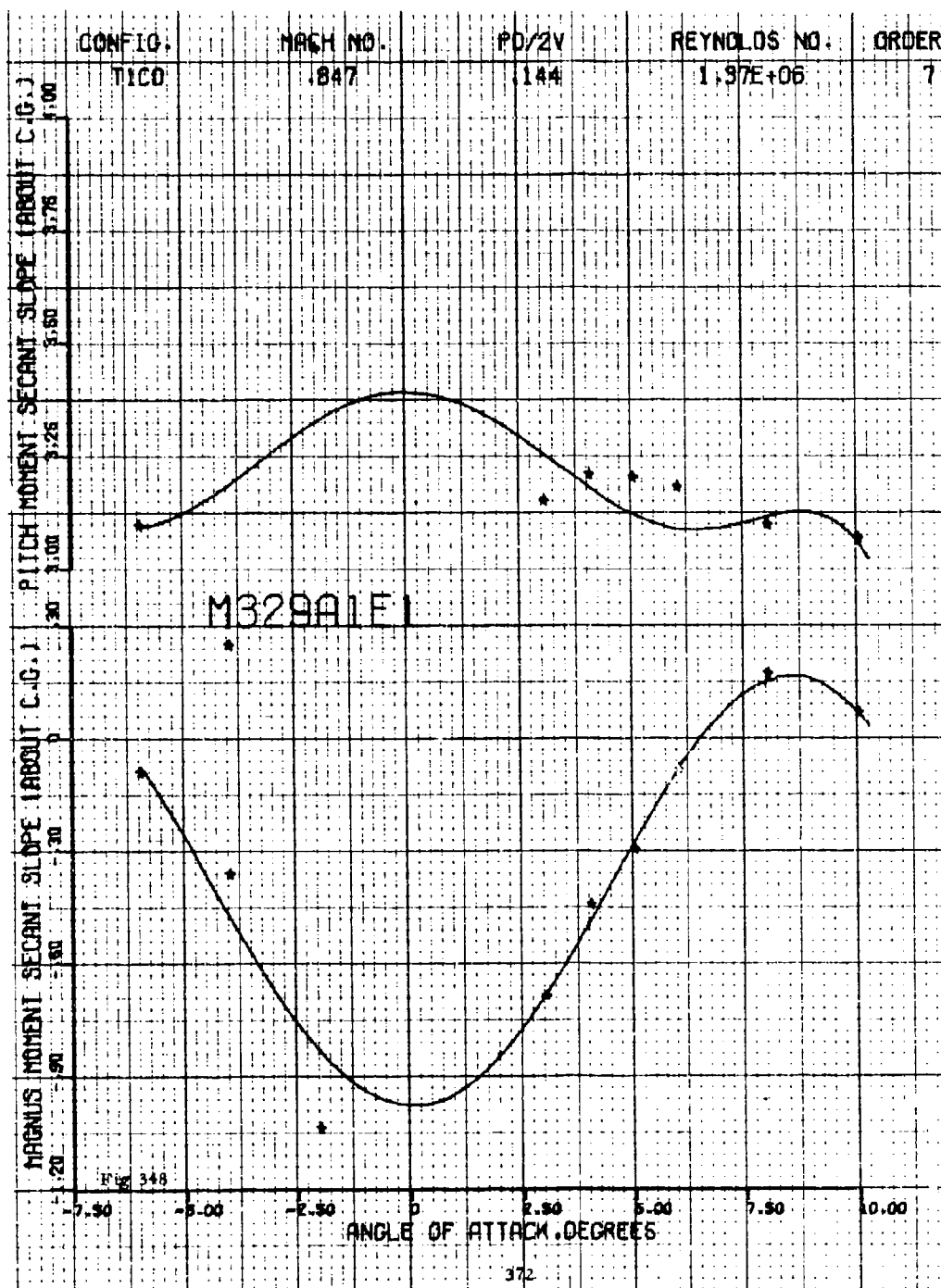


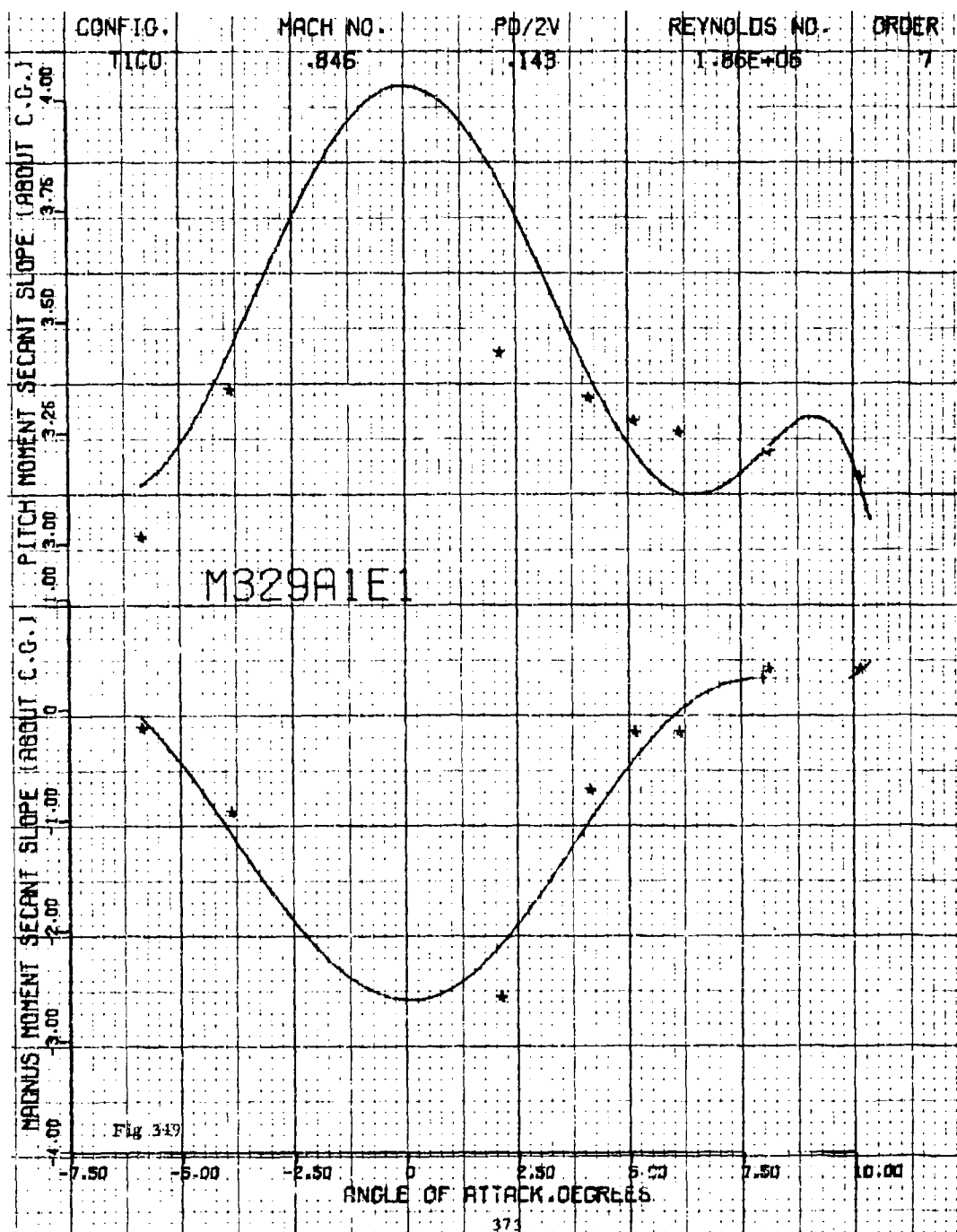


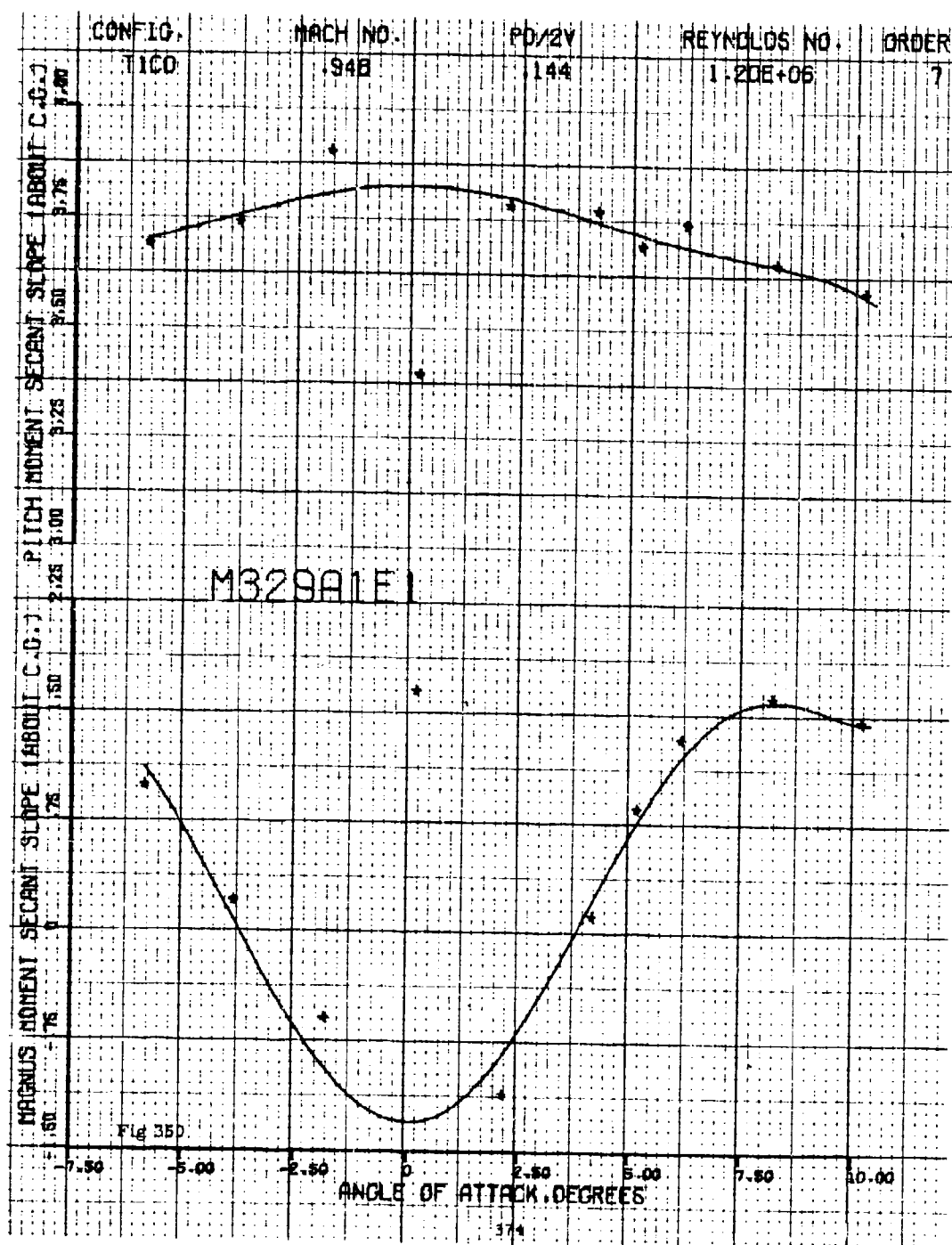


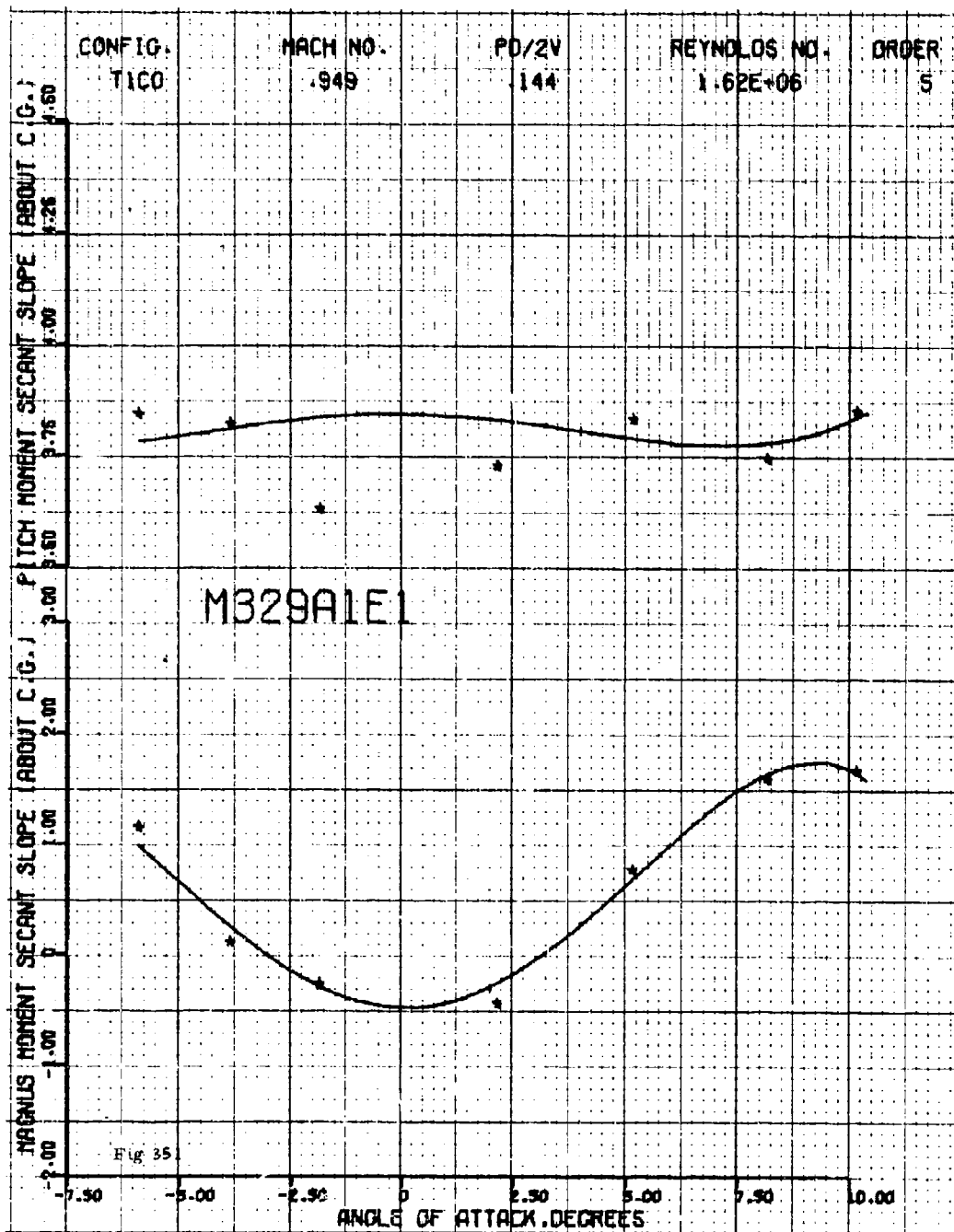


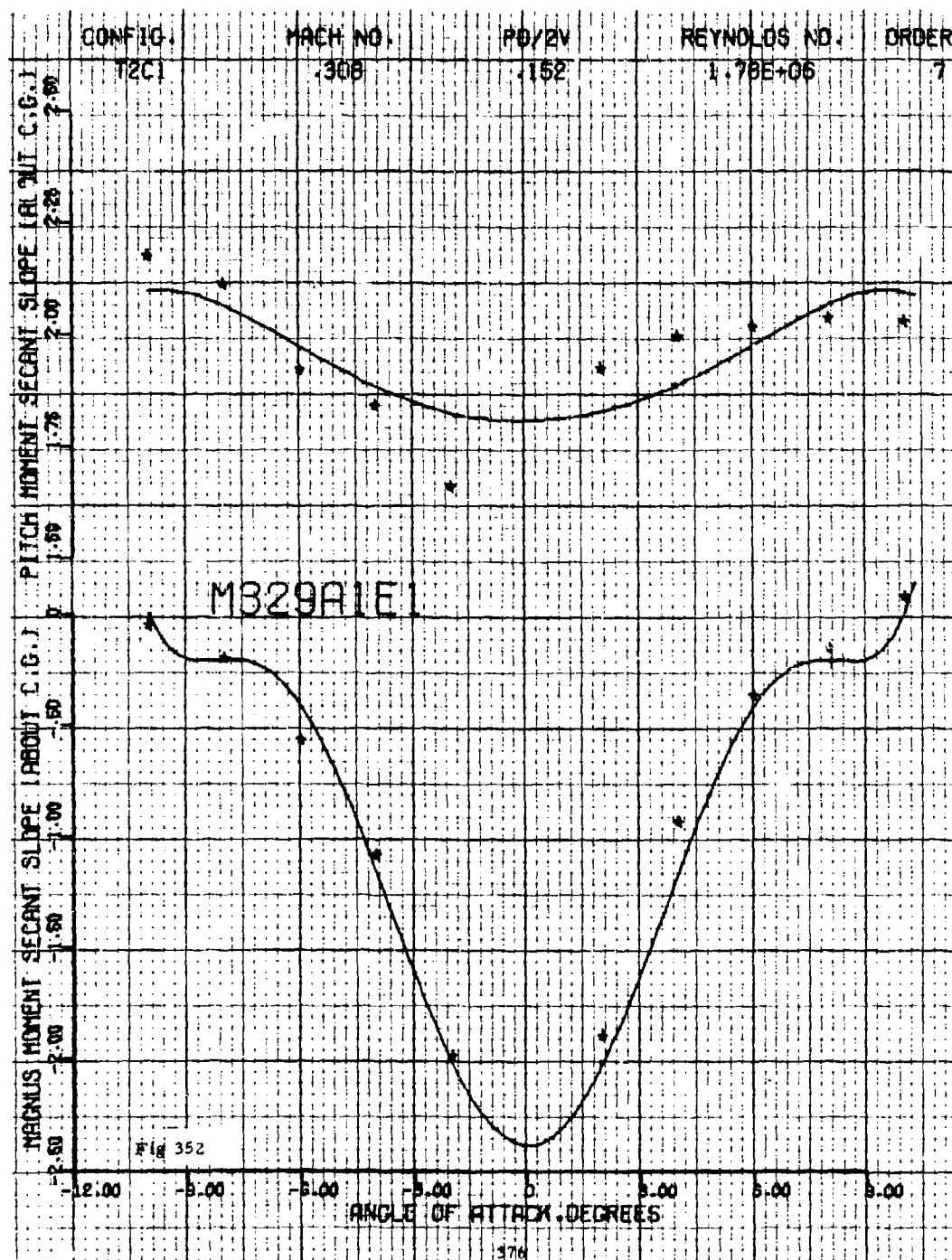


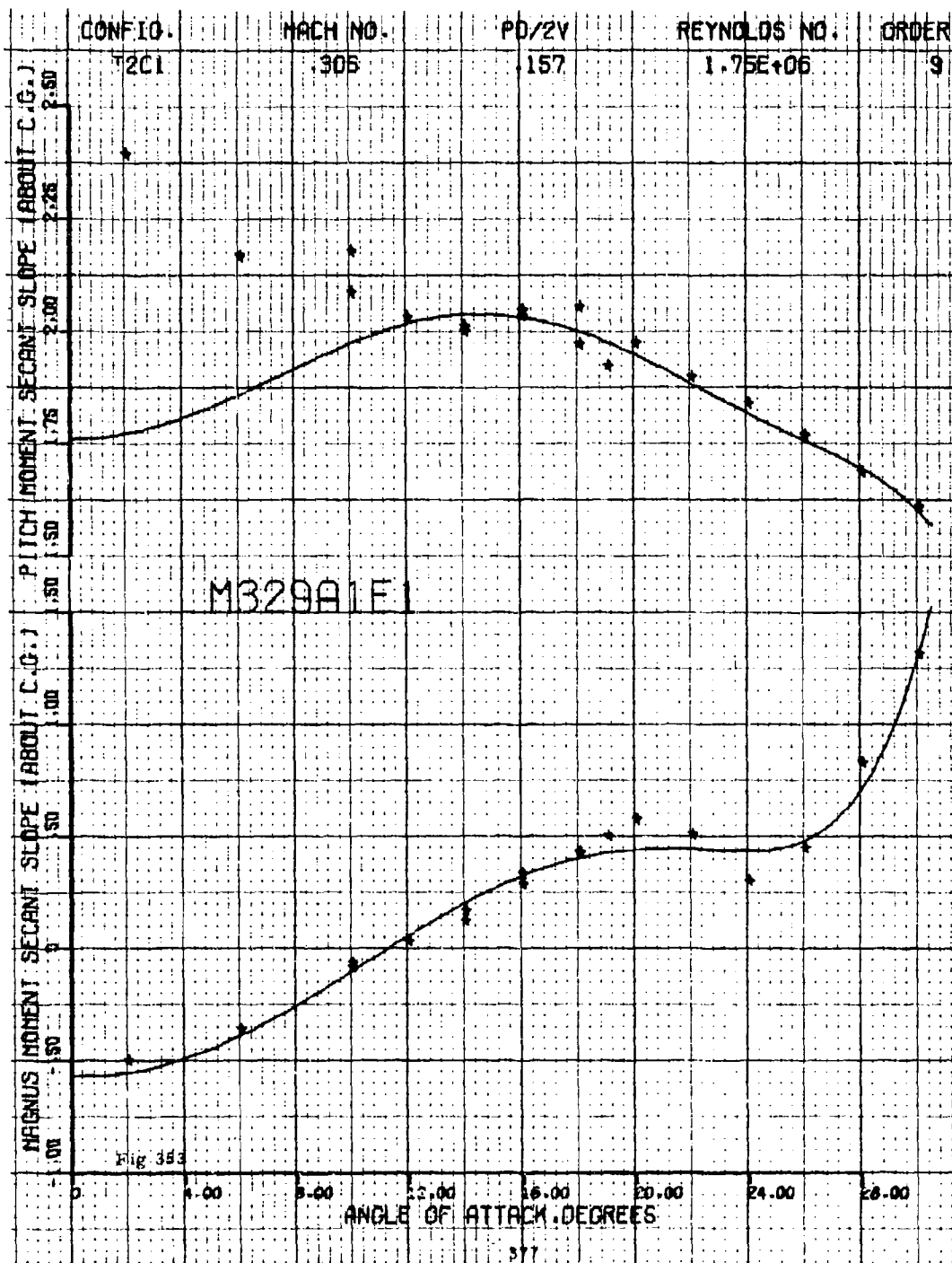


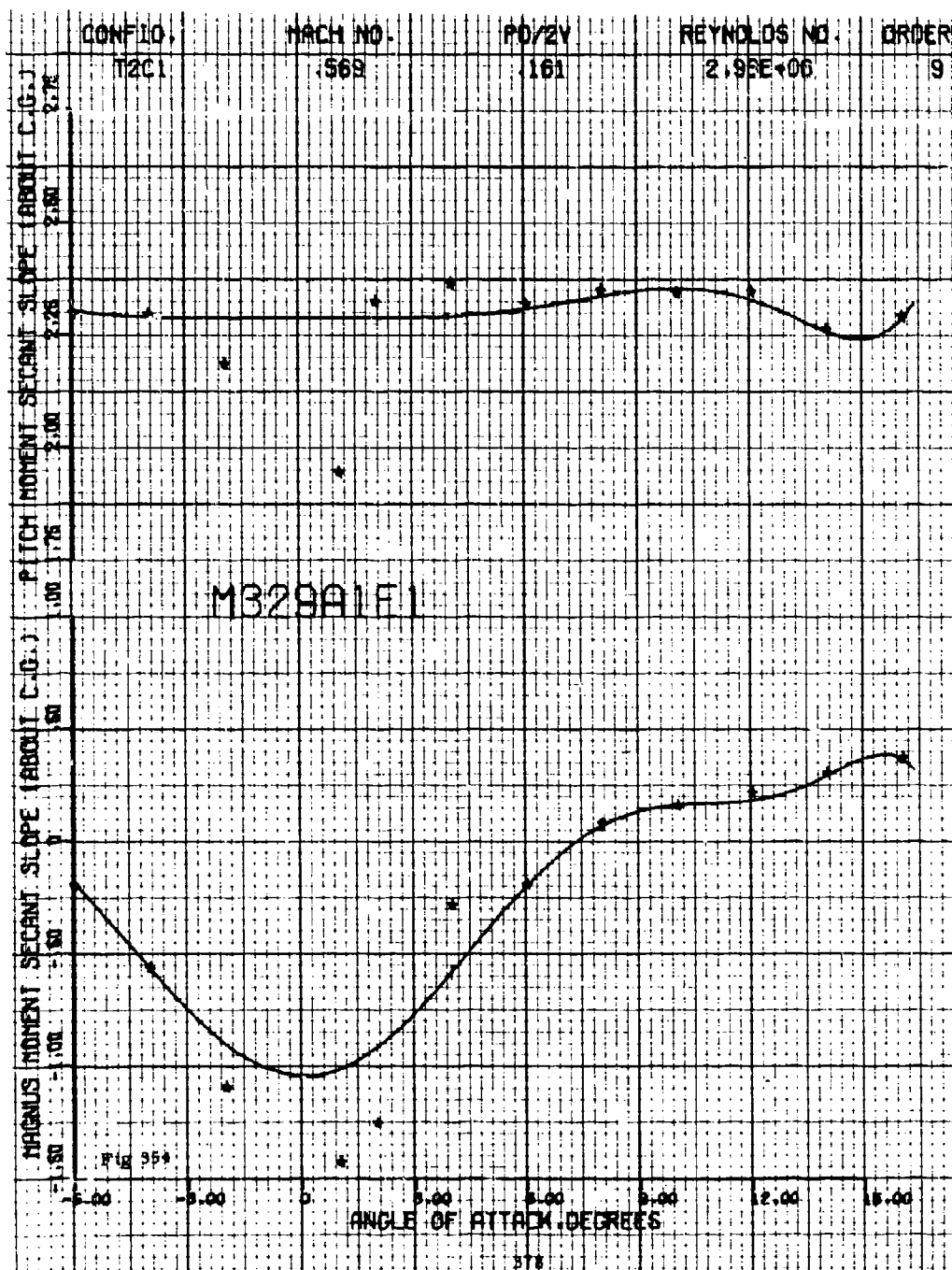


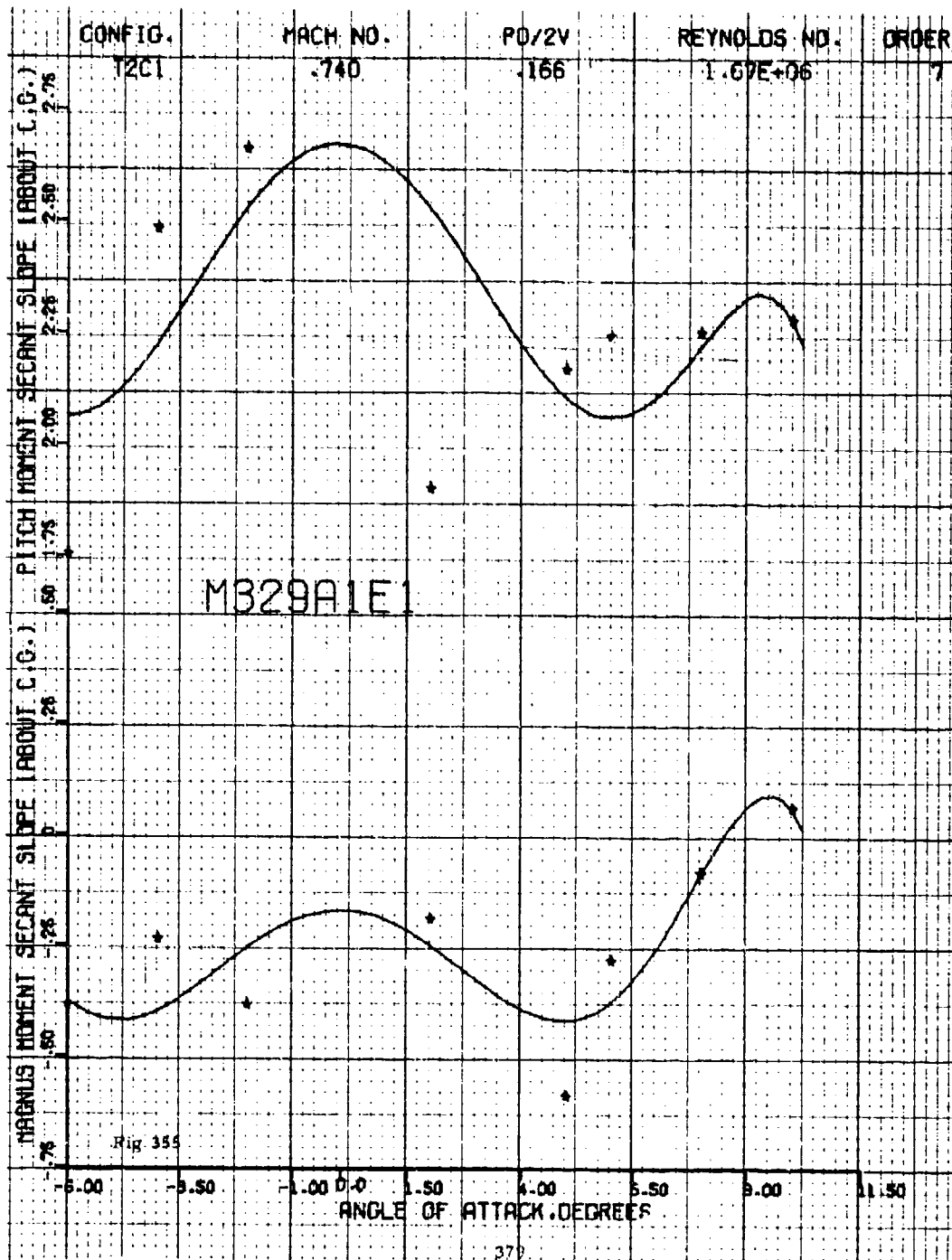


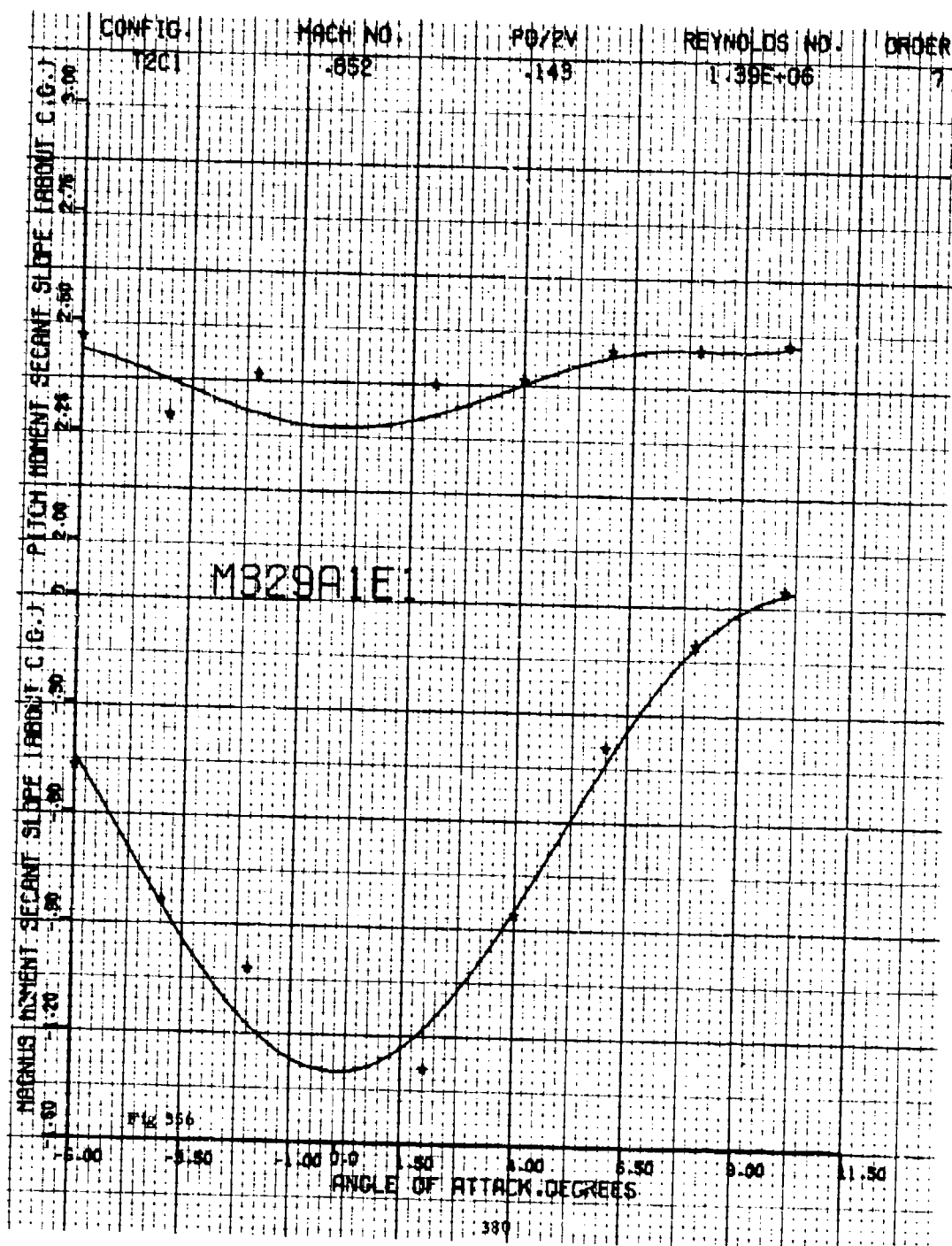


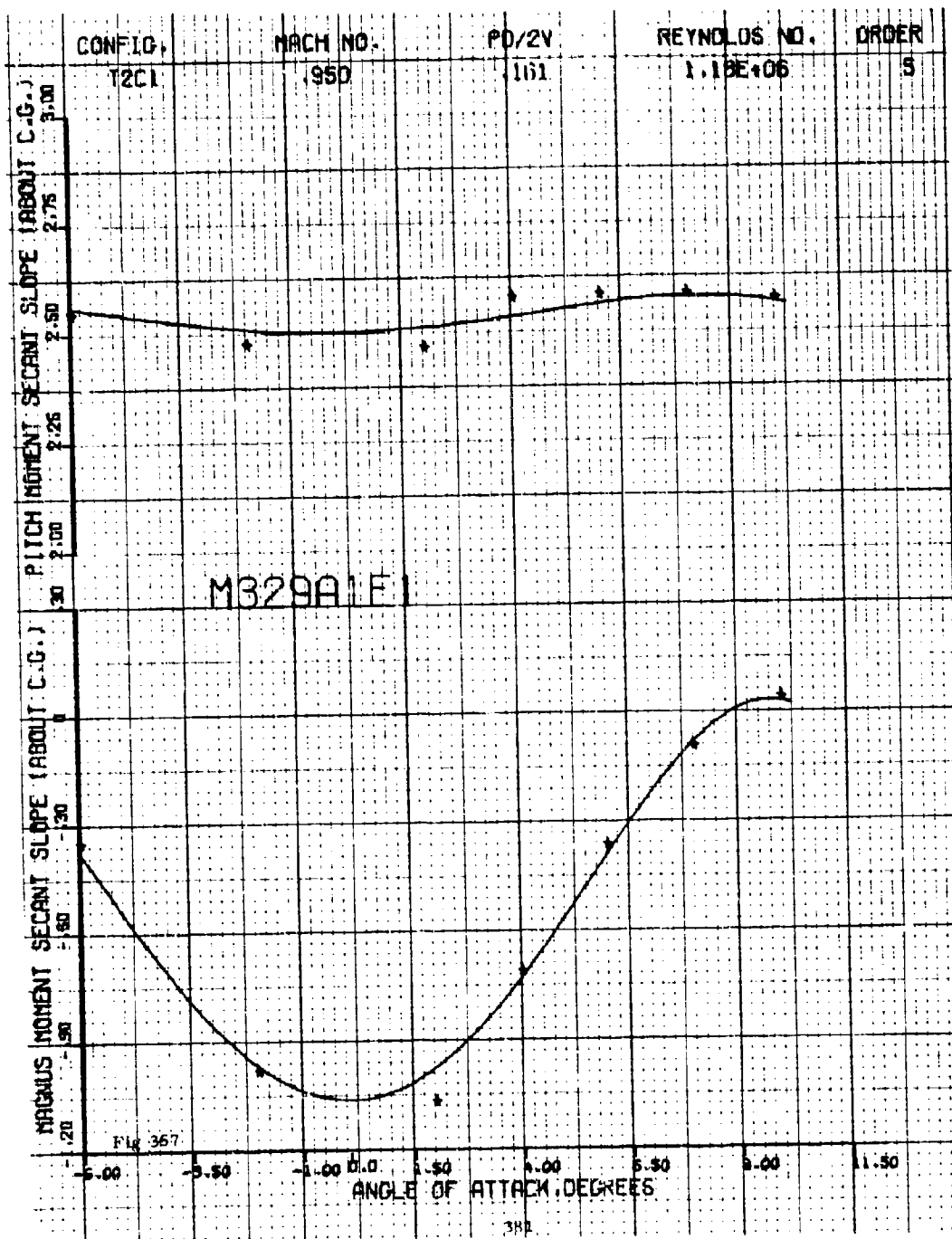












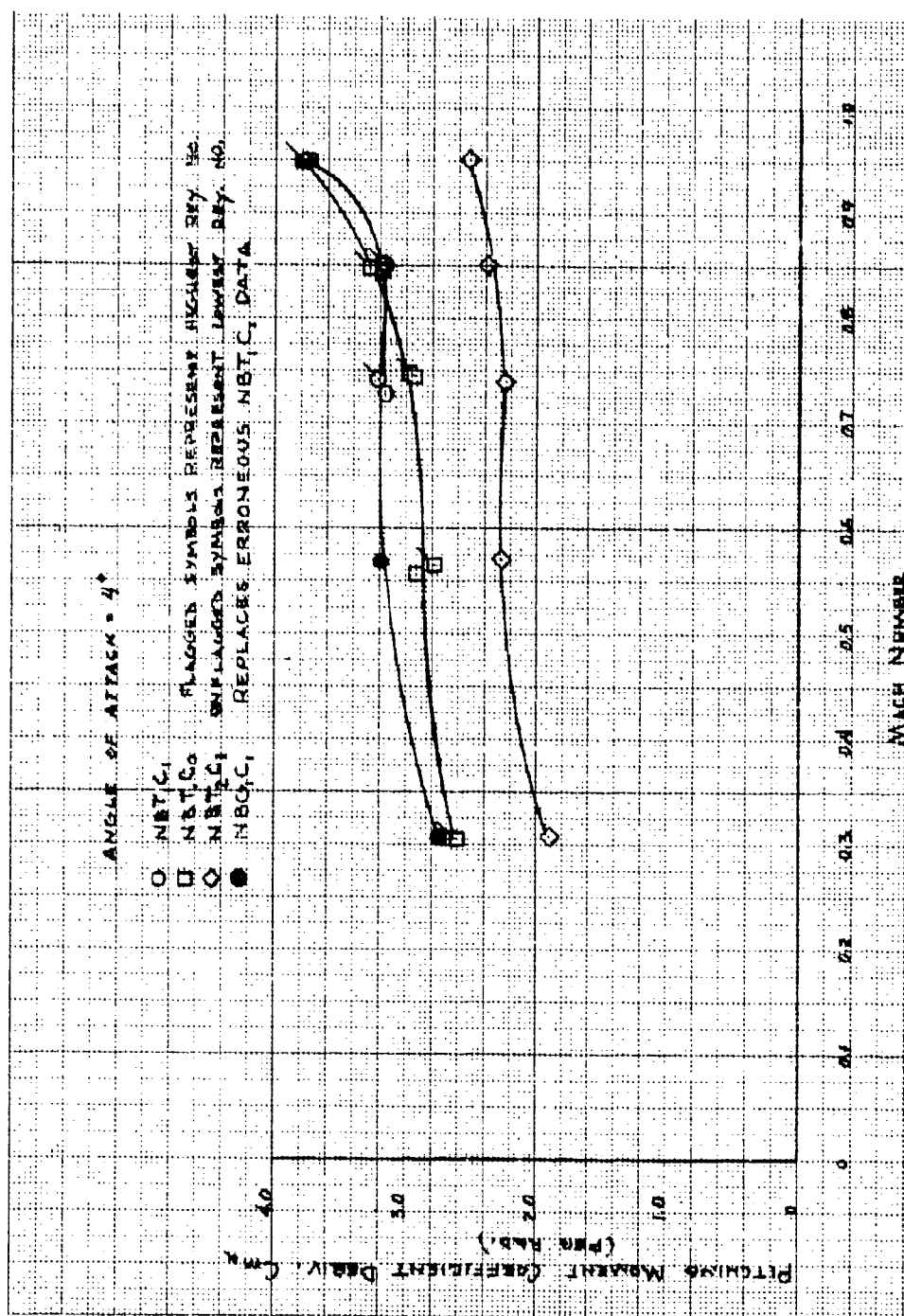


Fig 358 Pitching moment coefficient derivative vs Mach No.
(NBT₁C₁, NBT₁C₀, NBT₂C₁, NBT₂C₀)

Figures 359 and 360

Magnus moment coefficient derivative vs Mach No. .
(NBT_1C_1 , NBT_1C_0 , NBT_2C_1)

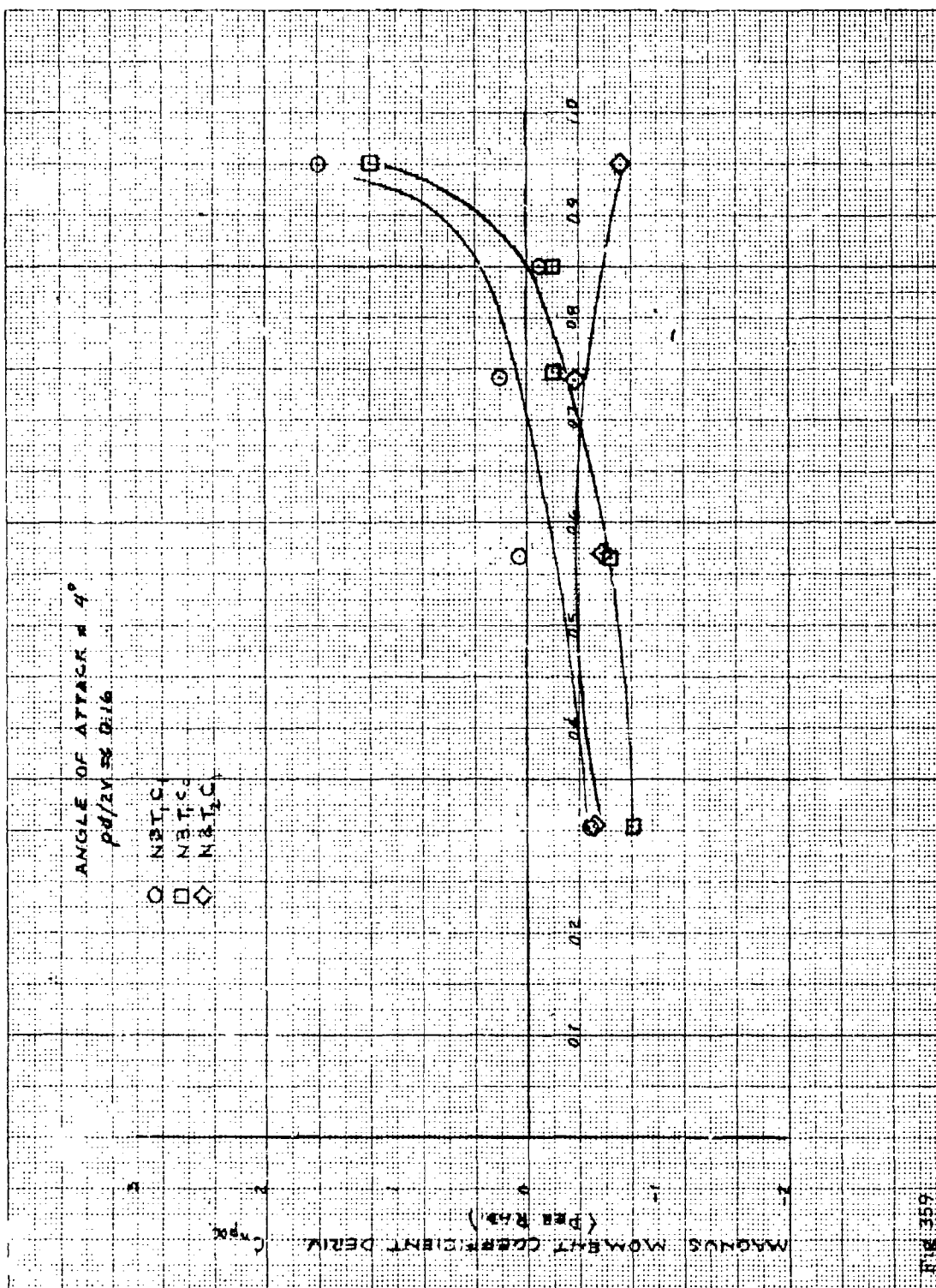
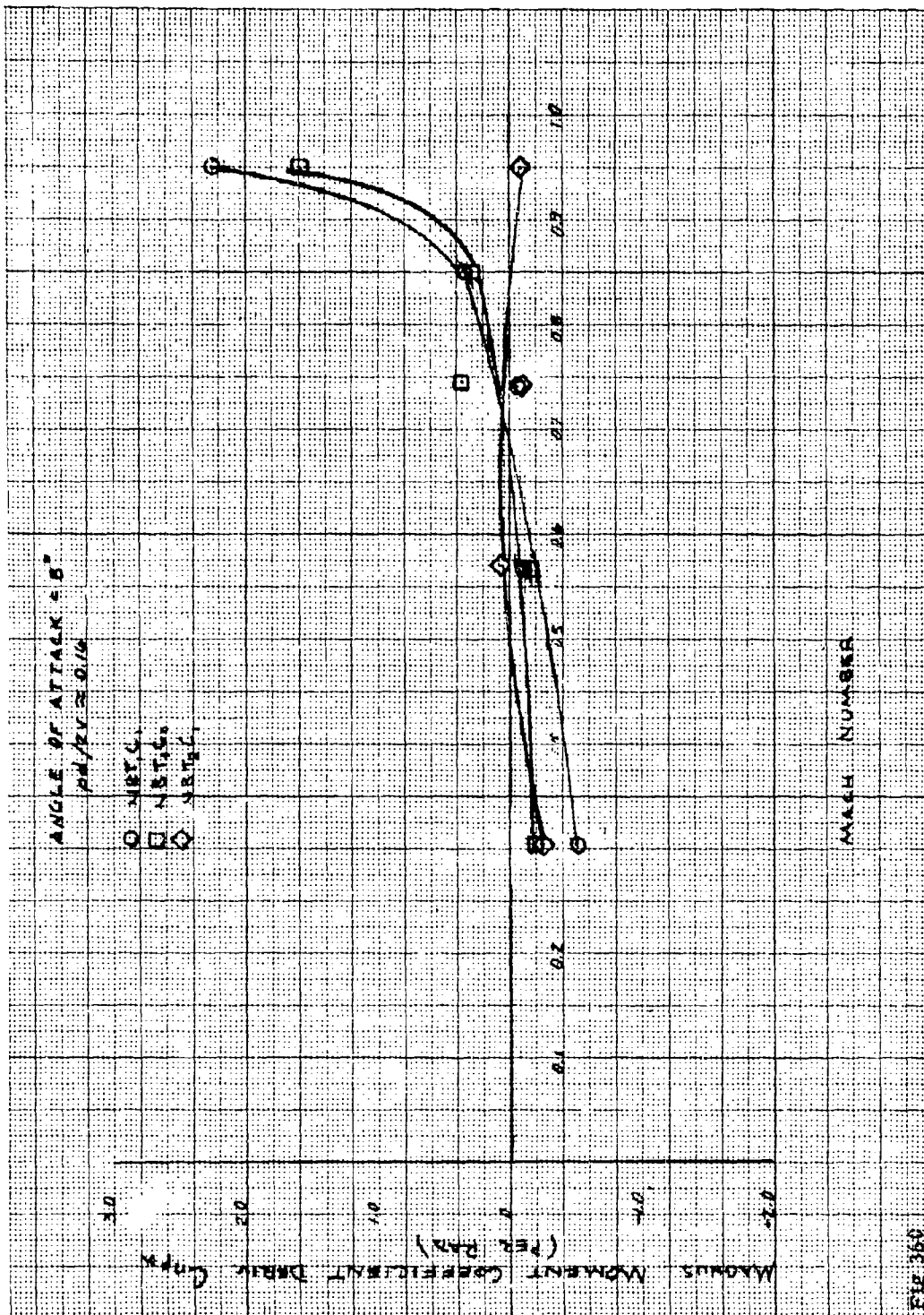


Fig 359



Figures 361 through 367

Magnus moment coefficient derivative vs $pd/2V$
($NBT_1 C_1$)

Preceding page blank

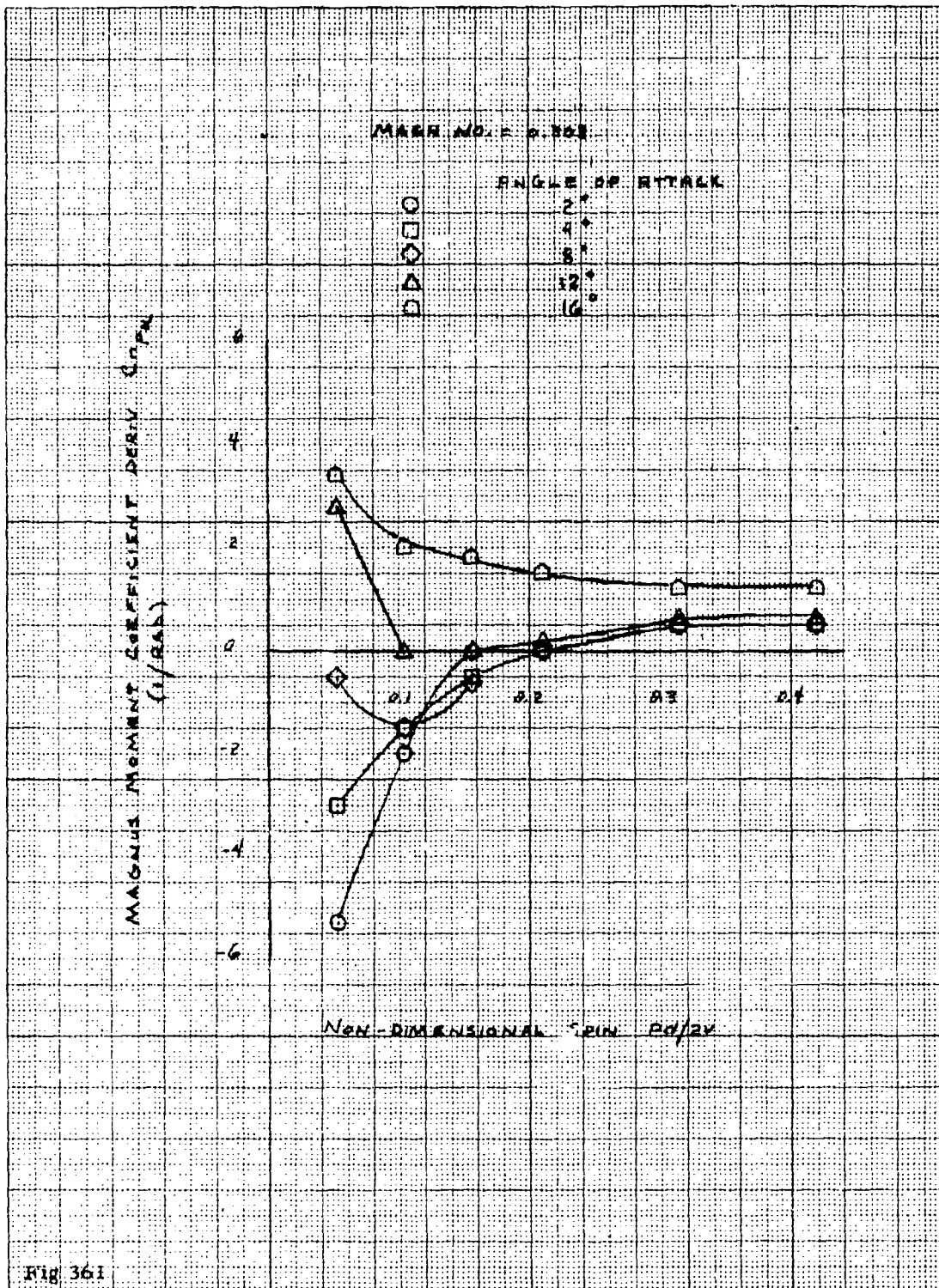


Fig 361

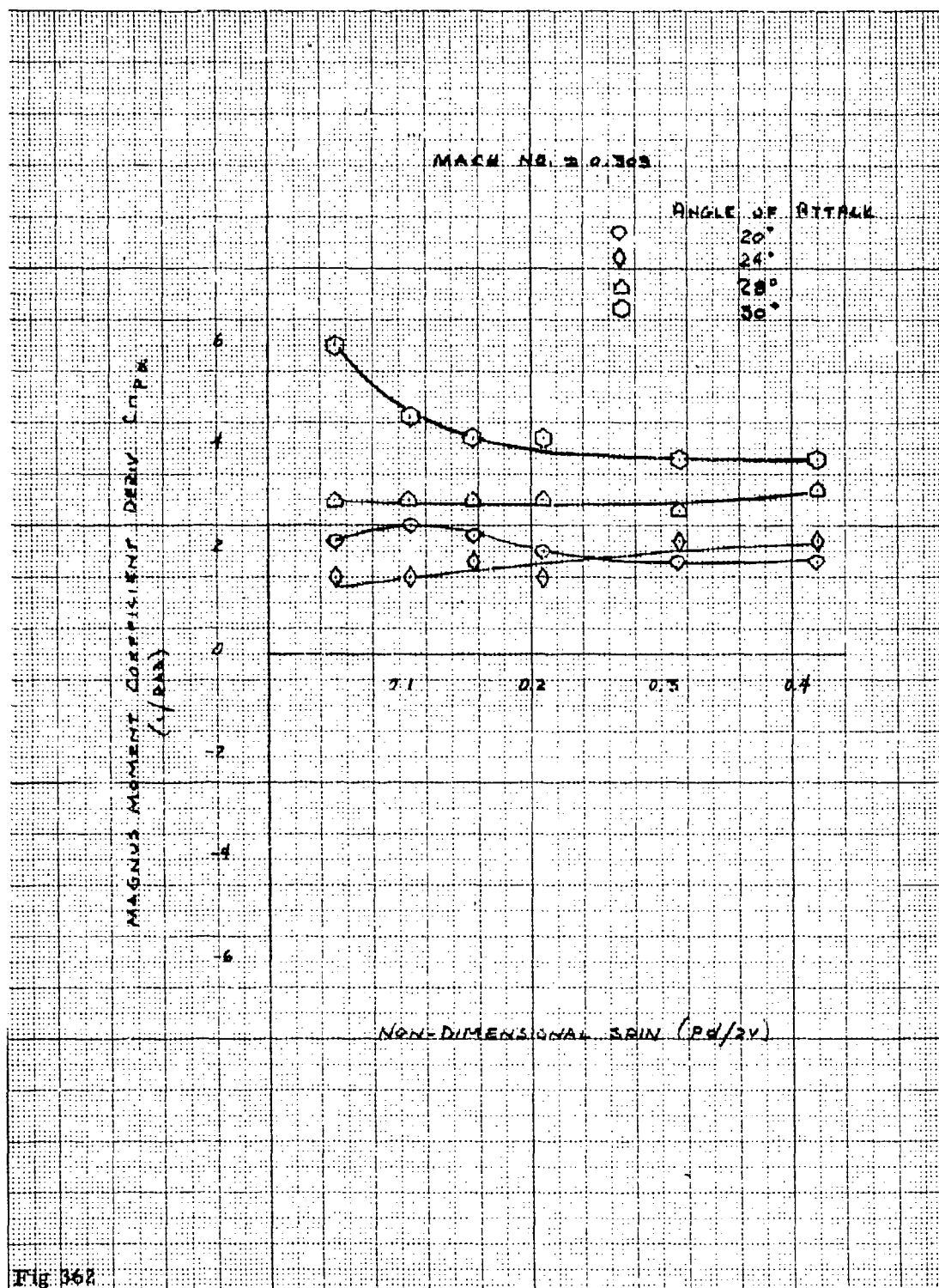


Fig 362

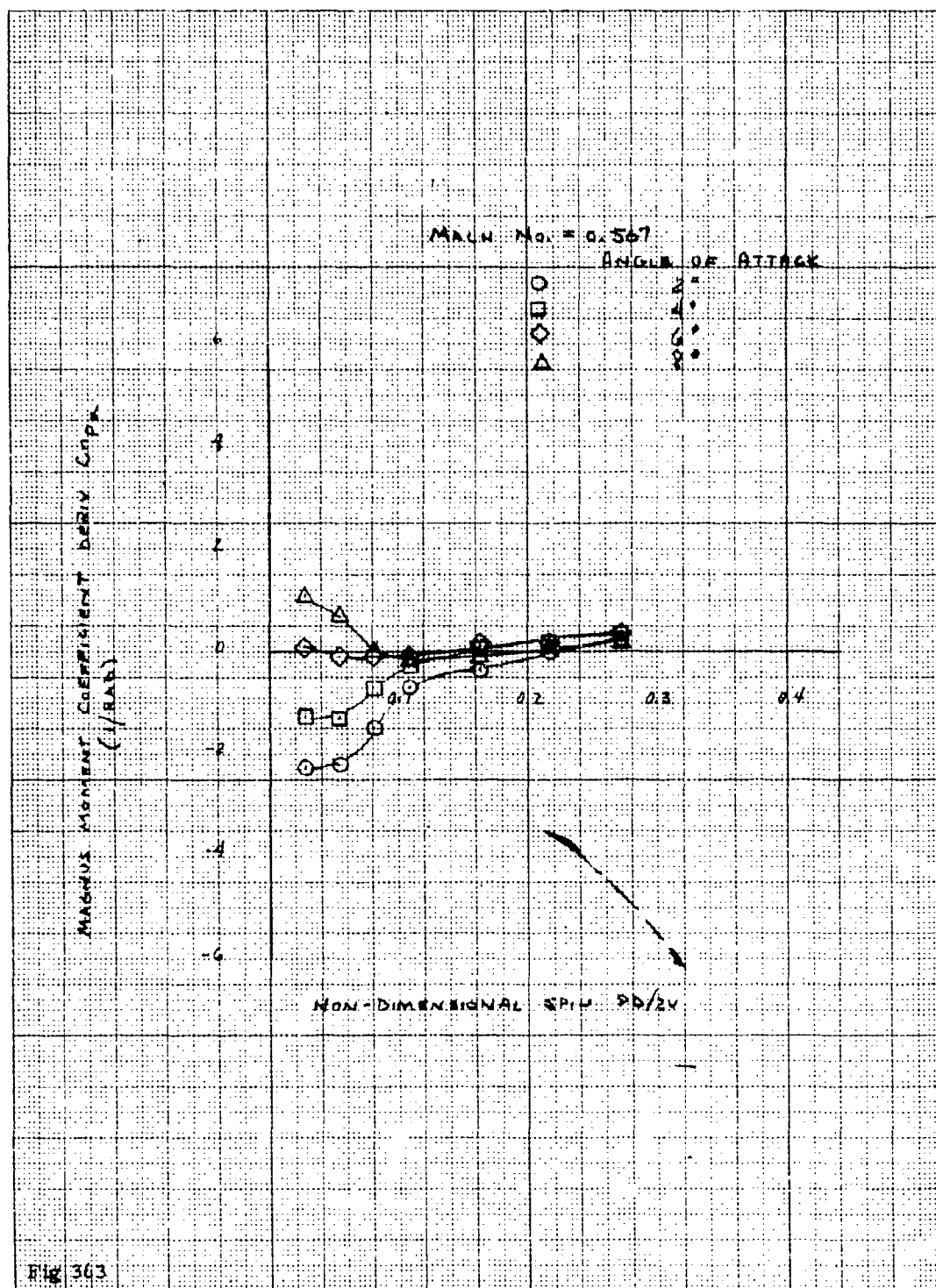


Fig 363

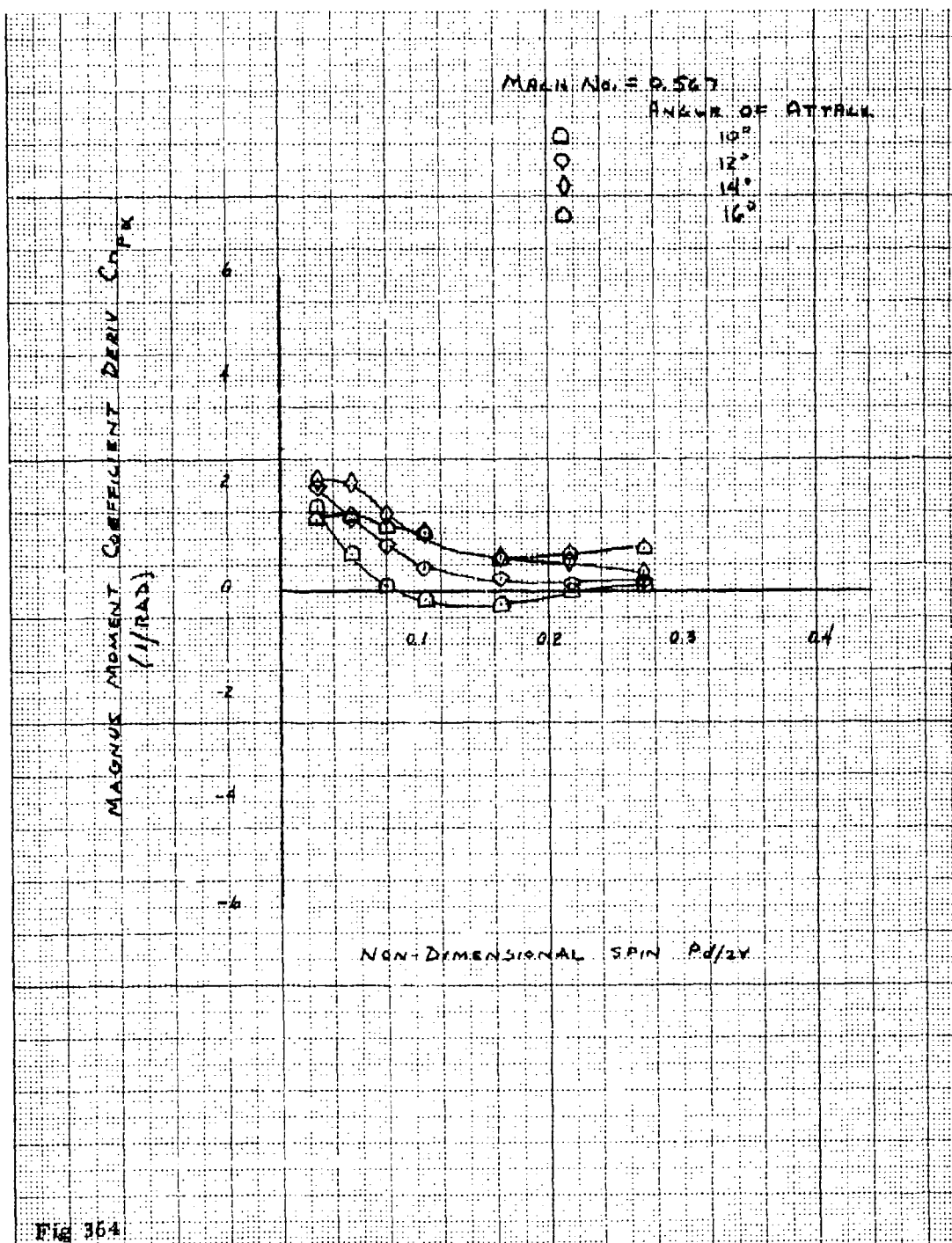


Fig 364

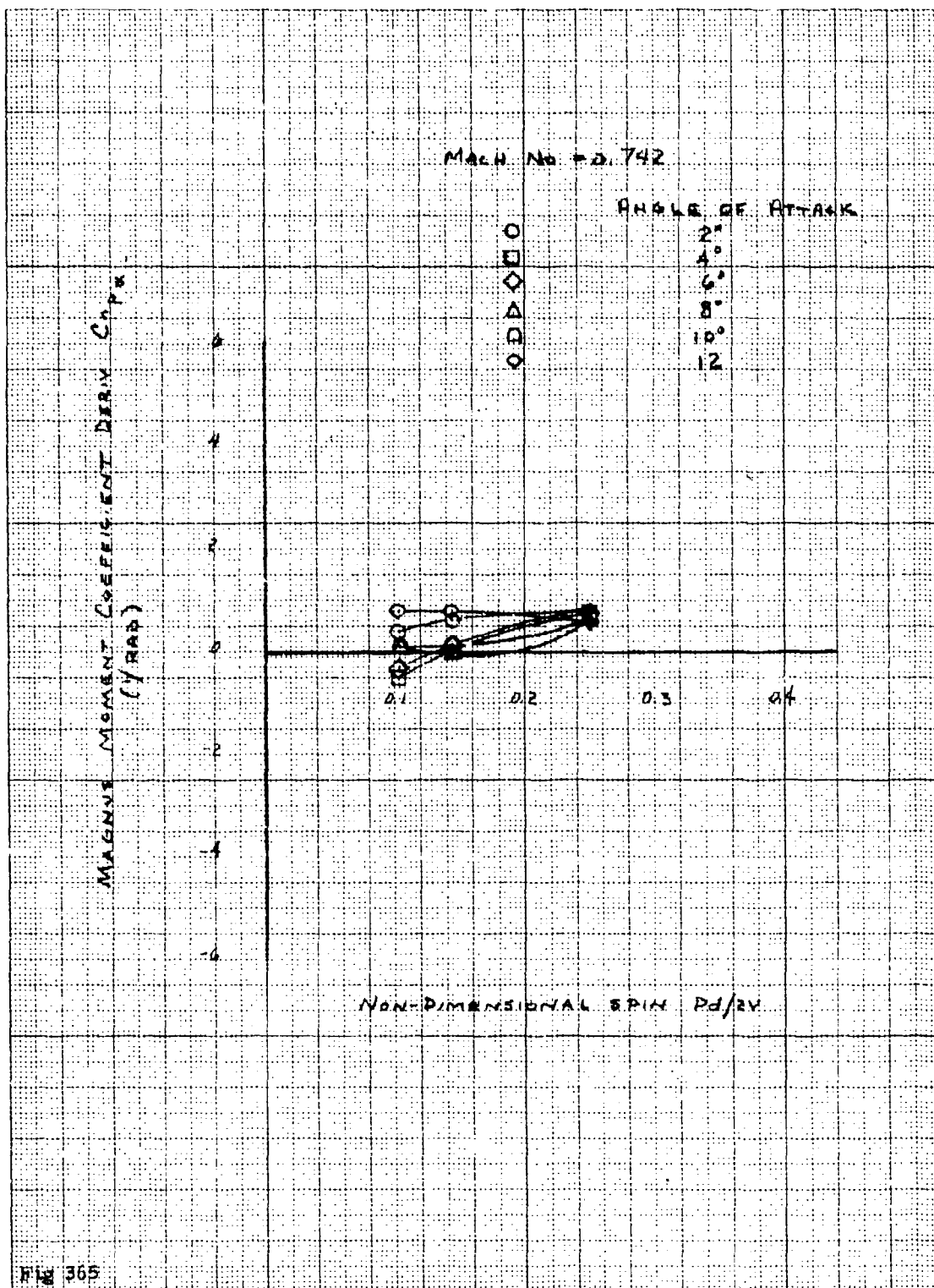


FIG 365

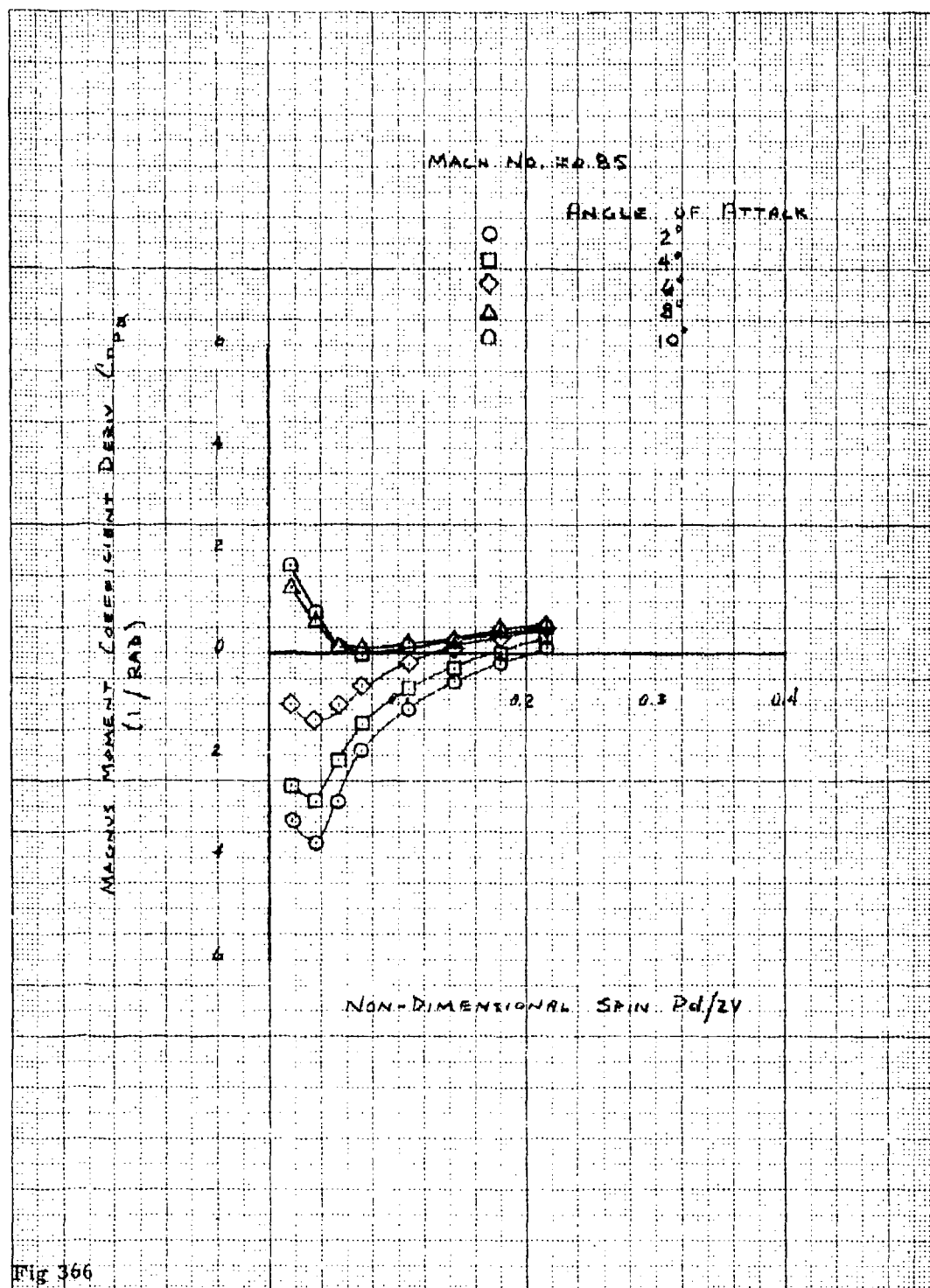


Fig 366

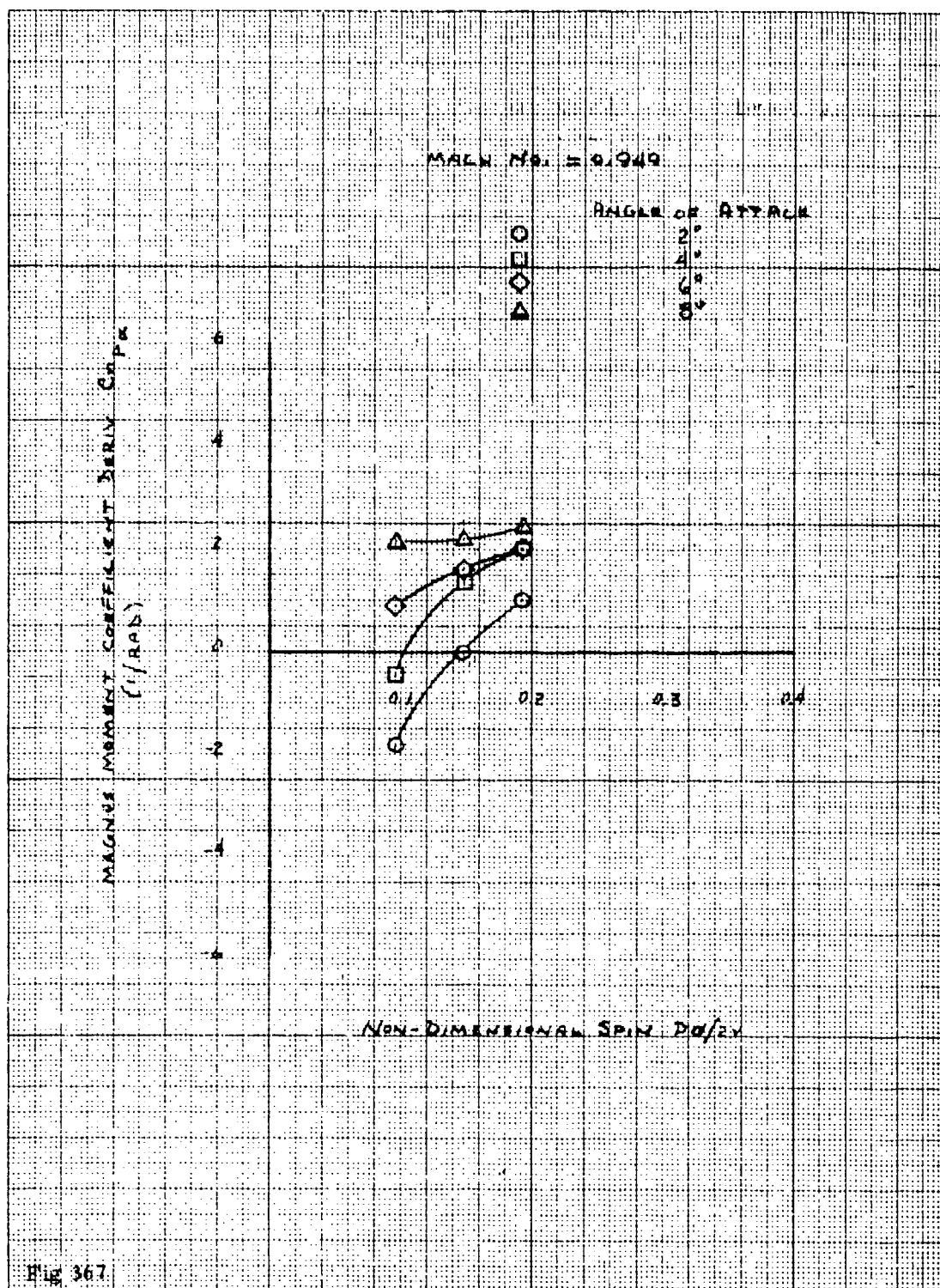
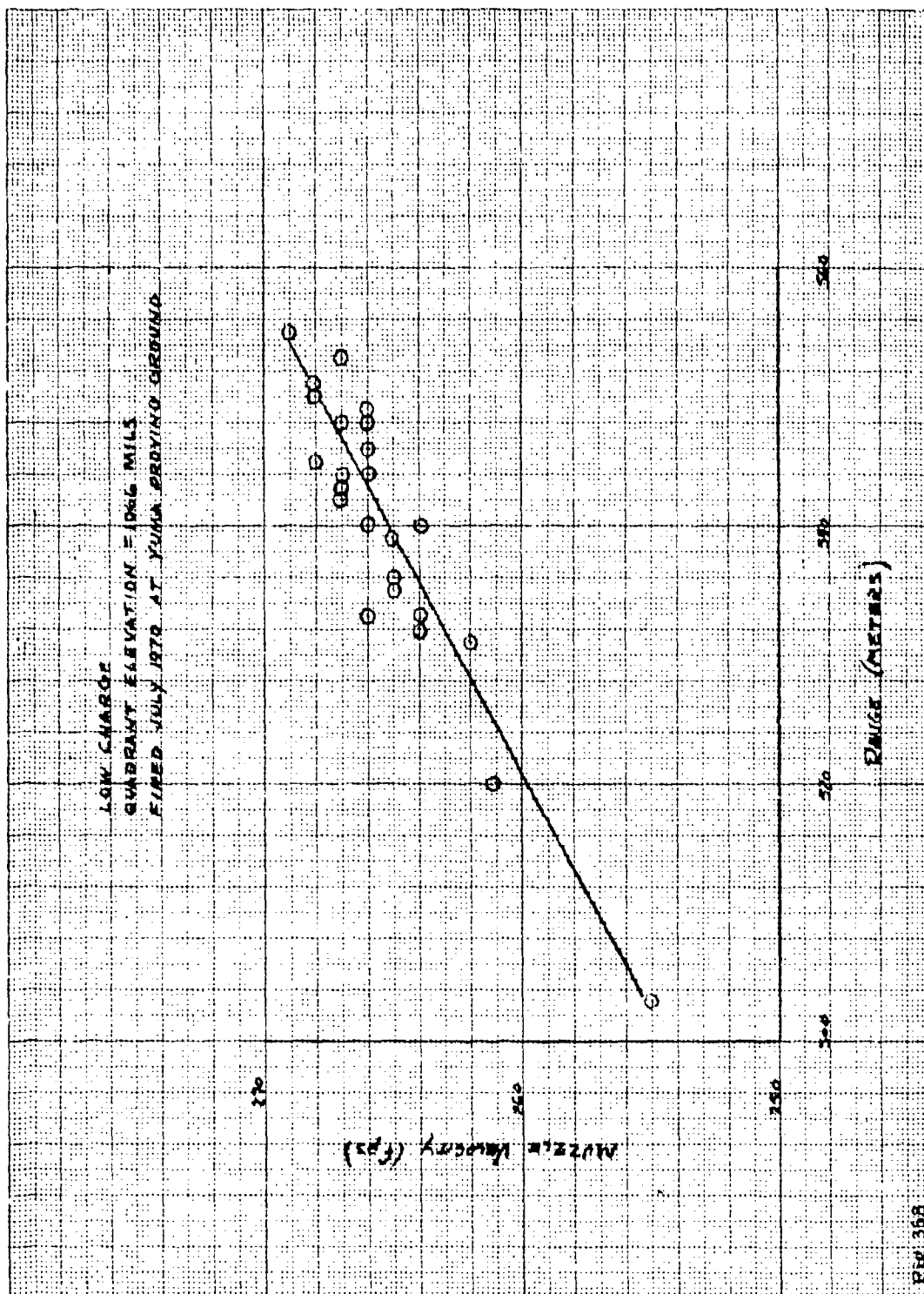
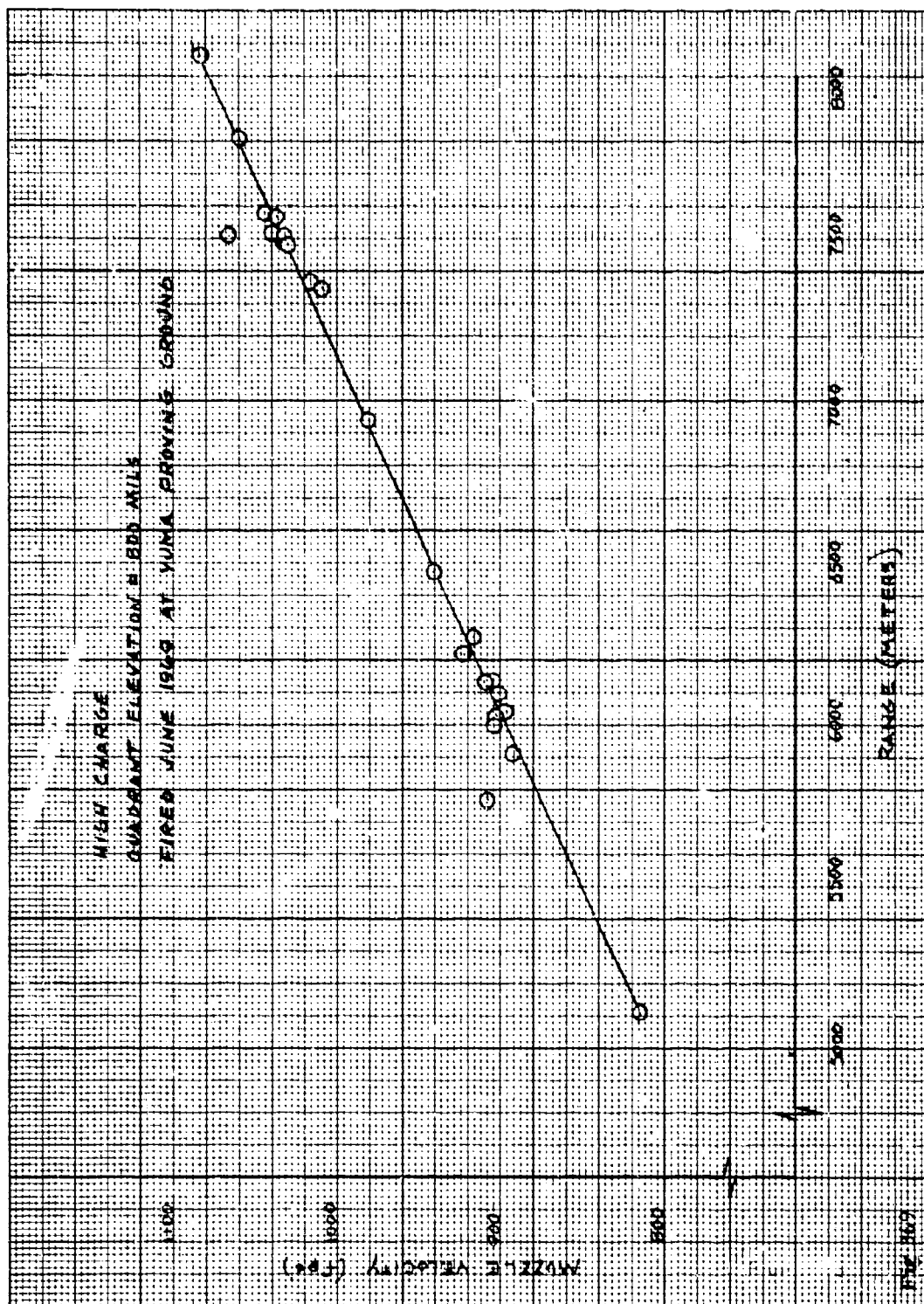


Fig 367

Figures 368 through 369

Muzzle velocity vs range for performance flight tests at
Yuma Proving Ground

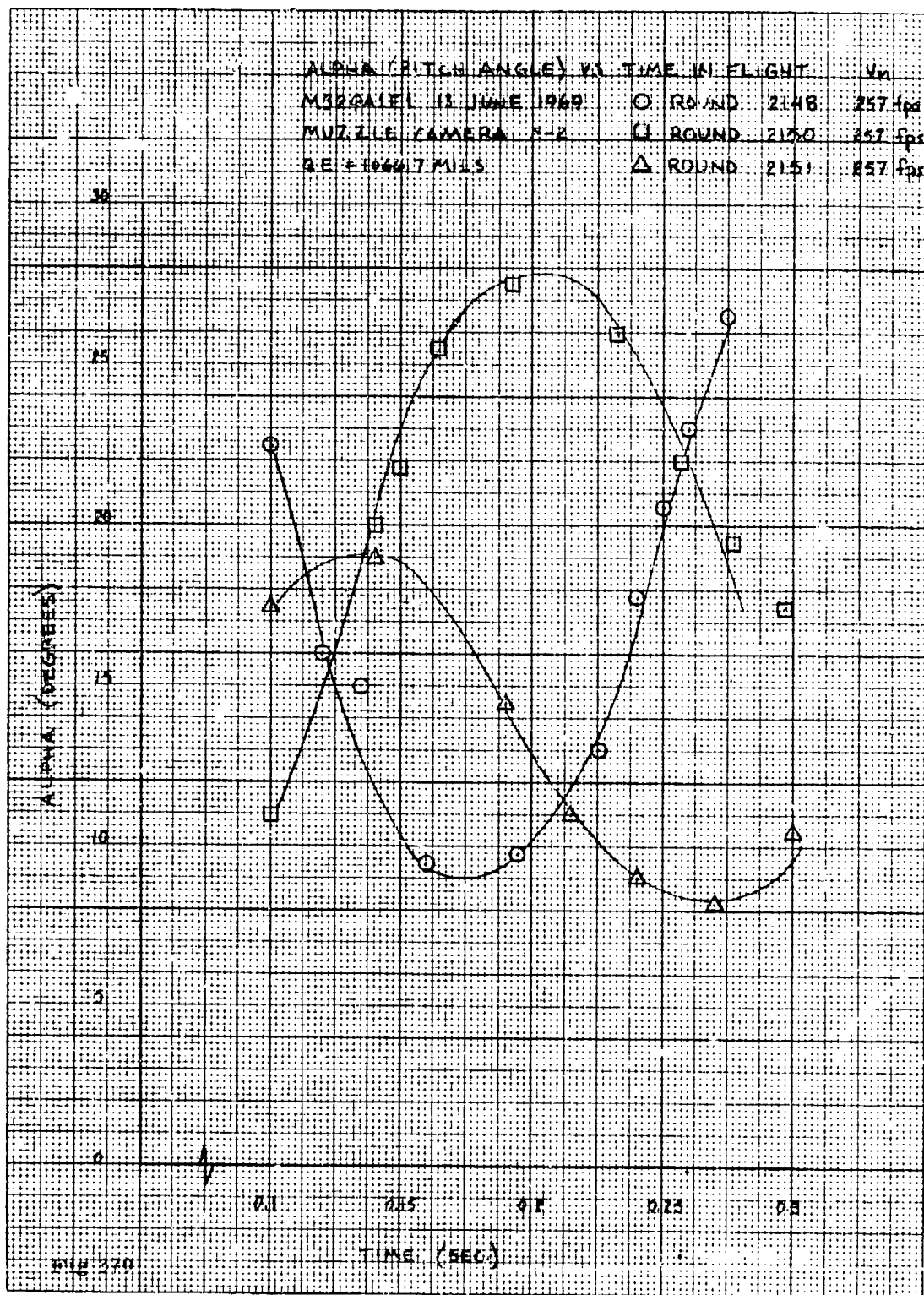


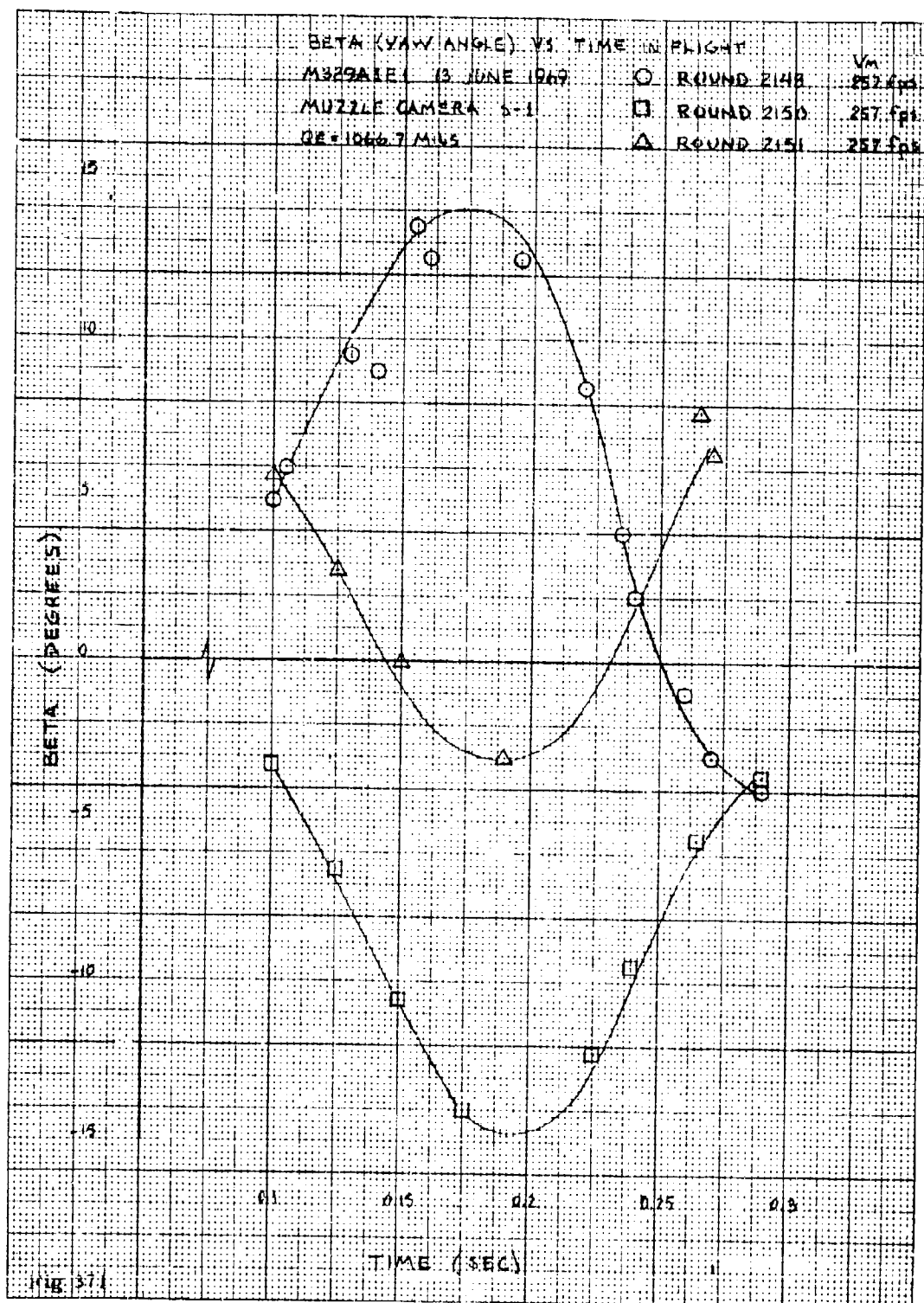


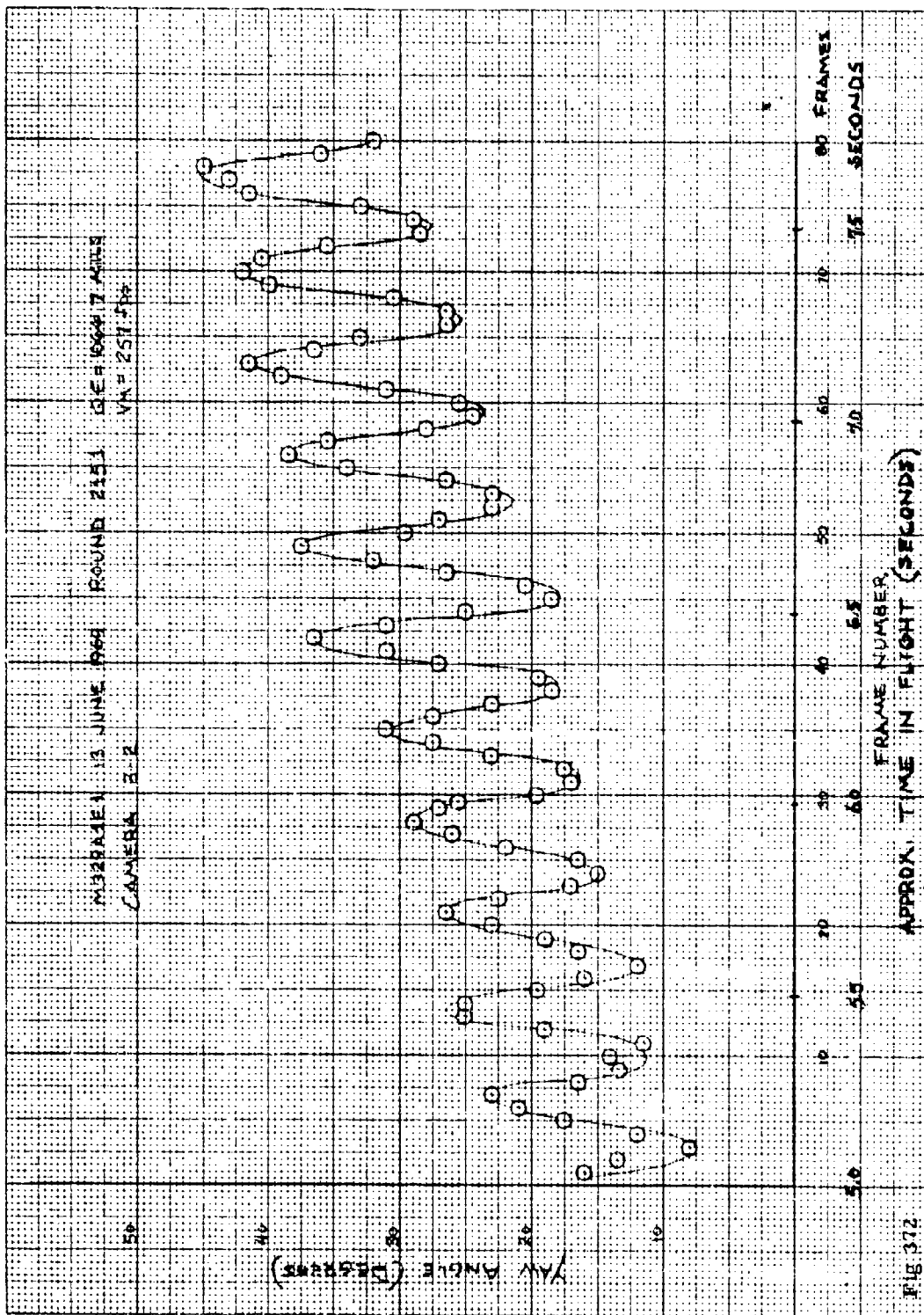
Figures 370 through 374

Yaw data translated from camera coverage shown in Figure 8

Preceding page blank







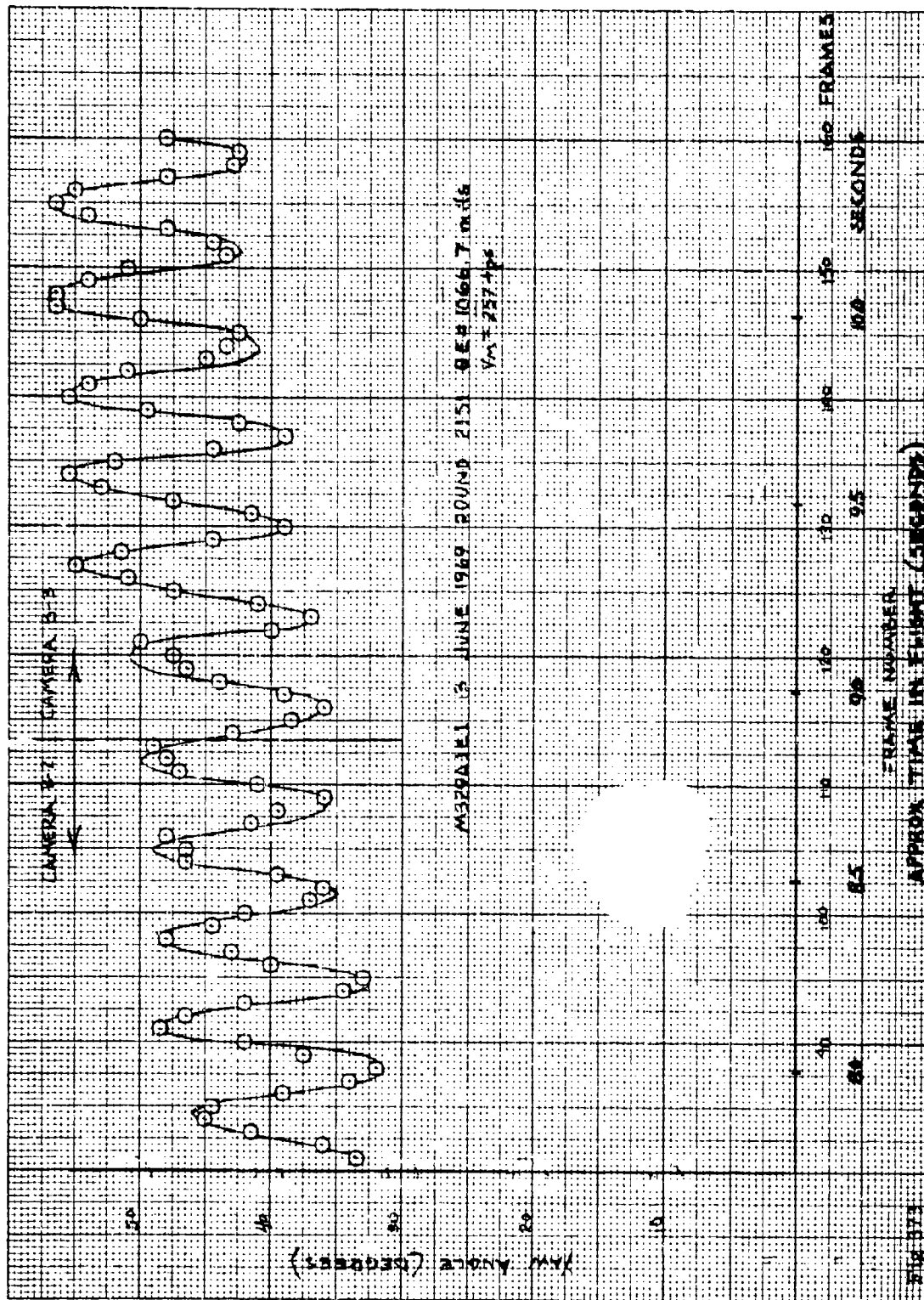




Fig 375 M329A1E1 projectile fired at low charge, with obturator still attached

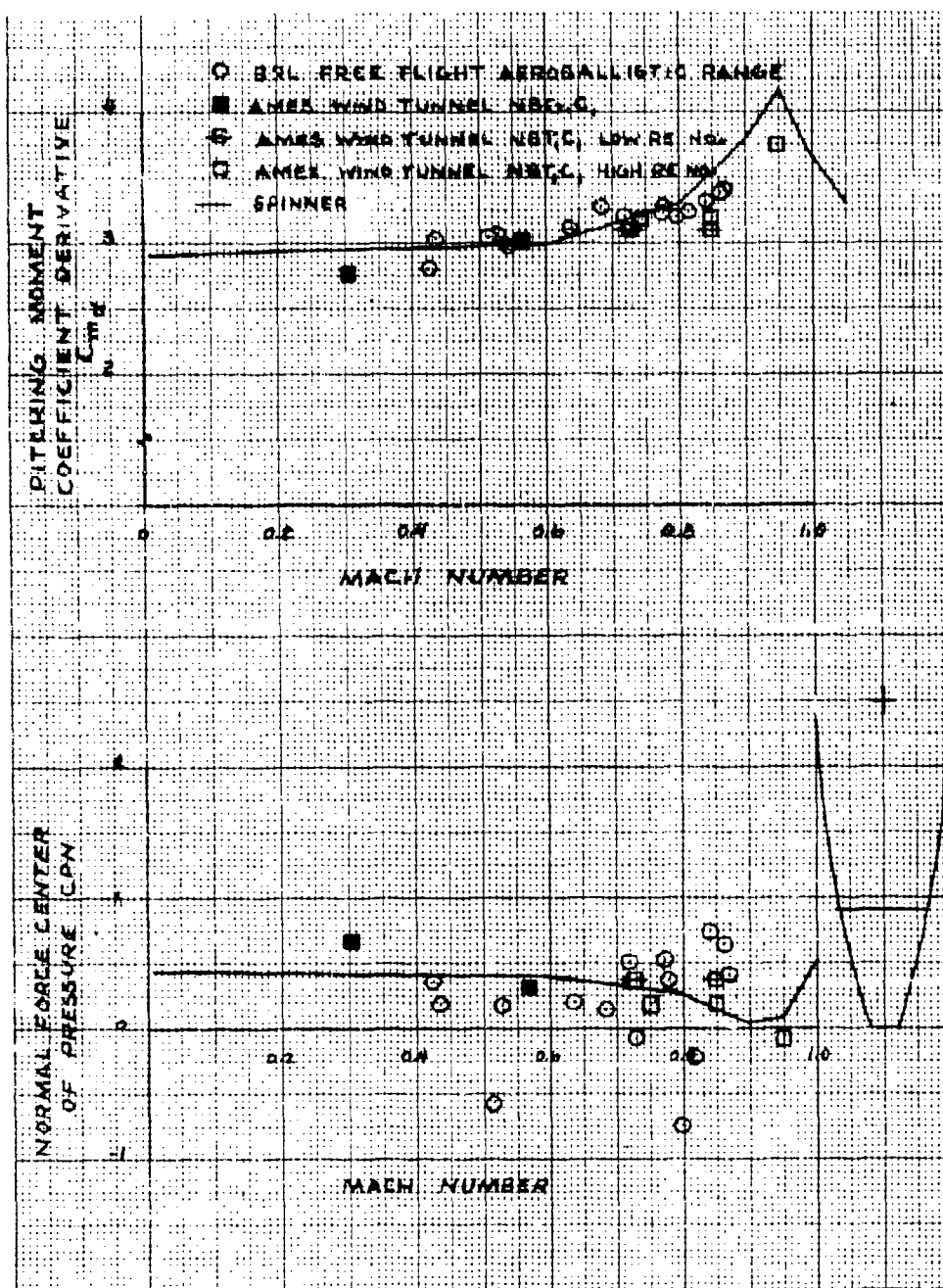
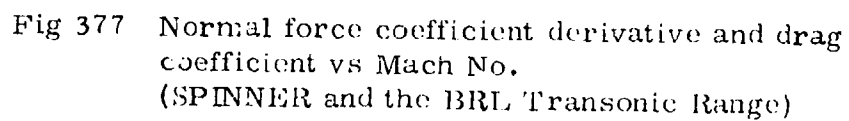


Fig 376 Pitching moment coefficient derivative and normal force center of pressure vs Mach No. (SPINNER and the BRL Transonic Range)
 ($NBG_1 C_L$, $NBT_1 C_L$)



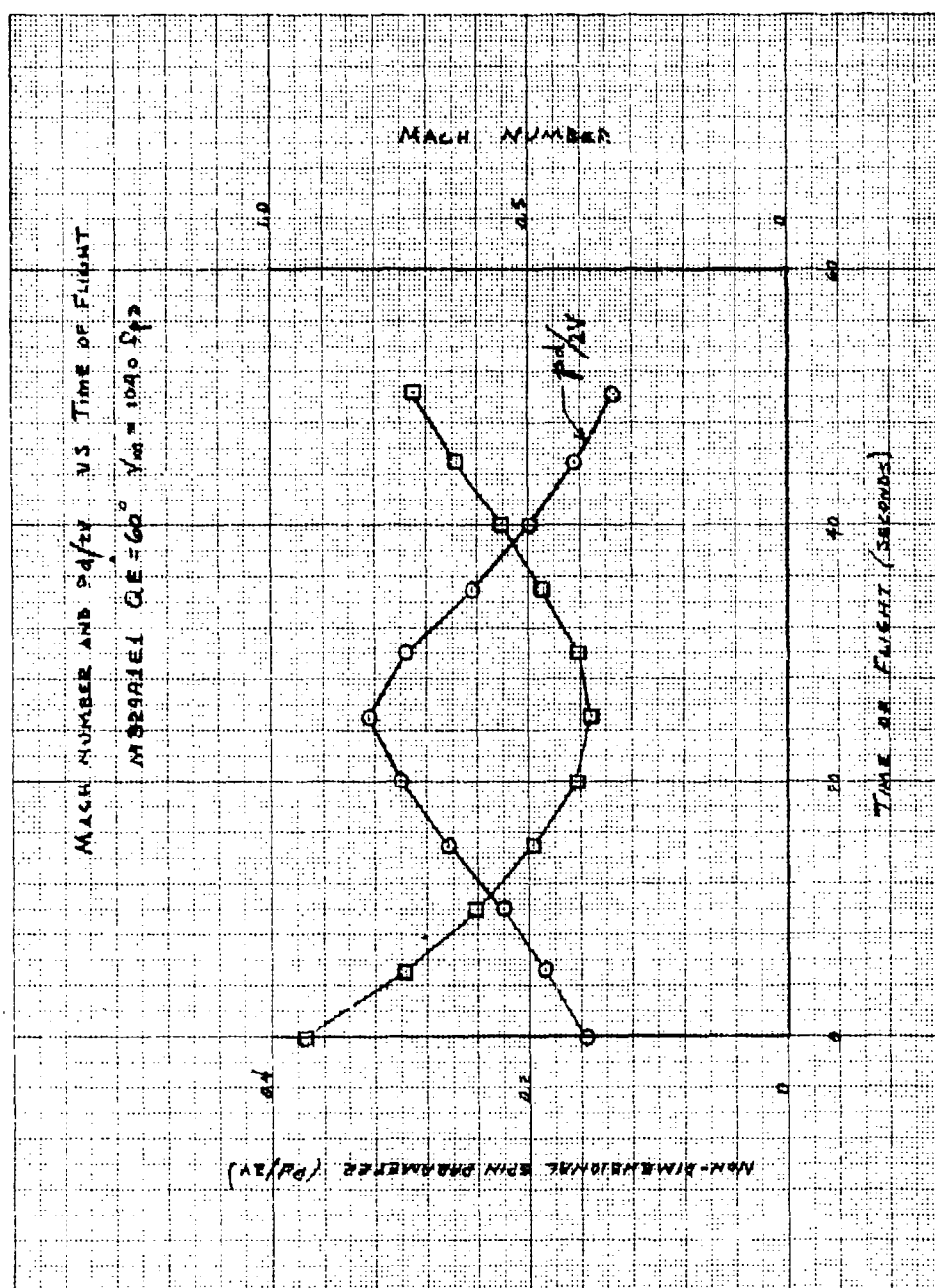


Fig 378 Mach No. and $pd/2V$ vs time of flight for M329A1E1 six-degree of freedom trajectory computer simulations. ($QE = 60^\circ$, $V_{muzzle} = 1040 \text{ fps}$)

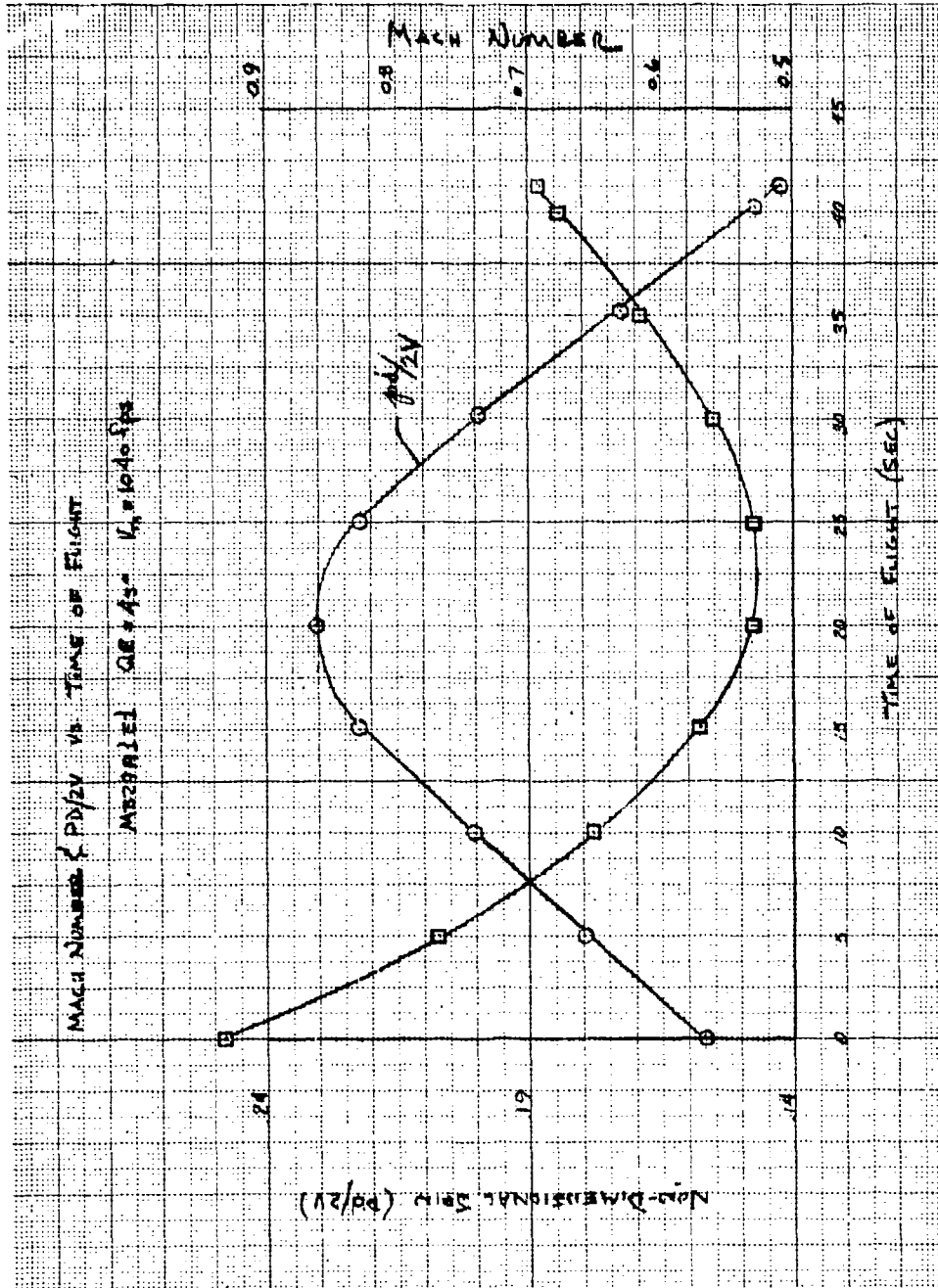


Fig 379 Mach No. and $pd/2V$ vs time of flight for M329A1E1 six-degree of freedom trajectory computer simulations. ($QE = 45^\circ$, $V_{\text{muzzle}} = 1040 \text{ fps}$)

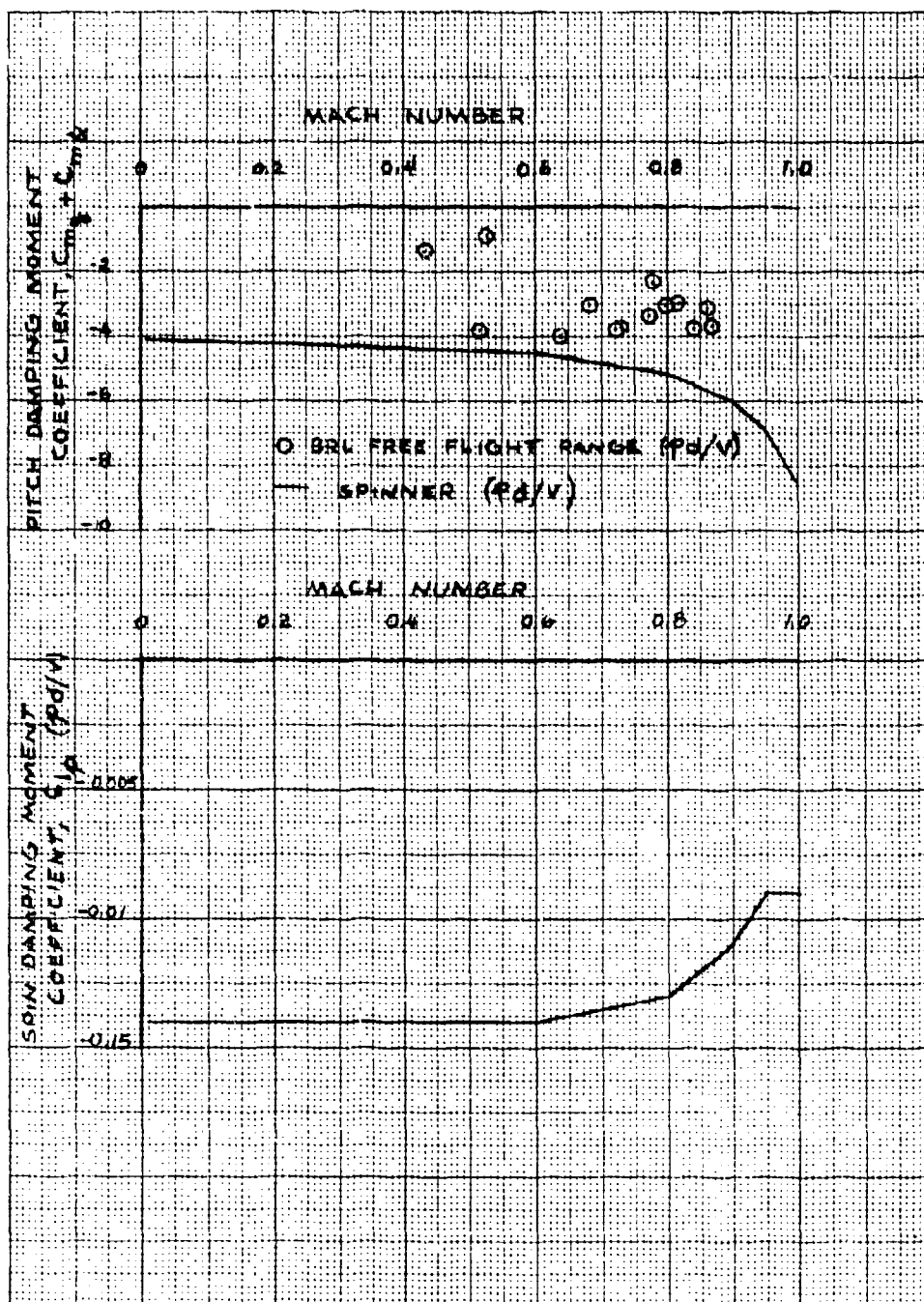


Fig 380 Pitch damping coefficient and spin damping coefficient vs Mach No.

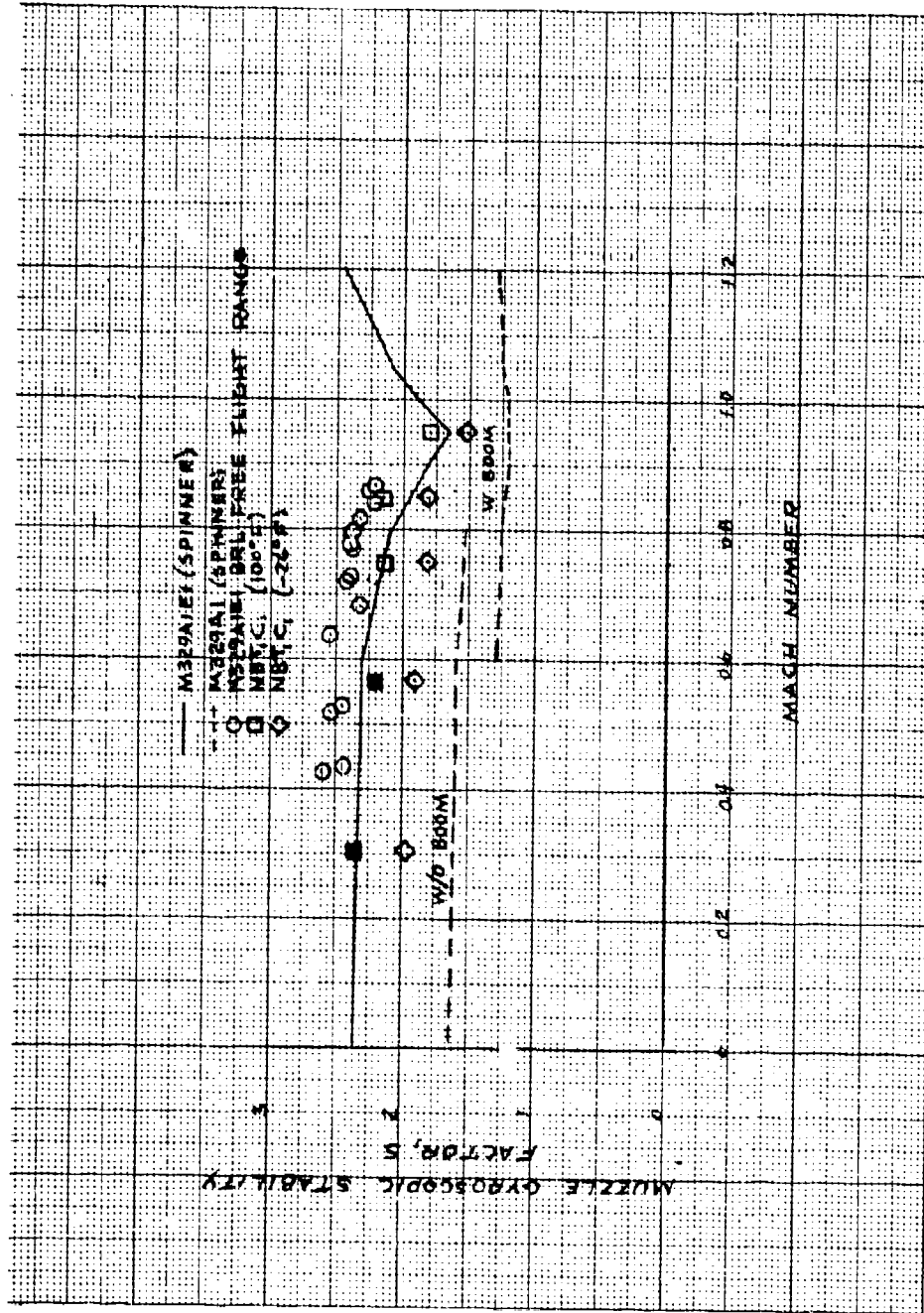


Fig 381 Muzzle gyroscopic stability factors vs Mach No.

Figures 382 through 386

Damping factors vs angle of attack for configuration
 NBT_1C_1 at various Mach numbers

Preceding page blank

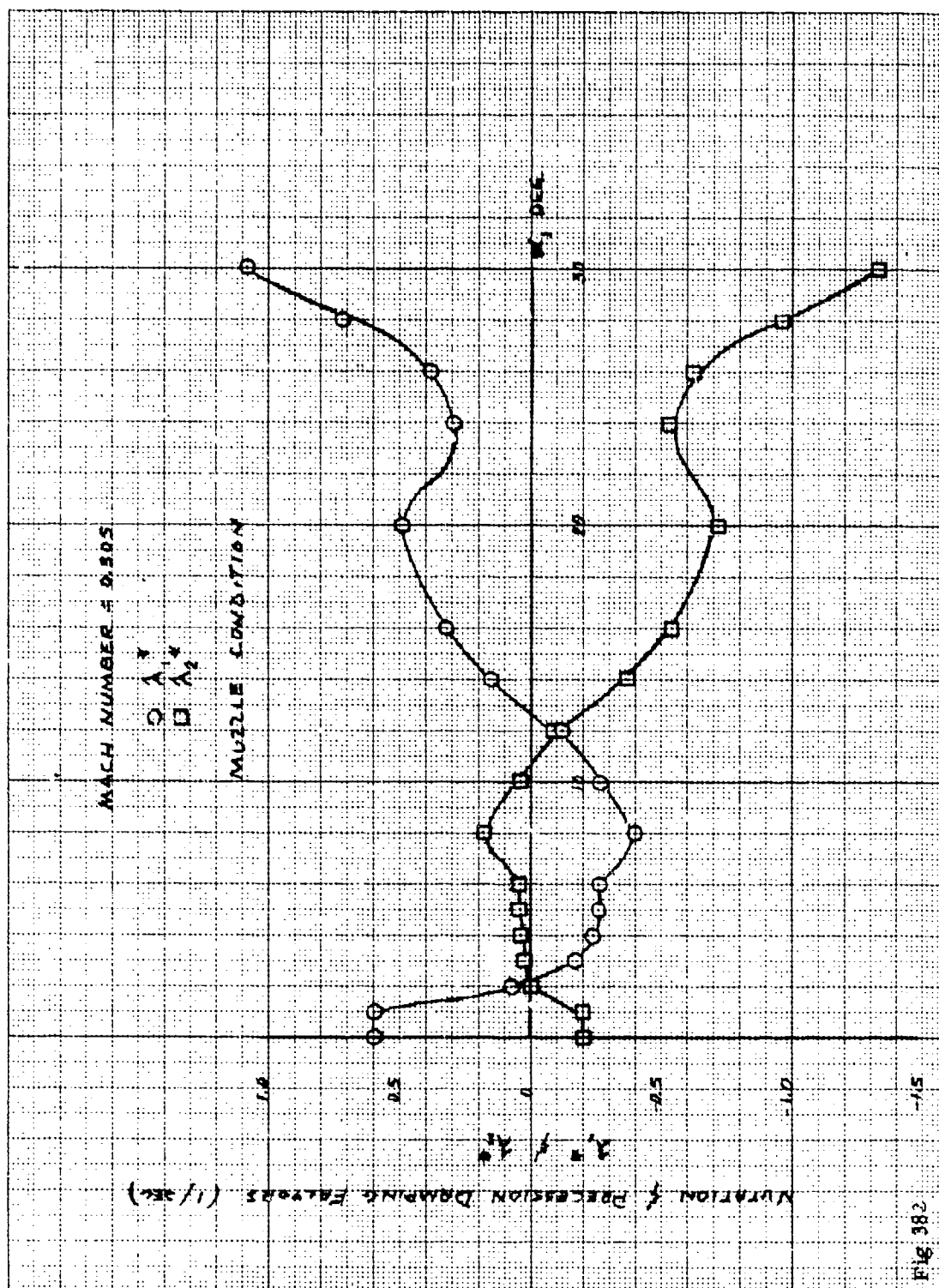


Fig. 382

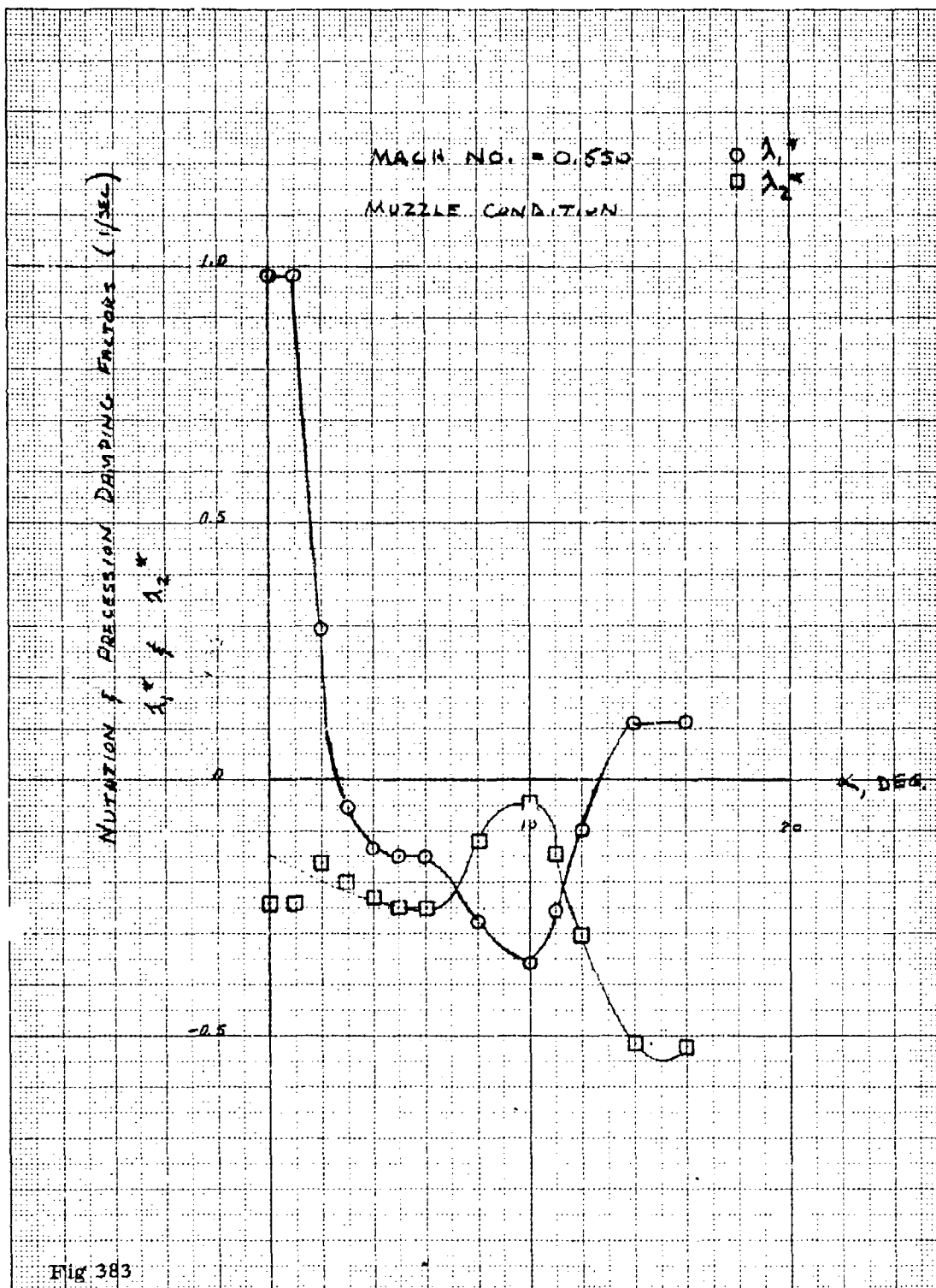


Fig 383

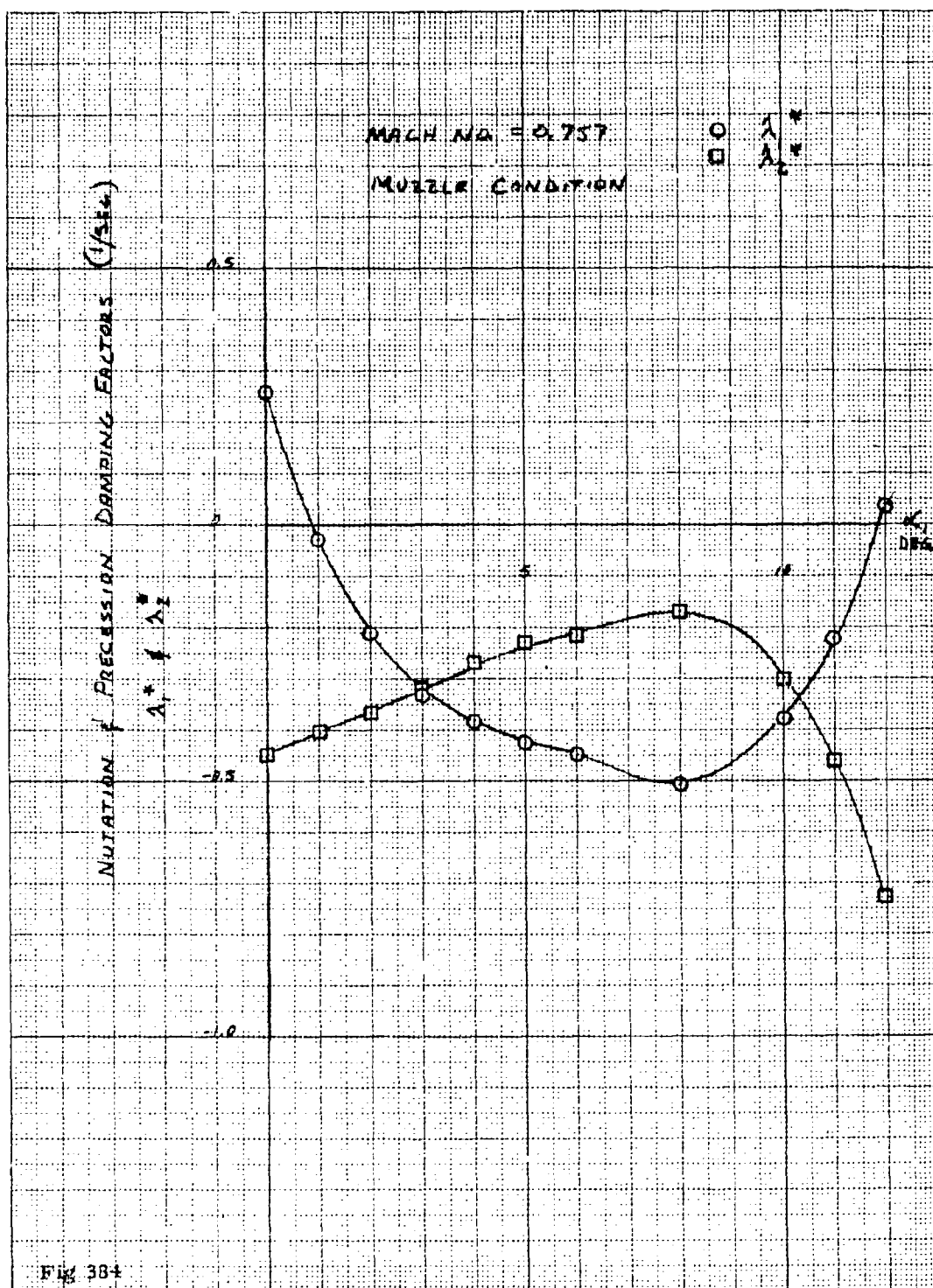


Fig 384

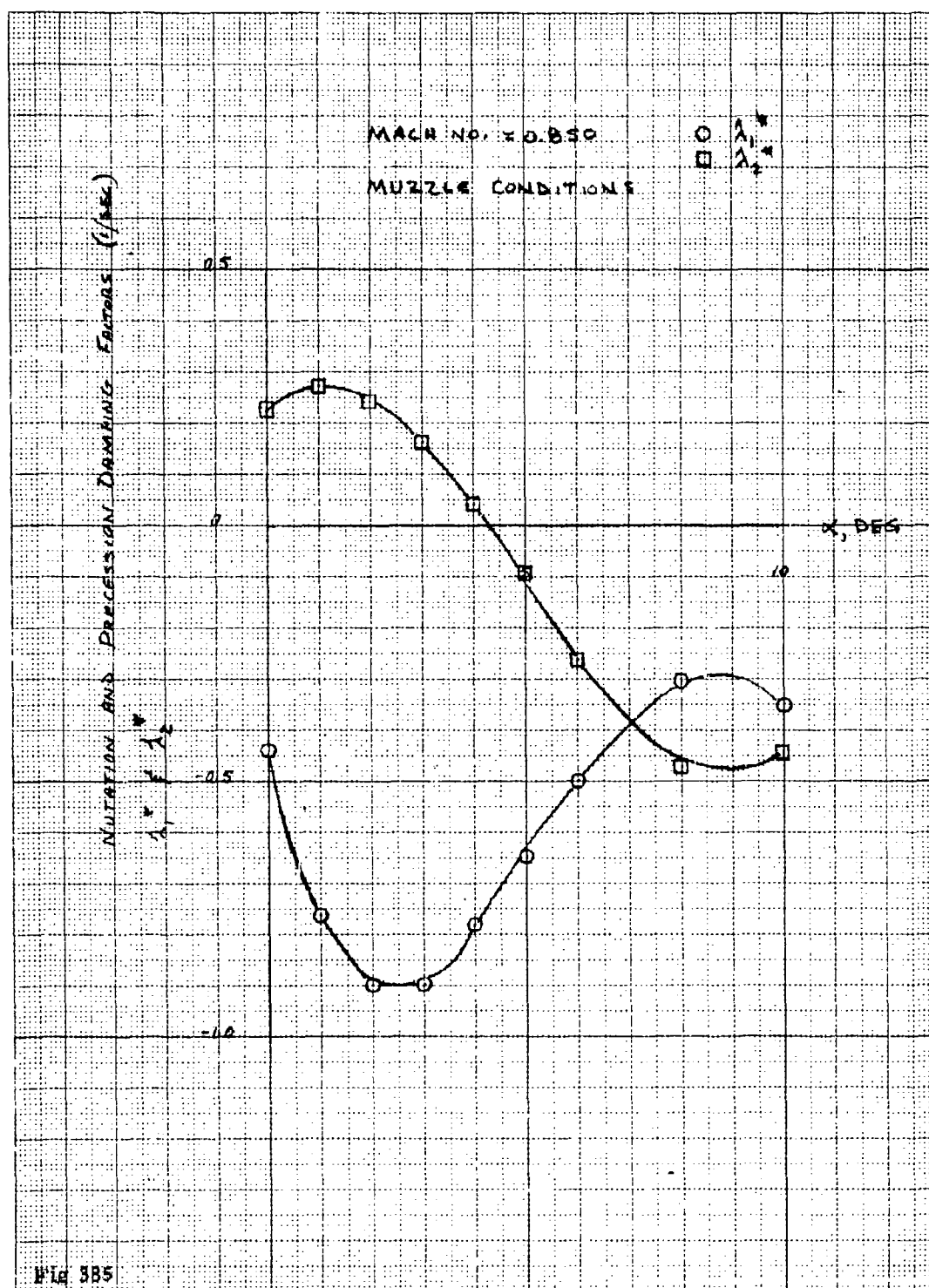
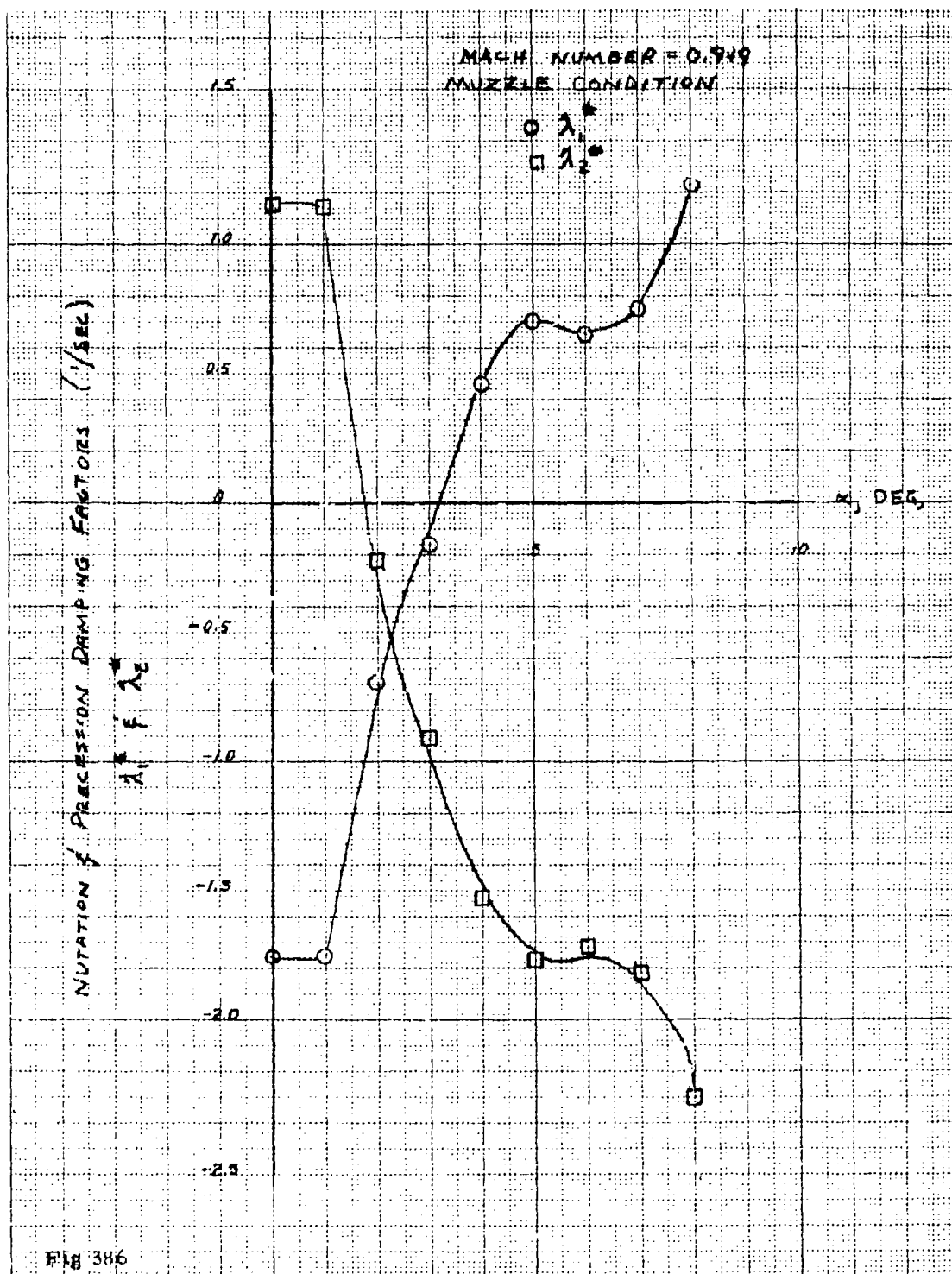
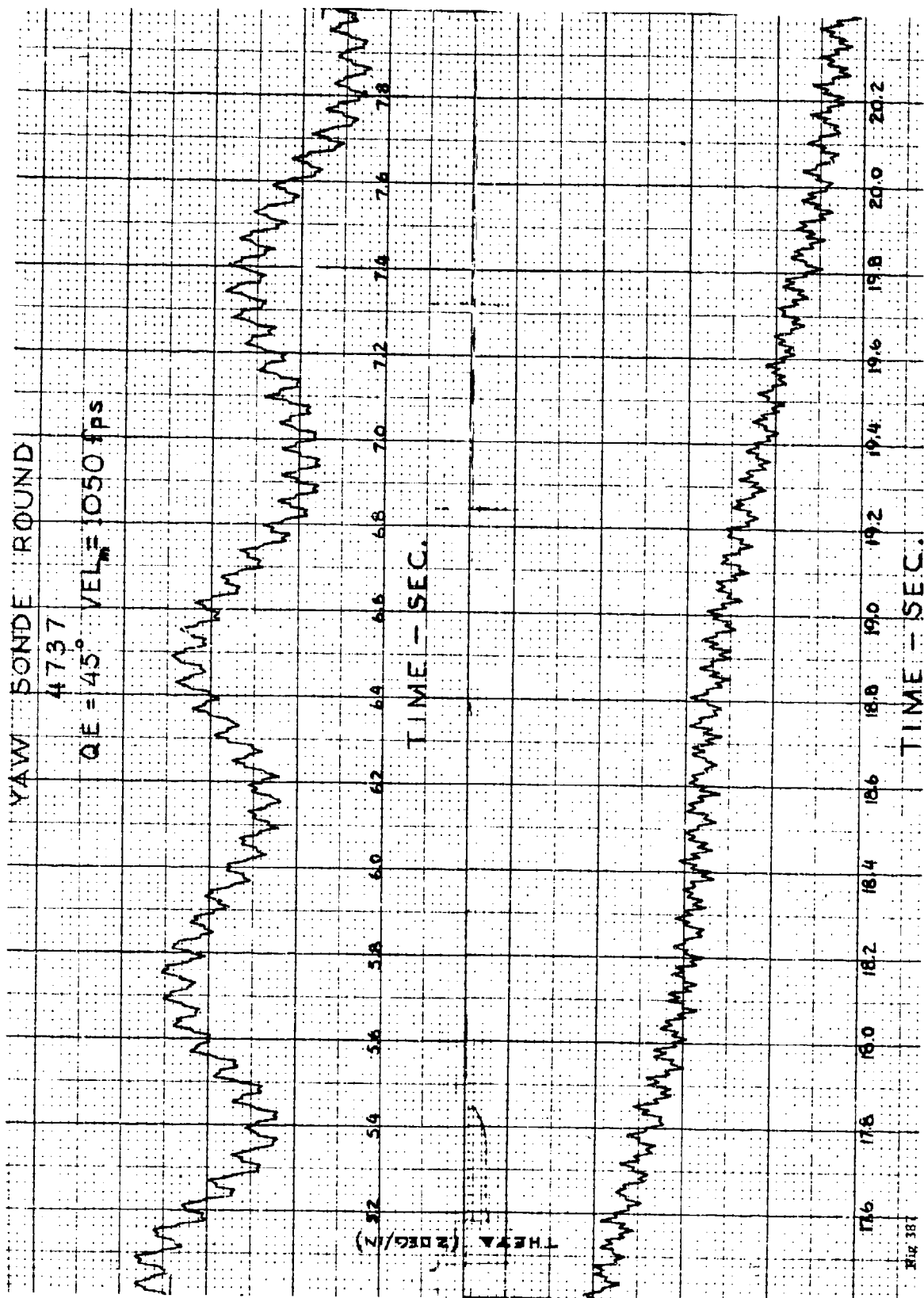


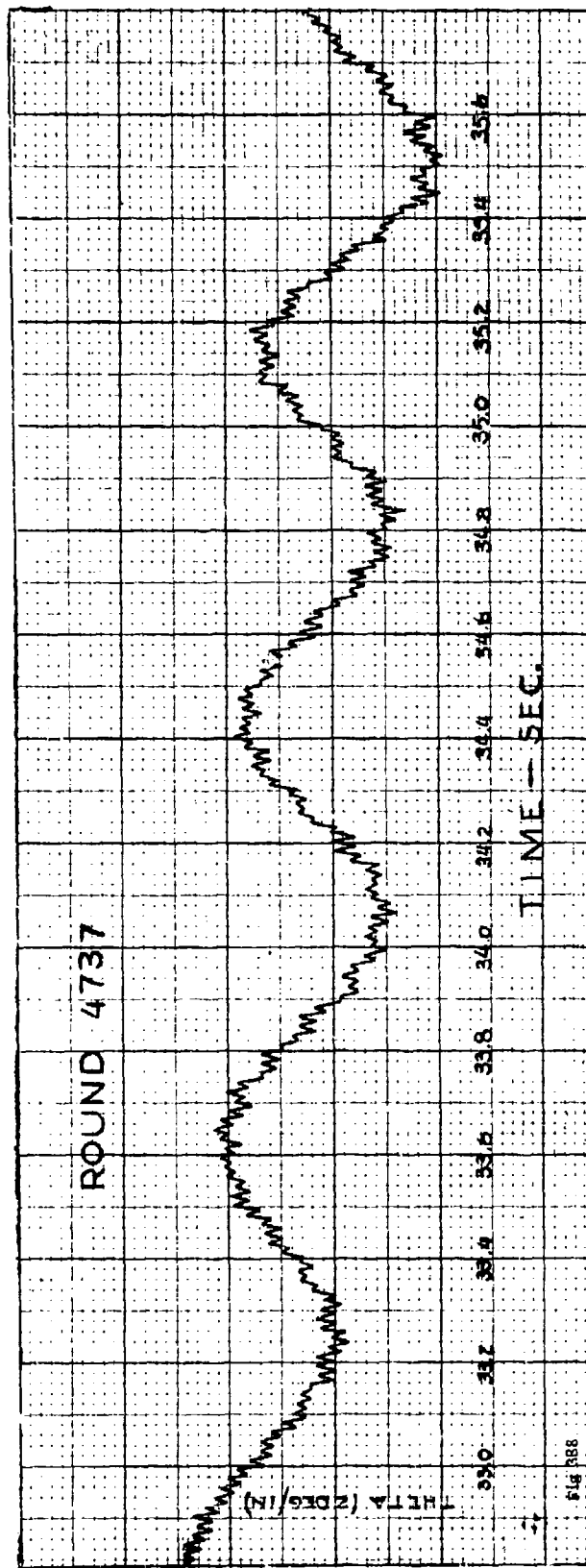
Fig 385



Figures 387 and 388

Solar aspect angle vs time of flight for M329A1E1
yaw sonde Round No. 4737



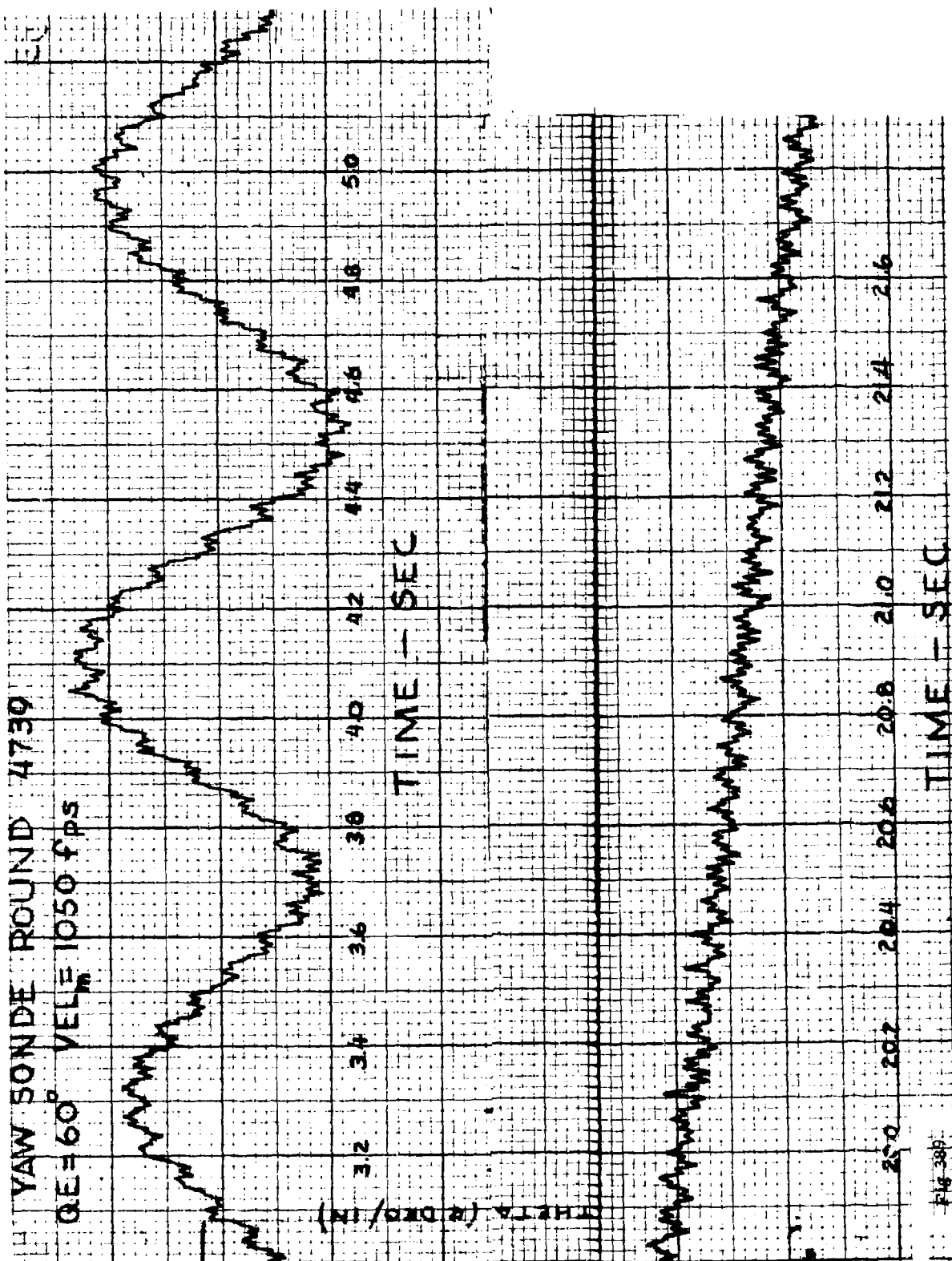


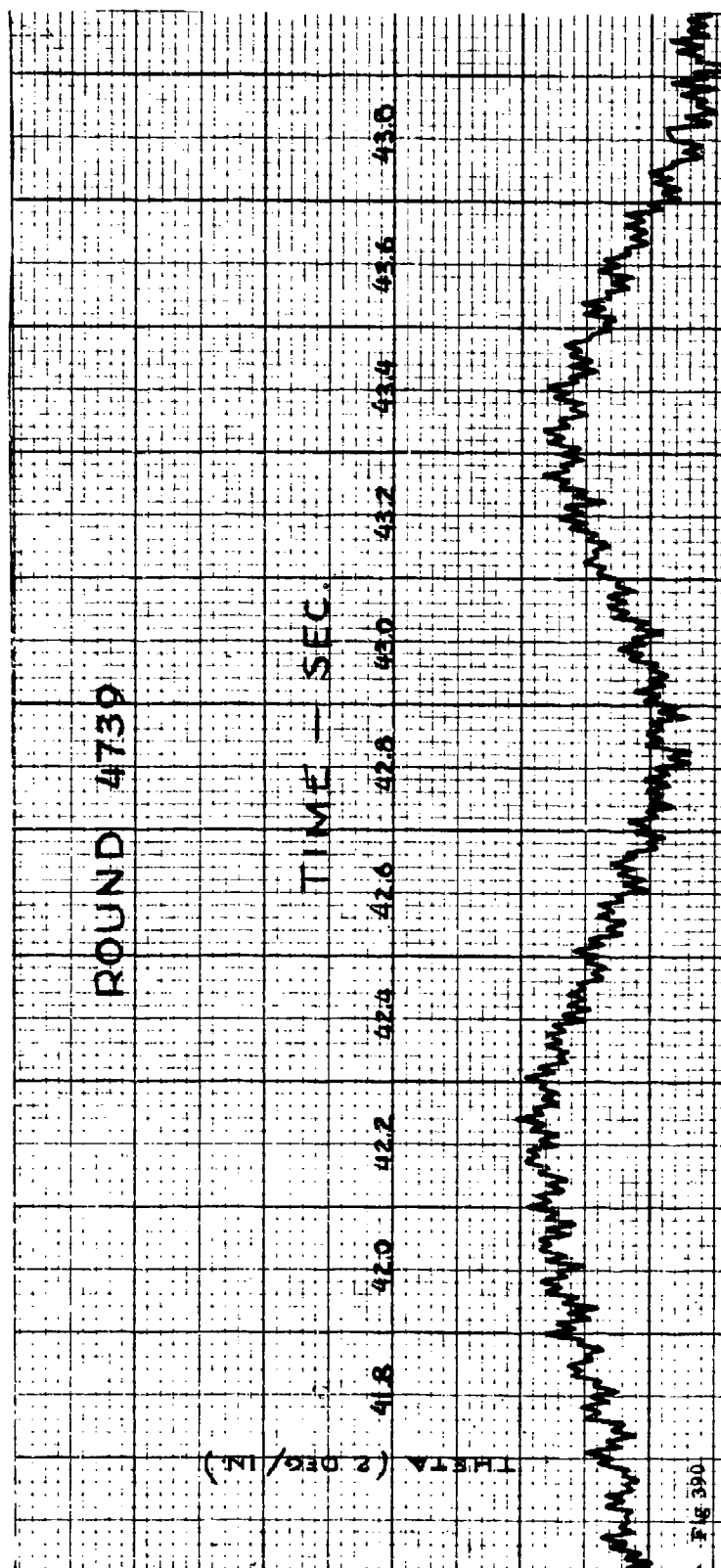
Figures 389 and 390

Solar aspect angle vs time of flight for M329A1E1
yaw sonde Round No. 4739

423

Preceding page blank





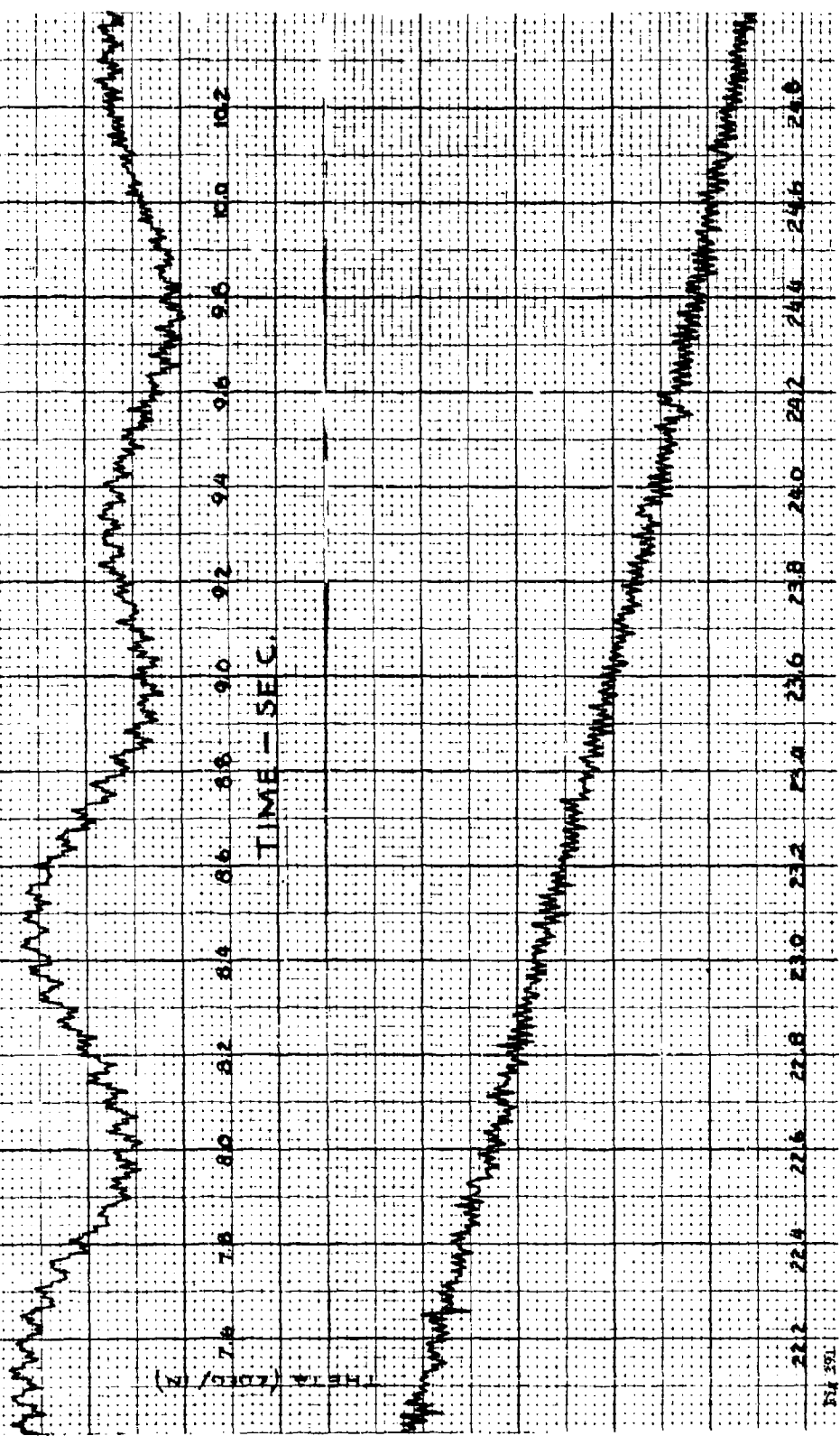
Figures 391 and 392

Solar aspect angle vs time of flight for M329A1E1
yaw sonde Round No. 4740

YAW SONDE ROUND

4740

QE=60° VEL_m=1050



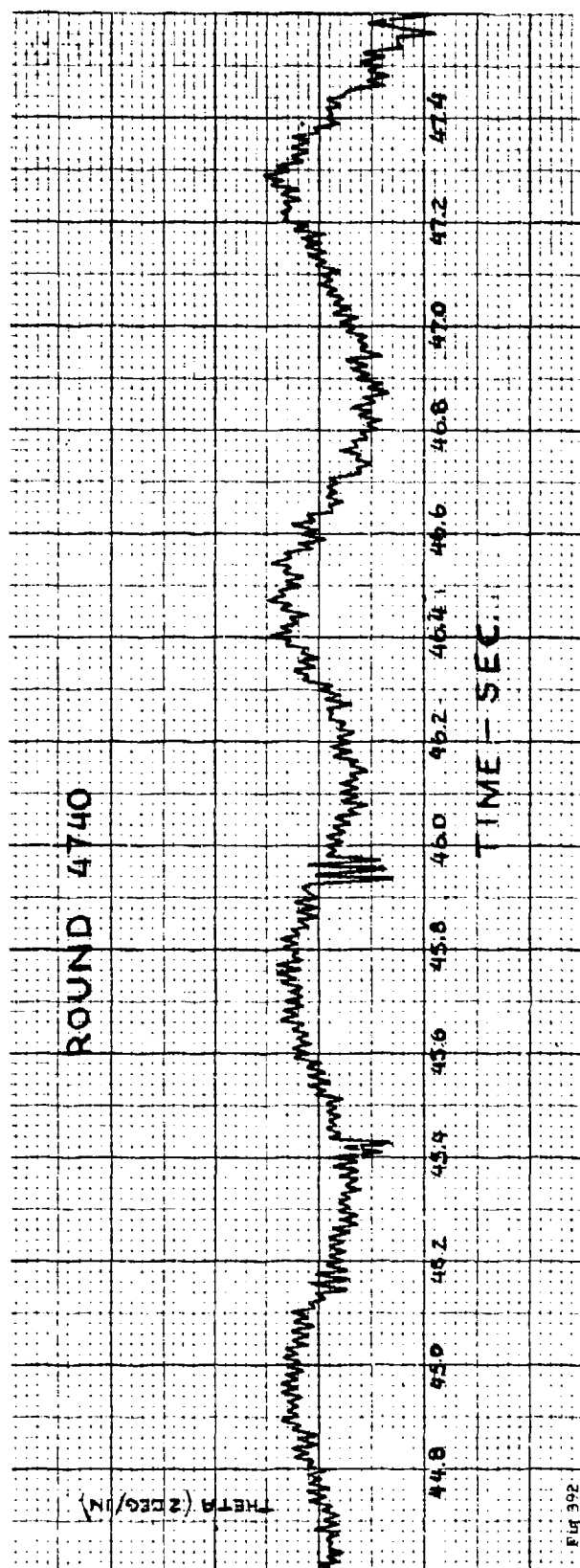


Fig 302